To subscribe for the book on amazon and ebay

Particle Beam Therapy:
contemporary trends and reviews

Editors: Huan Giap, Eric Y Chuang, Gary Y Yang

PARTICLE BEAM THERAPY:
CONTEMPORARY TRENDS AND REVIEWS

Edited by Huan Giap, MD, Ph.D
Eric Y Chuang, Sc.D
Gary Y Yang, MD

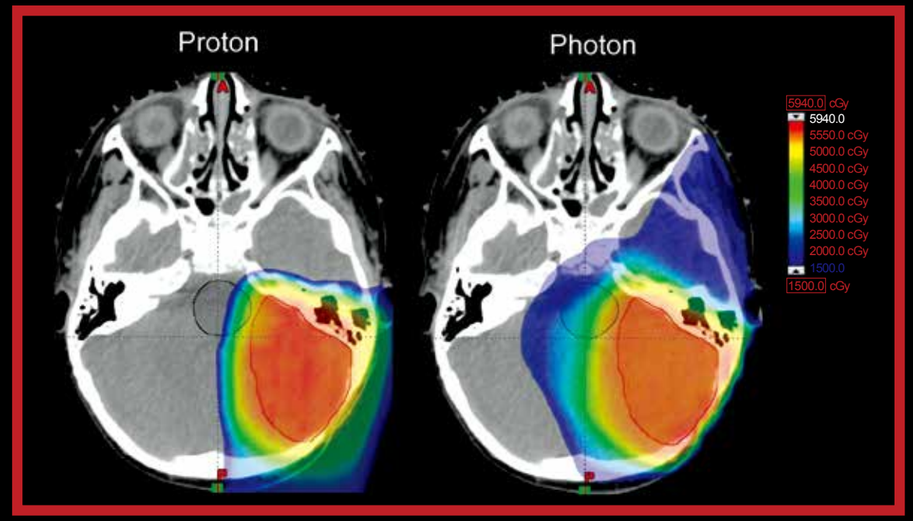

PBPC
Pioneer Bioscience Publishing Company

AME
Publishing Company

www.amepc.org

May 18 - 23, 2015

Manchester Grand Hyatt • San Diego, CA

Hosted by: Scripps Proton Therapy Center, University of California, San Diego & University of Maryland

54TH ANNUAL CONFERENCE OF THE

Particle Therapy Co-operative Group

Overview

The 2015 PTCOG annual meeting will be held in beautiful downtown San Diego, California. The theme for our 2015 conference will be The Modern Era of Particle Beam Therapy: Widening the Therapeutic Window for Better Patient Outcomes. As in the past, the conference will begin with the Educational Workshops taking place May 18-20th and be followed by the Scientific Meetings taking place May 21-23rd. The conference will feature plenary sessions, workshops, poster presentations and an extensive exhibition hall. Participants will also have an opportunity to visit the newly opened Scripps Proton Therapy Center and celebrate "San Diego style" at the Wednesday evening Gala.

Conference Highlights

- Plenary talks from nationally recognized experts
- More than fifty abstract presentations and hundreds of scientific posters
- Receptions and networking opportunities among colleagues
- Site visit to the newly opened Scripps Proton Therapy Center
- Mobile conference app with access to course materials and recordings from the convenience of your mobile device or computer

Conference Location

Manchester Grand Hyatt
One Market Place
San Diego, California 92101

619-232-1234

manchestergrand.hyatt.com

Discover a unique urban retreat in the heart of San Diego that the whole family will enjoy. The Hyatt hotel features an array of premium amenities including a bayside pool, city-view tennis courts and a serene spa. Manchester Grand Hyatt San Diego is distinctively heralded among the best hotels in San Diego and is conveniently located just minutes from the San Diego International Airport and attractions like the San Diego Zoo, Sea World, and Seaport Village. A specially priced block of rooms is on hold for our group until Friday, April 24, 2015 or until the room block fills, whichever comes first.

Accreditation

Scripps Health is accredited by the Accreditation Council for Continuing Medical Education (ACCME) to provide continuing medical education for physicians. This activity has been approved for *AMA PRA Category 1 Credit(s)*™.

Visit Our Website for Course Updates and Abstract Submission Dates
WWW.PTCOG54.ORG

For More Information
Scripps Conference Services & CME
11025 North Torrey Pines Rd., Ste. 200
La Jolla, CA 92037
858-652-5400
med.edu@scrippshealth.org

AME Publishing Company

FLAT A, 9/F Gold Shine Tower, 346-348 Queen's Road Central, Sheung Wan, Hong Kong.

Information on this title: www.amepc.org
For more information, contact info@amepc.org

First published 2014
Printed in AME Publishing Company

Huan Giap, Eric Y Chuang, Gary Y Yang
Particle Beam Therapy: contemporary trends and reviews
978-988-12997-4-1 (hardback)
978-988-12997-5-8 (eBook)

Particle Beam Therapy: contemporary trends and reviews

Contributors

EDITORS

Huan Giap, MD, Ph.D,
Professor, Department of Radiation Medicine and Applied Sciences,
University of California at San Diego,

Chief of GI, Lung, and Breast Service
Director of Clinical Research, Scripps Proton Therapy Center, San Diego, CA 92121, USA

Eric Y Chuang, Sc.D.,
Professor and Director,
Graduate Institute of Biomedical Electronics and Bioinformatics, National Taiwan University, Taipei, Taiwan

Gary Y. Yang, MD
Professor and Dell E. Webb Chair in Radiation Medicine, Department of Radiation Medicine, Loma Linda University Medical Center, Loma Linda, CA 92350, USA

AUTHORS

Bestoun Ahmed, MD
Department of Surgery, University of Florida College of Medicine, Jacksonville, FL 32206, USA

Michelle Alonso-Basanta, MD, Ph.D
Department of Radiation Oncology, Perelman School of Medicine, University of Pennsylvania, Philadelphia, PA 19104, USA

Shrikant Anant, Ph.D
Department of Molecular and Integrative Physiology, University of Kansas Cancer Center, University of Kansas Medical Center, Kansas City, KS 66160, USA

Stephen Avery, Ph.D
Department of Radiation Oncology, Perelman School of Medicine, University of Pennsylvania, Philadelphia, PA 19104, USA

Ziad T. Awad, MD
Department of Surgery, University of Florida College of Medicine, Jacksonville, FL 32206, USA

Eric J. Bernhard, Ph.D
Radiation Research Program, Division of Cancer Treatment and Diagnosis, National Cancer Institute, Bethesda, MD 20892, USA

Shanta Raj Bhattarai, Ph.D
Department of Radiation Oncology, The University of Texas M. D. Anderson Cancer Center, Houston, TX 77030, USA

Erik Blomquist, MD
Department of Radiology, Oncology and Radiation Science, Oncology, Uppsala University, Uppsala 75185, Sweden

Jordan M. Blum
Pharmacology & Cancer Biology, Duke University Medical Center, Durham, NC 27710, USA

Stefan Both, Ph.D
Department of Radiation Oncology, Hospital of the University of Pennsylvania, Philadelphia, PA 19104, USA

Aaron P Brown, MD
Department of Radiation Oncology, The University of Texas M. D. Anderson Cancer Center, Houston, TX 77030, USA

Viet Bui
University of Pennsylvania, Philadelphia, PA 19104, USA

Christian Bula
Center for Proton Therapy, Paul Scherrer IVilligen 5232, Switzerland

David A. Bush, MD
Department of Radiation Medicine, Loma Linda University Medical Center, Loma Linda, CA 92354, USA

Jacek Capala, MD
Radiation Research Program, Division of Cancer Treatment and Diagnosis, National Cancer Institute, Bethesda, MD 20892, USA

Andrew L. Chang, MD
Indiana University School of Medicine, IN, USA; Indiana University Health Proton Therapy Center, Bloomington, IN 46202, USA

Dev Kumar Chatterjee
Department of Radiation Oncology, The University of Texas M. D. Anderson Cancer Center, Houston, TX 77303, USA

Chee-Wai Cheng, Ph.D
Indiana University Health Proton Therapy Center, Bloomington, IN 47408, USA; Department of Radiation Oncology, Indiana University School of Medicine, Indianapolis, IN 46202, USA

Rovel J. Colaco, MD
University of Florida Proton Therapy Institute, Jacksonville, FL 32206, USA

C. N. Coleman, MD
Radiation Research Program, Division of Cancer Treatment and Diagnosis, National Cancer Institute, Bethesda, MD 20892, USA

Michael K. Cooper, MD
Department of Neurology, Vanderbilt University Medical Center, Nashville, TN 37212, USA; Neurology Service, Veterans Affairs TVHS, Nashville, TN 37212, USA

Indra J. Das, Ph.D
Indiana University Health Proton Therapy Center, Bloomington, IN 47408, USA; Department of Radiation Oncology, Indiana University School of Medicine, Indianapolis, IN 46202, USA

Prajnan Das, MD
Department of Radiation Oncology, U.T. M.D. Anderson Cancer Center, Houston, TX 77030, USA

Curtiland Deville, MD
Department of Radiation Oncology, The Hospital of the University of Pennsylvania, Philadelphia, PA 19104, USA

Parmeswaran Diagaradjane, Ph.D
Department of Radiation Oncology, The University of Texas M. D. Anderson Cancer Center, Houston, TX 77030, USA

Kate Dikeman
Department of Radiation Oncology, University of Louisville, Louisville, KY 40202, USA

Jeffrey Q Dinh
Division of Radiation Oncology, The University of Texas MD Anderson Cancer Center, Houston, TX 77030, USA

Jay F. Dorsey, MD, Ph.D
Department of Radiation Oncology, Perelman School of Medicine, University of Pennsylvania, Philadelphia, PA 19104, USA

Markus M. Fitzek, MD
Indiana University School of Medicine, IN, USA; Indiana University Health Proton Therapy Center, Bloomington, IN 46202, USA

Nataliya Getman
University of Florida Proton Therapy Institute, Jacksonville, FL 32206, USA

Bosco Giap
University of California at Los Angeles, Los Angeles, CA 90095, USA

Fantine N. Giap
Southern Methodist University, Dallas, TX 75275, USA

David R. Grosshans, MD, Ph.D
Division of Radiation Oncology, The University of Texas MD Anderson Cancer Center, Houston, TX 77030, USA

Stephen M. Hahn, MD
Department of Radiation Oncology, University of Pennsylvania, Philadelphia, PA 19104, USA

Meng W. Ho, MSc
Radiation Oncology, University of Florida Proton Therapy Institute, Jacksonville, FL 32206, USA

Bradford S. Hoppe, MD
University of Florida Proton Therapy Institute, Jacksonville, FL 32206, USA

James R. Howe, MD
University of Iowa Carver College of Medicine, Iowa City, IA 52242, USA

Qian Huang, MD, Ph.D
Department of Dermatology, Duke University Medical Center, Durham, NC 27710, USA

Soon N. Huh, Ph.D
Radiation Oncology, University of Florida Proton Therapy Institute, Jacksonville, FL 32206, USA

Josuha James, MS
Department of Radiation Oncology, University of Louisville, Louisville, KY 40202, USA

Martin Jermann, Ph.D
Paul Scherrer Institute, Villigen 5232, Switzerland

Jerry M. Jesseph, MD
Indiana University School of Medicine, Indianapolis, IN 46202, USA

Xun Jia, Ph.D
Center for Advanced Radiotherapy Technologies, Division of Medical Physics and Technology, Department of Radiation Medicine and Applied Sciences, University of California San Diego, La Jolla, CA 92037, USA

Daniel Y. Joh
Department of Radiation Oncology, Perelman School of Medicine, University of Pennsylvania, Philadelphia, PA 19104, USA

Gary D. Kao, MD
Department of Radiation Oncology, Perelman School of Medicine, University of Pennsylvania, Philadelphia, PA 19104, USA

Joseph I. Kang Jr, MD
Department of Radiation Medicine, Loma Linda University Medical Center, Loma Linda, CA 92354, USA

Ali Kassaee, Ph.D
Department of Radiation Oncology, University of Pennsylvania, Philadelphia, PA 19104, USA

Maura Kirk
Department of Radiation Oncology, University of Pennsylvania, Philadelphia, PA 19104, USA

David G. Kirsch, MD, Ph.D
Department of Radiation Oncology, Pharmacology & Cancer Biology, Duke University Medical Center, Durham, NC 27710, USA

Song-Chu Ko, MD
Indiana University School of Medicine, Indianapolis, IN, USA; Indiana University Health Proton Therapy Center, Bloomington, IN 46202, USA

Ritsuko Komaki, MD
Department of Radiation Oncology, The University of Texas MD Anderson Cancer Center, Houston, TX 77030, USA

Sunil Krishnan, MD
Department of Radiation Oncology, The University of Texas M. D. Anderson Cancer Center, Houston, TX 77030, USA

Hiroaki Kumada, Ph.D
Department of Radiation Oncology, University of Tsukuba, Tsukuba, Ibaraki Prefecture 305-0006, Japan

Deep Kwatra, Ph.D
Department of Molecular and Integrative Physiology, University of Kansas Medical Center, Kansas City, KS 66160, USA

Chang-Lung Lee, Ph.D
Department of Radiation Oncology, Duke University Medical Center, Durham, NC 27710, USA

Jihyoun Lee, MD
Department of Radiation Oncology, The University of Texas M. D. Anderson Cancer Center, Houston, TX 77030, USA; Soon Chun Hyang University Hospital, Yongsangu, Seoul 140-743, Republic of Korea

Richard Y. Lee, MD
Radiation Medicine, Roswell Park Cancer Institute, University at Buffalo, Buffalo, NY 14263, USA

Richard P. Levy, MD
Advanced Beam Cancer Treatment Foundation, 887 Wildrose Circle, Lake Arrowhead, CA 92352, USA

Chuan-Yuan Li, Ph.D
Department of Dermatology, Duke University Medical Center, Durham, NC 27710, USA

Fang Li, Ph.D
Department of Dermatology, Duke University Medical Center, Durham, NC 27710, USA

Mei Li, M.S.
Department of Radiation Oncology, Morristown Memorial Hospital, Morristown, NJ 07962, USA

Zuofeng Li, DSc
University of Florida Proton Therapy Institute, Jacksonville, FL 32206, USA

Alexander Lin, MD
Department of Radiation Oncology, University of Pennsylvania, Philadelphia, PA 19104, USA

Ted C. Ling, MD
Department of Radiation Medicine, Loma Linda University Medical Center, Loma Linda, CA 19104, USA

Xinjian Liu, Ph.D
Department of Dermatology, Duke University Medical Center, Durham, NC 27710, USA

Xing Qi Lu, Ph.D
Beth Israel Deaconess Medical Center, Harvard Medical School, Boston, MA 02215, USA

Anita Mahajan, MD
Division of Radiation Oncology, The University of Texas MD Anderson Cancer Center, Houston, TX 77303, USA

Akira Matsumura, MD
Department of Neurosurgery, University of Tsukuba, Tsukuba, Ibaraki Prefecture 305-0006, Japan

Yufang Ma
Department of Neurological Surgery, Vanderbilt University Medical Center, Nashville, TN 37232, USA

David Meer, Ph.D
Paul Scherrer Institut, Villigen 5232, Switzerland

Nancy P. Mendenhall, MD
University of Florida Proton Therapy Institute, Jacksonville, FL 32206, USA

William M. Mendenhall, MD
University of Florida Proton Therapy Institute, Jacksonville, FL 32206, USA

Laura Bonner Millar, MD
Department of Radiation Oncology, University of Pennsylvania, Philadelphia, PA 19104, USA

Michael Mills, Ph.D
Department of Radiation Oncology, University of Louisville, Louisville, KY 40202, USA

Masashi Mizumoto, MD, Ph.D
Department of Radiation Oncology, University of Tsukuba, Tsukuba, Ibaraki Prefecture 305-0006, Japan

Christopher G. Morris, M.S.
University of Florida Proton Therapy Institute, Jacksonville, Florida 32206, USA

Arno J. Mundt, MD
Center for Advanced Radiotherapy Technologies, Department of Radiation Medicine and Applied Sciences, University of California San Diego, La Jolla, CA 92037, USA

Kevin T. Murphy, MD
Department of Radiation Medicine and Applied Sciences, University of California San Diego, La Jolla, CA 92037, USA

Kei Nakai, MD
Department of Neurosurgery, University of Tsukuba, Tsukuba, Ibaraki Prefecture 305-0006, Japan

Wooi-Loon Ng
Department of Dermatology, Duke University Medical Center, Durham, NC 27710, USA

Romaine Charles Nichols, MD
University of Florida Proton Therapy Institute, Jacksonville, FL 32206, USA

Takashi Ogino
Medipolis Proton Therapy and Research Center, Ibusuki, Kagoshima 891-0304, Japan

Yoshiko Oshiro, MD
Department of Radiation Oncology, University of Tsukuba, Tsukuba, Ibaraki Prefecture 305-0006, Japan

Matthew B. Palmer, MD, Ph.D
Division of Radiation Oncology, The University of Texas MD Anderson Cancer Center, Houston, TX 77303, USA

Todd Pawlicki, Ph.D
Center for Advanced Radiotherapy Technologies, Division of Medical Physics and Technology, Department of Radiation Medicine and Applied Sciences, University of California San Diego, La Jolla, CA 92037, USA

Eros Pedroni, Ph.D
Paul Scherrer Institut, Villigen 5232, Switzerland

Pataje G.S. Prasanna, Ph.D
Radiation Research Program, Division of Cancer Treatment and Diagnosis, National Cancer Institute, Bethesda, MD 20892, USA

Carl J Rossi Jr, MD
Scripps Proton Therapy Center, 9730 Summers Ridge Road, San Diego CA 92121, USA

Sairos Safai
Center for Proton Therapy, Paul Scherrer Institut, Villigen 5232, Switzerland

Hideyuki Sakurai, MD
Department of Radiation Oncology, University of Tsukuba, Tsukuba, Ibaraki Prefecture 305-0006, Japan

Reinhard W. Schulte, MD
Department of Radiation Medicine, Translational Research, Loma Linda University Medical Center, Loma Linda, CA 92354, USA

Kambiz Shahnazi, Ph.D
Indiana University Health Proton Therapy Center, Bloomington, IN 47408, USA

Pankaj Kumar Singh, Ph.D
Department of Radiation Oncology, The University of Texas M. D. Anderson Cancer Center, Houston, TX 77030, USA

Heath Devin Skinner, MD, Ph.D
Department of Radiation Oncology, The University of Texas MD Anderson Cancer Center, Houston, TX 77030, USA

Jerry D. Slater, MD
Department of Radiation Medicine, Loma Linda University Medical Center, Loma Linda, CA 92354, USA

Shiv P. Srivastava
Purdue University, West Lafayette, and Reid Hospital, Richmond, IN 47374, USA

Helen B. Stone, Ph.D
Radiation Research Program, Division of Cancer Treatment and Diagnosis, National Cancer Institute, Bethesda, MD 20892, USA

Lova Sun
Department of Radiation Oncology, Perelman School of Medicine, University of Pennsylvania, Philadelphia, PA 19104, USA

Samuel Swisher-McClure, MD
Department of Radiation Oncology, University of Pennsylvania, Philadelphia, PA 19104, USA

Boong-Keng Kevin Teo, Ph.D
Department of Radiation Oncology, University of Pennsylvania, Philadelphia, PA 19104, USA

Allan F. Thornton, MD
Indiana University Health Proton Therapy Center, Bloomington, IN 47408, USA

Andrew Tsourkas, Ph.D
Department of Bioengineering, University of Pennsylvania, Philadelphia, PA 19104, USA

Koji Tsuboi, MD, Ph.D
Department of Radiation Oncology, University of Tsukuba, Tsukuba, Ibaraki Prefecture 305-0006, Japan

Neha Vapiwala, MD
University of Pennsylvania, Philadelphia, PA 19104, USA

Anand Venugopa, MD, Ph.D
Department of Molecular and Integrative Physiology, University of Kansas Medical Center, Kansas City, KS 66160, USA

Bhadrasain Vikram, MD
Radiation Research Program, Division of Cancer Treatment and Diagnosis, National Cancer Institute, Bethesda, MD 20892, USA

Jialiang Wang, Ph.D
Department of Neurological Surgery, Department of Cancer Biology, Vanderbilt University Medical Center, Nashville, TN 37232, USA

Ken Kang-Hsin Wang, Ph.D
University of Pennsylvania, Philadelphia, PA 19104, USA

Alon Witztum
Department of Radiation Oncology, Perelman School of Medicine, University of Pennsylvania, Philadelphia, PA 19104, USA

Mark Wolanski, Ph.D
Indiana University Health Proton Therapy Center, Bloomington, IN 47408, USA; Department of Radiation Oncology, Indiana University School of Medicine, Indianapolis, IN 46202, USA

Tatiana Wolfe
Department of Radiation Oncology, The University of Texas M. D. Anderson Cancer Center, Houston, TX 77030, USA

Rosemary S. Wong, Ph.D
Radiation Research Program, Division of Cancer Treatment and Diagnosis, National Cancer Institute, Bethesda, MD 20892, USA

Andrew J. Wroe, Ph.D
Department of Radiation Medicine, Translational Research, Loma Linda University Medical Center, Loma Linda, CA 92354, USA

Tetsuya Yamamoto, MD, Ph.D
Department of Neurosurgery, Department of Radiation Oncology, University of Tsukuba, Tsukuba, Ibaraki Prefecture 305-0006, Japan

Caitlyn Yeager
Department of Radiation Oncology, University of Pennsylvania, Philadelphia, PA 19104, USA

Robert Zaiden, MD
Medicine, University of Florida College of Medicine, Gainesville, FL 32610, USA

Ajlan Al Zaki
Department of Bioengineering, University of Pennsylvania, Philadelphia, PA 19104, USA

Li Zhao, Ph.D
Indiana University Health Proton Therapy Center, Bloomington, IN 47408, USA; Department of Radiation Oncology, Indiana University School of Medicine, Indianapolis, IN 46202, USA

Qingya Zhao, Ph.D
Indiana University Health Proton Therapy Center, Bloomington, IN 47408, USA; Department of Radiation Oncology, Parkview Health, Fort Wayne, IN 46845, USA

Mary Zimmerman, MD
Department of Dermatology, Duke University Medical Center, Durham, NC 27710, USA

Corresponding Editor
Nancy Q. Zhong

Executive Typesetting Editor
Chuyuan Xie

Table of Contents

Preface

Clinical

Physics and Biology

Editorial

Charged particle beam therapy: a new dawn for cancer treatment

Huan Giap[1], Eric Y Chuang[2], Gary Y Yang[3]

[1]The Scripps Proton Therapy Center, San Diego, CA, USA; [2]Graduate Institute of Biomedical Electronics and Bioinformatics, National Taiwan University, Taipei, Taiwan; [3]Department of Radiation Medicine, Loma Linda University Medical Center, Loma Linda, CA, USA

Correspondence to: Huan Giap, M.D, Ph.D. Scripps Proton Therapy Center, San Diego, CA, USA. Email: hbgiap@gmail.com.

Cancer is one of the leading causes of death worldwide. According to the World Health Organization (WHO), there are about 13 million new cases per year, and 8 million deaths annually, which account for 13% of all human deaths. This mortality rate has been projected to rise to 12 million by 2030 (2011 Global cancer statistics, CA: A Cancer Journal for Clinicians, Vol 62(2) p69-90, March/April 2011). The three major modalities for cancer treatments are surgery, chemotherapy, and radiotherapy. Since its discovery over the 110 years ago, the field of radiation therapy has progressed significantly and played an important role in cancer treatment. Like other fields in medicine, radiation therapy has depended most heavily on technology and science for its advancement. There have been continuing developments in discovery of various sources and different modes of radiation in laboratory, and transitioned scientific research into clinical practice. Charged particles with their favorable depth of dose distribution are ideal for treating tumors located inside the body. Despite its discovery and theoretical advantages were almost 60 years ago, the clinical implementation of charged particle beam therapy has been slow due to the cost and size requirement, and its use has been limited to physics research laboratories until the last few decades. The cooperation among research laboratories, academic medical centers, and private industries has improved the technology, affordability, and ease of implementation. There has been an evolution of charged particle beam therapy over the three frontiers: technology, radiobiology and clinical outcomes. At the time of this writing, there have been more than 100,000 patients treated with charged particle beam therapy worldwide at more than 40 centers. There are several dozen centers are currently being developed. These numbers are very small (<5%) comparing to the number of photon treatment centers, and only a small fraction of cancer patients will benefit from charged particle beam therapy. With all the potential advancements from physics and radiobiology, the field of charged particle beam therapy is still facing many challenges and is far from reaching its full capacity and application, especially how to improve patients' survival and quality of life as well as to be cost effective.

To address the importance of charged particle beam therapy, the editorial teams of Translational Cancer Research (TCR) and Journal of Gastroenterology Oncology journals have been making great efforts to collect the articles that were published in these two journals into these proceeding to go over this special topic of charged particle beam therapy. Contributors are experts from particle beam centers around the world. These peer-reviewed articles present the past experience, current status, and future directions for charged particle beam therapy. We divide the articles into two categories: Clinical and Physics/Biology. Several articles in the Physics/Biology, such as nanotechnology, represent the future trend of radiation therapy, not just particle beam therapy alone. We hope that this collection of articles will help clinicians, scientists, healthcare practitioners, and trainees to better understanding and appreciation of this new field with all the potentials and challenges. All technological challenges for particle beam therapy are similar to other radiation techniques, but they are at a greater magnitude and consequence. The history of radiation therapy has consistently showed that collaboration of clinicians, scientist, researchers, engineers and technology providers (vendors) has and can overcome lots of these challenges. This can be summarized by a quote from Theodore N Vail: "Real difficulties can be overcome, it is only the imaginary ones that are unconquerable".

We want to thank all the contributors for sharing their knowledge and expertise as well as their excellent research works in the creation of these articles. We are grateful to all the reviewers for their time and efforts. We also like to thank Varian Medical System for their financial support in sponsoring this publication. We appreciate the Pioneer

Science Publishing Company in its continuing commitment to solicit and publish high impact papers from world-renowned experts in cancer related medicine. Finally, our sincere gratitude is to the staff of Pioneer Science Publishing Company, particularly, Nancy Zhong, Katherine Ji, and Dr. Stephen Wang; their energy, professionalism, and perfectionism are contagious and have made this project a real joy.

Acknowledgements

Disclosure: The authors declare no conflict of interest.

Cite this article as: Giap H, Chuang EY, Yang GY. Charged particle beam therapy: a new dawn for cancer treatment. Transl Cancer Res 2012;1(3):125-126. DOI: 10.3978/j.issn.2218-676X.2012.10.11

Review Article

Historical perspective and evolution of charged particle beam therapy

Huan Giap[1], Bosco Giap[2]

[1]The Scripps Proton Therapy Center, [2]University of California at Los Angeles, USA

Correspondence to: Huan Giap, M.D, Ph.D. The Scripps Proton Therapy Center, Bosco Giap, University of California at Los Angeles, USA. Email: hbgiap@gmail.com.

DOI: 10.3978/j.issn.2218-676X.2012.10.09

Scan to your mobile device or view this article at: http://www.thetcr.org/article/view/595/html

History of charged particle beam therapy

Since Roentgen's discovery of X-ray 130 years ago, radiation has been used to treat various diseases including cancer (*Figures 1*,*2*). As much excitement seen in the early days when X-ray was found to be effective in shrinking tumors, it was also realized of the potential severe early and late adverse complications from the same treatment to nearby normal structures.

The early observations lead to further research and establishing one of the fundamental principle of radiotherapy, called "the therapeutic window", which compares the degree of tumor kill to the damages of surrounding normal structures (*Figure 3*).

The proton was discovered by Ernest Rutherford in the early 1900's. By irradiating nitrogen gas with (alpha) particles would lead to oxygen atoms and the dense nuclei of hydrogen atoms, which he named protons based on the Greek word "protos" which meant first. His conclusion was that the nitrogen atom was made up of some number of protons and electrons and can be transmuted into oxygen and a hydrogen nucleus. It was also discovered that charged particles (protons and light ions) have a finite range in matter. The interaction probability to cause ionization increases as they loose velocity along their paths, so that a peak of deposited dose occurs at a depth proportional to the energy of the charged particle. Beyond this peak, no further dose is deposited. This scientific phenomenon was described the William Bragg at that time (1). In 1930, the American physicist Ernest O. Lawrence and his associates were the first to invent cyclotron to accelerate proton to the energy high enough for cancer treatment applications. He invented the cyclotron in 1929 & developed it as a particle accelerator during the 1930s, winning the 1939 Nobel Prize for physics for this work. In 1931 he founded the Radiation Laboratory, later the Lawrence Berkeley Laboratory (*Figure 4*). In a decade later, his advanced version of the synchrocyclotron, which has 184-inch in diameter, is capable of producing 340 MeV protons (*Figure 5*) (2).

In 1946, Dr. Robert Rathburn Wilson wrote a seminal paper proposing the idea that proton beams could be used for cancer treatment (3) while he was in the Physics Department at Harvard University. He described the fundamental physical feature depth-dose curve of proton and heavy-charged particles in comparison with photon or X-rays. He described the way the particle beams deposit their energy as the beam enters the body en route to the tumor: smaller amount of energy is released first, and then much larger amount of the beam energy released at the end of its path (Bragg peak) and completely stops (*Figure 6*). The depth at which the particle beam stops can be controlled within millimeter precision by adjusting the beam energy using a rotating wheel of variable thickness, i.e., a range modulation wheel (RMW). This technique is still being used today, and it is a simple way of adding multiple Bragg peaks of variable energies and weights in order to spread the proton stopping region over the tumor volume. He did also play significant role in the development of nuclear weapons during World War II ("The Manhattan Project"); but afterwards, he chose to shift his focus of nuclear physics into medical application for the betterment of mankind. In addition to Wilson's being a very accomplished sculptor and architect, he was later responsible for the development of Fermi Laboratory and became its founding director (*Figure 7*).

Prior to treating human, the first investigations on

Figure 1 Wilhelm Conrad Roentgen's discovery of X-ray in 1895. (Credit: PHOTO RESEARCHERS/SCIENCE PHOTO LIBRARY)

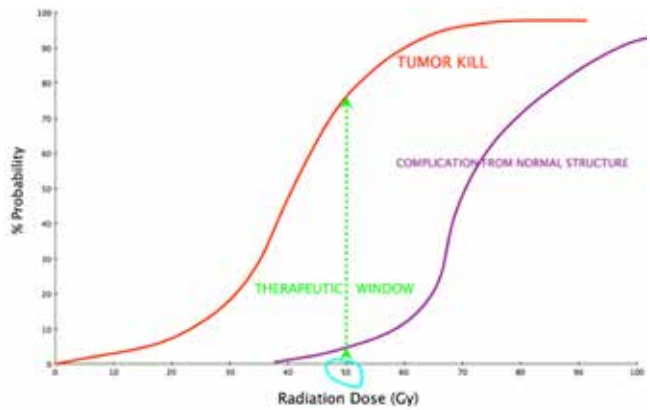

Figure 3 The fundamental of radiation therapy is to maximize the therapeutic window; i.e., increasing the ratio of probability of tumor control over the risk of causing complication. For an example, a dose of 50 Gy has a probability of 75% of "killing the tumor" and 5% chance of causing some complication from some normal structure

Figure 2 Roentgen ray therapy in 1900's. (Credit: PHOTO RESEARCHERS/SCIENCE PHOTO LIBRARY)

Figure 4 American physicist Ernest O. Lawrence [1901-1958], photographed in 1937 adjusting the ion source of his 60-inch cyclotron. Lawrence moved to the University of California at Berkeley in 1928. He invented the cyclotron in 1929 & developed it as a particle accelerator during the 1930s, winning the 1939 Nobel Prize for physics for this work. In 1931 he founded the Radiation Laboratory, later the Lawrence Berkeley Laboratory, & directed it until his death. (Credit: LAWRENCE BERKELEY LAB/SCIENCE PHOTO LIBRARY)

biological effects of protons were done on rodents by Cornelius Tobias and John Lawrence (brother of Ernest O Lawrence) using this 184-inch synchrocyclotron during the late 1940's and early 1950's (4). The first patients treated by protons was at the University of California, Berkeley in 1954 by the Lawrence "boys" (as they preferred to be called). The initial tumor targeted at was pituitary tumor since it could be located in 3-D using orthogonal plane X-ray films and rigid immobilization of the cranium (5). This was done some 20 years before the invent of CT scan. This isocentric technique forms the basis for stereotactic radiosurgery for many decades later. From 1954 to 1957, a total of thirty patients was treated with proton beam here. Due to better understanding of higher linear energy transfer (LET) and radiobiological equivalent (RBE) of heavier charged particle. In 1957, this synchrocyclotron was modified to accelerate Helium nuclei. By the time of the facility's closure in 1992, a total of 2,054 patients had been

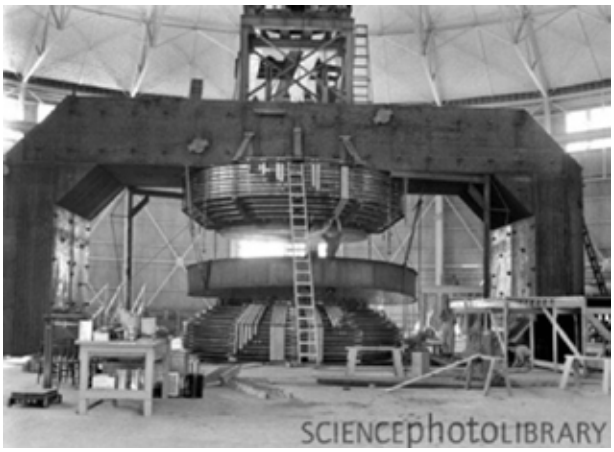

Figure 5 Engineers in 1942 working on the construction of the 184-inch synchrocyclotron at the Radiation Laboratory at the University of California, Berkeley, USA. This cyclotron was developed by the laboratory's director Ernest Orlando Lawrence. (Credit: LAWRENCE BERKELEY LAB/SCIENCE PHOTO LIBRARY)

Figure 7 Dr. Robert Rathburn Wilson, an American physicist, was the first to propose the use of proton beam therapy for cancer treatment in his seminal paper 1946. He is considered to be "the father of proton therapy". His other contribution to science included being a group leader of the Manhattan Project, a sculptor, and an architect of Fermi National Laboratory (Fermilab), where he was also the director from 1967-1978. He was pictured here in the ground breaking ceremony of FermiLab. (Credit. Scientific American)

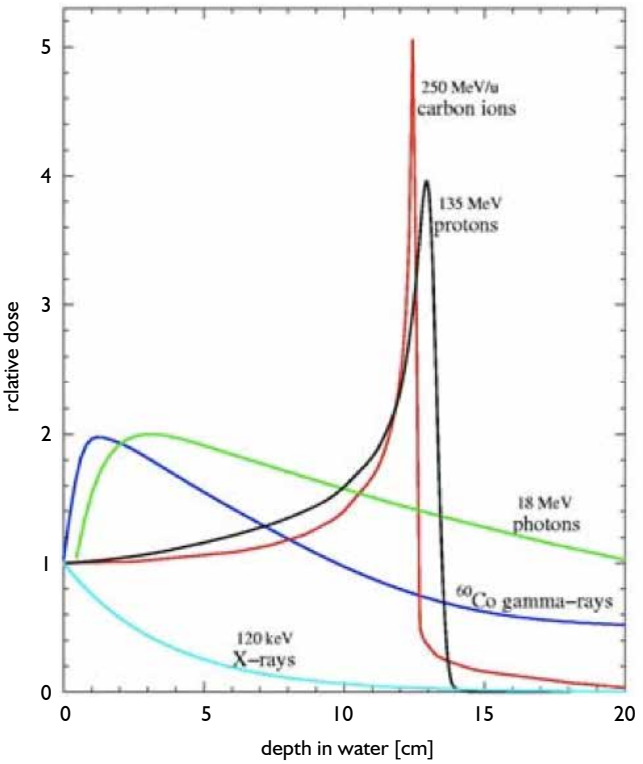

Figure 6 Percent depth dose versus depth in the patient's body. As proton beams enter the body, it loose some energy and deposits most of its energy at the end of its range (Bragg's peak) to the tumor. A range modulation wheel (RMW) is used to spread out the Bragg peaks of multiple proton beams at different energies over the tumor volume

treated with helium ions Concurrently, another particle beam facility was being developed in Uppsala, Sweden where they treated their first proton patient in 1957. The MGH-Harvard Cyclotron Laboratory was open in 1961, and then the Institute for Theoretical and Experimental Physics in Moscow in 1967. Over the next few decades, about 10 more facilities were open around the world. All these facilities were in physics laboratories with minimal infrastructure for patient care and support. Most of the patients treated at these facilities had intra-cranial or ocular tumors (*Figure 8*).

During the 1970's and 1980's, the primary technological development was the construction of the Bevatron at LBNL, a synchrotron-based facility that could accelerate charged particles ranging from helium ions to uranium nuclei. Otherwise, most of the scientific advancement in the delivery and technology of particle beam therapy in this era resulted from continuing to accumulate clinical data on

WHERE		PARTICLE	FIRST PATIENT	LAST PATIENT	PATIENT TOTAL	
Belgium	Louvain-la-Neuve	p	1991	1993	21	ocular tumors only
Canada	Vancouver (TRIUMF)	π^-	1979	1994	367	ocular tumors only
Germany	Darmstadt (GSI)	C-ion	1997	2009	440	
Japan	Tsukuba (PMRC, 1)	p	1983	2000	700	
Japan	Chiba	p	1979	2002	145	ocular tumors only
Japan	WERC	p	2002	2009	62	
Russia	Dubna (1)	p	1967	1996	124	
Sweden	Uppsala (1)	p	1957	1976	73	
Switzerland	Villigen PSI (SIN-Piotron)	π^-	1980	1993	503	
Switzerland	Villigen PSI (OPTIS 1)	p	1984	2010	5458	ocular tumors only
CA., USA	Berkeley 184	p	1954	1957	30	
CA., USA	Berkeley	He	1957	1992	2054	
CA., USA	Berkeley	ion	1975	1992	433	
IN., USA	Bloomington (MPRI, 1)	p	1993	1999	34	ocular tumors only
MA., USA	Harvard	p	1961	2002	9116	
NM., USA	Los Alamos	π^-	1974	1982	230	
					19790 Total	
				thereof	2054 He	
					1100 pions	
					440 C-ions	
					433 other ions	
					15763 protons	

Figure 8 Early particle beam physics facilities around the world and their patient statistics [Reference. Particle Beam Therapy Co-Operative Group (PTCOG) website, September 2012]

selected tumor sites. These included ocular tumors, brain and base-of-skull tumors, and then pediatric malignancies. During this period, due to the emergence of CT and MRI technologies and treatment planning algorithms and softwares, better 3-D targeting and treatment planning refined the delivery and verification of proton therapy. In parallel to the development of particle beam technology, there were major advancement in photon therapy, including the emergence of intensity-modulated radiation therapy (IMRT) in the late 1990's.

In 1990, the world first hospital-based proton therapy facility was built in Loma Linda. This effort was lead by Dr. James Slater with the support from Loma Linda University Medical Center (LLUMC) and a government grant. The facility houses a Fermi Lab-designed 250 MeV Synchrotron, a passive-beam nozzle, and four treatment vaults with three rotating gantries and one fixed beam room. This patient-dedicated center has treated the most patients with particle beam to date, more than 15,000 patients. Up to the late 1990, most patients treated with particle beam in the U.S. were considered "experimental" or "investigational" by Medicare and private insurance carriers; one of significant and non-scientific event that has popularized the use of proton therapy in the U.S. is the approval of proton-specific treatment delivery procedure codes from American Medical Association (AMA). This effort was lead by LLUMC and Massachusetts General Hospital (MGH). When this reimbursement rate was set by Medicare, the wording of "investigational" and "experimental" were removed from the domain of proton beam therapy. Like almost all technologies in radiation therapy, this approved reimbursement rate has provided financial incentives for a wave of hospitals and private sector in the U.S. to consider proton therapy due to the attractive rate of return of the investment. Concurrently, significant publications started to emerge on the superior clinical outcome of proton on clinical sites such as pediatric, eye, base of skull and spinal tumors. In the same period, there were availability of vendors offering commercial solutions for development of these facilities. These factors have lead to the rapid implementation of clinical centers in the U.S., Asia and Europe. This *Figure* (reference to PTCOG website as of Sept 24, 2012) shows the current particle beam facilities in the world. According to the PTCOG, the number of patients being treated with particle beam has recently exceeded 100,000 at 38 charged particle beam therapy centers worldwide (*Figure 9*).

Particle therapy facilities in operation (incl. patient statistics):

WHO, WHERE	COUNTRY	PARTICLE	S/C*, MAX. ENERGY (MeV)	BEAM DIRECTION	START OF TREATMENT	TOTAL PATIENTS TREATED	DATE OF TOTAL
ITEP, Moscow	Russia	p	S 250	1 horiz.	1969	4246	Dec-10
St.Petersburg	Russia	p	S 1000	1 horiz.	1975	1372	Dec-11
PSI, Villigen	Switzerland	p**	C 250	1 gantry, 1 horiz.	1996	1107	Dec-11
Dubna	Russia	p	C 200****	horiz.	1999	828	Dec-11
Uppsala	Sweden	p	C 200	1 horiz.	1989	1185	Dec-11
Clatterbridge	England	p	C 62	1 horiz.	1989	2151	Dec-11
Loma Linda	CA.,USA	p	S 250	3 gantry, 1 horiz.	1990	15000	Jan-11
Nice	France	p	C 65	1 horiz.	1991	4417	Dec-11
Orsay	France	p*****	C 230	1 gantry,2 horiz.	1991	5634	Dec-11
NRF - iThemba Labs	South Africa	p	C 200	1 horiz.	1993	521	Dec-11
IU Health PTC, Bloomington	IN.,USA	p	C 200	2 gantry, 1 horiz.	2004	1431	Dec-11
UCSF	CA.,USA	p	C 60	1 horiz.	1994	1391	Dec-11
HIMAC, Chiba	Japan	C-ion	S 800/u	horiz.,vertical	1994	6569	Dec-11
TRIUMF, Vancouver	Canada	p	C 72	1 horiz.	1995	161	Dec-11
HZB (HMI), Berlin	Germany	p	C 72	1 horiz.	1998	1859	Dec-11
NCC, Kashiwa	Japan	p	C 235	2 gantry	1998	772	Dec-10
HIBMC,Hyogo	Japan	p	S 230	1 gantry	2001	3198	Dec-11
HIBMC,Hyogo	Japan	C-ion	S 320/u	horiz.,vertical	2002	788	Dec-11
PMRC(2), Tsukuba	Japan	p	S 250	gantry	2001	2166	Dec-11
NPTC, MGH Boston	MA.,USA	p***	C 235	2 gantry, 1 horiz.	2001	5562	Oct-11
INFN-LNS, Catania	Italy	p	C 60	1 horiz.	2002	290	Dec-11
Shizuoka Cancer Center	Japan	p	S 235	3 gantry, 1 horiz.	2003	1175	Dec-11
STPTC, Koriyama-City	Japan	p	S 235	2 gantry, 1 horiz.	2008	1378	Dec-11
WPTC, Zibo	China	p	C 230	2 gantry, 1 horiz.	2004	1078	Dec-11
MD Anderson Cancer Center, Houston	TX.,USA	p***	S 250	3 gantry, 1 horiz.	2006	3400	Feb-12
UFPTI, Jacksonville	FL.,USA	p	C 230	3 gantry, 1 horiz.	2006	3461	Dec-11
NCC, Ilsan	South Korea	p	C 230	2 gantry, 1 horiz.	2007	810	Dec-11
RPTC, Munich	Germany	p**	C 250	4 gantry, 1 horiz.	2009	895	Dec-11
ProCure PTC, Oklahoma City	OK.,USA	p	C 230	1 gantry, 1 horiz, 2 horiz/60 deg.	2009	623	Dec-11
HIT, Heidelberg	Germany	p**	S 250	2 horiz.	2009	94	Dec-11
HIT, Heidelberg	Germany	C-ion**	S 430/u	2 horiz.	2009	568	Dec-11
UPenn, Philadelphia	PA.,USA	p	C 230	4 gantry, 1 horiz.	2010	433	Dec-11
GHMC, Gunma	Japan	C-ion	S 400/u	3 horiz., vertical	2010	271	Dec-11
IMP-CAS, Lanzhou	China	C-ion	S 400/u	1 horiz.	2006	159	Dec-11
CDH Proton Center, Warrenville	IL.,USA	p	C 230	1 gantry, 1 horiz, 2 horiz/60 deg.	2010	387	Dec-11
HUPTI, Hampton	VA., USA	p	C 230	4 gantry, 1 horiz.	2010	no data	start Aug-10
IFJ PAN, Krakow	Poland	p	C 60	1 horiz.	2011	11	Dec-11
Medipolis Medical Research Institute, Ibusuki	Japan	p	S 250	3 gantry	2011	180	Dec-11
CNAO, Pavia	Italy	C-ion, p	S 430/u	3 horiz/1 vertical	2011	5	Dec-11
ProCure Proton Therapy Center, New Jersey	NY., USA	p	C 230	4 gantry	2012	15	Apr-12

Figure 9 Current charged particle beam therapy centers in operation around the world (Taken from PTCOG website, September 24, 2012). There are more than 100,000 patients being treated with charged particle to date at 38 charged particle beam centers worldwide

In the U.S., there are currently ten centers in operations, and almost another ten facilities are under construction or being planned as shown geographically in *Figure 10*. With an approximate 1.5 million new cases of cancer in the U.S each year, and approximate half of those patients (about 750,000) will receive radiation therapy as part of their treatment. According to an analysis by Dr. James Cox, roughly about 15% will be the candidate for particle beam therapy, or about 100,000 cases annually in the U.S (6). More than 95% of these cancer patients currently receive their radiotherapy at over two thousands photon radiation facilities in the U.S.

Evolution in charged particle beam therapy

Over the past 100+ years, the field of radiation therapy has progressed over the three frontiers: technology, radiobiology and clinical trials. These principles also apply to charged particle therapy. In the following sections, the evolution, challenges, and future direction will be discussed.

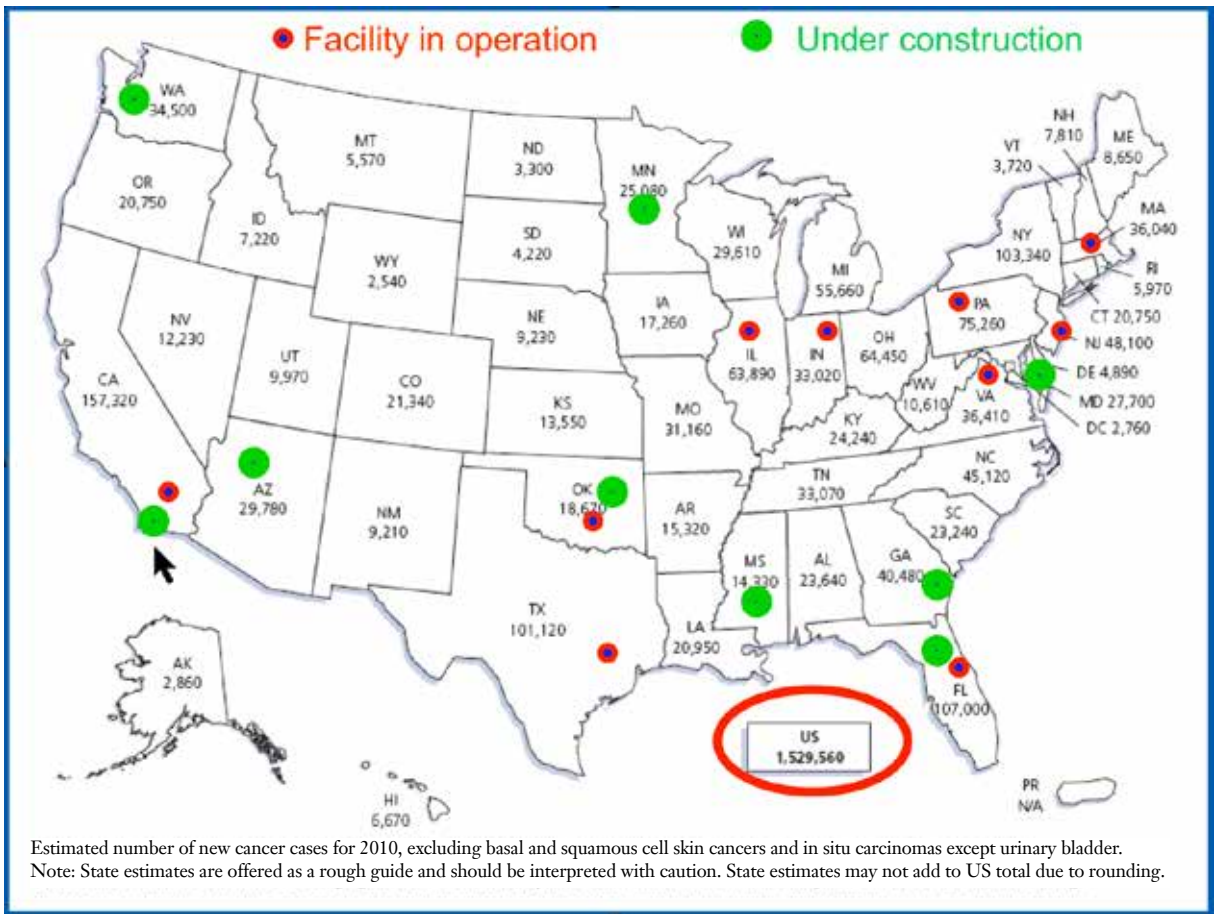

Figure 10 Current status of proton beam therapy centers in the U.S. As of September 2012, there are 10 clinical centers in operation, and about 10 being built or planned. The number in each state indicates the new cancer cases per year (2010 statistics)

Technological and scientific evolution of charged particle beam therapy

Comparing to other fields in medicine, radiation therapy (including charged particle beam therapy) has depended most heavily on technology and science for its advancement. There have been continuing development in many aspects of technologies to discover various sources and mode of radiation and transitioned from the physics laboratory into the clinical setting. The cooperation among research laboratories, academic medical centers, and private industries have continued to improve the technology, affordability, and ease of implementation. There are three areas that will be discussed in the details in the following sections.

Generation and delivery of charged particle beam

The fundamental principle of radiotherapy is the use of ionizing radiation to selectively damage and/or kill diseased cells at certain geometric target for some end clinical result with reasonable collateral damage of surrounding non-disease structures. The advancement of ionizing radiation is all about the discovery of reliable new types or sources of ionizing radiation with desirable physical characteristics that can be delivered to a human being for this principle. The field of radiation has evolved from low-energy X-rays to natural Cobalt-60 gamma rays, then bremstralung rays from electron linear accelerator in the MeV range, followed by modern day linear accelerator that generates photon in the 10 to 20 MV range. As discussed in the Introduction Section, the early scientists had discovered types of charged particles, how to accelerate their energy to achieve a certain useful clinical depth, how to deliver these particles precisely into a three-dimensional target volume inside human,

and how to plan and verify this treatment process. The components of the clinical particle beam center consists of:

(I) Accelerator

The accelerator (the "engine") accelerates charged particle beam from rest to a range of hundreds of MeV. Traditionally, two main types of accelerator are cyclotron and synchrotron, which are different physically on how they accelerate charged particles. There are historical differences and reason why each design was chosen. They both have advantages and disadvantages, and the discussion is beyond the scope of this article, and readers are referred to article by Dr. Al Smith (7). Newer generation of accelerators are superconducting cyclotrons and synchrocyclotrons, which have higher energy, more compact size, less power consumption, and higher beam extraction efficiency.

(II) Beam transport and energy selection system

The high energy charged particles will leave the accelerator at about 2/3 the speed of light and travel in vacuum in a very tightly collimated beamlet (few millimeters) to the treatment room. This part of the system will assure the beam quality, direct the beam to the right treatment room, and able to change the beam energy (to allow for different tissue penetration) at the timeframe of mili-second.

(III) Beam nozzle design

This very critical component will control the deposition of the charged particle in the patient in four dimensions: spatial (x,y,z) and temporal (time). The nozzle design defines the beam delivery technique. There are two general categories: passive scattering and spot scanning techniques. A detailed description can be found in the literature (8). The traditional passive scattering technique deposits an uniform dose to a 3-D target using charged particles with the same energy at the same time interval. A small focused uniform beamlet is "scattered" by some material to increase the beam size. The lateral dimension (x and y) of the target was shaped using a custom cut-out or block; the depth dimension (z) of the target was shaped using a compensator, which is a "negative" or mold shape of the target; all the dose is delivered to the target in some time interval of minutes. This is almost similar to the 3-D conformal treatment with photon. The passive scattering technique accounts for most of the current clinical data in particle beam therapy. It has several advantages: less expensive and easy to implement on the hardware; more "forgiving" for organ motion; easy treatment planning and plan verification. There are many disadvantages of the passive scattering technique: (i) Passive scattering technique does not use the charged particles efficiently. The majority of the particles generated is wasted due to scattering and never reach the target; (ii) There is high contamination of neutron generated due to these scattering particles. These neutrons are putting patients (particularly young patients) at risk for secondary malignancies later in life; (iii) The passive scattering technique requires fabrication of the 3-D compensators and block for each field in each patient. These adds time and cost to the treatment process. These devices have to be re-made each time there is a change in target size and shape; (iv) This technique treats the normal structure proximal to the target unintentionally; (v) Due to multiple scattering of the beam, the lateral penumbra of the field is increased (larger effective source size).

To unleash more potentials of charged particle therapy, these deficiencies should be addressed, and hence the rationales for the spot scanning technique or pencil beam scanning technique. In this technique, the Bragg peak of each beamlet from the accelerator is delivered into each voxel of the 3-D target. There are no scattering devices, and the 3-D placement (x,y,z) of these beamlets are done using scanning magnets and energy changes on the fly. A target with one liter in volume could contain around 10,000 or more voxels. The dose deposit to each voxel last few milliseconds and the whole process take about 1-2 minute for a 2 Gy dose. There are many versions (and names) of the spot scanning techniques with varying sophistication of the system. The most advanced spot scanning technique is intensity-modulated particle beam therapy (IMPT), where multiple pencil beam scanning fields are optimized simultaneously to produce a desired dose distribution to a 3-D target. IMPT allows for variation in beam energy and intensity. Overcoming the disadvantages of passive scattering technique, the newer spot scanning technique does present with challenges: (I) Treatment planning and verification are much more complicated; (II) Sensitive to organ motions; (III) More expensive and difficult technology to implement, particularly the control system; (IV) More clinical data are needed. More research and works are currently being done to address these challenges. There are also availability of "universal" "nozzle" which has ability to deliver both passive scattering and spot scanning techniques.

(IV) Patient positioning and verification system (PPVS)

The significant difference between a clinical and research facility is the patient positioning and verification system, which allows for accurate and comfortable patient setup and verification of dose delivery process. Robotics and automation have been introduced into the clinical facilities

in the past decade to allow for improved patient transport, facility throughput, better patient positioning, and accurate setup.

(V) The control system

The control system ("the brain") is the most critical component of the clinical treatment facility. The control system involves in all steps of the treatment process to achieve a safe and accurate treatment to patients and protect the personnel. This system interacts with accelerator, treatment planning software, electronic medical record (EMR), the treatment control and dose monitoring at the treatment nozzle, patient positioning and verification system, electronic/magnetic components in the facility, radiation detection monitor system, and mechanical component (door sensor, collision system, etc.). The control system is the ultimate safety defense for a clinical facility and must be 100% functional.

Treatment planning software (TPS)

The advancement of charged particle therapy will not be at this stage if there are not such parallel progress in treatment algorithms, softwares, and computers. Unlike other local treatment modalities for cancer, TPS allows the radiation oncologists optimize for the best plan and double check it before the treatment is delivered. TPS models the actual dose deposition in the patients and automation by going over thousands of possible combinations of treatment parameters to derive the best plan. Comparing to photon treatment planning, charged particle beam therapy planning is more complicated due to the followings: (i) Tissue inhomogeneity and interfaces (bone/air, tissue/metallic prosthesis) can affect dose distribution significantly; (ii) Due to the finite range of charged particles, the tissue-equivalent distance obtained from imaging studies such as CT and/or MRI should be looked at carefully; (iii) Treatment planning for spot scanning beam with organ motion is challenging. As the newer technologies emerge for charged particle beam therapy, the demand for better and faster TPS and computers goes up. The current developments for TPS include: (i) more advanced calculation algorithms such as Monte Carlo modeling is preferred over traditional ray-tracing algorithm; (ii) accounting for organ motion; (iii) adaptive therapy to accommodate for the change in tumor size and surroundings during the course of treatment; (iv) image-guided radiation therapy; (v) plan robustness modeling to account for treatment uncertainty parameters; (vi) biological modeling to account for biological dose and effects; (vii) more objective plan evaluation to automating the treatment planning process; (viii) in-vivo dose verification using the information from gamma camera and modeling of PET emitters; (ix) modeling of small field dosimetry for stereotactic radiosurgery and stereotactic body radiation therapy applications.

Radiological imaging

Parallel with advances in technology and treatment planning software, imaging technologies and faster computers, progress in the field of radiological imaging such as CT, MRI, PET has provided advancement to the field of charged particle therapy. Better 3-D anatomical and functional imaging technologies help clinician better defining the target and critical structures, adapting the treatment plan to tumor response during the treatment course, and providing feedback via evaluating the tumor response and complications after treatment completion. As 2-D and 3-D anatomical imaging modalities such as kV radiographs, CT, and MRI are incorporated into the treatment planning and verification. The resolution of these imaging systems will guide the accuracy of the dose delivery system. Current research work are focusing on the use of functional imaging such as PET for charged particle therapy as a way of dose recording and verification system. This is based on the fact that high-energy charged particles interact with human tissue and produce positron emitters or PET isotopes (Carbon-11 and Oxygen-15 with a half-lives of 20 and 2 minutes, respectively). The PET activity can be characteristically related in 3-D to the dose delivered and biological effects. In-room PET camera imaging system has been developed to investigate this property (9).

Radiobiology of charged particle beam therapy

The amount of radiation deposition into tissue is measured by a physic quantity, called Gray (or Gy). One Gray is defined as the amount of energy (measured in Joule) deposited in a unit of tissue mass of one Kilogram. This measurable unit of dose in radiation therapy does not tell or predict what happens at the molecular or cellular level. Radiobiology is the field of science that connects the dot between deposited dose to clinical endpoint. This basic science provides us the understanding the biological effects of radiation at cellular levels, repair mechanism, and multiple interactions with oxygen level, micro- and macro-environment, and differential effects on various tumor types and normal tissues. If one follows the track of ionizing radiation as it enters a human body, the radiation ray gives

up its energy and causing ionization to tissues, which are then translated into the radio-biological effects (RBE). The amount of radiation transferred per unit track is described by a quantity called Linear Energy Transfer (LET). For a given type of radiation, RBE can be thought of as a conversion factor from the dose deposited in Gray into the some biological effects. The physical dose in Gray is what we can measure with instrumentation, but the end biological effects are of significant interests ("biological effectiveness"). For each radiation type, RBE depends several factors such as type of radiation (hence LET), the speed of the particle, tissue types, and the local micro-environments (oxygen level, etc.). Low LET radiation (or sparsely-ionizing radiation) such as photon or X-ray transfers much less ionization along the path; therefore, their RBE is low, and defined as 1.0. High LET radiation (or densely-ionizing radiation) such as carbon, helium, neon particles transfers more energy along its path, and significantly more at the end of the Bragg peak; therefore, their RBE is higher (range, 1.5-4). For example, for a sample amount of 1 Gray dose to a target, carbon beam with RBE =3 will have three times the biological effects as photon beam with RBE =1. Higher RBE radiation is more effective against radio-resistant and hypoxic tumors since they are more likely to cause cell injuries by double-strand breaks and clustered damages in the DNA. Proton beam has RBE slightly higher than photon, about 1.1 to 1.2, and is considered to be a low LET type of radiation. It is also worth noting that the value of RBE varies along the path of particle beam, higher at the Bragg peak are than plateau area, and this difference is higher for heavier charged particle. From the theoretical standpoints, heavier charged particles such as Carbon and Helium have advantages over proton due to: (i) their Bragg peak is more pronounced; (ii) they have higher RBE, hence more effective against hypoxic or radio-resistant tumors and better cell-cycle independent cell kill; (iii) they have sharper beam edge or lateral penumbra. Disadvantages of using heavier charged particle therapy are: (i) the equipment is more expensive; (ii) the fragmentation region (or the stopping distance beyond the Bragg peak) is greater than proton; (iii) clinical experience is less than proton; (iv) RBE varies over the path of the beam; and incorporating this bio-effectiveness into treatment planning is difficult.

Clinical trials in charged particle beam therapy

Since its discovery, radiation had been used for many other diseases beside cancer such as acnes, infection, hair loss, arthritis, etc. Unfortunately, lots of lessons of the inappropriate use of radiation had long-lasting and severe complications that had brought a negative image to the field. In the early day, the use of radiation (and other medical treatments) was up to the call of the practitioner, and lot of knowledge was not transferrable or reproducible. Formation of clinical studies have significantly advanced the medical field (and protecting the patients). Multi-center clinical studies through such organization as Radiation Therapy Co-Operative Group (RTOG) have defined the standard of care in radiation therapy. The well-conducted clinical trials have defined the appropriate disease/stage, the technique (dose, fractionation, constraints), interactions with other modalities (surgery, chemotherapy), and outcomes. As the number of clinical centers for charged particle beam increases and emergence of more sophisticated technologies, the clinical application of charged particle beam therapy is expanded to more tumor sites from traditional applications such as tumors at the orbits, base of skull, spine, and pediatric population. A recent effort of PTCOG to compile clinical trials in charged particle beam therapy was reported by Giap *et al*. (10,11) and listed at the PTCOG website. There are more than 60 clinical studies investigating tumors of various sites from ten centers. The compiled list of clinical protocols shows a diversified potential applications in cancers of the lung, head and neck, gastrointestinal tract, prostate, breast, brain, gynecologic sites, lymphoma, and recurrent tumors. These clinical trials will validate or invalidate the use of particle beam for these disease sites. The publication of clinical trials will enhance awareness and accelerate the patient accrual to provide the answers. The other benefit of these listings will be for clinicians who are planning new clinical trials basing on these information and to promote the collaboration among multi-centers in conducting these clinical studies. In the U.S., due to its higher cost, charged particle beam therapy has faced lots of pressure from government, insurance carriers, and photon treatment centers to justify its superiority over the conventional radiation treatment. With the Agency for Healthcare Research and Quality (AHRQ) from the government promotes Comparative Effectiveness Research (CER) for various treatment modalities for a given type of disease. CER is designed to inform healthcare decisions by provide evidence on clinical effectiveness, benefits, and side effects of different treatment options. All modalities of cancer treatment will have to produce these data to justify itself. Clinical studies will provide these data and identify a subset of cancer patients that would best be

served by charged particle beam therapy either by more effective in local control and/or less side effects and/or both.

Conclusions

This article provides a historical perspective of charged particle therapy over the last 80 years. As cancer becomes the leading cause of mortality and morbidity in the U.S. and the rest of the world, and majority of cancer death and suffering is due to insufficient local control of tumor. Radiation therapy including charged particle therapy has been and will continue to be an effective modality for cancer therapy. There is still room for improvement in cancer care since only roughly half of cancer patients are cured from their diseases. There are many emergent treatment modalities for cancer therapy, and there are many refinement of existing treatments. Charged particle beam therapy has come a long way based upon its fundamental physical advantages, although more sophisticated, computer-intensive improvements are actively being pursued. Any strategy that continues to rely exclusively on using spread-out Bragg peak techniques with passive scattering, without modernizing the delivery and planning techniques, will cause the field of charged particle beam therapy will fall behind. With the recent emergence of much-improved technology and the engagement of many major academic centers into the field, this is the time that the field of charged particle therapy should take a quantum leap forward to unleash all these potentials. Charged particle therapy will never completely replace other modalities of radiation therapy or local treatment modalities, but it has to continue to evolve and push the bar higher by producing the clinical evidence for treatment of various cancer types. Perhaps, we could learn from one of humanity's greatest artists, Michelangelo: "*The greater danger for most of us is not that our aim is too high and we miss it, but that it is too low and we reach it*".

Acknowledgements

The authors would like to express gratitude to Dr. Richard P Levy for the review and comments on this manuscript.
Disclosure: The author declares no conflict of interest.

References

1. Brown A, Suit H. The centenary of the discovery of the Bragg peak. Radiother Oncol 2004;73:265-8.
2. Lawrence E, Livingston M. The production of high speed protons without the use of high voltages. Phys Rev 1931;38:834.
3. Wilson RR. Radiological use of fast protons. Radiology 1946;47:487-91.
4. Tobias CA, Anger HO, Lawrence JH. Radiological use of high energy deuterons and alpha particles. Am J Roentgenol Radium Ther Nucl Med 1952;67:1-27.
5. Levy RP, Blakely EA, Chu WT, et al. The current status and future directions of heavy charged particle therapy in medicine. AIP Conf Proc 2008;1099:410-25.
6. Cox J. Presentation at RadOnc 2010 at University of Texas M.D. Anderson Cancer Center. March 2010.
7. Smith AR. Vision 20/20: proton therapy. Med Phys 2009;36:556-68.
8. Gottschalk B, Pedroni E. Treatment delivery systems. In: DeLaney TF, Kooy HM. eds. Proton and Charged Particle Radiotherapy. Philadelphia: Lippincott Williams and Wilkins, 2008:33-49.
9. Nishio T, Miyatake A, Ogino T, et al. The development and clinical use of a beam ON-LINE PET system mounted on a rotating gantry port in proton therapy. Int J Radiat Oncol Biol Phys 2010;76:277-86.
10. Giap et al. Compilation of clinical trials in particle beam therapy. Presented at PTCOG 51 meeting in Seoul, South Korea, in May 2012.
11. Giap F, Levy R, Giap HB. Summary of on-going clinical protocols for proton and heavier-ion therapy. Proceedings the 22nd International Conference on the Application of Accelerators in Research and Industry (CAARI) 2012. In press by American Institute of Physics Conference Proceedings Series.

Cite this article as: Giap H, Giap B. Historical perspective and evolution of charged particle beam therapy. Transl Cancer Res 2012;1(3):127-136. DOI: 10.3978/j.issn.2218-676X.2012.10.09

Review Article

Particle therapy for central nervous system tumors in pediatric and adult patients

Jeffrey Q Dinh, Anita Mahajan, Matthew B Palmer, David R Grosshans

Division of Radiation Oncology, The University of Texas MD Anderson Cancer Center, Houston, TX, USA

Correspondence to: David R. Grosshans, MD, PhD. U.T. MD Anderson Cancer, Proton Therapy Center, 1840 Old Spanish Trail, Unit 1150, Houston, TX 77054, USA. Email: dgrossha@mdanderson.org.

Abstract: Radiation therapy has an established role in the treatment of many primary brain and spine tumors, both in adults and in children. However, adverse effects of radiotherapy arise when normal tissue is irradiated. As survival rates increase, limiting radiation-associated toxicities and thereby improving quality of life after treatment has become an increasing concern. Charged particles, such as protons and carbon ions, have unique physical properties, which differ from conventional photon-based treatments. These physical properties allow for superior dose-distributions, most notably sparing of normal tissues from unnecessary radiation exposure. In this review, we highlight the potential advantages of particle therapy in the treatment of central nervous system tumors in adults and children.

Keywords: Particle therapy; brain tumor; protons; carbon ions

Submitted Sep 12, 2012. Accepted for publication Oct 18, 2012.
DOI: 10.3978/j.issn.2218-676X.2012.10.02
Scan to your mobile device or view this article at: http://www.thetcr.org/article/view/583/html

Introduction

Despite the efficacy of radiation therapy (RT) in the treatment of central nervous system (CNS) tumors, substantial concerns exist regarding adverse radiation effects. Concerns regarding long-term radiation effects, including soft tissue or bone deformities, vascular damage, endocrine deficits, heart or lung damage, progressive cognitive decline, or even secondary malignancies, are further heightened as survival rates increase.

The central tenants of radiotherapy are to deliver tumoricidal doses of radiation accurately to target volumes while minimizing unnecessary exposure of normal tissues. Historically, the overwhelming majority of radiation treatments have been delivered using photon-based techniques. Diagnostic imaging, treatment planning, and tailored dose delivery have all advanced dramatically in recent decades, but the physical limitations of photon interactions within the body may now preclude further sparing of normal tissues.

Particle therapy is most commonly delivered using either protons or carbon ions. Both share the physical advantages of particle therapy in that beyond the Bragg peak, exit dose is essentially eliminated. In comparison with photon-based therapies, including intensity modulated radiation therapy (IMRT) or stereotactic treatments, radiation dose to normal tissues will virtually always be less, especially in the low dose regions. While both protons and carbon ions spare normal tissues, there are distinct biological differences between these particles. The concept of relative biological effectiveness (RBE) describes the cell killing capacity of various forms of radiation in relation to photons, leading to the creation of the term Gy(RBE) as the unit used to describe the physical dose (in Gy) times the determined RBE value. Carbon ions have a much higher RBE than protons, which could negatively impact exposed normal tissues adjacent to or within the target volume, as would be the case with craniospinal (CSI) irradiation, for example. Therefore, experience using proton therapy is rapidly expanding in the treatment of pediatric tumors, but greater caution applies to the use of carbon ions in this population. However, the higher RBE may be advantageous for treatment of tumors considered to be resistant to

conventional radiation. Indeed, for adults, there are numerous ongoing studies in this area. In this review, we will highlight the potential advantages of particle therapy when used for central nervous system tumors in both adults and children. We will present selected dosimetric studies, but focus on published clinical data supporting the use of particle treatments.

Particle therapy for pediatric brain tumors

Toxicities have been well-documented in long-term survivors of childhood cancers. The Childhood Cancer Survivor Study, funded by the National Cancer Institute, has systematically documented the long-term effects of treatment for childhood cancers in more than 14,000 survivors. Among these, over 1,800 survivors of CNS malignancies were included. In patients treated with radiotherapy, the cumulative incidence of secondary CNS malignancies was 7.1% at 25 years *vs.* 1% in patients not receiving radiation (1,2). Secondary malignancies include such tumors as meningiomas, thyroid tumors, and sarcomas, and these may contribute to the excess late mortality observed as compared with the general population (2). Therapeutic radiation exposure also contributed to endocrine, neurologic and neurocognitive deficits (3). Notably, a documented, dose-dependent relationship was also found between radiation and increased unemployment rates and decreased rates of marriage (4).

Medulloblastoma

Medulloblastomas represent one of the most common malignant CNS tumors in children. The high potential for subclinical dissemination throughout the brain and spinal column necessitates larger-field irradiation. In the United States, children over the age of 3 are typically treated with CSI, with dose selected based on set risk factors, including documented metastatic disease or residual tumor measuring >1.5 cm^2. Following CSI, an additional boost is delivered to the tumor bed plus margin or to the entire posterior fossa. Although there are ongoing attempts to reduce radiotherapy doses and volumes for medulloblastoma treatment, omission of radiotherapy has been associated with increased rates of recurrence and decreased survival (5).

As exposure of normal tissues to exit dose is unavoidable using photon therapy, many practitioners view CSI as a clear indication for proton therapy (PT). Comparative treatment plans demonstrate the complete sparing of structures distal to the spinal field using PT (*Figure 1A*). The potential adverse effects of irradiating these distal tissues are only now being realized. A retrospective study of 4,122 5-year childhood-cancer survivors found that individuals receiving an average of 5 Gy to the heart had a 12.5 relative risk over the general population for developing cardiovascular disease (6). Although clinical studies examining long-term clinical outcomes in patients treated with CSI using particles have yet to be performed, there have been several dosimetric studies. Lee *et al.* compared dose volume histograms (DVHs) in a prototypical patient receiving CSI with different treatment modalities, and found that the percentage of the heart receiving at least 10 Gy(RBE) was 65% with photons, 10% with electrons and 0% with protons (7).

Several studies have shown that PT, when utilized for the boost treatment following CSI, can significantly reduce dose to non-target structures (*Figure 1B*) (8). Comparative DVH's looking at the volume of cochlea receiving more than 20 Gy(RBE) during posterior fossa boost irradiation were 34% for PT, 87% for IMRT, and 89% for 3D-conformal radiotherapy (3D-CRT). Similarly, the volume of the hypothalamic-pituitary axis receiving more than 10 Gy(RBE) was 21% for protons, 81% for IMRT, and 91% for 3D-CRT. Dosimetric comparisons in another pediatric medulloblastoma case at MGH showed similar dose-sparing to the cochlea and pituitary when using proton therapy (9). Early clinical data from MD Anderson evaluating ototoxicity corroborates the clinical significance of these dosimetric studies (10). Nineteen patients with grossly intact hearing were evaluated 1 year following PT with only a single patient experiencing greater than grade 2 ototoxicity; more than half had no measurable hearing deficit. These clinical results compare favorably with ototoxicity after CSI using photons, including IMRT (11,12).

Given the large volumes irradiated with CSI and the high cure rates for medulloblastoma, secondary malignancies are a significant concern in long-term survivors. Using data from the International Commission on Radiologic Protection, Publication 60, to create a model for risk of cancer induction and normal tissue complication (13), two studies have shown the potential to reducing secondary malignancies using particle therapy. Miralbell *et al.* found PT was able to reduce the expected incidence of secondary malignancies by 8 to 15 fold compared with either IMRT or conventional photon therapy (14).

Similarly, a review of comparative treatment plans for five children with medulloblastoma found that the risk

Figure 1 A dosimetric comparison of proton and photon treatment plans for a child treated with craniospinal radiation. A. Sagittal images of proton and photon plans are depicted with the excess dose deposited from photon treatment highlighted on the right; B. Transverse images of proton and photon based boost plans. Dose to the brainstem and temporal lobes is reduced with protons

for secondary malignancy was lowest using intensity-modulated proton therapy (IMPT) (4%), followed by intensity-modulated electron therapy (IMET) (15%), conventional photon therapy (20%), and electron therapy (21%) (15). Investigators at MGH presented preliminary results suggesting a reduced incidence of secondary cancers in pediatric patients treated with protons at the Harvard Cyclotron, based upon a retrospective study

compared with photon patients extracted from the SEER database (16).

Ependymomas

Radiation also plays a crucial role in the management of ependymomas, but with typically much more limited field sizes restricted to those areas at highest risk for disease recurrence (i.e., the tumor bed). Nonetheless, cognitive deficits remain a challenge. Merchant *et al.* analyzed data from 88 patients who received the standard treatment for ependymomas to create a model to predict IQ, finding that increased doses to the total brain and to supratentorial volumes were predictive of lower intelligence (17). MacDonald *et al.* have published data on the clinical outcomes of 17 patients treated with proton therapy, in addition to performing a dosimetric comparison of IMPT, passive-scatter proton therapy (PSPT) and IMRT (18). At a median of 26 months after radiation, local control, progression free survival, and overall survival were 86%, 80%, and 89%, respectively, comparable to traditional photon-based treatments but without any significant toxicity yet observed (19,20). In comparing dose distributions in a patient with an infratentorial ependymoma, advantages of proton therapy were clearly demonstrated. The dose received by 50% of the whole brain was <0.1 Gy(RBE) for IMPT, <0.1 Gy(RBE) for PSPT, and 2 Gy for IMRT; the temporal lobe received 2 Gy(RBE) using IMPT, 4 Gy(RBE) with PSPT, and 16 Gy from IMRT. According to Merchant's model (17), these dose reductions seen in PSPT and IMPT for whole brain and temporal lobes suggest reduced adverse effects on IQ and reading ability, respectively. MacDonald's analysis also showed that PT was able to reduce cochlea doses significantly [0.1 Gy(RBE) for IMPT, 2 Gy(RBE) for PSPT, 37 Gy for IMRT], indicating that PT would be expected to preserve hearing (21). Similarly, dose sparing to the hypothalamus observed with PT may potentially avoid life-long endocrine deficits.

A small percentage of pediatric ependymomas arise within the spine, where surgical resection is the standard of care, yielding long-term control rates of >84% after complete resection (22). The management of incompletely resected spinal ependymomas is less certain, perhaps resulting from the low incidence of spinal ependymomas leading to less available data. Several studies have reported excellent control with subtotal resection alone, thereby recommending deferring adjuvant RT in most cases to avoid toxicities associated with spinal radiation (22,23). Other studies, however, have reported significantly improved control rates with adjuvant RT (24-26).

PT may offer a potential solution for incompletely resected spinal ependymomas. In eight cases of spinal ependymoma treated with adjuvant proton therapy at MD Anderson, Amsbaugh *et al.* reported 100% rates of local control, progression-free survival and overall survival at mean follow-up of 26 months, and with no Grade 3 or higher side-effects thus far observed (27).

Craniopharyngiomas

Although craniopharyngiomas are histologically benign lesions of the sellar region, they have a high propensity for local recurrence. Attempting to avoid RT by obtaining a gross total resection, however, often results in significant surgical morbidity and mortality (28,29). Consequently, the standard treatment has typically been maximal safe resection followed by adjuvant RT. Neurocognitive and endocrine deficits are the most common sequelae of radiotherapy in this location (30).

Boehling *et al.* studied the dosimetric advantages of proton therapy, highlighting the potential for improving cognitive outcomes by sparing of the hippocampal formations with IMPT (31). Given that these tumors are known to undergo cystic changes during the course of radiotherapy, however, caution must be utilized with employing modalities such as IMPT (32).

Two studies have published clinical outcomes of pediatric craniopharyngiomas treated with PSPT. Luu *et al.* retrospectively analyzed 16 patients treated with fractionated PT at Loma Linda, 12 of which were undergoing salvage therapy for tumor recurrence (33). At a mean follow-up of 60.2 months, local control was achieved in 14 patients (93.3%). Toxicities included one patient with pan-hypopituitarism after repeat resection and PT, another suffered from a cerebrovascular accident but fully recovered, and a third developed a posterior fossa meningioma 59 months after PT. Although cognitive function was not specifically reported in this study, neurocognitive deficits associated with radiotherapy of craniopharyngiomas are expected to decrease with PT based on lower doses to the supratentorial brain (34). Fitzek *et al.* have also reported promising functional outcomes on pediatric craniopharyngiomas treated using combined photon and proton therapy (35). All five patients in this series finished high school and were leading independent lives; three (treated at age 8.2, 16.7 and 16.8) were attending or had

completed college. Only one had learning difficulties, but these were comparable to his pre-radiotherapy status.

Germ cell tumors

Germ cell tumors can be subdivided histologically into germinomas or non-germinatous germ-cell tumors (NGGCT). Germinomas are more sensitive to radiotherapy and were historically treated with CSI with >90% durable response rate (36). However, due to considerable morbidity associated with CSI, whole-ventricle radiotherapy (WVRT) followed with a boost dose to the involved field has become the standard of treatment for localized, midline tumors. There is also the potential for reduction of radiation doses using pre-radiotherapy chemotherapy (37). In contrast to germinomas where disease control rates are high, NGGCTs carry a less favorable prognosis with recurrences and dissemination throughout the craniospinal axis being common. As such, a multimodality approach for NGGCTs is commonly employed with chemotherapy, CSI, and surgical resection all playing important roles (38).

A study from MGH has provided initial clinical data on the utility of proton therapy for treatment of germ cell tumors (39). Twenty-two patients, 13 with germinomas and 9 with NGGCT, were treated using 3D-CPT. At a median follow-up of 28 months, there was only one recurrence found in the peritoneum in a patient who did not have a complete response to chemotherapy. No new neurocognitive or auditory deficits were identified post-radiotherapy. Using a patient that received WVRT as a representative case to compare DVHs, proton therapy demonstrated dose-sparing: the left temporal lobe received 12.9 Gy(RBE) with IMPT, 20.5 Gy with IMRT, and 13.8 Gy with 3D-CPT. Although the lens dose using IMRT was low, no measurable lens dose was received using either 3D-CPT or IMPT, suggesting a further benefit of lowered risk of cataracts formation.

Gliomas

Pediatric gliomas comprise a clinically and histologically diverse group of tumors. Fortunately, the majority of pediatric gliomas are low-grade pilocytic astrocytomas which are typically managed with maximal safe surgical resection. If disease progression is documented post-operatively, chemotherapy is often utilized as a temporizing measure, thereby delaying radiotherapy in younger children. Still, RT is necessary for certain patients, including unresectable lesions or in cases of tumor progression after resection.

A study from Loma Linda has shown proton therapy to be an attractive option for treatment of pilocytic astrocytomas (40). Twenty-seven patients with low-grade astrocytomas were treated using fractionated proton therapy, with 25 of them being treated after sub-total resection. At mean follow-up of 39 months, 6 cases had failed locally [local control (LC) =78%], and 4 patients died from tumor progression [overall survival (OS) =85%]. For unresectable, centrally located astrocytomas (n=15), LC was achieved in 87%. With substantial dose-sparing to the cochlea, temporal lobe, pituitary, and contralateral optic nerve, the investigators found no significant short-term complications after proton therapy.

Optic pathway gliomas (OPGs) represent another area where PT could be particularly useful. The current trend is to utilize radiotherapy for older patients and chemotherapy for younger patients, again, in an attempt to delay radiotherapy and mitigate radiation-related toxicities (41,42). However, children treated with chemotherapy prior to radiotherapy may have worse visual outcomes compared to children treated primarily with radiotherapy (43). A study at Loma Linda demonstrated dosimetric advantage of PT in the treatment of seven pediatric OPGs by reducing doses to critical structures (44). PT reduced relative doses to the optic chiasm (by 11%), pituitary gland (by 13%), and bilateral temporal lobes (by 39%) compared to 3D-CRT. Additionally, PT was able to reduce the dose to the contralateral optic nerve by 47%. Accordingly, PT may make radiotherapy a more attractive option for younger OPG patients when radiation is necessary.

High-grade gliomas represent 6.5% of all childhood CNS neoplasms (45). In a study at Loma Linda consisting of 28 children with various brain tumors treated with proton therapy, 4 exhibited tumor progression (46). Two patients with high-grade (Grade 3 or 4) gliomas died after a mean of 13 months. Due to the poor control rates with both photon and PT for high-grade gliomas, future PT plans may use dose-escalation to attempt improved control rates.

Atypical tertatoid/rhabdoid tumors

Atypical teratoid/rhabdoid tumors (AT/RT) are estimated to represent 2-3% of primary pediatric CNS tumors. AT/RT is a relatively new histologic identity with an aggressive course and poor outcomes (47-49). Several studies have used aggressive chemotherapy regimens utilizing increased dose-intensity and intrathecal administration with promising

response rates (50,51). Given that the incidence of AT/RTs is highest in patients under three, practitioners often attempt to avoid radiation in fear of potential toxicities. However, delaying the initiation of radiation may lead to poor outcomes. A study in Taiwan (52) involving 17 patients who were managed with primary surgery with subsequent radiotherapy demonstrated that patients with increased latency between surgery and radiation did not fare as well as those that received radiation earlier. In another study of 22 cases of AT/RT (53), there were only 2 long-term survivors, both of whom received radiotherapy as part of the primary treatment. Based on an extensive literature review on AT/RT, Squire *et al.* (54) suggests that radiation should be employed as part of initial therapy in select cases, and there is currently a multi-institutional protocol in place for AT/RT that includes risk-adapted RT in the initial therapy for selected children under three (55). With the current trend towards using radiotherapy in the primary treatment in younger and therefore more radiosensitive patients, limiting the radiation doses becomes even more essential.

Particle therapy for adult brain tumors

Adults receiving radiotherapy for CNS tumors generally face many of the same side-effects as does the pediatric population, such as visual deficits, ototoxicity, cerebrovascular accidents, neurocognitive impairment, and increased risk of secondary malignancies (56). Although many consider the adult CNS to be more radiation resistant than that of children, radiation-induced cognitive impairment is known to occur in up to 50-90% of adults within 6-months after radiation for brain tumors (57-59). Adults that receive radiotherapy for CNS tumors face significant effects on quality of life with the most commonly reported symptoms being fatigue, mood changes, and cognitive dysfunction (60,61). Therefore, reducing doses of radiation to the normal tissues in the adult brain should also be a priority.

Pituitary adenomas

Pituitary adenomas are benign tumors found in the sella turcica, three quarters of which present with functional symptoms resulting from hormone over-secretion. Radiotherapy offers the potential for cure even if the lesion is unresectable, and is typically used after medical and surgical therapies have failed. Moreover, medical therapy may require life-long treatment, and tumors may become refractory to medical management.

Two primary dose schedules are commonly used in radiotherapy for pituitary adenomas. Stereotactic radiosurgery (SRS) delivers a high-dose single radiation treatment (typically 15 to 20 Gy), whereas fractionated schedules deliver 45-54 Gy over 5-6 weeks. SRS may normalize hormone levels of functional adenomas faster than does conventional fractionated RT (62). However, the use of SRS may be limited in larger tumors located in close proximity to critical structures, such as the optic chiasm, because of the high fractional doses prescribed. Several institutions have started performing proton stereotactic radiosurgery (PSRS) to take advantage of the favorable dose-distribution properties to achieve decreased risk of toxicity.

MGH has studied PSRS in the treatment of GH- and ACTH-secreting tumors. Of 22 patients with residual GH-secreting tumors after trans-sphenoidal resection who were then treated using PSRS with a median dose of 20 Gy(RBE), a complete response (CR), defined as sustained (≥3 months) normalization of IGF-1, was seen in 59% of patients after a median of 42 months post-radiotherapy (63). In another study, 38 patients with Cushing's disease or Nelson's syndrome were treated with PSRS for persistence of symptoms and elevated cortisol levels following trans-sphenoidal resection (64). At median follow-up of 62 months, CR was achieved in all 5 cases of Nelson's syndrome, and 52% (17/33) of Cushing's disease cases, with median time to CR being 18 months after PSRS. In both studies, the CR rate and time to CR was comparable to previous SRS studies (65-73). There were no cases of visual disturbance, seizure activity, or other clinical signs of brain injury, but both studies showed slightly higher rates of hypopituitarism after PSRS when compared with other SRS studies.

Meningiomas

Meningiomas are the most common benign CNS tumors in adults and portend a generally favorable prognosis, with 90% classified as WHO Class I. Surgery is the mainstay of the therapy, but radiotherapy is used as adjuvant therapy in cases of partial resection, or with high-grade or recurrent lesions. Radiotherapy can also be utilized as definitive treatment for lesions in locations where resection is not possible. Long-term control rates with current radiotherapy techniques are >90% (74). With the expected long-term survival, improving functional status and limiting toxicities

are objectives of treatment.

Given the proximity of skull base meningiomas to critical structures, particle therapy provides an opportunity to reduce toxicities. Wenkel *et al*. studied 46 patients with benign base-of-skull meningiomas treated with a combination of photon and proton therapy, reporting a recurrence-free rate of 100% and 88% at 5 and 10 years, respectively (75). Four patients in this series experienced ophthalmic toxicities. In retrospect, doses to the optic nerve in these four patients were found to have exceeded the threshold of 54 Gy(RBE) after the doses were recalculated following a calibration error. Patients that did not receive >54 Gy(RBE) to the optic nerve did not experience any ophthalmic toxicity. This highlights the need for high quality physics support given the increased complexity of particle therapy.

Noël *et al*. studied functional outcomes of 51 patients with skull base meningiomas treated with a combination of photons and proton therapy (76). Four-year LC and OS rates were 98% and 100% respectively. Although two patients (3.9%) suffered from Grade 3 side effects, 68.8% of eye-related symptoms improved after radiotherapy, and 67% of other miscellaneous symptoms improved, comparing favorably with photon studies reporting functional outcomes (77-80). Weber *et al*. from the Paul Scherrer Institute studied 39 cases treated only with protons, using a pencil-beam scanning (PBS) technique (81). At least 10 patients in this series had WHO Grade II/III meningiomas, and the average tumor volumes were larger than most other series. LC and OS at 5 years were 84.8% and 81.8%, respectively, for all histology types, and were 100% for benign histology. The 5-year Grade 3/4 toxicity-free survival was 84.5%. Those patients that experienced higher-grade toxicities were those who presented with large tumor volumes and/or with meningiomas of the optic tract. These results appear to support the use of particle therapy for meningiomas, especially for lesions in close proximity to critical structures.

Vestibular schwannoma

Vestibular schwannomas are benign intracranial tumors of the myelin-forming cells of the vestibulocochlear nerve. As many vestibular schwannomas are found incidentally on imaging studies, and only 43-46% of tumors show any growth (with an average rate of 1.2-1.9 mm per year), observation is a reasonable option for many patients (82). For tumors that require treatment, surgery and radiotherapy can both be used as first-line modalities. Surgery offers excellent control rates, but definitive radiotherapy is also a therapeutic option that offers excellent tumor control rates of greater than 90%. While vestibular schwannomas treated with radiotherapy may have a reported lower incidence of adverse effects, including hearing loss and facial nerve palsies, compared with microsurgery, direct comparison is difficult to make as tumors treated with microsurgery tend to be larger in volume (83).

Harsh *et al.* used a PSRS protocol prescribing 12 Gy(RBE) to the tumor and limiting brainstem dose to 12 Gy(RBE). They found LC rates of 94%, trigeminal and facial nerve preservation in 95.3%, and hearing preservation in 33.3% (84). Low rates of hearing preservation were thought to be due to an older patient population (mean age =67) and surgical resections prior to radiotherapy, which may have increased susceptibility to cranial nerve damage. Bush *et al*. used a fractionated protocol prescribing 54-60 Gy(RBE) in 30 to 33 fractions (85). At mean follow-up of 34 months, LC was 100%, and no trigeminal or facial nerve toxicities were observed, with 31% maintaining useful hearing. Using the α-β model to compare doses of FSRT and SRS studies, this fractionated protocol prescribed roughly 40% more dose than the PSRS regimen, suggesting that a lower fractionated dose might resulted in better preservation of hearing while maintaining good LC. Vernimenn *et al.* used a hypo-fractionated proton therapy [26 Gy(RBE) over 3 fractions] to treat a group of patients with an average tumor volume of 5.3 cm^3, which is among the largest studied in this group of tumors (86). At a mean follow-up of 72 months, hearing preservation was 42%, trigeminal and facial nerve preservation rates were 93% and 90.5%, respectively, and the 5-year LC rate was 98%, suggesting that this hypo-fractionated protocol was a good option for large, inoperable tumors. Baummert *et al*. compared dose distributions of photon and particle therapy and found that high-dose conformality was equal, but that proton therapy lowered the integral dose, concluding that particle therapy may be particularly useful for larger lesions.

Glioblastoma mutliforme

Glioblastoma multiforme (GBM) is the most common primary malignant brain tumor in adults. Early studies dating from 1978 demonstrated that radiotherapy after resection more than doubled overall survival to 8.0 months compared to 3.2 months with observation alone, establishing the effectiveness of radiotherapy in management of GBM (87). With the current standard, post-surgical, teomozolamide-based chemoradiotherapy, overall

median progression-free survival is approximately 7 months, with OS of 15 months (88). Current recommendations for RT include dosages up to 60 Gy given in daily fractions of 2 Gy to the enhancing area of the tumor with 1-2 cm margins. Using this standard radiotherapy regimen, however, 80-90% of tumors recur within 2 cm of the original lesion.

In an effort to improve tumor control, several studies have used proton therapy to escalate doses up to 90 Gy(RBE). Using a combination of photons and protons, MGH treated 23 GBM patients to a total dose of 90 Gy(RBE) to the gross tumor volume, 64.8 Gy(RBE) to the 2-cm margin encompassing the gross tumor volume, and 50.4 Gy(RBE) to area of surrounding edema plus 2-cm margins using accelerated fractionation (89). Stratified by RTOG prognostic classes, this plan consistently increased median survival time to 23, 17, and 14 months for RTOG Classes III, IV and V, respectively. This compares with the 17.9, 11.1, and 8.9 months median survival for respective classes seen in previous RTOG trials using standard doses of RT with chemotherapy (90). Of the 23 patients treated to these high doses, only one had tumor recurrence within the dose-escalated region. Despite the better control in the high-dose region and increased median survival, all patients in whom tissue was obtained (n=7) developed radiation necrosis, and neurological deterioration was observed in most patients.

A more recent study from Tsukuba also dose-escalated to 96.6 Gy(RBE) over 56 fractions, obtaining a median survival of 21.6 months in 21 patients, most having RTOG Class IV GBM (91). Stratifying by size of the enhancing tumor, it was found that acute side-effects were tolerable with smaller tumor volumes. However, this study was not able to comment on late-effects of the radiation, because it was difficult for imaging to distinguish between tumor recurrence and necrosis. These studies demonstrate dose-escalation up to 96 Gy(RBE) with proton therapy provides effective LC and offers some increase in median survival. At such high doses, however, the radiation necrosis experienced represents a significant toxicity and may limit quality of life benefits. Nonetheless, when combined with concurrent chemotherapy, particle therapy at intermediate doses may yet play an important role in the treatment of these aggressive tumors. Mizoe *et al.* used carbon ion RT to provide a boost of 16.8-24.8 Gy(RBE) to the tumor volume with concurrent nimustine hydrochloride in 32 patients. Median survival was 17 months and progression-free survival ranged from 7-19 months, depending on the dose of carbon-ion boost to the tumor. The incidence of late-toxicities appears low, with only four patients experiencing Grade 2 brain reactions. European investigators are also actively studying the potential utility of carbon ions, utilizing their inherently higher RBE in an attempt to overcome radiation resistance for gliomas and other brain tumors (92,93).

Discussion and future directions

Particle therapy promises to expand the therapeutic ratio for radiotherapy. The central tenants of radiation therapy remain treatment of the tumor and sparing of normal tissues. Given the high implementation costs, however, substantial controversy remains. In calculating the cost effectiveness of various radiation modalities, it is of great importance to consider the potential implications of late adverse effects. Indeed, several studies have used models to demonstrate the potential cost-benefits of particle therapy (94-97). These studies concluded that, when used to treat carefully selected patients, particle therapy has the potential to be cost saving through decreased toxicities and increased quality of life.

Another major criticism of particle therapy is the lack of clinical evidence showing benefit in efficacy and toxicity compared with the best photon therapy. For many years, the number of trials will be limited due to the lack of proton treatment facilities and the small number of patients at each site. In 2002, only two proton therapy facilities were in operation in the US. Currently, there are only ten proton centers operational in the US. As clinical evidence accumulates, it is hoped that the long-term cost benefits of normal tissue sparing will be realized.

There are several developing areas in particle therapy which may offer even greater benefit. To date, the majority of published studies on particle therapy for CNS tumors have used PSPT. Active-scanning techniques, including IMPT, may offer improved conformity while maintaining dose sparing of normal tissues. Active scanning, by not requiring the scattering foils used for passive scattering, creates fewer neutrons at beam delivery, thereby further minimizing the risk of inducing secondary malignancies. As scanning-beam treatments are implemented, there may also be an opportunity for biologic treatment planning with proton therapy, as the RBE of proton beams may increase at the most distal edge, although to a much lesser extent than is observed with heavier particles (98,99). Although carbon-ion RT may also offer increased efficacy for radiation-resistant tumors, there are currently only a few institutions

worldwide offering carbon-ion RT, and none in the US.

As more institutions adopt particle therapy, the potential of particle therapy is expected to translate into improved outcomes over photon therapy. Published data are quite promising, but much still remains to be learned about the role of particle therapy.

Acknowledgements

Disclosure: The authors declare no conflict of interest.

References

1. Mertens AC, Yasui Y, Neglia JP, et al. Late mortality experience in five-year survivors of childhood and adolescent cancer: the Childhood Cancer Survivor Study. J Clin Oncol 2001;19:3163-72.
2. Armstrong GT, Liu Q, Yasui Y, et al. Long-term outcomes among adult survivors of childhood central nervous system malignancies in the Childhood Cancer Survivor Study. J Natl Cancer Inst 2009;101:946-58.
3. Armstrong GT, Stovall M, Robison LL. Long-term effects of radiation exposure among adult survivors of childhood cancer: results from the childhood cancer survivor study. Radiat Res 2010;174:840-50.
4. Ellenberg L, Liu Q, Gioia G, et al. Neurocognitive status in long-term survivors of childhood CNS malignancies: a report from the Childhood Cancer Survivor Study. Neuropsychology 2009;23:705-17.
5. Thomas PR, Deutsch M, Kepner JL, et al. Low-stage medulloblastoma: final analysis of trial comparing standard-dose with reduced-dose neuraxis irradiation. J Clin Oncol 2000;18:3004-11.
6. Tukenova M, Guibout C, Oberlin O, et al. Role of cancer treatment in long-term overall and cardiovascular mortality after childhood cancer. J Clin Oncol 2010;28:1308-15.
7. Hein PA, Gladstone DJ, Bellerive MR, Hug EB. Importance of protocol target definition on the ability to spare normal tissue:an IMRT and 3D-CRT planning comparison for intraorbital tumors. Int J Radiat Oncol Biol Phys. 2005 Aug 1;62(5):1540-8.
8. Lee CT, Bilton SD, Famiglietti RM, et al. Treatment planning with protons for pediatric retinoblastoma, medulloblastoma, and pelvic sarcoma: how do protons compare with other conformal techniques? Int J Radiat Oncol Biol Phys 2005;63:362-72.
9. St Clair WH, Adams JA, Bues M, et al. Advantage of protons compared to conventional X-ray or IMRT in the treatment of a pediatric patient with medulloblastoma. Int J Radiat Oncol Biol Phys 2004;58:727-34.
10. Moeller BJ, Chintagumpala M, Philip JJ, et al. Low early ototoxicity rates for pediatric medulloblastoma patients treated with proton radiotherapy. Radiat Oncol 2011;6:58.
11. Huang E, Teh BS, Strother DR, et al. Intensity-modulated radiation therapy for pediatric medulloblastoma: early report on the reduction of ototoxicity. Int J Radiat Oncol Biol Phys 2002;52:599-605.
12. Polkinghorn WR, Dunkel IJ, Souweidane MM, et al. Disease control and ototoxicity using intensity-modulated radiation therapy tumor-bed boost for medulloblastoma. Int J Radiat Oncol Biol Phys 2011;81:e15-20.
13. ICRP Publication 60: 1990 Recommendations of the International Commission on Radiological Protection 1991.
14. Miralbell R, Lomax A, Cella L, et al. Potential reduction of the incidence of radiation-induced second cancers by using proton beams in the treatment of pediatric tumors. Int J Radiat Oncol Biol Phys 2002;54:824-9.
15. Mu X, Björk-Eriksson T, Nill S, et al. Does electron and proton therapy reduce the risk of radiation induced cancer after spinal irradiation for childhood medulloblastoma? A comparative treatment planning study. Acta Oncol 2005;44:554-62.
16. Chung CS, Keating N, Yock TY, et al. Comparative analysis of second malignancy risk in patients treated with proton therapy versus conventional photon therapy. Int J Radiat Oncol Biol Phys 2008;72:8.
17. Merchant TE, Kiehna EN, Li C, et al. Radiation dosimetry predicts IQ after conformal radiation therapy in pediatric patients with localized ependymoma. Int J Radiat Oncol Biol Phys 2005;63:1546-54.
18. MacDonald SM, Safai S, Trofimov A, et al. Proton radiotherapy for childhood ependymoma: initial clinical outcomes and dose comparisons. Int J Radiat Oncol Biol Phys 2008;71:979-86.
19. Weber DC, Zilli T, Do HP, et al. Intensity modulated radiation therapy or stereotactic fractionated radiotherapy for infratentorial ependymoma in children: a multicentric study. J Neurooncol 2011;102:295-300.
20. Schroeder TM, Chintagumpala M, Okcu MF, et al. Intensity-modulated radiation therapy in childhood ependymoma. Int J Radiat Oncol Biol Phys 2008;71:987-93.
21. Merchant TE, Gould CJ, Xiong X, et al. Early neuro-otologic effects of three-dimensional irradiation in children with primary brain tumors. Int J Radiat Oncol Biol Phys 2004;58:1194-207.
22. Benesch M, Weber-Mzell D, Gerber NU, et al.

Ependymoma of the spinal cord in children and adolescents: a retrospective series from the HIT database. J Neurosurg Pediatr 2010;6:137-44.
23. Lonjon M, Goh KY, Epstein FJ. Intramedullary spinal cord ependymomas in children: treatment, results and follow-up. Pediatr Neurosurg 1998;29:178-83.
24. O'Sullivan C, Jenkin RD, Doherty MA, et al. Spinal cord tumors in children: long-term results of combined surgical and radiation treatment. J Neurosurg 1994;81:507-12.
25. Merchant TE, Kiehna EN, Thompson SJ, et al. Pediatric low-grade and ependymal spinal cord tumors. Pediatr Neurosurg 2000;32:30-6.
26. Al-Halabi H, Montes JL, Atkinson J, et al. Adjuvant radiotherapy in the treatment of pediatric myxopapillary ependymomas. Pediatr Blood Cancer 2010;55:639-43.
27. Amsbaugh MJ, Grosshans DR, McAleer MF, et al. Proton therapy for spinal ependymomas: planning, acute toxicities, and preliminary outcomes. Int J Radiat Oncol Biol Phys 2012;83:1419-24.
28. Steňo J, Bízik I, Steňo A, et al. Craniopharyngiomas in children: how radical should the surgeon be? Childs Nerv Syst 2011;27:41-54.
29. Becker KL. Craniopharyngiomas. In: Becker KL. eds. Principles and Practice of Endocrinology and Metabolism. Philadelphia, PA: Lippincott Williams & Wilkins, 2000:957.
30. Crom DB, Smith D, Xiong Z, et al. Health status in long-term survivors of pediatric craniopharyngiomas. J Neurosci Nurs 2010;42:323-8; quiz 329-30.
31. Boehling NS, Grosshans DR, Bluett JB, et al. Dosimetric comparison of three-dimensional conformal proton radiotherapy, intensity-modulated proton therapy, and intensity-modulated radiotherapy for treatment of pediatric craniopharyngiomas. Int J Radiat Oncol Biol Phys 2012;82:643-52.
32. Beltran C, Roca M, Merchant TE. On the benefits and risks of proton therapy in pediatric craniopharyngioma. Int J Radiat Oncol Biol Phys 2012;82:e281-7.
33. Luu QT, Loredo LN, Archambeau JO, et al. Fractionated proton radiation treatment for pediatric craniopharyngioma: preliminary report. Cancer J 2006;12:155-9.
34. Merchant TE, Hua CH, Shukla H, et al. Proton versus photon radiotherapy for common pediatric brain tumors: comparison of models of dose characteristics and their relationship to cognitive function. Pediatr Blood Cancer 2008;51:110-7.
35. Fitzek MM, Linggood RM, Adams J, et al. Combined proton and photon irradiation for craniopharyngioma: long-term results of the early cohort of patients treated at Harvard Cyclotron Laboratory and Massachusetts General Hospital. Int J Radiat Oncol Biol Phys 2006;64:1348-54.
36. Maity A, Shu HK, Janss A, et al. Craniospinal radiation in the treatment of biopsy-proven intracranial germinomas: twenty-five years' experience in a single center. Int J Radiat Oncol Biol Phys 2004;58:1165-70.
37. Aoyama H, Shirato H, Ikeda J, et al. Induction chemotherapy followed by low-dose involved-field radiotherapy for intracranial germ cell tumors. J Clin Oncol 2002;20:857-65.
38. Jennings MT, Gelman R, Hochberg F. Intracranial germ-cell tumors: natural history and pathogenesis. J Neurosurg 1985;63:155-67.
39. MacDonald SM, Trofimov A, Safai S, et al. Proton radiotherapy for pediatric central nervous system germ cell tumors: early clinical outcomes. Int J Radiat Oncol Biol Phys 2011;79:121-9.
40. Hug EB, Muenter MW, Archambeau JO, et al. Conformal proton radiation therapy for pediatric low-grade astrocytomas. Strahlenther Onkol 2002;178:10-7.
41. Laithier V, Grill J, Le Deley MC, et al. Progression-free survival in children with optic pathway tumors: dependence on age and the quality of the response to chemotherapy--results of the first French prospective study for the French Society of Pediatric Oncology. J Clin Oncol 2003;21:4572-8.
42. Petronio J, Edwards MS, Prados M, et al. Management of chiasmal and hypothalamic gliomas of infancy and childhood with chemotherapy. J Neurosurg 1991;74:701-8.
43. Awdeh RM, Kiehna EN, Drewry RD, et al. Visual outcomes in pediatric optic pathway glioma after conformal radiation therapy. Int J Radiat Oncol Biol Phys 2012;84:46-51.
44. Fuss M, Hug EB, Schaefer RA, et al. Proton radiation therapy (PRT) for pediatric optic pathway gliomas: comparison with 3D planned conventional photons and a standard photon technique. Int J Radiat Oncol Biol Phys 1999;45:1117-26.
45. Dohrmann GJ, Farwell JR, Flannery JT. Astrocytomas in childhood: a population-based study. Surg Neurol 1985;23:64-8.
46. McAllister B, Archambeau JO, Nguyen MC, et al. Proton therapy for pediatric cranial tumors: preliminary report on treatment and disease-related morbidities. Int J Radiat

Oncol Biol Phys 1997;39:455-60.
47. Packer RJ, Biegel JA, Blaney S, et al. Atypical teratoid/rhabdoid tumor of the central nervous system: report on workshop. J Pediatr Hematol Oncol 2002;24:337-42.
48. Burger PC, Yu IT, Tihan T, et al. Atypical teratoid/rhabdoid tumor of the central nervous system: a highly malignant tumor of infancy and childhood frequently mistaken for medulloblastoma: a Pediatric Oncology Group study. Am J Surg Pathol 1998;22:1083-92.
49. Rorke LB, Packer RJ, Biegel JA. Central nervous system atypical teratoid/rhabdoid tumors of infancy and childhood: definition of an entity. J Neurosurg 1996;85:56-65.
50. Weinblatt M, Kochen J. Rhabdoid tumor of the central nervous system. Med Pediatr Oncol 1992;20:258.
51. Olson TA, Bayar E, Kosnik E, et al. Successful treatment of disseminated central nervous system malignant rhabdoid tumor. J Pediatr Hematol Oncol 1995;17:71-5.
52. Chen YW, Wong TT, Ho DM, et al. Impact of radiotherapy for pediatric CNS atypical teratoid/rhabdoid tumor (single institute experience). Int J Radiat Oncol Biol Phys 2006;64:1038-43.
53. Tekautz TM, Fuller CE, Blaney S, et al. Atypical teratoid/rhabdoid tumors (ATRT): improved survival in children 3 years of age and older with radiation therapy and high-dose alkylator-based chemotherapy. J Clin Oncol 2005;23:1491-9.
54. Squire SE, Chan MD, Marcus KJ. Atypical teratoid/rhabdoid tumor: the controversy behind radiation therapy. J Neurooncol 2007;81:97-111.
55. Kieran MW. A Single-Arm, Open Label Limited-Institutional Phase II Study of Multi-Agent Intrathecal and Systemic Chemotherapy With Radiation Therapy for Children < or = 18 Years With Newly Diagnosed Central Nervous System Atypical Teratoid/Rhabdoid Tumor. 2004: DFCI.
56. al-Mefty O, Kersh JE, Routh A, et al. The long-term side effects of radiation therapy for benign brain tumors in adults. J Neurosurg 1990;73:502-12.
57. Meyers CA, Brown PD. Role and relevance of neurocognitive assessment in clinical trials of patients with CNS tumors. J Clin Oncol 2006;24:1305-9.
58. Johannesen TB, Lien HH, Hole KH, et al. Radiological and clinical assessment of long-term brain tumour survivors after radiotherapy. Radiother Oncol 2003;69:169-76.
59. Crossen JR, Garwood D, Glatstein E, et al. Neurobehavioral sequelae of cranial irradiation in adults: a review of radiation-induced encephalopathy. J Clin Oncol 1994;12:627-42.
60. Gleason JF Jr, Case D, Rapp SR, et al. Symptom clusters in patients with newly-diagnosed brain tumors. J Support Oncol 2007;5:427-33, 436.
61. Meyers CA, Weitzner MA, Valentine AD, et al. Methylphenidate therapy improves cognition, mood, and function of brain tumor patients. J Clin Oncol 1998;16:2522-7.
62. Kong DS, Lee JI, Lim do H, et al. The efficacy of fractionated radiotherapy and stereotactic radiosurgery for pituitary adenomas: long-term results of 125 consecutive patients treated in a single institution. Cancer 2007;110:854-60.
63. Petit JH, Biller BM, Coen JJ, et al. Proton stereotactic radiosurgery in management of persistent acromegaly. Endocr Pract 2007;13:726-34.
64. Petit JH, Biller BM, Yock TI, et al. Proton stereotactic radiotherapy for persistent adrenocorticotropin-producing adenomas. J Clin Endocrinol Metab 2008;93:393-9.
65. Castinetti F, Nagai M, Dufour H, et al. Gamma knife radiosurgery is a successful adjunctive treatment in Cushing's disease. Eur J Endocrinol 2007;156:91-8.
66. Devin JK, Allen GS, Cmelak AJ, et al. The efficacy of linear accelerator radiosurgery in the management of patients with Cushing's disease. Stereotact Funct Neurosurg 2004;82:254-62.
67. Cho CB, Park HK, Joo WI, et al. Stereotactic Radiosurgery with the CyberKnife for Pituitary Adenomas. J Korean Neurosurg Soc 2009;45:157-63.
68. Höybye C, Grenbäck E, Rähn T, et al. Adrenocorticotropic hormone-producing pituitary tumors: 12- to 22-year follow-up after treatment with stereotactic radiosurgery. Neurosurgery 2001;49:284-91; discussion 291-2.
69. Castinetti F, Taieb D, Kuhn JM, et al. Outcome of gamma knife radiosurgery in 82 patients with acromegaly: correlation with initial hypersecretion. J Clin Endocrinol Metab 2005;90:4483-8.
70. Attanasio R, Epaminonda P, Motti E, et al. Gamma-knife radiosurgery in acromegaly: a 4-year follow-up study. J Clin Endocrinol Metab 2003;88:3105-12.
71. Pollock BE, Nippoldt TB, Stafford SL, et al. Results of stereotactic radiosurgery in patients with hormone-producing pituitary adenomas: factors associated with endocrine normalization. J Neurosurg 2002;97:525-30.
72. Voges J, Kocher M, Runge M, et al. Linear accelerator radiosurgery for pituitary macroadenomas: a 7-year follow-up study. Cancer 2006;107:1355-64.

73. Jezková J, Marek J, Hána V, et al. Gamma knife radiosurgery for acromegaly--long-term experience. Clin Endocrinol (Oxf) 2006;64:588-95.
74. Minniti G, Amichetti M, Enrici RM. Radiotherapy and radiosurgery for benign skull base meningiomas. Radiat Oncol 2009;4:42.
75. Wenkel E, Thornton AF, Finkelstein D, et al. Benign meningioma: partially resected, biopsied, and recurrent intracranial tumors treated with combined proton and photon radiotherapy. Int J Radiat Oncol Biol Phys 2000;48:1363-70.
76. Noël G, Bollet MA, Calugaru V, et al. Functional outcome of patients with benign meningioma treated by 3D conformal irradiation with a combination of photons and protons. Int J Radiat Oncol Biol Phys 2005;62:1412-22.
77. Debus J, Wuendrich M, Pirzkall A, et al. High efficacy of fractionated stereotactic radiotherapy of large base-of-skull meningiomas: long-term results. J Clin Oncol 2001;19:3547-53.
78. Dufour H, Muracciole X, Métellus P, et al. Long-term tumor control and functional outcome in patients with cavernous sinus meningiomas treated by radiotherapy with or without previous surgery: is there an alternative to aggressive tumor removal? Neurosurgery 2001;48:285-94; discussion 294-6.
79. Takanashi M, Fukuoka S, Hojyo A, et al. Gamma knife radiosurgery for skull-base meningiomas. Prog Neurol Surg 2009;22:96-111.
80. Shin M, Kurita H, Sasaki T, et al. Analysis of treatment outcome after stereotactic radiosurgery for cavernous sinus meningiomas. J Neurosurg 2001;95:435-9.
81. Weber DC, Schneider R, Goitein G, et al. Spot scanning-based proton therapy for intracranial meningioma: long-term results from the Paul Scherrer Institute. Int J Radiat Oncol Biol Phys 2012;83:865-71.
82. Smouha EE, Yoo M, Mohr K, et al. Conservative management of acoustic neuroma: a meta-analysis and proposed treatment algorithm. Laryngoscope 2005;115:450-4.
83. Arthurs BJ, Fairbanks RK, Demakas JJ, et al. A review of treatment modalities for vestibular schwannoma. Neurosurg Rev 2011;34:265-77; discussion 277-9.
84. Harsh GR, Thornton AF, Chapman PH, et al. Proton beam stereotactic radiosurgery of vestibular schwannomas. Int J Radiat Oncol Biol Phys 2002;54:35-44.
85. Bush DA, McAllister CJ, Loredo LN, et al. Fractionated proton beam radiotherapy for acoustic neuroma. Neurosurgery 2002;50:270-3; discussion 273-5.
86. Vernimmen FJ, Mohamed Z, Slabbert JP, et al. Long-term results of stereotactic proton beam radiotherapy for acoustic neuromas. Radiother Oncol 2009;90:208-12.
87. Walker MD, Alexander E Jr, Hunt WE, et al. Evaluation of BCNU and/or radiotherapy in the treatment of anaplastic gliomas. A cooperative clinical trial. J Neurosurg 1978;49:333-43.
88. Stupp R, Mason WP, van den Bent MJ, et al. Radiotherapy plus concomitant and adjuvant temozolomide for glioblastoma. N Engl J Med 2005;352:987-96.
89. Fitzek MM, Thornton AF, Rabinov JD, et al. Accelerated fractionated proton/photon irradiation to 90 cobalt gray equivalent for glioblastoma multiforme: results of a phase II prospective trial. J Neurosurg 1999;91:251-60.
90. Curran WJ Jr, Scott CB, Horton J, et al. Recursive partitioning analysis of prognostic factors in three Radiation Therapy Oncology Group malignant glioma trials. J Natl Cancer Inst 1993;85:704-10.
91. Mizumoto M, Tsuboi K, Igaki H, et al. Phase I/II trial of hyperfractionated concomitant boost proton radiotherapy for supratentorial glioblastoma multiforme. Int J Radiat Oncol Biol Phys 2010;77:98-105.
92. Combs SE, Kieser M, Rieken S, et al. Randomized phase II study evaluating a carbon ion boost applied after combined radiochemotherapy with temozolomide versus a proton boost after radiochemotherapy with temozolomide in patients with primary glioblastoma: the CLEOPATRA trial. BMC Cancer 2010;10:478.
93. Rieken S, Habermehl D, Haberer T, et al. Proton and carbon ion radiotherapy for primary brain tumors delivered with active raster scanning at the Heidelberg Ion Therapy Center (HIT): early treatment results and study concepts. Radiat Oncol 2012;7:41.
94. Lundkvist J, Ekman M, Ericsson SR, et al. Economic evaluation of proton radiation therapy in the treatment of breast cancer. Radiother Oncol 2005;75:179-85.
95. Lundkvist J, Ekman M, Ericsson SR, et al. Proton therapy of cancer: potential clinical advantages and cost-effectiveness. Acta Oncol 2005;44:850-61.
96. Lundkvist J, Ekman M, Ericsson SR, et al. Cost-effectiveness of proton radiation in the treatment of childhood medulloblastoma. Cancer 2005;103:793-801.
97. Pommier P, Lievens Y, Feschet F, et al. Simulating demand for innovative radiotherapies: an illustrative model based on carbon ion and proton radiotherapy. Radiother Oncol 2010;96:243-9.

98. Paganetti H, Olko P, Kobus H, et al. Calculation of relative biological effectiveness for proton beams using biological weighting functions. Int J Radiat Oncol Biol Phys 1997;37:719-29.
99. Calugaru V, Nauraye C, Noël G, et al. Radiobiological characterization of two therapeutic proton beams with different initial energy spectra used at the Institut Curie Proton Therapy Center in Orsay. Int J Radiat Oncol Biol Phys 2011;81:1136-43.

Cite this article as: Dinh JQ, Mahajan A, Palmer MB, Grosshans DR. Particle therapy for central nervous system tumors in pediatric and adult patients. Transl Cancer Res 2012;1(3):137-149. DOI: 10.3978/j.issn.2218-676X.2012.10.02

Review Article

Stereotactic radiosurgery with charged-particle beams: technique and clinical experience

Richard P. Levy[1], Reinhard W. M. Schulte[2]

[1]Advanced Beam Cancer Treatment Foundation, 887 Wildrose Circle, Lake Arrowhead, CA 92352-2356 USA; [2]Department of Radiation Medicine, Loma Linda University Medical Center, Loma Linda, CA, 92354, USA

Correspondence to: Richard Levy, MD, PhD. PO Box 2356, Lake Arrowhead, CA 92352-2356 USA. Email: RPL1616@AOL.com.

Abstract: Stereotactic radiosurgery using charged-particle beams has been the subject of biomedical research and clinical development for almost 60 years. Energetic beams of charged particles of proton mass or greater (e.g., nuclei of hydrogen, helium or carbon atoms) manifest unique physical and radiobiological properties that offer advantages for neurosurgical application and for neuroscience research. These beams can be readily collimated to any desired cross-sectional size and shape. At higher kinetic energies, the beams can penetrate entirely through the patient in a similar fashion to high-energy photon beams but without exponential fall-off of dose. At lower kinetic energies, the beams exhibit increased dose-deposition (Bragg ionization peak) at a finite depth in tissue that is determined by the beam's energy as it enters the patient. These properties enable highly precise, 3-dimensional placement of radiation doses to conform to uniquely shaped target volumes anywhere within the brain.

Given the radiosurgical requirements for diagnostic image acquisition and fusion, precise target delineation and treatment planning, and millimeter- or even submillimeter-accurate dose delivery, reliable stereotactic fixation and immobilization techniques have been mandatory for intracranial charged particle radiosurgery. Non-invasive approaches initially used thermoplastic masks with coordinate registration made by reference to bony landmarks, a technique later supplemented by using vacuum-assisted dental fixation and implanted titanium fiducial markers for image guidance. More-invasive stereotaxis has utilized surgically fixed reference frames, including those that can be removed and reconnected days later to sockets that have been implanted in the outer table of the patient's skull.

Since 1954 more than 15,000 neurosurgical patients and 12,000 ocular patients worldwide have been treated with stereotactic charged-particle radiosurgery for various localized and systemic malignant and nonmalignant disorders. Therapeutic efficacy has been demonstrated clearly for the treatment of selected intracranial disorders and for uveal melanomas. Its role in the treatment of subfoveal neovascularization and as boost therapy for primary brain tumors are the subjects of ongoing investigation. Charged-particle radiosurgery is particularly advantageous for the conformal treatment of large and/or irregularly shaped target volumes, and for the treatment of lesions located adjacent to sensitive organs at risk, as well as for children due to their increased sensitivity to intellectual deficits and secondary malignancies from ionizing radiation.

Keywords: Radiosurgery; charged-particle beams

DOI: 10.3978/j.issn.2218-676X.2012.10.04

Scan to your mobile device or view this article at: http://www.thetcr.org/article/view/596/html

Introduction

The application of charged-particle radiation to stereotactic radiosurgery has been the subject of biomedical research and clinical development for almost 60 years (1,2). In 1946, Wilson (3) first proposed the clinical use of charged-particle beams because of their unique physical properties.

After completion of the 184-inch synchrocyclotron at the University of California at Berkeley, Lawrence Berkeley National Laboratory (LBNL) in 1947 (4), Tobias and colleagues (5) began studies of the radiobiological effects of narrow beams of protons, deuterons and helium ions. Particular attention was paid to the reaction of normal brain tissues to charged-particle irradiation for subsequent clinical application to radiosurgery (6). The range of medical applications was constrained initially by the limitations of available neuroradiological techniques for stereotactic localization, image correlation, and treatment planning (2). Early clinical trials were therefore restricted to selective destruction of small, well-defined target volumes that could be localized accurately by existing neuroradiological procedures. Stereotactic irradiation of the pituitary gland was among the earliest applications, because localization of the *sella turcica* bone structure at the skull base could be accomplished reliably with plain radiographs.

The very first human treatments with charged-particle beams in 1954 were delivered with a radiosurgical technique: defined as carefully delineating intracranial target volumes, stereotactically localizing these volumes within a rigidly immobilized patient, and hitting these targets with millimeter accuracy using isocentrically focused radiation beams delivered with high fractional doses. The initial clinical trials used high doses of protons (and then helium ions) to ablate the pituitary gland for palliative treatment of metastatic breast cancer by means of pituitary-hormone suppression (7,8). Charged-particle radiosurgery was then applied to the pituitary-ablation treatment of proliferative diabetic retinopathy (9), and to the treatment of pituitary adenomas (10,11). With the development of improved techniques of stereotaxis and cerebral angiography, charged-particle radiosurgery was applied to the treatment of arteriovenous malformations (AVMs) (12-14).

In the mid-1970s, the advent and rapid evolution of high-resolution computed X-ray tomography (CT) enabled much improved calculation of the three-dimensional (3D)-depth-dose distribution of charged particle beams (15). When these dose-localization improvements were coupled with the higher-quality anatomic definition of magnetic resonance imaging (MRI) (16), it became possible to extend the use of charged-particle beams to a much wider variety of life-threatening disorders, including many types of cancer throughout the body, and to conventionally fractionated radiation therapy (RT). Some 100,000 patients worldwide have now been treated with charged-particle beams at more than 30 institutions (17). The experience with standard fractionation protocols of charged-particle therapy will be discussed elsewhere in this edition of Translational Cancer Research. This review will be limited to describing the worldwide clinical experience with charged-particle radiosurgery in the treatment of more than 15,000 intracranial patients and in more than 12,000 ocular patients.

Physical properties of charged-particle beams

Charged-particle beams of proton mass or greater (e.g., helium, carbon, and neon ions) manifest unique physical properties, first observed by Bragg in 1904 (18), that can be used to place a high dose of radiation preferentially within the boundaries of a deeply located intracranial target volume (*Figure 1*) (2). These include: (I) a well-defined, energy-specific range that can be modulated so that the beam stops at the distal edge of the target, resulting in little or no dose beyond the target; (II) an initial region of low dose (the plateau ionization region) as the beam penetrates through matter, which is followed deep within the tissue by a sharp and narrow region of high dose (the Bragg peak) at the end of the beam range that can be adjusted in that dimension to conform to the width of the target; and (III) very sharp lateral edges that can readily be made to conform to the projected cross-sectional contour of the target so that little or no dose is absorbed by the adjacent normal tissues.

Synchrotron and/or cyclotron charged-particle accelerators are able to produce monoenergetic beams with ranges in tissue of 30 cm or more that can be modified precisely to specification by adjusting beam-output energy or by interposing energy-absorbing filters of appropriate design and thickness in the beam path, providing considerable flexibility in choice of beam directions for stereotactic treatment planning (19). Assuming exact knowledge of charged particle energy at the entry point and the physical properties of the intervening tissues, each charged-particle beam can be aimed stereotactically in 3D to place an individually shaped, high-dose region precisely within the brain. Beam ports from several coplanar or non-coplanar entry angles are selected to intersect within the target volume, resulting in a much lower dose to immediately adjacent and intervening normal brain tissues. Accurate prediction of charged particle range is therefore an important prerequisite for charged particle therapy, which makes the more uniform, motionless brain a prime application for charged particle radiosurgery.

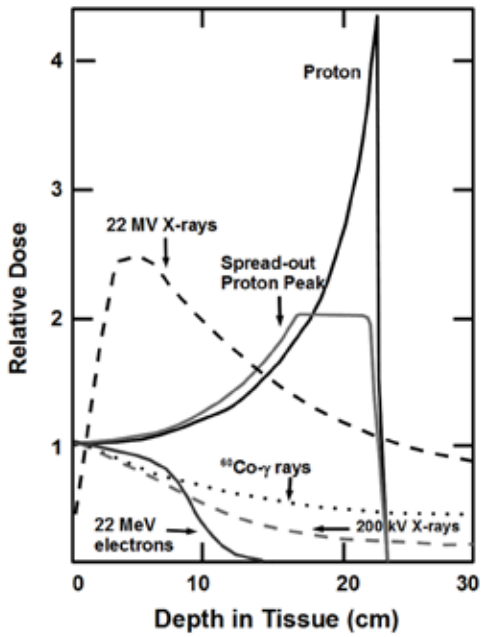

Figure 1 Relative dose as a function of depth in tissue is shown for 22 MV X-rays, 200 kV X-rays, ^{60}Cobalt-γ rays, 22 MeV electrons, an unmodulated proton-beam plateau and Bragg ionization peak, and a spread-out proton Bragg peak modulated by absorbing filters in the beam path

Radiobiological properties of charged particles

An important topic of ongoing radiobiological interest has been the quality of ionization density along the particle trajectory, described by linear energy transfer (LET) as a function of particle velocity. The relative biological effectiveness (RBE) value at any given location in the path of the particle depends on the specific particle and its velocity at that location. Sparsely ionizing (low LET) radiation (with RBE values close to 1.0) is a property of all photon beams, as well as electrons with energies in the MeV range, and heavier charged particles such as pions, protons, and helium nuclei of high energy (>10 MeV per nucleon). Heavier ions (e.g., carbon) have higher ionization densities and RBE even at higher energies, which offer them a radiobiological advantage (RBE >2 in the Bragg peak region).

As protons (RBE=1.1) and helium ions (RBE=1.3) in the energy range used for radiosurgery have radiobiological properties very similar to photons, the primary advantage of using such particles is the ability to conform the delivered RT dose in 3D much more tightly to the designated target volume than is possible with photons. Therefore, expected normal tissue complications with these charged particles will be lower for a biologically equivalent dose to the target volume. Alternatively, a more aggressive, higher dose can be given to the target, while the dose to normal tissue can be kept at the same acceptable levels.

Some 15% to 20 % of tumor histologies, however, are relatively radioresistant to low-LET irradiation, even at high doses. In these cases, the greater RBE of high-LET RT has shown great promise in the clinic and in the laboratory setting. Historically, neutrons were the first high-LET radiation used for many tumor types. Unfortunately, difficulties in conforming the neutron dose to the delineated target (i.e., adequately sparing critical adjacent normal tissues) severely limited the kinds of tumors for which this treatment could be applied. Beams of heavier charged particles (ranging from carbon to argon nuclei), however, exhibit high-LET radiation within their Bragg peaks, thereby integrating high RBE (about 3.0 for carbon) with excellent 3D dose conformity (20-22).

The radiobiological property underlying this RBE effect is that the higher-LET radiation is much more likely to cause clustered DNA damage, including double-strand breaks associated with additional breaks or base lesions in the targeted cells (23-25); by comparison, low-LET protons and X-ray beams typically cause more single-strand DNA breaks or double strand breaks that are not associated with additional DNA damage. The significance of complex double-strand DNA damage is that affected tumor cells are much less able to repair their DNA and survive high-LET treatment. This less-repairable DNA damage also appears to explain some other descriptions of enhanced cell death seen with high-LET RT that have been historically ascribed to the circumstances of reduced oxygen enhancement ratio or to less variation in sensitivity through the cell cycle (26-30). While normal cells may also suffer some double-strand damage with this technique, the preponderance of single-stranded and non-complex double-stranded DNA damage is much more repairable in the lower LET region of the plateau-ionization region where the normal tissues lie outside of the tumor target (31,32).

Another matter receiving increasing attention is the best method for integrating RBE information with the physical dose distribution. Historically, for simplicity, a simple RBE factor (1.1 for protons and 1.3 for helium nuclei) at a single reference point in the Bragg peak has been recorded. However, since heavier ions exhibit a wider range of RBE at different positions throughout the RT field, and protons and helium ions have an enhanced RBE at low energies (the last few millimeters before they stop), more detailed analysis is desirable. On a voxel-by-voxel basis, RBE values depend

upon the variables of the specific ion used, dose per fraction, beam energy of the primary beam and its fragments, position within the Bragg-peak depth-dose curve, and the particular cell types or endpoints under consideration. In order to cope with this problem, the Local Effect Model (LEM), developed at GSI in Darmstadt, Germany, is a biophysical theory that attempts to incorporate these complex variables on a voxel-by-voxel basis, by integrating a non-linear response function over an inhomogeneous microscopic dose distribution (28,33,34). The required biological parameters for LEM include the experimental data on the response to sparsely ionizing radiation of the specific tumor and the adjacent normal tissues, and the size of the cell nucleus as the critical target. The required physical parameters include the atomic numbers of the primary beam and its nuclear fragments, and the velocity of the particles at different voxels in the field. These LEM calculations have been incorporated into the so-called "TRIP" treatment planning system for ion therapy, and have been used for 10 years with patients at GSI to calculate RBE values for all treated voxels, typically yielding local RBE values ranging from 2 to 4 in the target volume (35). While LEM has been applied extensively to carbon therapy at GSI with great success, it is now also being used to predict the incidence of late complications. LEM can also be adapted for use with low-LET particles, i.e., protons and helium ions, in order to predict the higher RBE values in the distal spread-out Bragg peak. The LEM-calculated treatment plan calculated to deliver a uniform biologically effective dose across a target volume typically requires a very heterogeneous physical dose delivery, unique for each beam-entry angle and fractional dose, mandating active beam-scanning dose delivery to accommodate the prescribed physical dose heterogeneity. Thus, very intensive computer calculation is required to optimize the LEM bio-effective treatment plan. A model similar to LEM has been developed in Japan by Kase *et al.* (36), based on the Microdosimetric Kinetic Model (MKM) of Hawkins that was elaborated from the theory of dual radiation action of Kellerer and Rossi (37). Both LEM and MKM conceptually follow some of the original ideas of Katz *et al.* (38). Two recent papers report the specification of carbon-ion doses at NIRS (39) and the treatment-planning strategy at Heidelberg (40).

Technique for charged-particle radiosurgery

Reliable stereotactic immobilization is required for both diagnostic imaging and millimeter-accurate dose delivery. It is imperative to reproduce both the translational coordinates (x, y, z), as well as the rotational degrees of pitch, yaw and roll, if complex target volumes are to be irradiated with adequate dose shaping. In the early era of charged-particle radiosurgery at LBNL, this was accomplished non-invasively using a thermoplastic mask to immobilize the patient within a relocatable stereotactic frame that was attached to the various imaging couches and then to the treatment-positioning table. The very first radiosurgical treatments in 1954 were performed at LBNL using protons, but in 1957 the Berkeley machine was modified to accelerate helium nuclei, and subsequent radiosurgery patients were treated with helium ions. As the mid-1950s were about 20 years before CT was invented, considerable uncertainty prevailed at that time in predicting particle beam range within the patients. Therefore, the radiosurgery method employed in those early years required that rigidly immobilized patients were treated with isocentrically intersecting arcs of high-energy proton and helium-ion beams that were used in a plateau shoot-through technique placing the Bragg peak beyond the patient's distal surface, depositing that peak dose into the treatment table or into the walls of the treatment room—an early precursor to stereotactic photon radiosurgery (2).

At that time, accurate intracranial target delineation was limited to the pituitary gland, whose position within the midline structure of the *sella turcica* could be visualized readily by orthogonal plain radiographs. As increasingly sophisticated radiological imaging became available, image-fusion technology was developed to register cerebral angiograms and/or MRI with CT scans for improved target delineation of other intracranial lesions and for more-precise computerized treatment planning. Patient positioning verification for treatment was made by correlating digitally reconstructed radiographs with radio-opaque fiducial landmarks, such as adjacent bone structures. This immobilization technique was later supplemented at the Loma Linda University Medical Center (LLUMC) Proton Treatment Center by using vacuum-assisted dental fixation to assist the reliability of repositioning and by implanting titanium markers into the skull's outer table for improved fiducial correlation with orthogonal radiographs for image guidance. Surgically attached stereotactic, cranial-halo reference frames have also been utilized, including frames that can be removed and reconnected days later to sockets that have been inserted into the outer table of the patient's skull. At Harvard University, the Stereotactic Alignment System for Radiosurgery (STAR) was designed as an isocentric patient-positioning system with 6 degrees of freedom to enable a full spherical range of beam entry angles from a horizontal beam line (41). The STAR system has also proved to be an invaluable positioning device for fractionated proton treatment of cranial and skull base

tumors. Based on the prior experience with advanced patient positioners for charged particle radiosurgery, all proton radiosurgery treatments at LLUMC are now performed with a robotic patient positioner that has 6 degrees of freedom.

Given the complexity of establishing accurate target delineation using image-fusion technology, and the multi-disciplinary evaluation required to optimize therapy recommendations, a strong argument can be made for using a relocatable stereotactic immobilization system. This relocatable frame approach also allows multi-fraction stereotactic treatment for larger and/or more eloquently located target volumes, as well as enabling multi-institutional collaboration. Additionally, removing the time-urgency of progressing to treatment permits a more thorough assessment of treatment planning options and quality-assurance testing.

Beginning in the mid-1970s with the advent of CT scanning, acquisition of voxel-specific, electron-density data (i.e., Hounsfield units) enabled more accurate depth-dose calculation of charged-particle stopping powers in heterogeneous tissue within the patients and heralded the dawn of Bragg peak radiosurgery with its much tighter dose conformity to intracranial target volumes. The narrow Bragg peak profile had to be adapted to the larger treatment volumes, initially using the so-called "spread out Bragg peak" (SOBP) technique developed at Berkeley and Harvard (42). SOBP's were produced in analogous fashion to conventional photon therapy, using scattering foil systems, range-shifting absorbers, collimators, apertures and compensators to produce radiation fields that were more closely shaped to the target volume - but still not nearly as precisely as the 3D-conformity of modern beam-scanning techniques. Intracranial sites treated with radiosurgical technique expanded to include various benign tumors, as well as some primary and metastatic malignant tumors (43).

Although not traditionally categorized as representing stereotactic radiosurgery, charged-particle treatment of ocular diseases, including subfoveal macular degeneration and uveal melanoma, meets the definition of the term by requiring single- or limited-fraction external-beam irradiation of a target volume with millimeter accuracy. For these ocular lesions, treatment is given with a single fixed horizontal beam with the patient's head immobilized while in an upright-seated position. Using a low-energy (typically, 70 MeV) proton beam, a single dose of 14-24 Gy (RBE) is applied to the retinal vascular abnormality of wet macular degeneration, and five fractions of a similar daily dose are applied to ocular melanoma (44). In each case, surgically placed metal clips at the posterior aspect of the globe serve as fiducial references for beams-eye-view X-ray alignment, with the eyelids held retracted by clips. With the patient staring at a precisely positioned light source, the margin of the iris is delineated with ink drawn onto a monitor screen whose video camera is focused on the surface of the eye, with the treatment beam immediately paused if eye movement is observed.

Dose-volume histogram analysis

3D treatment planning calculations have been used to compare the dose distributions for different techniques of stereotactic radiosurgery of intracranial target volumes, examining dose-volume histograms and integral doses to the target and to normal brain (45). In this analysis, the radiation doses to normal brain structures adjacent to and remote from the target volume were demonstrated to be relatively low with stereotactic charged-particle Bragg peak radiosurgery when compared with photon radiosurgery techniques that use focused beams of X-rays or gamma rays; this difference becomes especially marked in the treatment of larger intracranial lesions (*Figure 2*). Very similar conclusions were reached by other investigators performing comparative dose-volume studies (46,47).

When irradiation of subfoveal neovascularization or ocular melanoma was evaluated by comparative analysis of the integral dose deposited in normal tissue, employing X-ray-based systems increased the integral dose to adjacent tissues (e.g., brain, pituitary gland) by a factor of 20 as compared to proton irradiation (48).

Clinical applications

A comprehensive review of the clinical experience and results in the field of charged-particle radiosurgery is beyond the scope of this brief review, and interested readers are referred to other manuscripts (1,2,43). Selected historically significant or representative studies have therefore been summarized and/or cited for further reference.

Pituitary gland

Charged-particle radiosurgery of the pituitary gland, historically its first clinical application, has proven to be a highly effective method for treatment of a variety of endocrine and metabolic hormone-dependent conditions, alone or in combination with surgical hypophysectomy and/or medical therapy in more than 3,500 patients worldwide. This includes patients with metastatic breast carcinoma and

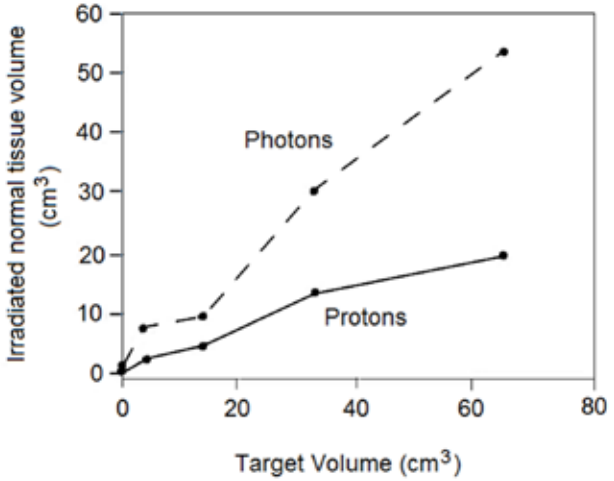

Figure 2 The volume of brain tissue (cm^3) outside the target volume that receives 80% or more of the dose delivered to the target volume plotted as a function of target volume (cm^3). These data are derived from dose-volume histograms for defined target volumes using photon irradiation (cobalt-60 gamma rays or X-ray) and proton (155 MeV/u) irradiation for stereotactic radiosurgery of target volumes ranging from 0.5 to 65 cm^3. Treatment plans were designed to place the 90% isodose line at the lesion periphery. Spheres of 1, 2, 3, 4, and 5 cm diameter correspond to volumes of 0.5, 4.1, 14, 33, and 65 cm^3, respectively. From the smallest to the largest volumes examined, focused photon irradiation (upper curve) results in the irradiation of 2 to 3 times more normal brain tissue surrounding the target volume compared with proton irradiation (lower curve) [Adapted from reference (45)]

diabetic retinopathy, as well as hormone-secreting tumors such as acromegaly, Cushing's disease, Nelson's syndrome, and prolactin-secreting adenomas.

In the early years of the LBNL charged particle program, before anti-estrogen therapy became available, pituitary ablation for treatment of metastatic breast carcinoma was achieved with 180 to 270 Gy stereotactic proton or helium-ion plateau irradiation (2). Although this total dose was divided into six to eight fractions over two to three weeks, we consider this therapy to be radiosurgical in nature, as each individual treatment consisted of at least 30 Gy. Given the long-term pain relief from bone metastases that was achieved in many patients, this procedure was also employed with favorable results by proton centers in Moscow (49), Leningrad (50), and Boston (2). Pituitary ablation was also achieved with doses of 80 to 150 Gy for treatment of proliferative diabetic retinopathy, but with mixed clinical results (2,50,51).

For hormone-secreting tumors, before the development of trans-sphenoidal hypophysectomy, doses of 30 to 50 Gy were delivered in 3 or 4 fractions to the central core of the pituitary gland, while preserving a narrow rim of functional pituitary tissue. This treatment resulted in reliable control of tumor growth and suppression of hyper-secretion in a great majority of the patients. For example, mean serum growth hormone levels in a cohort of 234 patients with acromegaly treated with helium-ion radiosurgery decreased by nearly 70% in one year, continued to decrease thereafter, and remained normal throughout more than 10 years of follow-up (52).

Similar results were found with proton radiosurgery for acromegaly (10,53), and for treatment of Cushing's disease and prolactinoma (2,11,54). Variable degrees of hypopituitarism occurred in as many as one-third of cases, but endocrine deficiencies were readily corrected with appropriate hormone supplemental therapy. The reader is referred to references (2) and (55) for comprehensive reviews of this subject.

Arteriovenous malformations

Charged-particle radiosurgery has also been applied to the treatment of intracranial AVMs in more than 3,000 patients worldwide since 1965 (2,13,14,16). While many AVMs are amenable to neurosurgical removal or endovascular embolization followed by surgery, surgical removal may involve high risks for the malformations located in deep or eloquent regions of the brain and for large lesions with multiple arterial supply or deep venous drainage. Moreover, these techniques, when possible, are not always completely successful because of the position or complexity of the malformation. The goal of radiosurgical treatment is to induce localized endothelial cell proliferation, vascular wall thickening, and thrombotic obliteration of the malformation while sparing normal adjacent brain structures. Given the complexity and variability of AVMs in terms of size and shape and the fact that many patients are children or young adults, the physical characteristics of charged-particle beams are uniquely advantageous for the radiosurgical treatment of these lesions. Bragg peak radiosurgery has the conformality required to treat eccentric and irregular AVMs of very large size (*Figure 3*), as well as to deliver sharp focal beams accurately to small lesions (e.g., in the brain stem or central nuclei) while protecting the adjacent critical nervous tissues and the rest of the normal brain (*Figure 2*) (1,2,16).

The most detailed report of charged-particle radiosurgery for AVM was that from the LBNL - Stanford University collaborative program (14). Here, 86 consecutive AVM

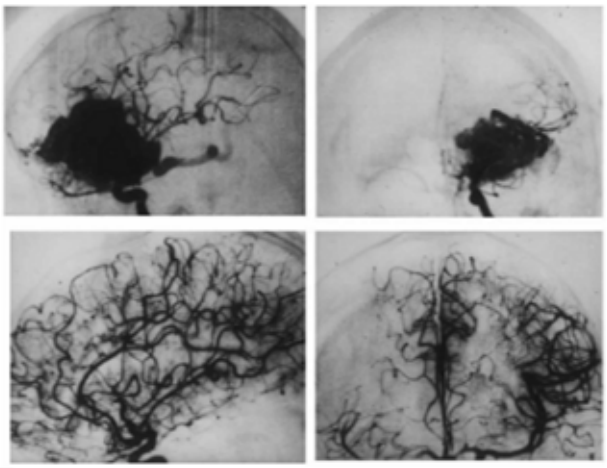

Figure 3 Cerebral angiograms in a 23-year-old man with a history of refractory seizures from a large (40 cm^3) left frontotemporal AVM. Upper: lateral and anteroposterior views of the internal carotid artery angiogram demonstrate the AVM supplied by branches of the anterior and middle cerebral artery circulations. The vascular steal is prominent. Lower: comparable view taken 18 months after helium-ion radiosurgery [dose, 28 Gy (RBE)] demonstrates complete obliteration of the AVM. Normal cerebral blood flow has been restored, with marked reversal of the vascular steal. (From Levy RP, Fabrikant JL, Frankel KA, Phillips MH, Lyman JT. Charged-particle radiosurgery of the brain. Neurosurg Clin North Am 1990;1:980, with permission.)

patients (47 females, 39 males) ranging in age at the time of treatment from 9 to 69 years (mean, 33 years) were treated with helium-ion radiosurgery. Almost half of these patients (44%) had AVMs located in the brain stem, corpus callosum, thalamus, or basal ganglia, and most of the remainder had large malformations in eloquent areas of the cerebrum — the sensory, motor, language, or visual areas of the cortex. One-quarter of the AVMs were larger than 25 cm^3.

In an evaluation carried out 24-72 months after radiosurgery, clinical outcome was graded as excellent in 58% and good in 36% of patients. In 63% of patients presenting with seizures and in 68% of patients presenting with headaches, there was an improvement in these symptoms. Two years after radiosurgery, angiographically demonstrated complete obliteration of the AVM occurred in 70%, partial closure (10% to 99% obliteration) occurred in 23%, and minimal or no change occurred in 7% of patients. Three years after treatment, 92% of patients had complete AVM obliteration, 4% had partial obliteration, and 4% experienced minimal or no change. The rate and extent of obliteration appeared to be a threshold phenomenon directly related to the AVM volume and the radiation dose. Smaller AVMs (<4 cm^3) had higher rates of obliteration than larger ones and became thrombotic more rapidly and more completely than intermediate-sized (4 to 25 cm^3) and larger (>25 cm^3) lesions. However, full obliteration was observed 3 years following radiosurgery in 70% of AVMs >25 cm^3.

Comparable results have been achieved with proton radiosurgery of AVMs after the LBNL-Stanford University helium radiosurgery program was transferred to LLUMC in 1993 and was continued there with protons. The experience with multimodality treatment (embolization and/or surgery performed at Stanford University and radiosurgery at LBNL or LLUMC) of very large ("giant") AVMs was reported in 2003 (56). In 47 of 53 patients, radiosurgery was part of the multimodality treatment plan, and 40 of these patients were treated with helium ion or proton radiosurgery, while seven patients received photon (linear accelerator) radiosurgery. Of the 53 patients, 19 (36%) were cured, 4 (8%) achieved nearly complete (90%) obliteration, 29 (55%) had less than 90% obliteration; one patient was lost to follow-up. The long-term, treatment-related morbidity rate in this series was 15%. These results are remarkable, given that these large AVMs had been previously thought to be incurable at an acceptable rate of long-term morbidity. A multimodality approach with embolization, radiosurgery, and surgery as part of a staged procedure is probably necessary to achieve better results than those that can be accomplished with radiosurgery alone in these very large AVMs.

We recently analyzed the outcome of 40 patients with AVMs of small and intermediate size (<15 cm^3) treated with proton radiosurgery alone at the LLUMC Proton Treatment Center. Patients were treated with a single or two fractions of proton radiosurgery to a dose of 25 Gy (RBE) to isocenter, corresponding to a marginal dose of 20 Gy (80%). The not-yet-published results of this analysis can be summarized as follows: out of the 29 patients with complete long-term imaging follow-up, the average AVM volume was 6.4 cm^3 (range, 1-14.7 cm^3). Complete angiographic obliteration rate was achieved in 69% (20/29). This includes 4 patients who failed their initial course of treatment and were successfully salvaged with a second course of proton radiosurgery, in which the dose was lowered to 20 Gy (RBE). The obliteration rates for AVMs <4 cm^3 and 4-15 cm^3 were 100% (9/9) and 55% (11/20), respectively. Two patients (7%) with AVMs larger than 10 cm^3, including one after a second course of radiosurgery, developed a new onset of persistent weakness, which was attributed to the radiosurgery. All other patients

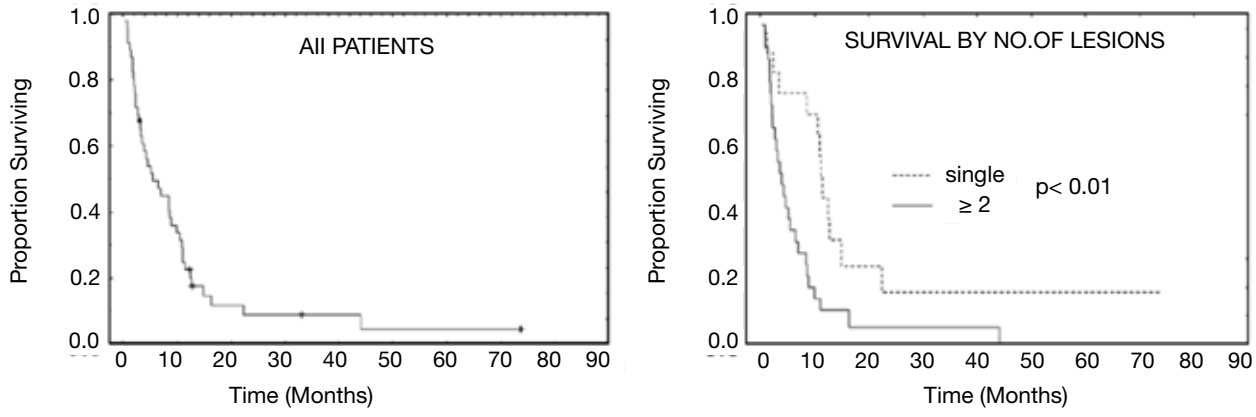

Figure 4 Kaplan-Meyer survival curves for 46 patients treated with proton radiosurgery at LLUMC (unpublished data). The left diagram shows the survival of all patients and the right diagram shows the survival of patients with a single metastasis and two or more metastases, respectively

had an excellent neurological outcome.

Additional single-institution reports of small series of AVMs treated with proton radiosurgery have appeared in the literature over the last 10 years, and the reader is referred to references (57-59) for additional information on this subject.

Brain metastases

At LLUMC and at other proton facilities, protocols have been developed and implemented for stereotactic radiosurgery of brain metastases, a condition with an annual incidence in the U.S. similar to that of primary prostate cancer. Most patients treated with protons at LLUMC for this condition are individuals who were first treated for their primary disease in our department and then developed secondary metastases subsequently or during their primary treatment.

Indications for proton radiosurgery of brain metastases in the LLUMC experience are adjuvant treatment of remaining metastases immediately following whole-brain radiation therapy (WBRT) and/or surgery (30%), salvage treatment for new or residual brain metastases more than one month after the primary treatment for metastatic disease (50%), and radiosurgery as the primary treatment modality, mostly for single or solitary metastases to the brain (20%). The Kaplan-Meyer survival curves of the first 46 consecutive patients with brain metastases treated at LLUMC are shown in *Figure 4*. On multivariate analysis, single versus multiple metastases at the time of treatment was the only prognostic factor associated with a better survival outcome (median survival: 15 versus 9 months, P<0.01).

Of interest, there were two long-term survivors in the LLUMC series of 46 patients. Long-term survival has also been reported in a single-institution report from the Cleveland Clinic including 1,288 patients diagnosed with brain metastases and treated with WBRT, surgery, and/or stereotactic radiosurgery (60). In that series thirty-two patients (2.5%) survived more than 5 years.

In the LLUMC experience, the use of proton radiosurgery for brain metastases can be of advantage if the patent returns for retreatment of a single metastasis or oligo-metastatic disease a few months after the first radiosurgery treatment. This scenario is more common now that primary radiosurgery is being practiced more frequently due to the fear of mental decline after WBRT. *Figure 5* shows the MRI of a patient treated consecutively for two asynchronous metastases with an interval of 6 months between the two treatments. Due to the proximity of the two metastases, the lack of dose beyond the Bragg peak was clearly an advantage for the repeated radiosurgery.

Benign tumors

At LLUMC, various benign tumors, including pituitary adenomas, acoustic neuromas and meningiomas have been successfully treated by protons with conventional fractionation schedules [1.8 Gy (RBE) per fraction] (61-63). For all tumor histologies, long-term radiological local control rates were higher than 90%. Good outcomes with local control rates consistently above 90%, and thus comparable to the results with conventional fractionation, have also been achieved following charged-particle radiosurgery with 1-3 fractions for acoustic neuromas (64,65) and a single dose for meningiomas (66).

Related to hearing preservation, the question whether

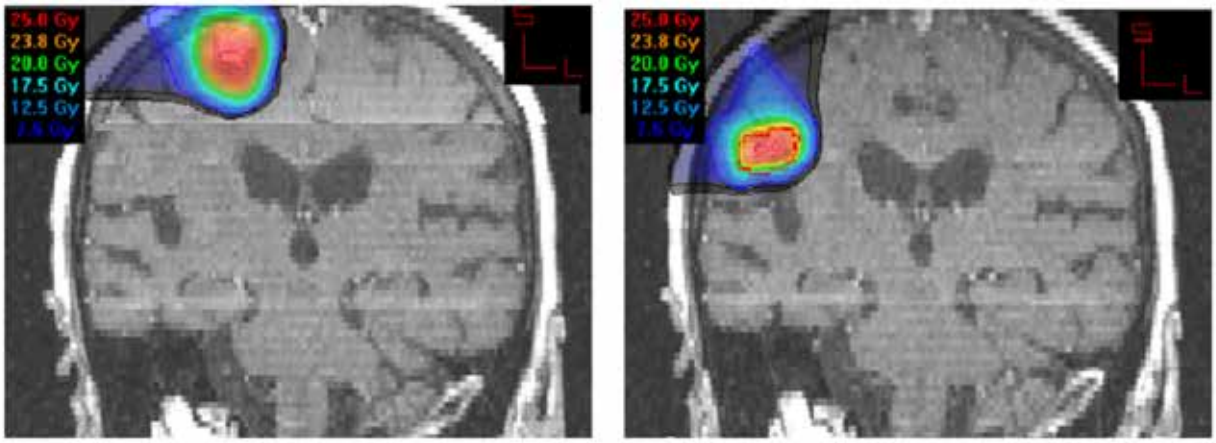

Figure 5 Isodose plans of a patient with metastatic breast cancer treated with two stereotactic proton radiosurgery treatments separated by 6 months. No WBRT was given in this patient. The plan on the left shows the first treatment plan; the plan on the right shows the second treatment plan after local recurrence in the same area. Both lesions were treated to a marginal treatment dose of 20 Gy (RBE). Note that initial brain metastasis had completely regressed at the time of retreatment

acoustic neuromas are better treated with stereotactic radiation therapy rather than radiosurgery remains open as various groups have been struggling with defining the best dose that leads to an acceptable hearing preservation with either technique. For example, the investigators at the Massachusetts General Hospital (MGH) reduced their maximum single-fraction proton radiosurgery dose to the target volume from 17.1 Gy (RBE) down to 13.3 Gy (RBE) in 1999 (64). In their 2003 review, only one of five patients treated at either dose retained functional hearing with longer audiometric follow-up (64). The authors concluded that patients with acoustic neuromas are better treated with fractionated stereotactic RT than single-dose radiosurgery. At LLUMC, only 31% of patients with initially useful hearing retained it during a mean follow-up period of 34 months after fractionated RT to 54 Gy (RBE) (62). A newer but not-yet-published analysis from the same institution shows a clear trend of improved hearing preservation after the dose had been reduced to 50.4 Gy (RBE) with 1.8 Gy per fraction, but longer follow-up will be needed to confirm that the high rates of local control are maintained.

Ocular irradiation - Age-related macular degeneration

Proton-beam irradiation for the "wet" form of age-related macular degeneration (AMD), which is associated with subfoveal neovascularization, showed favorable initial results in a small Phase I/II trial with a single dose of 8 Gy (RBE) performed at LLUMC (67). The rationale for this treatment was based on the observed sensitivity to irradiation of proliferating endothelial cells in culture (68), and the relative resistance to irradiation of the retina and choroid. Proton irradiation is ideally suited for this task, since a satisfactory dose to the neovascular membrane can be delivered in a few minutes, using a single anterior oblique proton field to deliver a therapeutic dose. The proton beam stops without entering the brain or reaching the opposite eye. Subsequent results of a non-randomized study comparing the efficacy of a single dose of 8 Gy (RBE) to a single dose of 14 Gy (RBE) in 21 and 27 patients, respectively, showed that a dose of 14 Gy (RBE) was more effective in halting visual loss: actuarial lesion control at 21 months was 36% for 8-Gy (RBE) patients and 89% for 14-Gy (RBE) patients (69). However, 11 eyes in the 14 Gy group experienced some radiation retinopathy, with the onset between 3 and 30 months, although only one patient developed a severe visual loss at 15 months after proton treatment (70).

Ciulla and colleagues (71) examined the effect of proton irradiation on neovascular membranes associated with AMD in a randomized, prospective, sham-controlled, double-blind study. Thirty-seven patients were randomly assigned to 16 Gy (RBE) proton irradiation delivered in two equal fractions or to sham control treatment. However, recruitment was stopped after 37 patients had been enrolled, citing ethical reasons regarding randomization to sham treatment when FDA approval of the photosensitizer Visudyne in combination with photodynamic laser therapy was anticipated. When the results in the control and proton

irradiation were analyzed, proton irradiation was associated with a trend toward stabilization of visual acuity, without reaching statistical significance.

Another randomized controlled trial (n=166) conducted at the MGH (72) evaluated the safety and visual outcomes after proton therapy to either 16 Gy (RBE) or 24 Gy (RBE) for subfoveal neovascular patients with AMD in two equal fractions. The investigators found no significant differences in rates of visual acuity or complications between the two study arms, but suggested that proton beam therapy may be useful as an adjuvant therapy or as an alternative for patients who decline or are not appropriate for approved therapies.

Ocular irradiation - Uveal melanomas

Episcleral radionuclide plaque brachytherapy and charged-particle RT are established eye- and vision-sparing alternatives to enucleation in patients with uveal melanomas (73). At LLUMC and other centers with proton eye-beam lines, 14 Gy (RBE) (the dose used for subfoveal neovascularization in a single fraction, as described above) is given five times for a total dose of 70 Gy (RBE) for treatment of uveal melanomas. About 12,000 patients worldwide have now been treated using this scheme of hypo-fractionated proton therapy for uveal melanomas, and local tumor control rates in excess of 95% (in smaller tumors) have been achieved consistently for this lesion that is generally considered to be radiation resistant to standard fractionation.

Charged-particle RT has been performed with proton beams (74) and helium ion beams (20) since the mid-1970s. In 1988, Munzenrider and colleagues from the MGH (75) reported on the outcomes in 1006 uveal melanoma patients treated with proton beams at the Harvard Cyclotron. Eye retention rates at 60 months were 89.1±3.0% for the entire group, and 97±3.7%, 92.7±3.1%, and 78.3±7.0% in patients with small, intermediate, and large tumors, respectively. Significantly greater enucleation rates were subsequently observed in patients with large tumors than in those with intermediate tumors ($P \leq 0.0001$), in patients with tumor height >8 mm relative to those with tumors ≤8 mm ($P \leq 0.0001$), with tumor diameter >16 mm compared to ≤16 mm, ($P \leq 0.0001$), and with tumor involvement of the ciliary body compared to involvement of the choroid only ($P \leq 0.0001$).

A separate analysis of 562 patients with pretreatment visual acuity of 20/200 or better, treated at the Harvard Cyclotron over a 10-year period, investigated prognostic factors for visual loss after proton radiosurgery to 70 Gy (RBE) in 5 fractions (76). Of 562 eyes, 363 (64.6%) contained tumors within 2 disc diameters (DD) of the disc or fovea. Two-year actuarial rates of loss of useful vision (worse than 20/200) among patients with tumors near the disc or fovea were 47%, compared with 28% for patients with tumors located farther from both structures.

Seeking to determine whether reducing the proton dose from 70 Gy (RBE) to 50 Gy (RBE) would decrease radiation-induced complications without compromising local control, the MGH/Harvard team subsequently conducted a randomized, double-blind study in 188 patients with small or medium-sized choroidal melanomas (<15 mm in diameter and <5 mm in height) within 4 DD of the optic disc or macula (77). Although the proportion (55%) of patients retaining visual acuity (VA) of at least 20/200, and the local and metastatic failure rates, were similar in the two dose groups at 5 years, patients treated to a lower dose had significantly less visual field loss.

In Europe, the largest experience in treating uveal melanomas with protons has been accumulated at the Paul Scherrer Institute in Switzerland starting in 1984. In 1999, the treatment outcomes of 2,435 uveal melanomas in 2,432 patients treated with proton beam RT between March 1984 and December 1998 were analyzed (78). The median follow-up time was 40 months. Initially, treatment had started with the application of 70 Gy (RBE) in 4 fractions, which was subsequently lowered to 65 Gy, then to 63 Gy, and finally to 60 Gy. At the time of analysis, most patients had been treated with 60 Gy (RBE) in 4 fractions. The largest tumor diameter ranged from 4 to 26 mm, and tumor thickness ranged from 0.9 to 15.6 mm. There was a trend to improved local control at 5 years over time from 90.6±1.7% for patients treated before 1988 to 98.9±0.6% for patients treated after 1993, which was attributed to changes in the treatment procedure. Of the 2,435 patients, 73 (3%) required a second treatment (proton beam RT, enucleation or brachytherapy) for tumor regrowth. Cause-specific survival at 10 years was 72.6±1.9% for patients with controlled tumors compared with 47.5±6.5% for those with recurrent tumors. The main prognostic factors for reduced local tumor control were large ciliary body tumors and male gender as well as technical factors, including eyelids within the treatment field and inadequate positioning of tantalum clips for tumor localization before treatment. In a later analysis (79), the overall eye retention rates at 5, 10, and 15 years after treatment were reported as 88.9%, 86.2%, and 83.7%, respectively. Enucleation was related to larger tumor size (mainly tumor height), proximity of posterior tumor margin to optic disc, male gender, high intraocular pressure, and large degree of retinal detachment at treatment time.

Similar results were also reported after helium-ion RT

for uveal melanomas. Char *et al.* prospectively investigated 218 patients treated at LBNL between 1978 and 1984 (80). Ten years following treatment, 46 eyes (22.4%) had been enucleated, and most enucleations (37 of 46) were due to anterior-segment ocular complications. The overall, 10-year local control rate was 95.4%, but 51 patients (23.4%) died from metastatic disease. For patients with tumors less than 6 mm in height and more than 3 mm distant from the optic nerve or fovea, 13 of 18 (72%) retained VA greater than 20/40. By contrast, only 11% of the patients that did not meet these criteria retained a good level of VA. The same group of investigators also reported on a prospective trial in which patients with uveal melanoma were randomized to receive helium-ion irradiation (n=86) or iodine-125 (n=98) brachytherapy (81). Tumor diameter was <15 mm and tumor thickness <10 mm in all patients. Local recurrence rate after 125I brachytherapy was significantly higher than after helium-ion irradiation (13% *vs*. 0%). Enucleation was also required more frequently after brachytherapy (relative risk =1.99; 95% confidence interval, 0.78-5.78), but more anterior-segment complications occurred following helium-ion RT, and there was no difference in overall survival.

At LLUMC, a retrospective review of 78 patients with 60 medium-sized (base <16 mm, apex 3-10 mm) and 18 large-sized (base ≥16 mm, apex ≥10 mm) choroidal melanomas was performed in the early 2000s (82). With a median follow-up of 34 months, the 5-year local control rate was 90.5±3.7%, and metastases-free and disease-specific survival rates were 76.2±6.7% and 75.6±7.6%, respectively. Eye retention was achieved in 75.3% and useful (better than 20/200) VA persisted in 49.1% of surviving patients. Prognostic factors for loss of the affected eye due to complications were close proximity to the optic disc (P=0.003) and large tumors involving the ciliary body (P=0.041). Prognostic factors for VA outcome were initial VA (P=0.001), doses to optic disc (P=0.001) and fovea (P=0.022) higher than 35 Gy (RBE), tumor proximity to the optic disc (P=0.034), and retinal detachment (P<0.001). Diameter of the tumor base was significantly related to metastases-free survival (P=0.02) and overall survival (P=0.033), but that did not impact local control, eye retention, or VA.

Other large series of uveal melanomas treated with 5 fractions of proton beam RT were reported by the centers in Nice, France (83), and Clatterbridge, UK (84), and the interested reader is referred to their reports.

Summary

Stereotactic charged-particle radiosurgery has now been successfully employed for almost 60 years in the clinical treatment of more than 15,000 intracranial patients and 12,000 ocular patients. Treated disorders include pituitary tumors, vascular malformations, primary and metastatic malignant brain tumors, various other benign brain tumors, uveal melanomas, and subfoveal neovascularization. The unique physical properties of charged particles make this method particularly advantageous for the conformal treatment of large and/or irregularly shaped lesions or for the treatment of lesions located in front of or adjacent to sensitive brain structures.

The role of heavier charged particles (e.g., carbon nuclei) as high-LET, radiosurgical boost therapy for the treatment of radioresistant brain tumors is the subject of ongoing investigation. Technological improvements in charged particle therapy described elsewhere in this edition of Translational Cancer Research are likely to lead to further applications and improved outcomes in charged particle radiosurgery.

Acknowledgements

Disclosure: The authors have no potential conflicts of interest related to the information contained herein.

References

1. Fabrikant JI, Levy RP, Steinberg GK, et al. Charged-particle radiosurgery for intracranial vascular malformations. Neurosurg Clin N Am 1992;3:99-139.
2. Levy RP, Fabrikant JI, Frankel KA, et al. Charged-particle radiosurgery of the brain. Neurosurg Clin N Am 1990;1:955-90.
3. Wilson RR. Radiological use of fast protons. Radiology 1946;47:487-91.
4. Brobeck WM, Lawrence EO, MacKenzie KR, et al. Initial performance of the 184 inch cyclotron of the University of California. Phys Rev 1947;71:449-50.
5. Tobias CA, Anger HO, Lawrence JH. Radiologic use of high energy deuterons and alpha particles. Am J Roentgenol 1952;67:1-27.
6. Rodriguez A, Levy RP, Fabrikant JI. Experimental central nervous system injury after charged-particle irradiation. In: Gutin PH, Leibel SA, Sheline GE. eds. Radiation Injury to the Nervous System. New York: Raven Press, 1990:149-82.
7. Lawrence JH. Proton irradiation of the pituitary. Cancer 1957;10:795-8.
8. Lawrence JH, Tobias CA, Born JL, et al. Heavy-particle

irradiation in neoplastic and neurologic disease. J Neurosurg 1962;19:717-22.
9. Lawrence JH, Tobias CA, Linfoot JA, et al. Heavy particles, the Bragg curve and suppression of pituitary function in diabetic retinopathy. Diabetes 1963;12:490-501.
10. Kjellberg RN, Shintani A, Franzt AG, et al. Proton beam therapy in acromegaly. N Engl J Med 1968;278:689-95.
11. Linfoot JA, Lawrence JH, Born JL, et al. The alpha particle or proton beam in radiosurgery of the pituitary gland for Cushing's disease. N Engl J Med 1963;269:597-601.
12. Fabrikant JI, Lyman JT, Hosobuchi Y. Stereotactic heavy-ion Bragg peak radiosurgery: method for treatment of deep arteriovenous malformations. Br J Radiol 1984;57:479-90.
13. Kjellberg RN, Hanamura T, Davis KR, et al. Bragg peak proton-beam therapy for arteriovenous malformations of the brain. N Engl J Med 1983;309:269-74.
14. Steinberg GK, Fabrikant JI, Marks MP, et al. Stereotactic heavy-charged particle Bragg peak radiation for intracranial arteriovenous malformations. N Engl J Med 1990;323:96-101.
15. Phillips MH, Singh RP, Castro JR, et al. Treatment planning for heavy charged particle radiotherapy. Int J Radiat Oncol Biol Phys 1991;20:881-9.
16. Chen GT, Kessler M, Chuang FYS, et al. Image correlation of MRI and CT in treatment planning for radiosurgery of intracranial vascular malformations. Int J Radiat Oncol Biol Phys 1979;5:1809-19.
17. Giap FN, Levy RP, Giap HB. Summary of ongoing clinical protocols for proton and heavier ion therapy. Am Inst Phys Conference Proceedings. Proceedings the 22nd International Conference on the Application of Accelerators in Research and Industry (CAARI) 2012. In press by American Institute of Physics Conference Proceedings Series 2012.
18. Bragg WH, Kleeman R. On the ionization curve of radium. Philos Mag 1904;S6:726-38.
19. Levy RP, Fabrikant JI, Frankel KA, et al. Stereotactic heavy-charged-particle Bragg peak radiosurgery for the treatment of intracranial arteriovenous malformations in childhood and adolescence. Neurosurgery 1989;24:841-52.
20. Castro JR, Quivey JM, Lyman JT, et al. Current status of clinical particle radiotherapy at Lawrence Berkeley Laboratory. Cancer 1980;46:633-41.
21. Blakely EA. Current issues in low and high LET medical radiobiology. In: Amaldi U, Larsson B. eds. Hadrontherapy in Oncology. Paris, Iune: Int Congr Series. Elsevier Science,1994:693-701.
22. Kraft G. Tumor therapy with heavy charged particles. Progr Part Nucl Phys 2000;45:473-544.
23. Roots R, Holley W, Chaterjee A, et al. The formation of strand breaks in DNA after high-LET irradiation: a comparison of data from in vitro and cellular systems. Int J Radiat Biol 1990;58:55-69.
24. Hirayama R, Furusawa Y, Fukawa T, et al. Repair kinetics of DNA-DSB induced by X-rays or carbon ions under oxic and hypoxic conditions. J Radiat Res (Tokyo) 2005;46:325-32.
25. Hada M, Georgakilas AG. Formation of clustered DNA damage after high-LET irradiation: a review, J Radiat Res 2008;49:203-10.
26. Blakely EA, Ngo FQH, Curtis SB, et al. Heavy-ion radiobiology: cellular studies. Adv Radiat Biol 1984;11:295-389.
27. Tauchi H, Komatsu K. Cell cycle and LET dependence for radiation-induced mutation: a possible mechanism for reversed dose-rate effect. J Radiat Res (Tokyo) 1999;40:45-52.
28. Scholz M, Kraft G. Calculation of heavy ion inactivation probabilities based on track structure, X-ray sensitivity and target size. Radiat Prot Dosim1994;52:29-33.
29. Blakely EA, Chang PY, Lommel L. Cell-cycle-dependent recovery from heavy-ion damage in G1-phase cells. Radiat Res Suppl 1985;8:S145-57.
30. Lücke-Huhle C, Blakely EA, Chang PY, et al. Drastic G2 arrest in mammalian cells after irradiation with heavy-ion beams. Radiat Res 1979;79:97-112.
31. Ando K, Koike S, Uzawa A, et al. Repair of skin damage during fractionated irradiation with gamma rays and low-LET carbon ions. J Radiat Res (Tokyo) 2006;47:167-74.
32. Blakely EA, Kronenberg A. Heavy-ion radiobiology: new approaches to delineate mechanisms underlying enhanced biological effectiveness. Radiat Res 1998;150:S126-45.
33. Elsässer T, Scholz M. Improvement of the local effect model (LEM) --- implications of clustered DNA damage. Radiat Prot Dosimetry 2006;122:475-7.
34. Elsässer T, Krämer M, Scholz M. Accuracy of the Local Effect Model for the prediction of biologic effects of carbon ion beams in-vitro and in-vivo. Int J Radiat Oncol Biol Phys 2008;71:866-72.
35. Krämer M, Jäkel O, Haberer T, et al. Treatment planning for heavy-ion radiotherapy: physical beam model and dose optimization. Phys Med Biol 2000;45:3299-317.
36. Kase Y, Kanai T, Matsufuji N, et al. Biophysical calculation of cell survival probabilities using amorphous track structure models for heavy-ion irradiation. Phys Med Biol 2008;53:37-59.
37. Kellerer AM, Rossi HH. A generalized formulation of dual radiation action.Radiat Res 2012;178:AV204-13.

38. Katz R, Anderson B, Homayoonfar M, et al. Inactivation of cells by heavy ion bombardment. Radiat Res 1971;47:402-25.
39. Matsufuji N, Kanai T, Kanematsu N, et al. Specification of carbon ion dose at the National Institute of Radiological Sciences (NIRS). J Radiat Res 2007;48:A81-6.
40. Jäkel O, Schulz-Erner D, Debus J. Specifying carbon ion doses for radiotherapy: the Heidelberg approach. J Radiat Res 2007;48:A87-95.
41. Chapman P. The STAR radiosurgery program at Harvard and MGH- the successful optimization of resources at two facilities. PTCOG48; Heidelberg, Germany, 2009.
42. Chu WT, Ludewigt BA, Renner TR. Instrumentation for treatment of cancer using proton and light-ion beams. Rev Sci Instr 1993;64:2055-122.
43. Harsh G, Loeffler JS, Thornton A, et al. Stereotactic proton radiosurgery. Neurosurg Clin N Am 1999;10:243-56.
44. Gragoudas E, Li W, Goitein M, et al. Evidence-based estimates of outcome in patients treated for intraocular melanoma. Arch. Ophthalmol 2002;120:1665-71.
45. Phillips MH, Frankel KA, Lyman JT, et al. Comparison of different radiation types and irradiation geometries in stereotactic radiosurgery. Int J Radiat Oncol Biol Phys 1990;18:211-20.
46. Verhey LJ, Smith V, Serago CF. Comparison of radiosurgery treatment modalities based on physical dose distributions. Int J Radiat Oncol Biol Phys 1998;40:497-505.
47. Baumert BG, Lomax AJ, Miltchev V, et al. A comparison of dose distributions of proton and photon beams in stereotactic conformal radiotherapy of brain lesions. Int J Radiat Oncol Biol Phys 2001;49:1439-49.
48. Moyers MF, Galindo RA, Yonemoto LT, et al. Treatment of macular degeneration with proton beams. Med Phys 1999;26:777-82.
49. Minakova EI, Vasil'eva NN, Svyatukhina OV. Irradiation of the hypophysis with single large dose of high energy protons for advanced breast carcinoma (in Russian). Med Radiol (Mosk) 1977;22:33-9.
50. Konnov B, Melnikov L, Zargarova O, et al. Narrow proton beam therapy for intracranial lesions. In: Heikkinen E, Kiviniitty K. eds. International Workshop on Proton and Narrow Photon Beam Therapy. Oulu, Finland, University of Oulu Printing Center, 1989:48-55.
51. Kjellberg RN, McMeel JW, McManus NL, et al. Pituitary suppression in diabetic retinopathy by proton beam in surgically "unfit" patients. In: Goldberg MF, Fine SL. eds. Symposium on the Treatment of Diabetic Retinopathy. Arlington: US Public Health Service Publication No. 1890. 1968:249-76.
52. Lawrence JH, Linfoot JA. Treatment of acromegaly, Cushing disease and Nelson syndrome. West J Med 1980;133:197-202.
53. Petit JH, Biller BMK, Coen JJ, et al. Proton stereotactic radiosurgery in management of persistent acromegaly. Endocr Pract 2007;13:726-34.
54. Petit JH, Biller BM, Yock TI, et al. Proton stereotactic radiotherapy for persistent adrenocorticotropin-producing adenomas. J Clin Endocrinol Metab 2008;93:393-9.
55. Levy RP, Fabrikant JI. Clinical applications of stereotactic radiosurgery. In: Phillips MH. eds. Physical Aspects of Stereotactic Radiosurgery. New York: Plenum, 1993:239-78.
56. Chang SD, Marcellus ML, Marks MP, et al. Multimodality treatment of giant intracranial arteriovenous malformations. Neurosurgery 2003;53:1-11.
57. Vernimmen FJ, Slabbert JP, Wilson JA, et al. Stereotactic proton beam therapy for intracranial arteriovenous malformations. Int J Radiat Oncol Biol Phys 2005;62:44-52.
58. Ito Y, Okumura T, Suzuki K, et al. Long-term outcome of proton beam radiosurgery for arteriovenous malformations larger than 30 mm in diameter. Neurol Med Chir (Tokyo) 2011;51:624-9.
59. Hattangadi JA, Chapman PH, Bussière MR, et al. Planned two-fraction proton beam stereotactic radiosurgery for high-risk inoperable cerebral arteriovenous malformations. Int J Radiat Oncol Biol Phys 2012;83:533-41.
60. Chao ST, Barnett GH, Liu SW, et al. Five-year survivors of brain metastases: a single-institution report of 32 patients. Int J Radiat Oncol Biol Phys 2006;66:801-9.
61. Ronson BB, Schulte RW, Han KP, et al. Fractionated proton beam irradiation of pituitary adenomas. Int J Radiat Oncol Biol Phys 2006;64:425-34.
62. Bush DA, McAllister CJ, Loredo LN, et al. Fractionated proton beam radiotherapy for acoustic neuroma. Neurosurgery 2002;50:270-3.
63. Slater JD, Loredo LN, Chung A, et al. Fractionated proton radiotherapy for benign cavernous sinus meningiomas. Int J Radiat Oncol Biol Phys 2012;83:e633-7.
64. Weber DC, Chan AW, Bussiere MR, et al. Proton beam radiosurgery for vestibular schwannoma: tumor control and cranial nerve toxicity. Neurosurgery 2003;53:577-86.
65. Vernimmen FJ, Mohamed Z, Slabbert JP, et al. Long-term results of stereotactic proton beam radiotherapy for acoustic neuromas. Radiother Oncol 2009;90:208-12.
66. Halasz LM, Bussière MR, Dennis ER, et al. Proton stereotactic radiosurgery for the treatment of benign meningiomas. Int J Radiat Oncol Biol Phys 2011;81:1428-35.
67. Yonemoto LT, Slater JD, Friedrichsen EJ, et al. Phase I/

II study of proton beam irradiation for the treatment of subfoveal choroidal neovascularization in age-related macular degeneration: treatment techniques and preliminary results. Int J Radiat Oncol Biol Phys 1996;36:867-71.
68. Mao XW, Archambeau JO, Kubínová L, et al. Quantification of rat retinal growth and vascular population changes after single and split doses of proton irradiation: translational study using stereology methods. Radiat Res 2003;160:5-13.
69. Yonemoto LT, Slater JD, Blacharski P, et al. Dose response in the treatment of subfoveal choroidal neovascularization in age-related macular degeneration: results of a phase I/II dose-escalation study using proton radiotherapy. J Radiosurgery 2000;3:47-54.
70. Flaxel CJ, Friedrichsen EJ, Smith JO, et al. Proton beam irradiation of subfoveal choroidal neovascularisation in age-related macular degeneration. Eye (Lond) 2000;14:155-64.
71. Ciulla TA, Danis RP, Klein SB, et al. Proton therapy for exudative age-related macular degeneration: a randomized, sham-controlled clinical trial. Am J Ophthalmol 2002;134:905-6.
72. Zambarakji HJ, Lane AM, Ezra E, et al. Proton beam irradiation for neovascular age-related macular degeneration. Ophthalmology 2006;113:2012-9.
73. Shields CL, Shields JA, Gündüz K, et al. Radiation therapy for uveal malignant melanoma. Ophthalmic Surg Lasers 1998;29:397-409.
74. Gragoudas ES, Goitein M, Koehler AM, et al. Proton irradiation of small choroidal malignant melanomas. Am J Ophthalmol 1977;83:665-73.
75. Munzenrider JE, Gragoudas ES, Seddon JM, et al. Conservative treatment of uveal melanoma: probability of eye retention after proton treatment. Int J Radiat Oncol Biol Phys 1988;15:553-8.
76. Seddon JM, Gragoudas ES, Egan KM, et al. Uveal melanomas near the optic disc or fovea. Visual results after proton beam irradiation. Ophthalmology 1987;94:354-61.
77. Gragoudas ES, Lane AM, Regan S, et al. A randomized controlled trial of varying radiation doses in the treatment of choroidal melanoma. Arch Ophthalmol 2000;118:773-8.
78. Egger E, Schalenbourg A, Zografos L, et al. Maximizing local tumor control and survival after proton beam radiotherapy of uveal melanoma. Int J Radiat Oncol Biol Phys 2001;51:138-47.
79. Egger E, Zografos L, Schalenbourg A, et al. Eye retention after proton beam radiotherapy for uveal melanoma. Int J Radiat Oncol Biol Phys 2003;55:867-80.
80. Char DH, Kroll SM, Castro J. Long-term follow-up after uveal melanoma charged particle therapy. Trans Am Ophthalmol Soc 1997;95:171-87.
81. Char DH, Quivey JM, Castro JR, et al. Helium ions versus iodine 125 brachytherapy in the management of uveal melanoma. A prospective, randomized, dynamically balanced trial. Ophthalmology 1993;100:1547-54.
82. Fuss M, Loredo LN, Blacharski PA, et al. Proton radiation therapy for medium and large choroidal melanoma: preservation of the eye and its functionality. Int J Radiat Oncol Biol Phys 2001;49:1053-9.
83. Caujolle JP, Mammar H, Chamorey E, et al. Proton beam radiotherapy for uveal melanomas at Nice teaching hospital: 16 years' experience. Int J Radiat Oncol Biol Phys 2010;78:98-103.
84. Wilson MW, Hungerford JL. Comparison of episcleral plaque and proton beam radiation therapy for the treatment of choroidal melanoma. Ophthalmology 1999;106:1579-87.

Cite this article as: Levy RP, Schulte RW. Stereotactic radiosurgery with charged-particle beams: technique and clinical experience. Transl Cancer Res 2012;1(3):159-172. DOI: 10.3978/j.issn.2218-676X.2012.10.04

Review Article

Proton beam therapy for intracranial and skull base tumors

Masashi Mizumoto, Yoshiko Oshiro, Koji Tsuboi

Department of Radiation Oncology, University of Tsukuba, Tsukuba, Ibaraki, Japan

Correspondence to: Masashi Mizumoto, M.D, Ph.D. Tennoudai 1-1-1, Tsukuba, Ibaraki, Japan. Email: mizumoto1717@hotmail.com.

Abstract: Radiotherapy is widely used for treating malignant and benign intracranial or skull base tumors because of the difficulty in performing wide or complete tumor resection due to the involvement of eloquent areas, vital vessels, or cranial nerves. Similarly, local radiotherapy with conventional methods may sometimes be inefficient for treating brain tumors because the tolerance doses for the optic nerves, eyes, and brainstem are strictly limited. Under the circumstances, particle radiotherapy with proton or carbon ion beams has excellent dose localization to the target volume owing to the sharp Bragg peak ionization in the human body. With this property, it is possible to deliver higher doses to tumors of various shapes while preserving the surrounding critical brain structures. Although the efficacy of proton beam therapy (PBT) has been suggested for skull base chordoma and unresectable meningioma, further clinical evidence is required for optimization and standardization of the therapy. In refractory tumors such as glioblastoma multiforme and anaplastic meningioma, it is necessary to deliver high doses to improve tumor control. Under these circumstances, protons or carbon ions have potential to deliver sufficient doses to the target while keeping the healthy brain intact. In this context, we focus on the current status of proton beam radiotherapy for treating intracranial and skull base tumors.

Keywords: Proton beam therapy (PBT); brain tumor; glioma; meningioma; chordoma

doi: 10.3978/j.issn.2218-676X.2013.04.08

Scan to your mobile device or view this article at: http://www.thetcr.org/article/view/1120/html

Introduction

Surgical resection is the most fundamental treatment for brain tumors; however, it is sometimes difficult to put wide surgical margins because of damage in the surrounding normal brain tissues such as the cranial nerves, the brainstem, and others. This renders the roles of postoperative radiotherapy (PORT) important or even essential. Particle radiotherapy such as proton beam therapy (PBT) and carbon ion therapy has better dose distribution than photon radiotherapy owing to a narrow energy peak called Bragg peak. Because of this excellent physical property, particle radiotherapy is suitable for treating brain tumors because high doses can be delivered to the target while preserving the surrounding normal tissue. In addition, because it is possible to make irregular target fields, particle radiotherapy can enable us to deliver uniform doses to irregularly shaped tumors.

Proton beams are categorized as low linear energy transfer (LET) radiation with a biological effect of 1.1 times that of photon beams (1). In contrast, carbon ions have a higher biological effectiveness than protons or photons; their effectiveness is almost 2-3 times that of photon beams (2,3), and they may be effective for treating highly radioresistant tumors. In this review, we describe current findings, particularly on PBT for brain tumors, including glioblastoma (GBM), low-grade glioma (LGG), chordoma, and meningioma.

PBT for low-grade glioma

Sequential PORT is recommended in some cases of LGG, depending on the tumor location, extent of residual disease, and proliferative potency. However, the significance of PORT for LGG is still not very clear (4-6). In the EORTC 22845 trial, progression-free survival (PFS) was significantly

better in patients who received early PORT at a dose of 54 Gy in 30 fractions compared with that in patients who did not receive radiotherapy (P<0.0001); however, there was no significant difference in the overall survival (OS) (P=0.872) (5). The current recommended dose is 50-55 Gy in conventional fractions (1.8-2 Gy per fraction). Fitzek *et al*. used PBT in combination with photon beams at doses of 68.2 and 79.7 GyE for glioma of grades 2 and 3, respectively, with dose escalation. However, they were not able to improve the outcome significantly (7). In contrast, Hug *et al*. reported an improved visual status in 27 pediatric patients with LGG treated with PBT at a median dose of 55.2 Gy (RBE) at 1.8 Gy per fraction (8). With the use of PBT for adult LGG at a median dose of 54 Gy (RBE) at 1.8 Gy per fraction, Hauswald *et al*. found that tumor progression was noticed in only 1 patient and there was no severe toxicity (9).

The prognosis of patients with LGG is better compared with that of patients with high-grade glioma. The 5- and 10-year OS rates have been reported to be 58% and 32%, respectively, for astrocytoma (10) and 88% and 85%, respectively, for low-grade oligodendroglioma (11). Therefore, the quality of life after treatment is an important consideration for patients with LGG, particularly younger patients. The advantages of PBT in the preservation of the healthy brain and in the reduction of risk for secondary cancer in patients with pediatric brain tumors have been widely suggested (12-19). Further clinical analyses of not only neuro-functional preservation but also secondary cancer prevention are required to establish the efficacy of PBT in younger patients with LGG.

PBT for high-grade glioma

PORT improves OS of patients with high-grade glioma (HGG) (20). Postoperative photon radiotherapy of approximately 60 Gy in conventional fractions with concomitant and adjuvant temozolomide is currently the standard therapy (21). However, the prognosis is still not satisfactory, and it has shown little improvement in patients with GBM over the past decades. The median survival times (MSTs) of patients with HGG have been reported to be 11-18 months, and the 5-year survival rates have been reported to be less than 10% (20-24). Outcomes were not improved even high linear-energy transfer (LET) radiations were applied. MSTs of 13.9 and 9 months were reported using radiation with carbon, helium, and neon (25) and pions, respectively (26). In contrast, dose escalation has yielded favorable results. Fitzek *et al*. found that accelerated fractionation of 90 Gy (RBE) using conformal protons and photons improved local control and survival in GBM, with MST of the 23 cases being 20 months (27). In their report, tumor recurrence occurred most commonly in areas that received doses of 60-70 Gy (RBE) or less, and only 1 case showed recurrence within areas that received 90 Gy (RBE).

In patients with GBM, Tanaka *et al*. reported MSTs of 16.2 (12.8-19.6) and 12.4 (10.0-14.8) months and 2-year survival rates of 38.4% (23.5-53.3%) and 11.4% (0.0-25.3%) after treatment with high-dose conformal X-ray radiotherapy of 80-90 Gy and 60 Gy, respectively. The patients who received 60 Gy did not develop radiation necrosis (RN), whereas 9 patients who received higher doses (80-90 Gy) developed RN. In addition, Mizumoto *et al*. also found a survival benefit of hyperfractionated concomitant boost PBT with nimustine hydrochloride (ACNU) in patients with GBM (28). In this study, radiotherapy was conducted for 20 patients with GBM twice a day as follows: 1.8 Gy (RBE) for the tumor and surrounding edema in the morning and 1.65 Gy (RBE) for the gross tumor on gadolinium-enhanced MRI in the afternoon (6 h later) over 28 days; a total dose of 96.6 Gy (RBE) in 56 fractions was delivered to the tumor. Only 1 of 20 patients had recurrence within the 96.6 Gy (RBE) volume. The MST was 21.6 months and the 1- and 2-year PFS was 45.5% and 15.5%, respectively. RN occurred in 6 cases, and probable leukoencephalopathy was observed in 1 patient. Although dose escalation may be associated with an increased risk of RN, the development of RN might be inevitable in patients with GBM when considering its refractoriness. The findings of Fitzek *et al*. and Mizumoto *et al*. indicate that a total dose ≥90 GyE has the potential to control GBM. However, because the accurate evaluation of the area of tumor infiltration was difficult with MRI or CT, recurrence mainly occurred in the marginal area. This fact may indicate that the use of methionine positron emission tomography facilitates the evaluation of exact tumor invasion and improves the outcome.

Carbon ions are also of interest for the treatment of HGG. Mizoe *et al*. conducted a phase I/II study in 48 patients with HGG (16 with anaplastic astrocytoma and 32 with GBM) using photon and carbon ion therapy with ACNU (29). The radiation dose with photon beams was 50 Gy in 25 fractions, followed by carbon ion therapy. The doses of carbon ions were escalated in 10% incremental steps from 16.8 to 24.8 Gy, and a high dose was associated with good prognosis with MST of 26 months.

Suit *et al*. suggested 2 directions for future radiotherapy, i.e., the shrinkage of the irradiation field and expansion of a gap between radiosensitivity of tumor and normal tissues (30). In this regard, PBT or carbon ion therapy has considerable potential to achieve the shrinkage of the irradiation field, in particular, by developing intensity-modulated particle therapy (IMPT). A recent study on radiosensitivity showed the feasibility of radiotherapy in combination with not only temozolomide but also other molecular-targeted agents (31,32). Therefore, high-dose particle therapy in combination with recently developed molecular-targeted or radiosensitizing agents should be tried as a promising multimodal treatment for GBM. In addition, boron neutron capture therapy (BNCT) may permit the expansion of the radiosensitivity gap. This approach is based on a nuclear capture reaction that occurs when boron (^{10}B) is irradiated with neutrons of thermal energy to yield high-energy short-range α particles ($^{4}He^{2+}$) and recoiling lithium (^{7}Li) nuclei. Because ^{10}B is selectively taken up by cancer cells, theoretically, only cancer cells are destroyed by this treatment. The outcomes of patients with GBM treated with BNCT have been found to be favorable, with MSTs of 13-27 months (33-36).

PBT for skull base chordomas and chondrosarcomas

Chordomas are rare low-grade malignancies that often develop in the clival region. Because metastasis and dissemination are uncommon, local control by aggressive treatment is important for long-term survival. Although surgical resection is the first treatment choice, gross total resection is often difficult because of difficult access and proximity to critical structures. Therefore, adjuvant radiotherapy is almost essential for tumor control. The control of skull base chordomas or chondrosarcomas requires doses more than 56-70 Gy (37-39) that are beyond the tolerance of critical structures such as the optic nerve, chiasma, and brainstem. This makes the treatment with photon beams difficult, it has been reported that 5-year PFS with X-ray treatment remained 17-39% (40-43). In this regard, particle radiotherapy was shown to be superior to photons for delivering higher doses to the tumor while keeping lower doses to normal tissues in the clival region in the 1990s (29,44-50).

The use of PBT for treating chordoma dates back to the 1990s. In early studies, PBT was often conducted in combination with photon radiotherapy. For example, Munzenrider *et al*. treated 519 patients with skull base tumors, including 290 chordomas and 229 chondrosarcomas, with photon and proton radiotherapy at a total dose of 66-83 Gy (RBE) at 1.8-1.92 Gy per fraction, and 10-year local control rates (LCRs) for chordoma and chondrosarcoma were 54% and 88%, respectively. Similarly, Hug *et al*. treated 58 patients (33 with chordomas and 25 with chondrosarcomas) with a median total dose of 71.9 Gy (RBE) and 69.3 Gy (RBE) for chordoma and chondrosarcoma, respectively, at 1.8 Gy (RBE) per fraction and found that 5-year LCRs for chordoma and chondrosarcoma were 59% and 75%, respectively, with symptomatic late toxicities being observed in only 3 of the 58 patients.

Ares *et al*. reported the outcomes of 42 patients with skull base chordomas and 21 patients with chondrosarcomas treated with only PBT. The dose for chordoma and chondrosarcoma was 73.5 Gy (RBE) and 68.4 Gy (RBE), respectively, at 1.8-2.0 Gy (RBE) dose per fraction. The 5-year LCR was 81% and 94% for chordoma and chondrosarcoma, respectively, and severe toxicities were observed in 4 patients, resulting in 94% 5-year freedom from severe toxicity (44). In addition, Fuji *et al*. obtained a 3-year LCR and OS of 100% in 8 patients with skull base chordomas using a prescribed dose of 70 Gy (RBE) at 1.8 Gy (RBE) per fraction (51). In 96 patients with chordomas treated with carbon ion therapy at a median dose of 60 Gy (RBE) delivered in 20 fractions within 3 weeks, Shulz-Ertner *et al*. obtained a 5-year LCR of 70%. Meanwhile, grade 3 optic nerve neuropathy and fat plomb necrosis occurred in 4 patients and 1 patient, respectively (48). Mizoe *et al*. conducted a phase I/II study of carbon ion therapy for skull base chordoma with dose escalation in 4 steps of 4.8 Gy from 48 to 60.8 Gy (RBE) in 16 fractions and obtained a 5-year LCR of 100% without severe toxicities (52).

Recent development of photon radiotherapy has enabled us to achieve a confocal and precise dose distribution. Debus *et al*. performed stereotactic radiotherapy (SRT) in 37 patients at a dose of 66.6 Gy with a median fraction size of 1.8 Gy, whereas Foweraker *et al*. treated 9 chordoma patients with radiotherapy at a dose of 65 Gy in 39 fractions (53). In meta-analysis of these recent studies, most of which are small and retrospective, Maio *et al*. found that 5-year PFS and OS were 50.8% and 78.4%, respectively, and no significant differences in 5-year OS were observed among photon radiotherapy, gamma-knife surgery, PBT, and carbon ion therapy, but 5-year PFS was lower in gamma-knife surgery (54). Although doses of photons delivered were lower than those of protons

and carbon ions, these results suggest that chordoma may possibly be controlled when a sufficient dose is delivered, regardless of the radiation quality. Further progress both in photon and particle radiotherapy is definitely required to overcome this radioresistant and invasive tumor that develop at the very complicated location.

Medial temporal lobe injury is another risk in particle radiotherapy of the middle and upper clival region, which results in amnesia with a specific memory impairment profile (55-57). Ten of 96 patients (10.4%) reportedly developed clinical symptoms or MRI changes in the temporal lobe after PBT at doses of 63-74 Gy (RBE) (58). Although a correlation between the occurrence of temporal lobe toxicities and tissue volume that received high doses has been suggested (58), a threshold dose for temporal lobe toxicity has not been clarified till date.

Collectively, at present, the treatment modality is selected on the basis of not only the tumor location, size, and shape but also the experiences of each institute. Although it takes at least 5 years to draw a meaningful result in chordomas and chondrosarcomas, clinical evidence with higher grades is highly desirable.

PBT for meningioma

Meningiomas are classified into 3 grades in the WHO classification. Most are benign or WHO grade I with an indolent course or a low rate of local recurrence. The first treatment choice for meningiomas is complete surgical resection. Condrao *et al*. found that 5- and 10-year LCRs after gross total resection (GTR) were 93% and 80%, respectively (59). However, complete resection with Simpson G-I or II is sometimes difficult owing to the location, size, and involvement of vial vessels or cranial nerves. In addition, it has been reported that subtotal resection (STR) is associated with a higher recurrence rate of 45-60% (60,61). In these patients, PORT significantly improves local control, although meningiomas are less sensitive to radiotherapy (61-64). Taylor *et al*. found that 69% of patients had recurrence after STR alone, compared with only 15% after PORT (P=0.01) (63).

As for atypical meningiomas, the role of PORT is not sufficiently proven; however, at present, PORT is recommended for all patients, regardless of GTR or STR (65-68). Since the revision of WHO grading criteria in 2000, there has been a significant increase in the number of meningiomas diagnosed as grade II (69,70). Among 114 patients diagnosed with WHO grade II meningioma, Mair *et al*. found a benefit of PORT only for patients who underwent STR (68). In contrast, Komotar *et al*. suggested that PORT improved local control even after GTR. They mentioned that recurrence was noticed only in 1 of 13 patients who received PORT, while it was noticed in 13 of 32 patients who did not receive PORT (P=0.085) (71). The typical dose for PORT is 50-54 Gy and 60 Gy for benign and atypical meningiomas, respectively. In addition, dose escalation may improve local control, particularly for atypical meningioma (72-74), and SRT is reportedly effective for treating small and unresectable meningiomas (75-79).

Hug *et al*. reported the outcomes of 31 patients with WHO grade 2 and 3 meningiomas treated with photon or combined proton-photon irradiation. The total doses ranged from 50 to 68 Gy (RBE) and 40 to 72 Gy (RBE) for grades 2 and 3 meningiomas, respectively. Local control was significantly improved with PBT compared with that with photon radiotherapy alone (P=0.025), and the survival rates for WHO grade 2 meningiomas were significantly improved by PBT and radiation doses >60 Gy (RBE) (74). Similarly, in a study of 24 patients with WHO II and III meningiomas treated by proton and photon beams with a median dose of 65.1 Gy (RBE), Boscos *et al*. found that survival was significantly associated with the total dose (72). In a recent report on the outcomes of 6 patients with WHO II and III meningiomas treated at doses of 68.4 Gy (RBE) and 72.0 Gy, respectively; Chan *et al*. observed local recurrence in 1 patient with WHO grade 3 meningioma but found no severe toxicity (73).

With regard to the use of SRT for meningiomas, Selch *et al*. found that 3-year PFS was 97.4% in a study of 41 cases of benign cavernous sinus meningioma (median tumor volume, 14.5 cc) treated with SRT (median dose, 50.4 Gy) after incomplete resection (77). In addition, in 12 cases of high-grade meningioma (tumor volume, 4.4 cc) treated with SRT at a mean marginal dose of 12-20 Gy, Kano *et al*. found that a marginal dose <20 Gy was a significant predictor (P=0.0139) of short-term tumor progression (5-year PFS, 29.4% *vs*. 63.1%) (79).

PBT is advantageous for treating tumors that are large or have a complex shape or for those adjacent to critical regions (80-85). Thus, in 46 patients with partially resected, biopsied, or recurrent meningiomas treated with a combination of photon and protons at median doses of 59 Gy (RBE), Wenkel *et al*. found that 5- and 10-year LCRs were 100% and 88%, respectively (84). IMRT also gives excellent dose distribution with the avoidance of surrounding organs (86). Kosaki *et al*. reported that

Table 1 Series of intracranial and skull base tumors treated by proton beam therapy

Authors [year]	Histology	Number of Patients	Mean dose (range) [Gy (RBE)]	Dose per fraction [Gy(RBE)]	Mean follow up (Month)	Local control (%)	Overall survival (%)
Fitzek *et al*. [2001]	Low grade glioma (Grade II)	7	68.2	1.92	61	N/A	71 (5 y)
Hug *et al*. [2002]	Low grade glioma	27	55.2	1.8	39.6	87	93
Hauswald *et al*. [2012]	Low grade glioma (Grade I/II)	19	54.0 [48.6-54]	1.8	N/A	N/A	N/A
Fitzek *et al*. [1999]	Glioblastoma	23	93.5 [81.6-94.2]	1.8-1.92 (2 Fx/day)	33	N/A	34 (2 y), 18 (3 y)
Mizumoto *et al*. [2010]	Glioblastoma	20	96.6	1.8 & 1.65 (2 Fx/day)	21.6	15.5 (2 y)	45.3 (2 y)
Hug *et al*. [1999]	Chordoma Chondrosarcoma	33 25	71.9 [66.6-79.2] 69.3 [64.8-72]	1.8	33.2	59 (5 y) 75 (5 y)	79.0 (5 y) 100 (5 y)
Munzenrider *et al*. [1999]	Chordoma Chondrosarcoma	290 229	66-83	1.8-1.92	41	73 (5 y), 54 (10 y) 98 (5 y), 94 (10 y)	80 (5 y), 54 (10 y) 91 (5 y), 88 (10 y)
Noel *et al*. [2001]	Chordoma Chondrosarcoma	34 11	66.7 [60-73]	1.8-2.0	31 (median)	83.1 (3 y) 90 (3 y)	91.2 (4 y) 60 (4 y)
Igaki *et al*. [2004]	Chordoma	13	72.0 [63-95]	2.0-3.5	69.3 (median)	66.7 (5 y)	44.2 (5 y)
Ares *et al*. [2009]	Chordoma Chondrosarcoma	42 22	73.5 [67-74] 68.4 [63-74]	1.8-2.0	38	81 (5 y) 94 (5 y)	62 (5 y) 91 (5 y)
Fuji *et al*. [2011]	Chordoma Chondrosarcoma	8 8	63 [50-70]	1.8	42 (median)	100 (3 y) 86 (3 y)	100 (3 y) 100 (3 y)
Yasuda *et al*. [2012]	Chordoma	40	68.9 [55-74]	N/A	62.3	70 (5 y)	83.4 (5 y)
Vernimmen *et al*. [2001]	Meningioma	18	20.3 [17.3-24.3] (ICRU reference dose)	3 fractions	40	88 (5 y)	N/A
Halasz *et al*. [2011]	Meningioma (benign)	50	10.0-15.5 (90% line)	10.0-15.5 (radiosurgery)	32 (median)	94 (3 y)	N/A
Weber *et al*. [2004]	Meningioma (benign+atypical)	16	56 [52.2-64]	1.8-2.0	34.1	91.7 (3 y)	92.7 (3 y)
Slater *et al*. [2012]	Meningioma (benign+atypical)	Total: 72 Grade I: 47 NP*: 21 Grade II: 4	50.4-66.6 (G1+NP) 54-70.2 (G2)	1.8	74	96 (5 y) G1+NP: 99 G2: 50	72 (5 y)

Table 1 *(continued)*

Table 1 (continued)

Authors [year]	Histology	Number of Patients	Mean dose (range) [Gy (RBE)]	Dose per fraction [Gy(RBE)]	Mean follow up (Month)	Local control (%)	Overall survival (%)
Hug *et al*. [2000]	Malignant meningioma	Total: 31 Atypical: 15 Malignant: 16	 62.5 [50.4-68.4] 58 [40-72]	1.8-2.0	59	 38 (5 y) 52 (5 y)	 89 (5 y) 51 (5 y)
Boskos *et al*. [2009]	Malignant meningioma	24	68	1.8-2.0	48	46.7 (5 y)	53.2 (5 y)
Chan *et al*. [2012]	Malignant meningioma	6	68.4 for Grade II 72.0 for Grade III	1.8	145	N/A	N/A

*NP, No pathology

the difference in dose distribution between IMRT and PBT for complex-shaped skull base meningiomas was very small. However, they mentioned that PBT allowed almost complete avoidance of the brainstem, while this region received 10-30% of the dose in IMRT (87). In an evaluation of the risk of a secondary tumor after radiotherapy for benign meningiomas, Arvot *et al*. found that PBT reduced this risk to less than half of that with photon radiotherapy (81). In addition, they also mentioned that PBT could significantly reduce the risk of neurocognitive, visual, and auditory complications. A summary of proton beam therapy for intracranial and skull base tumors is reported in *Table 1*.

Conclusions

The role of particle beam radiotherapy for intracranial and skull base tumors has not been fully established. However, it is clear that this method has 2 important advantages compared with photon radiotherapy. First, particle beam radiotherapy makes it possible to deliver a high dose to refractory tumors such as high-grade gliomas and anaplastic or atypical meningiomas, which can improve control rates of these tumors. Second, PBT can reduce the irradiated volume of normal brain tissues, thereby significantly reducing neurotoxicity. Therefore, particle beam radiotherapy is particularly advantageous for childhood brain tumors, low-grade gliomas, and benign meningiomas that require a long-term follow-up.

Acknowledgements

Disclosure: The authors declare no conflict of interest.

References

1. Paganetti H, Niemierko A, Ancukiewicz M, et al. Relative biological effectiveness (RBE) values for proton beam therapy. Int J Radiat Oncol Biol Phys 2002;53:407-21.
2. Koike S, Ando K, Oohira C, et al. Relative biologicaleffectiveness of 290 MeV/u carbon ions for the growth delay of a radioresistant murine fibrosarcoma. J Radiat Res 2002;43:247-55.
3. Kagawa K, Murakami M, Hishikawa Y, et al. Preclinical biological assessment of proton and carbon ion beams at Hyogo Ion Beam Medical Center. Int J Radiat Oncol Biol Phys 2002;54:928-38.
4. Shaw E, Arusell R, Scheithauer B, et al. Prospective randomized trial of low-versus high-dose radiation therapy in adults with supratentorial low-grade glioma: initial report of a North Central Cancer Treatment Group/ Radiation Therapy Oncology Group/Eastern Cooperative Oncology Group study. J Clin Oncol 2002;20:2267-76.
5. van den Bent MJ, Afra D, de Witte O, et al. Long-term efficacy of early versus delayed radiotherapy for low-grade astrocytoma and oligodendroglioma in adults: the EORTC 22845 randomised trial. Lancet 2005;366:985-90.
6. Karim AB, Maat B, Hatlevoll R, et al. A randomized trial on dose-response in radiation therapy of low-grade cerebral glioma: European Organization for Research and Treatment of Cancer (EORTC) Study 22844. Int J Radiat Oncol Biol Phys 1996;36:549-56.
7. Fitzek MM, Thornton AF, Harsh G 4th, et al. Dose-escalation with proton/photon irradiation for Daumas-Duport lower-grade glioma: results of an institutional phase I/II trial. Int J Radiat Oncol Biol Phys 2001;51:131-7.
8. Hug EB, Muenter MW, Archambeau JO, et al. Conformal

proton radiation therapy for pediatric low-grade astrocytomas. Strahlenther Onkol 2002;178:10-7.
9. Hauswald H, Rieken S, Ecker S, et al. First experiences in treatment of low-grade glioma grade I and II with proton therapy. Radiat Oncol 2012;7:189.
10. Shaw EG, Scheithauer BW, O'Fallon JR, et al. Mixed oligoastrocytomas: a survival and prognostic factor analysis. Neurosurgery 1994;34:577-82; discussion 582.
11. Lebrun C, Fontaine D, Ramaioli A, et al. Long-term outcome of oligodendrogliomas. Neurology 2004;62:1783-7.
12. Beltran C, Roca M, Merchant TE. On the benefits and risks of proton therapy in pediatric craniopharyngioma. Int J Radiat Oncol Biol Phys 2012;82:e281-7.
13. Boehling NS, Grosshans DR, Bluett JB, et al. Dosimetric comparison of three-dimensional conformal proton radiotherapy, intensity-modulated proton therapy, and intensity-modulated radiotherapy for treatment of pediatric craniopharyngiomas. Int J Radiat Oncol Biol Phys 2012;82:643-52.
14. Calaminus G, Göbel U, chrum J, et al. Proton beam therapy for loco-regional control of a recurrent mixed malignant germ cell tumor of the skull in a 22-month-old girl. Klin Padiatr 2010;222:175-9.
15. Hug EB, Sweeney RA, Nurre PM, et al. Proton radiotherapy in management of pediatric base of skull tumors. Int J Radiat Oncol Biol Phys 2002;52:1017-24.
16. Lee CT, Bilton SD, Famiglietti RM, et al. Treatment planning with protons for pediatric retinoblastoma,medu lloblastoma,and pelvic sarcoma: how do protons compare with other conformal techniques? Int J Radiat Oncol Biol Phys 2005;63:362-72.
17. MacDonald SM, Safai S, Trofimov A, et al. Proton radiotherapy for childhood ependymoma: initial clinical outcomes and dose comparisons. Int J Radiat Oncol Biol Phys 2008;71:979-86.
18. MacDonald SM, Trofimov A, Safai S, et al. Proton radiotherapy for pediatric central nervous system germ cell tumors: early clinical outcomes. Int J Radiat Oncol Biol Phys 2011;79:121-9.
19. St Clair WH, Adams JA, Bues M, et al. Advantage of protons compared to conventional X-ray or IMRT in the treatment of a pediatric patient with medulloblastoma. Int J Radiat Oncol Biol Phys 2004;58:727-34.
20. Walker MD, Green SB, Byar DP, et al. Randomized comparisons of radiotherapy and nitrosoureas for the treatment of malignant glioma after surgery. N Engl J Med 1980;303:1323-9.
21. Stupp R, Hegi ME, Mason WP, et al. Effects of radiotherapy with concomitant and adjuvant temozolomide versus radiotherapy alone on survival in glioblastoma in a randomised phase III study: 5-year analysis of the EORTC-NCIC trial. Lancet Oncol 2009;10:459-66.
22. Walker MD, Alexander E Jr, Hunt WE, et al. Evaluation of BCNU and/or radiotherapy in the treatment of anaplastic gliomas. A cooperative clinical trial. J Neurosurg 1978;49:333-43.
23. Kristiansen K, Hagen S, Kollevold T, et al. Combined modality therapy of operated astrocytomas grade III and IV. Confirmation of the value of postoperative irradiation and lack of potentiation of bleomycin on survival time: a prospective multicenter trial of the Scandinavian Glioblastoma Study Group. Cancer 1981;47:649-52.
24. Sandberg-Wollheim M, Malmström P, Strömblad LG, et al. A randomized study of chemotherapy with procarbazine, vincristine, and lomustine with and without radiation therapy for astrocytoma grades 3 and/or 4. Cancer 1991;68:22-9.
25. Castro JR, Saunders WM, Austin-Seymour MM, et al. A phase I-II trial of heavy charged particle irradiation of malignant glioma of the brain: a Northern California Oncology Group Study. Int J Radiat Oncol Biol Phys 1985;11:1795-800.
26. Greiner R, Blattmann H, Thum P, et al. Anaplastic astrocytoma and glioblastoma:pion irradiation with the dynamic conformation technique at the Swiss Institute for Nuclear Research (SIN). Radiother Oncol 1990;17:37-46.
27. Fitzek MM, Thornton AF, Rabinov JD, et al. Accelerated fractionated proton/photon irradiation to 90 cobalt gray equivalent for glioblastoma multiforme: results of a phase II prospective trial. J Neurosurg 1999;91:251-60.
28. Mizumoto M, Tsuboi K, Igaki H, et al. Phase I/II trial of hyperfractionated concomitant boost proton radiotherapy for supratentorial glioblastoma multiforme. Int J Radiat Oncol Biol Phys 2010;77:98-105.
29. Mizoe JE, Tsujii H, Hasegawa A, et al. Phase I/II clinical trial of carbon ion radiotherapy for malignant gliomas: combined X-ray radiotherapy, chemotherapy, and carbon ion radiotherapy. Int J Radiat Oncol Biol Phys 2007;69:390-6.
30. Suit H. The Gray Lecture 2001: coming technical advances in radiation oncology. Int J Radiat Oncol Biol Phys 2002;53:798-809.
31. Drappatz J, Norden AD, Wong ET, et al. Phase I study of vandetanib with radiotherapy and temozolomide for newly diagnosed glioblastoma. Int J Radiat Oncol Biol Phys

2010;78:85-90.
32. Prados MD, Chang SM, Butowski N, et al. Phase II study of erlotinib plus temozolomide during and after radiation therapy in patients with newly diagnosed glioblastoma multiforme or gliosarcoma. J Clin Oncol 2009;27:579-84.
33. Busse PM, Harling OK, Palmer MR, et al. A critical examination of the results from the Harvard-MIT NCT program phase I clinical trial of neutron capture therapy for intracranial disease. J Neurooncol 2003;62:111-21.
34. Henriksson R, Capala J, Michanek A, et al. Boron neutron capture therapy (BNCT) for glioblastoma multiforme: a phase II study evaluating a prolonged high-dose of boronophenylalanine (BPA). Radiother Oncol 2008;88:183-91.
35. Joensuu H, Kankaanranta L, Seppälä T, et al. Boron neutron capture therapy of brain tumors: clinical trials at the finnish facility using boronophenylalanine. J Neurooncol 2003;62:123-34.
36. Kawabata S, Miyatake S, Kuroiwa T, et al. Boron neutron capture therapy for newly diagnosed glioblastoma. J Radiat Res 2009;50:51-60.
37. Pearlman AW, Friedman M. Radical radiation therapy of chordoma. Am J Roentgenol Radium Ther Nucl Med 1970;108:332-41.
38. Rich TA, Schiller A, Suit HD, et al. Clinical and pathologic review of 48 cases of chordoma. Cancer 1985;56:182-7.
39. Noël G, Feuvret L, Calugaru V, et al. Chordomas of the base of the skull and upper cervical spine. One hundred patients irradiated by a 3D conformal technique combining photon and proton beams. Acta Oncol 2005;44:700-8.
40. Catton C, O'Sullivan B, Bell R, et al. Chordoma: long-term follow-up after radical photon irradiation. Radiother Oncol 1996;41:67-72.
41. Magrini SM, Papi MG, Marletta F, et al. Chordoma-natural history, treatment and prognosis. The Florence Radiotherapy Department experience (1956-1990) and a critical review of the literature. Acta Oncol 1992;31:847-51.
42. Romero J, Cardenes H, la Torre A, et al. Chordoma: results of radiation therapy in eighteen patients. Radiother Oncol 1993;29:27-32.
43. Fuller DB, Bloom JG. Radiotherapy for chordoma. Int J Radiat Oncol Biol Phys 1988;15:331-9.
44. Ares C, Hug EB, Lomax AJ, et al. Effectiveness and safety of spot scanning proton radiation therapy for chordomas and chondrosarcomas of the skull base: first long-term report. Int J Radiat Oncol Biol Phys 2009;75:1111-8.
45. Igaki H, Tokuuye K, Okumura T, et al. Clinical results of proton beam therapy for skull base chordoma. Int J Radiat Oncol Biol Phys 2004;60:1120-6.
46. Munzenrider JE, Liebsch NJ. Proton therapy for tumors of the skull base. Strahlenther Onkol 1999;175:57-63.
47. Yasuda M, Bresson D, Chibbaro S, et al. Chordomas of the skull base and cervical spine: clinical outcomes associated with a multimodal surgical resection combined with proton-beam radiation in 40 patients. Neurosurg Rev 2012;35:171-82; discussion 182-3.
48. Schulz-Ertner D, Karger CP, Feuerhake A, et al. Effectiveness of carbon ion radiotherapy in the treatment of skull-base chordomas. Int J Radiat Oncol Biol Phys 2007;68:449-57.
49. Stüer C, Schramm J, Schaller C. Skull base chordomas: management and results. Neurol Med Chir (Tokyo) 2006;46:118-24; discussion 124-5.
50. Takahashi S, Kawase T, Yoshida K, et al. Skull base chordomas: efficacy of surgery followed by carbon ion radiotherapy. Acta Neurochir (Wien) 2009;151:759-69.
51. Fuji H, Nakasu Y, Ishida Y, et al. Feasibility of proton beam therapy for chordoma and chondrosarcoma of the skull base. Skull Base 2011;21:201-6.
52. Mizoe JE, Hasegawa A, Takagi R, et al. Carbon ion radiotherapy for skull base chordoma. Skull Base 2009;19:219-24.
53. Foweraker KL, Burton KE, Maynard SE, et al. High-dose radiotherapy in the management of chordoma and chondrosarcoma of the skull base and cervical spine: Part 1--Clinical outcomes. Clin Oncol (R Coll Radiol) 2007;19:509-16.
54. Di Maio S, Temkin N, Ramanathan D, et al. Current comprehensive management of cranial base chordomas: 10-year meta-analysis of observational studies. J Neurosurg 2011;115:1094-105.
55. Cheung M, Chan AS, Law SC, et al. Cognitive function of patients with nasopharyngeal carcinoma with and without temporal lobe radionecrosis. Arch Neurol 2000;57:1347-52.
56. Baxendale S. Amnesia in temporal lobectomy patients: historical perspective and review. Seizure 1998;7:15-24.
57. Pehlivan B, Ares C, Lomax AJ, et al. Temporal lobe toxicity analysis after proton radiation therapy for skull base tumors. Int J Radiat Oncol Biol Phys 2012;83:1432-40.
58. Santoni R, Liebsch N, Finkelstein DM, et al. Temporal lobe (TL) damage following surgery and high-dose photon and proton irradiation in 96 patients affected by chordomas and chondrosarcomas of the base of the skull. Int J Radiat Oncol Biol Phys 1998;41:59-68.

59. Condra KS, Buatti JM, Mendenhall WM, et al. Benign meningiomas: primary treatment selection affects survival. Int J Radiat Oncol Biol Phys 1997;39:427-36.
60. Mirimanoff RO, Dosoretz DE, Linggood RM, et al. Meningioma: analysis of recurrence and progression following neurosurgical resection. J Neurosurg 1985;62:18-24.
61. Barbaro NM, Gutin PH, Wilson CB, et al. Radiation therapy in the treatment of partially resected meningiomas. Neurosurgery 1987;20:525-8.
62. Austin-Seymour M, Urie M, Munzenrider J, et al. Considerations in fractionated proton radiation therapy: clinical potential and results. Radiother Oncol 1990;17:29-35.
63. Taylor BW Jr, Marcus RB Jr, Friedman WA, et al. The meningioma controversy: postoperative radiation therapy. Int J Radiat Oncol Biol Phys 1988;15:299-304.
64. Glaholm J, Bloom HJ, Crow JH. The role of radiotherapy in the management of intracranial meningiomas: the Royal Marsden Hospital experience with 186 patients. Int J Radiat Oncol Biol Phys 1990;18:755-61.
65. Dziuk TW, Woo S, Butler EB, et al. Malignant meningioma: an indication for initial aggressive surgery and adjuvant radiotherapy. J Neurooncol 1998;37:177-88.
66. Milosevic MF, Frost PJ, Laperriere NJ, et al. Radiotherapy for atypical or malignant intracranial meningioma. Int J Radiat Oncol Biol Phys 1996;34:817-22.
67. Goldsmith BJ, Wara WM, Wilson CB, et al. Postoperative irradiation for subtotally resected meningiomas. A retrospective analysis of 140 patients treated from 1967 to 1990. J Neurosurg 1994;80:195-201.
68. Mair R, Morris K, Scott I, et al. Radiotherapy for atypical meningiomas. J Neurosurg 2011;115:811-9.
69. Pearson BE, Markert JM, Fisher WS, et al. Hitting a moving target: evolution of a treatment paradigm for atypical meningiomas amid changing diagnostic criteria. Neurosurg Focus 2008;24:E3.
70. Smith SJ, Boddu S, Macarthur DC. Atypical meningiomas: WHO moved the goalposts? Br J Neurosurg 2007;21:588-92.
71. Komotar RJ, Iorgulescu JB, Raper DM, et al. The role of radiotherapy following gross-total resection of atypical meningiomas. J Neurosurg 2012;117:679-86.
72. Boskos C, Feuvret L, Noel G, et al. Combined proton and photon conformal radiotherapy for intracranial atypical and malignant meningioma. Int J Radiat Oncol Biol Phys 2009;75:399-406.
73. Chan AW, Bernstein KD, Adams JA, et al. Dose escalation with proton radiation therapy for high-grade meningiomas. Technol Cancer Res Treat 2012;11:607-14.
74. Hug EB, Devries A, Thornton AF, et al. Management of atypical and malignant meningiomas: role of high-dose, 3D-conformal radiation therapy. J Neurooncol 2000;48:151-60.
75. Compter I, Zaugg K, Houben RM, et al. High symptom improvement and local tumor control using stereotactic radiotherapy when given early after diagnosis of meningioma. A multicentre study. Strahlenther Onkol 2012;188:887-93.
76. Henzel M, Gross MW, Hamm K, et al. Significant tumor volume reduction of meningiomas after stereotactic radiotherapy: results of a prospective multicenter study. Neurosurgery 2006;59:1188-94; discussion 1194.
77. Selch MT, Ahn E, Laskari A, et al. Stereotactic radiotherapy for treatment of cavernous sinus meningiomas. Int J Radiat Oncol Biol Phys 2004;59:101-11.
78. Liu JK, Forman S, Hershewe GL, et al. Optic nerve sheath meningiomas: visual improvement after stereotactic radiotherapy. Neurosurgery 2002;50:950-5; discussion 955-7.
79. Kano H, Takahashi JA, Katsuki T, et al. Stereotactic radiosurgery for atypical and anaplastic meningiomas. J Neurooncol 2007;84:41-7.
80. Slater JD, Loredo LN, Chung A, et al. Fractionated proton radiotherapy for benign cavernous sinus meningiomas. Int J Radiat Oncol Biol Phys 2012;83:e633-7.
81. Weber DC, Lomax AJ, Rutz HP, et al. Spot-scanning proton radiation therapy for recurrent, residual or untreated intracranial meningiomas. Radiother Oncol 2004;71:251-8.
82. Noël G, Bollet MA, Calugaru V, et al. Functional outcome of patients with benign meningioma treated by 3D conformal irradiation with a combination of photons and protons. Int J Radiat Oncol Biol Phys 2005;62:1412-22.
83. Vernimmen FJ, Harris JK, Wilson JA, et al. Stereotactic proton beam therapy of skull base meningiomas. Int J Radiat Oncol Biol Phys 2001;49:99-105.
84. Wenkel E, Thornton AF, Finkelstein D, et al. Benign meningioma: partially resected, biopsied, and recurrent intracranial tumors treated with combined proton and photon radiotherapy. Int J Radiat Oncol Biol Phys 2000;48:1363-70.
85. Halasz LM, Bussière MR, Dennis ER, et al. Proton stereotactic radiosurgery for the treatment of benign meningiomas. Int J Radiat Oncol Biol Phys

2011;81:1428-35.
86. Maclean J, Fersht N, Bremner F, et al. Meningioma causing visual impairment: outcomes and toxicity after intensity modulated radiation therapy. Int J Radiat Oncol Biol Phys 2013;85:e179-86.
87. Kosaki K, Ecker S, Habermehl D, et al. Comparison of intensity modulated radiotherapy (IMRT) with intensity modulated particle therapy (IMPT) using fixed beams or an ion gantry for the treatment of patients with skull base meningiomas. Radiat Oncol 2012;7:44.

Cite this article as: Mizumoto M, Oshiro Y, Tsuboi K. Proton beam therapy for intracranial and skull base tumors. Transl Cancer Res 2013;2(2):87-96. doi: 10.3978/j.issn.2218-676X.2013.04.08

Review Article

Boron neutron capture therapy for brain tumors

Tetsuya Yamamoto[1,2], Koji Tsuboi[2], Kei Nakai[1], Hiroaki Kumada[2], Hideyuki Sakurai[2], Akira Matsumura[1]

[1]Department of Neurosurgery, [2]Department of Radiation Oncology, University of Tsukuba, Ibaraki, Japan

Correspondence to: Tetsuya Yamamoto, M.D, Ph.D. Tennno-dai 1-1-1, Tsukuba City, Ibaraki 305-8575, Japan. Email: yamamoto.neurosurg@gmail.com.

Abstract: Boron neutron capture therapy (BNCT) is a unique method that can provide the delivery of tumor cell-selective high-linear energy transfer (LET) particle radiotherapy to tumor mass and the microscopic invasion while avoiding radiation damage to the surrounding normal brain tissue. The rationale of BNCT is based on the nuclear interaction of ^{10}B with thermal neutrons with the release of high LET α and ^{7}Li particles through the boron neutron capture reaction, ^{10}B(n, α) ^{7}Li. The very short path length (<9 μm) of α-particles and ^{7}Li enables high-LET irradiation of tumor cells without undesirable damage to ^{10}B-unloaded normal cells. Eight non-randomized prospective external beam BNCT trials for glioblastoma (GBM) have been performed over the past 15 years using two available boron drugs and neutron beams at nuclear reactors. The reported median time to progression and the median survival time are 6-12 and 12-27 mos, respectively. Optimization of dosage and boron delivery agents, the combined use of different boron agents, the combination of BNCT with other therapeutic modalities, and the development of in-hospital accelerator-based neutron sources are underway for the improvement of BNCT. In light of the existing clinical reports, there is a clear need for more evidence-based data.

Keywords: Boron neutron capture therapy; glioblastoma; accelerator

doi: 10.3978/j.issn.2218-676X.2013.04.11

Scan to your mobile device or view this article at: http://www.thetcr.org/article/view/1119/html

Introduction

Glioblastoma (GBM) is a common malignant brain tumor in adults, and many recur within several months and show fatal progression within 2 years after the initial treatment. Extensive resection of the contrast-enhancing part of a tumor under image-guided surgery using fluorescence with 5-aminolevulinic acid, neuronavigation, and intraoperative magnetic resonance imaging (MRI) is shown to be beneficial for prolongation of the post-operative survival time (1,2). Aggressive cyto-reductive surgery is not indicated for the tumor in the eloquent brain. Invading cells are evident at distances of 2 to 3 cm or even further from the main tumor mass of GBM, which can be clinically identified by the contrast enhancement area on a magnetic resonance image. Thus, post-operative adjuvant therapies are essential for the treatment of post-surgical residual tumor mass and microscopic invading tumor cells in the patients with GBM.

Among several chemotherapeutic agents for malignant glioma (3,4), the effectiveness of temozolomide or carmustine wafers has been shown. For example, the EORTC clinical trial provided Class I evidence that the concomitant and adjuvant use of temozolomide with the conventional radiotherapy leads to a modest but significant survival advantage (median survival time, or MST: 14.6 mos) compared to the conventional radiotherapy alone (MST 12.1 mos), approximately with 25% of the patients surviving longer than 24 mos (5).

Two prospective studies provided Class II evidence and also showed modest benefits of carmustine wafers for GBM patients (4). In the report of Westphal *et al.* (6), a subanalysis of 207 GBM patients showed that the carmustine wafer group had a longer mean survival (13.5 mos) than the placebo group (11.4 mos). In a study by Valtonen *et al.* (7), regarding the survival of the 27 GBM patients among the whole series of 32 patients, the group that received carmustine wafers had a longer mean survival (53.3 wks) than the placebo wafer group (39.9 wks). Because of the limited benefits produced by standard (conventional) radiotherapy and chemotherapy

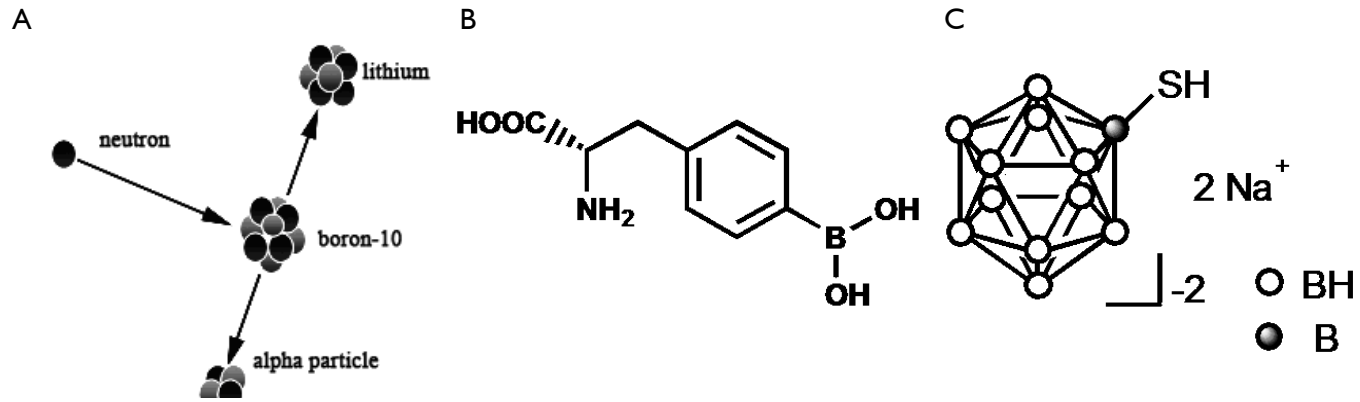

Figure 1 Neutron capture reaction of ^{10}B (A) and currently available boron delivery agents: boronophenylalanine *p*-dihydroxyboryl-phenylalanine (BPA, B) and borocaptate sodium sulfhydryl borane $Na_2B_{12}H_{11}SH$ (BSH, C)

to date, there has been also significant interest in new entity of radiotherapy and targeted molecular agents for the treatment of GBM.

Dose escalation studies using conventional X-ray fractionation, stereotactic radiosurgery, fractionated proton beam radiation, or other conformal radiotherapies have shown median survival times which vary from 9.5 to 26 mos (8,9). These studies and their failure analyses imply that at least 90 Gy must be delivered to achieve local control of GBM. Such a high-dose of radiation exceeds the accepted tolerance of normal brain tissue. Thus, high-dose radiation must be delivered with the upmost selectivity for tumor cells, to minimize radiation damage to the surrounding normal brain. Tumor-cell selectivity at the microscopic level is thus desirable. BNCT has been indicated primarily for GBM because of the theoretical selective sterilization of microscopic invading cells in the brain.

Boron neutron capture therapy (BNCT)

Boron neutron capture therapy (BNCT) has been proposed to provide tumor cell-selective high-linear energy transfer particle radiotherapy. The nuclear reaction between boron-10 (^{10}B) and thermal neutrons releases high LET α and ^{7}Li particles through the boron neutron capture reaction, $^{10}B(n, \alpha)\ ^{7}Li$ (*Figure 1*). The very short path length (<9 μm) of α-particles and ^{7}Li enables high-LET irradiation of ^{10}B-loaded tumor cells, minimizing undesirable damage to ^{10}B-unloaded normal cells. The effectiveness of BNCT is highly dependent on the amount of these particles and the selectivity of the boron compound in tumor cells. In BNCT clinical study, the minimum tumor dose of gross tumor volume (GTV) was around 30 Gy (10).

Although low-energy thermal neutrons (<0.53 eV) are captured most efficiently by ^{10}B nuclei, the shallow penetration limits their usefulness. For external beam BNCT, it is essential to use epithermal neutrons, which lose energy during the penetration of normal tissue (e.g., skin, cranium) and convert to thermal neutrons. Most commonly in BNCT for brain tumors, epithermal neutron beam irradiation is performed at a research reactor, and in a single fraction (*Figure 2*).

To deliver ^{10}B, two boron drugs, p-dihydroxyboryl-phenylalanine (BPA) and sulfhydryl borane $Na_2B_{12}H_{11}SH$ (BSH), are currently available for BNCT clinical studies (*Figure 1*). Positron emission tomography (PET) is used to estimate the ^{10}B concentration and to determine the eligibility of a patient for BNCT, by calculating the lesion-to-normal (L/N) ratio of ^{18}F-labeled BPA. The uptake in ^{11}C-methionine-PET, which has been more extensively studied for cancer diagnoses, is shown to have a linear correlation with that of ^{18}F-BPA-PET (*Figure 3*), indicating the potential application of ^{11}C-methionine-PET for BNCT dose planning and candidate selection (11). Before neutron irradiation, boron compounds (BSH and/or BPA) are administered intravenously, and then blood samples are drawn serially after the intravenous injection of the boron agent to measure their level in the blood.

Neutron source for BNCT: from reactor to accelerator

The major issues in BNCT research concern the neutron sources, boron compounds, and clinical applications.

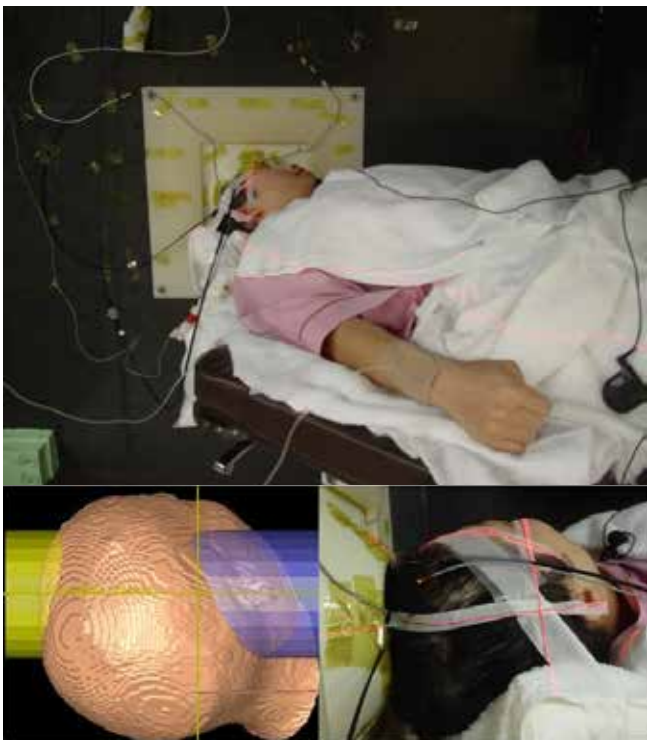

Figure 2 Neutron irradiation room and head positioning at Japan Research Reactor No. 4 (JRR-4). The patient's head position is fixed under the laser-guided positioning device in the neutron irradiation room. The relation between the beam direction and the patient's head position is also shown

BNCT research has been conducted for more than 60 years using nuclear research reactors. The first clinical studies for malignant brain tumors were performed at Brookhaven National Laboratory (BNL) and Massachusetts Institute of Technology (MIT) in 1950s and 1960s. In these early BNCT trials, low-energy thermal neutron beams were used for irradiation; however, because of shallow penetration, BNCT with thermal neutrons required craniotomy, to allow the neutrons to reach deeper regions of the brain.

In the 1990s, external beam BNCT using higher-energy (0.53-10 keV) epithermal neutrons was initiated using the Brookhaven Medical Research Reactor (BMRR) at BNL and a High Flux Reactor (HFR) at Petten, the Netherlands. This extended the therapeutic range deeper into the brain from 4 to 8 cm, and allowed the application of nonoperative external beam irradiation (12).

A typical research reactor for BNCT has only one irradiation port fixed in the side wall of the irradiation room, and this limits achieving desirable dose distribution compared to the current multiple field irradiation or conformation radiotherapy. The locations of research reactors usually require the transfer of the patient from a hospital, and this is unusually not possible until a few weeks after surgery. In Japan, the availability of machine time is limited by research projects, maintenance, and inspections. To resolve these nuclear reactor limitations, in-hospital accelerator-based neutron sources have been developed

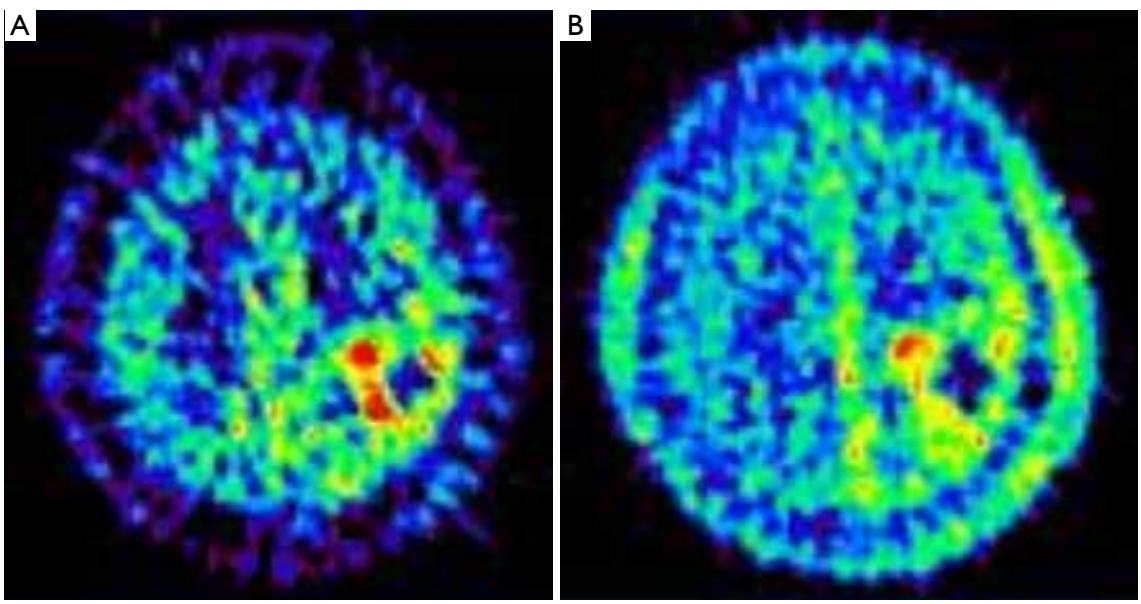

Figure 3 ^{11}C-Methionine-PET (A) and ^{18}F-BPA-PET (B) of a left frontal glioblastoma (GBM). Similar uptake is shown at the posteromedial wall of the surgical cavity

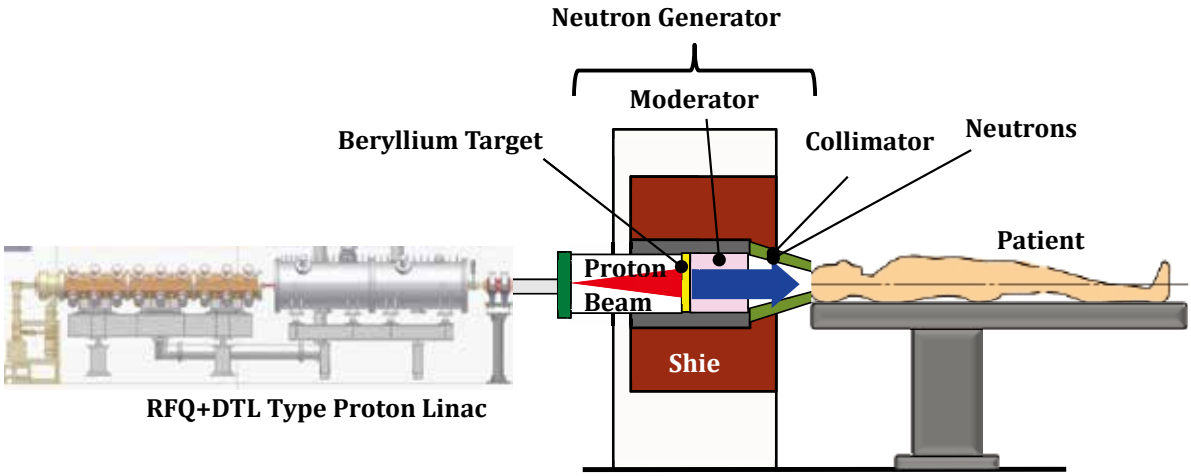

Figure 4 Schematic drawing of the linac-based beryllium target accelerator BNCT system which is under development in Tsukuba, Japan. Reduced proton energy (8 MeV) and current (10 mA) of a radio-frequency quadrupole (RFQ) linac and a drift-tube-linac (DTL) as proton accelerators minimize activation of the target and other materials of the neutron generator device, but are high enough to generate an epithermal neutron flux >1.0^9 n/cm^2/s. A schematic drawing of the linac-based BNCT device is also shown

and are now providing neutron beams for clinical study of BNCT. The accelerator BNCT system consists of a proton accelerator, target, moderator, collimator, and irradiation room, and neutrons are provided by the reaction of the target material (Be, Li, etc.) and the accelerated protons (*Figure 4*). The first clinical trial of BNCT for brain tumors using the beryllium target accelerator system was initiated at KURRI in Japan in late 2012.

Boron compound and delivery system

A variety of boron delivery agents have been investigated to date, including amino acids, porphyrins, nanoparticles, polyamines, biochemical precursors, DNA-binding agents, sugars, antisense agents, peptides, proteins, monoclonal antibodies, and liposomes. However, there are only two boron delivery agents available for clinical BNCT trials for malignant glioma: ^{10}B-enriched BPA and BSH (*Figure 1*). ^{10}B constructs 20% of natural nonradioactive boron and has high efficiency in capturing thermal neutrons to generate boron neutron capture reaction, ^{10}B(n, α) ^{7}Li (13). Successful BNCT is dependent on the selective accumulation and absolute level of ^{10}B atoms in tumor cells.

These boron delivery agents must be as safe as glucose, and drug administration of gram-order is commonly needed to achieve a high enough intracellular boron level to sterilize tumor cells. A boron delivery agent should be non-toxic at the clinically effective doses, achieve at least 10-30 μg ^{10}B/g of tumor, have high tumor/brain and tumor/blood concentration ratios, and show rapid clearance from the blood circulation and normal tissues (but persist in the tumor). They should also be water soluble and chemically stable (14).

BPA has structural characteristics similar to those of a melanin precursor, and promising clinical results were shown in a pilot study of BNCT for skin melanoma (14). BPA is usually administered intravenously as a soluble fructose complex, BPA-F, at doses ranging from 250 to 900 mg BPA/kg. BPA can penetrate across the blood-brain barrier into the normal brain, and is actively transported through the tumor cell membrane due to the elevated rate of amino acid transport in proliferating cells. Although the uptake of BPA depends highly on individual tumors, high tumor-to-normal-BPA-uptake ratios (2.1-7.1) were demonstrated in an ^{18}F-BPA-PET study of newly diagnosed GBMs (15).

BSH biodistribution studies have suggested that BSH is distributed through passive diffusion from the blood to tumor tissues via the disrupted blood-brain barrier. The boron concentration in the normal brain with an intact blood-brain barrier remains minimal, whereas the tumor ^{10}B concentration is related to both the tumor vessel density and the blood ^{10}B level. Tumor-to-blood boron concentration ratios ranging from 0.5 to 1.0 have been reported in human patients treated with BSH-mediated BNCT (12). Vascular irritation, fever, skin reaction (erythema), and peripheral

vasoconstriction have been reported as probable adverse effects of BSH injection (10). Japanese clinical trials have used a combination of BPA and BSH based on experimental data which showed these different compounds accumulate in different subpopulations of tumor cells (12).

Clinical studies of BNCT

In a clinical trial using epithermal neutrons at the BNL in which 53 GBMs were irradiated to evaluate the safety and effectiveness of external beam BNCT (16,17), no major adverse events were found following the 2-h intravenous injection of BPA-F at a dose of 250 to 330 mg/kg. However, patients who received 330 mg/kg BPA showed precipitates in the urine. MST following one, two and three field (one fraction each) BNCT were 14.8, 12.1 and 11.9 mos, respectively. Two of the seven subjects received an average brain dose (ABD) of 8 Gy-Eq or above, using three fields, and had grade 3 CNS toxicity. An ABD of 6.2 Gy-Eq was associated with 50% incidence of somnolence. Other grade 3 radiation toxicity was ototoxicity (17,18).

In the clinical trial at Harvard/MIT (19), no adverse event was found in relation to the intravenous injection of 250 mg/kg over 1 h, 300 mg/kg over 1.5 h, and 350 mg/kg over 1.5 h. The tumors with volumes <60 cm^3 and >60 cm^3 were associated with a 19% and 67% incidence of developing grade 3 or higher toxicity, respectively. Experimental data suggest that a longer infusion time up to 6 hours may improve the homogeneity of boron accumulation in tumors in BPA-mediated BNCT (20,21). This method was applied to the phase II clinical trial at the Studsvik BNCT facility for 29 patients suffering from GBM, who received 900 mg/kg BPA-F in a 6-h infusion, where the average boron concentration in the blood was 24.7 μg/g (22,23). Four patients developed grade 3-4 toxic events including epileptic seizures, hematuria, thrombosis, and erythema. These events except for seizures may relate to BPA administration. The median progression free survival and median MST were 5.8 and 17.7 mos, respectively.

The Finnish phase I/II trial showed that the BPA dose level of 450 mg/kg was the optimal dose for further BNCT studies of newly diagnosed GBM (24,25). In that study, 290 mg/kg of BPA was infused over 2 h in the first 12 patients suffering from GBM using two fields, and the BPA dose to subsequent patients was escalated from 330 mg/kg (n=1) to 360 mg/kg (n=3), 400 mg/kg (n=3), 450 mg/kg (n=3), and 500 mg/kg (n=8). The maximum tolerated dose was reached at the BPA dose level of 500 mg/kg, where grade 3 (n=2) and grade 4 (n=1) CNS toxicity was found. Kankaanranta *et al*. (26) also reported a phase I dose escalation study for recurrent malignant glioma after initial treatment using X-ray fractionated radiotherapy at a dose of 50 to 61Gy, and they recommended up to 400 mg/kg L-BPA as a 2-h infusion. The MST values for the dose groups of 290, 330/360, 400, 450, and 500 mg BPA/kg were 13.4, 11.0, 16.9, 21.9 and 14.7 mos, respectively. The other studies' protocol using long-term infusions showed that the median time from BNCT treatment to tumor progression was 5.8 mos, and the MST after BNCT was 14.2 mos (22,23).

The longer perfusion method was also employed in a trial at Osaka Medical College (700 mg/kg for 6 h) (15). Experimental data also suggest that the combination of BNCT and photon radiation leads to significant gains in survival (21). In the trial conducted at Osaka Medical College, the first 10 patients suffering from GBM were administered 100 mg/kg of BSH and 250 mg/kg of BPA in a 1-h infusion (protocol 1), and the latter 11 patients were administered 100 mg/kg of BSH and 700 mg/kg of BPA in a 6-h infusion (protocol 2). A 2 Gy daily fraction of X-ray irradiation was added in protocol 2 for a total dose of 20 to 30 Gy. The MST for all patients and for protocol 2 patients were 15.6 and 23.5 mos, respectively (15).

In a trial at the University of Tsukuba and Tokushima University at Japan Research Reactor No. 4 (JRR-4) of the Japan Atomic Energy Agency (JAEA) (10), the low dose (250 mg/kg) of BPA was administered over 1 h and 5 g BSH /kg was infused over 1 h in 8 patients with a single irradiation field. These patients received additional photon radiation defining the signal abnormality in T2-weighted MRI after the completion of BNCT. The MST and the time to progression were 27.1 and 11.9 mos, respectively. The 1-year and 2-year survival rates were 87.5% and 62.5%, respectively. This small number of patients showed the most favorable outcome with BNCT to date and treatment was well tolerated without severe acute or subacute adverse events. Four of 15 patients showed delayed radiation necrosis and median survival time of 4 patients including 1 alive patient was 43.4 mos (15.1-76.0). Although it is not certain whether the additional photon irradiation has a role in the clinical response to BNCT, the survival of the small cohort seemed to be favorable.

The clinical studies for newly diagnosed GBM revealed that the median time to progression varies from 6 to 12 mos and the MST varies from 12 to 27 mos after BNCT as an initial treatment (10). More clinical data are needed to confirm

the effectiveness of this modality, although the existing results appear promising, and warrant further investigation. Future areas of research include clinical applications, the development of new boron delivery agents, and accelerator neutron sources.

Acknowledgements

This study was supported in part by the Grant-in-Aid for Society Collaboration from the Ministry of Education, Science and Culture, Japan (22591604).
Disclosure: The authors declare no conflict of interest.

References

1. Stummer W, Pichlmeier U, Meinel T, et al. Fluorescence-guided surgery with 5-aminolevulinic acid for resection of malignant glioma: a randomised controlled multicentre phase III trial. Lancet Oncol 2006;7:392-401.
2. Nimsky C, Ganslandt O, Buchfelder M, et al. Intraoperative visualization for resection of gliomas: the role of functional neuronavigation and intraoperative 1.5 T MRI. Neurol Res 2006;28:482-7.
3. Stewart LA. Chemotherapy in adult high-grade glioma: a systematic review and meta-analysis of individual patient data from 12 randomised trials. Lancet 2002;359:1011-8.
4. Fadul CE, Wen PY, Kim L, et al. Cytotoxic chemotherapeutic management of newly diagnosed glioblastoma multiforme. J Neurooncol 2008;89:339-57.
5. Stupp R, Mason WP, van den Bent MJ, et al. Radiotherapy plus concomitant and adjuvant temozolomide for glioblastoma. N Engl J Med 2005;352:987-96.
6. Westphal M, Hilt DC, Bortey E, et al. A phase 3 trial of local chemotherapy with biodegradable carmustine (BCNU) wafers (Gliadel wafers) in patients with primary malignant glioma. Neuro Oncol 2003;5:79-88.
7. Valtonen S, Timonen U, Toivanen P, et al. Interstitial chemotherapy with carmustine-loaded polymers for high-grade gliomas: a randomized double-blind study. Neurosurgery 1997;41:44-8; discussion 48-9.
8. Tanaka M, Ino Y, Nakagawa K, et al. High-dose conformal radiotherapy for supratentorial malignant glioma: a historical comparison. Lancet Oncol 2005;6:953-60.
9. Fitzek MM, Thornton AF, Rabinov JD, et al. Accelerated fractionated proton/photon irradiation to 90 cobalt gray equivalent for glioblastoma multiforme: results of a phase II prospective trial. J Neurosurg 1999;91:251-60.
10. Yamamoto T, Nakai K, Kageji T, et al. Boron neutron capture therapy for newly diagnosed glioblastoma. Radiother Oncol 2009;91:80-4.
11. Nariai T, Ishiwata K, Kimura Y, et al. PET pharmacokinetic analysis to estimate boron concentration in tumor and brain as a guide to plan BNCT for malignant cerebral glioma. Appl Radiat Isot 2009;67:S348-50.
12. Yamamoto T, Nakai K, Matsumura A. Boron neutron capture therapy for glioblastoma. Cancer Lett 2008;262:143-52.
13. Nielsen FH. Micronutrients in parenteral nutrition: boron, silicon, and fluoride. Gastroenterology 2009;137:S55-60.
14. Coderre JA, Turcotte JC, Riley KJ, et al. Boron neutron capture therapy: cellular targeting of high linear energy transfer radiation. Technol Cancer Res Treat 2003;2:355-75.
15. Kawabata S, Miyatake S, Kuroiwa T, et al. Boron neutron capture therapy for newly diagnosed glioblastoma. J Radiat Res 2009;50:51-60.
16. Chanana AD, Capala J, Chadha M, et al. Boron neutron capture therapy for glioblastoma multiforme: interim results from the phase I/II dose-escalation studies Neurosurgery 1999;44:1182-92; discussion 1192-3.
17. Diaz AZ. Assessment of the results from the phase I/II boron neutron capture therapy trials at the Brookhaven National Laboratory from a clinician's point of view. J Neurooncol 2003;62:101-9.
18. Coderre JA, Hopewell JW, Turcotte JC, et al. Tolerance of normal human brain to boron neutron capture therapy. Appl Radiat Isot 2004;61:1083-7.
19. Busse PM, Harling OK, Palmer MR, et al. A critical examination of the results from the Harvard-MIT NCT program phase I clinical trial of neutron capture therapy for intracranial disease. J Neurooncol 2003;62:111-21.
20. Yoshida F, Matsumura A, Shibata Y, et al. Cell cycle dependence of boron uptake from two boron compounds used for clinical neutron capture therapy. Cancer Lett 2002;187:135-41.
21. Barth RF, Coderre JA, Vicente MG, et al. Boron neutron capture therapy of cancer: current status and future prospects. Clin Cancer Res 2005;11:3987-4002.
22. Henriksson R, Capala J, Michanek A, et al. Boron neutron capture therapy (BNCT) for glioblastoma multiforme: a phase II study evaluating a prolonged high-dose of boronophenylalanine (BPA). Radiother Oncol 2008;88:183-91.
23. Sköld K, H-Stenstam B, Diaz AZ, et al. Boron Neutron Capture Therapy for glioblastoma multiforme: advantage of prolonged infusion of BPA-f. Acta Neurol Scand

2010;122:58-62.
24. Joensuu H, Kankaanranta L, Seppälä T, et al. Boron neutron capture therapy of brain tumors: clinical trials at the finnish facility using boronophenylalanine. J Neurooncol 2003;62:123-34.
25. Kankaanranta L, Koivunoro H, Kortesniemi M, et al. BPA-based BNCT in the treatment of glioblastoma multiforme. A dose escalation study. In: Zonta A, Altieri S, Roveda L, et al. eds. Proceedings of the 13th international congress of neutron capture therapy, EANA, Rome, 2008,30.
26. Kankaanranta L, Seppälä T, Koivunoro H, et al. L-boronophenylalanine-mediated boron neutron capture therapy for malignant glioma progressing after external beam radiation therapy: a Phase I study. Int J Radiat Oncol Biol Phys 2011;80:369-76.

Cite this article as: Yamamoto T, Tsuboi K, Nakai K, Kumada H, Sakurai H, Matsumura A. Boron neutron capture therapy for brain tumors. Transl Cancer Res 2013;2(2):80-86. doi: 10.3978/j.issn.2218-676X.2013.04.11

Review Article

Proton therapy for head and neck cancer: current applications and future directions

Alexander Lin, Samuel Swisher-McClure, Laura Bonner Millar, Maura Kirk, Caitlyn Yeager, Ali Kassaee, Boong-Keng Kevin Teo, Stephen M. Hahn

Department of Radiation Oncology, University of Pennsylvania, Philadelphia, PA, USA

Correspondence to: Alexander Lin, M.D. University of Pennsylvania, Department of Radiation Oncology, 3400 Civic Center Blvd., TRC 2 West, Philadelphia, PA, USA. Email: alexander.lin@uphs.upenn.edu.

Abstract: Radiation therapy is a standard treatment modality for head and neck cancer. However, delivery of radiation therapy to areas of disease in close proximity to critical normal structures, can potentially result in severe toxicity. While advances in conformal radiation techniques, like intensity-modulated radiation therapy (IMRT) have led to improvements in the therapeutic ratio, significant treatment-related morbidity still exists. Proton therapy is an emerging and promising treatment modality for head and neck cancers, because of the potential to improve organ sparing and/or safely escalate doses of radiation delivered. Localized radiation therapy to limited areas of the head and neck, such as for a lateralized salivary gland tumor, can be delivered with proton therapy using current techniques. Proton therapy to the bilateral neck, as required for locally-advanced disease, will require the development of intensity-modulated techniques, intensity-modulated proton therapy (IMPT), using pencil beam scanning. Determining the proper role of proton therapy for head and neck cancer should be done in the setting of clinical studies, with careful attention to quality assurance, and meaningful measures of disease control, toxicity and quality of life.

Keywords: Head and neck cancer; proton therapy; radiation therapy

doi: 10.3978/j.issn.2218-676X.2012.12.01

Scan to your mobile device or view this article at: http://www.thetcr.org/article/view/786/html

Radiation therapy for head and neck cancer: indications and challenges

External beam radiation therapy (EBRT) is a well-established therapeutic modality in the treatment of head and neck cancer, with more than 80% of patients diagnosed with head and neck cancer receiving EBRT as a portion of their therapy. For early-stage cancers, it is often used as the primary treatment, obtaining high local control rates with limited fields (1,2). For locally advanced cancers, it is the standard treatment for cancers not amenable to surgical resection, such as nasopharynx cancer (3), and as an organ-preserving alternative to surgery for cancers such as larynx cancer (4,5). In the post-operative setting for locally-advanced disease with high-risk pathologic features, adjuvant EBRT can improve locoregional control and survival when given alone (6), or in conjunction with chemotherapy (7-9).

EBRT to the head and neck is associated with acute and late toxicity. The need to irradiate areas of disease involvement, which are in close proximity to normal tissues, results in significant radiation exposure to these tissues, with toxicity observed early in the course of treatment. Dose to the oral mucosa results in mucositis, a common side effect which can cause severe pain, difficulty swallowing, and malnutrition due to the inability to eat. Other common acute effects include xerostomia and dysgeusia. These side effects can lead to hospitalization and treatment interruptions (10), which may ultimately adversely affect disease outcomes (11).

Late effects secondary to head and neck radiation are also of concern. Dose to the cochlea can cause hearing loss, particularly in those who have also received platinum-

based chemotherapy. Radiation exposure to the salivary glands causes chronic xerostomia, which can affect eating, communication, pain, and emotion (12), as well as increase the risk of developing dental caries. Patients receiving high doses of radiation to the mandible are at risk for mandibular osteoradionecrosis (13), especially if they require post-radiation dental extractions. Exposure of swallowing structures to radiation can lead to long-term dysphagia (14), aspiration, and chronic reliance on nutritional supplementation, such as via gastrostomy tube. Side effects of radiation to the neck include lymphedema, fibrosis, and hypothyroidism (15). Neck radiation can also potentially cause accelerated carotid atherosclerosis, as evidenced by an increased risk of ischemic stroke after RT in younger (16) and older patients (17). Due to the changing epidemiology of head and neck cancer, with an increasing proportion of younger patients developing human-papilloma virus (HPV) positive oropharynx cancer who are treated and cured at high rates (18), minimizing long-term radiation-related morbidity will become increasingly important.

Advances in photon-based external beam radiation therapy: 3-D conformal radiotherapy (3-D CRT) and intensity-modulated radiation therapy (IMRT)

Technical advancements in photon-based radiotherapy, such as with 3-D CRT and IMRT, allow for a more conformal deposition of the high-dose region and therefore, an improved therapeutic ratio. Three-dimensional conformal planning utilizes multiple radiation beams shaped by a static multileaf collimator in an effort to better conform radiation dose to the targets of interest. IMRT further improves this process, through the use of a dynamic multileaf collimator that can modulate both the shape and intensity of individual beams to create an optimal dose distribution to treat disease and further spare normal tissues (*Figure 1*). The addition of daily image guidance (IGRT) has led to a decrease in the planning target volume (PTV) for radiation, which has the potential of decreasing normal tissue exposure to high-dose radiation without compromising locoregional control (19).

Although direct comparisons of IMRT to conventional radiation are limited, the literature supports its use given the promising results obtained with respect to disease control, toxicity, and quality of life. The University of California-San Francisco has reported their experience of treating nasopharynx cancer with IMRT (20). A total of 35 patients were treated, and at a median follow-up of 21.8 months, locoregional control was 100%. An update of their experience, which included 67 patients with a median follow-up of 31 months, continued to show an excellent 4-year locoregional control rate of 98% (21). Compared to conventional radiation, IMRT is superior in its ability to reduce dose to critical normal organs. An example of this is sparing the parotid gland (*Figure 2*) to minimize risk of long-term xerostomia, which can impair quality of life (12). A matched case-control study comparing IMRT to standard radiotherapy for head and neck cancer found that xerostomia and quality of life improved over time (starting at 6 months post-treatment) after IMRT, but not after standard RT (22). A phase III multicenter trial (PARSPORT) randomized 94 patients to receive either IMRT or conventional RT and found that parotid-sparing IMRT significantly reduced the incidence of long-term xerostomia, and improved quality of life (23).

IMRT has also been used in the context of comprehensive nodal radiation of the neck to spare swallowing structures and minimize risk of long-term dysphagia (*Figure 3*). A prospective, clinical study of 73 patients with stage III or IV oropharynx cancer treated with concurrent chemotherapy and IMRT at the University of Michigan found that efforts to spare the pharyngeal constrictors with IMRT could be done safely (3-year locoregional control 96%), and effectively (only 1 patient was feeding tube dependent 12 months after completion of IMRT) (24). They reported that long-term measures of swallowing were only slightly worse than pre-therapy baseline levels, and found a correlation between the mean doses delivered to swallowing organs and long-term dysphagia (25). However, even with IMRT, toxicity remains a pertinent issue, with rates of long-term gastrostomy tube dependence as high as 20% (26), and impaired quality of life secondary to chronic xerostomia and dysphagia (27). Efforts to explore methods to decrease dose to normal tissues, such as with proton therapy, are therefore warranted.

Proton therapy: potential advantages

Unlike photon radiation, proton therapy offers the added advantages of less dose delivered to tissues proximal to the tumor and rapid dose fall off at the distal edge of the tumor (Bragg-Peak effect, *Figure 4*). This allows for potential gains with respect to normal organ sparing and provides opportunities for potential dose escalation. Applied in the treatment of head and neck cancer, proton therapy could be utilized in the following ways:

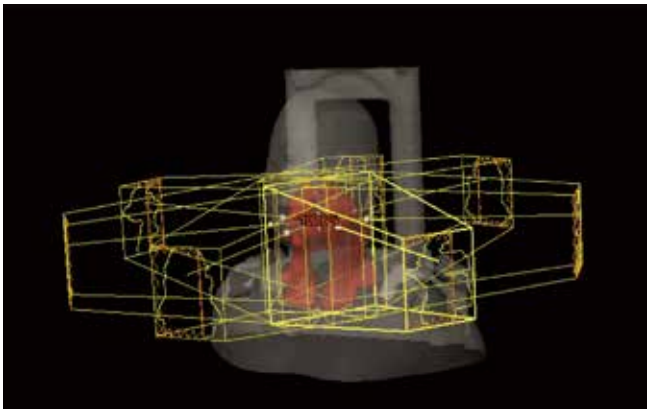

Figure 1 Patient with a stage IVa, base of tongue squamous cell carcinoma. IMRT plan for definitive radiotherapy to primary site and bilateral neck, using seven coplanar, equidistant beams with multileaf collimator

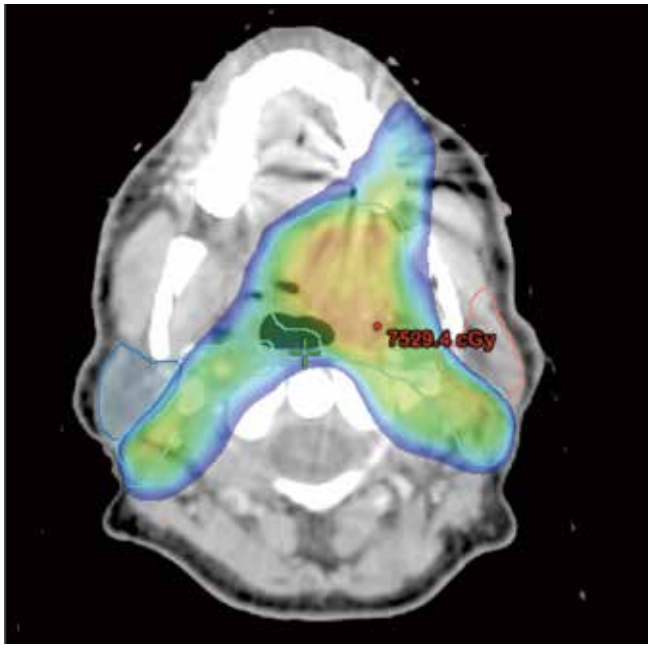

Figure 2 Stage IVa T4aN2aM0 squamous cell carcinoma of the left base of tongue, treated with definitive chemoradiation, using an IMRT technique (dose color wash set to lower limit of 57 Gy). The planning target volume (PTV, in light blue) is being covered with high dose, while the contralateral parotid gland (blue) is being spared to a mean dose of 25 Gy

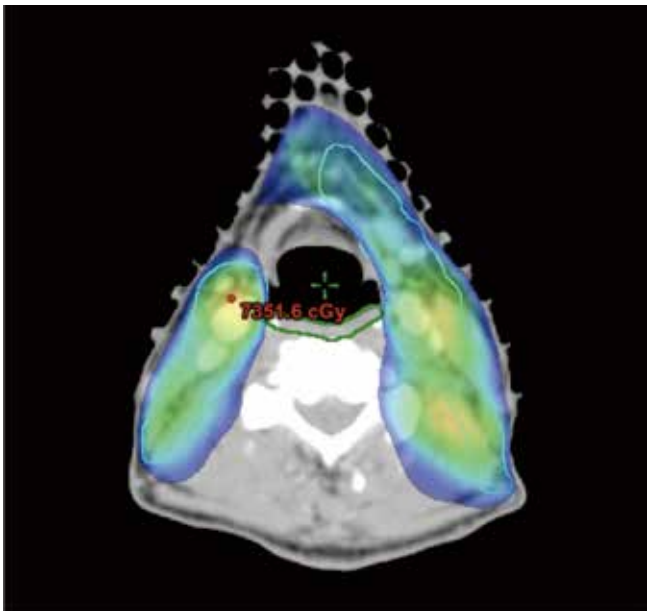

Figure 3 Sparing of swallowing structures. IMRT plan for the patient described in Figure 2 (dose color wash set to lower limit of 57 Gy). Even with elective nodal radiation of the bilateral necks (PTV in light blue), the midline, pharyngeal constrictors (green) are being spared to a mean dose of 48 Gy

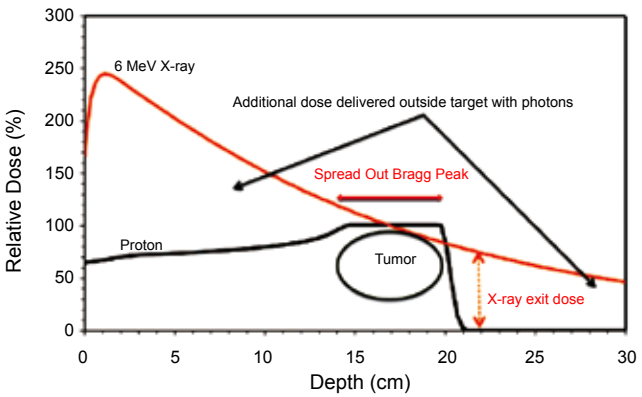

Figure 4 The physics of proton therapy. X-rays deliver a greater dose outside the target for the same dose within the target as protons

(I) Dose escalation for cancers where locoregional control is currently limited by an inability to adequately deliver therapeutic doses without excessive risk of toxicity.

(II) Minimizing exposure of normal tissues and decreasing toxicity in patients for whom long-term control is obtained with currently-prescribed doses, but at the cost of potential significant toxicity.

Multiple comparative planning studies have shown

that the dose distribution attainable with proton therapy appear superior to those possible with photon radiation. Two separate studies from the Paul Scherrer Institute, each derived from the CT scans of 5 patients treated for head and neck cancer, explored the potential benefits of proton radiotherapy compared to conventional treatment. The first study, in which 3-D conformal radiation was compared to IMRT and proton therapy (passively scattered and spot scanned), demonstrated that proton therapy provided the best dose homogeneity with respect to PTV coverage, as well as spinal cord and parotid gland sparing (28). The second study, a comparison of IMRT versus intensity-modulated proton therapy (IMPT) showed that critical organs were optimally spared with IMPT, with lower estimated secondary cancer risks as a result of lower integral dose received by normal tissue (29). Reduced second-malignancy risk also appears to be an advantage for non-IMPT, double-scatter proton therapy (30), even despite concerns about secondary neutrons from protons causing second malignancies. This risk should be significantly lower with the implementation of IMPT, given the reduced secondary neutron scatter associated with this technique.

For treatment of sinonasal tumors (for which adequate dose delivery is often limited due to the proximity of normal organs), proton-based planning was superior to conventional, conformal, as well as IMRT for normal organ sparing (31), while IMPT was superior to IMRT in sparing normal organs at both low- and high-dose levels (32). To study the potential gains with respect to long-term dysphagia, van der Laan *et al.* (33) conducted a comparative study in which IMPT plans were generated for 25 patients who were treated with IMRT to the bilateral neck for oropharynx or hypopharynx cancer. In an adaptive planning study, initial and re-simulation CT images from 10 patients with head and neck cancer were used to compare differences in doses to normal structures with non-adaptive and adaptive IMRT and IMPT replanning (34). Adaptive IMPT significantly reduced doses to multiple critical structures when compared against non-adaptive IMPT, and reduced doses to all critical structures when compared to non-adaptive and adaptive photon planning.

While planning studies clearly show the dosimetric advantages of proton therapy over photon radiation, clinical implementation and correlation to outcomes have been largely limited to small, single-institution series. Early results of local control appear promising, especially in anatomic sites in which organs at risk currently limit delivery of adequate photon doses. The Massachusetts General Hospital reported a 2-year locoregional control rate of 86% in their series of 20 patients with locally advanced sphenoid sinus malignancies treated with proton beam to a median dose of 76 Gy (35). Treatment appears well-tolerated, as evidenced by the published acute and late-toxicity rates. Tokuuye *et al*. reported toxicity results on 33 patients who received definitive proton therapy to a median dose of 76 Gy, at 2.8 Gy per fraction, with one (3%) and six (18%) patients experiencing > grade 3 acute and late toxicity, respectively (36). The Heidelberg ion therapy center published one of the largest series, in which 118 patients with skull base tumors were treated with proton and carbon ion radiotherapy (37). Few side effects were observed, which were mainly grade 1. The administration of large doses per fraction with protons also appears safe. In a pilot study of 14 patients with mucosal melanoma of the head and neck treated with proton therapy three times per week for 15 fractions to a total dose of 60 Gy, all patients were able to receive the full dose of therapy (38). Initial local control was 85.7%, and at a median follow-up of 3 years, there were no treatment-related deaths. Twenty-one percent of patients experienced grade 3 mucositis, 2 patients had unilateral decrease in visual acuity.

Although these data are encouraging, there are several factors which limit the ability to draw definitive conclusions regarding proton therapy. First, proton therapy is associated with uncertainties in dose delivery typically related to uncertainty regarding the precise location of the distal edge of the Bragg peak (39-42). Second, many of the dosimetric advantages of proton radiotherapy seen in planning studies were achieved with pencil-beam scanning and IMPT, a modality which still requires further technical development and ideally, means for *in vivo* range verification prior to clinical implementation. Third, worldwide, there are still relatively few proton therapy centers, which has limited the ability to treat and analyze a large number of patients and determine the most appropriate indications for proton therapy. Additional comparative effectiveness research is needed to best understand the benefit of proton therapy for specific patient populations and clinical conditions (43).

Current indications and future applications: the University of Pennsylvania experience

At our institution, there are several indications for delivering proton therapy for head and neck cancer. One indication is for treating patients with salivary gland cancers.

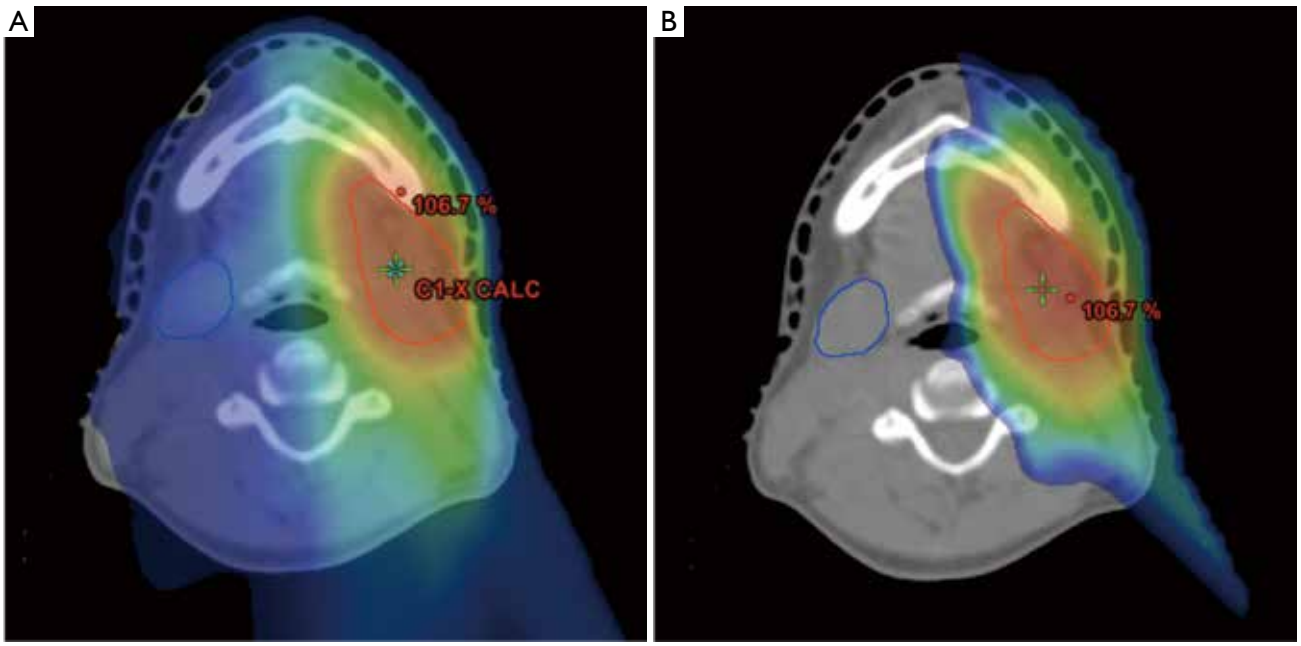

Figure 5 Patient with left submandibular gland adenoid cystic carcinoma. Tumor volume outlined in red, right submandibular gland in blue (dose color wash set at lower limit of 7 Gy). A. IMRT plan, with low dose delivered to the contralateral submandibular gland; B. Double scattering proton plan, with low dose limited to the ipsilateral neck

Previously, these patients were treated with IMRT, but are now currently treated with double scattering or uniform scanning proton therapy, as shown in *Figure 5*. When compared to IMRT, proton therapy can decrease dose to adjacent normal organs such as the brainstem, cochlea, temporal lobe, and the contralateral salivary glands. Other dosimetric advantages include limiting the area of low dose radiation delivered to normal tissues. These dosimetric gains could potentially translate to improved long-term results such as decreasing rates of chronic xerostomia and radiation-induced secondary malignancies. The potential decrease in radiation-induced malignancy with proton therapy is of particular importance, given the increasing incidence of oropharynx cancer (44), which is typically diagnosed in younger patients, and for whom long-term disease control is likely (18).

Pencil beam scanning is being used for the treatment of base of skull malignancies. Treatment of tumors at this particular site with conventional radiation has traditionally been limited by an inability to deliver adequate doses of radiation without exceeding constraints on critical structures in the brain and optic apparatus. Unlike double scattering or uniform scanning proton therapy, pencil beam scanning allows for enhanced conformal dose around critical structures through modulation of dose in depth, while retaining the rapid dose fall-off from the Bragg-Peak effect (*Figure 6*). For both of these indications, it is critical to enroll patients on clinical trials or registries to collect outcome data, thereby assessing the effectiveness and role of proton therapy.

Another indication is for reirradiation for recurrent head and neck cancer. Patients who require head and neck reirradiation generally have poor outcomes, with median survival typically less than 12 months, and reirradiation limited by treatment-related morbidity (45-48). Proton therapy, by potentially allowing for high-dose reirradiation while decreasing normal tissue exposure, may lead to improved outcomes. Lin *et al*. reported results on 16 patients reirradiated with protons for recurrent nasopharyngeal carcinoma (49), for which 2-year local control and overall survival were approximately 50%. Priority was given to minimizing toxicity (no patients experienced CNS toxicity) over tumor coverage. The 2-year survival was significantly higher in those with "optimal" dose-volume histogram coverage versus those with "suboptimal" coverage (83% and 17%, respectively, P=0.006). Patients who require head and neck reirradiation with proton therapy at the University of Pennsylvania are

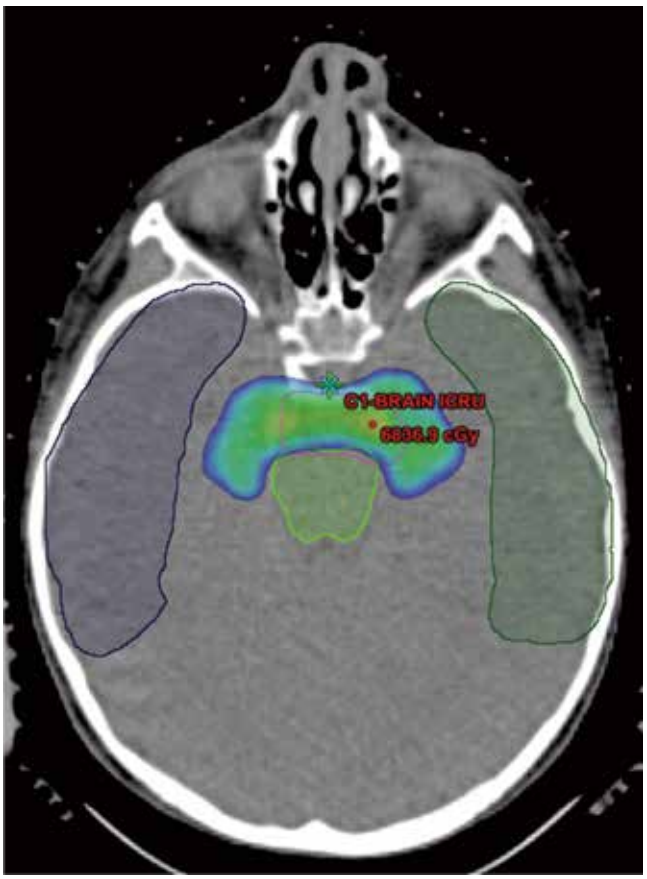

Figure 6 Pencil beam scanning proton plan for treatment to a skull base chordoma. The high-dose region is limited to the area of disease (red), sparing adjacent brainstem (green), as well as the bilateral temporal lobes (dark blue and dark green)

currently enrolled on clinical study, with the hopes that improving coverage of affected areas while minimizing normal tissue toxicity can improve clinical outcomes in a population that otherwise has limited options.

Current efforts include the development of pencil beam scanning proton therapy for treatment of the comprehensive, bilateral neck, which is required in the majority of patients with locally advanced mucosal squamous cell carcinoma of the head and neck. In order to take full dosimetric advantage of proton therapy, treatment requires a small beam spot size, which can be difficult to achieve when treating a superficial target, such as the neck. Presently at our institution, the minimum deliverable energy for pencil beam scanning is 100 MeV, requiring the use of a range shifter for treatment of targets that extend within 7.5 cm water-equivalent depth of the skin surface. There is a large air gap, typically greater than 30 cm, between the range shifter and patient surface through which spots scattered in the range shifter increase in size before reaching the target. The incorporation of a tissue-equivalent bolus that conforms and can be placed over the skin of the neck decreases the spot size of the beam at the depth of the neck lymphatics by eliminating the large air gap between the bolus and the patient. Dosimetric plans utilizing such a system show quite promising potential gains compared to IMRT, with possible further sparing of the swallowing structures (*Figure* 7), as well as the ability to protect structures not currently spared via IMRT, such as the submandibular glands (*Figure* 7). We plan to begin treatment of the comprehensive, bilateral neck within the next year by using such an approach. Other technical challenges specific to proton therapy include uncertainties in estimating proton stopping power from the planning CT image especially in cases with substantial CT image artifacts and sensitivity to anatomical changes such as patient setup or weight loss that may impact the dose distribution. Further research to quantify and minimize the impact of image artifacts is necessary to ensure robust proton therapy. Adaptive therapy and replanning during the course of therapy may be a clinical necessity in proton therapy given the dosimetric sensitivity to anatomical changes.

While from a dosimetric perspective, proton therapy appears superior to IMRT, it is still unclear whether these physical advantages translate to improved clinical outcomes. Therefore, the importance of enrolling patients who are to receive proton therapy on clinical studies cannot be overstated. These studies should have carefully described clinical endpoints, such as disease control, toxicity, and quality of life, and patients receiving proton therapy should ideally be compared to a control cohort receiving IMRT. At our institution, the goal is for all patients receiving proton therapy to be enrolled on a clinical study and/or registry. In patients receiving CNS or base of skull proton therapy, neuropsychiatric testing is performed routinely before, during and after treatment to assess the neurocognitive changes secondary to RT. In our pending implementation of bilateral neck proton therapy, we plan to assess patients with objective, functional swallow testing as well as with general, head and neck, and xerostomia-specific quality of life inventories prior, during, and after treatment. Results will then be compared to a matched cohort of patients receiving IMRT, in order to correlate dosimetric with clinical advantages.

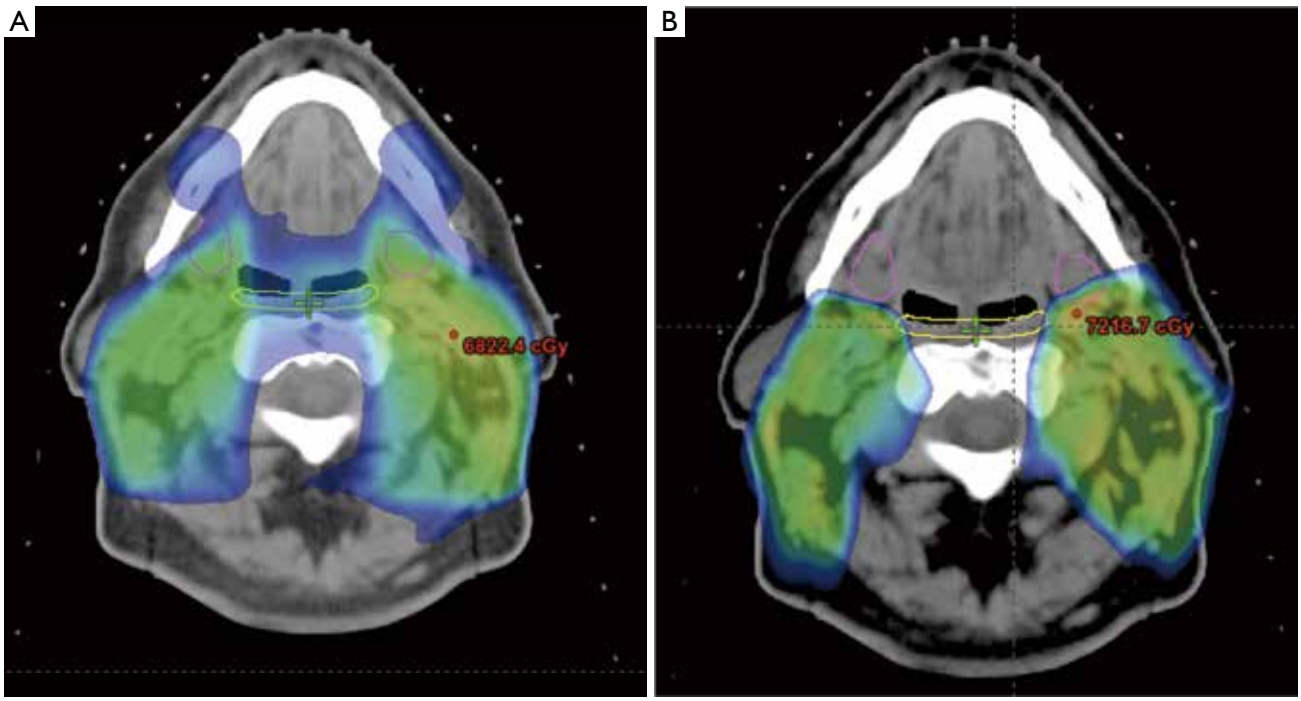

Figure 7 Patient with locally advanced larynx cancer treated with definitive chemoradiation (dose color wash set to lower limit of 45 Gy). A. Delivered IMRT plan, with areas of high dose exposure to the bilateral submandibular glands (pink) and pharyngeal constrictors (yellow); B. Pencil beam proton plan, with significant sparing of both submandibular glands (right submandibular gland mean dose 59 Gy with IMRT *vs.* 32 Gy with IMPT) and pharyngeal constrictors (mean dose 52 Gy with IMRT *vs.* 39 Gy with IMPT)

Conclusions

Proton therapy is a promising and emerging modality of radiation therapy for patients with head and neck cancers. The physical advantages inherent to protons, with rapid dose fall off, can yield improvements in the ability to escalate radiation dose, or to better spare organs at risk. Although emerging clinical data are promising, new techniques, such as pencil beam scanning and IMPT need to be developed further in order to overcome current limitations, and to potentially expand the indications under which proton therapy should be considered. Patients should ideally be treated on clinical study and compared, when possible, to a similar cohort of patients treated with IMRT.

Acknowledgements

Disclosure: None of the authors report any relevant disclosures or conflicts of interest as it pertains to this manuscript.

References

1. Yamazaki H, Nishiyama K, Tanaka E, et al. Radiotherapy for early glottic carcinoma (T1N0M0): results of prospective randomized study of radiation fraction size and overall treatment time. Int J Radiat Oncol Biol Phys 2006;64:77-82.
2. O'Sullivan B, Warde P, Grice B, et al. The benefits and pitfalls of ipsilateral radiotherapy in carcinoma of the tonsillar region. Int J Radiat Oncol Biol Phys 2001;51:332-43.
3. Al-Sarraf M, LeBlanc M, Giri PG, et al. Chemoradiotherapy versus radiotherapy in patients with advanced nasopharyngeal cancer: phase III randomized Intergroup study 0099. J Clin Oncol 1998;16:1310-7.
4. Induction chemotherapy plus radiation compared with surgery plus radiation in patients with advanced laryngeal cancer. The Department of Veterans Affairs Laryngeal Cancer Study Group. N Engl J Med 1991;324:1685-90.
5. Forastiere AA, Goepfert H, Maor M, et al. Concurrent chemotherapy and radiotherapy for organ preservation in advanced laryngeal cancer. N Engl J Med 2003;349:2091-8.

6. Lundahl RE, Foote RL, Bonner JA, et al. Combined neck dissection and postoperative radiation therapy in the management of the high-risk neck: a matched-pair analysis. Int J Radiat Oncol Biol Phys 1998;40:529-34.
7. Bernier J, Domenge C, Ozsahin M, et al. Postoperative irradiation with or without concomitant chemotherapy for locally advanced head and neck cancer. N Engl J Med 2004;350:1945-52.
8. Cooper JS, Pajak TF, Forastiere AA, et al. Postoperative concurrent radiotherapy and chemotherapy for high-risk squamous-cell carcinoma of the head and neck. N Engl J Med 2004;350:1937-44.
9. Bernier J, Cooper JS, Pajak TF, et al. Defining risk levels in locally advanced head and neck cancers: a comparative analysis of concurrent postoperative radiation plus chemotherapy trials of the EORTC (#22931) and RTOG (# 9501). Head Neck 2005;27:843-50.
10. Trotti A, Bellm LA, Epstein JB, et al. Mucositis incidence, severity and associated outcomes in patients with head and neck cancer receiving radiotherapy with or without chemotherapy: a systematic literature review. Radiother Oncol 2003;66:253-62.
11. Cox JD, Pajak TF, Marcial VA, et al. Interruptions adversely affect local control and survival with hyperfractionated radiation therapy of carcinomas of the upper respiratory and digestive tracts. New evidence for accelerated proliferation from Radiation Therapy Oncology Group Protocol 8313. Cancer 1992;69:2744-8.
12. Lin A, Kim HM, Terrell JE, et al. Quality of life after parotid-sparing IMRT for head-and-neck cancer: a prospective longitudinal study. Int J Radiat Oncol Biol Phys 2003;57:61-70.
13. Tsai CJ, Hofstede TM, Sturgis EM, et al. Osteoradionecrosis and Radiation Dose to the Mandible in Patients With Oropharyngeal Cancer. Int J Radiat Oncol Biol Phys 2013;85:415-20.
14. Eisbruch A, Lyden T, Bradford CR, et al. Objective assessment of swallowing dysfunction and aspiration after radiation concurrent with chemotherapy for head-and-neck cancer. Int J Radiat Oncol Biol Phys 2002;53:23-8.
15. Smith GL, Smith BD, Garden AS, et al. Hypothyroidism in older patients with head and neck cancer after treatment with radiation: a population-based study. Head Neck 2009;31:1031-8.
16. Dorresteijn LD, Kappelle AC, Boogerd W, et al. Increased risk of ischemic stroke after radiotherapy on the neck in patients younger than 60 years. J Clin Oncol 2002;20:282-8.
17. Smith GL, Smith BD, Buchholz TA, et al. Cerebrovascular disease risk in older head and neck cancer patients after radiotherapy. J Clin Oncol 2008;26:5119-25.
18. Ang KK, Harris J, Wheeler R, et al. Human papillomavirus and survival of patients with oropharyngeal cancer. N Engl J Med 2010;363:24-35.
19. Chen AM, Farwell DG, Luu Q, et al. Evaluation of the planning target volume in the treatment of head and neck cancer with intensity-modulated radiotherapy: what is the appropriate expansion margin in the setting of daily image guidance? Int J Radiat Oncol Biol Phys 2011;81:943-9.
20. Sultanem K, Shu HK, Xia P, et al. Three-dimensional intensity-modulated radiotherapy in the treatment of nasopharyngeal carcinoma: the University of California-San Francisco experience. Int J Radiat Oncol Biol Phys 2000;48:711-22.
21. Lee N, Xia P, Quivey JM, et al. Intensity-modulated radiotherapy in the treatment of nasopharyngeal carcinoma: an update of the UCSF experience. Int J Radiat Oncol Biol Phys 2002;53:12-22.
22. Jabbari S, Kim HM, Feng M, et al. Matched case-control study of quality of life and xerostomia after intensity-modulated radiotherapy or standard radiotherapy for head-and-neck cancer: initial report. Int J Radiat Oncol Biol Phys 2005;63:725-31.
23. Nutting CM, Morden JP, Harrington KJ, et al. Parotid-sparing intensity modulated versus conventional radiotherapy in head and neck cancer (PARSPORT): a phase 3 multicentre randomised controlled trial. Lancet Oncol 2011;12:127-36.
24. Feng FY, Kim HM, Lyden TH, et al. Intensity-modulated chemoradiotherapy aiming to reduce dysphagia in patients with oropharyngeal cancer: clinical and functional results. J Clin Oncol 2010;28:2732-8.
25. Eisbruch A, Kim HM, Feng FY, et al. Chemo-IMRT of oropharyngeal cancer aiming to reduce dysphagia: swallowing organs late complication probabilities and dosimetric correlates. Int J Radiat Oncol Biol Phys 2011;81:e93-9.
26. Ingle CJ, Yip K, Caskie V, et al. Intensity modulated radiotherapy (IMRT) in the management of locally advanced oropharyngeal squamous cell carcinomata (SCC): disease control and functional outcome using the therapy outcome measure (TOM) score--report from a single U.K. institution. Head Neck Oncol 2010;2:28.
27. Langendijk JA, Doornaert P, Verdonck-de Leeuw IM, et al. Impact of late treatment-related toxicity on quality of life among patients with head and neck cancer treated with radiotherapy. J Clin Oncol 2008;26:3770-6.

28. Cozzi L, Fogliata A, Lomax A, et al. A treatment planning comparison of 3D conformal therapy, intensity modulated photon therapy and proton therapy for treatment of advanced head and neck tumours. Radiother Oncol 2001;61:287-97.
29. Steneker M, Lomax A, Schneider U. Intensity modulated photon and proton therapy for the treatment of head and neck tumors. Radiother Oncol 2006;80:263-7.
30. Yoon M, Ahn SH, Kim J, et al. Radiation-induced cancers from modern radiotherapy techniques: intensity-modulated radiotherapy versus proton therapy. Int J Radiat Oncol Biol Phys 2010;77:1477-85.
31. Mock U, Georg D, Bogner J, et al. Treatment planning comparison of conventional, 3D conformal, and intensity-modulated photon (IMRT) and proton therapy for paranasal sinus carcinoma. Int J Radiat Oncol Biol Phys 2004;58:147-54.
32. Lomax AJ, Goitein M, Adams J. Intensity modulation in radiotherapy: photons versus protons in the paranasal sinus. Radiother Oncol 2003;66:11-8.
33. van der Laan HP, van de Water TA, van Herpt HE, et al. The potential of intensity-modulated proton radiotherapy to reduce swallowing dysfunction in the treatment of head and neck cancer: A planning comparative study. Acta Oncol 2012. [Epub ahead of print].
34. Simone CB 2nd, Ly D, Dan TD, et al. Comparison of intensity-modulated radiotherapy, adaptive radiotherapy, proton radiotherapy, and adaptive proton radiotherapy for treatment of locally advanced head and neck cancer. Radiother Oncol 2011;101:376-82.
35. Truong MT, Kamat UR, Liebsch NJ, et al. Proton radiation therapy for primary sphenoid sinus malignancies: treatment outcome and prognostic factors. Head Neck 2009;31:1297-308.
36. Tokuuye K, Akine Y, Kagei K, et al. Proton therapy for head and neck malignancies at Tsukuba. Strahlenther Onkol 2004;180:96-101.
37. Rieken S, Habermehl D, Nikoghosyan A, et al. Assessment of early toxicity and response in patients treated with proton and carbon ion therapy at the Heidelberg ion therapy center using the raster scanning technique. Int J Radiat Oncol Biol Phys 2011;81:e793-801.
38. Zenda S, Kawashima M, Nishio T, et al. Proton beam therapy as a nonsurgical approach to mucosal melanoma of the head and neck: a pilot study. Int J Radiat Oncol Biol Phys 2011;81:135-9.
39. Minohara S, Endo M, Kanai T, et al. Estimating uncertainties of the geometrical range of particle radiotherapy during respiration. Int J Radiat Oncol Biol Phys 2003;56:121-5.
40. Engelsman M, Kooy HM. Target volume dose considerations in proton beam treatment planning for lung tumors. Med Phys 2005;32:3549-57.
41. Lu HM. A potential method for in vivo range verification in proton therapy treatment. Phys Med Biol 2008;53:1413-24.
42. Lu HM. A point dose method for in vivo range verification in proton therapy. Phys Med Biol 2008;53:N415-22.
43. Bekelman JE, Shah A, Hahn SM. Implications of comparative effectiveness research for radiation oncology. Practical Radiation Oncology 2011;1:72-80.
44. Marur S, D'Souza G, Westra WH, et al. HPV-associated head and neck cancer: a virus-related cancer epidemic. Lancet Oncol 2010;11:781-9.
45. De Crevoisier R, Bourhis J, Domenge C, et al. Full-dose reirradiation for unresectable head and neck carcinoma: experience at the Gustave-Roussy Institute in a series of 169 patients. J Clin Oncol 1998;16:3556-62.
46. Salama JK, Vokes EE, Chmura SJ, et al. Long-term outcome of concurrent chemotherapy and reirradiation for recurrent and second primary head-and-neck squamous cell carcinoma. Int J Radiat Oncol Biol Phys 2006;64:382-91.
47. Langer CJ, Harris J, Horwitz EM, et al. Phase II study of low-dose paclitaxel and cisplatin in combination with split-course concomitant twice-daily reirradiation in recurrent squamous cell carcinoma of the head and neck: results of Radiation Therapy Oncology Group Protocol 9911. J Clin Oncol 2007;25:4800-5.
48. Spencer SA, Harris J, Wheeler RH, et al. Final report of RTOG 9610, a multi-institutional trial of reirradiation and chemotherapy for unresectable recurrent squamous cell carcinoma of the head and neck. Head Neck 2008;30:281-8.
49. Lin R, Slater JD, Yonemoto LT, et al. Nasopharyngeal carcinoma: repeat treatment with conformal proton therapy--dose-volume histogram analysis. Radiology 1999;213:489-94.

Cite this article as: Lin A, Swisher-McClure S, Millar LB, Kirk M, Yeager C, Kassaee A, Teo BK, Hahn SM. Proton therapy for head and neck cancer: current applications and future directions. Transl Cancer Res 2012;1(4):255-263. doi: 10.3978/j.issn.2218-676X.2012.12.01

Review Article

Proton radiotherapy in the treatment of lung cancer

Heath Devin Skinner, Ritsuko Komaki

Department of Radiation Oncology, The University of Texas MD Anderson Cancer Center, Houston, TX, USA

Correspondence to: Heath Devin Skinner. The University of Texas MD Anderson Cancer Center, 1515 Holcombe Blvd, Unit 97, Houston, TX 77030, USA. Email: hskinner@mdanderson.org.

Abstract: Radiation therapy for lung cancer often leads to treatment-related pneumonitis or lung fibrosis, especially when given with concurrent chemotherapy. These side effects can impair quality of life and negatively affect treatment outcomes. With the advent of proton radiotherapy comes the possibility of reducing these toxicities by minimizing the amount of non-target tissue that is irradiated. Protons have significantly different physical characteristics that can make their use advantageous over standard photon radiotherapy. Multiple retrospective reviews and phase I/II studies have linked the use of protons with fewer side effects in at least some patients with lung cancer, and randomized trials comparing proton therapy with photon treatments are ongoing. Technologic advances may allow for even further minimization of toxicity associated with radiation therapy. In this review, we discuss the current state of proton therapy for the management of lung cancer as well as challenges and opportunities for further development of this treatment modality.

Keywords: Radiation therapy; lung cancer; protons

doi: 10.3978/j.issn.2218-676X.2012.12.02

Scan to your mobile device or view this article at: http://www.thetcr.org/article/view/787/html

Introduction

Ever since the first attempts to treat malignancy with radiotherapy were made in the early 1900s, delivering a tumorcidal dose of radiotherapy while minimizing toxicity to nearby normal tissues has always been a challenge. Initially, tumors could be targeted only via direct or near-direct contact with a radiotherapy source. With the advent of Cobalt-60 radiation sources and, later, linear accelerators, therapeutic radiation could be delivered to virtually any site in the body. However, the dose that can be delivered to the tumor continues to be limited by normal tissue constraints. Fundamentally, this is determined by the physical characteristics of standard photon or electron radiotherapy. Photons, which include standard X-rays, and electrons deposit the radiation dose over the entire track of the beam; after peaking at a physically determined depth in water (or tissue), the deposited dose decreases slowly. For example, as shown in *Figure 1*, the maximum dose of radiation delivered by a standard 6 MV photon beam is at a depth of 1.5 cm in water. For electrons of similar energies, the depth at which maximum dose is delivered (D_{max}) is even less. This dose distribution is reasonable for superficial tumors, but for tumors more than 1.5 cm below the surface of the skin, for one radiation beam, the normal tissue proximal to the tumor will be treated to a higher dose than the tumor itself. This physical reality is compensated for in standard radiotherapy by the use of multiple beams that converge at the level of the tumor. With more advanced planning techniques, such as intensity-modulated radiotherapy (IMRT), the intensity of each beam can be altered by using a computer-determined "best solution" for all beams to maximize tumor dose while sparing surrounding normal tissue. Despite these significant advances, standard radiotherapy continues to be limited by the generally inalterable physical characteristics of a photon (or electron) beam. This has led to interest in other forms of radiotherapy with different beam characteristics. Here we focus primarily on proton radiotherapy, the most common charged particle therapy in clinical use for lung cancer in the United States.

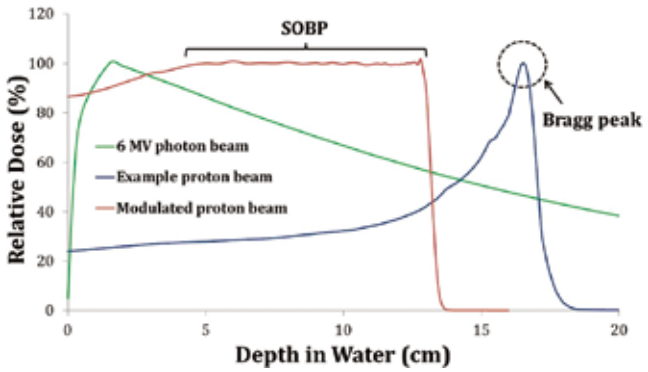

Figure 1 Depth-dose characteristics of proton and photon beams. The example proton beam is of a higher energy than the SOBP for clarity

Physical characteristics of proton beams

As previously stated, photon beams reach their maximum dose (D_{max}) at a known depth in tissue, a known physical property determined by the beam energy. Higher photon energies lead to greater D_{max} at the expense of increased fall-off dose as well as increased possibility of neuton scattering. However, charged particles such as protons have minimal ionization along their beam path, meaning that the dose delivered to any point along the beam path is minimal and the entrance dose for any particular proton beam is less than that for a comparable photon beam. Instead, the vast majority of dose in a charged particle beam is deposited near the end of the beam path, when the particles have nearly stopped (*Figure 1*). This phenomenon was initially observed as early as 1904, and has been dubbed the "Bragg peak" for its discoverer William Henry Bragg (1). By modulating the proton energy, the depth of the Bragg peak, or point of maximal radiation dose delivery, can be altered. However, the area of the Bragg peak for any one proton energy is too narrow for clinical use, requiring the use of a summed proton beam of multiple energies, resulting in the so-called "spread-out Bragg peak" (*Figure 1*).

A concept useful in comparing forms of radiotherapy is that of relative biologic effectiveness (RBE). Simply stated, this is a ratio between a standard dose of radiation (typically 250 kVp X-rays) and the dose of the test radiation required to produce the same biologic effect. Although the concept is fairly simple, derivation of the RBE is a complex process, depending upon a number of variables including the type of tissue being studied, the degree of hypoxia within the tissue, the type of radiation being used, the dose delivered, and the energy lost over the beam path (linear energy transfer or LET). Historically, the RBE for a variety of different types of radiation has been determined primarily by *in vitro* and preclinical studies. For clinical use, the RBE for a proton beam (within the Bragg peak) is generally assumed to be 1.1 (2,3), meaning that for every 1 Grey (Gy), the biological effectiveness of a proton beam is similar to what is seen with 1.1 Gy of standard X-rays. This has led to the use of the term cobalt-Grey equivalent (CGE) when describing doses or proton therapy. Thus 74 CGE is equivalent to 67.3 Gy delivered by protons. Although the RBE/CGE concept provides a clinically useful value, several caveats must be borne in mind. The RBE is thought to vary slightly over the breadth of a Bragg peak. Specifically, the experimentally determined RBE values within a proton beam generally increase over the Bragg peak and are highest in the final millimeters (4-8). This effect is recognized in the course of routine clinical treatments by the recommendation that no proton beam should terminate in a critical normal structure. RBE also varies as a function of the tissue irradiated; *in vivo* preclinical models have predicted average values ranging from 0.7 to 1.6 (2). Examination of this variation in the RBE of a proton beam has led to attempts to integrate this factor into treatment planning (9-11).

Clinical use of proton therapy in lung cancer

The use of proton radiotherapy has grown substantially, particularly over the past decade, with 10 facilities using this modality in the United States alone. The unique characteristics of proton radiotherapy has led to its use being championed to allow both sparing of normal tissue and increasing the radiation dose delivered to targets heretofore limited by proximity to adjacent normal surrounding structures. Particular interest in proton radiotherapy has been expressed for the treatment of lung cancer. The standard therapy for locally advanced lung cancer involves a combination of radiation and chemotherapy delivered concurrently, typically to radiation doses of 60-70 Gy. However, treatment in this dose range can be quite toxic, leading to significant pulmonary injury (mainly pneumonitis and fibrosis) as well as esophagitis and other toxic effects (12). Any damage to the lungs in patients with lung cancer tends to be exacerbated by a lack of pulmonary reserve, as many patients present with some form of chronic obstructive disease from cigarette smoking and many require supplemental oxygen even before radiotherapy. The findings regarding the value of dose-escalation in these patients is somewhat conflicting (13,14).

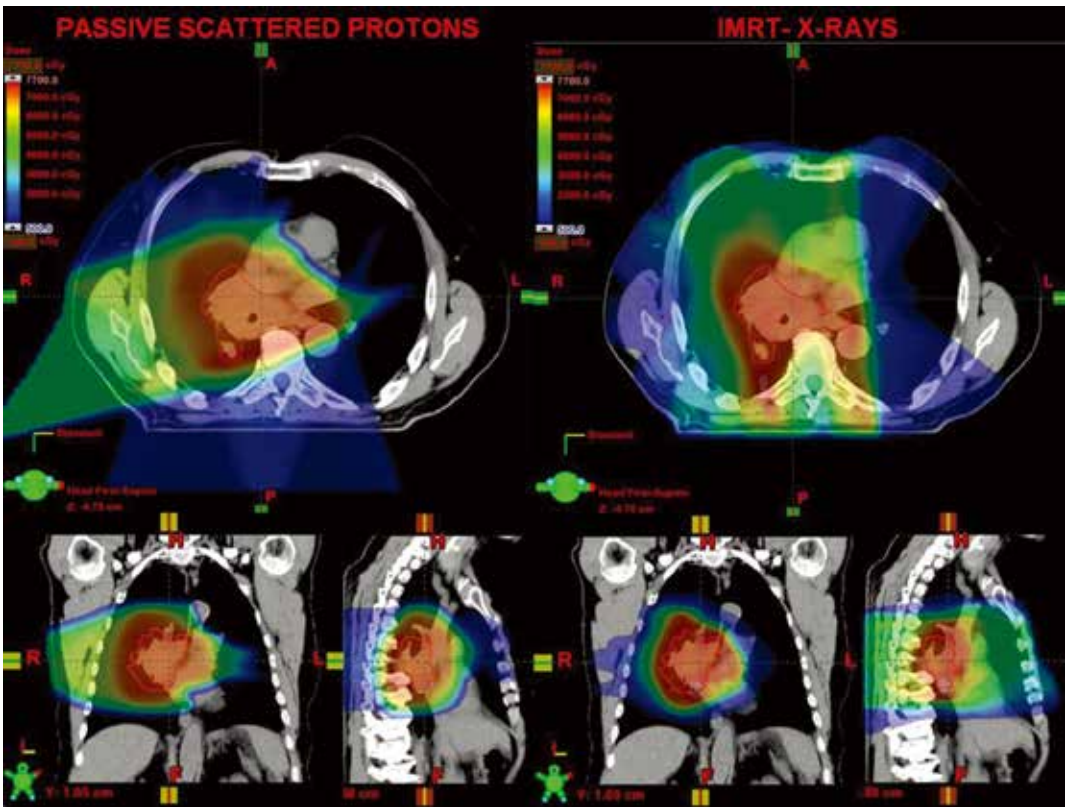

Figure 2 Example of comparison plans for the treatment of lung cancer between passive scatter proton radiotherapy and IMRT

One possibility for this disparity could be treatment-related toxicity; in other words, although tumor control may be increased in patients treated with higher radiation doses, the commensurate increase in toxicity and toxicity-related death can mask any potential benefit. Hence the desire for a radiation treatment modality that can minimize radiation dose to critical structures (e.g., the lungs) while allowing the possibility of dose escalation to the target. One such modality that attempts to achieve this goal is proton beam therapy.

Several planning studies have been done to compare the dose to normal surrounding structures associated with either photon or proton radiotherapy. Generally, in these studies, proton beam therapy has shown benefits over standard conformal radiotherapy; specifically, the dose to the uninvolved lung can in some cases be superior to that provided via conventional radiotherapy (15-17) or IMRT (15,17). Examples of a typical plan for passive scatter proton radiotherapy and one for IMRT are shown in *Figure 2*. Proton radiotherapy may also have advantages over photon-based stereotactic radiotherapy for smaller tumors in terms of sparing normal tissue (15,18-20). However, the benefit from the use of protons from the dosimetric perspective is not universal. Because of the uncertainty of the exact range of the Bragg peak, particularly in hypodense tissues such as lung, the use of additional margin of high-dose radiation may be required, leading to a higher dose to critical structures, particularly when they are close to the target (21). Further, because many tumors have irregular borders and involve the mediastinum, highly conformal IMRT may provide an advantage in regard to normal tissue sparing compared with the traditional passive-scatter approach to proton radiotherapy (22).

Dosimetric studies aside, a growing body of literature details the clinical experience of using charged particle therapy for lung cancer. Several institutions have generated significant data from the use of proton radiotherapy as monotherapy. One of the earliest published studies reported the investigators' experience in treating mainly early-stage non-small cell lung cancer (NSCLC) with a proton boost after traditional photon radiotherapy. In that study of 37 patients, the local control rate was 87%, and only 2 patients developed symptomatic pneumonitis (23). Studies of stereotactic or hypofractionated proton-based radiotherapy

for early-stage lung cancer have shown similar local control rates for small, peripheral lesions (24-27). However, in the same studies, local control rates for larger lesions have been less favorable, falling in the range of 40% to 60%. Toxicity in these studies has been minimal; in a phase I/II trial recently completed at MD Anderson Cancer Center involving a dose of 87.5 CGE, the rates of symptomatic pneumonitis and esophagitis were 11% and 6% (27).

Less information is available regarding combinations of proton radiotherapy with concurrent chemotherapy for locally advanced lung cancer. The guiding principle for radiotherapy to the lung has been to increase the dose to the point of maximum tolerability, as a radiation dose-response relationship has been observed for locally advanced lung cancer (13). However, any dose escalation must take into account the significant toxicity associated with thoracic radiotherapy. In fact, the most recent national trial of dose-escalated thoracic radiotherapy initiated by the RTOG led to the premature closure of the high-dose treatment group (74 Gy) because of the absence of any observed survival benefit (14). Although the final toxicity data from this trial were not available when this review was written, it is worth noting that 7 patients died in the high-dose group versus 3 in the control group (treated to 60 Gy). Thus, it seems that significant caution should be observed in attempting dose escalation of thoracic radiotherapy when that therapy involves conventional methods. However, a recent retrospective review of concurrent platinum-based chemotherapy and proton radiotherapy noted particularly low rates of pneumonitis (2%) and esophagitis (5%) compared with those rates in a similar group of patients treated to a lower dose (63 Gy) by either 3-dimensional conformal radiotherapy or IMRT (28). Further investigation of these results in a phase II trial showed similarly positive results, with local control rates of close to 80% and pneumonitis and esophagitis rates of around 2% and 11% (29). These results are also being evaluated further in a Bayesian randomized trial of image-guided proton radiotherapy compared with photon radiotherapy for patients with locally advanced lung cancer.

Despite the dosimetric evidence and some clinical data supporting the use of proton radiotherapy for the treatment of lung cancer, significant challenges remain. First, treatment planning using proton radiotherapy is complicated by the inherent motion of the lung. Unlike photon radiotherapy, protons are drastically affected by the material through which they pass. Thus tissue densities must be accounted for during treatment planning. However the motion of the lung - and consequently the motion of the tumor - during the respiratory cycle can make this challenging, particularly in light of the finite range of protons. Although proton radiotherapy is appealing in the context of sparing normal structures, any changes in the path of the beams during respiration could change the range of the proton beam significantly, leading to marginal misses of the target or increased dose to surrounding normal structures. This problem has been addressed in several planning studies [reviewed in (30)], and a variety of different approaches are being used to minimize this problem. In one such approach, "smearing" the target volume artificially increases the volume targeted in an attempt to ensure good coverage despite small changes arising from motion during the respiratory cycle. This problem of appropriate targeting is further amplified by changes in the tumor itself during radiotherapy: tumors can shrink or become more cavitary in response to radiotherapy, which again changes the density of the tissue traversed by the proton beam and altering its range. At MD Anderson Cancer Center, we have tried to minimize this problem by obtaining images throughout the course of the radiotherapy and modifying the plans ("adaptive planning") if the tumor responds significantly.

Further difficulties arise from highly irregular targets. As noted previously, IMRT can in many cases provide more conformal treatment for large irregular lesions. In an initial dosimetric comparison between IMRT and proton radiotherapy as part of the above-mentioned randomized protocol, IMRT was found to have a dosimetric advantage in many cases (31). One possible solution to the problem of conformality is the use of some form of modulated proton radiotherapy. Conventional proton radiotherapy ("passive scatter") uses material to scatter the beam over a large area, with a rotating wheel placed in the beam path to allow generation of a spread-out Bragg peak. This approach basically delivers a uniform dose over the extent of the target, but does not allow generation of irregular contours for the dose to be delivered. The concept of "pencil beam" proton radiotherapy is being investigated to improve upon this dose distribution; in this technique, the dose can be "painted" over any particular target by the use of pencil beams of protons directed at small segments of an individual target. Although this approach can improve the conformal coverage of irregular targets, in some situations it can be less robust than use of a passive scatter beam, because the accuracy of scanning beam proton radiotherapy is affected to an even greater extent by organ motion (32). Studies of the use of scanning beam technology for the treatment of

lung cancer are ongoing.

Finally, cautions have been raised regarding the problem of unintended neutron dose when using proton radiotherapy. The production of secondary neutrons may be of particular concern for passive scatter beams, in which a physical component is placed in the beam path, because these scattered neutrons may themselves be carcinogenic. Although this could be of significant import for younger populations, patients with lung cancer tend to be older, and risk estimates for carcinogenesis are highest for young patients (33). Further, the magnitude of neutrons generated by passive scatter beams is debated in the literature (34). Regardless, the advent of scanning beam technology has greatly reduced the possible risk of neutron scatter in the use of proton beam radiotherapy (33).

Future challenges and opportunities

The advent of proton radiotherapy for lung cancer brings with it an opportunity to minimize the toxicity of current standard-of-care therapy. At present, this possibility is being investigated in at least one randomized trial in which the benefits of passive scatter proton radiotherapy are being compared with those of IMRT. Further prospective studies are also ongoing to compare the benefits of stereotactic proton radiotherapy with those of standard 3D-conformal stereotactic radiotherapy. So, what further challenges and opportunities remain? One major criticism of proton radiotherapy for the treatment of lung cancer is its cost. The development of proton radiotherapy capability requires a significant cost outlay for any institution. Moreover, a treatment course of proton radiotherapy is significantly more expensive at the current time than is a comparable course of IMRT. Although this cost will likely decrease with time, proton radiotherapy remains an expensive treatment option. However, the costs of proton radiotherapy for lung cancer must be weighed against the costs of toxicity associated with therapy. In fact, in one cost-effectiveness model involving only recent studies, proton radiotherapy was found to be cost-effective for the management of selected cases of lung cancer (35). This finding underscores the idea that merely calculating treatment costs does not completely measure the value of any particular therapy.

With regard to technology, the current "cutting edge" in proton radiotherapy delivery is the development of intensity modulation. As noted previously, one of the disadvantages of passive beam proton radiotherapy is the inability to conform to a highly irregular target or to allow dose-painting within the irradiated field. Scanning beam technology removes this disadvantage. Moreover, one could conceivably generate treatment plans that take advantage of the increased RBE at the Bragg peak by deliberately encompassing a radioresistant area of a tumor (e.g., an hypoxic area) within the Bragg peak of each scanning beam. Theoretically, this approach would lead to improved response without incurring any toxicity associated with dose escalation. However, as noted previously, scanning beam technology for proton delivery is highly dependent on precise planning software and improved motion management. As these technologies improve, true intensity modulation of protons in the treatment of lung cancer will become a reality.

In summary, the current state of proton beam radiotherapy or intensity-modulated proton beam radiotherapy for lung cancer is one of optimism. Prospective trials of proton radiotherapy are ongoing, and those findings, as they mature, will be valuable in further clarifying the role of proton radiotherapy for the management of this deadly disease.

Acknowledgements

Disclosure: The authors declare no conflict of interest.

References

1. Bragg W. On the ionization of various gasses by the alpha particles of radium. Proc Phys Soc 1907;20:523-50.
2. Paganetti H, Niemierko A, Ancukiewicz M, et al. Relative biological effectiveness (RBE) values for proton beam therapy. Int J Radiat Oncol Biol Phys 2002;53:407-21.
3. International Commission on Radiation Units and Measurements. Prescribing, recording, and reporting proton-beam therapy (ICRU report 78). Bethesda, MD.
4. Wouters BG, Lam GK, Oelfke U, et al. Measurements of relative biological effectiveness of the 70 MeV proton beam at TRIUMF using Chinese hamster V79 cells and the high-precision cell sorter assay. Radiat Res 1996;146:159-70.
5. Bettega D, Calzolari P, Chauvel P, et al. Radiobiological studies on the 65 MeV therapeutic proton beam at Nice using human tumour cells. Int J Radiat Biol 2000;76:1297-303.
6. Tang JT, Inoue T, Inoue T, et al. Comparison of radiobiological effective depths in 65-MeV modulated proton beams. Br J Cancer 1997;76:220-5.
7. Courdi A, Brassart N, Hérault J, et al. The depth-

dependent radiation response of human melanoma cells exposed to 65 MeV protons. Br J Radiol 1994;67:800-4.
8. Matsuura T, Egashira Y, Nishio T, et al. Apparent absence of a proton beam dose rate effect and possible differences in RBE between Bragg peak and plateau. Med Phys 2010;37:5376-81.
9. Frese MC, Wilkens JJ, Huber PE, et al. Application of constant vs. variable relative biological effectiveness in treatment planning of intensity-modulated proton therapy. Int J Radiat Oncol Biol Phys 2011;79:80-8.
10. Carabe A, Moteabbed M, Depauw N, et al. Range uncertainty in proton therapy due to variable biological effectiveness. Phys Med Biol 2012;57:1159-72.
11. Jones B, Underwood TS, Dale RG. The potential impact of relative biological effectiveness uncertainty on charged particle treatment prescriptions. Br J Radiol 2011;84:S61-9.
12. O'Rourke N, Roqué I Figuls M, et al. Concurrent chemoradiotherapy in non-small cell lung cancer. Cochrane Database Syst Rev 2010;(6):CD002140.
13. Partridge M, Ramos M, Sardaro A, et al. Dose escalation for non-small cell lung cancer: analysis and modelling of published literature. Radiother Oncol 2011;99:6-11.
14. Bradley JD, Paulus R, Komaki R, et al. A randomized phase III comparison of standard-dose (60 Gy) versus high-dose (74 Gy) conformal chemoradiotherapy +/– cetuximab for stage IIIa/IIIb non-small cell lung cancer: Preliminary findings on radiation dose in RTOG 0617. Int J Radiat Oncol Biol Phys 2011;81: abstr LBA2.
15. Chang JY, Zhang X, Wang X, et al. Significant reduction of normal tissue dose by proton radiotherapy compared with three-dimensional conformal or intensity-modulated radiation therapy in Stage I or Stage III non-small-cell lung cancer. Int J Radiat Oncol Biol Phys 2006;65:1087-96.
16. Lee CH, Tait D, Nahum AE, et al. Comparison of proton therapy and conformal X-ray therapy in non-small cell lung cancer (NSCLC). Br J Radiol 1999;72:1078-84.
17. Nichols RC, Huh SN, Henderson RH, et al. Proton radiation therapy offers reduced normal lung and bone marrow exposure for patients receiving dose-escalated radiation therapy for unresectable stage iii non-small-cell lung cancer: a dosimetric study. Clin Lung Cancer 2011;12:252-7.
18. Macdonald OK, Kruse JJ, Miller JM, et al. Proton beam radiotherapy versus three-dimensional conformal stereotactic body radiotherapy in primary peripheral, early-stage non-small-cell lung carcinoma: a comparative dosimetric analysis. Int J Radiat Oncol Biol Phys 2009;75:950-8.
19. Hoppe BS, Huh S, Flampouri S, et al. Double-scattered proton-based stereotactic body radiotherapy for stage I lung cancer: a dosimetric comparison with photon-based stereotactic body radiotherapy. Radiother Oncol 2010;97:425-30.
20. Wang C, Nakayama H, Sugahara S, et al. Comparisons of dose-volume histograms for proton-beam versus 3-D conformal x-ray therapy in patients with stage I non-small cell lung cancer. Strahlenther Onkol 2009;185:231-4.
21. Seco J, Panahandeh HR, Westover K, et al. Treatment of non-small cell lung cancer patients with proton beam-based stereotactic body radiotherapy: dosimetric comparison with photon plans highlights importance of range uncertainty. Int J Radiat Oncol Biol Phys 2012;83:354-61.
22. Zhang X, Li Y, Pan X, et al. Intensity-modulated proton therapy reduces the dose to normal tissue compared with intensity-modulated radiation therapy or passive scattering proton therapy and enables individualized radical radiotherapy for extensive stage IIIB non-small-cell lung cancer: a virtual clinical study. Int J Radiat Oncol Biol Phys 2010;77:357-66.
23. Bush DA, Slater JD, Bonnet R, et al. Proton-beam radiotherapy for early-stage lung cancer. Chest 1999;116:1313-9.
24. Bush DA, Slater JD, Shin BB, et al. Hypofractionated proton beam radiotherapy for stage I lung cancer. Chest 2004;126:1198-203.
25. Iwata H, Murakami M, Demizu Y, et al. High-dose proton therapy and carbon-ion therapy for stage I nonsmall cell lung cancer. Cancer 2010;116:2476-85.
26. Nihei K, Ogino T, Ishikura S, et al. High-dose proton beam therapy for Stage I non-small-cell lung cancer. Int J Radiat Oncol Biol Phys 2006;65:107-11.
27. Chang JY, Komaki R, Wen HY, et al. Toxicity and patterns of failure of adaptive/ablative proton therapy for early-stage, medically inoperable non-small cell lung cancer. Int J Radiat Oncol Biol Phys 2011;80:1350-7.
28. Sejpal S, Komaki R, Tsao A, et al. Early findings on toxicity of proton beam therapy with concurrent chemotherapy for nonsmall cell lung cancer. Cancer 2011;117:3004-13.
29. Chang JY, Komaki R, Lu C, et al. Phase 2 study of high-dose proton therapy with concurrent chemotherapy for unresectable stage III nonsmall cell lung cancer. Cancer 2011;117:4707-13.
30. Liao Z, Lin SH, Cox JD. Status of particle therapy for

lung cancer. Acta Oncol 2011;50:745-56.
31. Mohan R, Zhang X, Matney J, et al. IMRT vs. passively scattered proton therapy (PSPT) for locally advanced non-small cell lung cancer (LA NSCLC) randomized trial - is there equipoise? Int J Radiat Oncol Biol Phys 2010;78:S201-2.
32. Schippers JM, Lomax AJ. Emerging technologies in proton therapy. Acta Oncol 2011;50:838-50.
33. Brenner DJ, Hall EJ. Secondary neutrons in clinical proton radiotherapy: a charged issue. Radiother Oncol 2008;86:165-70.
34. Paganetti H, Bortfeld T, Delaney TF. Neutron dose in proton radiation therapy: in regard to Eric J. Hall (Int J Radiat Oncol Biol Phys 2006;65:1-7). Int J Radiat Oncol Biol Phys 2006;66:1594-5; author reply 1595.
35. Grutters JP, Pijls-Johannesma M, Ruysscher DD, et al. The cost-effectiveness of particle therapy in non-small cell lung cancer: exploring decision uncertainty and areas for future research. Cancer Treat Rev 2010;36:468-76.

Cite this article as: Skinner HD, Komaki R. Proton radiotherapy in the treatment of lung cancer. Transl Cancer Res 2012;1(4):264-270. doi: 10.3978/j.issn.2218-676X.2012.12.02

Review Article

Proton therapy for gastrointestinal cancers

Ted C. Ling, Joseph I. Kang, Jerry D. Slater, Gary Y. Yang

Department of Radiation Medicine, Loma Linda University Medical Center, Loma Linda, California, USA

Correspondence to: Gary Y. Yang, MD. Department of Radiation Medicine, Loma Linda University Medical Center, 11234 Anderson Street, B121, Loma Linda, CA 92354, USA. Email: gyang@llu.edu.

Abstract: Proton beam therapy provides an opportunity to deliver ionizing radiation with improved dose conformity. It has gained popularity as a means of more localized radiation delivery. However, proton therapy data are still lacking, as there are still relatively few proton treatment centers worldwide. This paucity of data is particularly evident in gastrointestinal (GI) cancers. Most GI cancers are located in close proximity to or abut critical organs. The ability to deliver an appropriate dose to a target in this area is challenging; normal organ toxicities often limit the amount of radiation that can be delivered to achieve a therapeutic dose. The modern trend in treatment of GI cancers is toward multimodality treatment. However, there is an increased risk of toxicity when combining modalities such as radiotherapy, chemotherapy, and surgery, thus placing an even greater emphasis or normal-tissue toxicities.

Improvements in radiation treatment techniques over the past few decades have allowed dose escalation with improved normal-tissue sparing. The driving force behind improving treatment conformity is the significant short- and long-term morbidity of normal tissue toxicity during and after radiation treatment. The degree of normal-tissue sparing within individuals undergoing radiation treatment is highly variable and depends on tumor type and region. Tumors of the esophagus, for example, are surrounded by lung and spinal cord, while anal cancers are in close proximity to the bladder and rectum. Each subsite of the GI tract requires different techniques and approaches to maximize normal-organ sparing while delivering adequate amounts of radiation to the tumor. The physical properties of proton radiation may offer a distinct benefit in treating GI malignancies.

Keywords: Proton; radiation; esophageal cancer; gastric cancer; pancreatic cancer; rectal cancer; anal cancer

DOI: 10.3978/j.issn.2218-676X.2012.09.01

Scan to your mobile device or view this article at: http://www.thetcr.org/article/view/543/html

Introduction

Proton radiation therapy has gained popularity over the past few decades as a means of optimizing radiation treatment. In the field of radiation oncology there is an ever-present impetus to improve tumor killing while minimizing side effects. This is achieved by delivering higher doses of radiation to the tumor while sparing normal surrounding tissues. The most important factor in determining the success of this optimization, or therapeutic ratio, is tight control of dose conformality. However, the magnitude of normal tissue sparing in various regions of the body is variable due to specific individual anatomy. There is, in fact, evidence that patients with high-grade acute organ toxicity during multimodality treatment seem to benefit in regard to tumor response and prognosis (1-3). This places an even greater emphasis on the need to lower radiation exposure to organs at risk. There is still a paucity of data involving the use of proton therapy in gastrointestinal malignancy due to a relative lack of clinically available proton treatment facilities worldwide.

Most of the radiation given with conventional X-ray, or photon, therapy is deposited along the entrance and exit of the beam path. In contrast, protons are small charged particles that travel only a finite distance in tissue. Most of an accelerated proton's energy is deposited as a Bragg peak

at the end of the beam path. The depth of this Bragg peak can be modulated by either varying the proton beam energy or adding compensators to the treatment gantry. Therefore, the integral dose is greatly reduced since there is no exit dose and the entrance dose is greatly reduced relative to the Bragg peak. The ability to dose-escalate at the tumor while maintaining low toxicity in normal tissues may improve the therapeutic ratio of radiation treatment. The kidneys, for example, are often involved in the radiation fields when treating gastric or pancreatic cancer. There is evidence of decline in relative renal function following kidney irradiation (4). The degree of dysfunction correlates with the amount of radiation received. These adverse outcomes emphasize the importance of sparing normal tissue from dose during radiation therapy. The use of proton therapy for treating gastrointestinal (GI) malignancy is still a topic of many ongoing studies. Nonetheless, the opportunity to improve dose distribution to highly critical organs within the abdominal cavity presents itself as a major topic of interest. We present an overview of proton therapy contributions in the role of treating esophageal, gastric, pancreatic, and rectal malignancy.

Esophageal cancer

Esophageal cancer accounts for 5% of all GI cancers worldwide. It is the sixth leading cause of death from cancer worldwide. There is a male predominance, with the highest prevalence in Asia. The percentage and overall incidence of adenocarcinoma histology is increasing in comparison to squamous cell carcinoma histology. Tobacco, alcohol, gastroesophageal reflux (GERD), and Plummer-Vinson syndrome are known risk factors for esophageal cancer. Barrett's esophagus is an established risk factor associated with a 9-fold risk of developing adenocarcinoma of the distal esophagus (5).

Treatment options are guided by disease stage. Early stage tumors with minimal invasion have very low risk of distant metastases. They are often treated with surgical resection of the tumor. Early stage tumors with deeper invasion are generally managed with esophagectomy. Concurrent chemotherapy and radiation may be considered in patients who are not surgical candidates. Locally advanced disease is managed with up-front concurrent chemoradiation followed by re-evaluation for possible esophagectomy. Concurrent chemoradiation is considered the standard of care, yielding increased survival benefit when compared to radiation alone (6). Meta-analyses have also demonstrated increased survival benefit when chemoradiation is administered pre-operatively as compared to pre-operative chemo alone or no pre-operative treatment (7). Furthermore, available data suggest improvement in local control and a possible survival improvement with the use of post-operative chemoradiation as well as post-operative radiation alone (8).

The esophagus is located in the posterior mediastinum in close proximity to several critical structures, namely lung, spinal cord, and heart. Minimizing toxicities to these critical structures decreases overall treatment morbidity and mortality to the patient. However, a margin large enough to cover the areas of tumor and involved lymph nodes must be accounted for in the radiation field. This puts surrounding organs at greater risk. Lung dose is a major risk factor for toxicity during irradiation for esophageal cancer. It is often necessary to use several beams oriented at oblique angles in order to keep spinal cord dose within tolerance (*Figures 1*,*2*,*3*,*4*). This results in a significant amount of radiation dose received by the lung, leading to subsequent radiation pneumonitis and post-operative pulmonary complications in some patients.

A recent phase III randomized prospective trial compared surgery alone with pre-operative concurrent chemotherapy using carboplatin and taxol given with 41.4 Gy conventional X-radiation (9). The standard radiation dose in most North American studies is 50.4 Gy, but despite the reduced dose regimen in this study the authors found improved median and overall survival in the pre-operatively treated arm compared to surgery alone. A dose of 41.4 Gy allowed the authors to use an anterior-posterior beam arrangement to spare integral dose in the lung while keeping the spinal cord dose within tolerance. The dosimetric properties of proton therapy could potentially allow safe dose escalation to 50.4 Gy or above while simultaneously sparing integral dose to the lungs and keeping the spinal cord dose within tolerance. A series of esophageal patients at M.D. Anderson Cancer Center treated with either IMRT or proton therapy found improved dose toxicity profiles when protons were used (10). While the dosimetric advantage of protons is clear, the reported clinical experience using proton beams is limited. Nonetheless several studies do report fewer interruptions during treatment due to radiation esophagitis and hematologic toxicities (11,12). The use of intensity-modulated proton beam therapy (IMPT) is the topic of several new trials in the management of esophageal cancer.

Gastric cancer

Gastric cancer has seen a sharp decrease in incidence

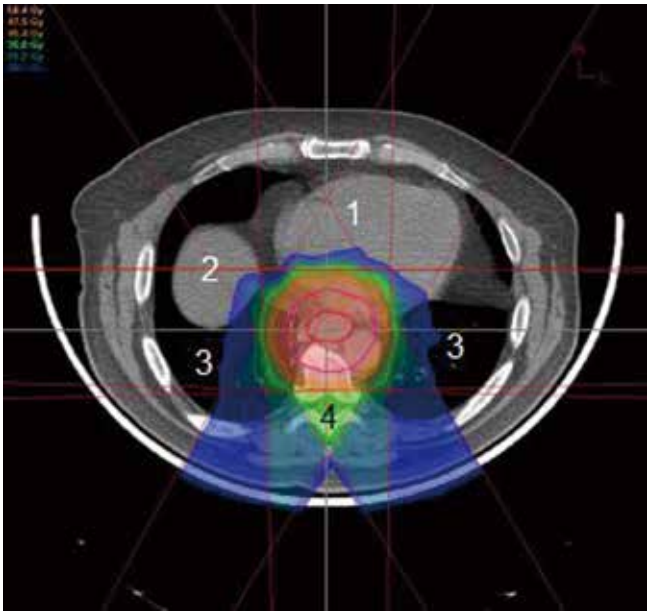

Figure 1 Axial view of posterior oblique proton beams treating the esophagus. After reaching the esophagus the dose drops off immediately. This minimizes radiation dose received by the heart and lungs; 1. heart; 2. liver; 3. lung; 4. spinal cord

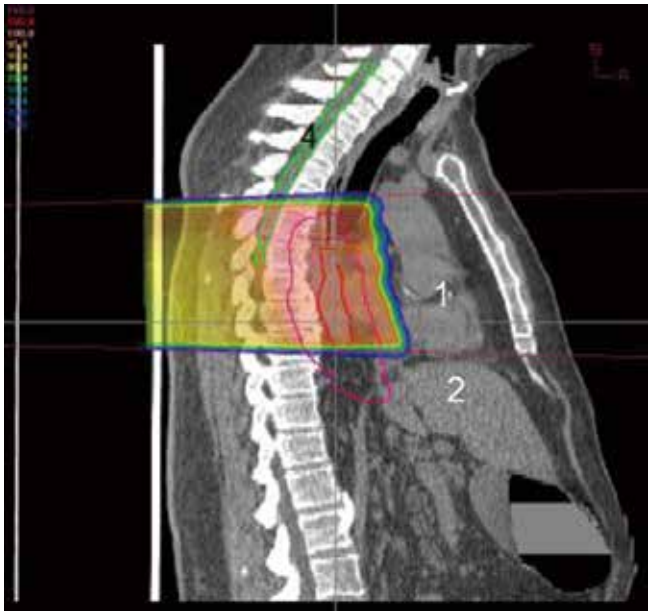

Figure 2 Sagittal view of posterior proton beam entering the body and stopping after reaching the esophagus; 1. heart; 2. liver; 4; spinal cord

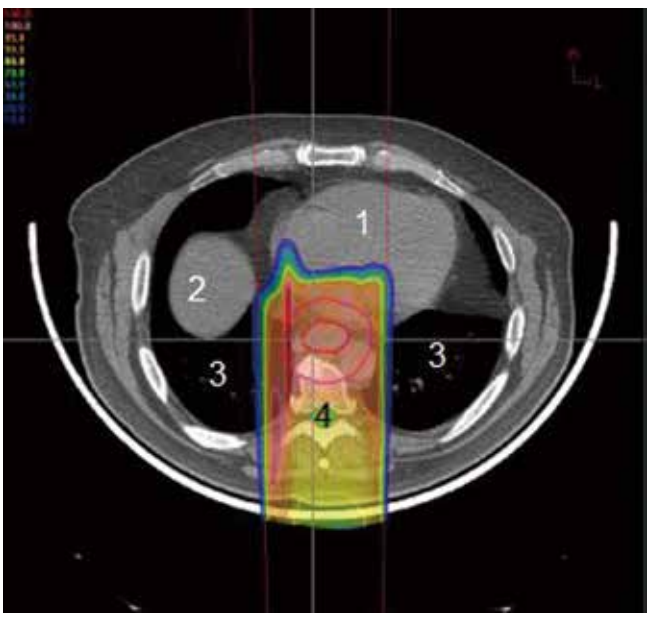

Figure 3 Axial view of single posterior proton beam treating esophagus; Red. esophagus; Magenta. margin around the esophagus; 1. heart; 2. liver; 3. lung; 4. spinal cord

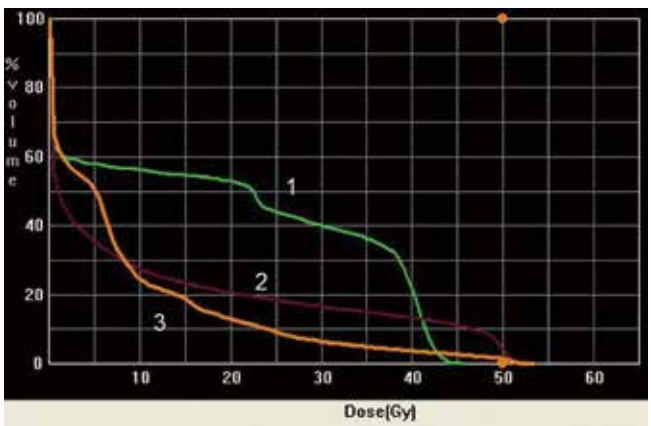

Figure 4 Dose-volume histogram for treatment plan seen in figures 1-3 showing the amount of dose received by each organ; 1. heart; 2. liver; 3. lung

in Western countries over the past 60 years. However, the incidence of gastro-esophageal and proximal gastric tumors is increasing. It is the third most common cancer in the world and the second leading cause of cancer deaths worldwide. There is a slight male predominance, with the median age of diagnosis at 65 years. The highest death rates from gastric cancer are reported in Asia and South America. Known risk factors are smoked and salted food, pernicious anemia, and Helicobacter Pylori infection. Adenocarcinoma comprises the vast majority of gastric cancer histology. Positron emission tomography (PET) has achieved an increasing role in the diagnosis and staging of gastric cancers and is used as an option for greater specificity in characterizing suspected gastric tumor (13). Anatomic imaging, however, remains the standard recommendation.

Surgery has been the mainstay of treatment, although chemotherapy and radiation now have an established role. Tumors of the upper and middle third of the stomach generally require a total gastrectomy, while partial gastrectomy may be adequate for tumors located in the distal antrum. These considerations are highly variable and specific to each patient. Achieving negative margins and thorough lymph node assessment is critical in gastric cancer treatment, as the majority of recurrences are locoregional (14).

Today, the standard of care for gastric cancer is tri-modality treatment or, in some institutions, perioperative chemotherapy. Surgery, chemotherapy, and radiation together all play an increasingly important role. Several landmark trials investigated the role of chemoradiation in relation to surgery. The INT0116 trial demonstrated an overall survival benefit (HR 1.32, P=0.0046) when surgery is followed by a combination of chemoradiation (15). Gastric cancer recurrence is largely locoregional in nature. Post-operative radiation therapy is generally given to the surgical bed and surrounding lymph node regions. This results in large radiation fields that put nearby organs at risk, including lungs, liver, kidney, and small intestine. Little or no clinical prospective data exist regarding proton therapy in gastric cancer. The inherent dosimetric advantage that proton therapy provides should serve as an opportunity for improving the post-gastrectomy bed normal-organ toxicities.

Pancreatic cancer

Despite being only the tenth most common cancer worldwide, pancreatic cancer is the fourth leading cause of cancer mortality. It is found primarily in Western countries. Known risk factors include tobacco use, ionizing radiation, and diets high in animal fat. The incidence has been stable over the past 20 years but has increased 3-fold since 1920. It is seen more frequently in African Americans and males, with a peak incidence at 70 to 80 years of age. The most common histologic cell type is adenocarcinoma, with mucinous, serous, and neuroendocrine histologies comprising less than 10% of cases. Although elevated in some benign conditions, the tumor marker CA 19-9 is often used as a pretreatment prognostic indicator. A decreasing value after pancreatic cancer treatment is associated with better survival (16).

As a whole, pancreatic cancer carries a very poor prognosis. Nearly 80% of newly diagnosed cases are stage IV disease. Its 5-year overall survival rate is among the lowest of all cancers. Over 80% of patients who undergo surgery will have recurrence. Historically, surgery with or without chemotherapy has been the mainstay of pancreatic cancer. Chemotherapy alone has not been shown to be curative in GI malignancies. However, some promising survival data are associated with the concurrent administration of intense cytotoxic chemotherapy regimens such as fluorouracil, irinotecan, and oxaliplatin (FOLFIRINOX) (17). The role of novel molecularly targeted agents is a topic of active investigation as well. When pre-operative chemotherapy or chemoradiation is administered, it is critical to assess for disease response to this treatment. Patients with disease progression during pre-operative therapy likely will not benefit from surgery and an extremely morbid surgery may be prevented (18). Patients deemed resectable typically undergo pancreaticoduodenectomy, or Whipple's Procedure, followed by chemoradiation. There is evidence for a survival benefit in giving post-operative chemoradiation over post-operative chemotherapy alone (19,20). Aside from extended survival, post-operative chemoradiation has been seen to improve performance status, reduce the amount of hospital stay, and facilitate greater pain relief (21). However, a consensus has not yet been reached defining the exact role of radiation in pancreatic cancer.

Since the value of radiation therapy in this disease has not been firmly established it is difficult to estimate the number of cases suitable for proton-beam therapy. Radiation dose escalation has shown disease control benefits for various cancer sites. Though systemic relapse is still a predominant feature, dose escalation has been shown to increase long-term disease control (22). Improvements in radiation treatment techniques, particularly in IMRT, have allowed dose escalation with acceptable normal tissue toxicitites (23). Few pancreatic proton

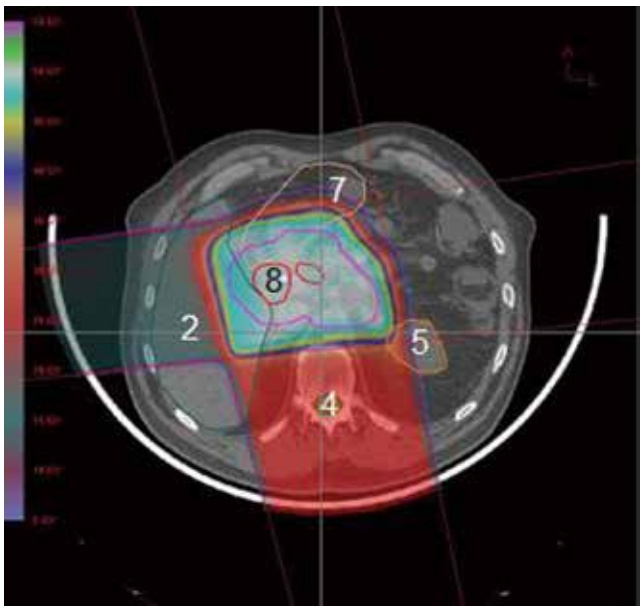

Figure 5 Axial view of right oblique and posterior oblique proton beam entering the body to treat the postoperative pancreatic bed. The posterior beam is more heavily weighed and the dose from both beams drop off after the postoperative bed is reached; 2. liver; 4. spinal cord; 5. left kidney; 7. duodenum; 8. surgical clips

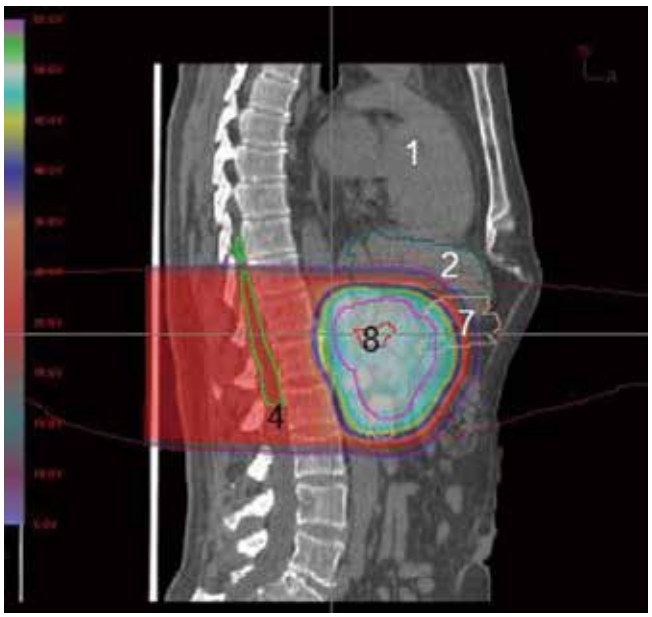

Figure 6 Sagittal view of posterior oblique proton beam targeting postoperative pancreatic bed. This minimizes radiation dose to the liver, stomach, and bowel; 1. heart; 2. liver; 4. spinal cord; 7. duodenum; 8. surgical clips

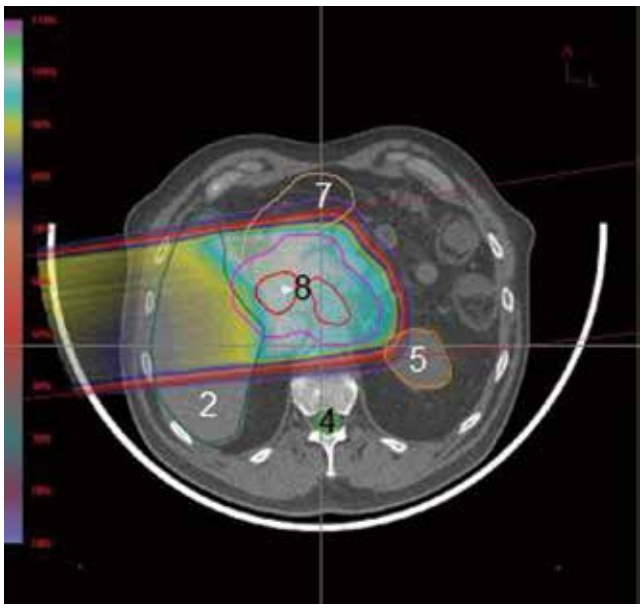

Figure 7 Axial view of right oblique proton beam targeting postoperative pancreatic bed; 2. liver; 4. spinal cord; 5. left kidney; 7. duodenum; 8. surgical clips

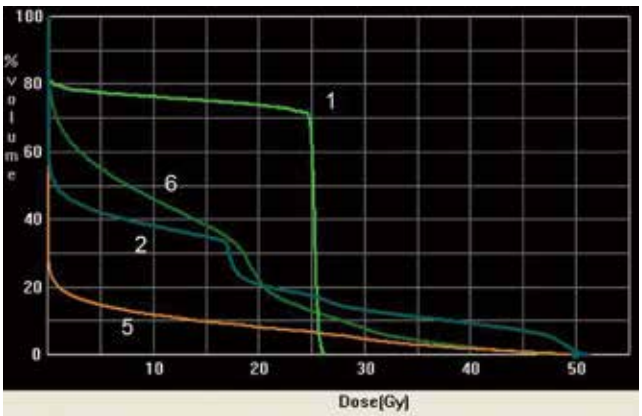

Figure 8 Dose-volume histogram for treatment plan seen in figures 5-7 showing the amount of dose received by each organ; 1. heart; 2. liver; 5. left kidney; 6. right kidney

dosimetric data are available, but one study did demonstrate the dosimetric feasibility of five fractions of 5 Gy delivered as pre-operative pancreatic cancer treatment (24)

The pancreas is located in the retroperitoneum, closely abutting several critical organs. A proton beam's unique qualities would seem to lend itself well to such a situation (*Figures 5*,*6*,*7*,*8*). One study compared target coverage and dose-volume histograms of proton therapy plans to various 3D conformal and IMRT photon plans (25). The proton therapy plans demonstrated significantly lower integral doses. In particular, the rapid downstream falloff of dose for tumors near the ligament of Treitz enabled complete coverage of the planning target volume while staying within acceptable normal-tissue toxicity limits. In Japan concurrent proton therapy with high-dose gemcitabine has been studied, showing high feasibility and tolerability (26). The frequency of grade 3 or higher acute GI toxicities was low even when using doses as high as 70.2 GyE. Major late toxicities varied, depending on pancreatic tumor position relative to organ anatomy. Nonetheless, they were significantly reduced when using a field-in-field technique, as in this study. Proton therapy will continue to be a major focal point of investigation in future pancreatic cancer dose-escalation studies.

Rectal cancer

The incidence of rectal cancer is equally distributed between males and females. The median age of diagnosis is the seventh decade. Associated risks factors include high-fat, low-fiber diets; animal fat; red meat; and inflammatory bowel disease. A number of gene mutations also are associated with a high risk of colon cancer. The colon and rectum are divided by the rectosigmoid junction at the level of the S3 vertebra. The rectum begins below this junction. In planning treatment for colorectal cancer one must take into account the highly variable lymph node drainage patterns, depending on the level of involvement in the colon or rectum.

The mainstay of treatment for rectal cancer remains surgery. Historically, however, surgery alone has yielded high cure rates only in early-stage rectal cancers. The addition of post-operative radiation improved local control rates but did not improve overall survival. When chemotherapy was combined with radiation, an improvement in local control, distant failures, and overall survival was seen (27). Unfortunately, many patients who undergo surgery are unable to complete chemoradiation. Therefore, interest grew in pre-operative chemoradiation therapy. The German rectal cancer study compared pre-operative with post-operative chemoradiation and found no difference in survival rates. Pre-operative chemoradiation, however, demonstrated improved local control rates and significantly improved toxicity rates (28). Many institutions now consider pre-operative chemoradiation to be the standard of care in rectal cancer.

Isacsson *et al*. initially demonstrated dosimetric advantages with proton therapy in inoperable rectal cancer patients (29). Three dose plans were made for each of six patients: one proton plan, one X-ray plan, and one mixed plan with X-ray beams followed by a proton beam boost. They demonstrated that the treatment plans involving proton beams showed superior dosimetric coverage of the target volumes. Wolff *et al*. performed a treatment planning comparison study for rectal cancer using various treatment modalities (30). Twenty-five patients with locally advanced rectal cancer were treated with pre-operative chemoradiation. The radiation was planned out using either Intensity modulated radiation therapy (IMRT), RapidArc with two arcs (full gantry rotation around the patient), 3D conformal therapy, and proton therapy. Consistently, improved systematic sparing of normal tissues as seen in the proton therapy plans while providing adequate coverage to the target regions.

Protons showed reliable and reproducible dosimetric advantages in these rectal cancer cases. The ability to spare nearby bladder, small bowel, and other normal tissue indicates an opportunity for an improved therapeutic ratio in locally advanced rectal cancers.

Anal cancer

The past three decades has seen a marked increase in the incidence of anal cancer. Overall it is still a relatively rare malignancy, comprising less than 2% of all gastrointestinal cancers. It is seen nearly twice as often in women than in men. The mean age of diagnosis is between ages 55 and 65. Human papilloma virus (HPV) infection is strongly associated with anal squamous cell carcinoma, which comprises over 75% of cases. It is thought that HPV infection, particularly HPV-16, 18 may in fact be a requisite for disease formation. Anal cancer is associated with AIDS, although, unlike cervical cancer, it is not an AIDS-defining illness. Other risk factors include cigarette smoking, multiple sexual partners, and a history of anal warts.

Historically, abdominoperineal resection (APR) was

the standard treatment for anal cancer. This required a permanent colostomy. However, in 1973 a Wayne State study showed that pre-operative chemoradiation utilizing Fluorouracil (5-FU) and Mitomycin could induce complete pathologic responses in over 80% of patients, thus obviating the need for surgery (31). Numerous trials have established concurrent chemoradiation as superior to radiation alone (32,33). Surgical resection alone may still play a role in certain early-stage tumors with favorable characteristics. Surgery is sufficient with anal margin cancers in which the sphincter can be spared. Nonetheless, definitive chemoradiation is considered standard treatment by many institutions.

The advent of IMRT for anal cancer marked a considerable advance in treatment. Ongoing studies investigating the role of IMRT in anal cancer demonstrated promising clinical response rates with significantly better skin and normal organ toxicities as compared to conventional techniques (34). The pelvis is a tightly packed region of the body with numerous critical structures in intimate proximity to one another. Acute toxicities occur fairly frequently during treatment. Although some authorities suggest a dosimetric improvement of proton therapy over photon therapy in locally advanced anal cancer, very limited data are available for proton therapy in this disease. Traditional scanning beam techniques for proton therapy have field size limitations that make definitive proton treatment for anal cancer technically challenging. Intensity-modulated proton therapy (IMPT) techniques do not have the same field size limitations. IMPT may allow for treating anal cancer with protons with the potential of further decrease in adverse events, particularly late effects. Future studies should investigate ways to ensure adequate homogeneous coverage while sparing organs at risk.

Conclusions

Proton therapy shows great potential to increase therapeutic tolerance for patients with gastrointestinal malignancies. Numerous studies have demonstrated the capability to reliably reproduce the dosimetric quality of conventional conformal plans. Furthermore, improved beam conformality reduces the toxicity of surrounding organs at risk. This would lead to lower rates of late toxicity. Combined modality regimens have become the standard of treatment for a great majority of GI tract cancers. Reduction in radiation toxicity to organs at risk with proton therapy may allow the use of other systemic therapy or combination of therapies deemed too toxic when combined with conventional radiotherapy. Additionally, beam conformality with normal-tissue sparing becomes increasingly important in accordance with the general trend of finding ways to dose escalate. The possibility of decreasing radiation dose to organs at risk may also help facilitate chemotherapy dose escalation or allow for new chemotherapy combinations, which were previously deemed too toxic. The therapeutic ratio is the key parameter clinicians try to maintain in utilizing radiation therapy. Another major challenge for the future is proper identification of indications for proton therapy as a treatment modality. Proton centers are still relatively few in number; accordingly, outcomes are still fairly limited. Nonetheless, it is likely that the use of proton therapy will play a decisive role in the context of ongoing intensified combined modality treatments for GI cancers.

Acknowledgements

The author would like to thank William Preston, Ed.D for his assistance with manuscript preparation.
Disclosure: The authors declare no conflict of interest.

References

1. Wolff HA, Bosch J, Jung K, et al. High-grade acute organ toxicity as positive prognostic factor in primary radio(chemo)therapy for locally advanced, inoperable head and neck cancer. Strahlenther Onkol 2010;186:262-8.
2. Wolff HA, Gaedcke J, Jung K, et al. High-grade acute organ toxicity during preoperative radiochemotherapy as positive predictor for complete histopathologic tumor regression in multimodal treatment of locally advanced rectal cancer. Strahlenther Onkol 2010;186:30-5.
3. Wolff HA, Raus I, Jung K, et al. High-grade acute organ toxicity as a positive prognostic factor in primary radiochemotherapy for anal carcinoma. Int J Radiat Oncol Biol Phys 2011;79:1467-78.
4. May KS, Yang GY, Khushalani NI, et al. Association of Technetium (99m) MAG-3 renal scintigraphy with change in creatinine clearance following chemoradiation to the abdomen in patients with gastrointestinal malignancies. J Gastrointest Oncol 2010;1:7-15.
5. Cook MB, Wild CP, Everett SM, et al. Risk of mortality and cancer incidence in Barrett's esophagus. Cancer Epidemiol Biomarkers Prev 2007;16:2090-6.
6. Cooper JS, Guo MD, Herskovic A, et al. Chemoradiotherapy of locally advanced esophageal cancer:

long-term follow-up of a prospective randomized trial (RTOG 85-01). Radiation Therapy Oncology Group. JAMA 1999;281:1623-7.
7. Gebski V, Burmeister B, Smithers BM, et al. Survival benefits from neoadjuvant chemoradiotherapy or chemotherapy in oesophageal carcinoma: a meta-analysis. Lancet Oncol 2007;8:226-34.
8. Jabbour SK, Thomas CR Jr. Radiation therapy in the postoperative management of esophageal cancer. J Gastrointest Oncol 2010;1:102-11.
9. van Hagen P, Hulshof MC, van Lanschot JJ, et al. Preoperative chemoradiotherapy for esophageal or junctional cancer. N Engl J Med 2012;366:2074-84.
10. Lin SH, Komaki R, Liao Z, et al. Proton beam therapy and concurrent chemotherapy for esophageal cancer. Int J Radiat Oncol Biol Phys 2012;83:e345-51.
11. Zhang X, Zhao KL, Guerrero TM, et al. Four-dimensional computed tomography-based treatment planning for intensity-modulated radiation therapy and proton therapy for distal esophageal cancer. Int J Radiat Oncol Biol Phys 2008;72:278-87.
12. Welsh J, Gomez D, Palmer MB, et al. Intensity-modulated proton therapy further reduces normal tissue exposure during definitive therapy for locally advanced distal esophageal tumors: a dosimetric study. Int J Radiat Oncol Biol Phys 2011;81:1336-42.
13. Hopkins S, Yang GY. FDG PET imaging in the staging and management of gastric cancer. J Gastrointest Oncol 2011;2:39-44.
14. Gunderson LL, Sosin H. Adenocarcinoma of the stomach: areas of failure in a re-operation series (second or symptomatic look) clinicopathologic correlation and implications for adjuvant therapy. Int J Radiat Oncol Biol Phys 1982;8:1-11.
15. Macdonald JS, Smalley SR, Benedetti J, et al. Chemoradiotherapy after surgery compared with surgery alone for adenocarcinoma of the stomach or gastroesophageal junction. N Engl J Med 2001;345:725-30.
16. Tian F, Appert HE, Myles J, et al. Prognostic value of serum CA 19-9 levels in pancreatic adenocarcinoma. Ann Surg 1992;215:350-5.
17. Moertel CG, Frytak S, Hahn RG, et al. Therapy of locally unresectable pancreatic carcinoma: a randomized comparison of high dose (6000 rads) radiation alone, moderate dose radiation (4000 rads + 5-fluorouracil), and high dose radiation + 5-fluorouracil: The Gastrointestinal Tumor Study Group. Cancer 1981;48:1705-10.
18. Kotowski A, Ma WW. Emerging therapies in pancreas cancer. J Gastrointest Oncol 2011;2:93-103.
19. Wang F, Kumar P. The role of radiotherapy in management of pancreatic cancer. J Gastrointest Oncol 2011;2:157-67.
20. Klaassen DJ, MacIntyre JM, Catton GE, et al. Treatment of locally unresectable cancer of the stomach and pancreas: a randomized comparison of 5-fluorouracil alone with radiation plus concurrent and maintenance 5-fluorouracil--an Eastern Cooperative Oncology Group study. J Clin Oncol 1985;3:373-8.
21. Shinchi H, Takao S, Noma H, et al. Length and quality of survival after external-beam radiotherapy with concurrent continuous 5-fluorouracil infusion for locally unresectable pancreatic cancer. Int J Radiat Oncol Biol Phys 2002;53:146-50.
22. Willett CG, Del Castillo CF, Shih HA, et al. Long-term results of intraoperative electron beam irradiation (IOERT) for patients with unresectable pancreatic cancer. Ann Surg 2005;241:295-9.
23. Brown MW, Ning H, Arora B, et al. A dosimetric analysis of dose escalation using two intensity-modulated radiation therapy techniques in locally advanced pancreatic carcinoma. Int J Radiat Oncol Biol Phys 2006;65:274-83.
24. Kozak KR, Kachnic LA, Adams J, et al. Dosimetric feasibility of hypofractionated proton radiotherapy for neoadjuvant pancreatic cancer treatment. Int J Radiat Oncol Biol Phys 2007;68:1557-66.
25. Bouchard M, Amos RA, Briere TM, et al. Dose escalation with proton or photon radiation treatment for pancreatic cancer. Radiother Oncol 2009;92:238-43.
26. Terashima K, Demizu Y, Hashimoto N, et al. A phase I/II study of gemcitabine-concurrent proton radiotherapy for locally advanced pancreatic cancer without distant metastasis. Radiother Oncol 2012;103:25-31.
27. Thomas PR, Lindblad AS. Adjuvant postoperative radiotherapy and chemotherapy in rectal carcinoma: a review of the Gastrointestinal Tumor Study Group experience. Radiother Oncol 1988;13:245-52.
28. Sauer R, Becker H, Hohenberger W, et al. Preoperative versus postoperative chemoradiotherapy for rectal cancer. N Engl J Med 2004;351:1731-40.
29. Isacsson U, Montelius A, Jung B, et al. Comparative treatment planning between proton and X-ray therapy in locally advanced rectal cancer. Radiother Oncol 1996;41:263-72.
30. Wolff HA, Wagner DM, Conradi LC, et al. Irradiation with protons for the individualized treatment of patients with locally advanced rectal cancer: a planning study with

clinical implications. Radiother Oncol 2012;102:30-7.
31. Nigro ND, Seydel HG, Considine B, et al. Combined preoperative radiation and chemotherapy for squamous cell carcinoma of the anal canal. Cancer 1983;51:1826-9.
32. Northover J, Glynne-Jones R, Sebag-Montefiore D, et al. Chemoradiation for the treatment of epidermoid anal cancer: 13-year follow-up of the first randomised UKCCCR Anal Cancer Trial (ACT I). Br J Cancer 2010;102:1123-8.
33. Bartelink H, Roelofsen F, Eschwege F, et al. Concomitant radiotherapy and chemotherapy is superior to radiotherapy alone in the treatment of locally advanced anal cancer: results of a phase III randomized trial of the European Organization for Research and Treatment of Cancer Radiotherapy and Gastrointestinal Cooperative Groups. J Clin Oncol 1997;15:2040-9.
34. Meyer J, Czito B, Yin FF, et al. Advanced radiation therapy technologies in the treatment of rectal and anal cancer: intensity-modulated photon therapy and proton therapy. Clin Colorectal Cancer 2007;6:348-56.

Cite this article as: Ling TC, Kang JI, Slater JD, Yang GY. Proton therapy for gastrointestinal cancers. Transl Cancer Res 2012;1(3):150-158. DOI: 10.3978/j.issn.2218-676X.2012.09.01

Review Article

Proton therapy for hepatocellular carcinoma

Ted C. Ling, Joseph I. Kang, David A. Bush, Jerry D. Slater, Gary Y. Yang

Department of Radiation Medicine, Loma Linda University Medical Center, CA 92354, USA

Correspondence to: Gary Y. Yang, MD. Department of Radiation Medicine, Loma Linda University Medical Center, 11234 Anderson Street, B121, Loma Linda, CA 92354, USA. Email: gyang@llu.edu.

Abstract: Proton radiotherapy has seen an increasing role in the treatment of hepatocellular carcinoma (HCC). Historically, external beam radiotherapy has played a very limited role in HCC due to a high incidence of toxicity to surrounding normal structures. The ability to deliver a high dose of radiation to the tumor is a key factor in improving outcomes in HCC. Advances in photon radiotherapy have improved dose conformity and allowed dose escalation to the tumor. However, despite these advances there is still a large volume of normal liver that receives a considerable radiation dose during treatment. Proton beams do not have an exit dose along the beam path once they enter the body. The inherent physical attributes of proton radiotherapy offer a way to maximize tumor control via dose escalation while avoiding excessive radiation to the remaining liver, thus increasing biological effectiveness. In this review we discuss the physical attributes and rationale for proton radiotherapy in HCC. We also review recent literature regarding clinical outcomes of using proton radiotherapy for the treatment of HCC.

Keywords: Proton radiotherapy; hepatocellular carcinoma (HCC)

DOI: 10.3978/j.issn.1000-9604.2012.10.09

Scan to your mobile device or view this article at: http://www.thecjcr.org/article/view/1185/1530

Introduction

Hepatocellular carcinoma (HCC) is one of the most significant causes of cancer mortality worldwide (1,2). It generally has a poor prognosis as it is an aggressive tumor often found concomitantly in the setting of cirrhosis. The presence of cirrhosis, hepatitis B, and hepatitis C are key risk factors (3), but HCC is a complex disease involving many patient factors. There are several risk stratification systems which aim to address the challenge of determining prognosis and outcomes of HCC (4). Ultimately, HCC is a rapidly infiltrating malignancy with patients presenting with large, multifocal tumors with vessel invasion. Thus, there is a strong impetus to develop better methods of local treatment for HCC.

Treatment of HCC is most effective in the early stages of disease, but diagnosing early-stage HCC is often difficult since symptoms are vague. Surveillance programs are recommended for individuals with any of the aforementioned key risk factors (5-7) and diagnosis may be established with biopsy or radiographic studies alone. Once the diagnosis of HCC has been established, surgical resection should be the first consideration as it has shown to provide the best long-term survival (8). Unfortunately, most HCC patients do not qualify for surgery due to a number of medical comorbidities. Nor do they meet the strict eligibility for liver transplantation. There is high morbidity and many HCC patients are too ill to tolerate these surgeries (9-11). Several other local treatments are available for unresectable HCC or for tumor down-staging while awaiting liver transplantation. Other ablative therapies include transarterial chemoembolization (TACE), alcohol injection, cryotherapy, radiofrequency ablation, and focused ultrasound therapy. Nonetheless, the patient suitability of each of these local therapy remains rather limited (12).

It is apparent that an effective local-regional therapy is needed which can be applied to a broad range of patients. The 5-year survival rate for patients diagnosed with HCC remains poor at approximately 3-5% (13). The role of

external beam radiotherapy has historically been considered ineffective for treating HCC because the doses of radiation necessary to cure HCC far exceeded liver tissue tolerance to radiation. There is accumulating evidence that dose escalation can improve both tumor response and survival in HCC patients (14,15). One particularly challenging aspect of HCC is the fact that radiotherapy is guided not only by the characteristics of the tumor but also by the function of the cirrhotic liver. Modern three-dimensional radiotherapy techniques have allowed clinicians to increase dose conformity while escalating dose to the tumor while sparing more normal liver, thus, largely avoiding radiation-induced liver disease (RILD). Several reports have shown that high-dose irradiation to a portion of the liver could be delivered safely with reasonable treatment efficacy (16,17). Charged particle therapy, in particular proton therapy, shows great promise in treating HCC since it allows for tumor dose escalation while sparing critical normal structures.

Characteristics of proton therapy

Proton therapy, among other charged-particle therapies, offers distinct dosimetric advantages in comparison to photon radiotherapy. The depth dose characteristics of these two beams are qualitatively different. Due to physical laws, photons are absorbed exponentially in a specific tissue whereas protons exhibit a finite range depending on the initial proton energy.

A proton beam loses its energy via coulombic interactions with electrons as it traverses tissue. The energy loss of a proton beam per unit path length is small until the end of the beam range. Near the end of the proton range the residual energy over the beam is lost over a very short distance and the beam itself comes to rest. This results in a distinctive sharp rise in the dose absorbed by the tissue, known as the "Bragg peak". The low-dose region located between the Bragg peak and the beam entrance is called the "plateau", with its dose being approximately 30% to 40% of the maximum dose.

The Bragg peak is narrow in nature. This poses a problem when it comes to irradiating larger targets. To overcome this, clinical proton beams are modulated to extend the length of the Bragg peak. Several beams of similar energy are closely spaced and superimposed to create a region of uniform dose over length of the target. These extended regions are called "spread-out Bragg peaks" (18).

The rationale for proton therapy in HCC

The above mentioned physical characteristics of proton beams confer significant dosimetric advantages as compared to photon radiotherapy. The extent of scatter which accounts for lateral penumbra of the beam is less in proton beams when compared with photon beams. The dose delivered to tissues by a proton beam rises to a maximum value at a particular depth and then falls off exponentially to lower doses once the Bragg peak depth has been reached. This dosimetric advantage can be seen for each individual beam in a proton radiotherapy treatment plan. This allows for improvements in dose conformity and sparing of normal organs around the liver including the remaining uninvolved liver, heart, spinal cord, kidneys, bowel, and stomach. Proton radiotherapy is also able to completely spare one kidney more often than photon radiotherapy. More modern treatment techniques such as intensity-modulated proton therapy (IMPT) allow for more conformal high dose delivery while sparing nearby tissues at risk. Dose comparison studies have shown significantly reduced dose toxicity to regular tissues when compared to photon plans equivalent target coverage (19). IMPT has also demonstrated considerable sparing of normal liver tissue in comparison to photon-based intensity-modulated radiation therapy (IMRT) (20)

Dose conformity aside, proton radiotherapy delivers lower integral dose to tissue when compared to photon radiotherapy. Many HCC patients have severe liver disease with low functional reserve. Therefore, it is critical to limit the integral dose to the liver as much as possible. Modern photon therapy techniques such as intensity-modulated radiation therapy (IMRT) may achieve prescription conformity similar to that of a proton treatment plan, but the amount of dose scattered to the remainder of the liver is still higher owing to the physical nature of photon beams. There is evidence that normal liver function is significantly positively correlated to the percentage of normal that is not irradiated (21). Reduction of integral dose to remaining liver may help preserve liver function, decrease the risk of secondary malignancies, and also allow for future retreatment of the liver.

HCC radiation treatment planning with proton therapy

The unique physical properties of proton beams pose challenges not encountered in photon radiotherapy. Unlike photon beams, a distal beam edge must be defined for a proton beam. Since the majority of a proton beam's dose is delivered at the end of its range at the Bragg peak it is

crucial to define accurately where the beam stops. The use of compensators in the treatment gantry allows the physician to control the location of the beam's distal edge. A "smearing algorithm" is then applied to ensure dose coverage along the entire extent of the target region. However, due to variations in daily patient setup a certain amount of normal tissue beyond the distal extent of the target will receive some dose of radiation. At some institutions, 4-dimensional CT treatment planning is utilized which takes into account the patient's free breathing. One method is a breath-hold technique whereby the patient is asked to inhale deeply and hold his breath until the scan is complete. Other institutions apply a respiratory gating technique which maps a sinusoidal pattern of the patient's respiratory motion. The beam is then synced and turned during the same phase of each breathing cycle. Image acquisition during the portal venous and arterial enhancement phases may show differences in tumor and normal tissue attenuation. Thus, it is essential for each institution to develop a scanning protocol that allows for optimal target delineation (22).

The aforementioned variation in daily patient set-up and target motion is a challenge encountered in photon radiotherapy as well. However, range uncertainty is a unique problem encountered by proton radiotherapy. In the setting of external beam radiotherapy there is variable beam attenuation seen in the beam path. This occurs when the radiation beam traverses tissues of different density along its path. Proton beams deposit nearly all its energy within the tissue with very little exit dose. These range uncertainties stem from artifacts in computed tomography (CT) scans and errors in converting CT Hounsfield units into proton stopping power. These errors occur due to changes in organ motion during normal respiration or variations in daily set-up. For example, a high-density rib adjacent to air-filled lung moving into and out of the beam path during normal respiration creates uncertainty in the beam path. A similar phenomenon may be seen if the beam traverses loops of bowel which shift position each day. Ultimately, this range uncertainty may result in areas of target and normal tissues unexpectedly being overdosed or underdosed.

The relative biological effective (RBE) of proton beams, as compared with photons, is assigned a value of 1.1 by consensus at most institutions. This means that a physical dose of 1 Gy delivered using a proton beam is considered biologically equivalent to 1.1 Gy delivered using a photon beam. The assignment of relative biological effectiveness (RBE) is dependent on a number of biological endpoints which are often unpredictable (23,24). Because of this unpredictability and the aforementioned issue of range uncertainty, beam arrangements are often selected so that they do not stop directly in front of critical organs or structures.

From a dosimetric standpoint, liver tumors have a benefit of being located within a relatively homogenous liver organ. There is less variable density within the liver itself. On that same note, however, dose conformality may be restricted if the beam angle selection to confined to only those that travel entirely through liver tissue. Doing so may also increase the integral dose delivered to the normal liver since the beam is traversing more normal liver tissue and the proximal extent of the beam is often less conformal than the distal extent. However, dose conformality with sparing of adjacent normal liver may lend itself to post treatment dosimetic verification utilizing CT changes in order to assess geometric accuracy of treatment delivery (25).

Dose constraint models for proton-based planning

The liver is a relatively radiosensitive organ which has a limited ability to tolerate the significant dose needed to control HCC. Radiation induced liver disease (RILD) is a clinically defined entity that occurs in the liver after being exposed to high doses of radiotherapy. It is associated with a 2- to 4-fold increase in hepatic enzymes, ascities, fatigue, and anicteric hepatomegaly. The normal tissue complication probability model for RILD developed at the University of Michigan has found widespread application in clinical practice. However, this model is based on RILD that arose in patients treated with hyperfractionated photon radiotherapy (26). Many proton radiotherapy protocols for HCC utilize hypofractionated treatment regimens which are not well-represented by this model.

Another biological model based on the equivalent uniform dose (EUD) was developed by the proton radiotherapy group at Massachusetts General Hospital (27). In this model the 2-dimensional information from the dose-volume histogram (DVH) of inhomogenously irradiated liver is expressed as a single dose value. The EUD expresses mean dose while taking into account volume irradiated. Early application of this model found tumor dose escalation to be limited by adjacent non-liver normal tissues, such as biliary stenosis, rather than liver toxicity.

Aside from reducing the risk of RILD, patients with cirrhosis often undergo advancement of their Child-Pugh score after a course of radiotherapy to the liver. This

portends to worse outcomes and decreased quality of life. The volume of normal liver sparing has been associated with a decreased risk of advancing Child-Pugh class in cirrhotic patients (28). Other structures in the beam path such as ribs post a risk of late post-radiotherapy complication. Rib fracture has been reported as a late complication following external beam radiotherapy. One series looked at 310 ribs which were irradiated during a course of hypofractionated proton radiotherapy (29). Twenty-seven (8.7%) of these irradiated patientsdeveloped rib fracture. The volume of rib receiving at least 60 Gy (V60) was found to be the most statistically significant parameter predicting late rib fractures. Other parameters which were found useful for estimating rib fracture risk were V30, V120, and maximum dose (Dmax) to a point.

There are also reports of a two-step surgical treatment which involves the surgical placement of a spacer into the gastrointestinal tract (30). The intent of the spacer is to create a firm, reproducible separation between the radiation target and adjacent normal tissues. Of course, placement of this spacer as a second surgery will expose the patient to the additional risks also seen in other surgeries. The variety of tissue-sparing precautions selected for any individual patient must take into account medical comorbidities and underlying conditions. Nonetheless, it is evident that great care must be taken while findings ways to assess and limit normal organ toxicity during hypofractionated proton radiotherapy.

Clinical outcomes of HCC treated with proton radiotherapy

Many of the studies looking at the use of proton radiotherapy in liver tumors were performed in Asia (31). One of the first large retrospective series was presented by Chiba *et al*. (32). In this series 162 patients were treated with proton radiotherapy, all treatments delivered with hypofractionated regimens (3.5-5 CGE) with total doses ranging from 50 CGE (10 fractions) to 84 CGE (24 fractions) with a median dose of 72 CGE in 16 fractions over 29 days. Portal vein thrombus was seen in 25 patients (15%). At a median follow-up interval of 31.7 months, the 5-yearlocal control rate was 86.9% and overall survival rate was 23.5%. However, over 50% of deaths were due to complications from cirrhosis rather than tumor progression. The acute side effects in this study were limited primarily to liver enzyme elevation. Only 3% of the patients experienced grade 2 or higher late toxicity. Several recent retrospective studies show similar overall survival and local control rates in a similar population (33,34).

More recently, Komatsu *et al*. reported on the retrospective review of 343 consecutive patients with HCC treated at the Hyogo Ion Beam Medical Center with proton or carbon ion therapies (35). For the 285 patients for which both proton and carbon ion beams were available, treatment planning with both modalities were performed and the better treatment plan was selected based on dosimetric criteria. A total of 242 patients were treated with proton therapy using 8 different dose and fractionation protocols from 2001-2009. Pooled results show for proton therapy show 5 year local control rates of 90.2% with 5 year overall survival of 38%. Results of carbon ion therapy appear non-inferior, but limitations with treatment delivery resulted in the majority of patients (66%) being treated with proton therapy.

Patients with portal venous thrombosis may especially benefit from the dosimetric advantages offered by proton radiotherapy. Larger volumes of liver often need to be irradiated in the setting of portal venous thrombosis. Many of these patients have poor functional reserve remaining in the liver and photon therapy may result in unacceptable toxicity. A series of 35 patients with HCC portal venous thrombosis received treatment of 50 to 72 CGE which resulted in local control rates of over 45% at 2 years. Only 3 of these patients developed severe acute toxicity (36). The excellent conformality of proton beams may open up the possibilities for retreatment in the case of HCC progression or for synchronous tumors arising elsewhere in the liver. The Tsukuba proton radiotherapy group has reported on the efficacy, feasibility, and safety of HCC retreatment in a series of 27 patients with 68 total lesions (37). The median dose delivered was 66 CGE in 16 fractions with a median time interval of 24 months between the first and second course of treatment. They reported a 5-year local control rate of 87.8% and 5-year overall survival rate of 56%.

As mentioned before, cirrhotic patients have very little functional reserve in the liver and are at high risk for hepatic insufficiency. A study examining proton therapy in HCC showed correlation with grade of cirrhosis and toxicity. One third of the patients in this study had Child-Pugh class B cirrhosis with a 40% rate of grade 3 toxicity and 27% of patients eventually developing hepatic insufficiency (38). Damage to the alimentary tract is another cause of great concern as the doses necessary to control HCC are high and often greater than bowel tolerance. One series of 47 patients with HCC located within 2 cm of the alimentary

tract underwent treatment of 72.6 CGE in 22 fractions or 77 CGE in 35 fractions (39). After a median follow-up period of 23 months the overall survival was 50% and progression free survival 88.1%. Grade 2 and 3 alimentary tract hemorrhage was observed in 6.4% and 2.1% of patients, respectively. Beams were edited off of bowel in this study to avoid excess radiation delivered to the alimentary tract.

Prospective data for the use of proton radiotherapy in HCC is rather limited. One randomized study from Japan looking at 30 patients with local HCC reported a 3 year overall survival rate of 62% and local control rate of 95%. All tumors in this study did not invade into the gastrointestinal tract. Well-compensated hepatitis C was present in 90% of the patients with bilirubin <3.0 mg/dL. The dose delivered was 76 CGE in 20 fractions to the tumors which were entirely encompassed within the target volume (38). Another more recent randomized study of 51 patients in Japan reported a 5 year overall survival of 38.7% and local control of 87.8%. A dosing scheme of 66 CGE in 10 fractions was delivered to the tumor. This study included larger tumors as well as patients with symptomatic hepatitis C infections. Approximately two-thirds of the patients in this study had received prior local therapy as well (40).

One of the larger prospective studies was a phase II trial examining outcomes of proton radiotherapy in HCC patients with cirrhosis demonstrated a 66% 2-year overall survival rate after delivering 76 CGE in 3.8 CGE daily fractions (36). Loma Linda University reported results of the largest prospective phase II trial describing the use of proton radiotherapy in patients with HCC. Patients without cirrhosis, with extrahepatic metastases, tense ascites, or greater than 3 liver lesions were excluded. Patients were eligible regardless of tumor size, transplant candidacy, or alpha-fetoprotein (AFP) level. All patients had documented stability of ascites. Fluctuating levels of ascites could impact treatment planning by altering the path of beam attenuation. Shifting fluid content during the course of treatment due procedures such as a paracentesis would affect the targeting of treatment volumes. As such, all patients were required to have documented stability of ascitic fluid levels prior to treatment. Preliminary results were initially reported with 34 cases of unresectable HCC were treated with 63 CGE in 15 fractions (41). The 2-year overall survival rate was 55% and the local control rate was 75%. Mild acute radiation-induced toxicity was noted in 60% of patients but no radiation induced liver disease (RILD) was observed. Patients continued to be enrolled on this trial and updated results were recently reported (42). In this report, 42 additional patients were accrued for a total of 76 evaluable patients. Median progression-free survival for the entire group was 36 months, with a 60% 3-year progression free survival in patients within the Milan criteria. Eighteen patients subsequently underwent liver transplantation, with 6 explants showing complete pathological complete response and 7 explants showing only microscopic residual. The overall survival rate was significantly better in patients receiving liver transplant in comparison to those who did not, 70% *vs*. 10%, respectively.

Post treatment toxicity was minimal with no patients exhibiting RILD or significant changes in MELD scores. Grade 2 GI toxicity was noted in 5 patients with GI bleeding and/or endoscopic evidence of ulceration. All cases were managed medically without surgical intervention. All 5 cases were observed in the first 30 patients as greater care was taken to reduce field margins when tumors occurred adjacent to the bowel after the toxicities were observed. Overall, this is the largest prospective study reported with extensive follow-up that shows that proton therapy is safe and effective for the treatment of HCC. A randomized control trial is underway, comparing proton therapy to transarterial chemoembolization.

Overall, proton radiotherapy has demonstrated some of the most promising outcomes in terms of HCC treatment. The potential for toxicity in treating HCC is highly variable based on the location of the tumor within the liver and baseline liver function. The dosimetric advantages seen with proton radiotherapy appear to allow more feasible tumor dose escalation.

Conclusions

Historically, radiation therapy did not play a prominent role in HCC treatment. Earlier radiation techniques often delivered substantial doses to the liver causing a high incidence of RILD. The liver has a rather limited ability to tolerate substantial doses of radiation. Computerized and three-dimensional treatment planning has allowed better dose conformity thus allowing dose escalation to the tumor. The distinctive physical properties of proton beams confer unique advantages over photon radiotherapy. Many HCC patients have a number of morbidities which make them non-candidates for surgical resection or transplantation. The excellent toxicity profiles and durable in-field local control rates make proton radiotherapy an attractive option for localized HCC.

In principle, it is likely that the greater sparing of uninvolved liver using proton radiotherapy may be safer in patients with cirrhosis or poor liver reserve. The importance of normal liver-sparing is also evident in patients with portal venous thrombosis, since they often require greater volumes of liver to be irradiated. Centrally located lesions or lesions located near critical structures such as vessels may be especially suitable for proton radiotherapy. Proton radiotherapy is becoming increasingly available globally. Nearly 30 clinical proton radiotherapy facilities have been established worldwide. The integration of proton radiotherapy into treatment algorithms requires a great deal of multidisciplinary collaboration and highly individualized optimization for each patient. Nevertheless, there is accumulating evidence demonstrating the safety and efficacy of proton radiotherapy for liver-directed HCC therapy.

Acknowledgements

Disclosure: The authors declare no conflict of interest.

References

1. Bosch FX, Ribes J, Díaz M, et al. Primary liver cancer: worldwide incidence and trends. Gastroenterology 2004;127:S5-S16.
2. Venook AP, Papandreou C, Furuse J, et al. The incidence and epidemiology of hepatocellular carcinoma: a global and regional perspective. Oncologist 2010;15:5-13.
3. Jiang X, Pan SY, de Groh M, et al. Increasing incidence in liver cancer in Canada, 1972-2006: Age-period-cohort analysis. J Gastrointest Oncol 2011;2:223-31.
4. Marrero JA, Kudo M, Bronowicki JP. The challenge of prognosis and staging for hepatocellular carcinoma. Oncologist 2010;15:23-33.
5. Lau WY, Lai EC. Hepatocellular carcinoma: current management and recent advances. Hepatobiliary Pancreat Dis Int 2008;7:237-57.
6. Al Ustwani O, Iancu D, Yacoub R, et al. Detection of circulating tumor cells in cancers of biliary origin. J Gastrointest Oncol 2012;3:97-104.
7. Liu JH, Chen PW, Asch SM, et al. Surgery for hepatocellular carcinoma: does it improve survival? Ann Surg Oncol 2004;11:298-303.
8. Page AJ, Kooby DA. Perioperative management of hepatic resection. J Gastrointest Oncol 2012;3:19-27.
9. Aragon RJ, Solomon NL. Techniques of hepatic resection. J Gastrointest Oncol 2012;3:28-40
10. May KS, Yang GY, Khushalani NI, et al. Association of Technetium (99m) MAG-3 renal scintigraphy with change in creatinine clearance following chemoradiation to the abdomen in patients with gastrointestinal malignancies. J Gastrointest Oncol 2010;1:7-15.
11. Munireddy S, Katz S, Somasundar P, et al. Thermal tumor ablation therapy for colorectal cancer hepatic metastasis. J Gastrointest Oncol 2012;3:69-77.
12. Llovet JM, Burroughs A, Bruix J. Hepatocellular carcinoma. Lancet 2003;362:1907-17.
13. Bruix J, Sherman M, Practice Guidelines Committee, et al. Management of hepatocellular carcinoma. Hepatology 2005;42:1208-36.
14. Matsuzaki Y. Powerful radiotherapy for hepatocellular carcinoma. J Gastroenterol Hepatol 1999;14:1025-33.
15. Cheng JC, Chuang VP, Cheng SH, et al. Local radiotherapy with or without transcatheter arterial chemoembolization for patients with unresectable hepatocellular carcinoma. Int J Radiat Oncol Biol Phys 2000;47:435-42.
16. Dawson LA, McGinn CJ, Normolle D, et al. Escalated focal liver radiation and concurrent hepatic artery fluorodeoxyuridine for unresectable intrahepatic malignancies. J Clin Oncol 2000;18:2210-8.
17. Park HC, Seong J, Han KH, et al. Dose-response relationship in local radiotherapy for hepatocellular carcinoma. Int J Radiat Oncol Biol Phys 2002;54:150-5.
18. Schulte RW, Wore AJ. New developments in treatment planning and verification of particle beam therapy. Transl Cancer Res 2012;1:184-95.
19. Wang X, Krishnan S, Zhang X, et al. Proton radiotherapy for liver tumors: dosimetric advantages over photon plans. Med Dosim 2008 Winter;33:259-67.
20. Petersen JB, Lassen Y, Hansen AT, et al. Normal liver tissue sparing by intensity-modulated proton stereotactic body radiotherapy for solitary liver tumours. Acta Oncol 2011;50:823-8.
21. Mizumoto M, Okumura T, Hashimoto T, et al. Proton beam therapy for hepatocellular carcinoma: a comparison of three treatment protocols. Int J Radiat Oncol Biol Phys 2011;81:1039-45.
22. Li Z. Toward robust proton therapy planning and delivery. Transl Cancer Res 2012;1:217-26.
23. Gerweck LE, Kozin SV. Relative biological effectiveness of proton beams in clinical therapy. Radiother Oncol 1999;50:135-42.
24. Dale RG, Jones B, Cárabe-Fernández A. Why more needs

to be known about RBE effects in modern radiotherapy. Appl Radiat Isot 2009;67:387-92.
25. Fukumitsu N, Hashimoto T, Okumura T, et al. Investigation of the geometric accuracy of proton beam irradiation in the liver. Int J Radiat Oncol Biol Phys 2012;82:826-33.
26. Dawson LA, Normolle D, Balter JM, et al. Analysis of radiation-induced liver disease using the Lyman NTCP model. Int J Radiat Oncol Biol Phys 2002;53:810-21.
27. Niemierko A. Reporting and analyzing dose distributions: a concept of equivalent uniform dose. Med Phys 1997;24:103-10.
28. Mizumoto M, Okumura T, Hashimoto T, et al. Evaluation of liver function after proton beam therapy for hepatocellular carcinoma. Int J Radiat Oncol Biol Phys 2012;82:e529-35.
29. Kanemoto A, Mizumoto M, Okumura T, et al. Dose-volume histogram analysis for risk factors of radiation-induced rib fracture after hypofractionated proton beam therapy for hepatocellular carcinoma. Acta Oncol 2012. [Epub ahead of print].
30. Komatsu S, Hori Y, Fukumoto T, et al. Surgical spacer placement and proton radiotherapy for unresectable hepatocellular carcinoma. World J Gastroenterol 2010;16:1800-3.
31. Ling TC, Kang JI, Slater JD, et al. Proton therapy for gastrointestinal cancers. Transl Cancer Res 2012;1:150-8.
32. Chiba T, Tokuuye K, Matsuzaki Y, et al. Proton beam therapy for hepatocellular carcinoma: a retrospective review of 162 patients. Clin Cancer Res 2005;11:3799-805.
33. Sugahara S, Oshiro Y, Nakayama H, et al. Proton beam therapy for large hepatocellular carcinoma. Int J Radiat Oncol Biol Phys 2010;76:460-6.
34. Nakayama H, Sugahara S, Tokita M, et al. Proton beam therapy for hepatocellular carcinoma: the University of Tsukuba experience. Cancer 2009;115:5499-506.
35. Komatsu S, Fukumoto T, Demizu Y, et al. Clinical results and risk factors of proton and carbon ion therapy for hepatocellular carcinoma. Cancer 2011;117:4890-904.
36. Sugahara S, Nakayama H, Fukuda K, et al. Proton-beam therapy for hepatocellular carcinoma associated with portal vein tumor thrombosis. Strahlenther Onkol 2009;185:782-8.
37. Hashimoto T, Tokuuye K, Fukumitsu N, et al. Repeated proton beam therapy for hepatocellular carcinoma. Int J Radiat Oncol Biol Phys 2006;65:196-202.
38. Kawashima M, Furuse J, Nishio T, et al. Phase II study of radiotherapy employing proton beam for hepatocellular carcinoma. J Clin Oncol 2005;23:1839-46.
39. Nakayama H, Sugahara S, Fukuda K, et al. Proton beam therapy for hepatocellular carcinoma located adjacent to the alimentary tract. Int J Radiat Oncol Biol Phys 2011;80:992-5.
40. Fukumitsu N, Sugahara S, Nakayama H, et al. A prospective study of hypofractionated proton beam therapy for patients with hepatocellular carcinoma. Int J Radiat Oncol Biol Phys 2009;74:831-6.
41. Bush DA, Hillebrand DJ, Slater JM, et al. High-dose proton beam radiotherapy of hepatocellular carcinoma: preliminary results of a phase II trial. Gastroenterology 2004;127:S189-93.
42. Bush DA, Kayali Z, Grove R, et al. The safety and efficacy of high-dose proton beam radiotherapy for hepatocellular carcinoma: a phase 2 prospective trial. Cancer 2011;117:3053-9.

Cite this article as: Ling TC, Kang JI, Bush DA, Slater JD, Yang GY. Proton therapy for hepatocellular carcinoma. Chin J Cancer Res 2012;24(4):361-367. DOI: 10.3978/j.issn.1000-9604.2012.10.09

Review Article

Stereotactic body proton therapy for liver metastases

Joseph I. Kang Jr, Ted C. Ling, Jerry D. Slater, Gary Y. Yang

Department of Radiation Medicine, Loma Linda University Medical Center, Loma Linda, CA, USA

Correspondence to: Joseph I. Kang Jr, MD, PhD. Department of Radiation Medicine, Loma Linda University Medical Center, 11234 Anderson Street, B121, Loma Linda, CA 92354, USA. Email: jikang@llu.edu.

Abstract: Although surgical resection is the gold standard, stereotactic body radiotherapy (SBRT) is often the preferred treatment for metastatic liver tumors due to size, multi-focality, tumor distribution or patient co-morbidities limiting surgical options. The major dose-limiting concern in the use of SBRT for liver tumors is the risk of radiation-induced liver disease (RILD). This can limit the number of patients who may be candidates for conventional SBRT. The use of protons for SBRT is potentially attractive given the dosimetric advantages inherent to proton radiotherapy potentially offering a way to maximize tumor control via dose escalation while avoiding excessive radiation to the remaining liver and other organs at risk. In this review we discuss the physical attributes and rationale for stereotactic body proton therapy (SBPT) for the treatment of liver metastases.

Keywords: Proton therapy; radiation therapy; liver metastases; stereotactic body radiation therapy; stereotactic ablative body radiation

doi: 10.3978/j.issn.2218-676X.2012.12.03

Scan to your mobile device or view this article at: http://www.thetcr.org/article/view/789/html

Introduction

Liver metastases are a common occurrence for metastatic disease from many primary sites with estimates that 40-50% of all malignancies are complicated by liver metastases (1). Colorectal cancer is one of the most common solid malignancies to metastasize to the liver with approximately 20% of the estimated 150,000 patients diagnosed yearly in the United States with liver involvement at presentation and up to an additional 60% who develop liver metastases (2,3). Aggressive treatment of liver metastases may prolong survival in certain scenarios. Hepatic resection of liver metastases from colorectal cancer has become an accepted standard therapy for patients deemed operable with reported 5-year survival of 50-60% in selected series (3-8). The benefit of local therapy in non-colorectal liver metastases is less defined, but long-term survival has been reported after liver metastases resection from sarcoma, breast cancer, and other primary sites (9). Local control of hepatic metastases appears to be a major determinant of overall survival. However, 80-90% of patients are either patients with lesions that are surgically not resectable or are medically inoperable patients at the time of diagnosis (10). Therefore, there is an important role for a treatment that can provide the equivalent of tumor resection with minimal morbidity.

Stereotactic body radiotherapy (SBRT) delivers an ablative regimen of highly focused external beam radiotherapy that targets one or more discrete extracranial lesions. Published reports using SBRT to treat liver metastases have shown actuarial local control rates ranging from 50-100% with higher doses associated with better local control (11-18). Studies to date have been small but encouraging with the best results thus far showing no local failures at 2 years after 60 Gy in 5 fractions (13). A multi-institutional phase I/II study of SBRT for liver metastases showed the safety of dose escalation from 36 Gy up to 60 Gy in 3 fractions with a 2 year actuarial in-field local control rates of 92% (11). Lesions smaller than 3 cm had a 100% local control at 2 years. Although liver metastases from primary colorectal cancer represents the largest group treated with SBRT, many studies report a broad variety of tumor types treated with this technique with no apparent difference in local control.

Toxicities reported from these studies have been limited, and no acute SBRT-related deaths have been reported in studies reviewed. In a study of 141 lesions in the setting of metastatic colorectal cancer, there was a death from liver failure in a patient receiving >10 Gy to 60% of the liver (median 14.4 Gy) and a colon perforation warranting surgery (17). Given the 20-30 times higher incidence of liver metastases compared to primary liver cancer and the high likelihood of repeat treatments given the natural history of metastatic disease, proton therapy shows promise since it allows for similar tumor dose coverage for adequate local control while simultaneously limiting dose to critical normal structures including the normal liver parenchyma (1-3).

Characteristics of proton therapy

Proton therapy offers distinct dosimetric advantages in comparison to photon radiotherapy. The depth dose characteristics of proton and photon beams are qualitatively different. Due to physical laws, photons are absorbed exponentially in a specific tissue whereas protons exhibit a finite range depending on the initial proton energy. The energy of a proton beam is attenuated via coulombic interactions with electrons as it traverses tissue. The energy loss of a proton beam per unit path length is small until the end of the beam range. Towards the end of the proton range the remaining energy is lost over a very short distance and the beam itself comes to rest. This results in a characteristic steep rise in the dose absorbed by the tissue, known as the "Bragg peak". The low-dose region located between the Bragg peak and the entrance of an unmodulated beam is called the "plateau", with its dose being approximately 30% to 40% of the maximum dose.

The Bragg peak is narrow in nature. This presents a problem when irradiating wider targets. To overcome this, clinical proton beams are modulated to extend the length of the Bragg peak. Several beams of similar energy are closely spaced and superimposed to create a region of uniform dose over length of the target. These extended regions are called "spread-out Bragg peaks."

The rationale for stereotactic body proton therapy for liver metastases

The above mentioned physical characteristics of proton beams confer significant dosimetric advantages as compared to photon radiotherapy. The extent of scatter which accounts for lateral penumbra of the beam is less in proton beams than photon beams for typical treatment depths and beam energies. The dose delivered to tissues by a proton beam rises to a maximum value at a specified depth and then falls off exponentially to no dose once the Bragg peak depth has been reached. This dosimetric advantage can be seen for each individual beam in a proton radiation treatment plan. This permits improvements in dose conformity and sparing of normal organs around the liver including the remaining uninvolved liver, heart, spinal cord, kidneys, bowel, and stomach.

In addition to improved dose conformity, proton radiotherapy delivers lower integral dose to tissue when compared to photon radiotherapy. Modern photon therapy techniques such as intensity-modulated radiation therapy (IMRT) may achieve prescription conformity similar to that of a proton treatment plan, but the amount of dose scattered to the remainder of the liver is still higher due to the spreading out of the low dose volume seen with IMRT. There is evidence that normal liver function is significantly correlated to the percentage of normal liver that is not irradiated (19). This decreased integral dose to normal liver is more critical in patients with hepatocellular carcinoma who tend to have underlying cirrhosis, but may be clinically significant in patients with liver metastases particularly in patients with prior partial hepatectomy. Reduction of integral dose to remaining liver may help preserve liver function, decrease the risk of secondary malignancies, and also allow for future retreatment of the liver.

Radiation treatment planning with proton therapy

The unique physical properties of proton beams present challenges not seen in photon based radiotherapy. Unlike photon beams, a distal beam edge must be defined for a proton beam. Since the majority of a proton beam's dose is delivered at the end of its range at the Bragg peak it is critical to accurately delineate where the beam stops. Compensators in the treatment gantry allow the physician to control the location of the proton beam's distal edge. A "smearing algorithm" is then applied to ensure dose coverage along the entire extent of the target region. However, due to variations in daily patient setup and internal organ motion, a certain amount of normal tissue beyond the distal extent of the target will receive some dose of radiation.

At some institutions, 4-dimensional CT treatment planning is utilized which takes into account the patient's free breathing. Other institutions apply a respiratory gating technique which maps a sinusoidal pattern of the

patient's respiratory motion. The beam is then synced and turned during the same phase of each breathing cycle. At Loma Linda University, we employ a voluntary deep inspiration breath hold technique (SDX inc.) when treating liver lesions where the patient can independently monitor his/her breathing pattern and reproduce the effective breath hold using a spirometer and audio/visual feedback. Image acquisition during the portal venous and arterial enhancement phases may show differences in tumor and normal tissue attenuation. Thus, it is essential for each institution to develop a scanning protocol that allows for optimal target delineation.

Variation in daily patient set-up and target motion is a challenge encountered in photon radiotherapy as well. But range uncertainty is a unique problem encountered by proton radiotherapy. Variable beam attenuation can occur when the proton beam traverses tissues of different density along its path. A proton beam deposits nearly all its energy within the tissue with very little exit dose. These range uncertainties stem from artifacts in computed tomography (CT) scans and errors in converting CT Hounsfield units into proton stopping power. Additional errors occur due to changes in organ motion during normal respiration or variations in daily set-up. For example, a high-density rib adjacent to air-filled lung moving into and out of the beam path during normal respiration creates uncertainty in the beam path. A similar phenomenon may be seen if the beam traverses loops of bowel which shift position each day. Ultimately, this range uncertainty may result in areas of target and normal tissues unexpectedly being overdosed or underdosed. Because of the unpredictability of the relative biological effectiveness at the distal edge and the aforementioned issue of range uncertainty, beam arrangements are often selected so that they do not stop directly in front of critical organs or structures.

From a dosimetric standpoint, liver tumors have a benefit of being located within a relatively homogenous liver organ. There is less variable density within the liver itself. However, dose conformality may be restricted if the beam angle selection is confined to a path that travels entirely through liver tissue. Doing so may also increase the integral dose delivered to the normal liver since the beam is traversing more normal liver tissue and the proximal extent of the beam is often less conformal than the distal extent.

SBPT treatment planning comparisons for liver metastases

Several treatment planning comparison studies have been reported showing improved normal tissue dosimetry of proton based stereotactic body radiotherapy compared to photon based stereotactic body radiotherapy in the treatment of liver, lung and adrenal lesions (20-23). However, only one study compared these techniques in the treatment of liver tumors reporting a treatment planning comparison on 10 patients with solitary liver metastasis treated with multi-field SBRT that were re-planned with IMRT and proton pencil beam scanning techniques (20). The spared liver volume for the proton based plan was significantly higher compared to IMRT in all 10 patients and the mean liver dose was lower with the proton based plans (median 9.1 *vs.* 20.0 Gy; P<0.005).

Clinical outcomes for SBPT

There have been no reported outcomes using stereotactic body proton therapy yet, but protons have been used to treat hepatocellular carcinoma using various hypofractionated regimens (24-27). The largest reported prospective phase II study using proton radiotherapy for hepatocellular carcinoma (HCC) was done here at Loma Linda University Medical Center. Between 1998 and 2006, 76 patients with HCC were treated with proton radiotherapy with minimal acute toxicity, no reported radiation induced liver disease, and 3-year progression-free survival of 60% (26). Although all patients had cirrhosis, there were no reported dose limiting toxicity using doses of 63 Gray Equivalents (GyE) in 15 fractions showing the safety of such a treatment modality when normal tissue constraints are met.

At the time of this review, there are 2 active prospective clinical trials for proton based stereotactic body radiotherapy for liver metastases (28,29). Massachusetts General Hospital is conducting a non-randomized phase II trial comparing proton based and photon based stereotactic body radiotherapy techniques with individualized dose determined by size and location of tumor(s) given over 2-3 fractions (28). Here at Loma Linda University, we are conducting a phase I study to determine the feasibility and safety of stereotactic body proton therapy in patients with liver metastases followed by a phase II study to determine the efficacy of such treatment on local control (29). Patients will receive 3 fractions of SBPT starting at 12 GyE/fraction (total, 36 GyE), increased by 4 GyE/fraction for each subsequent dose group to 20 GyE/fraction (total, 60 GyE) according to standard phase I design. Treatment plans from first 2 patients on protocol

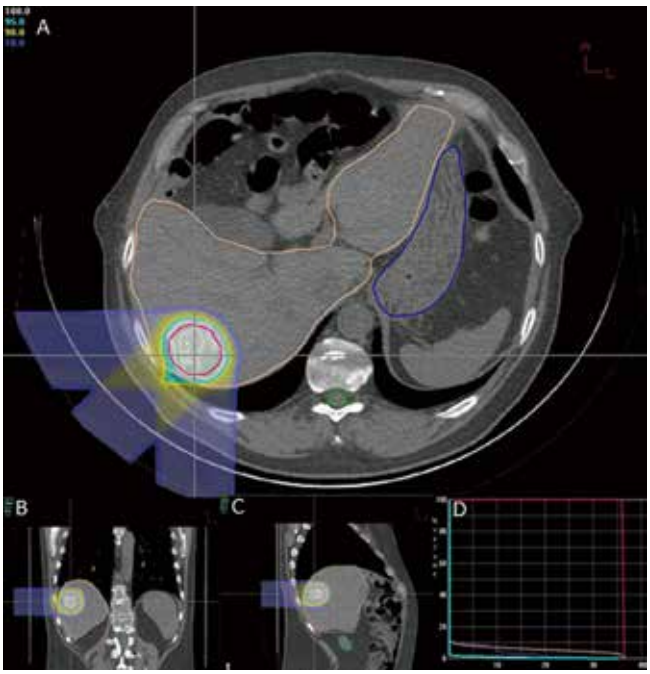

Figure 1 Stereotactic body proton plan. 77 year old female with recurrent stage II colorectal cancer with distant metastases status post liver resection in 2011 now with solitary liver metastases. Two proton fields, Right lateral and Right posterior oblique used to deliver 36 Gy in 3 fractions over 1 week. GTV (red), ITV expansion (pink), Liver (tan), right kidney (dark green), duodenum (light blue). Axial (A), Sagittal (B), Coronal (C) views. Isodose lines: Light blue (95%); Yellow (90%) Purple (10%). Dose volume histograms (D) of ITV overlapping with GTV showing high dose conformity to target and limited dose to organs at risk. Other organs at risk (not shown) including heart, lungs, spinal cord, contralateral kidney, etc. had negligible dose

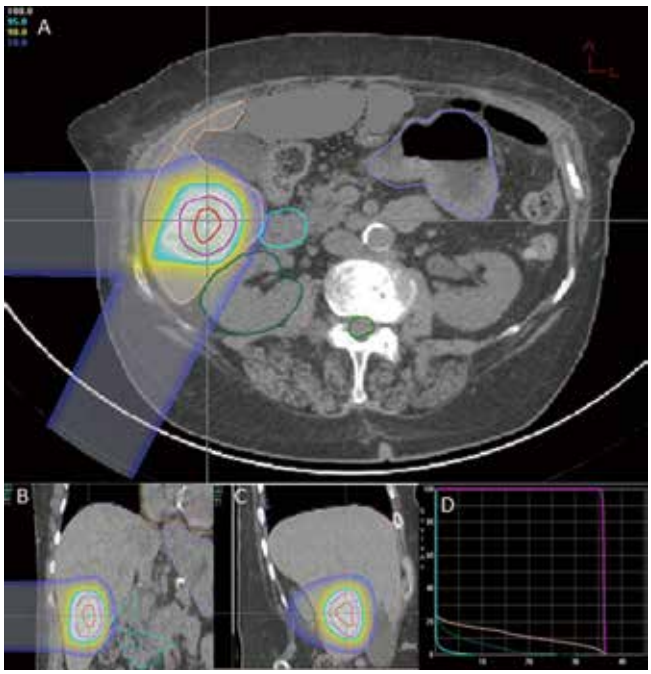

Figure 2 58 year old male with recurrent stage IV colorectal cancer with solitary liver metastases. Three proton fields, Right lateral, Right posterior oblique, Posterior fields used to deliver 36 GyE in 3 fractions over 1 week. ITV expansion (pink), Liver (tan), stomach (dark blue). Axial (A), Sagittal (B), Coronal (C) views. Isodose lines: Light blue (95%); Yellow (90%) Purple (10%). Dose volume histograms (D) showing ITV (pink), Liver (tan), body wall (purple), ipsilateral lung (light blue) with high dose conformity to target and limited dose to organs at risk

on dose level 1 show high dose conformity to target with limited dose to nearby organs at risk (*Figures 1,2*). The phase II portion of the study will evaluate local control at 2 years with the maximally tolerated dose from the phase I portion.

In patients with metastatic liver disease, aggressive local therapy using modern radiotherapy techniques are promising and project to have a substantial role in the treatment of unresectable liver metastases. The dosimetric advantage of proton therapy may lead to improved clinical outcomes with less morbidity. As yet, there are no clinical data to confirm this assertion. Reports from current clinical trials and experiences from other proton centers are eagerly anticipated.

Acknowledgements

Disclosure: The authors declare no conflict of interest.

References

1. Choti MA, Bulkley GB. Management of metastatic disease. In: Schiff ER, Sorrell MR, Maddrey WC. eds. Diseases of the liver. New Delhi: Lippincott-Raven, 1999:1319-33.
2. Bhattacharya R, Rao S, Kowdley KV. Liver involvement in patients with solid tumors of nonhepatic origin. Clin Liver Dis 2002;6:1033-43, x.
3. Choti MA, Sitzmann JV, Tiburi MF, et al. Trends in long-term survival following liver resection for hepatic colorectal metastases. Ann Surg 2002;235:759-66.
4. Fong Y, Fortner J, Sun RL, et al. Clinical score for predicting recurrence after hepatic resection for metastatic

colorectal cancer: analysis of 1001 consecutive cases. Ann Surg 1999;230:309-18; discussion 318-21.
5. Shah SA, Bromberg R, Coates A, et al. Survival after liver resection for metastatic colorectal carcinoma in a large population. J Am Coll Surg 2007;205:676-83.
6. House MG, Ito H, Gönen M, et al. Survival after hepatic resection for metastatic colorectal cancer: trends in outcomes for 1,600 patients during two decades at a single institution. J Am Coll Surg 2010;210:744-52, 752-5.
7. Robertson DJ, Stukel TA, Gottlieb DJ, et al. Survival after hepatic resection of colorectal cancer metastases: a national experience. Cancer 2009;115:752-9.
8. Reddy SK, Barbas AS, Marroquin CE, et al. Resection of noncolorectal nonneuroendocrine liver metastases: a comparative analysis. J Am Coll Surg 2007;204:372-82.
9. Groeschl RT, Nachmany I, Steel JL, et al. Hepatectomy for noncolorectal non-neuroendocrine metastatic cancer: a multi-institutional analysis. J Am Coll Surg 2012;214:769-77.
10. Small R, Lubezky N, Ben-Haim M. Current controversies in the surgical management of colorectal cancer metastases to the liver. Isr Med Assoc J 2007;9:742-7.
11. Rusthoven KE, Kavanagh BD, Cardenes H, et al. Multi-institutional phase I/II trial of stereotactic body radiation therapy for liver metastases. J Clin Oncol 2009;27:1572-8.
12. Lee MT, Kim JJ, Dinniwell R, et al. Phase I study of individualized stereotactic body radiotherapy of liver metastases. J Clin Oncol 2009;27:1585-91.
13. Rule W, Timmerman R, Tong L, et al. Phase I dose-escalation study of stereotactic body radiotherapy in patients with hepatic metastases. Ann Surg Oncol 2011;18:1081-7.
14. Goodman KA, Wiegner EA, Maturen KE, et al. Dose-escalation study of single-fraction stereotactic body radiotherapy for liver malignancies. Int J Radiat Oncol Biol Phys 2010;78:486-93.
15. Herfarth KK, Debus J, Wannenmacher M. Stereotactic radiation therapy of liver metastases: update of the initial phase-I/II trial. Front Radiat Ther Oncol 2004;38:100-5.
16. Wulf J, Guckenberger M, Haedinger U, et al. Stereotactic radiotherapy of primary liver cancer and hepatic metastases. Acta Oncol 2006;45:838-47.
17. Hoyer M, Roed H, Traberg Hansen A, et al. Phase II study on stereotactic body radiotherapy of colorectal metastases. Acta Oncol 2006;45:823-30.
18. van der Pool AE, Méndez Romero A, Wunderink W, et al. Stereotactic body radiation therapy for colorectal liver metastases. Br J Surg 2010;97:377-82.
19. Mizumoto M, Okumura T, Hashimoto T, et al. Proton beam therapy for hepatocellular carcinoma: a comparison of three treatment protocols. Int J Radiat Oncol Biol Phys 2011;81:1039-45.
20. Petersen JB, Lassen Y, Hansen AT, et al. Normal liver tissue sparing by intensity-modulated proton stereotactic body radiotherapy for solitary liver tumours. Acta Oncol 2011;50:823-8.
21. Macdonald OK, Kruse JJ, Miller JM, et al. Proton beam radiotherapy versus three-dimensional conformal stereotactic body radiotherapy in primary peripheral, early-stage non-small-cell lung carcinoma: a comparative dosimetric analysis. Int J Radiat Oncol Biol Phys 2009;75:950-8.
22. Hoppe BS, Huh S, Flampouri S, et al. Double-scattered proton-based stereotactic body radiotherapy for stage I lung cancer: a dosimetric comparison with photon-based stereotactic body radiotherapy. Radiother Oncol 2010;97:425-30.
23. Scorsetti M, Mancosu P, Navarria P, et al. Stereotactic body radiation therapy (SBRT) for adrenal metastases : a feasibility study of advanced techniques with modulated photons and protons. Strahlenther Onkol 2011;187:238-44.
24. Bush DA, Kayali Z, Grove R, et al. The safety and efficacy of high-dose proton beam radiotherapy for hepatocellular carcinoma: a phase 2 prospective trial. Cancer 2011;117:3053-9.
25. Fukumitsu N, Sugahara S, Nakayama H, et al. A prospective study of hypofractionated proton beam therapy for patients with hepatocellular carcinoma. Int J Radiat Oncol Biol Phys 2009;74:831-6.
26. Kawashima M, Furuse J, Nishio T, et al. Phase II study of radiotherapy employing proton beam for hepatocellular carcinoma. J Clin Oncol 2005;23:1839-46.
27. Nakayama H, Sugahara S, Tokita M, et al. Proton beam therapy for hepatocellular carcinoma: the University of Tsukuba experience. Cancer 2009;115:5499-506.
28. ClinicalTrials.gov; Identifier: NCT01239381
29. ClinicalTrials.gov; Identifier: NCT01697371

Cite this article as: Kang JI Jr, Ling TC, Slater JD, Yang GY. Stereotactic body proton therapy for liver metastases. Transl Cancer Res 2012;1(4):271-275. doi: 10.3978/j.issn.2218-676X.2012.12.03

Original Article

Proton therapy may allow for comprehensive elective nodal coverage for patients receiving neoadjuvant radiotherapy for localized pancreatic head cancers

Richard Y. Lee[1], Romaine C. Nichols Jr[2], Soon N. Huh[2], Meng W. Ho,[2] Zuofeng Li[2], Robert Zaiden[3], Ziad T. Awad[4], Bestoun Ahmed[3], Bradford S. Hoppe[2]

[1]Radiation Medicine, Roswell Park Cancer Institute, University at Buffalo, NY, USA; [2]Radiation Oncology, University of Florida Proton Therapy Institute, USA; [3]Medicine, University of Florida College of Medicine, USA; [4]Surgery, University of Florida College of Medicine, USA

Correspondence to: Romaine C. Nichols Jr, MD. University of Florida Proton Therapy Institute, 2015 North Jefferson St., Jacksonville, FL 32206, USA. Email: rnichols@floridaproton.org.

Background: Neoadjuvant radiotherapy has the potential to improve local disease control for patients with localized pancreatic cancers. Concern about an increased risk of surgical complications due to small bowel and gastric exposure, however, has limited enthusiasm for this approach. Dosimetric studies have demonstrated the potential for proton therapy to reduce intestinal exposure compared with X-ray-based therapy. We sought to determine if neoadjuvant proton therapy allowed for field expansions to cover high-risk nodal stations in addition to the primary tumor.

Methods: Twelve consecutive patients with nonmetastatic cancers of the pancreatic head underwent proton-based planning for neoadjuvant radiotherapy. Gross tumor volume was contoured using diagnostic computed tomography (CT) scans with oral and intravenous contrast. Four-dimensional planning scans were utilized to define an internal clinical target volume (ICTV). Five-mm planning target volume (PTV) expansions on the ICTV were generated to establish an initial PTV (PTV1). A second PTV was created using the initial PTV but was expanded to include the high-risk nodal targets as defined by the RTOG contouring atlas (PTV2). Optimized proton plans were generated for both PTVs for each patient. All PTVs received a dose of 50.4 cobalt gray equivalent (CGE). Normal-tissue exposures to the small bowel space, stomach, right kidney, left kidney and liver were recorded. Point spinal cord dose was limited to 45 CGE.

Results: Median PTV1 volume was 308.75 cm^3 (range, 133.33-495.61 cm^3). Median PTV2 volume was 541.75 cm^3 (range, 399.44-691.14 cm^3). In spite of the substantial enlargement of the PTV when high-risk lymph nodes were included in the treatment volume, normal-tissue exposures (stomach, bowel space, liver, and kidneys) were only minimally increased relative to the exposures seen when only the gross tumor target was treated.

Conclusions: Proton therapy appears to allow for field expansions to cover high-risk lymph nodes without significantly increasing critical normal-tissue exposure in the neoadjuvant setting.

Keywords: Proton therapy; pancreatic; dosimetry; neoadjuvant radiotherapy

doi: 10.3978/j.issn.2078-6891.2013.043

Scan to your mobile device or view this article at: http://www.thejgo.org/article/view/1395/2275

Background

Pancreatic cancer is the fifth leading cause of cancer mortality in the United States. In 2011, there were an estimated 44,030 new cases and 37,660 deaths (1). Curative therapy for patients with nonmetastatic disease necessarily includes extirpative surgery. Unfortunately, the surgical literature suggests a local-regional failure rate ranging from 50% to 80% for patients undergoing pancreaticoduodenectomy (2,3). Recognizing this concern, postoperative radiotherapy has been offered in an effort to increase the likelihood of local disease control. While the shortcomings of these studies have been well-described in

the oncologic literature (4), the results of studies by the European Study Group for Pancreatic Cancer (ESPAC) suggest that postoperative X-ray-based radiotherapy fails to offer an improvement in survival over surgery and chemotherapy alone (5). The problems with postoperative radiation therapy are that (I) radiotherapy cannot be delivered until several weeks after surgery because of postoperative convalescence and (II) postoperative radiotherapy doses are limited by the large volume of transposed small bowel in the radiotherapy target volume.

Preoperative neoadjuvant radiotherapy would potentially avoid these problems. A drawback of preoperative X-ray-based radiotherapy, however, is that small bowel and gastric exposure in the neoadjuvant setting can complicate an already challenging major surgical intervention. Several dosimetric studies suggest that proton therapy has the potential to improve the therapeutic index over X-ray-based radiotherapy by reducing such normal-tissue exposure (6-10). Various clinical outcome studies also suggest low rates of gastrointestinal toxicity when protons are used to treat pancreatic cancers (11,12). Although many published studies on the use of neoadjuvant radiotherapy for patients with pancreatic cancer targeted the primary tumor and ***selective*** regional nodes (13-15), others only targeted the gross tumor with no specific effort to cover regional lymph nodes (16,17). In this setting, some nodal targets are ostensibly omitted in an effort to limit gastrointestinal toxicity, even though nodal metastases may be identified in 39% to 71% of these patients (3,18,19) at the time of surgery. The current study was undertaken to assess the feasibility of leveraging the improved therapeutic index of protons to deliver comprehensive elective nodal irradiation in the neoadjuvant setting.

Methods

Twelve consecutive patients with nonmetastatic cancers of the pancreatic head underwent treatment planning for neoadjuvant chemoradiation at our institution. Patients were immobilized using a standard wing-board and a lower extremity stabilizer. Four-dimensional computed tomography (CT) without contrast and three-dimensional CT with oral and intravenous contrast was performed. Patients were imaged on a Philips Brilliance large-bore CT scanner with a 60-cm field of view and 1-mm slices (Philips Healthcare, Amsterdam, the Netherlands). Gross tumor volume was contoured and guided by diagnostic CT scans with contrast, magnetic resonance imaging (MRI), and positron emission tomography (PET)-CT. Four-dimensional planning scans were utilized to define an internal clinical target volume (ICTV). Five-mm planning target volume (PTV) expansions were generated to establish the final PTV (labeled the PTV1) for the gross disease.

A second planning target volume (PTV2) was created using the initial PTV expanded to include the high-risk nodal targets as defined by the Radiation Therapy Oncology Group (RTOG) contouring atlas (20). Elective nodal expansions were based on either (I) the most proximal 1.0 to 1.5 cm of the celiac artery (CA); (II) the most proximal 2.5 to 3.0 cm of the superior mesenteric artery (SMA); (III) the portal vein segment extending from the bifurcation to the confluence with either the superior mesenteric vein (SMV) or splenic vein (SV); and (IV) the aorta from the most cephalad contour of either the celiac axis or portal vein to the bottom of the L2 vertebral body. If the gross tumor volume (GTV) contour extended to or below the bottom of L2, the aorta contour was extended towards the bottom of L3. To achieve elective nodal expansions on the CTV, the CA, SMA, and portal vein were expanded by 1.0 to 1.5 cm in all directions and the aortic region of interest was expanded 2.5 to 3.0 cm to the right, 1.0 cm to the left, 2.0 to 2.5 cm anteriorly, and 0.2 cm posteriorly towards the anterior edge of the vertebral body. The goal of the asymmetric expansion was to include the prevertebral nodal regions (retroperitoneal space) from the top of the portal vein or celiac axis (whichever was most superior) to the bottom of L2 (or L3 if the GTV location was too low).

Proton plans were generated on a Varian Eclipse 8.9 planning system (Varian Medical Systems Inc., Palo Alto, CA).

The proton treatment table top was inserted into the CT images manually and aligned with the CT table top so that the proton range and skin dose could be correctly calculated. A CT-Hounsfield unit to proton relative stopping-power conversion curve was used for proton range calculations. An effort was made to account for patient setup variability, respiratory motion, and delivery uncertainties, both by using appropriate distal and proximal margins to account for uncertainties in stopping-power conversion and by evaluating the presence of bowel and stomach contents in beam paths. The distal and proximal margins for each treatment field were estimated to be 2.5% of the beam range to the distal/proximal PTV plus 1.5 mm. Distal and proximal median spread-out Bragg peak (SOBP) expansions of 8 mm (range, 6-9 mm) and 10 mm (range, 8-12 mm) smearing margins were utilized for each beam.

Field apertures were designed to conform to the PTV in the beam's-eye view, with an aperture margin adequate to account for the beam penumbrae (typically 10 mm uniformly around the PTV) depending on the beam range, except for edits that may have been necessary to avoid critical organs such as the kidneys. Range compensators

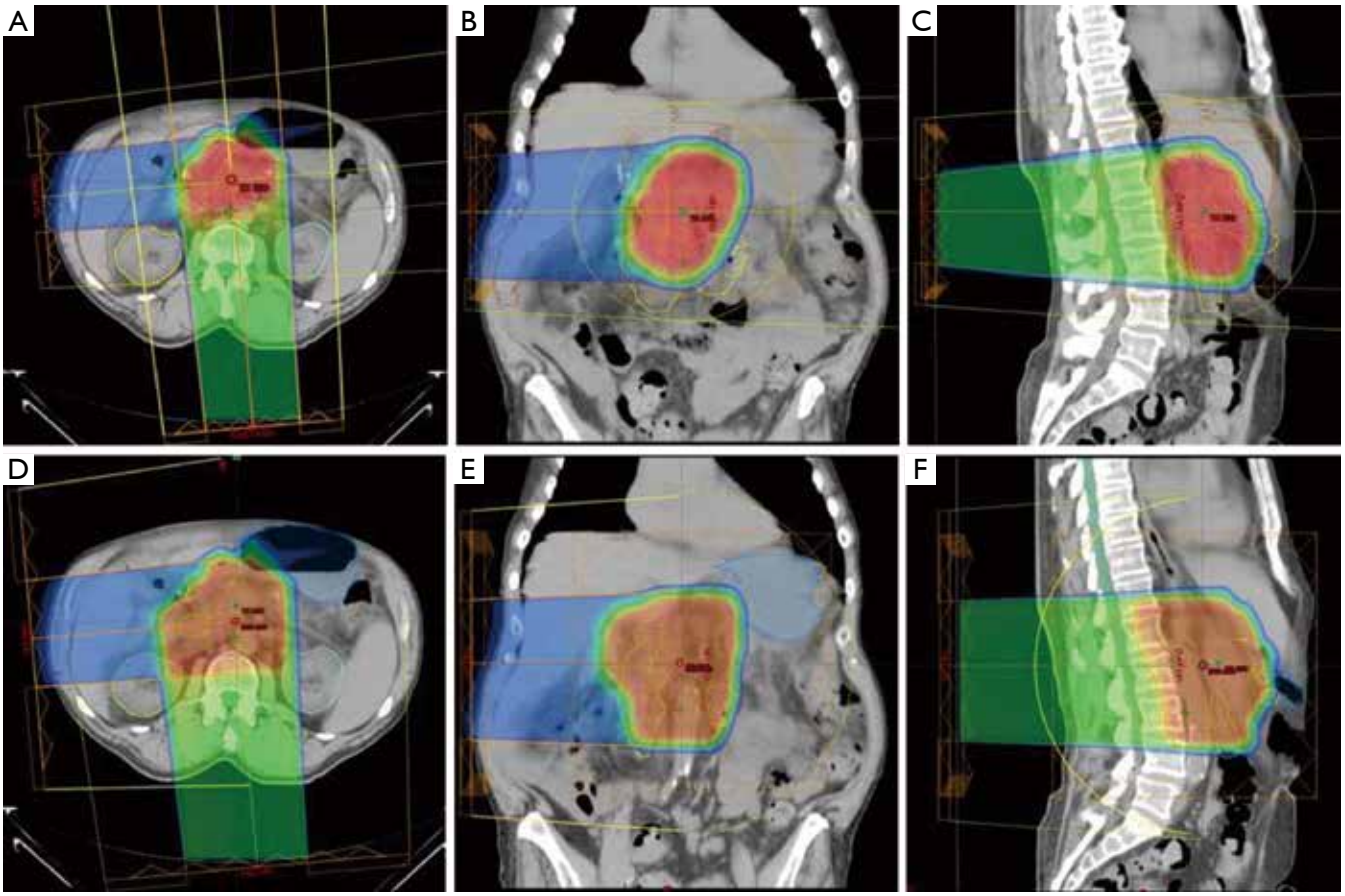

Figure 1 Typical field configurations used to treat pancreatic cancers with protons. A heavily weighted (75% of the target dose) posterior or posterior-oblique field is combined with a more lightly weighted (25% of target dose) right lateral-oblique field. Since the posterior beam is unlikely to pass through an air-filled space on its way to the retroperitoneal target, there is very little uncertainty in its range. Although the treatment plans that include the elective nodes irradiate a larger volume, because of the conformality of the proton dose distribution and posterior location of the target relative to the small bowel space, the elective plans were not associated with meaningfully increased small bowel or gastric exposure compared to the plans treating the gross disease alone. A. Axial (Gross tumor only); B. Coronal (Gross tumor only); C. Sagital (Gross tumor only); D. Axial (Elective nodes included); E. Coronal (Elective nodes included); F. Sagital (Elective nodes included).

were constructed with Lucite using median parameters for smearing margins and border smoothing of 6 and 8 mm, respectively.

A 2-field approach was utilized on all patients (posterior oblique: right lateral oblique) with a 3-to-1 weighting to the posterior field while limiting the spinal cord dose to less than 46 CGE. The heavy weighting of the posterior field allowed for coverage of the retroperitoneal region with minimal dose to the small bowel space anteriorly and to the body of the stomach left of the midline. Since no air-filled space (i.e., small bowel) would be situated in the beam path between the posterior proton source and the targeted tissues, there would be very little range uncertainty for the dose delivered from this field. The more lightly weighted right lateral-oblique field allowed for the degree of spinal cord sparing described above without delivering excessive dose to the liver. Since the lateral field had the potential to pass through a possibly air-filled small bowel space, however, the SOBP was generously expanded proximally and distally to compensate for the associated range uncertainty. This expansion did not result in meaningfully increased normal-tissue exposure due to the low dose delivered (approximately 12.6 Gy at 0.45 Gy per fraction).

Both PTV1 and PTV2 were prescribed to a total dose of 50.4 CGE; 95% of all PTVs received 100% of the target dose and 100% of the PTVs received at least 95% of the target dose. Normal tissue goals of particular interest were as follows: right kidney V18 to <70%; left kidney V18 Gy to <30%; small bowel/stomach V20 Gy to <50%, V45 Gy to <15%, V50 Gy to <10%, and V54 Gy <5%; liver V30 Gy to <60%; and spinal cord maximum to <46 Gy. Typical proton plans are illustrated in *Figure 1*.

Results

The median PTV1 volume was 270.7 cm^3 (range, 133.33-495.61 cm^3). Median PTV2 volume was 541.75 cm^3 (range, 399.44-691.14 cm^3). All proton plans achieved the assigned PTV coverage. The median and range of normal-tissue exposures for each set of treatment plans are shown in *Table 1*.

All 12 plans that treated the PTV1 volumes (gross tumor only) met all of the previously described normal tissue goals. Eight of the 12 plans that targeted the PTV2 volumes (gross tumor plus high-risk nodes) met all constraints. Of the 4 PTV2 plans that did not meet constraints, one failed to meet the bowel space constraint (V54, 9.6%; V50, 10.6%) constraint, one failed to meet the right kidney (V18, 85.5%) and bowel space constraints (V54, 17.1%; V50, 20.2%; V45, 23.8%), one failed to meet the gastric constraint (V50, 15.5%; V45, 23.9%), and one failed to meet the right kidney (V18, 75.8%) and gastric constraints (V50, 10.6%; V45, 19.0%).

Discussion

Various reports in the contemporary literature describe the use of neoadjuvant radiotherapy with or without chemotherapy for nonmetastatic resectable or marginally resectable pancreatic cancers (13-17). *Table 2* presents a review of this literature. Neoadjuvant therapies provide numerous theoretical and practical advantages over postoperative treatment:

(I) Malignant cells are more likely to oxygenate preoperatively, allowing radiation to be more effective through the production of radicals causing DNA damage;

(II) Preoperative treatment may reduce the likelihood of tumor spillage, dissemination, or implantation at the time of surgery;

(III) Since the irradiated bowel is likely to be resected at the time of pancreaticoduodenectomy, patients treated with preoperative radiotherapy may experience less long-term nutritional problems compared to patients irradiated postoperatively;

(IV) With neoadjuvant therapy, there is no delay between systemic therapy and surgery, as opposed to adjuvant therapy where the delay is caused by postoperative recovery, possibly reducing the control of distant metastases;

(V) Neoadjuvant therapies may effectively downstage marginally resectable tumors and render them resectable.

These theoretical advantages are promising, but, to date, there are no randomized trials that directly compare neoadjuvant and adjuvant therapies.

In a phase 1 clinical trial, Hong *et al.* demonstrated the feasibility of hypofractionated neoadjuvant proton therapy with concomitant capecitabine for patients with resectable adenocarcinoma of the pancreatic head (11). Fifteen patients received doses ranging from 30 GyE in 10 fractions over 2 weeks to 25 GyE in 5 fractions over 1 week. Chemotherapy consisted of capecitabine at 825 mg/m^2 twice daily. No dose-limiting toxicities were observed. Evaluation of 30-day postoperative mortality and morbidity showed no deaths or anastomotic leaks. Limited elective nodal irradiation was offered. Of note, 10 of 11 patients undergoing surgery had positive lymph nodes in the operative specimen.

Nichols *et al.* reported negligible weight loss and gastrointestinal toxicity in a group of 20 patients treated with conventionally fractionated protons and concomitant capecitabine (1,000 mg orally twice-daily) (12). Patients had marginally resectable (N=5), resected (N=5), or unresectable (N=10) disease and received planning target volume (PTV) proton doses ranging from 50.40 to 59.40 CGE. No elective nodal irradiation was offered to the patients with measurable gross disease. The median PTV volume was 406 cm^3 (range, 244 to 1,811 cm^3). For the 17 patients treated with a 2-field plan (posterior oblique and right lateral oblique) which minimized gastric and small bowel exposure, the median weight loss was only 1.1l bs (range, gain of 10.4 lbs to loss of 14.1 lbs) over the course of treatment. No patient experienced grade 2 or greater GI toxicity.

Conclusions

Protons allow for substantial gastric and small bowel sparing compared with X-rays in the setting of neoadjuvant radiotherapy for pancreatic cancer. This normal-tissue sparing offers the potential to reduce the risk of perioperative complications. As such, surgeons evaluating patients with resectable disease may ultimately be more willing to accept neoadjuvant radiotherapy if protons are to be used.

Additionally, in the majority of the cases we evaluated, we were able to expand the neoadjuvant radiotherapy field to safely cover both the gross tumor and the high-risk regional lymph nodes without significantly increasing the volume of critical normal tissues irradiated.

In light of this dosimetric data, as well as our clinical data showing a virtual absence of gastrointestinal toxicity when protons are used to treat pancreatic cancer, our current trial in development for neoadjuvant radiotherapy for patients with resectable and marginally resectable disease offers 50.40 CGE over 28 fractions to the above-described PTV2 volume with concomitant capecitabine (1,000 mg orally

Table 1 Median and range of normal-tissue exposures for each set of treatment plans

	Right kidney	Left kidney	Stomach				Bowel space				Liver
	V18	V18	V20	V45	V50	V54	V20	V45	V59	V54	V30
Gross tumor only	22.7% (0-68%)	3.9% (0-28%)	5.0% (0-33%)	1.1% (0-25%)	0.2% (0-18%)	0% (0-0.1%)	12.7% (4-26%)	4.7% (1-16%)	2.3% (0-12%)	0% (0-0.1%)	4.3% (1-14%)
Elective nodes included	34.6% (13-86%)	11.4% (1-31%)	7.5% (0-40%)	2.4% (0-24%)	1.3% (0-15%)	0% (0-0.9%)	17.5% (7-38%)	10% (3-24%)	7.2% (0-17%)	0.3% (0-17%)	8.3% (3-22%)

Table 2 Neoadjuvant trials for borderline resectable pancreatic cancers

		RT prescription	Target coverage	Chtx	OS	DFS	LR	DM
ECOG (12 institutions) (13)	n=53	39.6 Gy/22 fx; 10.8 Gy/ 6 fx	GTV + [2-3] cm; Porta hepatis\Celiac; GTV + [1-2] cm	96 h iv 5-FU; 1,000 mg/m^2 days 2-5 & 29-32 and mitC 10 mg/m^2 (IV) bolus day 2	2 y OS: 27%	MDFS: 8.5 m	17%	79%
Duke (16)	n=111	45 Gy/25 fx; Boost 540 cGy to the tumor bed	NR	5-5FU alone; --bolus mitC; --iv cisplatin; 5-FU, mitC, and CDDP	2 y OS: 32%; MS not reached @ F/U of 16 m	NR	18%	>20%
Fox chase (U Penn) (14)	n=89; Resectable; (n=40)	39.6 Gy/22 fx; 10.8 Gy/6 fx	GTV + [2-3] cm; Porta hepatis\Celiac; GTV + [1-2] cm	On day 2 RT, bolus mitC (10 mg/m^2) followed by a 96-h cont iv 5-FU (1,000 mg/m^2/day); On day 28 96 h course 5-FU	MS: 20 m	MDFS: 20 m	16%	84%
Harvard (15)	n=70	50.4 Gy/28 fx	The primary tumor plus regional lymph nodes were targeted in all patient	--Gem: 1,000 mg/m^2/w for 3 w, then 1 w off followed by CRT: cont iv 5-FU or Xeloda; --CRT alone	MS, NC-CRT: 18.7 m; CRT: 12.4 m (P=0.02)	MPFS, NC-CRT: 11.4 m; CRT: 6.7 m (P=0.02)	LR, NC-CRT: 23%; MP: 4.1 m. CRT: 25%; MP: 6.4 m	DM, NC-CRT: 77%; MP: 5.4 m. CRT: 65%; MP: 2.7 m
MD Anderson (17)	n=90	30 Gy/10 fx	The primary tumor and gross adenopathy were treated with a 3-cm block margin cranially and caudally and a 2-cm block; margin radially	--Gem (750 mg/m^2) & CDDP (30 mg/m^2) q2w for 4 doses; --CRT: 4 qw iv Gem (400 mg/m^2) combined w\RT; --Gem 400 mg/m^2 qw, 7 w	Overall: 5 y OS, 18%; MS, 17.4 m. Resected: 5 y OS, 30%; MS, 31 m; Unresected: 5 y OS, 18%; MS, 10.5 m	Overall: MPFS, 13.2 m	LR: 65%; MP:8.9 m	50%

RT, radiotherapy; Chtx, chemotherapy; OS, overall survival; DFS, disease-free survival; LR, local recurrence; DM, distant metastasis; Gy, Grey; fx, fractions; LN, lymph node; FU, fluorouracil; iv, intravenous; MS, median survival; NR, not reported; ECOG, Eastern Cooperative Oncology Group; GTV, gross target volume; h, hours; mitC, mitomycin C; y, years; MDFS, median disease-free survival; CDDP, cisplatin; CT, computed tomography; lat, lateral; ant, anterior; CTV, clinical target volume; PTV, planning target volume; CRT, chemo-radiation therapy; NC-CRT, Neoadjuvant chemotherapy followed by chemo-radiation; MPFS, median progression-free survial; q2w, every 2 weeks; qw, weekly; w, week; d, day; m, month; F/U, follow-up; MP, median time to progression; GEM, Gemcitabine; NR, not reported; NC-CRT, neoadjuvant chemotherapy followed by chemoradiation.

twice daily). If normal-tissue constraints cannot be met, a reduction in volume (to PTV1) will be made after 45.00 CGE (or as low as 39.60 CGE, if necessary).

Acknowledgements

Disclosure: The authors declare no conflict of interest.

References

1. Siegel R, Ward E, Brawley O, et al. Cancer statistics, 2011: the impact of eliminating socioeconomic and racial disparities on premature cancer deaths. CA Cancer J Clin 2011;61:212-36.
2. Tepper J, Nardi G, Sutt H. Carcinoma of the pancreas: review of MGH experience from 1963 to 1973. Analysis of surgical failure and implications for radiation therapy. Cancer 1976;37:1519-24.
3. Kayahara M, Nagakawa T, Ueno K, et al. An evaluation of radical resection for pancreatic cancer based on the mode of recurrence as determined by autopsy and diagnostic imaging. Cancer 1993;72:2118-23.
4. Abrams RA, Winter KA, Regine WF, et al. Failure to adhere to protocol specified radiation therapy guidelines was associated with decreased survival in RTOG 9704--a phase III trial of adjuvant chemotherapy and chemoradiotherapy for patients with resected adenocarcinoma of the pancreas. Int J Radiat Oncol Biol Phys 2012;82:809-16.
5. Neoptolemos JP, Stocken DD, Friess H, et al. A randomized trial of chemoradiotherapy and chemotherapy after resection of pancreatic cancer. N Engl J Med 2004;350:1200-10.
6. Hsiung-Stripp DC, McDonough J, Masters HM, et al. Comparative treatment planning between proton and X-ray therapy in pancreatic cancer. Med Dosim 2001;26:255-9.
7. Kozak KR, Kachnic LA, Adams J, et al. Dosimetric feasibility of hypofractionated proton radiotherapy for neoadjuvant pancreatic cancer treatment. Int J Radiat Oncol Biol Phys 2007;68:1557-66.
8. Nichols RC Jr, Huh SN, Prado KL, et al. Protons offer reduced normal-tissue exposure for patients receiving postoperative radiotherapy for resected pancreatic head cancer. Int J Radiat Oncol Biol Phys 2012;83:158-63.
9. Johansson J, Isacsson U, Glimelius B. In regard to Zurlo et al., IJROBP 2000;48:277-288. Int J Radiat Oncol Biol Phys 2001;50:279-80.
10. Zurlo A, Lomax A, Hoess A, et al. The role of proton therapy in the treatment of large irradiation volumes: a comparative planning study of pancreatic and biliary tumors. Int J Radiat Oncol Biol Phys 2000;48:277-88.
11. Hong TS, Ryan DP, Blaszkowsky LS, et al. Phase I study of preoperative short-course chemoradiation with proton beam therapy and capecitabine for resectable pancreatic ductal adenocarcinoma of the head. Int J Radiat Oncol Biol Phys 2011;79:151-7.
12. Nichols RC Jr, George TJ, Zaiden RA Jr, et al. Proton therapy with concomitant capecitabine for pancreatic and ampullary cancers is associated with a low incidence of gastrointestinal toxicity. Acta Oncol 2013;52:498-505.
13. Hoffman JP, Lipsitz S, Pisansky T, et al. Phase II trial of preoperative radiation therapy and chemotherapy for patients with localized, resectable adenocarcinoma of the pancreas: an Eastern Cooperative Oncology Group Study. J Clin Oncol 1998;16:317-23.
14. Meszoely IM, Wang H, Hoffman JP. Preoperative chemoradiation therapy for adenocarcinoma of the pancreas: The Fox Chase Cancer Center experience, 1986-2003. Surg Oncol Clin N Am 2004;13:685-96, x.
15. Arvold ND, Ryan DP, Niemierko A, et al. Long-term outcomes of neoadjuvant chemotherapy before chemoradiation for locally advanced pancreatic cancer. Cancer 2012;118:3026-35.
16. White RR, Tyler DS. Neoadjuvant therapy for pancreatic cancer: the Duke experience. Surg Oncol Clin N Am 2004;13:675-84, ix-x.
17. Varadhachary GR, Wolff RA, Crane CH, et al. Preoperative gemcitabine and cisplatin followed by gemcitabine-based chemoradiation for resectable adenocarcinoma of the pancreatic head. J Clin Oncol 2008;26:3487-95.
18. Griffin JF, Smalley SR, Jewell W, et al. Patterns of failure after curative resection of pancreatic carcinoma. Cancer 1990;66:56-61.
19. Showalter TN, Winter KA, Berger AC, et al. The influence of total nodes examined, number of positive nodes, and lymph node ratio on survival after surgical resection and adjuvant chemoradiation for pancreatic cancer: a secondary analysis of RTOG 9704. Int J Radiat Oncol Biol Phys 2011;81:1328-35.
20. Abrams RA, Goodman KA, Ben-Josef E, et al. Pancreas atlas: consensus panel contouring atlas for the delineation of the clinical target volume in the postoperative treatment of pancreatic cancer. Available online: http://www.rtog.org/CoreLab/ContouringAtlases/PancreasAtlas.aspx

Cite this article as: Lee RY, Nichols RC Jr, Huh SN, Ho MW, Li Z, Zaiden R, Awad ZT, Ahmed B, Hoppe BS. Proton therapy may allow for comprehensive elective nodal coverage for patients receiving neoadjuvant radiotherapy for localized pancreatic head cancers. J Gastrointest Oncol 2013;4(4):374-379. doi: 10.3978/j.issn.2078-6891.2013.043

Original Article

Protons offer reduced bone marrow, small bowel, and urinary bladder exposure for patients receiving neoadjuvant radiotherapy for resectable rectal cancer

Rovel J. Colaco, Romaine Charles Nichols, Soon Huh, Nataliya Getman, Meng Wei Ho, Zuofeng Li, Christopher G. Morris, William M. Mendenhall, Nancy P. Mendenhall, Bradford S. Hoppe

University of Florida Proton Therapy Institute, Jacksonville, Florida, USA

Correspondence to: Romaine Charles Nichols, MD. University of Florida Proton Therapy Institute, 2015 North Jefferson St., Jacksonville, FL, 32206, USA. Email: rnichols@floridaproton.org.

Background: To assess the potential benefit of proton therapy (PT) over photon therapy, we compared 3-dimensional conformal radiotherapy (3DCRT), intensity-modulated radiotherapy (IMRT), and PT plans in patients undergoing neoadjuvant chemoradiation for resectable rectal cancer at our institution.

Methods: Eight consecutive patients with resectable (T2-T3) rectal cancers underwent 3DCRT, IMRT, and 3-dimensional conformal PT treatment planning. Initial target volumes (PTV1) were contoured using the Radiation Therapy Oncology Group anorectal atlas guidelines. Boost target volumes (PTV2) consisted of the gross rectal tumor plus a uniform 2-cm expansion. Plans delivered 45 Gray (Gy) or Cobalt Gray Equivalent (CGE) to the PTV1 and a 5.4-Gy (CGE) boost to the PTV2. Ninety-five percent of the PTVs received 100% of the target dose and 100% of the PTVs received 95% of the target dose. Standard normal-tissue constraints were utilized. Wilcoxon paired t-tests were performed to compare various dosimetric points between the 3 plans for each patient.

Results: All plans met all normal-tissue constraints and were isoeffective in terms of PTV coverage. The proton plans offered significantly reduced median normal-tissue exposure over the 3DCRT and IMRT plans with respect to pelvic bone marrow at the V5Gy, V10Gy, V15Gy, and V20Gy levels and the small bowel space at the V10Gy and V20Gy levels. The proton plans also offered significantly reduced median normal-tissue exposure over the 3DCRT plans with respect to the small bowel at the V30Gy and V40Gy levels and the urinary bladder at the V40Gy level.

Conclusions: By reducing bone marrow exposure, PT may reduce the acute hematologic toxicity of neoadjuvant chemoradiation and increase the likelihood of uninterrupted chemotherapy delivery. Bone marrow sparing may also facilitate the delivery of salvage chemotherapy for patients who subsequently develop hematogenous metastasis. Reduced small bowel exposure using PT may also reduce toxicity and possibly facilitate the use of more-aggressive chemotherapy with radiotherapy.

Keywords: Proton therapy; particle therapy; dosimetry; rectal cancer; gastrointestinal cancer

doi: 10.3978/j.issn.2078-6891.2013.041

Scan to your mobile device or view this article at: http://www.thejgo.org/article/view/1291/2660

Introduction

The introduction of neoadjuvant therapy through short and long courses of radiation therapy for resectable rectal cancer has resulted in reduced relapse rates (1-3). Adding chemotherapy to preoperative long-course radiation has been shown to be superior to radiation alone (2), while preoperative chemoradiation (CRT) results in lower relapse rates and better sphincter preservation than postoperative CRT (3). As a result, preoperative CRT is now a standard of care in locally advanced rectal cancer. Nevertheless, despite

neoadjuvant CRT, recurrence rates of locally advanced rectal cancer remain high with systemic recurrence in up to 30% to 40% of patients (1,3).

Historically, radiation was delivered using 3-dimensional conformal radiotherapy (3DCRT) techniques in a 3- or 4-field arrangement. The introduction of intensity-modulated radiation therapy (IMRT) has resulted in improved conformality; however, despite this improvement, organs outside of the planning target volume (PTV), including the bladder, small bowel, and pelvic bone marrow, may still receive a significant radiation dose.

Conventional photon radiation uses X-rays to deliver the dose to the target volume. X-ray therapy, however, results in a significant entrance and exit dose along the path of beam delivery in addition to subsequent dose to normal tissue. Compared to X-ray therapy, proton therapy is a form of charged-particle therapy that allows delivery of the equivalent X-ray dose or dose escalation while sparing normal tissue. More specifically, the properties of the spread-out Bragg peak (SOBP) allow improved sparing of non-targeted organs, with proton beams conformed to fit the exact depth and shape of the required target. Reducing the volume and exposure of normal pelvis and bone marrow to radiation will likely reduce long-term toxicity and preserve pelvic bone marrow, which is increasingly important in the setting of systemic recurrences where patients may require multiple lines of myelosuppressive chemotherapy.

In this study, we sought to compare proton therapy plans for patients treated with neoadjuvant CRT to IMRT and 3DCRT plans in an attempt to quantify the dosimetric benefit of proton therapy in a cohort of patients receiving neoadjuvant CRT.

Materials and methods

Under an institutional review board-approved study, 8 consecutive patients with resectable rectal cancers underwent treatment planning with 3DCRT, IMRT, and conformal proton therapy. All patients were simulated in the prone position with a full bladder and imaged on a Phillips Brilliance (Phillips Healthcare, Andover, MA) large-bore computed tomography (CT) scanner with a 60-cm field-of-view and 1-mm slices.

Target volumes and dose constraints

Initial target volumes (PTV1) were contoured using the guidelines in the Radiation Therapy Oncology Group (RTOG) anorectal atlas (4). The initial clinical target volume (CTV) consisted of the gross tumor volume (GTV) as determined by a combination of physical examination, colonoscopy, and diagnostic CT and/or magnetic resonance imaging (MRI) scan plus the entire mesorectum, including the perirectal fat and presacral space along with the internal iliac lymph nodes. Boost target volumes (PTV2) consisted of the GTV plus a 2-cm uniform expansion. The dose delivered to the PTV1 was 45 Gray (Gy) or Cobalt Gray Equivalent (CGE) in 25 fractions with a boost of 5.4 CGE in 3 fractions to the PTV2, resulting in a total dose of 50.4 CGE over 28 fractions.

Target goals were similar to those used in the RTOG 0822 protocol for resectable rectal cancer. For each treatment phase, 95% of the PTV received 100% of the target dose and 100% of the PTV received 95% of the target dose. Per the normal-tissue constraints, no more than 180 cm^3 of small bowel received greater than 35 Gy, while no more than 40% of the femoral heads received greater than 40 Gy; V40Gy for the bladder was less than 40%.

3DCRT plans delivered the target doses via a standardized 3-field (posterior/anterior, right lateral, and left lateral) approach with a 2-to-1 field weighting by dose contributed to the target volume. IMRT plans delivered the initial 45 Gy following the planning and dose delivery guidelines of the RTOG 0822 protocol and a 5.4-Gy boost by following the same field angles as the initial plan. PT plans utilized a 3-field approach similar to the 3DCRT plans with a heavier weighting of the posterior field relative to the right and left lateral fields (3.1 to 1 to 1). To avoid excess skin toxicity, the maximum dose permitted to 1 cm^2 of skin was 35 Gy. To account for air within the rectum when designing the proton plan, the Hounsfield units were overridden for the circumferential air-filled portion of the rectum.

Representative colorwash dose distributions for typical proton therapy, IMRT and 3DCRT plans are shown in *Figure 1*.

Statistics

Descriptive statistics (median and range) were used to characterize the disease-specific and dosimetric points of interest. A Wilcoxon signed rank sum test for nonparametric paired data was used to compare the 3DCRT and IMRT plans with the proton plans for the various dosimetric points, and to establish statistical significance, $P \leq 0.05$ (WinStat Microsoft Excel, Microsoft, Redmond, WA).

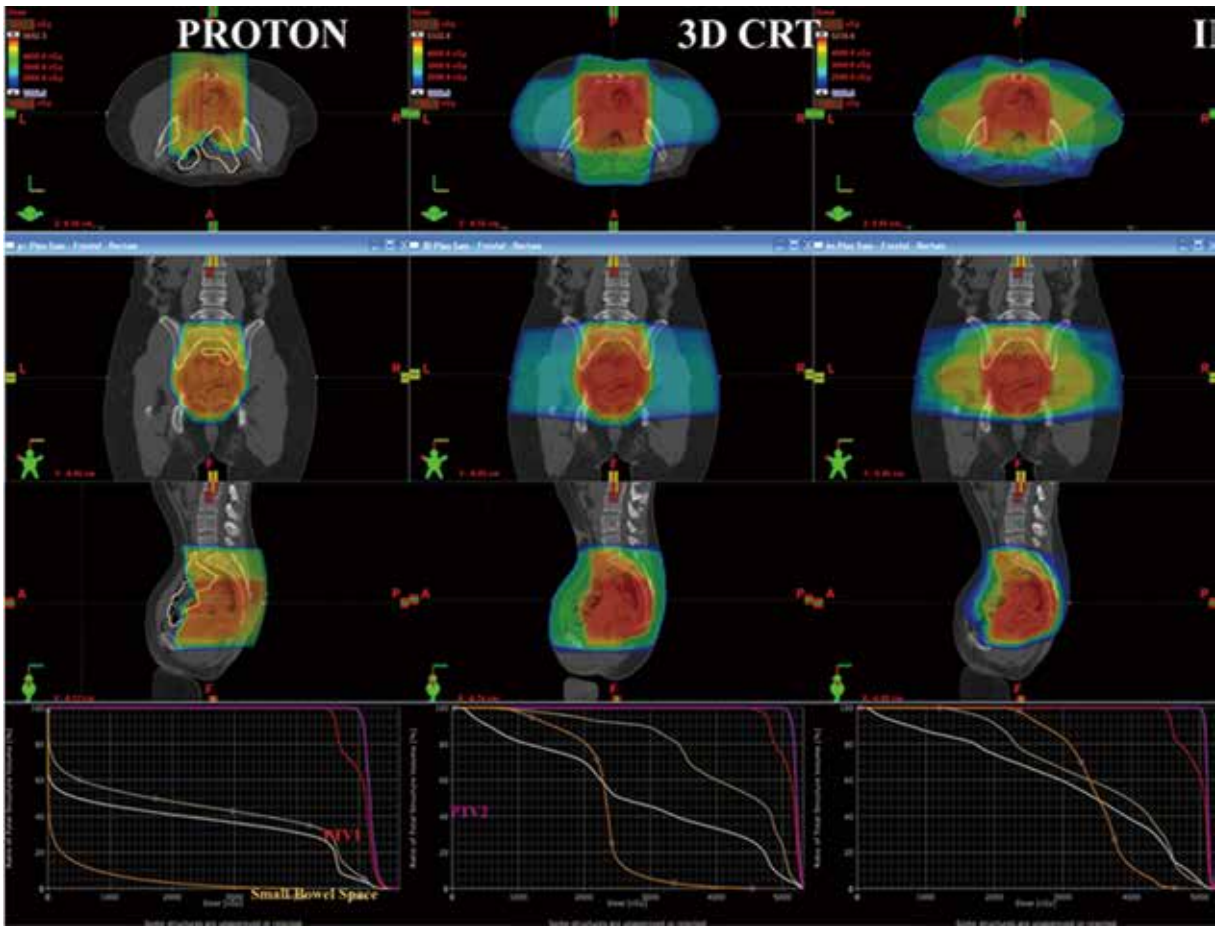

Figure 1 Colorwash dose distributions for typical proton therapy, IMRT and 3DCRT plans for a patient with resectable rectal cancer.

Results

Target volume coverage

All 3DCRT, IMRT, and proton plans met all normal-tissue constraints and were isoeffective in terms of PTV coverage.

Pelvic bone marrow dosimetry

The results for median pelvic bone marrow dosimetry comparing the 3 plans are shown in *Table 1*. At all dose levels evaluated, proton plans offered significantly reduced pelvic bone marrow exposure over 3DCRT and IMRT.

Small bowel and bladder dosimetry

The results for small bowel and bladder dosimetry are shown in *Table 2*. Proton therapy was statistically superior to 3DCRT with regard to small bowel exposure at all evaluated dose levels and with regard to the urinary bladder at the V40Gy level. The superiority of proton therapy over IMRT with regard to small bowel exposure was limited to the V10Gy and V20Gy levels. There was no significant improvement with protons compared to IMRT with regard to urinary bladder exposure.

Discussion

We present the first known dosimetric study comparing 3DCRT, IMRT, and proton therapy plans for neoadjuvant CRT for resectable rectal cancer. The results show superior bone marrow sparing for proton therapy over IMRT and 3DCRT and better sparing of small bowel with proton therapy, particularly at low-dose thresholds.

As a result of its dosimetric advantages in certain tumors, such as childhood cancers (5-10) and skull base tumors (11-13), proton therapy is a well-established radiotherapy

Table 1 Median pelvic bone marrow exposure for 3DCRT versus IMRT versus proton therapy plans (range in parentheses)

	PBM V5Gy [%]	PBM V10Gy [%]	PBM V15Gy [%]	PBM V20Gy [%]
3DCRT	88 [79-100]	81 [70-100]	77 [64-99]	73 [60-95]
IMRT	88 [81-100]	82 [70-99]	76 [70-96]	67 [49-93]
PT	70 [60-95]	43 [38-63]	37 [31-58]	32 [29-55]
PT *vs.* 3DCRT	P=0.0156	P=0.0156	P=0.0156	P=0.0156
PT *vs.* IMRT	P=0.0156	P=0.0156	P=0.0156	P=0.0156

Abbreviations: 3DCRT, 3-dimensional conformal radiation therapy; IMRT, intensity-modulated radiation therapy; PBM, pelvic bone marrow; PT, proton therapy.

Table 2 Median small bowel and bladder normal-tissue exposures for each planning technique

	Small bowel V10Gy (cm^3)	Small bowel V20Gy (cm^3)	Small bowel V30Gy (cm^3)	Small bowel V40Gy (cm^3)	Bladder V40Gy (%)	Bladder V50Gy (%)
3DCRT	91	55	35	27	41	19
IMRT	90	56	29	19	29	12
PT	45	39	32	22	31	13
PT *vs.* 3DCRT	P=0.0156	P=0.0156	P=0.0156	P=0.0156	P=0.016	P=NS
PT *vs.* IMRT	P=0.0156	P=0.0156	P=NS	P=NS	P=NS	P=NS

Abbreviations: 3DCRT, 3-dimensional conformal radiation therapy; IMRT, intensity-modulated radiation therapy; NS, not significant; PT, proton therapy.

treatment technique. Furthermore a growing body of evidence is emerging indicating superior dosimetric profiles and sparing of normal tissue over 3DCRT, IMRT, or both in various other tumor sites, including lung tumors (14-16), lymphoma (17,18) and upper gastrointestinal (GI) tumors (19,20).

While radiation therapy for rectal cancer is a long-established practice and neoadjuvant CRT is a standard of care in the management of operable locally advanced rectal cancer (2,3,21,22), preoperative radiation is still delivered in most cancer centers using 3DCRT. Neoadjuvant CRT with 3DCRT, however, results in non-trivial rates of acute and late treatment toxicity from treatment as well as significant local and distant recurrence rates. In the German study (3) comparing pre- and postoperative CRT in which preoperative CRT was given to a dose of 50.4 Gy with 5 fluourouracil (5-FU) concurrent chemotherapy, the incidence of acute grade 3+ toxicity was 27% with a late grade 3+ toxicity rate at the 5-year follow-up in the preoperative group of 14%. In an updated report of this study (23), at the 11-year follow-up, the 10-year rate of cumulative local recurrence was 7.1% and the rate of distant metastases 29.8%.

In the Sauer study, 6% of patients in the preoperative group experienced grade 3+ haematological toxicity. In addition, with approximately 30% to 40% of patients recurring at 10 years, a large proportion of patients receiving neoadjuvant CRT will likely require future salvage chemotherapy. Thus, the significant sparing of bone marrow seen in our study with proton therapy over both IMRT and 3DCRT ($P<0.05$ for V5, V10, V15, and V20 for proton therapy versus IMRT and proton therapy versus 3DCRT) may be of substantial benefit. Indeed, sparing bone marrow through the use of proton therapy may reduce the compromise of delivery of CRT in the acute setting while preserving bone marrow function ahead of several lines of myelosuppressive chemotherapy that are delivered in the salvage setting (3).

Proton therapy offers the potential to reduce acute and late bowel toxicity from CRT compared to IMRT or 3DCRT in the treatment of rectal cancer. In our study, proton therapy plans had statistically significant superior sparing of the small bowel compared to both IMRT and 3DCRT for both V10 and V20. Although the median V30 and V40 for IMRT was slightly less than with proton therapy, this was not statistically significant. In this regard,

by reducing the low-dose bowel volume irradiated, proton therapy may better allow for dose escalation or avoidance of treatment interruptions in the acute setting.

Current research in the neoadjuvant setting revolves around adding new chemotherapy agents to radiation: capecitabine has been shown to be equally efficacious as infusional 5-FU in the treatment of colon cancer (24,25) and the effectiveness of agents such as oxaliplatin, irinotecan, and bevacuzimab has led to these agents being piloted in early-phase trials of neoadjuvant rectal cancer.

Nevertheless, bowel toxicity can be a limiting factor in this setting; indeed, the phase II randomized RTOG 0247 trial comparing neoadjuvant radiation combined with capecitabine and oxaliplatin versus capecitabine and irinotecan was temporarily suspended due to excess grade 3+ GI toxicity from both the chemotherapy and the radiation. Several studies have shown a potential benefit with IMRT compared to 3DCRT in rectal cancer with regard to the small bowel dose (26,27). Such studies are the foundation to the hypothesis for the RTOG 0822 study, which involves using IMRT with concurrent multiagent chemotherapy to reduce small bowel exposure and therefore acute GI toxicity, thus enabling better dose delivery and dose escalation of concurrent chemotherapy. Similarly, proton therapy may permit additional small bowel sparing, allow chemotherapy dose escalation, and increased patient compliance.

Proton therapy plans in our study utilized a 3-field approach with uniform scanning. This field arrangement was chosen to avoid the excess skin dose with a single posterior field plan. Furthermore, uniform scanning allowed delivery of the dose to a greater depth in the pelvis than would be possible with double-scattered protons. Advancements in proton therapy, such as the introduction of pencil-beam scanning and with it intensity-modulated proton therapy, may result in proton therapy offering further dosimetric advantages over and above those seen in our study and may merit further investigation as intensity-modulated proton therapy becomes increasingly available.

Conclusions

In this small series of patients with rectal cancer undergoing neoadjuvant CRT for rectal cancer, proton therapy plans offered superior sparing of bone marrow and the small bowel compared to both IMRT and 3DCRT. The dosimetric advantages seen with proton therapy may therefore merit further investigation as a means of limiting the acute toxicity of neoadjuvant CRT and preserving both bone marrow and bowel function in advance of future myelosuppressive chemotherapy in the relapse setting.

Acknowledgements

Disclosure: The authors declare no conflict of interest.

References

1. Improved survival with preoperative radiotherapy in resectable rectal cancer. Swedish Rectal Cancer Trial. N Engl J Med 1997;336:980-7.
2. Gérard JP, Conroy T, Bonnetain F, et al. Preoperative radiotherapy with or without concurrent fluorouracil and leucovorin in T3-4 rectal cancers: results of FFCD 9203. J Clin Oncol 2006;24:4620-5.
3. Sauer R, Becker H, Hohenberger W, et al. Preoperative versus postoperative chemoradiotherapy for rectal cancer. N Engl J Med 2004;351:1731-40.
4. Myerson RJ, Garofalo MC, El Naqa I, et al. Elective clinical target volumes for conformal therapy in anorectal cancer: a radiation therapy oncology group consensus panel contouring atlas. Int J Radiat Oncol Biol Phys 2009;74:824-30.
5. Miralbell R, Lomax A, Cella L, et al. Potential reduction of the incidence of radiation-induced second cancers by using proton beams in the treatment of pediatric tumors. Int J Radiat Oncol Biol Phys 2002;54:824-9.
6. Kozak KR, Adams J, Krejcarek SJ, et al. A dosimetric comparison of proton and intensity-modulated photon radiotherapy for pediatric parameningeal rhabdomyosarcomas. Int J Radiat Oncol Biol Phys 2009;74:179-86.
7. Yock T, Schneider R, Friedmann A, et al. Proton radiotherapy for orbital rhabdomyosarcoma: clinical outcome and a dosimetric comparison with photons. Int J Radiat Oncol Biol Phys 2005;63:1161-8.
8. St Clair WH, Adams JA, Bues M, et al. Advantage of protons compared to conventional X-ray or IMRT in the treatment of a pediatric patient with medulloblastoma. Int J Radiat Oncol Biol Phys 2004;58:727-34.
9. Lee CT, Bilton SD, Famiglietti RM, et al. Treatment planning with protons for pediatric retinoblastoma, medulloblastoma, and pelvic sarcoma: how do protons compare with other conformal techniques? Int J Radiat Oncol Biol Phys 2005;63:362-72.
10. Krengli M, Hug EB, Adams JA, et al. Proton radiation therapy for retinoblastoma: comparison of various

intraocular tumor locations and beam arrangements. Int J Radiat Oncol Biol Phys 2005;61:583-93.
11. Weber DC, Rutz HP, Pedroni ES, et al. Results of spot-scanning proton radiation therapy for chordoma and chondrosarcoma of the skull base: the Paul Scherrer Institut experience. Int J Radiat Oncol Biol Phys 2005;63:401-9.
12. Munzenrider JE, Liebsch NJ. Proton therapy for tumors of the skull base. Strahlenther Onkol 1999;175 Suppl 2:57-63.
13. Hug EB, Loredo LN, Slater JD, et al. Proton radiation therapy for chordomas and chondrosarcomas of the skull base. J Neurosurg 1999;91:432-9.
14. Chang JY, Zhang X, Wang X, et al. Significant reduction of normal tissue dose by proton radiotherapy compared with three-dimensional conformal or intensity-modulated radiation therapy in Stage I or Stage III non-small-cell lung cancer. Int J Radiat Oncol Biol Phys 2006;65:1087-96.
15. Nichols RC, Huh SN, Henderson RH, et al. Proton radiation therapy offers reduced normal lung and bone marrow exposure for patients receiving dose-escalated radiation therapy for unresectable stage iii non-small-cell lung cancer: a dosimetric study. Clin Lung Cancer 2011;12:252-7.
16. Colaco RJ, Huh S, Nichols RC, et al. Dosimetric rationale and early experience at UFPTI of thoracic proton therapy and chemotherapy in limited-stage small cell lung cancer. Acta Oncol 2013;52:506-13.
17. Hoppe BS, Flampouri S, Su Z, et al. Effective dose reduction to cardiac structures using protons compared with 3DCRT and IMRT in mediastinal Hodgkin lymphoma. Int J Radiat Oncol Biol Phys 2012;84:449-55.
18. Hoppe BS, Flampouri S, Li Z, et al. Cardiac sparing with proton therapy in consolidative radiation therapy for Hodgkin lymphoma. Leuk Lymphoma 2010;51:1559-62.
19. Nichols RC Jr, Huh SN, Prado KL, et al. Protons offer reduced normal-tissue exposure for patients receiving postoperative radiotherapy for resected pancreatic head cancer. Int J Radiat Oncol Biol Phys 2012;83:158-63.
20. Nichols RC Jr, George TJ, Zaiden RA Jr, et al. Proton therapy with concomitant capecitabine for pancreatic and ampullary cancers is associated with a low incidence of gastrointestinal toxicity. Acta Oncol 2013;52:498-505.
21. Bosset JF, Collette L, Calais G, et al. Chemotherapy with preoperative radiotherapy in rectal cancer. N Engl J Med 2006;355:1114-23.
22. Bujko K, Nowacki MP, Nasierowska-Guttmejer A, et al. Long-term results of a randomized trial comparing preoperative short-course radiotherapy with preoperative conventionally fractionated chemoradiation for rectal cancer. Br J Surg 2006;93:1215-23.
23. Sauer R, Liersch T, Merkel S, et al. Preoperative versus postoperative chemoradiotherapy for locally advanced rectal cancer: results of the German CAO/ARO/AIO-94 randomized phase III trial after a median follow-up of 11 years. J Clin Oncol 2012;30:1926-33.
24. Twelves C, Gollins S, Grieve R, et al. A randomised cross-over trial comparing patient preference for oral capecitabine and 5-fluorouracil/leucovorin regimens in patients with advanced colorectal cancer. Ann Oncol 2006;17:239-45.
25. Twelves C, Wong A, Nowacki MP, et al. Capecitabine as adjuvant treatment for stage III colon cancer. N Engl J Med 2005;352:2696-704.
26. Duthoy W, De Gersem W, Vergote K, et al. Clinical implementation of intensity-modulated arc therapy (IMAT) for rectal cancer. Int J Radiat Oncol Biol Phys 2004;60:794-806.
27. Guerrero Urbano MT, Henrys AJ, Adams EJ, et al. Intensity-modulated radiotherapy in patients with locally advanced rectal cancer reduces volume of bowel treated to high dose levels. Int J Radiat Oncol Biol Phys 2006;65:907-16.

Cite this article as: Colaco RJ, Nichols RC, Huh S, German N, Ho MW, Li Z, Morris CG, Mendenhall WM, Mendenhall NP, Hoppe BS. Protons offer reduced bone marrow, small bowel, and urinary bladder exposure for patients receiving neoadjuvant radiotherapy for resectable rectal cancer. J Gastrointest Oncol 2014;5(1):3-8. doi: 10.3978/j.issn.2078-6891.2013.041

Editorial

Rectal cancer: do protons have prospects?

Prajnan Das

Department of Radiation Oncology, U.T. M.D. Anderson Cancer Center, Houston, TX, USA

Correspondence to: Prajnan Das, M.D., M.S., M.P.H. Department of Radiation Oncology, The University of Texas M. D. Anderson Cancer Center, 1515 Holcombe Boulevard, Unit 97, Houston, TX 77030, USA. Email: PrajDas@mdanderson.org.

doi: 10.3978/j.issn.2078-6891.2013.047

Scan to your mobile device or view this article at: http://www.thejgo.org/article/view/1536/2659

Preoperative chemoradiation and preoperative short course radiotherapy have widely been accepted as standards of care for stage II and III rectal cancer. However, pelvic radiotherapy can lead to significant rates of acute and late toxicity. Advances in radiation therapy technique and newer radiation therapy modalities could potentially reduce acute and late toxicity rates, by limiting radiation exposure to normal tissues. In this issue, Colaco *et al.* report a dosimetric study comparing proton therapy with 3-dimensional conformal radiotherapy (3D-CRT) and intensity modulated radiation therapy (IMRT), in an effort to lower treatment-related toxicity (1).

Colaco *et al.* report that proton therapy reduced bone marrow exposure and small bowel exposure, compared to both IMRT and 3D-CRT. Proton therapy also reduced bladder exposure, compared to 3D-CRT, but not compared to IMRT. Their findings are similar to that reported by previous studies on proton therapy for rectal cancer, which also showed that proton therapy reduced normal tissue exposure compared to 3D-CRT and IMRT (2-4). However, all of these studies have been dosimetric analyses and not clinical evaluations. While proton therapy does appear to reduce normal tissue exposure, it remains unknown whether this reduction will lead to differences in acute and late toxicity.

Clinical studies, ideally prospective trials, will be necessary to evaluate the role of proton therapy in the neoadjuvant treatment of rectal cancer. However, it will be difficult to design such studies. Treatment-related toxicity in rectal cancer patients is multifactorial, arising from the combination of chemotherapy, radiation therapy and surgery. Hence, it may be difficult to discern the contribution of radiation therapy to toxicity. If the use of proton therapy leads to only a modest-sized reduction in toxicity, then a large sample size will be required to demonstrate the benefit of proton therapy. Furthermore, long follow-up will be required to evaluate late toxicity. Similar challenges have made it difficult to evaluate the role of IMRT for rectal cancer. While multiple dosimetric studies have shown that IMRT reduces normal tissue exposure, only a limited number of retrospective studies have shown reductions in acute toxicity; furthermore, a prospective study did not show a significant difference in acute toxicity with the use of IMRT compared to conventional radiotherapy (5-8).

Proton therapy for rectal cancer may be associated with certain technical challenges. For example, proton range is highly dependent on the stopping power of different substances; proton range is much higher in air than in tissue. Changes in rectal gas volume may therefore affect proton range, leading to either undercoverage of the target or overexposure of normal tissues. In Colaco *et al.*'s study, Hounsfield units were overridden for air in the rectum. Hence, this study did not account for uncertainties arising from rectal gas. Further studies are needed on such technical factors.

Proton therapy may have a potential role in some specific clinical situations. Proton therapy may reduce the risk of second malignancies in patients undergoing radiation therapy for rectal cancer at a young age. Proton therapy may also have a role in reirradiation for rectal cancer, in patients previously treated with pelvic radiation therapy. While it is difficult to develop clinical trials for such uncommon indications, retrospective studies may help us better understand the role of proton therapy in these situations.

Studies on proton therapy have explored one way of decreasing radiation-related toxicity: reduction in the dose

to normal tissues. However, another way of decreasing toxicity could be patient selection, i.e., reduction in the number of patients treated with radiation therapy. A large phase II/III trial (PROSPECT) is currently comparing standard preoperative chemoradiation versus induction chemotherapy and selective radiotherapy for rectal cancer. A prospective European trial (MERCURY) has indicated that MRI could be used to identify patients likely to have a good outcome with surgery alone without preoperative radiotherapy (9). In the future, more selective use of radiation may help lower treatment-related toxicity in rectal cancer patients.

In summary, Colaco *et al.* have presented an intriguing dosimetric study on the role of proton therapy for the treatment of rectal cancer. Clinical studies will be needed to further elucidate the potential role of proton therapy.

Acknowledgements

Disclosure: The author declares no conflict of interest.

References

1. Colaco RJ, Nichols RC, Huh S, et al. Protons offer reduced bone marrow, small bowel, and urinary bladder exposure for patients receiving neoadjuvant radiotherapy for resectable rectal cancer. J Gastrointest Oncol 2014;5:3-8.
2. Tatsuzaki H, Urie MM, Willett CG. 3-D comparative study of proton vs. x-ray radiation therapy for rectal cancer. Int J Radiat Oncol Biol Phys 1992;22:369-74.
3. Wolff HA, Wagner DM, Conradi LC, et al. Irradiation with protons for the individualized treatment of patients with locally advanced rectal cancer: a planning study with clinical implications. Radiother Oncol 2012;102:30-7.
4. Palmer M, Mok H, Ciura K, et al. Dose Reduction to Small Bowel and Other Relevant Structures in Rectal Carcinoma with Proton Therapy. Int J Radiat Oncol Biol Phys 2012;84:S846.
5. Mok H, Crane CH, Palmer MB, et al. Intensity modulated radiation therapy (IMRT): differences in target volumes and improvement in clinically relevant doses to small bowel in rectal carcinoma. Radiat Oncol 2011;6:63.
6. Samuelian JM, Callister MD, Ashman JB, et al. Reduced acute bowel toxicity in patients treated with intensity-modulated radiotherapy for rectal cancer. Int J Radiat Oncol Biol Phys 2012;82:1981-7.
7. Garofalo M, Moughan J, Hong T, et al. RTOG 0822: A Phase II Study of Preoperative (PREOP) Chemoradiotherapy (CRT) Utilizing IMRT in Combination with Capecitabine (C) and Oxaliplatin (O) for Patients with Locally Advanced Rectal Cancer. Int J Radiat Oncol Biol Phys 2011;81:S3-4.
8. Jabbour SK, Patel S, Herman JM, et al. Intensity-modulated radiation therapy for rectal carcinoma can reduce treatment breaks and emergency department visits. Int J Surg Oncol 2012;2012:891067.
9. Taylor FG, Quirke P, Heald RJ, et al. Preoperative high-resolution magnetic resonance imaging can identify good prognosis stage I, II, and III rectal cancer best managed by surgery alone: a prospective, multicenter, European study. Ann Surg 2011;253:711-9.

Cite this article as: Das P. Rectal cancer: do protons have prospects? J Gastrointest Oncol 2014;5(1):1-2. doi: 10.3978/j.issn.2078-6891.2013.047

Review Article

Proton beam radiation therapy of prostate cancer - history, results, and future directions

Carl J Rossi Jr

Scripps Proton Therapy Center, 9730 Summers Ridge Road, San Diego CA 92121, USA

Correspondence to: Carl J Rossi Jr, MD. Scripps Proton Therapy Center, 9730 Summers Ridge Road, San Diego CA 92121, USA. Email: Rossi.carl@scrippshealth.org.

Abstract: Proton beam radiation therapy of organ-confined prostate cancer now constitutes one of the most commonly treated malignancies with this modality. This paper will provide a concise review of the history of proton beam therapy of prostate cancer, discuss the most recently published clinical data, examine the future uses of proton beam radiotherapy in prostate cancer treatment, and seek to place proton beam therapy in the context of other technological evolutions in radiation oncology.

Key Words: Protons; prostate cancer; dose-escalation

DOI: 10.3978/j.issn.2218-676X.2012.10.06

Scan to your mobile device or view this article at: http://www.thetcr.org/article/view/597/html

Introduction

Prostate cancer continues to present a major oncologic dilemma for the developed world. In the United States there were an estimated 240,000 new cases diagnosed in 2011, with approximately 33,000 deaths from this disease (1) . Prostate cancer is the second leading cause of cancer deaths among American men and accounts for approximately 10% of all cancer related deaths in men. A similar incidence and death rate is seen in Western Europe, with the lowest reported incidence being in Eastern/Southern Asia. Beginning in the early 1990's the discovery and use of Prostate Specific Antigen (PSA) as a screening tool has led to both an increase in the number of cases being diagnosed and a decrease in the proportion of men being diagnosed with advanced disease. This encouraging trend towards diagnosis with organ-confined disease has prompted the development and refinement of treatment methods directed at the prostate in the entirely reasonable hope of providing long-term disease free survival and cure.

From the standpoint of radiotherapy virtually all technical advances in prostate cancer treatment have been implemented to reduce normal tissue toxicity by limiting the volume of adjacent bladder and rectum which receive moderate to high doses of radiation. A direct consequence of this improvement in dose conformity has been dose escalation (2), a concept which has been tested and confirmed in one proton beam-based prospective randomized trial.

The unique physical properties inherent in proton beams makes them particularly attractive to the radiation oncologist, for they permit a reduction in "integral dose" (defined as the total radiation dose given to the patient) over and above anything which can be achieved with photon-based external beam treatment systems (3-5).

Initial proton beam treatment results

The ability to use proton therapy to treat deep organs was, and remains, greatly dependent on the concurrent development and refinement of cross-sectional imaging technology [CT, MRI] and modern computers, hence it is not surprising that proton beam therapy of prostate cancer did not commence until the late 1970's. Beginning in 1977, Shipley and associates at the Massachusetts General Hospital [MGH] initiated a Phase I trial in which proton beam radiotherapy was used to give a boost dose to patients with locally advanced disease that were also receiving photon radiotherapy. At that time, this boost dose was felt to be over and above what could be safely given with existing 2-dimensional photon technology. Seventeen

Table 1 Patient characteristics in initial LLU trial (adapted from Slater *et al*. 1998)

	Patients
T-stage	
1A/1B	28
1C	91
2A	157
2B	173
2C	157
3	37
Gleason score	
2-5	232
6-7	324
8-10	54
Initial PSA	
≤4.0	53
4.1-10.0	280
10.1-20.0	175
>20	85

patients with stage T2-T4 disease received a perineally-directed proton beam boost of 20-26 GyE (given at a rate of 1.8-2 GyE/day) following treatment to the prostate and pelvis to a dose of 50.4 Gy with 10 MV photons given via a four-field box approach. A perineal approach was chosen because this was the only anatomical pathway that allowed the 160 MeV proton beam generated by the Harvard Cyclotron to reliably encompass the entire prostate gland. Acutely, the treatment was well tolerated and after a follow up period ranging from 12-27 months no severe late rectal reactions were noted (6).

These favorable toxicity results led directly to the initiation of a prospective randomized trial designed to test the benefits of proton beam dose escalation in patients with locally advanced disease. Patients with stage T3-T4 tumors were chosen as it was felt that this group stood to gain the most benefit from high doses. All patients received 50.4 Gy to the prostate and pelvis with megavoltage photons, administered via a four-field box-technique. They were then randomly assigned to receive either an additional 16.8 Gy of photons (for a total prostate dose of 67.2 Gy) or 25.2 GyE of protons for a total prostate dose of 75.6 Gy. Adjuvant hormonal therapy was not permitted. The limited availability of the Harvard Cyclotron affected patient accrual; nonetheless, two hundred and two patients were eventually enrolled, with one hundred and three being treated in the high dose arm and ninety nine in the standard dose arm.

With a median follow up of 61 months there were no differences seen in overall survival, disease-specific survival, total relapse-free survival, or local control between the arms. Patients with high-grade tumors who were treated on the high dose arm did experience a trend towards improvement in local control at five and eight years (92% and 77% *vs*. 80% and 60%, P=0.089). Patients whose digital rectal exams normalized following treatment and who underwent subsequent prostate biopsy revealed a lower positive biopsy rate in the high dose arm (28% *vs*. 45%) and, perhaps most surprisingly, the local control rates for patients with Gleason grade 4-5 tumors (57 patients total) were significantly better at five and eight years in the high dose patients (94% & 84% *vs*. 68% & 19%, P=0.001). High dose treatment was associated with an increase in late grade 1-2 rectal bleeding (32% *vs*. 12%, P=0.02) (7).

These results have been erroneously cited by some as evidence that proton-beam dose escalation is of doubtful utility (8). However, it must be noted that the patients treated in this trial were at a high risk of not only local failure but of distant failure and therefore it is not surprising that overall survival was unaffected. In addition, patients with these adverse characteristics would not, if diagnosed today, receive radiotherapy as monotherapy and instead would be treated with a multi-modality approach (9-12). What the trial did demonstrate is that (I) high dose radiotherapy did decrease local failure, and this decrease was most profound in those patients with the most aggressive tumors and (II) Dose-escalation by means of a perineal proton beam (an approach which has largely been abandoned today as higher energy proton beams have become available) can be performed safely with acceptable toxicity.

The completion in 1990 of the world's first hospital-based proton treatment center at Loma Linda University Medical Center [LLUMC] marked the beginning of a transition in proton beam therapy from the research laboratory setting to clinical radiation oncology (13). Beginning in late 1991 prostate patients at LLUMC were treated on a clinical trial who's goal was to confirm the efficacy and toxicity data generated at MGH. Between December 1991 and December 1995 643 patients were treated to total prostate radiation doses of 74-75 GyE. Patients who were deemed to be at a low risk for occult nodal metastasis were treated with lateral proton beams alone while those who were felt to benefit from elective nodal radiation received 45 Gy to the pelvis with 18-23 MV photons delivered via a multifield

Table 2 Predictors of biochemical failure-from Slater *et al*. 1998

		% Disease-free survival @ 5 years	Univariate P	Multivariate P
Initial PSA	≤4.0	100		
	4.1-10.0	88	<0.001	0.001
	10.1-20.0	68		
	>20.0	48		
Gleason	2-5	82		
	6-7	76	<0.001	0.007
	8-10	48		
T stage	1A/1B	79		
	1C	94		
	2A	87	<0.001	0.003
	2B	73		
	2C	59		
	3	59		

3-D conformal technique. Patient characteristics are shown in *Table 1*.

With a median follow up of 43 months, the overall biochemical disease-free survival [bNED] rate was 79% as per the American Society for Therapeutic Radiology and Oncology [ASTRO] definition of three successively rising PSA values above a nadir equating to biochemical failure. The risk of biochemical failure was strongly dependent on the pre-treatment PSA with five-year bNED survival rates varying from 53% in patients with pre-treatment PSA's of 20-50 to 100% with PSA's of <4.1. BNED survival was also significantly influenced by post-treatment PSA nadir. A multi-variant analysis of failure predictors demonstrated that initial stage, PSA, and Gleason Score were all strong predictors of biochemical failure at five years (*Table 2*). Acute toxicity was minimal and all patients completed the prescribed course of radiotherapy. Proctitis remained the most common late toxicity with Grade 2 proctitis occurring in 21% of patients at three years; for the majority of patients this represented a single episode of rectal bleeding. No > Grade 3 GI toxicity was seen. Grade 2 GU toxicity (primarily gross hematuria) was seen in 5.4% of patients at three years, with two patients developing Grade 3 bladder toxicity. No significant difference in late toxicity was seen between those patients treated with protons alone and those receiving pelvic x-ray therapy (14).

An update of the initial LLUMC experience was published in 2004. This study encompassed 1,255 patients with stage T1-T3 disease who were treated with proton beam radiotherapy alone (i.e., no prior or concurrent hormonal therapy) to a dose of 74-75 GyE. As was seen in the earlier trial initial PSA, Gleason Grade, and PSA nadir were all strong predictors of bNED survival. Treatment continued to be well tolerated with rates of RTOG Grade >3 GI/GU late morbidity of <1% (15).

PROG/ACR95-09 randomized dose-escalation trial

Beginning in 1996, LLUMC and MGH embarked on the Proton Radiation Oncology Group/American College of Radiology [PROG/ACR] 95-09 trial, a prospective, randomized dose-escalation study for patients with organ-confined prostate cancer. This study was designed to test the hypothesis that a dose escalation from 70.2 to 79.2 GyE would result in a statistically significant decrease in local failure, biochemical failure, and overall survival. Eligibility criteria included stage T1b-T2b disease (as per the 1992 American Joint Committee on Cancer staging system), a PSA of <15 ng/mL, and no evidence of metastatic disease on imaging studies (bone scan, abdominal-pelvic CT scan). All Gleason scores were allowed, but no prior or concurrent androgen-deprivation therapy was permitted. Pre-treatment patient characteristics are shown in *Table 3*.

Patients were randomly assigned to receive a total prostate dose of 70.2 or 79.2 GyE. Radiotherapy was administered sequentially in two phases. In Phase I, conformal proton beams were used to treat the prostate alone. Depending on randomization either 19.8 or 28.8 GyE in 11 or 16 fractions was delivered. The clinical target volume [CTV] was the

Table 3 PROG/ACR 9509 patient characteristics-from Zietman *et al.* 2005

Characteristic	#Patients [% of group]	
	70.2 GyE [n=197]	79.2 GyE [n=195]
Age, years		
50-59	43 [21.8]	37 [19.0]
60-69	92 [46.7]	103 [52.8]
70-79	61 [31.0]	55 [28.2]
≥80	1 [0.5]	0
Race		
White	176 [89.3]	178 [91.3]
Hispanic	4 [2.0]	7 [3.6]
Black	12 [6.1]	5 [2.6]
Other	5 [2.5]	5 [2.6]
PSA level, ng/mL		
<4.0	24 [12.2]	21 [10.8]
4-10.0	145 [73.6]	145 [74.3]
10-15	28 [14.2]	29 [14.9]
Median [range]	6.3 [1.2-14.7]	6.2 [0.67-14.3]
Combined gleason score		
2-6	148 [75.1]	147 [75.4]
7	30 [15.2]	30 [15.4]
8-10	18 [9.1]	15 [7.7]
Unknown	1 [0.5]	3 [1.5]
Tumor stage		
T1b	1 [0.5]	0
T1c	120 [60.9]	120 [61.5]
T2a	43 [21.8]	50 [25.6]
T2b	33 [16.8]	25 [12.8]
Node stage		
N0	0	2 [1.0]
NX	197 [100]	193 [99.0]
Risk group		
Low	111 [56.4]	116 [59.5]
Intermediate	68 [34.5]	61 [31.3]
High	18 [9.1]	15 [7.7]
Not classified	0	3 [1.5]

prostate plus a 5 mm margin. Beam arrangement was facility dependent with patients at LLUMC being treated with lateral proton beams of 225-250 MeV energy, while at MGH a perineal 160 MeV proton beam was employed. Before each proton beam treatment session a water balloon was inserted into the rectum and inflated with 100 mL of saline; this served the dual purpose of distending the rectum lumen to decrease the volume of rectum receiving any radiation and minimizing prostate motion.

In the second phase of treatment all patients received 50.4 Gy of photons given in twenty-eight 1.8 Gy fractions. The CTV was the prostate and seminal vesicles. No effort was made to include the pelvic lymphatics. Three-dimensional planning was used on all patients and photon energies of 10-23 MV were employed. The use of photons for a portion of the treatment was done solely to allow both institutions to participate in this trial, for at the time the trial commenced MGH patients were still restricted to treatment at the Harvard Cyclotron Laboratory and the limited throughput of that facility meant that the most efficient use of protons was as a boost and not as monotherapy. A total of 393 patients were randomized between January 1996 and December 1999.

The results of the trial were initially published in 2005 (16), with an update in 2010. At a median follow-up of 8.9 years there is a persistent and statistically significant increase in biochemical freedom from relapse amongst patients randomized to the high dose arm (*Figure 1*). This difference was seen when using both the ASTRO and the more recent Phoenix definition (17) (in which biochemical failure = a PSA elevation of >2 ng/mL above a nadir). Subgroup analysis showed a particularly strong benefit in 10-year bNED survival amongst the "low risk" patients (defined as PSA <10 ng/mL, and Gleason score <7 and stage < T2b), with 92.2% of high dose patients being disease free *vs.* 78.8% for standard dose (P=0.0001). A strong trend towards a similar finding was seen in the intermediate risk patients but this has not reached statistical significance (*Figure 2*). In addition, patients in the standard dose arm are twice as likely to have been started on androgen deprivation therapy as high dose patients (22 *vs.* 11, P=0.47) with such treatment usually being initiated due to a rising PSA. To date, there is no difference in overall survival between the arms (18).

As was seen in the previously reported proton trials treatment was well tolerated. Only 2% of patients in both arms have experienced late GU toxicities of Grade >3 and 1% have experienced late GI toxicity of Grade >3. Interestingly, as opposed to what has been reported in some photon-based randomized dose escalation trials high dose radiotherapy delivered via a conformal proton beam boost did not result in an increase in late Grade >3 GI morbidity amongst the high dose patients (*Table 4*). This encouraging finding has been confirmed by a patient-reported sensitive Quality of Life instrument which did not report any greater

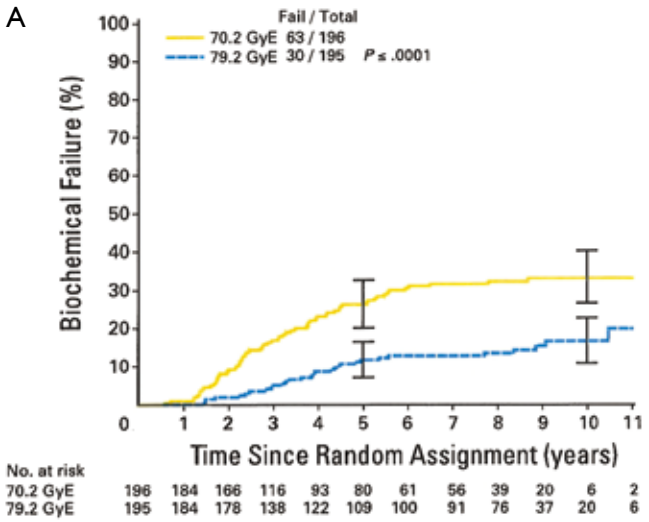

Figure 1 Biochemical failure for all patients. A. represents failure as per the American Society for Therapeutic Radiology and Oncology Definition; B. represents failure as per the Phoenix Definition. Adapted from Zietman, 2010

morbidity than the physician-reported scores, and which revealed equal and high satisfaction with quality of life between both arms (19).

Thus, the PROG/ACR 9509 trial provides "Level One" evidence verifying the importance of radiation dose-escalation in organ confined prostate cancer and while this study was not designed to directly compare the efficacy of conformal proton beam radiotherapy against other conformal techniques or modalities it does demonstrate that conformal proton beam radiotherapy is an effective treatment for this disease, with minimal risk of experiencing

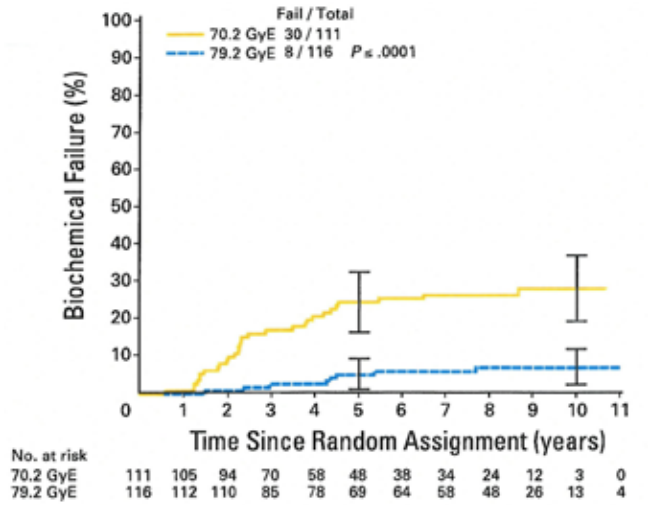

Figure 2 Biochemical failure for low-risk patients. A. as per ASTRO definition. B. as per Phoenix definition. Adapted from Zietman, 2010

severe treatment-induced toxicity.

University of Florida experience

The University of Florida Proton Therapy Institute opened in the summer of 2006 with prostate cancer treatment commencing at that time. From August, 2006 to October 2007 patients were treated on one of three prospective trials: 78 GyE/39 fractions for low-risk disease, dose escalation from 78-82 GyE for intermediate-risk disease, and 78 GyE with concomitant taxotere, followed by androgen-deprivation therapy, for high-risk disease. Preliminary GI and GU toxicity data was reported in 2010 with a minimum of two year follow up. Forty-two percent of the patients experienced Grade 2+ GU symptomatology requiring management after treatment, including four transient Grade 3 symptoms (all of which occurred in patients who required medical or surgical management of GU symptoms prior to radiotherapy). The overwhelming majority of Grade 2 symptoms (98%) were retentive symptoms requiring treatment with alpha-blockers. Multivariate analysis suggested that Grade 2+ GU toxicities were correlated with pre-treatment prostatitis, pre-treatment International Prostate Symptom Score [IPSS] score and, as time progressed, with patient age and pre-treatment GU symptom management. This strongly suggests that the predominant predictors of early GU toxicity were pre-treatment clinical factors.

Table 4 Acute and late GU and GI toxicity. From Zietman *et al.* 2010

Toxicity	Assigned dose																P
	70.2 GyE (n=196)								79.2 GyE (n=195)								
	Grade 1		Grade 2		Grade 3		Grade 4		Grade 1		Grade 2		Grade 3		Grade 4		
	No.	%	No.	%	No.	%	No.	%	No.	%	No.	%	No.	%	No.	%	
Acute																	
GU	72	37	100	51	5	3	0	0	56	29	117	60	4	2	1	1	0.0745
GI	76	39	87	44	2	1	0	0	50	26	123	63	2	1	0	0	0.0006
Late																	
GU	82	42	44	22	4	2	0	0	88	45	52	27	3	2	0	0	0.7934
GI	68	35	25	13	0	0	0	0	79	41	46	24	2	1	0	0	0.0895

GI toxicities were considerably less common, 10% of the patients experiencing a cumulative incidence of Grade 2+ GI toxicities over the first two years post-treatment, including a single Grade 3 toxicity. Univariate analysis revealed a significant correlation between Grade 2 or higher GI toxicity and the percentage of rectal wall receiving radiation doses from 40-80 GyE, and the percentage of rectum receiving 10-80 GyE, while multivariate analysis revealed the rectal wall V70 correlated with the cumulative incidence of Grade 2+ rectal bleeding and/or proctitis at 24 months. The authors concluded that treatment was well tolerated with minimal and acceptable GI/GU toxicity, again mirroring the results from other proton centers (20).

ACR 0312 trial

Following the completion of patient accrual to the PROG/ACR9509 randomized trial, LLUMC and MGH opened a Phase II dose-escalation study designed to determine the toxicity and efficacy of proton-beam based dose escalation in patients with organ-confined disease. The ACR 0312 trial delivered a total dose of 82 GyE/41 fractions to the prostate, with the initial 50 GyE also including the caudal 2 cm of the seminal vesicles. PTV volumes were identical to those used in the PROG 9509 patients. The trial enrolled eighty-five patients who were treated between May 2003 and March 2006. The rate of acute GI/GU > Grade 3 complications were 1%. With a median follow up of 31.6 months six patients have developed a late Grade 3 GI/GU toxicity with one additional patient developing Grade 4 toxicity. The median time to Grade 3+ toxicity was 9.5 months with an estimated rate of Grade 3+ toxicity at eighteen months of 6%. Dose-Volume Histogram [DVH] analysis of the radiation dose to the anterior rectal wall failed to reveal a demonstrable association between dose to various volumes of the anterior wall and the risk of subsequently developing a Grade 2+ late rectal toxicity. The authors noted that the observed late morbidities compare favorably with that reported in IMRT dose-escalation studies, but that the dose of 82 GyE/41 fractions may represent the safe limit of what can be delivered with passive-scattered proton beams. They speculated that further dose-escalation should be possible with the forthcoming implementation of intensity modulated proton beams and real-time image-guided proton treatment delivery (21).

Japan

The Hyogo Ion Beam Medical Center began treating prostate patients with proton radiation in April 2001. Between 2001-2002 a series of Phase I-II protocols were performed to verify treatment techniques and assess toxicity. Once these revealed minimal toxicity proton beam therapy passed into general clinical use (22). In 2003-2004, 287 patients with stage T1-T4 N0 M0 prostate cancer were treated with lateral proton beams to a dose of 74 GyE in 37 fractions. Planning margins were similar to those used at the US proton centers, although a rectal balloon was not used. Patient characteristics are shown in *Table 5* (23). Seventy-one percent of the patients also received androgen-deprivation therapy.

The observed morbidities are shown in *Table 6*. Mirroring the US experience, Grade 3 GU toxicities were extremely rare, and no Grade 4 events occurred. On Univariate analysis CTV size and patient age were significantly associated with a greater incidence of Grade >2 GU morbidity. Multivariate analysis confirmed that large CTV's [P=0.001] and the use of androgen suppression therapy [P=0.017] independently

Table 5 Patient characteristics. From Mayahara *et al.* 2007

Characteristic	Patient [% of group]
Age [y]	
<70	146 [51]
≥70	141 [49]
T stage	
T1c	107 [37]
T2a	81 [28]
T2b	39 [14]
T3	59 [21]
T4	1 [0.3]
Gleason score	
2-6	91 [32]
7	161 [56]
8-10	26 [9]
Unknown	9 [3]
Initial PSA ng/mL	
<10	135 [47]
10.0-19.9	79 [28]
20-49.9	53 [18]
≥50	20 [7]
Risk group [MSKCC]	
Favorable	62 [22]
Intermediate	100 [35]
Unfavorable	125 [43]
Use of AAT	
No	83 [29]
Yes	204 [71]

Abbreviations: MSKCC = Memorial Sloan-Kettering Cancer Center; AAT = Androgen Ablation Therapy

predicted acute GU Grade 2-3 morbidity. These acute toxicities were comparable to those seen in published IMRT, 3-D conformal, and Brachytherapy series.

Protons *vs.* IMRT

In a widely quoted 2012 study, Sheets and colleagues at the University of North Carolina performed a comparison of prostate cancer patients treated with IMRT to those receiving 3-D conformal radiation therapy or proton beam treatment. The study reviewed patients from the SEER and Medicare databases who were treated between 2000 and 2007. Disease-free status was assessed by the need for additional cancer therapy and late morbidity was assessed by the need for additional diagnostic and/or therapeutic procedures to address radiation-induced problems.

The authors concluded that while IMRT was superior to 3-D conformal radiation therapy in terms of disease-free status and late morbidity, proton beam therapy carried with it (as compared to IM RT) an increased risk of late gastrointestinal morbidity for no therapeutic gain (24).

I believe that there are substantial methodological flaws in the study, which could easily explain the observed results:

(I) The authors made no attempt to account for likely 10-15% difference in radiation dose between the proton and IMRT patients. During the time period encompassed by this study, the "typical" IMRT radiation dose was between 70-74 Gray, the largest series of randomized data favoring dose escalation in prostate cancer was not published until 2005 and even after this paper was published it still took several years for the radiation oncology community to accept the increased external beam radiation dose of 79-81 Gray as "standard". In contrast, all the proton patients analyzed in this trial were treated at a single SEER institution, and all received a minimum radiation dose of 79.2 Gray, with many receiving 80-81 Gray. As has been previously published late gastrointestinal morbidity is highly dependent upon both total radiation dose and normal-organ delineation (13,25), so the difference in late gastrointestinal morbidity between the proton beam and IMRT patients can be easily explained simply by the higher radiation dose routinely given to the proton beam patients.

(II) In contrast to the situation prevalent in the community, all of the proton beam patients were treated on protocols that called for close and regular follow-up with particular attention being paid to gastrointestinal issues, and which mandated gastrointestinal evaluation for any late gastrointestinal complaints. Since this study did not analyze severity of gastrointestinal issues but only the need for additional diagnostic and/or therapeutic procedures, this inherent bias in the proton patients towards protocol-mandated gastrointestinal referral can explain the greater number of gastrointestinal event seen in the proton beam patients.

(III) No attempt was made by the authors to analyze any potential differences in prostate gland and rectal wall coverage between the IMRT and Proton patients via a dose-volume-histogram analysis. Indeed, the authors fail to comment on any of the technical aspects of the two different types of radiotherapy analyzed. Were identical treatment margins used on all patients? How was the dose proscribed? What immobilization, if any was used? Was image-guidance

Table 6 Acute GU and GI morbidities as per NCI-CTC. From Mayahara *et al*. 2007. Patient # [% of group]

	Grade 0	Grade 1	Grade 2	Grade 3	Grade 4
Toxicity					
Dysuria	52 [18]	134 [47]	101 [35]	0	0
Frequency	69 [24]	179 [62]	36 [13]	3 [1]	0
Retention	204 [71]	73 [25]	9 [3]	1 [0.3]	0
Hematuria	231 [81]	50 [17]	5 [2]	1 [0.3]	0
GU overall	18 [6]	154 [54]	111[39]	4 [1]	0
Proctitis	282 [98]	5 [2]	0	0	0
Bleeding	0	0	0	0	0
GI overall	282 [98]	5 [2]	0	0	0

employed and if so what type? When one considers the heterogeneous nature of the IMRT patients who were treated at multiple facilities versus the homogeneous nature of the proton patients, all of whom were treated at a single center with well-defined and adhered to protocols for dose prescription, patient immobilization, and daily positioning, these technical factors become even more important as they could easily in and of themselves result in the difference in morbidity noted between the two groups.

All this serves to illustrate the risks and potential inaccuracies inherent in attempting to use large patient registries to perform a detailed data analysis. Unfortunately, papers such as the Sheets paper, once published, are often quoted as having "proved" a particular point when in fact they have done nothing substantive to settle the issue. The definitive way to answer the protons *vs*. IMRT question would be to perform a prospective randomized trial but this is no more likely to occur than were randomized 3-D conformal X-ray *vs*. IMRT trials when the latter technology was first being introduced, and for the same reason-randomizing patients to potentially receive more of a toxic substance (radiation) whose toxicity is beyond questioning and which is of no benefit whatsoever to the patient is ethically suspect and in all likelihood such a trial would, if attempted, fail to reach its accrual goal (26).

Hypofractionation

Modern radiobiologic theory predicts that prostate cancer has a low "alpha/beta ratio". This is a numeric description of the sensitivity of a particular tissue to radiation fraction size. For example, tissues with a low alpha/beta ratio are more sensitive to changes in fraction size than those with a high alpha-beta ratio, with most estimates for prostate cancer cells being in the range of 1.5-2.0 (27). This is substantially lower than the alpha/beta ratio of 3-4 that has been assumed for late bladder/rectal toxicity. This difference in alpha/beta ratios implies that prostate cancer cells are more sensitive to changes in radiation fraction size than those of the bladder or rectum, meaning that by increasing the daily fraction size and reducing the total radiation dose one can potentially shorten the overall treatment time without compromising tumor control and without increasing the risk of incurring a late GI/GU injury.

Hypofractionation has a long-established history in proton beam therapy, and is now routinely used in proton beam treatment of ocular melanomas, intracranial metastasis, arterial-venous malformations (28), lung cancer (29), and breast cancer (30). It also is being actively investigated in prostate cancer, although to date this investigation has employed primarily IMRT-based approaches (31-34). There is an emerging body of data supporting its safety and efficacy in this setting to the point that at least one prominent radiation biologist has declared that hypofractionation should be considered the treatment of choice for prostate cancer (35).

At the time of this writing there are at least four hypofractionated conformal proton beam treatment protocols actively accruing patients in the USA. At LLUMC, a Phase I-II trial of 60 GyE/20 fractions (which is designed to be isoeffective with 81 GyE/ 45 fractions, if one assumes an alpha/beta ratio of 1.5 for prostate cancer) began accruing patients in 2009. Eligibility is limited to "low risk" patients (PSA <10 ng/mL, Gleason <7, and Stage < T2b). Preliminary analysis indicates that treatment is well tolerated with no patient (n=50) experiencing a Grade >3 acute GI/GU complication. Post-treatment PSA decreases are consistent with expectations. At the University of Florida hypofractionation is being investigated in a similar protocol in which patients with low to intermediate-risk

prostate cancer are treated on a 5-week hypofractionated schedule to a total dose of 70 GyE/28 fractions for low-risk patients, and 72.5 GyE/29 fractions for intermediate risk patients. The Proton Collaborative Group is performing a Phase III randomized trial of standard *vs.* hypofractionated proton radiation in low-risk patients, while the University of Pennsylvania is performing a feasibility trial of "mildly hypofractionated" proton radiation therapy or IMRT in intermediate-risk patients.

Proton treatment-summary

The published peer-reviewed data conclusively demonstrates that conformal proton beam radiotherapy is extremely well tolerated and can produce bNED survival rates equivalent to other modern radiotherapy modalities, and to radical prostatectomy. Conformal proton beam dose-escalation has been tested in a prospective randomized trial and has been shown to improve bNED survival without [as opposed to what has been seen in some x-ray based trials (36)] concurrently increasing the risk of late Grade >3 GI/GU morbidity. However, attempts to escalate dose to 82 GyE have been met with a substantial increase in late GI morbidity; this may reflect the "limit" beyond which treatment with passive-scattered beams and their attendant substantial penumbra may not be safely possible, although it is likely that the pending introduction of intensity-modulated proton therapy [IMPT] via active beam scanning and the implementation of novel image-guided techniques will permit further increases in dose. Hypofractionation is currently being tested in protocols at several proton centers and preliminary data on the safety and efficacy of this technique will be available within the next 12-18 months.

Future directions

Prostate cancer is an excellent site in which to test and perfect the implementation of new treatment techniques and dose-fractionation schedules. Ongoing technical advances in proton beam therapy will lead to further dose-specificity within the target organ and a further reduction in normal tissue radiation dose. Development of these techniques, including IMPT and real-time particle beam IGRT, will require their testing in a large number of patients who have similar disease characteristics and anatomic constraints. Prostate cancer represents an excellent "test bed" for these important developments. It is an extremely common disease so large numbers of potential patients exist and, as opposed to some other common tumors (most notably lung cancer) it is typically diagnosed while confined to its organ of origin so that treated patients are likely to live for the many years post treatment required to perform a comprehensive analysis of late effects. Organ motion is minimal, which aids in the development of beam-scanning techniques that are inherently more sensitive to target motion than passive-scattered arrangements. That fact that tumor response can be assessed biochemically as opposed to clinically or radiologically means that the effects of alterations in treatment techniques on tumor can be analyzed (and potentially adjusted or even abandoned) far more rapidly than when less exacting measures are available. Lastly, in contrast to other sites like the base of skull, the prostate is adjacent to only two critical organs about which a good deal is already known concerning dose-volume effects and their impact on acute and late morbidity, thereby providing for a more accurate extrapolation of the effects of any potential treatment alterations than would be true of other, less frequently treated sites.

One of the often-voiced complaints about proton beam treatment is the cost of providing this therapy. This concern is commonly raised whenever any new treatment technology or, for that matter, any new technology, is introduced into society. In the health care arena, new technology is increasingly being met with the demand that the new method be subjected to randomized trials *vs.* existing treatment methods before the medical community and health care payers accept the new method.

This clamor for randomized data is not new, nor is it confined to the introduction of proton beam treatment. It is imperative to remember that virtually all other advancements in radiotherapy treatment technology, including the widespread embracement of IMRT, have not occurred only after this technology was first tested in prospective trials but solely because this technology promised a higher degree of dose conformality than its contemporaries. When considered from this perspective, proton beam therapy is best viewed as simply a further large step along the same road of technological advancement that has been followed diligently by radiation oncologists for the last century. A randomized proton/IMRT trial would expose (literally) one group of patients to an integral dose 3-4 times greater than the other, with no expected gain in terms of disease control. Attempts to convince educated patients to participate in such a study in meaningful numbers will be difficult at best may well prove to be impossible.

It is also quite likely that the cost of proton beam

radiation therapy (again, mirroring the cost of any new technology, with computers being a prime example) will inevitably decline as demand for this technology fosters the continuing development of newer, less expensive treatment units. Once the cost of proton beam treatment approximates that of IMRT arguments over relative efficacy will in all likelihood come to an abrupt end. In order for proton beam treatment to achieve this goal it has to be used for treatment of common cancers like prostate cancer. Again, this pathway is not new, and it simply follows the trail already blazed by other technologies, including IMRT.

The prostate represents perhaps the ideal proving ground for proton beam treatment. Rather than discourage its use on prostate cancer I believe that its use should be encouraged. The techniques perfected and lessons learned will serve to benefit all patients, including those treated with other radiotherapy modalities, and will add invaluable data to the widespread clinical implementation of proton beam radiotherapy.

Acknowledgements

Disclosure: The author declares no conflict of interest.

References

1. Mohler J, Bahnson RR, Boston B, et al. NCCN clinical practice guidelines in oncology: prostate cancer. J Natl Compr Canc Netw 2010;8:162-200.
2. Pickles T, Pollack A. The case for dose escalation versus adjuvant androgen deprivation therapy for intermediate risk prostate cancer. Can J Urol 2006;13:68-71.
3. Archambeau JO, Bennett GW, Levine GS, et al. Proton radiation therapy. Radiology 1974;110:445-57.
4. Archambeau JO, Bennett GW, Chen ST. Potential of proton beams for total nodal irradiation. Acta Radiol Ther Phys Biol 1974;13:393-401.
5. Loeffler JS, Smith AR, Suit HD. The potential role of proton beams in radiation oncology. Semin Oncol 1997;24:686-95.
6. Shipley WU, Tepper JE, Prout GR Jr, et al. Proton radiation as boost therapy for localized prostatic carcinoma. JAMA 1979;241:1912-5.
7. Shipley WU, Verhey LJ, Munzenrider JE, et al. Advanced prostate cancer: the results of a randomized comparative trial of high dose irradiation boosting with conformal protons compared with conventional dose irradiation using photons alone. Int J Radiat Oncol Biol Phys 1995;32:3-12.
8. Hanks GE. A question-filled future for dose escalation in prostate cancer. Int J Radiat Oncol Biol Phys 1995;32:267-9.
9. Roach M 3rd. Dose escalated external beam radiotherapy versus neoadjuvant androgen deprivation therapy and conventional dose external beam radiotherapy for clinically localized prostate cancer: do we need both? Strahlenther Onkol 2007;183:26-8.
10. Roach M 3rd, Bae K, Speight J, et al. Short-term neoadjuvant androgen deprivation therapy and external-beam radiotherapy for locally advanced prostate cancer: long-term results of RTOG 8610. J Clin Oncol 2008;26:585-91.
11. Roach M 3rd. Current status of androgen suppression and radiotherapy for patients with prostate cancer. J Steroid Biochem Mol Biol 1999;69:239-45.
12. Roach M 3rd. Neoadjuvant total androgen suppression and radiotherapy in the management of locally advanced prostate cancer. Semin Urol Oncol 1996;14:32-7; discussion 38.
13. Guckenberger M, Meyer J, Baier K, et al. Distinct effects of rectum delineation methods in 3D-conformal vs. IMRT treatment planning of prostate cancer. Radiat Oncol 2006;1:34.
14. Slater JD, Yonemoto LT, Rossi CJ Jr, et al. Conformal proton therapy for prostate carcinoma. Int J Radiat Oncol Biol Phys 1998;42:299-304.
15. Slater JD, Rossi CJ Jr, Yonemoto LT, et al. Proton therapy for prostate cancer: the initial Loma Linda University experience. Int J Radiat Oncol Biol Phys 2004;59:348-52.
16. Zietman AL, DeSilvio ML, Slater JD, et al. Comparison of conventional-dose vs high-dose conformal radiation therapy in clinically localized adenocarcinoma of the prostate: a randomized controlled trial. JAMA 2005;294:1233-9.
17. Abramowitz MC, Li T, Buyyounouski MK, et al. The Phoenix definition of biochemical failure predicts for overall survival in patients with prostate cancer. Cancer 2008;112:55-60.
18. Zietman AL, Bae K, Slater JD, et al. Randomized trial comparing conventional-dose with high-dose conformal radiation therapy in early-stage adenocarcinoma of the prostate: long-term results from proton radiation oncology group/american college of radiology 95-09. J Clin Oncol 2010;28:1106-11.
19. Talcott JA, Rossi C, Shipley WU, et al. Patient-reported long-term outcomes after conventional and high-dose combined proton and photon radiation for early prostate

cancer. JAMA 2010;303:1046-53.
20. Mendenhall NP, Li Z, Hoppe BS, et al. Early outcomes from three prospective trials of image-guided proton therapy for prostate cancer. Int J Radiat Oncol Biol Phys 2012;82:213-21.
21. Coen JJ, Bae K, Zietman AL, et al. Acute and late toxicity after dose escalation to 82 GyE using conformal proton radiation for localized prostate cancer: initial report of American College of Radiology Phase II study 03-12. Int J Radiat Oncol Biol Phys 2011;81:1005-9.
22. Hara I, Murakami M, Kagawa K, et al. Experience with conformal proton therapy for early prostate cancer. Am J Clin Oncol 2004;27:323-7.
23. Mayahara H, Murakami M, Kagawa K, et al. Acute morbidity of proton therapy for prostate cancer: the Hyogo Ion Beam Medical Center experience. Int J Radiat Oncol Biol Phys 2007;69:434-43.
24. Sheets NC, Goldin GH, Meyer AM, et al. Intensity-modulated radiation therapy, proton therapy, or conformal radiation therapy and morbidity and disease control in localized prostate cancer. JAMA 2012;307:1611-20.
25. Guckenberger M, Pohl F, Baier K, et al. Influence of rectum delineation (rectal volume vs. rectal wall) on IMRT treatment planning of the prostate. Strahlenther Onkol 2006;182:721-6.
26. Goitein M, Cox JD. Should randomized clinical trials be required for proton radiotherapy? J Clin Oncol 2008;26:175-6.
27. Fowler JF. The radiobiology of prostate cancer including new aspects of fractionated radiotherapy. Acta Oncol 2005;44:265-76.
28. Munzenrider JE, Austin-Seymour M, Blitzer PJ, et al. Proton therapy at Harvard. Strahlentherapie 1985;161:756-63.
29. Bush DA. Proton radiation therapy for lung cancer: is there enough evidence? Oncology (Williston Park) 2010;24:1052-7.
30. Bush DA, Slater JD, Garberoglio C, et al. Partial breast irradiation delivered with proton beam: results of a phase II trial. Clin Breast Cancer 2011;11:241-5.
31. Brenner DJ. Hypofractionation for prostate cancer radiotherapy--what are the issues? Int J Radiat Oncol Biol Phys 2003;57:912-4.
32. Pollack A, Hanlon AL, Horwitz EM, et al. Dosimetry and preliminary acute toxicity in the first 100 men treated for prostate cancer on a randomized hypofractionation dose escalation trial. Int J Radiat Oncol Biol Phys 2006;64:518-26.
33. Ritter M, Forman J, Kupelian P, et al. Hypofractionation for prostate cancer. Cancer J 2009;15:1-6.
34. Spyropoulou D, Kardamakis D. Review of hypofractionated radiotherapy for prostate cancer. ISRN Oncol 2012;2012:410892.
35. Fowler JF, Nahum AE, Orton CG. Point/Counterpoint. The best radiotherapy for the treatment of prostate cancer involves hypofractionation. Med Phys 2006;33:3081-4.
36. Kuban DA, Tucker SL, Dong L, et al. Long-term results of the M. D. Anderson randomized dose-escalation trial for prostate cancer. Int J Radiat Oncol Biol Phys 2008;70:67-74.

Cite this article as: Rossi CJ Jr. Proton beam radiation therapy of prostate cancer-history, results, and future directions. Transl Cancer Res 2012;1(3):173-183. DOI: 10.3978/j.issn.2218-676X.2012.10.06

Review Article

Clinical trials for charged particle beam therapy

Fantine N. Giap[1], Huan B. Giap[2], Martin Jermann[3], Bosco Giap[4], Richard P. Levy[2], Erik Blomquist[5]

[1]Southern Methodist University, Dallas, TX, USA; [2]Scripps Proton Therapy Center, San Diego, CA, USA; [3]Paul Scherrer Institute, Villigen, Switzerland; [4]University of California at Los Angeles, CA, USA; [5]Uppsala University, Uppsala, Sweden

Correspondence to: Huan B. Giap, M.D, Ph.D. Scripps Proton Therapy Center, San Diego, CA, USA. Email: hbgiap@gmail.com.

Abstract: Since 1954 when the very first patient was treated at Lawrence Berkeley National Laboratory with heavy-charged particles, more than 100,000 patients in total have now been treated with charged particle beam therapy. During the first several decades of this new modality, charged particle beam therapy was accessible only at a small number of institutions. More recently, however, this therapy has become available at a rapidly increasing number of facilities worldwide. This expansion of the discipline has led to the development of many more clinical trials, designed to optimize particle-beam therapy and to compare the results achieved with those resulting from other treatment methods. Presently, more than 50 clinical protocols worldwide are actively involved in the effort to improve our understanding of these clinical guidelines. The purpose of this brief review is to offer a broad overview of these protocols, highlighting the specific disease categories that are now being studied using proton and/or heavier-ion therapy, and how the parameters of dose-escalation, beam conformity, and RBE modeling are being evaluated for various disease sites and stages.

Keywords: Proton beam therapy; carbon therapy; heavier ions; clinical trials; charged particle therapy

doi: 10.3978/j.issn.2218-676X.2012.12.06

Scan to your mobile device or view this article at: http://www.thetcr.org/article/view/856/html

Introduction

After observing the depth-dose properties of protons accelerated by the first cyclotrons designed by Ernest Lawrence in the 1930s, Robert Wilson published in 1946 the seminal paper proposing the use of fast protons for radiation therapy in humans (1,2). Shortly thereafter, Lawrence finished building the 184-inch synchrocyclotron in the Berkeley hills at the future site of Lawrence Berkeley National Laboratory. The so-called "Big Machine" was capable of accelerating both protons and helium nuclei to the much higher kinetic energies needed for the depth of penetration required for human treatment. Since the first patient treated at LBNL in 1954 in the U.S. and at Gustav Werner Institute in Uppsala in 1957, protons and other heavier charged particles have been used increasingly to treat a greater variety of cancers and various nonmalignant conditions. Since then, more than 100,000 patients have been treated with charged particle beam therapy, of which 87,000+ are proton and 14,000 are carbon and other heavier ions (3).

Given the ability to focus the radiation dose conformably on an internal target lesion with less dose to surrounding normal tissues, particle-beam therapy has become more prevalently considered as a better radiation treatment option versus photon therapy. The achievable, 3-dimensional dose-precision with charged-particle irradiation benefits patients by improving local control with a more aggressive dose within the target volume and/or by causing less adverse sequelae to adjacent healthy tissues due to the smaller integral dose outside the target volume.

The technology of proton and heavier-ion therapy has improved clinically over the last few decades. As the therapy is relatively novel, however, standards of treatment for different cancers are currently evolving based upon numerous, ongoing clinical studies. Until the recent compilation of particle-beam-therapy protocols, these studies have been published in a wide variety of medical-science journals. By means of this brief summary, we hope

Table 1 Overview of clinical charged-particle protocols

Parameter	Number of protocols
Particle evaluated	
Carbon	5
Proton	59
Study category	
Randomized	5
Phase I/II	49
Phase III	3
Registry	6
Physics	4
Number of participating centers	
Single institution	58
Multiple institutions	6
Protocols examining combined modalities	21
Recruitment status	
Open	26
Closed	10
Unknown	28

to increase physician awareness of the available clinical trials and of the expanding, evidence-based data worldwide in particle-beam therapy.

Methods

The idea of compiling clinical protocols for proton and heavier-ion therapy was introduced and discussed at the Particle Beam Therapy Co-Operative Group (PTCOG) Publication Committee in May 2011. A standard template was then developed to include the following information: title, principle investigator, contact information, additional information, institution, study purpose, accrual information, primary and secondary aims, methods, eligibility, and exclusion criteria. The presented initiative was subsequently approved by the PTCOG Steering Committee.

The collection of clinical trials was accomplished by auditing the National Cancer Institute (NCI) www.clinicaltrials.gov website and through Steering Committee members (4). All radiation treatment protocols found were then individually examined, and the relevant information for all charged-particle studies was entered into the previously developed, formatted templates for tabulation and compilation. Any missing information at participating

Table 2 Participating centers

Center	Number of protocols
Univ. of Penn. Abramson Cancer Center	22
University of Florida Proton Therapy Institute	20
National Cancer Center of Korea	8
Mass. General Hospital: Francis Burr Proton Center	5
Univ. of Texas MD Anderson Cancer Center	6
Univ. of Heidelberg	3
Loma Linda Univ.	3
Proton Collaborative Group (Chicago, OKC, NJ)	2
Russian Scientific Center of Roentgeno-Radiology	2
St. Jude's Children's Hospital	2

institutions worldwide was gathered by email inquiry or left blank. All protocols were then organized by treatment site. Subsequently, the compilation was reviewed by PTCOG for accuracy and completeness. Additional protocols will be added as they are initiated.

Results

A total of 64 protocols were compiled from those available on the NCI website, from PTCOG members, and from email inquiries, representing the efforts of ten proton and/or heavier-ion therapy centers. The following tables summarize the compilation overview, list the participating institutions, and highlight the treatment sites and categories currently under investigation for response to charged-particle therapy.

Discussion

Table 1 lists 64 clinical protocols underway in 10 institutions. Proton therapy is being studied in 59 trials and carbon therapy in 5 trials. Multi-modality treatments (chemotherapy and also including X-ray therapy) are evaluated in 21 protocols. The majority are phase I/II studies, but 5 are prospective, randomized trials (three comparing proton versus carbon). Six have multi-center collaboration, and the rest are of single-institution variety. *Table 2* lists the number of clinical trials at each of the 10 centers, and *Table 3* lists them by disease site. The majority of trials are in the prostate [13], pediatric [8], CNS [9] and para-spinal [8] areas, but there are also a good number

Table 3 Treatment site or category

Type	Number of protocols
Pediatrics	8
Central nervous system (including base of skull)	9
Paraspinal (including sarcoma)	8
Head and neck	4
Thoracic	
Breast	5
Lymphoma	2
Lung	
Stage III	6
Stage I: stereotactic body irradiation	3
Gastrointestinal	
Esophagus	2
Stomach	1
Pancreas	4
Rectum	1
Liver (primary)	2
Liver metastases: stereotactic body irradiation	1
Prostate	
High risk	3
Intermediate and low risk	7
Hypo-fractionated treatment	1
Post-operative treatment	2
Gynecologic: peri-aortic lymph node recurrence	1
Testicular	1
Bladder	1
Other recurrence	2
General registry	3

involving breast [5] and lung [9]. For the breast studies, proton beam therapy is used in boost treatment and also in accelerated partial breast irradiation. For lung studies, proton beam therapy is used in treatment of advanced (stage III) lung cancer and also in early stage (I) as hypofractionation or as stereotactic body radiation therapy. For GI sites, proton beam therapy is used in variety of sites including liver, pancreas, rectum and esophagus.

Conclusions

Despite that more than 100,000 patients have been treated with particle beam over the last 60 years at more than 30 centers around the world, only a small percentage of these patients are treated on clinical trials. As increasing number of particle beam centers are in operation and being developed, the clinical indications for particle beam therapy need to go beyond the traditional uses such as pediatrics, ocular tumors, sarcoma, and base of skull tumors. The compiled list of clinical protocols shows a diversified potential applications in cancers of the lung, head and neck, gastrointestinal tract, prostate, breast, brain, gynecologic sites, lymphoma, and recurrent tumors. These clinical trials will validate or invalidate the use of particle beam for these disease sites. The compilation and posting of clinical trials will enhance awareness and accelerate the patient accrual to provide the answers. The other benefit of these listings will be for clinicians who are planning new clinical trials basing on these information, and we hope to promote multi-center collaboration. The authors believe that likely there may be more, now-unreported clinical trials currently underway, and we hope that these centers will recognize our efforts and contribute to this listing.

Acknowledgements

The authors wish to acknowledge members of the PTCOG for their assistance in compiling the data presented. The authors are also grateful to the 10 particle beam centers (listed in *Table 2*) who develop these clinical trials and contribute their time and effort to this listings.
Disclosure: The authors declare no conflict of interest.

References

1. Wilson RR. Radiological use of fast protons. Radiology 1946;47:487-91.
2. Suit HD, Chu W. History of Charged Particle Radiotherapy. In: Pine JW Jr. eds. Proton and Charged Particle Radiotherapy. Philadelphia: Lippincott Williams & Wilkins, 2008:1-7.
3. Available online: www.ptcog.web.psi.ch accessed on Jan 14, 2013.
4. Available online: www.clinicaltrials.gov

Cite this article as: Giap FN, Giap HB, Jermann M, Giap B, Levy RP, Blomquist E. Clinical trials for charged particle beam therapy. Transl Cancer Res 2012;1(4):276-278. doi: 10.3978/j.issn.2218-676X.2012.12.06

Review Article

Emerging evidence for the role of an endorectal balloon in prostate radiation therapy

Stefan Both, Curtiland Deville, Viet Bui, Ken Kang-Hsin Wang, Neha Vapiwala

University of Pennsylvania, Philadelphia, PA 19104, USA

Correspondence to: Stefan Both, PhD. 3400 Civic Center Blvd., Philadelphia, PA 19104, USA. Email: Stefan.Both@uphs.upenn.edu.

Purpose: To reassess and update the role of an endorectal balloon (ERB) in prostate radiotherapy (RT) based on emerging evidence by reviewing various aspects of treatment methodologies and clinical outcomes.

Methods and materials: A literature review based on a PubMed/MEDLINE database search using keywords such as: ERB, prostate RT, toxicities, real-time, image-guided radiotherapy (IGRT), radiofrequency-guided radiotherapy (RGRT), and inter- and intrafraction prostate motion for articles published over the past two years. Ten articles were identified and subdivided into three categories: (I) Issue of Motion, (II) Dosimetry, (III) Clinical Outcomes.

Results: With the advent of real-time prostate tracking, analysis of intrafraction motion as a function of treatment time for patients treated with a daily-ERB was performed and revealed an overall reduction in 3D prostate motion, especially in the anterior-posterior direction. Two different groups of authors found that this reduction in intrafraction prostate motion allowed for tighter internal margins. Dosimetric studies showed overall improved dose distributions which for proton therapy were maximized when using ERB-guided range verification for anteriorly oriented beams. Clinical outcomes showed favorable early GI toxicities however late toxicity results are still awaited.

Conclusions: Utilizing a daily-ERB shows favorable early GI toxicity as well as reduced prostate intrafraction motion based on real-time tracking data. Reduced intrafraction motion improves the feasibility to use anteriorly oriented proton beams, which may further improve dosimetry.

Keywords: Endorectal balloon (ERB); radiotherapy (RT); toxicities; image-guided radiotherapy (IGRT); radiofrequency-guided radiotherapy (RGRT)

DOI: 10.3978/j.issn.2218-676X.2012.10.10

Scan to your mobile device or view this article at: http://www.thetcr.org/article/view/600/html

Introduction

External beam radiation treatment is a well-established treatment modality for prostate cancer patients. Advancements in radiation treatment such as three-dimensional conformal radiation therapy (3DCRT), intensity-modulated radiotherapy (IMRT), and proton therapy (PT) have allowed for highly conformal dose distribution to the target and consequently improved normal tissue sparing when dose escalation was performed. Radiation doses greater than 70 Gy have demonstrated greater local tumor control and improved biochemical outcomes, therefore delivery of higher doses of radiation has been attempted in order to further improve outcomes (1,2). Although a direct relationship between the level of dose administered and outcome has been shown, dose escalation in prostate cancer radiation therapy (RT) was traditionally limited by the associated rectal toxicities.

Due to prostate motion and setup uncertainties and to avoid significant deviation from the prescribed dose, planning target volume (PTV) margins are applied to the clinical target volume (CTV) to ensure dosimetric coverage of the prostate (3). The CTV-to-PTV margin may also increase the risk of irradiating surrounding normal tissues such as the rectum and may lead to increased anorectal

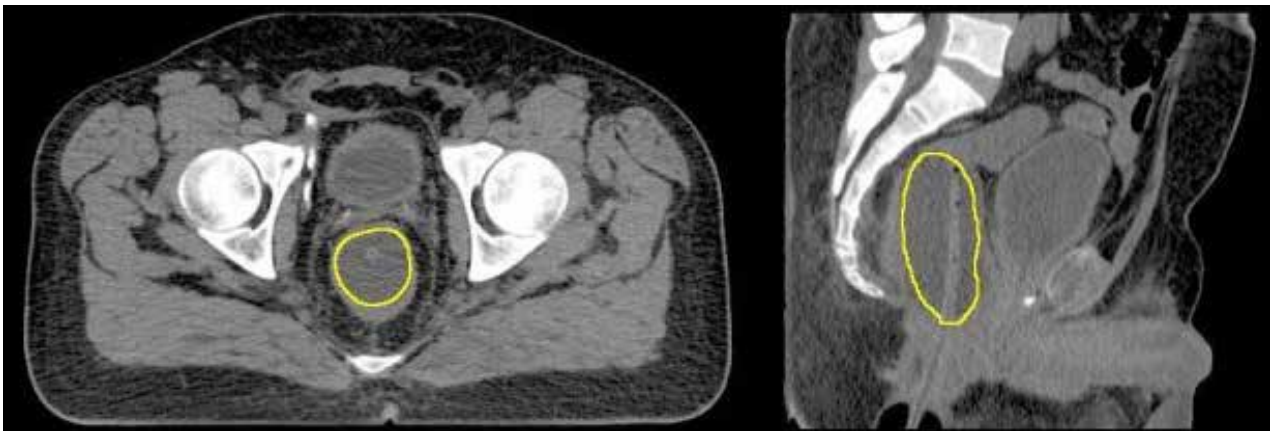

Figure 1 Contoured image of an endorectal balloon (100 mL water filled) in the axial (left) and sagittal (right) view

toxicity. The impact of PTV margins may be even more dramatic in the setting of stereotactic and hypofractionated prostate RT (4). Therefore, reducing the internal margin (IM) is critical in order to further escalate dose while the rate of rectum complications are maintained within clinically acceptable limits.

Particular to proton RT, the PTV also has to account for the range uncertainty present along the proton beam direction (5) and therefore, a beam orientation dependent PTV is defined. The traditional beam arrangement clinically employed in proton RT in prostate cancer has historically varied, from the perineal boost field (6), to parallel opposed, or slightly angled opposed fields (7). However, this paradigm may change if anteriorly oriented beams would be employed, as suggested by Tang *et al.* (8). Based on this work, the endorectal balloon (ERB), *Figure 1*, may have a particularly relevant role in range verification, required to ensure the safe delivery of daily proton RT utilizing this anterior beam arrangement.

An extensive literature review conducted by Smeenk *et al.* (9) demonstrated that the role of the ERB in prostate RT to improve prostate fixation, rectal sparing, and outcome is not entirely clear despite more than three decades since it was first described in the literature by Shipley *et al.* (6). The presumption is that the ERBs ability to reduce prostate intrafraction motion would allow for improved target localization, tighter IM, and decreased anorectal toxicity.

In order to clarify the role of a daily-ERB in prostate RT, Smeenk *et al.* identified the need for prospective clinical studies using real-time and imaging surveillance for position verification and methods to reduce gas and stool volumes (9). As the use of ERBs expands, the need to reexamine its role in prostate RT becomes even more critical. A PubMed/MEDLINE search using the keywords: ERB, prostate RT, toxicities, real-time, IGRT, RGRT, and interfraction and intrafraction prostate motion was performed in order to identify new publications related to the use of daily-ERB for prostate RT since the review of Smeenk *et al.* (9). Ten prospective and retrospective ERB studies have since been published and form the basis of this review (8,10-18).

The issue of motion

Radiofrequency-guided radiotherapy (RGRT) and *image-guided radiation therapy* (IGRT) have allowed for the use of advanced conformal RT techniques by monitoring interfraction and intrafraction tumor motion during treatment. IGRT utilizes specialized imaging such as a computed tomography (CT) scan, cone beam CT (CBCT) scan, ultrasound, or X-rays as a means to improve dose delivery. Technologies such as cine-magnetic resonance imaging (MRI), CT, and Calypso tracking systems (Calypso Medical Technologies Inc., Seattle, WA) have examined interfraction and intrafraction prostate motion, offline or online, relative to the patient treatment delivery. Calypso is the only in-beam real time tracking system which has been extensively used in the clinical setting for RGRT (19,20). Real-time prostate tracking during treatment delivery provides further insight into the role of daily-ERB in prostate intrafraction motion management.

Motion has been a critical factor during advanced prostate RT and was previously, generally managed using external and internal immobilization devices. External

anatomical variations are minimized by positioning the patient in a secure and reproducible manner based on indexed immobilization devices such as Knee-Lok and Foot-Lok cushions or personalized Vac-Lok body casts (CIVCO, Orange City, IA). Internal prostate fixation may be achieved using an air- or water-filled daily-ERB. Besides the external and internal immobilization devices, IGRT largely used in modern RT has been widely applied to prostate alignment based on implanted fiducial or prostate 3D representation.

Patient preparation for prostate RT may be particularly important as the prostate resides between organs with variable volumes such as the rectum and bladder. Intrafraction motion significantly hinders target localization as a result from rectal peristalsis, distention, and respiration (21,22). Studies using cine-MRI of non-ERB patient suggested that prostate motion is mostly due to the effect of gas pockets in the filled rectum (23).

The effect of stool and gas pockets on motion may affect the ERBs ability to reduce random intrafraction motions (10). Some advocate for patients' pretreatment bladder and bowel preparations, such as daily use of anti-gas tablets with meals beginning 1-2 weeks prior, laxative suppositories or enemas within 1-4 hours prior, and voiding followed by immediately drinking adequate fluid (approximately 16 ounces of water) to achieve full bladder filling 20-30 min prior to CT simulation. Recently, Wootton *et al.* retrospectively examined the effectiveness of an ERB with passive gas release conduit on the removal of rectal gas for prostate proton radiotherapy. Two groups of fifteen patients treated with standard ERB and gas-release ERB were analyzed based on lateral kilovoltage (KV) images and the results showed that the mean incidence of gas in the anterior and other regions differed at a statistically significant level (11). Although the main limitation of this study was the lack of volumetric data, the possibility to identify the gas anterior to the ERB based on the lateral KV for a large number of fractions allowed the authors to conclude in favor of the use of the gas-release ERB for patients undergoing proton RT which mostly occurs with two parallel opposed beams. A potential advantage of a daily-ERB is that it allows for standardization of the rectal volume to minimize the daily variability of the prostate position, leading to improved target localization over the course of treatment (12).

As mentioned previously, 4 of the 10 recent reports have evaluated the effect of ERB on reducing prostate intrafraction motion via RGRT (10,12-14). Both *et al.* (13) prospectively studied real-time prostate intrafraction motion as a function of treatment time to determine an optimal IM for ERB patients and addressed the patient-specific intrafraction motion. A daily-ERB (RadiaDyne, LLC, Houston, TX) was filled with 100 cc of water. All patients received 79.2 Gy to the PTV in 44 fractions of 1.8 Gy per fraction via IMRT or Varian RapidArc (Varian2300IX; Varian Medical Systems, Palo Alto, CA). The balloon position relative to the rectum canal was ensured through the use of an indexed ERB, positioned based on the value obtained at the time of simulation. Calypso tracking system was utilized to evaluate three-dimensional (3D), lateral (L), cranial-caudal (CC), and anterior-posterior (AP) displacements for a group of 24 patients with a total of 787 tracking sessions. The average percentage of time with 3D, L, CC, and AP prostate displacements >2, 3, 4, 5, 6, 7, 8, 9, and 10 mm in 1 minute intervals was calculated for up to 6 minutes of treatment time. 3D analysis showed that prostate motion is dependent on treatment time for displacements >2, 3, and 4 mm. Interestingly, displacements >5 mm showed time-independence, and the larger motions >6 mm were negligible within 6 minutes treatment time. The overall average time with prostate displacement >3 mm was 5%, suggesting that a 3 mm IM would sufficiently cover 95% of the treatment time within a 6 minute interval. Moreover, for treatment times longer than 6 minutes, a 5 mm IM may be considered to cover more than 95% of time due to the time-independence of the motion >5 mm observed. Directional analysis shown in this study illustrated negligible lateral prostate motion while the AP and CC motions were comparable. The authors also indicated that no obvious relationship exists between the percentage of time at displacement and the week of treatment course, indicating the use of an ERB obviates the correlation between bowel habit changes and rectal volume over the treatment course. Their findings suggested that use of a daily-ERB consistently stabilized prostate motion and prevented clinically significant displacements to occur.

Following the study of Both *et al.* (13), Wang *et al.* (14) further compared the intrafraction motion between 30 (1,008 sessions) ERB and 29 (1,061 sessions) non-ERB patients groups. The same patient preparations described by Both *et al.* (13) were applied to both groups. Large 3D motion (up to 1 cm or more) was noted in the non-ERB group. The motion increased as a function of time for displacements >2-8 mm for the non-ERB group and >2-4 mm for the ERB group. The authors also indicated that the percentage time distributions between the two groups were significantly different for motion >5 mm. The 3D symmetrical IM can be reduced

by 40% from 5 to 3 mm if an ERB is chosen as the internal immobilization device. Based on the similar directional analysis as described in Both *et al.* (13), this study showed that the percentage of time the prostate displaced in any direction was less in the ERB group than the non-ERB group, with a particularly large motion reduction shown in the anterior-posterior directions, which may allow for dose escalation while sparing surrounding normal tissues such as bladder and rectum (4,24). The motion patterns of the patients representing the worst-case scenario for both groups were analyzed in this study, which found that the percentage time of prostate displacements >3 up to 10 mm was consistently higher for the non-ERB patient group.

Smeenk *et al*. (10) investigated prostate intrafraction motion during RT and performed a one-to-one comparison of 15 ERB (567 sessions) to non-ERB patients (576 sessions). All patients received a total dose of 80 Gy in 2 Gy fractions and the ERB patients were applied with a 100 cc air-filled balloon (QLRAD B.V., Dalfsen, Netherlands). The intrafraction motions were analyzed in 150 second timeframes, using the Calypso system, at displacements >1, 3, 5, and 7 mm for 3D vector analysis to determine where motion was most volatile. The analysis showed displacements <5 mm were more frequent for both groups. However, after 150 seconds there was a linear increase of displacement with time, most notably for displacements >3 mm. There were significantly smaller variances of the percentages of 3D displacement >3, 5, and 7 mm when treated with an ERB. Intrafraction motion of 3D-vector deviations >1, 3, 5, and 7 mm were 57.7%, 7.0%, 0.7%, and 0.3% in the ERB group *vs.* 70.2%, 18.1%, 4.6%, and 1.4% in the non-ERB group after 10 minutes. Prostate interfraction motion was evaluated and they found insignificant interfraction variation between cohorts with and without a daily-ERB but there were significantly less intrafraction motions with an ERB (10,15). The data suggested a 5 mm IM to be sufficient for prostate intrafraction motion when using an ERB (10), as similarly indicated by Both *et al.* and Wang *et al.*

Hung *et al.* (12) investigated daily interfraction prostate motion comparing two cohorts of patients (14/15) treated with fiducial markers implanted in the prostate with and without daily-ERB. Based on portal imaging, the daily displacements necessary to place the prostate at the isocenter were determined and analyzed. The change in interfraction prostate motion over the course of treatment was reduced for the ERB group, however not statistically significant and therefore the use of daily image guidance was still recommended when daily-ERBs are employed.

Dosimetric studies

Two of the 10 recent reports have assessed the dosimetric consequences and potential benefit of ERB use. In the first, Smeenk *et al.* (15) investigated the dosimetric effect of the ERB on anorectal toxicities post-prostatectomy IMRT for 20 patients who underwent salvage IMRT treatment planning with a prescribed dose of 70 Gy with and without a 100 cc air-filled ERB (QLRAD B.V., Dalfsen, Netherlands). Comparative analysis reported significant reductions of the anal wall (Awall) dose-volume indicators except for V_{70Gy}, while the mean dose was reduced by an average of 6 Gy. The rectal wall (Rwall) V_{30}, V_{40}, and A_{40} were found to be significantly reduced as well. According to this dosimetric study the use of an ERB has the potential to spare the anorectal wall and in particular the Awall in high-dose post-prostatectomy IMRT.

In the second dosimetric study, Tang *et al.* (8) conducted a detailed dosimetric comparison among anterior, anterior-oblique, and lateral passive scattering proton beams for 10 patients treated with a daily-ERB has shown that the anterior-oriented beams can fully exploit the sharp distal penumbra to spare the rectum and provide superior dose distribution. The rectal volume that receives 95% of the prescription dose in the anterior beams is about 1/10 of that in the lateral beams. The mean dose of rectum and penile bulb can also be reduced by about a factor of two. Femoral heads are not included in the anterior-oriented beams and hence received negligible dose but the bladder received a much higher dose in the anterior beams. However, an optimal plan can be produced to significantly reduce the rectal dose without compromising the bladder dose by properly weighting all the available beams. In addition, the introduction of anterior-oriented fields allows for the possibility of either reducing treatment toxicity at current prescription doses or further dose escalation in the treatment of prostate cancer.

In order to correct for range uncertainty due to bladder volume variability when anterior beams are employed an array of dosimeters can be placed on the anterior surface of the ERB for the purpose of range verification as well as dose monitoring during treatment (8). An *in vivo* range verification method particularly for the passive scattering delivery system has shown millimeter accuracy in phantom tests (25,26). With a small amount of dose from a probing beam delivered to the detectors at the beginning of the treatment, the residual range of the probing beam can be determined, which is then used to adjust the treatment

beam. The pretreatment "range check" using detectors placed on the ERB makes the anterior-oriented proton beams clinically feasible and offer the ability to deliver improved dose distributions in proton prostate RT.

Clinical outcomes

The Smeenk *et al.* review (9) summarized the GI toxicity outcomes of patients treated with an ERB during radiotherapy for the potential benefit of prostate fixation, dose escalation, and anorectal sparing, as reviewed in *Table 1*, specifically for photon therapy. Since then 3 additional reports discussed below have examined clinical outcomes (20-22) in photon therapy. The first, also noted in *Table 1*, has reported clinical outcomes in terms of acute GI and GU toxicities using a water-filled ERB during IMRT (16).

Prostate proton therapy is delivered in conjunction with a water-filled daily-ERB to eliminate the dose heterogeneities in the beam. In contrast, photon radiation therapy reports indicate most commonly the use of air-filled ERBs for the benefit of anterior rectal wall sparing at the risk of diminished posterior target coverage. Song *et al.* (33) reviewed conventional treatment planning to address heterogeneity by comparing the dose calculations to a Monte Carlo simulation using the four-field box technique and found that the treatment planning system inferred higher dose regions resulting in potential under dosage of 3.4% mean dose for the posterior beam near the peripheral zone of the prostate, where up to 74% of the prostate cancer foci are located (34). Thus, a water-filled ERB, has more recently been employed during IMRT to reduce dose heterogeneity and potential dose calculation errors due to treatment planning algorithm limitations which could lead to diminished target coverage.

Deville *et al.* (16) reported the acute GI and GU toxicity rates for 100 prostate cancer patients undergoing image-guided intensity-modulated radiation therapy (IG-IMRT) with a daily endorectal water-filled balloon (ERB_{H2O}), using an indexed-lumen 100 cc ERB_{H2O} to 79.2 Gy in 1.8 Gy fractions. They found that Grade ≥2 GI and GU toxicity rates of 8% and 42%, respectively, compared favorably with (I) patients treated with IMRT using an ERB_{air} - for which there is only single institution data from the Baylor group, reporting rates of acute GI and GU toxicity of 18% and 35%, respectively, in 396 prostate cancer patients treated from 1997-2001 with mean dose 77 Gy (specifically 70 Gy in 2 Gy daily fractions prescribed to the 85% isodose line) IMRT using 100 cc ERB_{air} (35) - and (II) with the more extensively reported acute GI and GU toxicity rates for non-ERB prostate IMRT including their own institution at 13% and 50%, respectively (36).

In an in-depth analysis of anorectal toxicity, Smeenk *et al.*, recently investigated the relationship between anal and rectal DVH parameters and GI incontinence-related complaints such as urgency, incontinence, and frequency in 60 prostate cancer patients undergoing external beam RT (3- or 4-field 3DCRT or 5-field IMRT to 67.5 or 70 Gy in 2.25 or 2.5 Gy fractions) between 2000-2007 using anorectal manometry and barostat measurements to evaluate anal pressures, rectal capacity, and rectal sensory functions at least 90 days post-treatment (17). Half were treated with an 80 cc air-filled ERB. They found that in patients with (I) frequency - almost all rectal parameters were reduced, (II) urgency - several anal wall and rectal wall were predictive, such as the anal D_{mean} >38 Gy, and (III) incontinence - some anal wall parameters correlated. Patients treated with an ERB described significantly fewer complaints than patients treated without a balloon, which was therefore attributed to receiving lower doses to the Awall and Rwall.

In a related report, Smeenk *et al.*, retrospectively investigated the relationship between fecal incontinence-related complaints and individual pelvic floor muscles (the internal anal sphincter (IAS) muscle, the external anal sphincter (EAS) muscle, the puborectalis muscle (PRM), and the levator ani muscles (LAM), in addition to the Awall and Rwall in 48 patients undergoing prostate radiotherapy (3- or 4-field 3DCRT or 5-field IMRT to 67.5 or 70 Gy in 2.25 or 2.5 Gy fractions), 28 patients with an 80 or 100 cc air-filled ERB (18). They found that urgency was associated with several anal and rectal wall parameters, as well as doses to all separate pelvic floor muscles, while incontinence was associated mainly with doses to the EAS and PRM. Based on the dose-effect curves, they suggested the following mean doses to reduce the risk of urgency: ≤30 Gy to the IAS; ≤10 Gy to the EAS; ≤50 Gy to the PRM; and ≤40 Gy to the LAM. Finally, similar to the previous study, they found that patients treated with an ERB reported significantly less urgency and incontinence, attributed to significantly lower doses to the Awall, Rwall, and all pelvic floor muscles.

Conclusions

The emerging evidence of the role of ERB in prostate RT consist mainly of real-time tracking of the prostate motion with and without an ERB and showed a favorable reduction in the IM required when a daily-ERB was employed while

Table 1 Review of clinical toxicities for photon prostate radiotherapy using an endorectal balloon

Study	Number of patients	Therapy	ERB	Follow-up	Toxicity	DVH parameters and/or correlates
The (27)	116 [1997-1999]	IMRT 76 Gy (mean)	100 cc air-balloon	31.3 months (median)	GI: rectal Grade 1: 10.3% Grade 2: 6.9% Grade 3: 1.7%	Rectal mean: V65 =16.5% V70 =12.6% V75 =4.6%
The (28)	40 PPI *vs.* 125 PI retrospective, nonrandomized [1998-1999]	15 MV IMRT PPI: 64 Gy (mean: 69 Gy) PI: 70 Gy	100 cc air-balloon	Acute only	GU: PPI *vs.* PI Grade 0-1: 82.5% *vs.* 59% Grade 2: 17.5% *vs.* 40.8%	Bladder: Dmean: PPI > PI V65: PI > PPI
Goldner (29)	399 of 486 enrolled prospective multicenter trial [1999-2002]	4 field 3DCRT Low-inter: 70 Gy High: 74 Gy 87% neoadjuvant, 7 months ADT	40 cc air PTV = CTV+ 10 mm (5 mm post after 66 Gy)	65 months (median)	GI: Late crude side effect Grade 2/3: 23%/2% 5 yr actuarial late side effect Grade ≥2: 28%/30% GU: Late crude side effect Grade 2-3: 16%/2% 5 yr actuarial late side effect Grade ≥2: 19%/34%	-
Goldner (30)	166 (subset of 486) prospective multicenter trial [1999-2002]	4 field 3DCRT Low-inter: 70 Gy High: 74 Gy 87% neoadjuvant, 7 months ADT	40 cc air PTV = CTV +10 mm (5 mm post after 66 Gy)	Rectal sigmoidoscopy 12 and/or 24 months Median follow-up 40 months	GI Late rectal toxicity: Grade 0: 57% Grade 1: 11% Grade 2: 28% Grade 3: 3%	-
Woel (31)	46 Prospective, phase II [2001-2003]	4 field 15 MV 3DCRT 72 Gy (95% iso) ≈75.6 Gy (1.8 Gy) 6 months ADT	60 cc air ERB first 15 treatments only. PTV = CTV +5 mm PTV without balloon = CTV +15 mm	Acute only (up to 3 months from end of treatment)	Acute: medical intervention (i.e., RTOG grade ³ 2 equiv.) GI: Loose bm 11%, hemorrhoidal 20% GU: 50% Anal cutaneous skin: 70% No significant difference by 3 months.	-
D'Amico (4)	57 Prospective, phase II [2001-2004]	4 field 15 MV 3DCRT 75.6 Gy (1.8 Gy) 6 months ADT	60 cc air ERB first 15 treatments only. PTV = CTV +5 mm PTV without balloon = CTV +15 mm	Minimum 1 yr follow-up, median 1.8, max 3.3.	GI: 2-yr estimate Grade 3 rectal bleeding 10%, all in patients on anticoagulation and controlled with argon plasma coagulation. Grade 1: 18%	Rectal V70 median 3.7 cc
Van Lin (32)	48 ERB [24] *vs.* non-ERB [24] prospective, randomized [2002]	4 field 18 MV 3DCRT 67.5 Gy (2.25 Gy) 6 months ADT	80 cc air PTV = CTV +9 mm	30 months with repeat sigmoidoscopy at 3, 6, 12, 24 mo.	Acute GI: no Grade 3, non-ERB *vs.* ERB Grade 1: 50% *vs.* 46%, Grade 2: 29% *vs.* 29% (NS) Late GI: non-ERB *vs.* ERB Grade 1+ late rectal bleeding 58% *vs.* 21% (P=0.003)	ERB decreased Rectal wall V40+, as well as the percentage of areas showing high grade telengiectasias at 2 years.

Table 1 (*continued*)

Table 1 (*continued*)

Study	Number of patients	Therapy	ERB	Follow-up	Toxicity	DVH parameters and/or correlates
Deville (16)	100 retrospective [2008-2010]	IG-IMRT 79.2 Gy 40 patients Concurrent ADT	100 cc water-filled balloon PTV = CTV +10 mm, 6 mm post	Acute only	GI: max Grade 0, 1, 2 was 69%, 23%, 8% GU: max Grade 0, 1, 2 was 17%, 41%, 42%	Infield rectum associated with mean/median doses, D75, V30, V40. Infield bladder V20 associated with Grade 2 GU toxicity.

Abbreviations: ADT = androgen deprivation therapy; CTV = clinical target volume; DVH = dose-volume histogram; ERB = endorectal balloon; GI = gastrointestinal; GU = genitourinary; PI = primary; PPI = post-prostatectomy; PTV = planning target volume

the introduction of gas release ERBs seems promising. Dosimetric studies suggest improved dose distributions when the ERB is employed using parallel opposed beams and especially for anteriorly oriented beams with ERB guided range verification. The outcome study of Deville *et al.* presents promising finding for early GI toxicity with a water-filled ERB, however late toxicity data should be awaited. Correlative studies of late rectal function and anorectal dosimetry by Smeenk *et al.* provided clinical evidence for the dosimetric gains noted with an ERB. Further investigation of SV variation and involvement, rectal deformation, and stool and air contributions are merited and will likely comprise future directions.

Acknowledgements

Disclosure: The authors declare no conflict of interest.

References

1. King CR, Spiotto MT. Improved outcomes with higher doses for salvage radiotherapy after prostatectomy. Int J Radiat Oncol Biol Phys 2008;71:23-7.
2. Zelefsky MJ, Kollmeier M, Cox B, et al. Improved clinical outcomes with high-dose image guided radiotherapy compared with non-IGRT for the treatment of clinically localized prostate cancer. Int J Radiat Oncol Biol Phys 2012;84:125-9.
3. ICRU Report 62. Prescribing, Recording and Reporting Photon Beam Therapy (Supplement to ICRU Report 50). Bethesda: ICRU, 1999:ix+52.
4. D'Amico AV, Manola J, McMahon E, et al. A prospective evaluation of rectal bleeding after dose-escalated three-dimensional conformal radiation therapy using an intrarectal balloon for prostate gland localization and immobilization. Urology 2006;67:780-4.
5. ICRU Report 78. Prescribing, Recording, and Reporting Proton-Beam Therapy. International Commission on Radiation Units and Measurements 2007;7:1473-6691.
6. Shipley WU, Tepper JE, Prout GR Jr, et al. Proton radiation as boost therapy for localized prostatic carcinoma. JAMA 1979;241:1912-5.
7. DeLaney TF, Kooy HM. eds. Proton and charged particle radiotherapy. Philadelphia: Lippincott Williams & Wilkins, 2008.
8. Tang S, Both S, Bentefour H, et al. Improvement of prostate treatment by anterior proton fields. Int J Radiat Oncol Biol Phys 2012;83:408-18.
9. Smeenk RJ, Teh BS, Butler EB, et al. Is there a role for endorectal balloons in prostate radiotherapy? A systematic review. Radiother Oncol 2010;95:277-82.
10. Smeenk RJ, Louwe RJ, Langen KM, et al. An endorectal balloon reduces intrafraction prostate motion during radiotherapy. Int J Radiat Oncol Biol Phys 2012;83:661-9.
11. Wootton LS, Kudchadker RJ, Beddar AS, et al. Effectiveness of a novel gas-release endorectal balloon in the removal of rectal gas for prostate proton radiation therapy. J Appl Clin Med Phys 2012;13:3945.
12. Hung AY, Garzotto M, Kaurin D. Minimal benefit of an endorectal balloon for prostate immobilization as verified by daily localization. Med Dosim 2011;36:195-9.

13. Both S, Wang KK, Plastaras JP, et al. Real-time study of prostate intrafraction motion during external beam radiotherapy with daily endorectal balloon. Int J Radiat Oncol Biol Phys 2011;81:1302-9.
14. Wang KK, Vapiwala N, Deville C, et al. A study to quantify the effectiveness of daily endorectal balloon for prostate intrafraction motion management. Int J Radiat Oncol Biol Phys 2012;83:1055-63.
15. Smeenk RJ, Louwe RJ, Langen KM, et al. An endorectal balloon reduces intrafraction prostate motion during radiotherapy. Int J Radiat Oncol Biol Phys 2012;83:661-9.
16. Deville C, Both S, Bui V, et al. Acute gastrointestinal and genitourinary toxicity of image-guided intensity modulated radiation therapy for prostate cancer using a daily water-filled endorectal balloon. Radiat Oncol 2012;7:76.
17. Smeenk RJ, Hopman WP, Hoffmann AL, et al. Differences in radiation dosimetry and anorectal function testing imply that anorectal symptoms may arise from different anatomic substrates. Int J Radiat Oncol Biol Phys 2012;82:145-52.
18. Smeenk RJ, Hoffmann AL, Hopman WP, et al. Dose-effect relationships for individual pelvic floor muscles and anorectal complaints after prostate radiotherapy. Int J Radiat Oncol Biol Phys 2012;83:636-44.
19. Kupelian P, Willoughby T, Mahadevan A, et al. Multi-institutional clinical experience with the Calypso System in localization and continuous, real-time monitoring of the prostate gland during external radiotherapy. Int J Radiat Oncol Biol Phys 2007;67:1088-98.
20. Willoughby TR, Kupelian PA, Pouliot J, et al. Target localization and real-time tracking using the Calypso 4D localization system in patients with localized prostate cancer. Int J Radiat Oncol Biol Phys 2006;65:528-34.
21. Beard CJ, Kijewski P, Bussière M, et al. Analysis of prostate and seminal vesicle motion: implications for treatment planning. Int J Radiat Oncol Biol Phys 1996;34:451-8.
22. Little DJ, Dong L, Levy LB, et al. Use of portal images and BAT ultrasonography to measure setup error and organ motion for prostate IMRT: implications for treatment margins. Int J Radiat Oncol Biol Phys 2003;56:1218-24.
23. Ghilezan MJ, Jaffray DA, Siewerdsen JH, et al. Prostate gland motion assessed with cine-magnetic resonance imaging (cine-MRI). Int J Radiat Oncol Biol Phys 2005;62:406-17.
24. Smeenk RJ, van Lin EN, van Kollenburg P, et al. Anal wall sparing effect of an endorectal balloon in 3D conformal and intensity-modulated prostate radiotherapy. Radiother Oncol 2009;93:131-6.
25. Lu HM. A potential method for in vivo range verification in proton therapy treatment. Phys Med Biol 2008;53:1413-24.
26. Bentefour el H, Shikui T, Prieels D, et al. Effect of tissue heterogeneity on an in vivo range verification technique for proton therapy. Phys Med Biol 2012;57:5473-84.
27. Teh BS, Dong L, McGary JE, et al. Rectal wall sparing by dosimetric effect of rectal balloon used during intensity-modulated radiation therapy (IMRT) for prostate cancer. Med Dosim 2005;30:25-30.
28. Teh BS, Mai WY, Augspurger ME, et al. Intensity modulated radiation therapy (IMRT) following prostatectomy: more favorable acute genitourinary toxicity profile compared to primary IMRT for prostate cancer. Int J Radiat Oncol Biol Phys 2001;49:465-72.
29. Goldner G, Bombosch V, Geinitz H, et al. Moderate risk-adapted dose escalation with three-dimensional conformal radiotherapy of localized prostate cancer from 70 to 74 Gy. First report on 5-year morbidity and biochemical control from a prospective Austrian-German multicenter phase II trial. Strahlenther Onkol 2009;185:94-100.
30. Goldner G, Tomicek B, Becker G, et al. Proctitis after external-beam radiotherapy for prostate cancer classified by Vienna Rectoscopy Score and correlated with EORTC/RTOG score for late rectal toxicity: results of a prospective multicenter study of 166 patients. Int J Radiat Oncol Biol Phys 2007;67:78-83.
31. Woel R, Beard C, Chen MH, et al. Acute gastrointestinal, genitourinary, and dermatological toxicity during dose-escalated 3D-conformal radiation therapy (3DCRT) using an intrarectal balloon for prostate gland localization and immobilization. Int J Radiat Oncol Biol Phys 2005;62:392-6.
32. van Lin EN, Kristinsson J, Philippens ME, et al. Reduced late rectal mucosal changes after prostate three-dimensional conformal radiotherapy with endorectal balloon as observed in repeated endoscopy. Int J Radiat Oncol Biol Phys 2007;67:799-811.
33. Song JS, Court LE, Cormack RA. Monte Carlo calculation of rectal dose when using an intrarectal balloon during prostate radiation therapy. Med Dosim 2007;32:151-6.
34. Chen ME, Johnston DA, Tang K, et al. Detailed mapping of prostate carcinoma foci: biopsy strategy implications. Cancer 2000;89:1800-9.
35. Bastasch MD, Teh BS, Mai WY, et al. Tolerance of endorectal balloon in 396 patients treated with intensity-modulated radiation therapy (IMRT) for prostate cancer. Am J Clin Oncol 2006;29:8-11.

36. Deville C, Both S, Bui V, et al. Acute gastrointestinal and genitourinary toxicity of image-guided intensity modulated radiation therapy for prostate cancer using a daily water-filled endorectal balloon. Radiat Oncol 2012;7:76.

Cite this article as: Both S, Deville C, Bui V, Wang KK, Vapiwala N. Emerging evidence for the role of an endorectal balloon in prostate radiation therapy. Transl Cancer Res 2012;1(3):227-235. DOI: 10.3978/j.issn.2218-676X.2012.10.10

Editorial

Surgical organ displacement: what is the best "materials and methods" for proton radiotherapy?

Takashi Ogino

Medipolis Proton Therapy and Research Center, Ibusuki, Kagoshima, Japan

Correspondence to: Takashi Ogino. Higashikata 5188, Ibusuki, Kagoshima 891-0304, Japan. Email: Ogino-takashi@medipolis.org.

doi: 10.3978/j.issn.1000-9604.2013.04.03

Scan to your mobile device or view this article at: http://www.thecjcr.org/article/view/1859/3052

In the mid 1940s, Robert Wilson (1) hypothesized that a highly localized deposition of energy from a proton beam could be used to increase the radiation dose to tumors while minimizing radiation to adjacent normal tissues. The depth-dose distribution of a proton beam differs significantly from that of a photon beam. Protons show increasing energy deposition with penetration distance, reaching a maximum-named the Bragg peak-near the end of the range of the proton beam. In front of the Bragg peak, the dose level is modest compared to photon beams; beyond the Bragg peak, the dose decreases to nearly zero. By choosing the appropriate proton beam energy, the depth of the Bragg peak can be adjusted to match the depth and extent of the target volume. Therefore, excellent conformality can be achieved, in contrast to conventional or intensity-modulated radiotherapy (IMRT).

Protons have a higher linear energy transfer (LET) than photons, but their radiobiological properties do not differ substantially. In clinical applications, the absorbed dose is multiplied by a factor of 1.1 to convert the relative biological effectiveness (RBE) of a proton beam to cobalt gray equivalents (CGE) or gray equivalents (GyE) (2). In 1954, scientists at the Lawrence Berkeley Laboratory initiated the first studies of proton radiotherapy (PRT) to support Wilson's hypothesis. Therefore, PBT has been studied for over a half a century, and more than 83,000 patients worldwide are reported to have been treated with proton beams (3-7).

The most significant change to PRT occurred in the 1990s, when the Loma Linda University Medical Center began to use PRT clinically, and became the first hospital based medically dedicated proton therapy facility in the world (8). Since then, similar medically dedicated facilities have been constructed around the world. At present, almost 50 particle therapy facilities are operating worldwide, and it is estimated that the number of facilities will increase to 70-80 within 5-10 years. Despite these physical advantages, proximal and lateral dose is still the modest, and it never reaches to be zero. Therefore, if organs or structures that are sensitive to radiation located closely adjacent or abutting vulnerable, especially digestive tract, it is difficult to irradiate sufficient dose to the tumor.

The article by Jesseph and colleagues in *Translational Cancer Research* described their single-institution experience of the use of surgical organ displacement in the treatment of abdominal, pelvic, or retroperitoneal tumors by PRT (9). The aim of this intervention is to make a space between tumor and digestive tract in order to perform PRT with a curative intent. Their findings are noteworthy. All of the 15 patients who did surgical organ displacement obtained adequate displacement to allow successful proton treatment planning. Furthermore, there were no surgical complications. These methods described by Jesseph *et al.* might not only allow us to irradiate sufficient dose to the tumor, but also expand indication of PRT.

Materials

The ideal materials are not yet found. Patients' own tissue, such as omentum, is considered to be safe and effective, because it does not cause rejection reaction. Omentum is sometimes used in the treatment of liver or pancreatic cancer in Japan also.

How about artificial materials? Breast prosthesis and tissue expander Jesseph *et al.* used are originally developed for other purposes. The safety of these materials is

already confirmed. In Japan, Gore-tex sheet is commonly used (10,11), and use of breast prosthesis or tissue expander is rare. One of the problems is that some patients complain discomfort or pain by inserting artificial materials.

So, what is the ideal material? I would like to suggest that the density of the material should be water equivalent, because this enables us to calculate accurate dose distributions. The material remains as a spacer for a couple of months (at least treatment duration), then melt and disappear thereafter. Development of such a material is highly warranted.

Methods

Surgeons familiar with this surgical intervention might be quite few. Collaboration with radiation oncologists is essential at present. More education and understanding of surgical organ displacement to surgeons is needed.

Patients' own tissue might be leaved on, but artificial materials should sometimes be removed depend on patient's complaint. However, this intervention is not so easy, and it is not necessarily to be preferred because it involves invasive. The best methods require further investigation.

Finally, reimbursement of this procedure might be different by each country. In Japan, all of the cost (including the cost of insertion materials) and fee are not covered by social insurance at all. Therefore, patients have to pay all of them by themselves.

Despite these problems, surgical organ displacement and spacer insertion are quite effective methods in the field of PRT. There is still room for improvement, further research and development are needed.

Acknowledgements

Disclosure: The author declares no conflict of interest.

Cite this article as: Ogino T. Surgical organ displacement: what is the best "materials and methods" for proton radiotherapy? Chin J Cancer Res 2013;25(3):267-268. doi: 10.3978/j.issn.1000-9604.2013.04.03

References

1. Wilson RR. Radiological use of fast protons. Radiology 1946;47:487-91.
2. Ando K, Furusawa Y, Suzuki M, et al. Relative biological effectiveness of the 235 MeV proton beams at the National Cancer Center Hospital East. J Radiat Res 2001;42:79-89.
3. Schulz-Ertner D, Tsujii H. Particle radiation therapy using proton and heavier ion beams. J Clin Oncol 2007;25:953-64.
4. Brada M, Pijls-Johannesma M, De Ruysscher D. Proton therapy in clinical practice: current clinical evidence. J Clin Oncol 2007;25:965-70.
5. Olsen DR, Bruland OS, Frykholm G, et al. Proton therapy - a systematic review of clinical effectiveness. Radiother Oncol 2007;83:123-32.
6. Ramaekers BL, Pijls-Johannesma M, Joore MA, et al. Systematic review and meta-analysis of radiotherapy in various head and neck cancers: comparing photons, carbon-ions and protons. Cancer Treat Rev 2011;37:185-201.
7. Ogino T. Clinical evidence of particle beam therapy (proton). Int J Clin Oncol 2012;17:79-84.
8. Slater JM, Miller DW, Archambeau JO. Development of a hospital-based proton beam treatment center. Int J Radiat Oncol Biol Phys 1988;14:761-75.
9. Jesseph JM, Fitzek MM, Shahnazi K, et al. Surgical organ displacement for proton radiotherapy. Transl Cancer Res 2012;1:247-54.
10. Fukumoto T, Komatsu S, Hori Y, et al. Particle beam radiotherapy with a surgical spacer placement for advanced abdominal leiomyosarcoma results in a significant clinical benefit. J Surg Oncol 2010;101:97-9.
11. Komatsu S, Hori Y, Fukumoto T, et al. Surgical spacer placement and proton radiotherapy for unresectable hepatocellular carcinoma. World J Gastroenterol 2010;16:1800-3.

Review Article

New developments in treatment planning and verification of particle beam therapy

Reinhard W. Schulte, Andrew J. Wroe

Department of Radiation Medicine, Translational Research, Loma Linda University Medical Center, Loma Linda, CA, 92354, USA
Correspondence to: Reinhard W. Schulte, M.D., M.S. 11234 Anderson St., Loma Linda, CA 92354, USA. Email: rschulte@llu.edu.

Abstract: Charged particle beam therapy has been used for almost 60 years. During the initial 40 years, the medical use of protons and heavy ions was explored at accelerator laboratories in a limited number of patients and for a limited number of cancerous and non-cancerous disease conditions. After the development of computed tomography and 3D treatment planning, it was time to move charged particle therapy into the clinical realm. This happened in October 1991 when an ocular melanoma patient became the first patient to be treated at Loma Linda University Medical Center in California. Due to the increased awareness of the advantages of charged particle therapy and promising results of single-institution experiences, one currently observes a phase of rapid expansion of proton treatment centers throughout the world. A few of these centers are combined proton/carbon ion facilities. It is very important that the technological evolution of charged particle therapy will continue during this phase of clinical expansion to ensure that the increasing number of patients exposed to therapeutic charged particles will benefit most from the advantageous dose distributions that these particles afford. This report will give an overview of translational research activities related to planning and verification of proton therapy in which the authors have been involved for a number of years. While our activities focus on protons, these developments are to a large degree also applicable to carbon ion therapy.

Keywords: Proton therapy; proton computed tomography; range verification; immobilization

DOI: 10.3978/j.issn.2218-676X.2012.10.07
Scan to your mobile device or view this article at: http://www.thetcr.org/article/view/598/html

Introduction

Proton therapy is currently expanding its role in radiation therapy. In the U.S., there are at present 10 clinical proton treatment facilities, with 9 centers operating proton gantries, and 7 additional facilities in the planning and construction phase (1). Charged-particle beams heavier than electrons, including protons, helium and carbon ions, are distinguished from photon beams by the unique property of dose deposition at a precise depth, known as the Bragg peak, with a steep dose falloff beyond the peak. Thus, the integral dose to surrounding normal tissues is generally less compared with photon radiation therapy. Having fine control over the dose deposition in the patient allows for generation of very conformal dose distributions. Sparing of critical normal structures and minimizing integral dose to normal tissues appears most advantages in the central nervous system (CNS), where critical structures are densely packed and often abutted by gross tumor, and in children whose normal brain is very radiosensitive and who are at the highest risk of developing secondary cancers.

The wide-spread use of proton therapy in other body sites, in particular in prostate cancer, where it is in fact used most often, is currently controversial because no clear benefit over intensity modulated radiation therapy (IMRT) with photons has been demonstrated (2). While head-to-head trials comparing IMRT and proton therapy may be conducted in prostate cancer patients in the near future, where the wide use of proton therapy is most controversial, one should keep in mind that proton therapy is far from fully developed. Range uncertainties in proton therapy

that are amplified in body treatment sites due to material heterogeneity, organ deformation and internal motion can negatively impact the delivered dose distribution and are the subject of ongoing study and improvements. Closely related to this subject is the continued development of image guidance technology in the treatment room that ideally will provide feedback for in-room treatment plan modifications (adaptive proton therapy). It appears that full implementation of inversely planned intensity modulated proton beam therapy (IMPBT) with all its advantages will have to await these developments.

A related and often overlooked subject of interest in proton and heavy ion therapy is the immobilization of the patient. For the various anatomic sites, specific devices have to be developed that position and immobilize the patient reproducibly and effectively. In charged particle therapy, attention needs to be paid to minimize the proton water equivalent thickness (WET) of the immobilization devices in order to reduce the effect on proton beam penumbra and range uncertainty.

The next major step in therapeutic proton beam technology is to supplement passive beam delivery and shaping techniques with active proton beam scanning techniques. Proton beam scanning is currently being developed and implemented at major academic proton treatment centers. The major advantage of proton beam scanning as compared to passive beam delivery methods is the ability to perform inversely planned and optimized IMPBT. However, there are major technological hurdles to be overcome with proton beam scanning. In fact, most existing proton treatment centers continue to employ passive scattering systems.

In this contribution, the authors give an overview on developments undertaken by the translational medical physics and technology team at the James M. Slater Proton Treatment and Research Center at Loma Linda University Medical Center (LLUMC) to overcome some of the technical and conceptual hurdles currently encountered in proton and heavy ion therapy. While our developments are specifically geared towards improving proton therapy, they can be equally applied to heavy ion therapy.

Concepts and strategies

The classical strategy of planning and delivering a radiation treatment is to first scan the patient with X-ray computed tomography (CT) and to define the gross tumor and clinical target volumes (GTV and CTV) and organs at risk (OARs) with support of registered complementary imaging studies. At the time of the planning CT scan, the patient has been provided with appropriate immobilization support, and the position during the planning CT needs to be reproduced later in the treatment room.

Reproduction of the planned patient position and distribution of tissues relative to the beam is very important in proton therapy. Slight changes in the distribution of tissues relative to the beam due to setup errors, differences between the immobilization devices used during planning and treatment, and interim changes in patient or tumor anatomy, e.g., due to tumor shrinkage or weight changes, can have a noticeable influence on the resulting dose distribution at the time of treatment. Some of these uncertainties are random (e.g., variations in patient position); however, others, such as tumor shrinkage and weight loss or gain, are systematic and, therefore, may lead to a significant underdosing of tumor and overdosing of organs at risk since the range of the charged particle beams has changed compared to the original plan. This situation is further complicated when tumor sites are characterized by significant organ motion and deformation, such as intra-abdominal tumors, lung tumors, breast tumors, and even prostate tumors since the position of the prostate is influenced by the filling of bladder, rectum and small bowel. Uncertainties in range due to intra- and interfractional target motion can significantly modify the proton beam dose distribution and lead to cold spots and hot spots (3).

All the systematic and random errors combined require a considerable lateral margin to be added to the CTV to derive the internal target volume (ITV) and planning target volume (PTV). While this is also true in photon therapy, such as IMRT, distal uncertainty margins due to range errors are unique to charged particle therapy and are specific to each beam.

Organ motion is less of an issue in CNS and head and neck sites. However, there are considerable range uncertainties due to the presence of considerable bone and air inhomogeneity, CT artifacts from dental fillings, and tissue or tumor changes during the course of the treatment (e.g., in intra-orbital tumors or head and neck carcinomas).

The presence of range uncertainty in charge particle therapy has been known for a long time, and has been addressed in many ways, with the ultimate goal to reduce them to the fullest extent possible. Monte Carlo (MC) studies have been used to show the effect of inaccuracies resulting from conversion of Hounsfield units to relative stopping power (RSP) with respect to water in

analytical dose calculations as well as MC-based dose algorithms (4-6). A recent study, utilizing the change of bone marrow fat signal in MRI after proton treatment, demonstrated the range uncertainty encountered in posterior spinal proton fields in 10 patients (7). The mean overshoot was 1.9 mm (95% confidence interval, 0.8-3.1 mm) and exceeded 3 mm in four patients. In addition, there have been attempts to develop robust treatment planning algorithms that optimize beam direction to minimize range uncertainty (8-10).

At LLUMC, we have chosen to invest in the development of proton CT (pCT) as a promising technique to reduce systematic uncertainties in RSP determination related to the Hounsfield unit conversion (see below). Another interesting approach is the development of dual-energy CT scanners, which may provide better RSP estimates than single-energy CT scans (11). Yet the development of pCT presents additional advantages for proton therapy. One such advantage is the ability to provide similar or even better images with fewer artifacts than X-ray cone beam CT, making pCT useful for not only treatment planning but also pretreatment monitoring of patent setup. Besides cross-sectional anatomy, the pre-treatment pCT study also provides the RSP distribution of the patient and, in combination with fast computational hardware, may be able to check the adequacy of the treatment before its delivery, or even modify beam angles to optimize the treatment delivery. We currently have no data that supports these applications, but one should consider this for future research and development once pCT technology has been fully translated into clinical application.

While we were studying the application of radiation detectors typically employed in high-energy physics research, i.e., particle trackers and energy/range detectors (calorimeters), for proton CT, it became apparent that these detectors can also be used to monitor the proton radiation delivery by detecting primary or secondary particles generated during beam delivery. This led to the investigation of interaction vertex and proton scattering imaging during pencil beam scanning of charged particle beams, which will also be discussed below.

Lastly, one needs to pay meticulous attention to the immobilization devices that are used during CT scanning and treatment. Special immobilization devices for proton therapy have been developed that help to minimize additional range uncertainties and beam widening due to scattering. The importance of implementation of such devices will also be addressed in this contribution.

Proton CT

The standard approach to deal with range uncertainties in charged particle therapy is to add an additional range to each beam according to the expected range uncertainty, assuring target volume coverage (12). However, this can lead to unsatisfactory results by over-treating normal tissues. Initially, CT units used in charged particle treatment planning were calibrated with standard tissue substitutes (13). Schneider *et al.* (14) showed that this method is very sensitive to the choice of tissue substitutes and can lead to maximum range errors in the head in excess of 20 mm. These investigators developed a "stoichiometric calibration" method (15), which is based on data published in ICRP report 44 (16) for the calculation of Hounsfield values and RSP power. This is done after the dependence of the particular CT scanner on atomic composition has been measured with tissue substitutes. The stoichiometric method does not solve the problem that tissues of the same Hounsfield values can have different RSP. Schneider *et al.* (17) also showed that the "best" CT calibration was achieved when the CT of an individual patient was calibrated with proton radiography, which provides a composite "projection" image of integral RSP in proton beam direction. While this work pointed to the usefulness of RSP measurements as the basis for quality assurance of X-ray-CT-based charged particle treatment planning, it did not make the innovative step towards using protons themselves for CT planning.

Proton CT itself is not a new idea. It was originally suggested by Alan Cormack (18), who shared the Nobel Prize with Hounsfield for his seminal work on CT image reconstruction. He mentioned proton CT in his original paper as well as in his Nobel lecture (19). Driven by the clinical need for more proton range accuracy, a scientific pCT collaboration was formed by investigators from the Department of Radiation Medicine at LLUMC, University of California Santa Cruz (UCSC) (20), Brookhaven National Laboratory (BNL), and the State University of New York Stony Brook in 2003. A series of publications appeared during this exploratory (and mostly unfunded) period of 2003-2008 (21-27), documenting progress made in the conceptual and scientific understanding of the new pCT technology and pCT reconstruction.

The recent development of pCT has mostly become possible by application of the latest detector technology adapted from High Energy Physics (HEP). Silicon microstrip trackers and crystal calorimetry, commonly

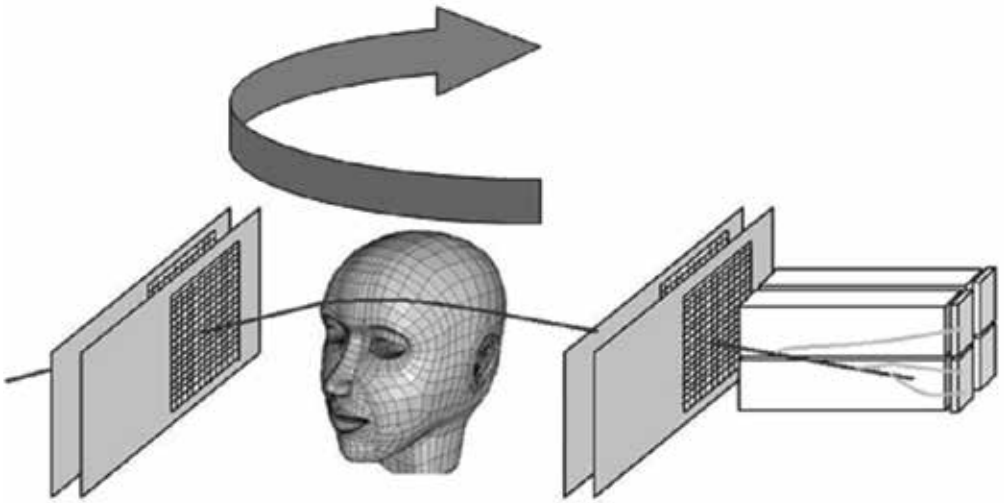

Figure 1 Schematic illustration of the first-generation pCT scanner. Protons are individually recorded by the four planes of position-sensitive silicon detectors which form the scanner reference system. These four planar detectors provide positions as well as angles of the protons in front and behind the object. A signal proportional to the energy of each outgoing proton is recorded with a segmented calorimeter in coincidence with its position and angle information. For a complete scan, the object is traversed by broad proton cone beam from many different projection angles

applied in HEP, allowed for the achievement of good spatial and energy resolution in the first generation prototype pCT scanner. For example, the silicon strip detectors in our Phase 1 scanner have a strip pitch of 228 μm, which allows to determine the position of protons at the level of each detector plane with better than 100 μm resolution. The crystal calorimeter has an intrinsic resolution of energy response of the order of 2%, which can be further improved by using a multi-stage plastic scintillator design in the Phase 2 scanner under construction.

Our conceptual approach to realizing pCT for treatment planning and image guidance originates from the approach described by Hanson *et al.* (28,29) and later work by Zygmanski *et al.* (30), although we deviate in some respect from these approaches, in particular in the implementation of reconstruction based on individual particle measurements. Our approach, outlined in more detail below, is based on a single-proton detection methodology; it uses a most likely path concept (24,27) to reconstruct along a curved path rather than a straight line, and iterative reconstruction algorithms to produce high-quality RSP reconstructions (31-33).

Proton CT offers the possibility to directly obtain the RSP distribution from proton energy measurements, which are then converted to a water equivalent pathlength (WEPL). Note that the WEPL of a proton through an object equals the line integral of RSP along the (not straight) proton path. With currently available detector technology, we have built the first generation of a pCT scanner whose design, originally proposed in (23) is shown in *Figure 1*. Individual protons are tracked before entering and after exiting the patient with two pairs of 2D sensitive silicon strip detectors (SSDs), providing information about proton position and direction at the boundaries of the image space. This allows the effects of multiple Coulomb scattering within the object to be accounted for in the estimation of an optimal trajectory or most likely path (MLP) (24,27).

In addition to tracking the position of individual protons, the energy lost by each proton after traversal of the image space is recorded in a calorimeter (an energy detector consisting of an array of cesium iodide (CsI) crystals). Using these measurements, one can obtain the WEPL, i.e., the path integral of relative stopping power along each path l, which is defined as

$$L = \int_l \rho dl \quad , \qquad [1]$$

where ρ is defined as the ratio of the local RSP of the tissue, S_{tissue}, to the RSP of water, S_{water}, thus

$$\rho = \frac{S_{\text{tissue}}}{S_{\text{water}}} \ . \qquad [2]$$

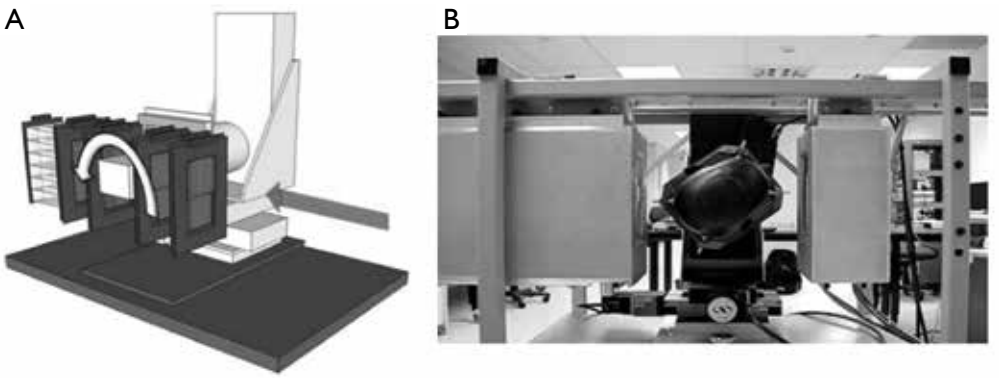

Figure 2 Schematic sketch (A) and view (B) of the first generation pCT scanner completed in 2011. The system consists of a front and rear module with a total of 4 silicon tracker planes and a crystal-calorimeter with an array of 18 CsI (Tl) crystals. The object (here a Rando head phantom) is rotating between the front- and rear-module on a precision rotational stage (Newport Corporation, Irvine, CA)

Assuming constant entry energy of the protons, the WEPL is strictly related to the energy of the outgoing protons. Thus, one can experimentally calibrate the scanner by relating the signal produced by the calorimeter to the WEPL of proton traversing a plate of polystyrene plates of known water-equivalent thickness, as recently described in (34).

In 2008, the Departments of Physics at Northern Illinois University and Radiation Medicine at LLUMC and the Santa Cruz Institute of Particle Physics (SCIPP) at UCSC received funding to build a Phase 1 preclinical head pCT scanner. The schematic layout of the Phase 1 pCT tracker and the device completed in 2011 are shown in *Figure 2*. It is comprised of front and rear SSD modules, consisting of 4 XY planes for full coordinate and direction data. The 18-crystal energy detector is integrated with the rear tracker modules. The scanner is mounted on a rail system that allows positioning of the detectors close to the phantom object that will rotate on a fixed, horizontal proton beam axis. The system also includes a precision microstage system for axial rotation and 3-axis translations. A more detailed description of this first generation pCT scanner can be found in (35).

The first generation pCT head scanner is not optimized for the high proton data rates that will be encountered in clinical operation. This is related to limitations of the data readout of the current data acquisition system and the rate limitations of the CsI energy detector. Another limitation is the relatively long image reconstruction time of up to 12 hours on conventional computing hardware. A third limitation of the Phase 1 scanner is its restricted sensitive area of 9 cm × 18 cm, which is suitable for head scans only.

The first 1.5 years of experience with the first generation scanner, which is currently mounted on one of the proton research beam lines at LLUMC, has shown that good quality RSP maps can be reconstructed but has also clearly demonstrated the technological limitations of this device. For example, *Figure 3* shows two RSP reconstructions obtained with the Lucy® phantom (Standard Imaging, Middleton, WI). The phantom consists of a 14-cm diameter polystyrene sphere that was equipped with cylindrical inserts of acrylic, bone-equivalent plastic, polystyrene, and air. As shown, spatial resolution has improved over time due to refinements in the reconstruction parameters, but also new artifacts have appeared which are related to differences in the responses of the different components of the CsI crystal matrix.

The Department of Radiation Medicine at LLUMC in collaboration with UCSC and the Department of Computer Science and Engineering at California State University San Bernardino (CSUSB) has received funding in 2011 to build the next generation pCT scanner, which will address the limitations of the first pCT scanner. The Department of Physics at Illinois University with Fermi National Accelerator Laboratory as collaborator has also received funding to build a Phase 2 scanner, albeit with somewhat different technology than the current Phase 1 scanner. A detailed description of the new scanner designs can be found in (36,37).

Figure 4 shows the schematic of the Phase 2 pCT scanner currently being built at LLUMC, CSUSB and UCSC. Without giving up the general concept shown in *Figure 1*, the LLUMC Phase 2 design will comprise a large-area silicon detector (9 cm by 36 cm) for the clinical pCT scanning with data acquisition rates increased by at least a

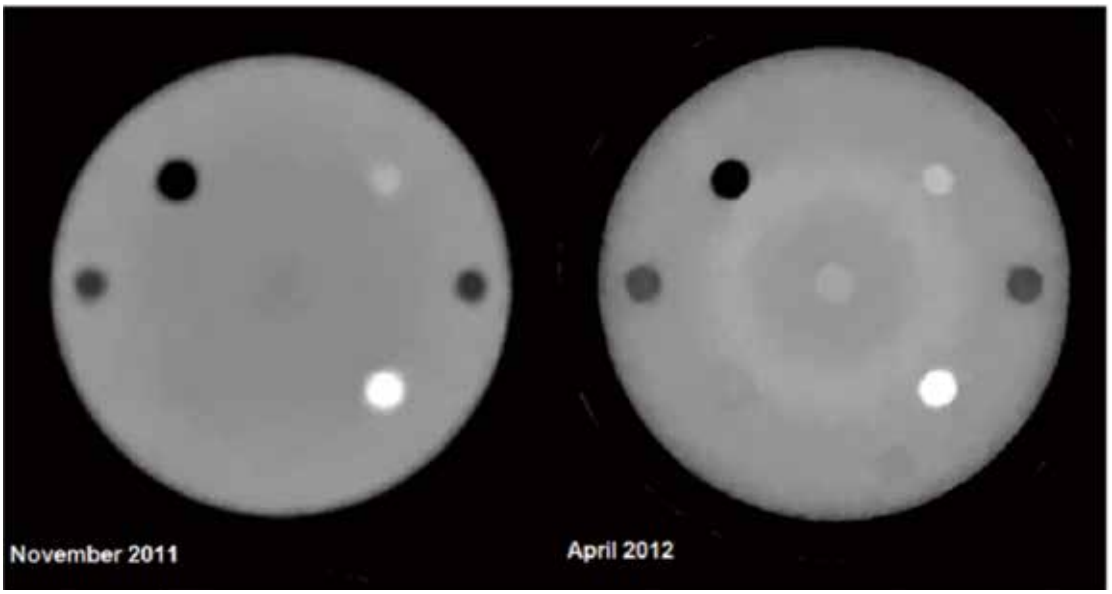

Figure 3 Cross sectional reconstructions of relative stopping power (RSP) of the Lucy® phantom through cylindrical inserts. The body of the Lucy sphere is made of polystyrene (RSP=1.035). The dark insert corresponds to air (RSP=0.05), the denser insert at the lower right to bone equivalent material (RSP=1.7), and the less dense insert in the upper right to acrylic (RSP=1.2). The right reconstruction, performed at a later time, shows improvement in resolution but also shows the presence of ring artifacts related to different responses of individual crystals in the calorimeter

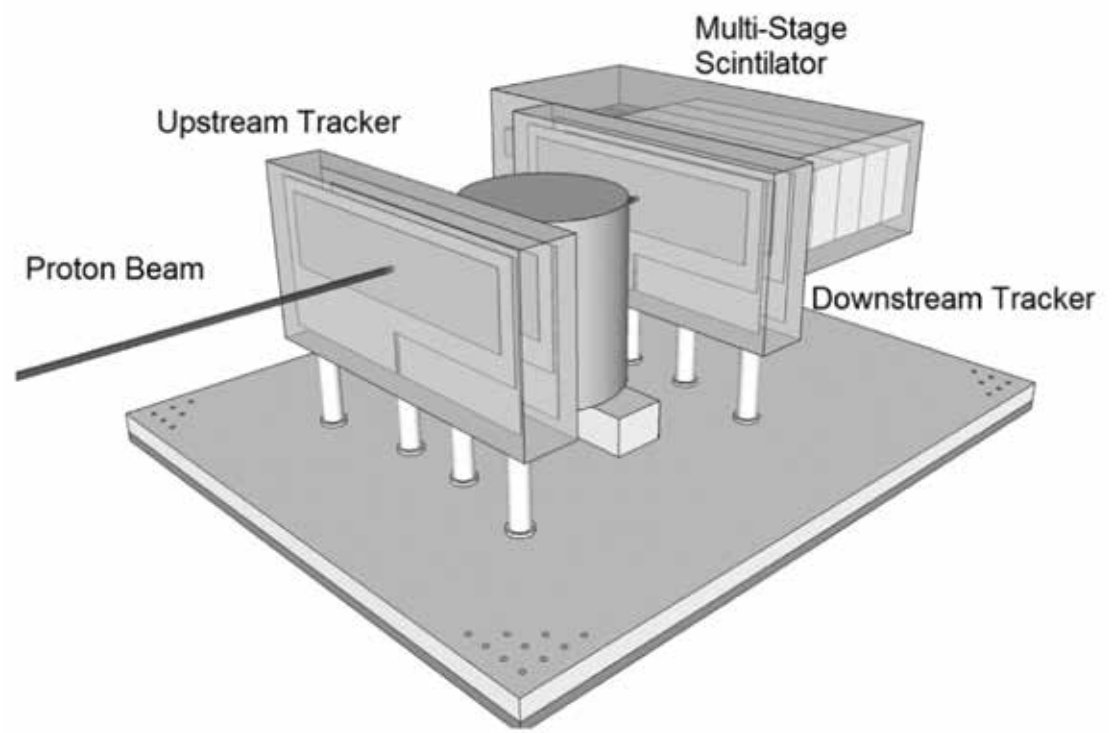

Figure 4 Schematic of the second generation (Phase 2) pCT scanner currently under construction. Different from Phase 1, the rotation stage is vertical rather than horizontal. The detector area will be expanded horizontally by a factor of two

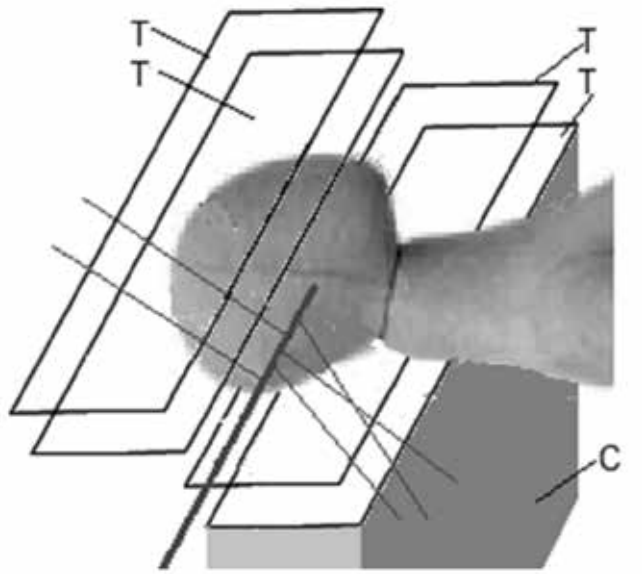

Figure 5 Principle of the large-angle scattered proton monitoring technique with two tracker telescopes with 4 position-sensitive planes (T). The protons scattered out of the primary beam (solid line) are detected by the trackers and their trajectory is back-tracked into the patient. The use of two telescopes increases the number of detected protons. With appropriate reconstruction techniques, the 3D position of the interaction points creating the scattered protons and thus the beam axis location can be inferred. In addition, one can also measure the energy of the tracked protons with a calorimeter (C) (here only shown in the lower half for clarity) to obtain additional data

factor of 10 from current rates to a sustained rate of about 2 MHz. The detectors will be mounted on a bread board with option of variable spacing relative to the phantom. The nominal distance between the inner silicon detectors will be 30 cm. The multi-segmented crystal energy detector will be replaced by a multi-stage scintillation (MSS) detector which has shown an intrinsic resolution of better than 1% in initial beam tests and provides a more uniform response.

After completion and acceptance testing of the Phase 2 pCT scanner, we will conduct a detailed performance evaluation of the pCT method using standard CT testing modules (Catphan® 600 phantom, The Phantom Laboratory, Inc., Salem, NY) including parameters such as image noise and noise power spectrum, field uniformity, high-contrast spatial frequency limits and modulation transfer function (MTF) measurements, low contrast detectability, and quantitative accuracy of CT numbers with materials of known RSP.

We will also evaluate the ability of the pCT scanning method to provide a more accurate proton range definition than currently possible with X-ray CT with a versatile proton range phantom, which will consist of a stack of radiochromic films (WET of 0.3 μm per film), embedded in the posterior fossa of a pediatric head phantom (CIRS). Proton pencil beams of known energy will be directed through different anatomical parts of the phantom and their observed range in the film stack will be compared to that predicted by pCT and X-ray CT-based treatment plans.

Large-angle proton scattering monitoring

Contemporary beam scanning nozzles contain monitors for the beam size, profile, position and beam intensity (38). The beam delivery control software receives signals from these beam monitors and frequently checks whether tolerances have been exceeded. Tolerance levels are generally much more stringent than for photon beam delivery, due to the sharpness of the rise and fall-off of dose in the Bragg peak. Since these monitors are located at considerable distance from the patient, the required accuracy of beam position is difficult to achieve. Very small deviations in the beam position at detector level can lead to relatively large deviations in the patient. In addition, there is no exact knowledge about loss of energy and intensity in beam modifying devices and immobilization devices that are located downstream from the monitoring detectors. Therefore, it would be very attractive to develop methods that allow for *online* monitoring of all relevant beam parameters as the beam enters and interacts with the patient.

Detecting and reconstructing the origin of large-angle scattered protons from primary proton pencil beams is a novel method investigated for fast and accurate proton beam monitoring. The principle, schematically shown in *Figure 5*, is based on the detection of distinct protons that are scattered out of primary beam due to elastic or inelastic nuclear interactions within the patient. A significant number of these scattered protons will be energetic enough to leave the patient, and their properties can be measured with particle detectors developed for pCT. Fast reconstruction of scattered proton tracks and their origin will primarily allow monitoring of beam position and size; the intensity of scattered protons will correlate with the primary beam intensity and energy, and hence these parameters could also be monitored with this technique.

First experiments demonstrating the potential of this

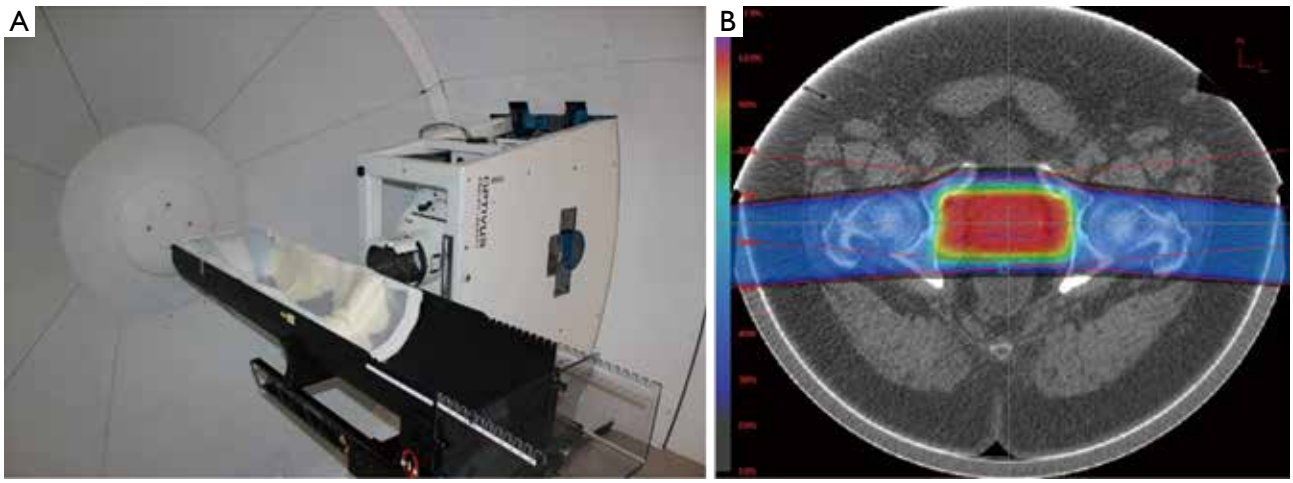

Figure 6 A pod immobilization system mounted to a six-degree of freedom robotic patient positioner at LLUMC (A); example of how pod immobilization maintains a consistent patient external contour minimizing the impact of the contour on range uncertainty (B)

monitoring technique were performed at the LLUMC proton treatment center and were presented at the 2008 IEEE Nuclear Science Symposium (39). A human head phantom was irradiated with 250 and 100 MeV proton pencil beams, and scattered protons were detected with a silicon microstrip tracker located near the phantom. Extrapolation of about 10^4 scattered proton tracks back to a focus plane inside the phantom demonstrated the feasibility of reconstructing the location of the pencil beam and estimating its axis inside the phantom with sub-millimeter accuracy. Although the slow readout system of the pCT tracker used in these first experiments did not permit measurement of the actual flux of the scattered protons, subsequent Geant4 Monte Carlo simulations of the experiment indicated that with fast and efficient particle detectors one could register 10^6-10^7 scattered protons per single proton beam spill of 10^{10} primary protons (33).

An additional preliminary feasibility test of the proton scattering monitoring technique was carried out at the LLUMC proton center using the Phase 1 proton CT scanner (see above). In particular, a phantom, consisting of a PMMA cylinder of 15 cm diameter filled with water, was exposed to 126 and 200 MeV proton pencil beams. Protons emerging from the phantom at 90 degrees with respect to the direction of the incoming beam were tracked in the four planes of silicon microstrip detectors of the scanner, while their energy was measured with the segmented CsI calorimeter. The beam position and its profile in the vertical plane were reconstructed by extrapolating the trajectories of reconstructed protons back to their point of origin along the beam axis. Using a sample of 11,500 reconstructed tracks from data taken with the 200 MeV beam, the vertical beam position was determined with a statistical accuracy of 0.07 mm and a realistic beam width of 3.60±0.11 mm was determined from the reconstructed vertical beam profile. The results of this test, though very limited in scope and event statistics, highlight the promising perspectives of the proposed technique.

Advances in proton immobilization

Immobilization is not a new concept in radiation therapy as it has been used over the years in photon and electron therapy to place the patient in a reproducible and stable position for treatment. This is no different in proton therapy, as the use of both external and internal immobilization impacts the ability to cover a target with the specific treatment dose. However, unlike in photon therapy, the third dimension of depth is very critical in proton beam delivery. Changes in patient contour or target position along the beam axis can impact the position of the distal edge of the Bragg peak relative to the tumor. Pod immobilization (see *Figure 6*) has been used extensively at LLUMC over the past 20 years in order to not only provide superior body immobilization but also control the reproducibility of the patient's external contour, especially on larger patients, hence removing a source of range uncertainty which can impact Bragg peak placement.

Figure 7 CT images of immobilization devices whose heterogeneity and lack of part-to-part reproducibility makes them unsuitable for proton therapy immobilization

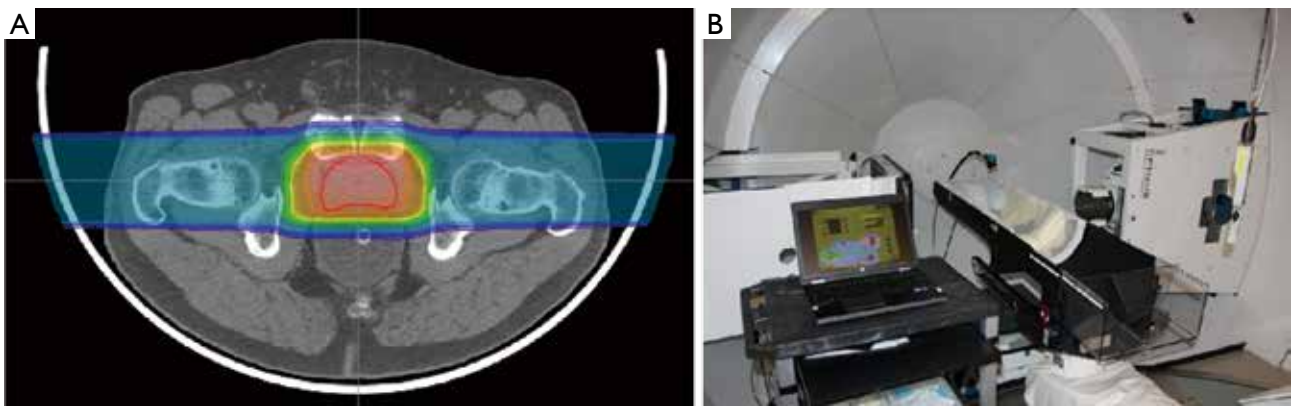

Figure 8 A. A proton prostate plan which utilizes a water-filled endo-rectal balloon to limit prostate motion during and between treatments; B. example of a spirometric device that assists in deep-inspiration breath-hold treatment delivery at LLUMC

It is important to realize that the distal edge placement of each proton beam is modified by any device placed upstream (closer to the beam source) of the patient, including immobilization devices. It is imperative that such devices are taken into account accurately by the treatment planning system, and that their water equivalent thickness (WET) is known precisely and verified using measured proton data. Devices that are non-uniform may change their internal composition between the time of the initial imaging for treatment planning and the time of patient treatment; similar attention must be paid to differences in the materials used for the purposes of planning and treatment delivery (*Figure 7*). Prior to clinical implementation all immobilization devices should be thoroughly evaluated including CT imaging, treatment planning system evaluation and measured WET data to ensure that the impact of the devices on the treatment process is understood.

Bragg peak placement is controlled using a range shifter in passive proton beam delivery or through dynamic changes in proton energy for active proton delivery. Regardless of the beam delivery method, the Bragg peak placement is determined by the location (or water equivalent depth) of the target relative to upstream anatomy, including bony structures or air cavities. Motion of the target relative to these anatomical structures can cause a mismatch between the range shifter or energy selected and the target's water equivalent depth, leading to either over-irradiation of normal tissue past the target or under-irradiation of the target itself. To minimize this mismatch, inter- and intra-fraction motion must be minimized to ensure the target is in the same location at the time of treatment that it was during CT imaging and treatment planning. For example, in prostate treatments this can be accomplished by asking the patient to maintain a modestly full bladder during imaging and treatment, and by placing an endorectal balloon (*Figure 8A*), as shown by our recent and yet unpublished study of 25 consecutive prostate cancer patients. For structures that are influenced by respiratory motion, including liver and intra-abdominal tumors, advances in spirometric and optical tracking systems allow for reproducible beam delivery during the respiratory cycle (*Figure 8B*).

As more proton therapy centers come online, a good understanding of immobilization devices and how these will impact the proton dose profile and its accuracy is necessary to maintain treatment efficacy. Centers using more than one radiation modality (e.g., protons and photon IMRT) also need to consider the functionality of their current immobilization devices and whether these devices are suited to proton therapy. Immobilization devices specifically developed for proton therapy may be the best solution in theory, but may prove too costly to maintain and place unnecessary burdens on staff training in practice. Further, immobilization devices used exclusively for proton therapy may limit use of other radiation modalities in patients that receive combined-modality treatments, as they require re-immobilization and re-scanning of patients as they are moved from one to the next treatment modality. As such, immobilization solutions that meet the needs of both the photon and proton treatment modalities should be considered, allowing for maximum treatment flexibility, while maintaining adequate patient immobilization.

Discussion and conclusions

Proton therapy is still an evolving radiation therapy modality. With an increasing number of patients treated worldwide, technological advancements in proton therapy are likely to occur at an increasing pace.

Range uncertainties due to tissue and immobilization device material heterogeneity and stopping power uncertainties are important challenges to overcome in proton therapy, in particular, if targets in moving and deformable organs are treated and more hypofractionated treatment protocols are being investigated in the clinic.

Reducing range uncertainties will support the development of clinical protocols based on inversely planned IMPBT. The IMPBT technology has additional challenges that will need input from multidisciplinary teams. We have proposed and are currently testing a new method for monitoring proton pencil beam delivery during active beam scanning, which is based on detecting large-angle scattered protons arising from the primary beam. Similar and complementary monitoring techniques using prompt gamma detection and post-treatment monitoring of positron emitter distribution created by nuclear interactions during treatment are likely to be further developed and integrated in the treatment room environment.

Suitable immobilization devices and techniques are also likely to continue to evolve. Rather than adopting existing devices and techniques that have been developed for primary application in photon radiation therapy, focus needs to shift to devices that address the special demands of charged particle therapy. Ideally, these devices will be part of a universal immobilization suite that can be employed for multi-modality treatments utilizing both proton and photon irradiation. Rather than focusing on proton beam gating, we believe that internal organ and tumor motion is best controlled by devices that restrict this motion and stabilize the treated organ. Therefore, we prefer the use of passive devices such as an endorectal balloon for prostate treatments and active breathing control in patients undergoing lung and abdominal proton therapy.

We have presented examples of ongoing translational research and development in proton therapy that are also applicable to carbon ion therapy. Forming research relationships with open exchange of ideas and research results is, in our opinion, the key to accelerated progress in this field. Appropriate technology transfer protocols should be developed that allow an efficient transition from the research environment to clinical application.

Summary

Charged particle therapy with protons and heavy ions started almost 60 years ago, but continues to evolve clinically and technologically. Important aspects that need to be addressed include the reduction of proton range uncertainty, the development of active beam scanning technology and its monitoring, and advanced immobilization techniques that take the special requirements of charged particle beams into account. Translational research activities are presented that focus on these areas.

Acknowledgements

The authors are supported by Grant No. 1R01EB013118-01 from the Institute of Biomedical Imaging and Bioengineering at the National Institutes of Health. The content of this paper is solely the responsibility of the authors and does not necessarily represent the official views of the National Institute of Biomedical Imaging and Bioengineering or the National Institutes of Health. The first author would also like to acknowledge financial support received by the United States - Israel Binational Science Foundation (BSF), grant Number 2009012. The Phase 1 proton CT development was partially funded by the U.S. Department of Defense Prostate Cancer Research Program Award No.

W81XWH-12-1-0122 to Northern Illinois University and the Department of Radiation Medicine.

Disclosure: This manuscript has not been submitted or published elsewhere. The authors have no potential conflicts of interest related to the information contained herein.

References

1. Particle therapy facilities in operation. Particle Therapy Co-Operative Group. Available online: http://ptcog.web.psi.ch/ptcentres.html
2. Allen AM, Pawlicki T, Dong L, et al. An evidence based review of proton beam therapy: the report of ASTRO's emerging technology committee. Radiother Oncol 2012;103:8-11.
3. Lomax AJ. Intensity modulated proton therapy and its sensitivity to treatment uncertainties 1: the potential effects of calculational uncertainties. Phys Med Biol 2008;53:1027-42.
4. Jiang H, Seco J, Paganetti H. Effects of Hounsfield number conversion on CT based proton Monte Carlo dose calculations. Med Phys 2007;34:1439-49.
5. España S, Paganetti H. The impact of uncertainties in the CT conversion algorithm when predicting proton beam ranges in patients from dose and PET-activity distributions. Phys Med Biol 2010;55:7557-71.
6. Paganetti H. Range uncertainties in proton therapy and the role of Monte Carlo simulations. Phys Med Biol 2012;57:R99-117.
7. Gensheimer MF, Yock TI, Liebsch NJ, et al. In vivo proton beam range verification using spine MRI changes. Int J Radiat Oncol Biol Phys 2010;78:268-75.
8. Chen W, Unkelbach J, Trofimov A, et al. Including robustness in multi-criteria optimization for intensity-modulated proton therapy. Phys Med Biol 2012;57:591-608.
9. Unkelbach J, Bortfeld T, Martin BC, et al. Reducing the sensitivity of IMPT treatment plans to setup errors and range uncertainties via probabilistic treatment planning. Med Phys 2009;36:149-63.
10. Unkelbach J, Chan TC, Bortfeld T. Accounting for range uncertainties in the optimization of intensity modulated proton therapy. Phys Med Biol 2007;52:2755-73.
11. Yang M, Virshup G, Clayton J, et al. Theoretical variance analysis of single- and dual-energy computed tomography methods for calculating proton stopping power ratios of biological tissues. Phys Med Biol 2010;55:1343-62.
12. Urie M, Goitein M, Wagner M. Compensating for heterogeneities in proton radiation therapy. Phys Med Biol 1984;29:553-66.
13. Chen GT, Singh RP, Castro JR, et al. Treatment planning for heavy ion radiotherapy. Int J Radiat Oncol Biol Phys 1979;5:1809-19.
14. Schneider U, Pedroni E. Proton radiography as a tool for quality control in proton therapy. Med Phys 1995;22:353-63.
15. Schneider U, Pedroni E, Lomax A. The calibration of CT Hounsfield units for radiotherapy treatment planning. Phys Med Biol 1996;41:111-24.
16. International Commission of Radiation Units and Measurements. Tissue Substitutes in Radiation Dosimetry and Measurements. ICRU Report 44, ICRU, Bethesda, MD, 1989.
17. Schneider U, Pemler P, Besserer J, et al. Patient specific optimization of the relation between CT-hounsfield units and proton stopping power with proton radiography. Med Phys 2005;32:195-9.
18. Cormack AM. Representation of a function by its line integrals, with some radiological applications. J Appl Phys 1963;34:2722-7.
19. Allan M. Cormack, Godfrey N. Hounsfield. The Nobel Prize in Physiology or Medicine 1979. Available online: http://nobelprize.org/nobel_prizes/medicine/laureates/1979/cormack-lecture.html
20. Sipala V, Bruzzi M, Bucciolini M, et al. A proton imaging device: Design and status of realization. Nucl Instrum Methods A 2010;612:566-70.
21. Sadrozinski HF-W, Bashkirov V, Bruzzi M, et al. Issues in proton computed tomography. Nucl Instrum Methods A 2003;511:275-81.
22. Johnson LR, Keeney B, Ross G, et al. Initial studies on proton computed tomography using a silicon strip detector telescope. Nucl Instrum Methods A 2003;514:215-23.
23. Schulte RW, Bashkirov V, Li T, et al. Conceptual design of a proton computed tomography system for applications in proton radiation therapy. IEEE Trans Nuc Sci 2004;51:866-72.
24. Williams DC. The most likely path of an energetic charged particle through a uniform medium. Phys Med Biol 2004;49:2899-911.
25. Schulte RW, Bashkirov V, Klock MC, et al. Density resolution of proton computed tomography. Med Phys 2005;32:1035-46.
26. Li T, Liang Z, Singanallur JV, et al. Reconstruction for proton computed tomography by tracing proton trajectories: a Monte Carlo study. Med Phys 2006;33:699-706.
27. Schulte RW, Penfold SN, Tafas JT, et al. A maximum

likelihood proton path formalism for application in proton computed tomography. Med Phys 2008;35:4849-56.
28. Hanson KM, Bradbury JN, Cannon TM, et al. Computed tomography using proton energy loss. Phys Med Biol 1981;26:965-83.
29. Hanson KM, Bradbury JN, Koeppe RA, et al. Proton computed tomography of human specimens. Phys Med Biol 1982;27:25-36.
30. Zygmanski P, Gall KP, Rabin MS, et al. The measurement of proton stopping power using proton-cone-beam computed tomography. Phys Med Biol 2000;45:511-28.
31. Penfold SN, Rosenfeld AB, Schulte RW, et al. A more accurate reconstruction system matrix for quantitative proton computed tomography. Med Phys 2009;36:4511-8.
32. Penfold SN, Schulte RW, Censor Y, et al. Total variation superiorization schemes in proton computed tomography image reconstruction. Med Phys 2010;37:5887-95.
33. Penfold SN. Image reconstruction and Monte Carlo simulations in the development of proton computed tomography for applications in proton radiation therapy. Ph.D. thesis, University of Wollongong, 2010.
34. Hurley RF, Schulte RW, Bashkirov VA, et al. Water-equivalent path length calibration of a prototype proton CT scanner. Med Phys 2012;39:2438-46.
35. Hurley RF, Schulte RW, Bashkirov VA, et al. The phase I proton CT scanner and test beam results at LLUMC. T Am Nucl Soc 2012;106:63-6.
36. Schulte RW, Bashkirov V, Johnson R, et al. T Am Nucl Soc 2012;106:59-62.
37. Zutshi V. Overview of the NIU/Fermilab Phase 2 proton CT project. T Am Nucl Soc 2012;106:67-8.
38. Flanz J. Particle Beam Scanning. In: Paganetti H. eds. Proton Therapy Physics. Boca Raton, FL: CRC Press/ Taylor & Francis, 2011:158-89.
39. Bashkirov VA. Proton Computed Tomography: a Status Update. Presented at the Special Focus Workshop: Innovative Techniques for Hadron Therapy. 2008 IEEE Nuclear Science Symposium, Medical Imaging Conference. 2008.

Cite this article as: Schulte RW, Wroe AJ. New developments in treatment planning and verification of particle beam therapy. Transl Cancer Res 2012;1(3):184-195. DOI: 10.3978/j.issn.2218-676X.2012.10.07

Review Article

Improving the precision and performance of proton pencil beam scanning

Sairos Safai, Christian Bula, David Meer, Eros Pedroni

Paul Scherrer Institut, Switzerland

Correspondence to: Safai Sairos, PhD. Paul Scherrer Institut 5232 Villigen PSI, Switzerland. Email: sairos.safai@psi.ch.

Abstract: In this report we present the technical features of Gantry 2, the new second generation scanning system of PSI. On the basis of the experience and success with the first prototype, Gantry 1, built in the 90s for introducing pencil beam scanning and IMPT into the field of proton therapy, we have recently implemented a new system capable of offering much faster repainted conformal scanning for being able to treat moving targets with scanning under image guidance, the next challenge in the field of proton therapy.

The new technical developments are conducted in parallel to the ongoing basic commissioning of Gantry 2, which should go into operation with usual discrete spot scanning for treating static targets in 2013.

The innovative layout of Gantry 2 and the integration in the treatment area of the basic equipment for image guidance are presented. Noteworthy are the sliding CT within reach of the patient table and the unique new Beam's-Eye-View X-ray fluoroscopy system for taking images in the beam direction synchronized with the proton beam delivery.

The first preliminary results with the development of much faster scanning modes look very encouraging. We can change the beam energy with the beam line within 80 ms for typical 0.5 cm range steps. We can deliver whole fluence-shaped energy layers within a time of the order of 100 ms. Dose lines are painted by changing the velocity of the scan magnets. The instantaneous dose rate of the pencil beam can be varied dynamically as well. The dose is precisely controlled with a feedback loop connecting the main gantry beam monitor with a vertical deflector plate at the ion source.

These new fast scanning modes should be used for providing scanning with repainting, gating and tracking for treating moving targets. The goal is to develop pencil beam scanning as a universal beam delivery solution capable of treating optimally all possible clinical indications for proton therapy. Scanning could then completely replace the old beam delivery methods based on passive scattering from the market.

The long term projects of Gantry 2 should represent the new contributions of PSI to the proton therapy field in the next 5-10 years, by providing direct translational cancer research from the physics laboratory into industry and clinics.

Keywords: Proton therapy; conformal therapy; dynamic therapy; moving targets; image guidance

DOI: 10.3978/j.issn.2218-676X.2012.10.08

Scan to your mobile device or view this article at: http://www.thetcr.org/article/view/599/html

Introduction

Due to the finite range of particle beams and the excellent dose localization in depth with a characteristic dose maximum at the location where the beam stops, the so-called Bragg peak, proton and ion therapy provide an improved capability of shaping the dose conformally to the target volume with a significant dose sparing of healthy tissues surrounding the tumour as compared to conventional therapy with photons.

Another advantage of charged particle beams is given by the possibility to scan a small pencil beam laterally by magnetic deflection and in depth by changing the energy

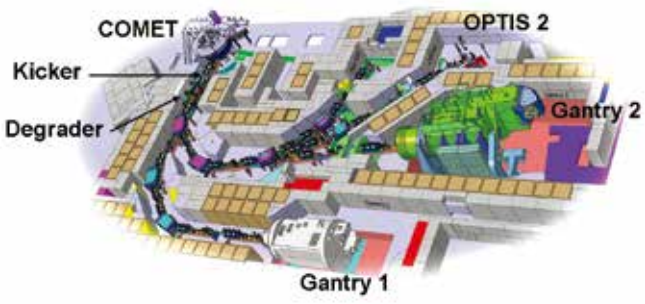

Figure 1 PROSCAN layout with the COMET cyclotron, the fast kicker magnet to switch the beam on and off, the energy degrader system and the beam line to the treatment areas Gantry 1, Gantry 2 and OPTIS 2

of the beam as a method for painting the dose dynamically. The Paul Scherrer Institut (PSI) has committed itself to the development of *pencil beam scanning* for over three decades, starting in the 80s with pion beams (1), in 1992 with the realization of the first proton scanning gantry in the world (Gantry 1) operational since 1996 (2) and recently with the installation of a new prototype (3) Gantry 2, which is currently being commissioned (4). The goal is to bring the scanning technology close to the physical limits using a new next generation gantry. By providing new advanced beam delivery techniques we should expand the spectrum of the clinical applications treated with pencil beam scanning to include moving targets. This shall be the main goal of our centre in terms of translational research from accelerator physics to clinics over the next decade.

The main topic of this report is to present the technical characteristics of the new Gantry 2 in view of the potential of this system for new future translational research.

In Section 2, we briefly describe the history and the technical status of the proton facility at PSI with emphasis on the technical features of the first prototype Gantry 1, which provided the necessary experience and background for the current and future developments of Gantry 2.

In section 3, we discuss why further developments of proton pencil beam scanning are needed.

Section 4 is focused on the conceptual design of the new Gantry 2.

Section 5 presents the advancement of the scanning technology for achieving very fast scanning techniques designed for treating moving targets with scanning in conjunction with image guidance.

In section 6, we briefly mention the potential clinical indications for Gantry 2.

Conclusions can be found in section 7.

Scanning experience with the first prototype Gantry 1

The technological innovation of PSI in the field of particle therapy in the 90s was the introduction of pencil beam scanning, a method where narrow pencil beams are superimposed laterally and in depth to achieve a dose distribution conformal to the target volume while sparing the surrounding healthy tissue as much as possible (2).

The first prototype implementing this technique is named PSI's Gantry 1. During the past 16 years, more than 800 patients have been treated successfully, most of them for tumours in the skull base region. PSI developed at Gantry 1 and introduced in the clinical program *intensity modulated proton therapy* (IMPT) (5), the equivalent of intensity modulated therapy with photons (IMRT). A paediatric program was started in 2000 in collaboration with the University of Zurich, based on the idea that children should profit most from proton therapy. Children under the age of 5 years are treated under anaesthesia. Being a great success, this program now makes up one third of all patient treatments.

Gantry 1 was designed for parasitic operation at PSI's 590 MeV ring cyclotron. By connecting the Gantry 1 beam line to a new dedicated cyclotron COMET (6) in 2006 (*Figure 1*), two major limitations of the first decade of clinical operation were eliminated, namely considerable current instabilities of the split and degraded beam and long yearly shutdowns due to the maintenance of the main accelerator of PSI. Since its introduction, COMET has been operating reliably with patients treated at 5 days a week all year long and without shutdowns longer than 3 days.

Gantry 1 implements *discrete spot scanning* where the beam is turned off while moving from one spot position to the next. This approach allows controlling the spot parameters like position and dose under static conditions and was chosen to cope with the beam instabilities present during the first years of operation. Individual spots of variable length are applied at a rate of up to 200 spots/s.

The fine adjustment of the proton energy is achieved with a so-called range shifter, a device located in the gantry nozzle in front of the patient, consisting of 40, 4.5 mm water equivalent, polyethylene plates which can be inserted individually in the beam. This method has the advantage of working with an invariant fixed depth dose profile, but multiple Coulomb scattering (MCS) of the protons in the

Table 1 Time characteristic of the three scan axes of Gantry 1 and Gantry 2. Also shown is the time needed to apply a 2 Gy dose box of 1 litre (10×10×10 cm^3) in discrete spot scanning mode with and without repainting. Note that the beam ON time is always 90 s regardless of the number of repaintings

Comparing scanning speeds		Gantry 1	Gantry 2
1st scan axis	Device	sweeper magnet	T-sweeper magnet
	time/step	5 ms	2 ms
2nd scan axis	Device	range shifter	U-sweeper magnet
	time/step	50 ms	2 ms
3rd scan axis	Device	patient table	degrader, beam line
	time/step	1 s	80 ms
10,000 spots, ~1 liter box, 90 s beam ON, ~2 Gy	single paint	3 min	1 min 50 s
	4 repaintings	7 min 30 s	2 min 50 s
	9 repaintings	15 min	4 min 30 s

range shifter plates make the beam width very sensitive to the air gap between nozzle and the patient surface and can lead to a fast degradation of the lateral dose fall-off with increasing nozzle-patient distance (7).

Laterally, the beam is scanned magnetically along one axis with a sweeper magnet located upstream from the last 90° bending magnet. With such an upstream scanning mode, the beam optics can be designed to provide parallel scanned pencil beams at the target location (apparent source at the infinite). The second lateral scan axis is realized by moving the patient, i.e., the target volume, with the patient-table. The speed of this mechanical movement is limited and contributes substantially to the overall dead-time of the system. The scanning system is Cartesian in all three dimensions.

The scan sequence to move the beam on a 3D-grid of 5 mm step size is dictated by the scan speed of the three axis: lateral with sweeper magnet (5 ms/step), in-depth with range shifter (50 ms/step) and lateral with patient-table (1 s/step). The resulting time to treat a 1 litre volume with 2 Gy with discrete spot scanning is 3 min with a duty factor of 50% (*Table 1*). Due to the use of the motion of the patient-table as a scanning axis, substantial volumetric repainting (defined later) with this scanning performance is not practical and therefore Gantry 1 is limited in its application to non-moving targets.

Motivation for further developments in spot scanning

To understand the reasons to further push the pencil beam scanning technology we must first compare this technology with the more traditional method of passive scattering, which is based on a uniform scattered broad beam and where the dose is shaped with fixed collimators and compensators.

The major advantages of scanning, as we have learned from Gantry 1 (8), are the following:

With scanning one can provide a true 3D-dose conformation with variable modulation of the range as opposed to fixed range modulation of scattering, which delivers unnecessary full dose outside the target. With scanning there is no need to fabricate and mount patient-field specific hardware in the beam line in front of the patient. One can thus deliver multiple fields in sequence without the need for personnel to enter the room to change equipment in between fields. This reduces treatment time and makes the use of many field directions easier.

Scanning can deliver not only homogeneous dose fields [so called single field uniform dose, i.e., SFUD (9)] but can also provide non-homogeneous dose distributions with planned dose shaping within the target (non-uniform dose fields NUDF). Planned non-homogenous dose fields can be combined within a simultaneous optimization of fields to obtain superior dose distributions (multiple field optimization). In the 90s this approach was named intensity modulated proton therapy to indicate its similarity with IMRT. IMPT has been pioneered at our institute with the Gantry 1 system, where it has been the only IMPT capable system for over a decade (5).

With scanning, all protons in the pencil beam are stopped in the tumour, hence, scanning provides the best possible efficiency of utilization of the beam. This results in a lower neutron background (10) and a lower activation of

elements in the nozzle and in the whole beam line.

Other points to be more explicitly demonstrated with the new Gantry 2 system are the following:

Planned NUDF, delivered by pencil beam scanning, should be used in the future for providing *biological dose targeting* (dose shaped within the target according the biologically measured distribution of tumour activity).

Scanning is usually delivered without placing individual hardware in the beam line in front of the patient, while scatterers and compensators are needed with scattering. Since the amount of material in the nozzle is almost negligible — Gantry 2 works with variable beam energy instead of a range shifter — in general we expect to have a sharper lateral dose fall-off as with scattering. At low energies (<100 MeV), the use of collimation added on top of conformal scanning is possibly the best solution. Both alternatives, scanning alone for deep seated tumours and scanning in combinations with collimation for shallower depths, are expected to be superior to scattering.

With scanning it should be easier to provide more robust field patching techniques (against inter-field shifts) than with scattering by adding adjacent fields with overlapping smooth dose transition regions.

Presently the major disadvantage of scanning is its specific sensitivity to organ motion; a problem common to any dynamic therapy including IMRT in conventional therapy. This issue was already anticipated in the early 90 s with Gantry 1 (11). Interferences of the motion of the target with the motion of the beam can produce significant dose errors spoiling the homogeneity of the dose distribution within the target. At PSI this is the main reason why we have only been able to treat non-moving target to date (tumours in the head, spinal chord and lower pelvis).

A possible remedy to the organ motion problem of scanning is to realize much faster scanning techniques in order to apply the dose to the target very quickly and as repeatedly as possible (*repainting*), approaching as much as possible the repainting capability of scattering, which is the basis of the success of this technique in the context of organ motion.

Other methods under consideration aim at reducing the extent of organ motion itself by synchronizing dose delivery with a given phase interval of the breathing cycle (*gating*). This approach not only reduces the dose homogeneity errors within the target, but also allows reducing the safety margins at the border of the tumour, at the potential cost of increasing treatment delivery time.

The motion-reduction methods being discussed at PSI are based on scanning in connection with *breath hold* - *gating* - or *tracking* techniques. A very fast scanning technique should in any case help for repainting the target repeatedly within the same daily session with any of these approaches (12).

Although scanning will never reach the same rate of repainting as scattering, it could represent a better approach to image-guided proton therapy, since it can provide a tighter conformation of the dose to the target with a beam delivery method, which can be adapted very quickly to the instant target motion. During beam delivery tumour-motion tracking could be done by shifting the position of the following in real time: spots, whole irradiated energy layers and/or whole irradiated volume.

The new scanning gantry prototype at PSI: Gantry 2

To overcome the limitations of Gantry 1, Gantry 2 was designed with the goal of much faster scanning to support volumetric dose repainting and a smaller spot size to improve the lateral dose fall-off.

Technical specification

A substantial improvement of the beam spot size is achieved by avoiding the use of a range shifter in the nozzle. In Gantry 2 the proton range is controlled by adjusting the beam energy dynamically with the degrader system and the beam line upstream from the gantry. This approach minimizes the material and the associated MCS in the nozzle, but also results in range dependent depth dose profiles. Special care has been taken to make the beam energy changes as fast as possible by using low mass multiple carbon wedges in the degrader and laminated magnets for the beam line. This allows beam energy changes in 80 ms for typical range steps of 5 mm water equivalent.

The scanning speed is dramatically improved over that of Gantry 1 by scanning both lateral axes magnetically. As in Gantry 1, the sweeper magnets are installed upstream from the last bending magnet, which is designed such that the scanned pencil beams are parallel in both directions at the iso-centre over a scanning area of 12×20 cm^2. This upstream parallel scanning (*Figure 2*) not only allows a compact gantry design but also reduces the complexity of therapy planning. This is especially the case for large effective field sizes where multiple scanning areas can be patched together with overlapping regions with smooth dose gradients to render the patching insensitive to target motion.

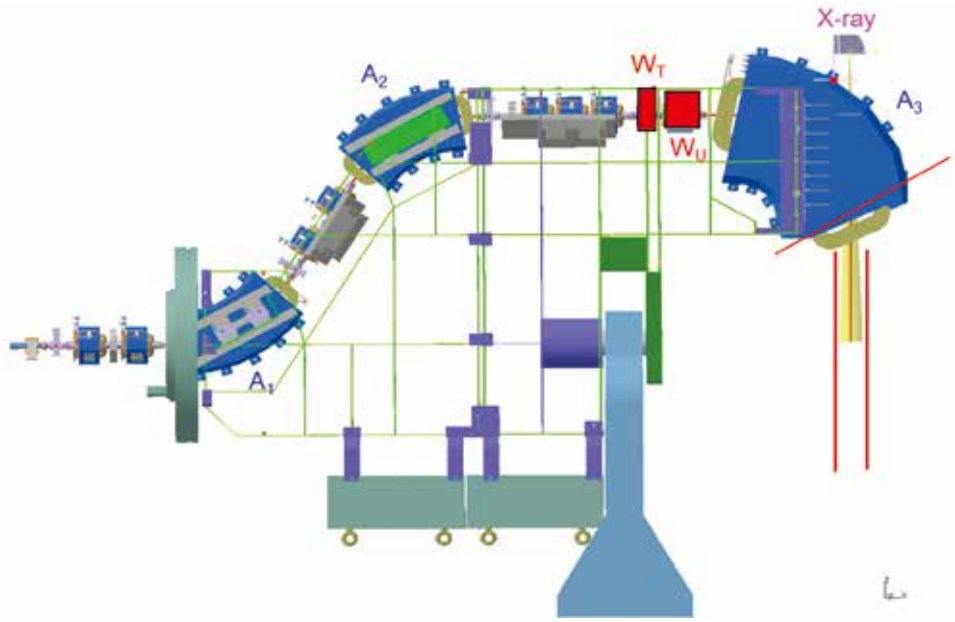

Figure 2 The Gantry 2 beam line with the bending magnets A1 and A2 deflecting the beam away from the gantry rotation axis, the two upstream sweeper magnets W_T and W_U and the final 90° bending magnet A3. Also indicated is the position of the X-ray tube of the Beam's-Eye-View system

The sweeper magnets scan the beam at the iso-centre with a speed of 2 cm/s along one axis (transverse to the magnets, referred to as T-axis) and 0.5 cm/s along the other axis (dispersive direction, referred to as U-axis). The overall dead-time between spots given by setting the sweepers, verifying spot parameters and logging data is 2 ms per 5 mm step. Due to the higher speed of the lateral motion compared to the changes of the range, the dose is applied in iso-energy layers. The faster scanning of Gantry 2 results in a dead-time of 20 s for the 2 Gy 1 litre box single painted spot scanning example compared to the 90 s of Gantry 1 (*Table 1*), which makes moderate volumetric repainting feasible already in the simplest discrete spot scanning mode.

Gantry 2 will start its clinical operation with the discrete spot scanning mode analogous to Gantry 1. However, the goal of Gantry 2 is to demonstrate the potential of new scanning methods by pushing the scanning speed to the physical limits with new delivery techniques like line or contour scanning. From start the control system was designed for highest flexibility in order to support both clinical operation and new research projects, including future developments. It is based on two independent systems: a delivery system which steers the dose application (beam energy, lateral beam position, beam current and dose) and a verification system to measure and verify these critical parameters by independent detectors and diverse methods.

System realization

The mechanical and room layout of Gantry 2

During the conceptual phase particular attention was given to the gantry- and room-layout to allow an effective patient-handling and the installation of modern imaging equipment.

The mechanical layout of Gantry 2 is characterized by a gantry rotation ranging from –30° to 180°. Since the missing degrees can be easily compensated by rotating the patient-table this solution does not compromise the choices of the incident beam angles. The important advantage of this configuration is the integration of a fixed false floor covering the gantry pit (with exception of the rolling cover of the slit where the nozzle rotates) which permits easy access to the patient in every treatment situation (*Figure 3*). The medical-staff can have a direct and close contact with the patient for reassurance or rescue in case of emergency. This layout also simplifies the work of the medical physicists and developers, who can easily install their equipment on top of the patient-table and effectively verify that the equipment is correctly positioned.

We are pleased to observe that this layout has been

Figure 3 Photograph of Gantry 2 treatment room with gantry-angle set to +20°. Visible on the left are the patient-table, the false fixed floor around the patient-table for easy access to the patient, the extractable nozzle, the rolling cover where the nozzle rotates and the BEV. Note that the BEV is extracted with the imager positioned along the proton beam direction just downstream from the patient. Noteworthy on the right is the sliding-CT, with the rails clearly visible on the floor. A white protective film is currently covering the floor and patient-table prior to treatment of first patient

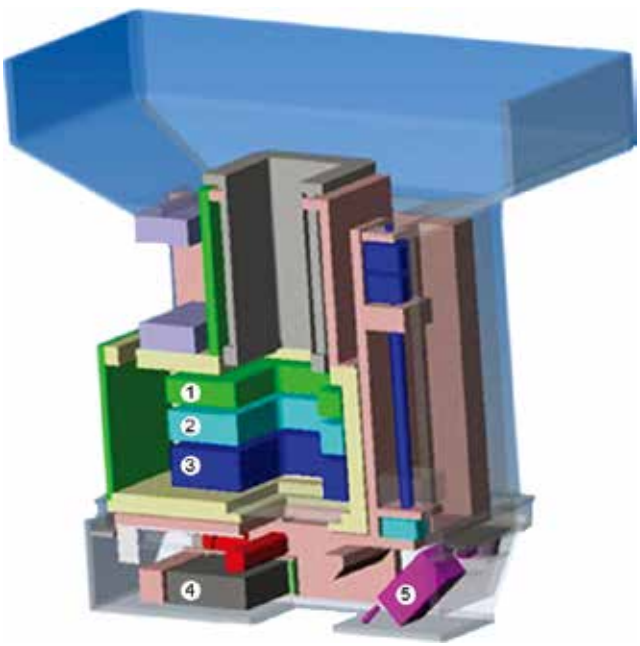

Figure 4 Cross section of the nozzle, containing two dose-monitors [1 and 2] and a strip monitor for beam position detection [3]. Underneath the monitors we have a removable pre-absorber [4], that is used to treat shallow tumours (below 4 g/cm^2), and means for mounting optional collimators and compensators. In addition we have lasers and a visual camera [5] for observing and positioning the patient from within the nozzle

recently adopted by several vendors in the proton therapy field.

The nozzle (*Figure 4*) was specifically designed to improve the precision of the treatment by keeping the pencil beam size as small as possible. The short distance between vacuum window and iso-centre of 86 cm reduces the effect of scattering in air without compromising beam size at low energies. The three monitors in the nozzle (two dose-monitors and one strip chamber for measuring beam position) are fixed to a movable support that can be extracted to reduce the air-gap between nozzle and patient with a range of motion of 27 cm. On the same support, a 2.5 cm thick graphite pre-absorber is mounted just before the nozzle exit-window and can be moved in and out of the beam as desired under remote control. Beam size, and in turn lateral penumbra, can therefore be minimized by extracting the nozzle so to reduce the effect of scattering in the monitors and particularly in the pre-absorber. If required, collimators/apertures can be mounted on the nozzle to improve furthermore the lateral penumbra for shallow tumours. The slim shape of the nozzle additionally helps to reduce the air-gap. All included we have shown that the beam size (sigma) in air can be kept below 5 mm for all energies down to 70 MeV (*Figure 5*).

The mechanical support of the gantry has been designed to be very robust and reliable in order to offer reproducible

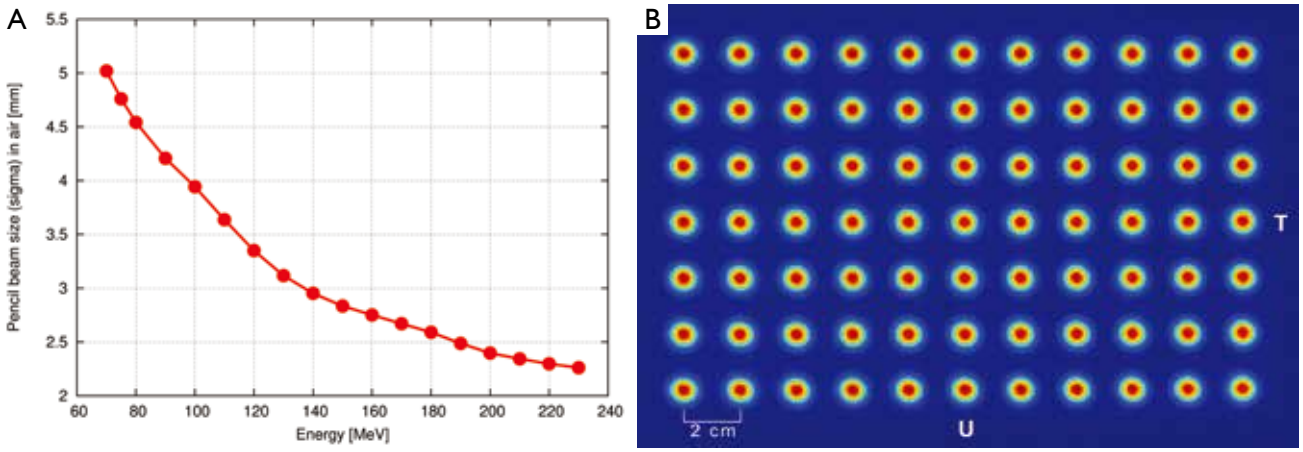

Figure 5 A. Pencil beam size (sigma) as a function of energy in air at iso-centre. Sigma (σ) is related to the full-width-half-maximum (FWHM) as follows, FWHM =2.355σ. B. 150 MeV pencil beams on a scintillating screen at iso-centre for different transversal positions recorded with a CCD-camera

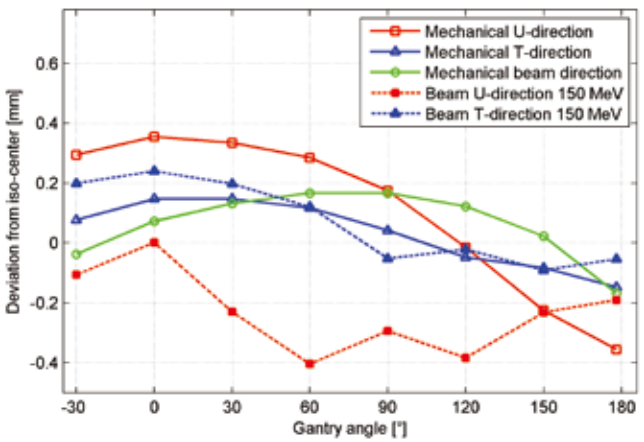

Figure 6 Mechanical deviations from the iso-centre in all three dimensions. The biggest displacements were observed in the U-direction for 0° and 180° due to the weight of the last bending magnet (45 tons). The graph also shows the deviations for the beam position at iso-centre for a 150 MeV beam; note that no angular dependent tuning was necessary to achieve this precision

movements. Therefore, one very important check is to measure the mechanical deformation of the gantry for different gantry angles. Measurements of the deviation from the ideal iso-centre are shown in *Figure 6* and are within a window of 0.8 mm for all angles. This mechanical behaviour is reflected in the achieved accuracy of the measured beam position for different gantry angles. If required the residual position-errors can be further improved with angle-dependent beam tuning corrections. Three fan lasers (LAP lasers) mounted on the walls of the treatment room are aligned to the mechanical iso-centre and to the three room-axes. The mechanics for the extraction of the nozzle has also shown to be very accurate so that additional lasers could be mounted in the nozzle itself and aligned to the room-lasers at iso-centre. Both room- and nozzle-lasers are the main instrument used to position the dosimetric equipment.

The imaging equipment in the treatment room

The large floor surface of over 50 m^2 provides a comfortable working environment making it possible to install an in-room CT for patient setup and verification as shown in *Figure 3*.

The installed Siemens Sensation Open CT-on-Rail has a large bore (82 cm) and a 24/40-slice configuration with 4DCT capability. The particularity of the equipment is that the CT gantry moves on rails while the table stays still during image acquisition. Therefore the same patient table used for proton irradiation can be used for CT acquisition. After positioning, a simple table rotation brings the patient from the CT to the treatment position. If space is not a concern we are convinced that CTs are the best solution for an in-room patient positioning rather than C-arms, cone-beam CTs or orthogonal X-rays. As a matter of fact, besides offering 3D volumetric matching of soft-tissue and bony structures, CT images allow us to perform accurate dose calculations to verify dosimetrically the impact of patient positioning corrections. This is an important advantage compared to cone-beam CTs.

The other innovative imaging approach with Gantry

2 is the installation of a Beam's-Eye-View (BEV) X-ray fluoroscopy system, which will be used to verify patient positioning and is part of a grant study for treating moving-targets. The X-ray tube is mounted on the back of the last bending magnet and X-rays are shined through a hole in the return yoke along the proton direction (*Figure 2*). This realisation was possible only because the last bending magnet has a large gap due to the choice of upstream scanning. The 150 kV X-ray tube can be operated in fluoroscopy mode and the field size at the iso-centre is 20×25 cm^2. The digital flat panel (Varian PaxScan 4020E) is mounted on an extractable support (*Figure 3*). Similar to a portal imaging device on a conventional linac, the BEV can acquire X-ray images synchronised with proton irradiation and provide information of the transversal location of the tumour and the nearby bony structures. This information can be used for image-guided radiation therapy to gate, track, or QA the beam delivery.

Patient-handling and remote control

The control room for both Gantry 2 and the imaging equipment is located outside the treatment room. The aim is to operate all moving components, such as patient-table and gantry-rotation, remotely as well as patient positioning and beam delivery, in order to improve efficiency. To prevent harmful movement under safety regulation the gantry patient positioning system defines virtual walls recognized by the system itself and uses collision plates around the nozzle. In addition, several dome cameras are installed in the room, which can observe the patient under different angles.

Development of advanced scanning technique: preliminary results

Compared to the traditional scattering technique the major disadvantage of the scanning technique is the increased sensitivity to organ motion. Moving the target during the application of individual spots can disturb the homogeneity of the dose distribution. Several mitigation techniques are proposed and discussed e.g., gating, repainting, tracking and breath-hold (13,14).

For us, one of the most promising approaches to tackle organ motion is repainting in combination with - when needed - gating or breath-hold (12). The basic idea of repainting is that the full dose distribution of an irradiation is applied repeatedly in several iterations such that possible interferences of neighbouring spots are statistically smeared out. The dose per spot is reduced according to the number of repaintings in order to get the same final dose distribution.

Thus, one of the preconditions for efficient repainting is to have very fast scanning with minimal dead-time. Most of the dead-time of discrete spot scanning can be avoided by painting the dose continuously along lines, meanders or contours. The most efficient mode should be achieved by painting the dose of a whole energy-layer without interrupting the beam delivery. With the help of the sweeper magnets and a typical line separation of 0.5 cm, a rectangular energy layer of 10×10 cm^2 can be painted in continuous mode as fast as 125 ms at maximum speed. For precise dose painting one can shape the dose by changing the velocity of moving the beam position and/or by changing dynamically the intensity of the beam. These are the major topics which we plan to explore in the future developments of Gantry 2.

In order to provide a full conformal dose distribution it is also necessary to provide a varying proton flux along the scanned lines. For a typical target the proton flux along one line can vary up to a factor of 30.

A vertical deflector plate and several collimators were installed inside the proton accelerator close to the ion source so as to provide a very fast modulation of the beam intensity during scanning. Near the source the protons still have a very low kinetic energy and can thus be quickly deflected with an electrostatic field. Only the fraction of the initial beam emerging from the collimation system is then accelerated. By changing the voltage of the deflector plate it is thus possible to modulate the proton beam current in a reproducible and very fast way on the time scale of 100 µs.

A particular challenge in continuous scanning is the precise control of the dose along painted lines. Since the vertical deflector plate has the shortest latency in the whole system we decided to install a feed-back control loop acting on the vertical deflector and based on the signal of the primary dose monitor right in front of the patient. In this so-called time driven configuration a line scan runs completely deterministic according to a given table containing time, position and intensity data.

It should be remembered that 3D-conformal scanning requires the delivery of non-homogeneous proton fluences within an energy layer.

With Gantry 2 we have two complementary methods of painting non-homogeneous dose lines. Either the scan speed of the sweeper is kept constant and the intensity of the proton beam current follows the shape of the dose

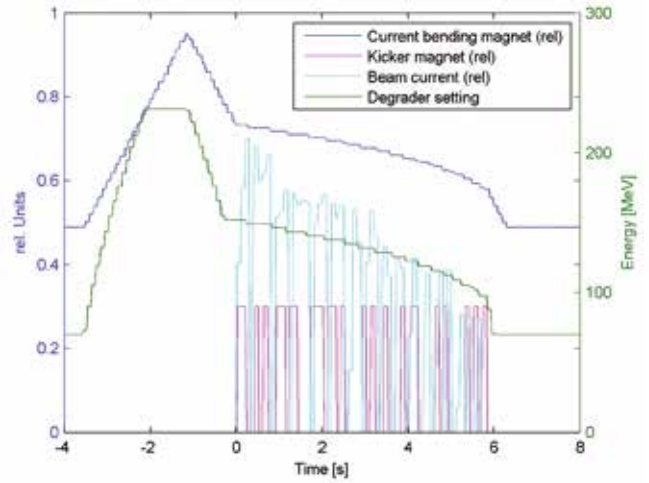

Figure 7 Recorded scan sequence for a spherical target of 0.5 litre using line scanning. The figure shows the current of the largest (90°) dipole, the status of the kicker magnet, extracted beam current (all relative) and the setting of the degrader system. The scan is completed in 6 seconds. The first 3.5 seconds are used to ramp the beam line

profile (intensity modulation), or the speed of the sweeper is modulated and the proton current is kept constant (speed modulation). A combination of those is possible as well.

Speed modulation at maximum beam current is most efficient for reducing treatment time since it works with a fully extracted beam. However critical situations could arise in this mode when portions of the dose line profile must be delivered, which are below the limit given by the maximum velocity of the sweepers.

Intensity modulation at maximum sweeper speed can easily handle very low doses but in turn it is limited by the maximum dose which can be delivered at maximum speed. The limit is given here by the maximal available extracted beam current.

In practice a combination of both modes will be used to get the most flexible and effective scan algorithm. Speed modulation is open-ended for modulating the dose on the high-dose side while intensity modulation better covers the low-dose side.

We intend to develop several repainting strategies. One of the most important characterizations is regarding the detailed sequence of changing the beam energy. For the so-called *layer repainting* mode, iso-energy layers are repeated in sequence without changing the beam energy which is set only once. For the so-called *volumetric repainting* each energy layer is single painted and the whole target volume is repainted several times including intermediate energy changes.

From simulations we feel confident that volumetric repainting brings additional benefits compared to layer repainting (12). However, volumetric repainting can be effectively implemented only if the beam energy can be switched rapidly. Fast energy change has been one of the main requirements for our facility. Due to dedicated power supplies for the magnets, laminated magnets and a fast mechanical degrader system we can provide energy switching times of about 80 ms for typical energy steps of 3 MeV.

Thanks to these fast energy changes we are also able to implement a very fast *uniform scanning* (iso-energy layers with uniform flux). The 3D- dose shaping can be achieved by using individual collimator-compensator pairs mimicking the method used with passive scattering. In an experiment (15), we were able to conformally irradiate a 1 litre target with 1 Gy with 48 repaintings applied on the most distal layer in 30 s and thereby getting closer to the repainting conditions of the scattering technique. The flexibility of the scanning system brings additional advantages, e.g., better proximal conformity to the target volume. We could show that scanning can simulate scattering fairly well including variable modulation of the range. The opposite is not true, since scattering cannot simulate scanning and cannot provide IMPT.

The main focus of the new developments with Gantry 2 remains however the delivery of fast conformal line scanning with volumetric repainting to cope with moving organs. In another experiment, a spherical target of 0.5 litre was irradiated with 0.1 Gy in pure line scanning mode. 18 different proton energies were delivered in sequence. The overall scan was completed within 6 s (*Figure* 7). To get the typical field dose of 1 Gy the whole scan sequence must be repeated 10 times. This is equivalent to 10 volumetric repaintings and would require only 60 s.

The possibility to irradiate the whole target volume within 5-10 s opens the door to the idea of treating small lung nodules as a whole with scanning within a single breath hold, and to repeat the treatment many times on the same daily fraction. This could include image guidance applied to the whole volume. The idea would be to take advantage of the increased scanning speed of Gantry 2 for reducing a complex dynamic treatment into a simple sequence of fully applied static treatments.

Possible clinical indications to be treated with Gantry 2

Static tumours will be treated on Gantry 2 with discrete spot scanning as with Gantry 1, but with improved dose

precision by using smaller pencil beam sizes. The main improvement results from the dynamic variable energy of the beam line of Gantry 2. Brain tumours, head and neck targets and tumours near the spinal cord could particularly benefit from this improvement.

For very superficial tumours we will provide the option to use scanning with added collimation. One could think to use this approach also for eye treatments, e.g., for retinoblastoma and for treating children under anaesthesia in supine position. The use of a gantry in horizontal position with a patient chair coupled to the patient table could then be seen as an alternative of building an extra horizontal beam line dedicated to eye treatments at new proton therapy facilities.

We also expect to be able to treat moving targets with scanning. Moving targets in the trunk will be treated by applying multiple repaintings (tumours in the lower pelvis like rectum, cervix, pancreas - or breast tumours with lymph nodes involvement). Lung and liver could be treated by repeating whole dose volumes painted within a single breath-hold (but gating and tracking could be developed and used as well if necessary).

Very large tumours like medulloblastoma are planned to be treated in one sequence by making use of the remote-controlled patient-table and by taking advantage of the two dimensional parallelism of the scanned beam.

In the end the overall goal is to provide a system which is potentially capable of treating any valid indication for proton therapy with a well-designed basic scanning system with minimal hardware.

Conclusions

Over the years PSI has contributed very substantially to the development of the field of proton therapy by introducing the first conformal proton pencil beam scanning system in the world. In this context we would like to mention the work of our Japanese colleagues in the 80 s with low energy scanning proton beams (16) and the parallel work of GSI with scanning ion beams (17). The first scanning system of PSI has been realized on a very compact gantry (Gantry 1), capable of delivering multiple fields in one go. The experience with this system has been very positive, especially in the context of delivering simultaneous field optimization, i.e., IMPT. Today IMPT is considered a necessary development for being able to compete with IMRT in conventional therapy. As a result of these developments, the whole community and the industrial providers of proton therapy systems are now switching to scanning beams.

There is, however, still a lot of new scanning developments which are potentially worth being done. To this goal we have developed Gantry 2 capable of delivering scanning with a much higher speed and with enhanced capability to adapt the dose delivery to image guidance and to cope also with the motion of internal organs. In this report, we have presented the technical features of the new system and sketched the main ideas for potential clinical applications of scanning. The goal has been to design a system capable of delivering the dose with the highest possible precision for treating essentially any clinical indication including moving targets and for providing biological dose targeting.

The Gantry 2 system has been realized with minimal dose shaping and monitoring equipment in order to have a flexible and fully software-based approach to proton beam delivery. We believe that this technology will render passive scattering obsolete, also in view of the fact that scattering can be replaced with fast highly repainted uniform scanning techniques.

The scope of the Gantry 2 project is to bring, very similarly as with Gantry 1 in the past, a next significant contribution into the future of the field of proton therapy.

Acknowledgements

We would like to thank the entire team of the Center of Proton Therapy of PSI for their engagement.
Disclosure: Some of the ideas presented in this report are protected by patent applications. As a government institution, our institute is not involved in providing commercial systems.

References

1. Pedroni E. Therapy planning System for the SIN Pion Therapy Facility. In: Burger G, Broerse JJ. eds. Treatment planning for external beam therapy with Neutrons. Munich: Urban & Schwarzenberg, 1981:60-9.
2. Pedroni E, Bacher R, Blattmann H, et al. The 200-MeV proton therapy project at the Paul Scherrer Institute: conceptual design and practical realization. Med Phys 1995;22:37-53.
3. Pedroni E, Bearpark R, Böhringer T, et al. The PSI Gantry 2: a second generation proton scanning gantry. Z Med Phys 2004;14:25-34.
4. Pedroni E, Meer D, Bula C, et al. Pencil beam

characteristics of the next-generation proton scanning gantry of PSI: design issues and initial commissioning Results. Eur Phys J Plus 2011;126:66.
5. Lomax AJ, Boehringer T, Coray A, et al. Intensity modulated proton therapy: a clinical example. Med Phys 2001;28:317-24.
6. Schippers JM, Dölling R, Duppich J, et al. The SC cyclotron and beam lines of PSI's new protontherapy facility PROSCAN. Nucl Instr Meth B 2007;261:773-6.
7. Lomax AJ, Böhringer T, Bolsi A, et al. Treatment planning and verification of proton therapy using spot scanning: initial experiences. Med Phys 2004;31:3150-7.
8. Pedroni E, Scheib S, Böhringer T, et al. Experimental characterization and physical modelling of the dose distribution of scanned proton pencil beams. Phys Med Biol 2005;50:541-61.
9. Lomax AJ. Intensity Modulated Proton Therapy. In: Delaney T, H Kooy H. eds. Proton and charged particle radiotherapy. Boston: Lippincott, Williams and Wilkins, 2008.
10. Schneider U, Agosteo S, Pedroni E, et al. Secondary neutron dose during proton therapy using spot scanning. Int J Radiat Oncol Biol Phys 2002;53:244-51.
11. Phillips MH, Pedroni E, Blattmann H, et al. Effects of respiratory motion on dose uniformity with a charged particle scanning method. Phys Med Biol 1992;37:223-34.
12. Zenklusen SM, Pedroni E, Meer D. A study on repainting strategies for treating moderately moving targets with proton pencil beam scanning at the new Gantry 2 at PSI. Phys Med Biol 2010;55:5103-21.
13. Knopf A, Bert C, Heath E, et al. Special report: workshop on 4D-treatment planning in actively scanned particle therapy--recommendations, technical challenges, and future research directions. Med Phys 2010;37:4608-14.
14. Rietzel E, Bert C. Respiratory motion management in particle therapy. Med Phys 2010;37:449-60.
15. Zenklusen SM, Pedroni E, Meer D, et al. Preliminary investigations for the option to use fast uniform scanning with compensators on a gantry designed for IMPT. Med Phys 2011;38:5208-16.
16. Kawachi K, Kanai T, Matsuzawa H, et al. Three dimensional spot beam scanning method for proton conformation radiation therapy. Acta Radiol Suppl 1983;364:81-8.
17. Haberer T, Becher W, Schardt D, et al. Magnetic scanning system for heavy ion therapy. Nucl Instrum Methods Phys Res 1993;330:296-305.

Cite this article as: Safai S, Bula C, Meer D, Pedroni E. Improving the precision and performance of proton pencil beam scanning. Transl Cancer Res 2012;1(3):196-206. DOI: 10.3978/j.issn.2218-676X.2012.10.08

Review Article

Proton therapy dose calculations on GPU: advances and challenges

Xun Jia[1,2,3], Todd Pawlicki[1,2,3], Kevin T. Murphy[3], Arno J. Mundt[1,3]

[1]Center for Advanced Radiotherapy Technologies, [2]Division of Medical Physics and Technology, [3]Department of Radiation Medicine and Applied Sciences, University of California San Diego, La Jolla, CA 92037, USA

Correspondence to: Xun Jia. Center for Advanced Radiotherapy Technologies, University of California San Diego, La Jolla, CA 92037, USA. Email: xunjia@ucsd.edu.

DOI: 10.3978/j.issn.2218-676X.2012.10.03

Scan to your mobile device or view this article at: http://www.thetcr.org/article/view/582/html

Proton therapy can allow higher dose conformality compared to conventional radiation therapy. Radiation dose calculation has an integral role in the success of proton radiotherapy. An ideal dose calculation method should be both accurate and efficient. Over the years, a number of dose calculation methods have been developed. To overcome the high computational burden of these algorithms, or to further speed them up for advanced applications, e.g., inverse treatment planning, graphics processing units (GPUs) have recently been employed to accelerate the proton dose calculation process. In this paper, we will review a set of available GPU-based proton dose calculation algorithms including a pencil-beam method, a simplified Monte Carlo (MC) simulation method, a track-repeating MC method, and a full MC simulation method. The advantages and limitations of these methods will be discussed. We will also propose a dose calculation method via solving the Boltzmann transport equations, which is expected to be of the same level of accuracy as a MC method but could be more efficient on GPU.

Introduction

Cancer radiation therapy aims at delivering a prescribed radiation dose to cancerous targets, while sparing the surrounding organs at risk and normal tissues by conventional high-energy X-ray beams or by particle beams such as protons. A proton beam, due to its unique way of depositing dose, has clinical advantages over X-ray beams. As a proton beam travels through a patient, it forms a sharp maximum, the Bragg peak (1,2), at the end of its range as a result of the phenomenon that the energy deposition increases with penetration depth. One can control the peak location by varying the beam energy, and then assemble a set of peaks to form a plateau called Spread-Out Bragg Peak (SOBP). Favorable dose distributions with a relatively homogeneous region and steep dose fall-offs can therefore be easily achieved, resulting in greater dose localization than can be produced by conventional photon beams. Hence, dose escalation can be performed while mitigating radiation toxicity in surrounding normal tissues.

Dose calculation plays a critical role in a proton therapy treatment. Generally speaking, a clinically desirable dose engine should attain the following features. First, it has to be accurate. The sharp dose fall-off at the distal end of a proton beam makes the dose distribution extremely sensitive to dose calculation error. Inaccuracies in the calculations of proton penetration can easily shift the SOBP, which leads to under coverage of the target and over dose to surrounding health tissues. It has been reported that the proton range uncertainty due to dose calculation methods alone is about 2-3%. This estimated error excludes uncertainties in other practical issues encountered in dose calculation such as CT image calibration and conversion to tissue properties. Efficiency is another crucial requirement for proton dose calculation. In the time-critical clinical environment, not only does a fast dose engine ensure a smooth workflow, but also it offers planners opportunities to fine tune treatment parameters to select the most beneficial set of parameters for each individual patient. Efficient and accurate dose calculations have become even more critical lately in those novel technologies where repeated dose calculations are necessary, for instance, in intensity-modulated proton therapy (3,4) and 4D treatment planning (5,6).

Yet, it is quite difficult, if not impossible, to develop dose calculation techniques that meet both of these two requirements. In practice, it usually means prolonged computation time, if one prefers a highly accurate dose calculation result. One example is the Monte Carlo (MC) simulation method, where the accuracy is ensured by faithful simulation of particle transport. The computation time required to attain a level of acceptable accuracy prohibits its applications in clinical practice. It has been reported that it takes a few hours to compute the dose for a patient with 2.5% relative uncertainty using the MC method on a typical computer (7). In another calculation approach where computation time is also critical, pencil beam (PB) models can be used in conjunction with empirical data tables (8-10). The accuracy of PB methods is, however, compromised by the simplifying assumptions built into them. To date, there is no dose calculation engine that attains the accuracy and speed required for the clinical setting. Hence, despite the apparent advantages of proton therapy, its potential is highly limited by unsatisfactory dose calculation algorithms, potentially making the treatment delivered to patients suboptimal.

One practical approach to achieve the combined accuracy and efficiency is to utilize more powerful computational hardware. Recently, the development of general-purpose graphics processing unit (GPU) hardware and software has been rapidly progressing for the purposes of massively parallel scientific computing, resulting in enormous, affordable, and readily accessible computational power that are particularly suitable for routine clinical uses. Specific to dose calculation problems in radiotherapy, GPU has been utilized to speed up pencil-beam algorithms (11,12), superposition-convolution algorithms (13,14), and MC simulations (15-22). With these efforts, the calculation time of MC-based proton dose calculation has been greatly shortened. This also indicates that it is affordable to consider more complex physics in the dose calculation process, resulting in considerably enhanced calculation accuracy, especially in cases with complicated geometry and large heterogeneities.

In this paper, we will review a set of current state-of-the-art GPU-based dose calculation methods with emphases on their implementations, current status, and potential improvements. A promising algorithm based on the Boltzmann transport equation will also be proposed. The rest of this paper is organized as follows: Section 2 will give a brief introduction about GPUs and Section 3 will discuss three groups of GPU-based dose calculation algorithms, Section 4 will conclude the paper with discussions.

Graphics processing unit

A graphics processing unit (GPU) is a specialized hardware in a computer system designed to accelerate the processing of graphics information. In a modern desktop workstation, it is usually in the form of a separate card plugged onto the motherboard. The advantages of a GPU over a conventional computational hardware, e.g., central processing unit (CPU), come from its large number of processing units. For instance, an NVIDIA Tesla C2050 GPU that is manufactured specifically for scientific computing purposes contains 448 thread processors. Although the clock speed of each of them is relatively lower than that of a CPU, the combined processing power of them is over 1 Tflops, much larger than what can be achieved by a CPU. All of these GPU threads share the use of a common piece of memory space called global memory, and some of them are grouped together, share the so-called shared memory, which offers a much higher speed than the global memory. *Figure 1* depicts the structure of a typical computer workstation with a GPU installed.

GPU follows a SIMD (single instruction multiple data) (23) design in its execution scheme. As such, a GPU executes a program in groups of 32 parallel threads termed *warps*. If the paths for threads within a warp diverge due to, *e.g.*, some *if-else* statements, the warp serially executes one thread at a time, while putting all other threads in an idle state. Thus, high computation efficiency is only achieved when all threads in a warp process together along a same execution path. Under this structure, some operations are essentially GPU-friendly while others are not. An example in this category include vector and matrix operations, as different GPU thread can process different matrix entries in the same operational fashion but with different data. It is for this reason that pencil-beam based dose calculation algorithms are suitable for GPU, as the calculation algorithms can be mathematically formulated as matrix-vector operations. In contrast, it is quite difficult to achieve high speed-up factors for MC dose calculations on a GPU, because the work paths on different threads are statistically independent and can be very different in an MC calculation.

Proton dose calculations on GPU

Pencil-beam method

Pencil-beam dose calculation algorithm for proton therapy

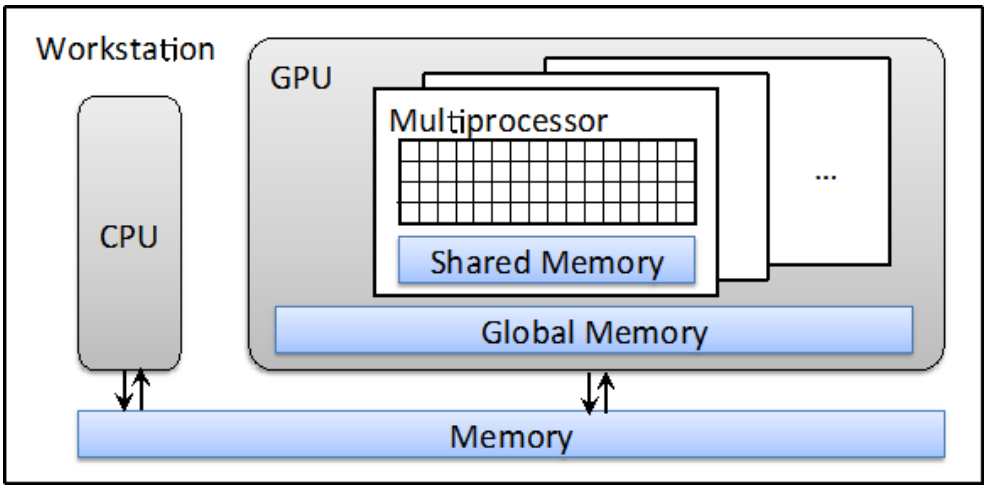

Figure 1 Illustration of the structure of a computer workstation that contains a GPU

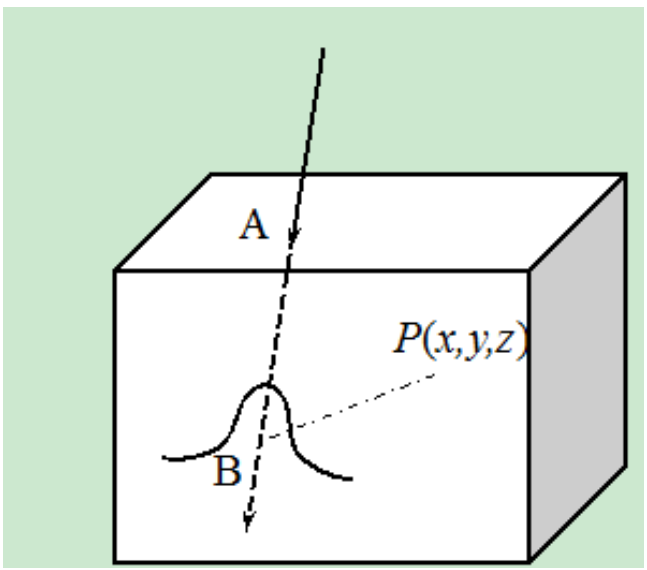

Figure 2 Illustration of the pencil-beam algorithm

has a long history (8-10,12). Because of its simplicity of calculation scheme and acceptable accuracy in most clinical settings, this method has been widely utilized in routine clinical applications for treatment planning purposes. The dose calculation algorithm starts from the assumption regarding the dose distribution of a pencil-beam. Take a commonly used Gaussian function kernel as an example; for a pencil-beam irradiated along the axis, the dose deposited at the point (x, y, z) can be written as

$$K(x,y,z) = p(d_{eff})\left(\frac{SSD+d_{eff}}{z}\right)^2 G(x,y,z), \quad [1]$$

where $p(d_{eff})$ is the depth dose distribution of a pencil-beam, which is usually determined from experiments in a water medium and d_{eff} is the water-equivalent length from the phantom surface A to the point B on the pencil-beam axis, see *Figure 2*. The second term corresponds to the inverse square correction, while the third one describes the dose spread out inside the plane perpendicular to the z axis and is empirically taken as a Gaussian function in this model

$$G(x,y,z) = \frac{1}{2\pi\sigma(z)}\exp[-\frac{x^2+y^2}{2\sigma^2(z)}]. \quad [2]$$

Note that the amount of beam spread is characterized by the quantity $\sigma(z)$, which is an increasing function of the depth z. Physically, this spread is due to the lateral scattering during the proton propagation. In practice, an empirical function form is usually employed which combines the contributions from two sources, namely the proton beam nozzle and the patient (9). Finally, with the dose deposition for a single proton beam given in Eq. [1], the dose distribution for a broad beam can be expressed as a summation over all the pencil-beams as

$$d(x,y,z) = \iint_{\Sigma} dx'dy'T(x',y')\,K(x-x',y-y',z), \quad [3]$$

where $T(x,y)$ parameterizes the pencil-beam intensity and the integral is carried out over an area Σ on which all the pencil beams pass through.

The computations can be decomposed into the following/g steps. First, a broad beam is divided into a set of pencil beams and ray-tracing calculation is performed along the central axis of each pencil beam to determine the water equivalent depth d_{eff}. Next, for each voxel, the dose is equal to the summation over the contributions from all the pencil beams, which can be easily evaluated by using Eq. [1]. In this step, the corresponding quantities such as $p(d_{eff})$ and $\sigma(z)$ are determined based on available data tables. It is straightforward to parallelize both of these two steps. The first one can be parallelized with each GPU thread responsible for a pencil beam, while the second step is accomplished by assigning each voxel to a thread. Because of the largely available number of GPU thread processors, the computational efficiency is extremely high for this method. For instance, it has been reported that the computational time is less than 1 second for most of the cases tested (12) on an NVIDIA Geforce GTX 480 GPU.

Apart from the apparent advantages of computational efficiency of this pencil-beam approach, it also provides dose distributions from each single pencil beam. Such important information is of critical importance for many clinical applications such as intensity-modulated proton therapy, where the intensity of each pencil beam is optimized to yield a desired dose distribution. It is for these reasons that pencil beam algorithms are currently widely employed in routine clinic for proton therapy treatment planning.

Yet, it should be noted that this method is only a temporary solution for proton dose calculation due to its questionable accuracy in some cases. In fact, the Eq. [3] is only a phenomenological description about how dose is deposited to the patient, and the physics of proton transport is missing here. In some cases with complicated geometry and/or large amount of tissue heterogeneity, the accuracy of this method could be significantly reduced. Even though a variety of pencil-beam models have been proposed over the years, it has been pointed out that no single pencil-beam model can result in correct dose in every situation (24). Another limiting factor of this model is the associated difficulties in commissioning, where the empirical data $p(d_{eff})$ and $\sigma(z)$ must be determined. In a typical approach, this commissioning step is treated as an optimization problem in which these data are determined by numerical algorithms so that the calculated dose matches measurements in some simple cases, *e.g.* water. This is a very tedious task, as $\sigma(z)$ goes to the denominator in an exponential term in Eq. [2] and a highly nonlinear system needs to be solved.

Monte Carlo method

Monte Carlo (MC) simulation is commonly regarded as the most accurate method for radiotherapy dose calculation due to its capability of faithfully transporting a particle according to the underlying physics and modeling the patient geometry and material properties. It has been demonstrated that the use of MC in proton therapy could lead to a significant reduction in treatment planning margins (25). As a statistical method, the precision of an MC dose calculation is governed by the total number of particles simulated and an enormously large number of particles are usually required. Hence, despite the great efforts devoted to accelerating the MC dose calculation process, such as using large-scale computational hardware and developing simplified algorithms (26-29), this method is still mainly applied for re-calculating existing treatment plans for research studies or for secondary dosimetric calculations that are not time sensitive. The unsatisfactory efficiency also impedes the progresses of advanced treatment techniques in proton therapy, such as MC-based treatment planning and adaptive proton radiotherapy. Recently, with the aim of increasing the efficiency of MC dose calculations, a number of research groups have developed a few packages on GPU. Here, three representative types of GPU-based MC methods will be discussed.

Simplified Monte Carlo simulation

The first approach to alleviate the high computational burden in a MC simulation is to employ some simplified physics. Motivited by this idea, Kohno *et al.* (27) developed a simplified MC method (SMC) for proton dose calculations. It was later implemented it on a GPU platform (19) and used for treatment planning. The SMC method begins by setting each individual proton with a location, a velocity direction, and a residual range in water. Once the transport starts, the proton travels through the voxelized geometry. At each voxel, there are two effects modeled. First, the proton's residual range is reduced according to the local material property and a corresponding amount of energy is deposited to the voxel, which is determined by a water equivalent model (30) based on the measured depth-dose distribution in water. Second, multiple Coulomb scattering of the proton is modeled, where the scattered angles are sampled from a normal distribution with a standard deviation given by Highland formula (31). This model contains a much simplified proton transport physics compared to what happens in reality. For example, as opposed to determining

dose deposition at each voxel according the actual physical interaction process, it is determined using the measured depth-dose distribution in water. This is essentially an effective model, as those real interactions occurring locally at the voxel are phenomenologically described and the net effect in terms of dose deposition is captured. This avoidance of sampling detailed interaction processes preserves the accuracy to an acceptable extent while greatly simplifies the model and increases the efficiency.

In terms of GPU implementation, this SMC algorithm is compatible with GPU's SIMD structure. This is because the proton transport process described above can be carried out by each GPU thread independently, where all of the threads repeated perform the same instructions but using different data according the current proton status. Moreover, high speed shared memory is utilized in the implementation. In terms of the achieved efficiency, a speed-up factor of 12-16 compared to CPU implementation has been observed in real clinical cases. Regarding the absolute dose calculation time, it was found that with 9-67 seconds, one can attain a clinically acceptable uncertainty on an NVIDIA Tesla C2050 GPU.

Track-repeating Monte Carlo simulation

Track-repeating is a variance technique utilized in MC simulations for dose calculations. In the context of proton transport, this technique was first utilized by Li *et al.* (26) and then recently implemented on a GPU platform (18,28). In this method, a database of proton transport histories is first generated in a homogeneous water phantom using an accurate MC code such as GEANT4 (32). Each particle trajectory consists of a set of steps, and for each step, the direction, step length, and energy loss are stored. The computational load for this step is not a practical issue, as this database preparation step is only performed once and the generated database will be repeated used later on. For a patient case, the track-repeating MC calculates dose distributions by repeating appropriate proton tracks in the database. As such, it first generates a proton at the surface of the phantom and selects a track in the database corresponding to this proton. The proton is then transported as if it follows this assigned track inside the patient. The underlying assumption is that the random numbers generated while transporting this proton are identical to what occurred when generating the track in the database, and hence leading to an identical trajectory. To account for the tissue heterogeneity of the patient, each step length and the scattering angle within this track is scaled according to the local properties of the non-water medium. The dose depositions recorded for the steps are added to the corresponding voxels.

This method is computationally efficient for two reasons. Regarding the transport process, it avoids the sampling of physical interactions on the fly. Hence, the majority of the computational burden in a MC simulation is eliminated. Yet, as the tracks are pre-generated by an accurate MC simulation, this simplification does not result in a significant degradation of dose calculation accuracy. In validation studies (14,24), it was discovered that the dosimetric results of this method agree with those from a full MC simulation using GEANT4 within 1% discrepancy. Second, regarding its advantages in the GPU context, this method is quite GPU-friendly. Each GPU thread essentially performs the same operations at all the time. Therefore, the full GPU power can be employed, leading to a high computational efficiency. The aforementioned 1% accuracy can be accomplished in less than 1 minute with a dual GPU system equipped with Geforce GTX 295 GPUs. A speedup of a factor of 75.5 with respect to the same CPU-based implementation has been reported.

Full Monte Carlo simulation

The accuracies achieved in the two MC codes discussed in Sections 3.2.1 and 3.2.2 is found to be sufficient for clinical applications in most of the cases. Yet, in those cases with unique situations of heterogeneity, a full MC simulation is still desired. Examples include those places where charge particle disequilibrium occurs or at interfaces between two mediums with quite distinct properties. It is challenging to develop a full MC dose calculation package for proton therapy on GPU. First, protons interact with human tissue through various types of interactions, but not all of them are necessary for dose calculations. Careful investigations with respect to how much detail one should include in the simulations are needed in order to balance accuracy and efficiency. Second, from the computational point of view, the inherent conflict between the GPU's SIMD processing scheme and the stochastic nature of a MC process poses a big challenge (16,17,33).

Only until recently has a full MC simulation package, gPMC, been developed for proton dose calculation on GPU (20). The distinction between this package and the above-mentioned packages is that it tracks a proton according to the realistic physical process on the fly. Specifically, proton propagation is modeled by a Class II condensed history simulation scheme using the continuous slowing

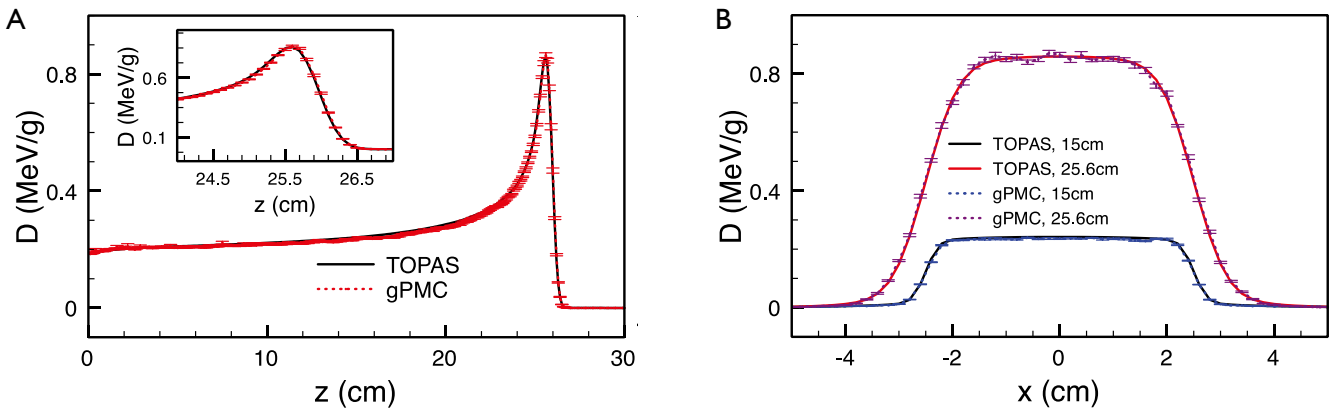

Figure 3 Depth dose curves (A) and lateral profiles (B) for a water phantom with a 200 MeV source, respectively. Inserts are zoomed-in views of the depth curves near the Bragg peak

down approximation. The proton is transported in a step-by-step fashion until its energy is below a user-defined cut-off energy or it exits the phantom region, where each step terminates at an interaction point, a voxel boundary, or a upper bound set by the user. Ionization, elastic, and inelastic proton nucleus interactions are considered. Energy straggling and multiple scattering are also modeled. As for nuclear interactions, gPMC follows an empirical strategy invented by Fippel and Soukup (29). Only proton-proton elastic interactions, proton-oxygen elastic, and inelastic interactions are included. The secondary protons generated in the proton-proton elastic interactions and in the proton-oxygen inelastic interactions are tracked by the same proton transport physics mentioned above. All other heavy charged particles are terminated and their energies are locally deposited. Charge-neutral particles produced in the proton-oxygen inelastic events are simply neglected.

gPMC performs dose calculations in a batched fashion. In each batch, a certain number of source protons and the produced secondary protons are transported and dose depositions are recorded. The results from different batches are then analyzed statistically to obtain the average dose to each voxel and the corresponding uncertainties. To further ensure the computational efficiency, a high-performance pseudo-random number generator CURAND developed by NVIDIA is utilized, which offers simple and efficient generation of high-quality pseudo-random numbers using the XORWOW algorithm. GPU texture memory is also employed to support hardware-based interpolation on the cross section and stopping power data.

The success of gPMC has been established by comparing the dose calculation results with those from TOPAS/Geant4 (34), a golden standard MC simulation package. For a set of cases ranging from homogeneous and inhomogeneous phantoms to a patient case, sufficient agreements between gPMC and TOPAS/Geant4 are observed. Specifically, gamma passing rate for a 2%/2 mm criterion is over 98.7% in the region with dose greater than 10% maximum dose in all cases. A comparison of the dose distributions computed by the two algorithms is shown in *Figure 3*. With respect to the efficiency, it takes only 6-22 sec to simulate 10 million source protons to yield ~1% relative statistical uncertainty on an NVIDIA C2050 GPU card, depending on the phantoms and the energy. This is an extremely high efficiency compared to the computational time of tens of CPU hours for TOPAS/Geant4.

One interesting issue discussed by Jia *et al.* is that there exists a memory writing conflict problem when using GPU for MC dose calculations (20). Because of the shared-memory programming mode of a GPU, a single dose counter allocated in the GPU's global memory is responsible for recording the dose information deduced by all GPU threads. When two threads happen to deposit dose information to a voxel at the same time, a memory writing conflict occurs and the energy deposition has to be serialized in order to obtain correct results. In practice, gPMC uses an atomic float addition function to serialize the dose addition. This function is called atomic in that, once a GPU thread is writing to a memory address, it takes the full control and no other threads can interfere with this process. However, this serialization apparently counteracts the available parallel processing power of a GPU. A higher frequency of conflict occurrences indicates a greater reduction of the overall efficiency. Even though

this memory writing conflict occurs also in x-ray beam dose calculations (15,16), it is, exacerbated in the context of proton beams. This is because protons travel almost along a straight line and a parading column of protons in a beam, especially in a small-size beam, marches in almost locked step with each other leading to a high possibility of memory writing conflicts. To date, there is no practical solution to this problem and careful investigations on this issue are needed.

Boltzmann transport

An alternative for proton dose calculations is to deterministically solve the Boltzmann transport equation (BTE) (35,36), which describes particle transport by a partial-differential-integral-equation formulated in phase space. It has been demonstrated that deterministic methods can compete with MC in terms of accuracy (37) as the latter is essentially a way of solving the BTE by statistical methods. Because of the absence of random fluctuations, the deterministic approach is well suited for evaluating small dose variations in a typical treatment. Moreover, this approach leverages the use of mature numerical algorithms ensuring both accuracy and efficiency. In the past, dose calculation packages via this deterministic approach for conventional high-energy photon therapy have been developed and applied in routine clinical practice (35,38-40). Its acceptance as an integral part of photon therapy clearly indicates its potential in proton therapy. Yet, the use of BTE for proton dose calculation is still under investigation. In the following we outline the use of BTE in proton dose calculations.

Let us consider a bounded region X, which contains a voxelized patient anatomy. The proton dose calculation problem is to compute the radiation dose deposited into each voxel under a proton beam configuration defined in a treatment plan. The beam configuration is characterized by the proton fluence at the boundary ∂X.. Let us further denote a proton fluence at location x with unit velocity direction Ω and energy E as $\psi(E,\Omega,x)$. Under the continuous slowing down approximation, the steady state BTE that administers the proton fluence ψ can be expressed as (41,42)

$$\begin{aligned} &\Omega \cdot \nabla\psi(E,\Omega,x) + \sigma(E,x)\psi = Q^{Sca}(E,\Omega,x) + \frac{\partial S(E,x)\psi}{\partial E}, \\ &\psi(E,\Omega,x) = \overline{\psi}(E,\Omega), n\cdot\Omega < 0, x \in \partial X, \end{aligned} \quad [4]$$

where $\overline{\psi}(E,\Omega)$, the Dirichlet condition of ψ on the inflow surface, is the specification of the proton fluence at the boundary ∂X, and n is the unit normal of the boundary surface. $S(E,x)$ and $\sigma(E,x)$ are the total stopping power and total cross section in the medium at x at energy E, respectively. The scattering term $Q^{Sca}(E,\Omega,x)$ is given by

$$Q^{Sca}(E,\Omega,x) = \int_0^\infty \mathrm{d}E' \int_{\Omega'\in S^2} d\Omega'\ \sigma(E,E';\Omega\cdot\Omega';x)\psi(E',\Omega',x), \quad [5]$$

where $\sigma(E,E';\Omega\cdot\Omega';x)$ is the differential cross section for the medium at x. Once the BTE is solved for ψ, a radiological quantity of interest such as dose at location x can be obtained by:

$$D(x) = \frac{1}{\rho(x)}\int_0^\infty \mathrm{d}E \int_{\Omega\in S^2} d\Omega\ \sigma_p(E,x)\psi(E,\Omega,x). \quad [6]$$

Here, $\sigma_p(E,x)$ is the cross section corresponding to the quantity of interest and $\rho(x)$ is the density.

The total cross section $\sigma(E,x)$ is the sum of all the cross sections for all interactions considered. In the energy range up to a few hundred MeV for proton therapy, ionizing collisions are the most important interactions in this model. Although nuclear reactions are significant for a typical clinical proton beam, a nuclear reaction of a proton within a material can be approximately treated as if the reaction was with water, as human tissue is approximately water-equivalent. Therefore, only proton-proton elastic scattering, proton-oxygen elastic scattering and proton-oxygen scattering are needed.

The BTE in [4] is too complicated to have a closed-form analytical solution. Yet, it is possible to solve it numerically. A typical approach is to employ the so called multi-group discretization of E and the discrete-ordinate discretization of Ω, yielding:

$$\begin{aligned} &\Omega_d \cdot \nabla\psi_{g,d}(x) + \sigma_g(x)\psi_{g,d}(x) = Q^{Sca}_{g,d}(x) + \frac{S_{g+1.2}\psi_{g+1,d} - S_{g-1/2}\psi_{g,d}}{\Delta E_g} \\ &\psi_{g,d}(x) = \overline{\psi}_{g,d'}, n\cdot\Omega_d < 0, x \in \partial X. \end{aligned} \quad [7]$$

where the indices d and g are used to label the descritized angular direction Ω and energy E, respectively. A forward finite difference scheme can be used to approximate the stopping power term $\partial(S\psi)/\partial E$, which is mathematically proven to be numerically stable. A further discretization of the spatial derivatives of ∇ using, *e.g.*, Diamond-Difference method (43) will result in a set of coupled linear equations. These equations can be solved via iterative approaches (44). Radiation dose will be computed using a discretized version of Eq. [6], once $\psi_{g,d}(x)$ is available.

Numerically solving the BTE on a GPU could be

extremely efficient. Not only are the matrix-vector operations within a BTE solver particularly favored by the GPU's SIMD processing scheme, it also avoids the memory conflict issue encountered in GPU-based MC simulations. This method combines the accuracy advantage of a MC method and avoids its limitations. Hence, it is very promising to develop a dose calculation engine via this approach with clinically desired features. Further investigations along this road are currently in progress.

Discussion and conclusions

In this paper, we have reviewed a set of currently available GPU-based dose calculation algorithms for proton therapy. For pencil-beam type algorithms, although an extremely high efficiency can be achieved on GPU, the unsatisfactory accuracy, especially in some complicated clinical cases, becomes a significant concern. With the continuous growth of computational power and developments of new algorithms, the pencil-beam algorithms may be gradually replaced. Among those MC simulation methods, the full MC one attains a well guaranteed accuracy, while its efficiency is limited to a certain extent due to the inherent conflict between the GPU SIMD structure and the MC randomness, as well as the memory writing conflict issue. On the other hand, even though the simplified MC or the track-repeating MC reduces the computational weight significantly, the gain in terms of absolute computation time is not particularly attractive (not to mention the potential degradation of precision). Finally, a new dose calculation method via solving the Boltzmann transport equation is presented. With all the relevant physics included in this model and the underlying matrix-vector operations in the numerical computation that are suitable for GPU parallel processing, it is promising for this method to achieve a combined accuracy and efficiency.

Despite the achieved efficiency so far, a few research directions could also be explored in near future to further accelerate proton dose calculations. These efforts will contribute significantly towards realizing some advanced proton therapy treatment techniques that are currently limited by the computational speed. From the hardware point of view, it is always possible to keep enhancing the efficiency with faster GPUs. For example, the recently available next generation NVIDIA GPUs in the Kepler family delivers almost three times higher peak processing powers than previous GPUs. Moreover, if a multi-GPU platform is available, many of the aforementioned methods can be further parallelized among GPUs. Especially for MC simulations, all the particle histories can be simply distributed among GPUs, which then execute simultaneously without interfering with each other. Due to the negligible overhead in this process, it is expected that a roughly linear scalability of the computation efficiency can be achieved with respect to the number of GPUs. In a recently work, it has been reported that this linear scalability holds at least on a quad-GPU system (16). Another direction worth exploring is to develop new algorithms. Algorithm-based acceleration is usually much more efficient in terms of boosting processing speed than hardware based acceleration. Nonetheless, the intellectual difficulty is large and will require a series of novel inventions. Especially in the GPU context; it is an interesting, difficult, and important research topic to design GPU-suitable algorithms.

In retrospect, GPU has been applied for proton dose calculations for only a few years. The tremendous achievements to date have already opened a new door to allow much advanced dose calculation techniques. It is reasonable to believe that with continuous efforts on this research topic more and more developments will soon become available that will inevitably contribute to this field and benefit patients under proton therapy treatments.

Acknowledgements

This work is supported in part by the University of California Lab Fees Research Program.
Disclosure: The authors declare no conflict of interest.

References

1. Miller DW. A review of proton beam radiation therapy. Med Phys 1995;22:1943-54.
2. Bonnett DE. Current developments in proton therapy: a review. Phys Med Biol 1993;38:1371-92.
3. Lomax AJ, Boehringer T, Coray A, et al. Intensity modulated proton therapy: a clinical example. Med Phys 2001;28:317-24.
4. Oelfke U, Bortfeld T. Inverse planning for photon and proton beams. Med Dosim 2001;26:113-24.
5. Paganetti H, Jiang H, Trofimov A. 4D Monte Carlo simulation of proton beam scanning: modelling of variations in time and space to study the interplay between scanning pattern and time-dependent patient geometry. Phys Med Biol 2005;50:983-90.

6. Kang Y, Zhang X, Chang JY, et al. 4D Proton treatment planning strategy for mobile lung tumors. Int J Radiat Oncol Biol Phys 2007;67:906-14.
7. Paganetti H, Jiang H, Parodi K, et al. Clinical implementation of full Monte Carlo dose calculation in proton beam therapy. Phys Med Biol 2008;53:4825-53.
8. Petti PL. Differential-pencil-beam dose calculations for charged particles. Med Phys 1992;19:137-49.
9. Lee M, Nahum AE, Webb S. An empirical method to build up a model of proton dose distribution for a radiotherapy treatment planning package. Phys Med Biol 1993;38:989-98.
10. Szymanowski H, Oelfke U. Two-dimensional pencil beam scaling: an improved proton dose algorithm for heterogeneous media. Phys Med Biol 2002;47:3313-30.
11. Gu X, Choi D, Men C, et al. GPU-based ultra-fast dose calculation using a finite size pencil beam model. Phys Med Biol 2009;54:6287-97.
12. Fujimoto R, Kurihara T, Nagamine Y. GPU-based fast pencil beam algorithm for proton therapy. Phys Med Biol 2011;56:1319-28.
13. Jacques R, Taylor R, Wong J, et al. Towards real-time radiation therapy: GPU accelerated superposition/ convolution. Comput Methods Programs Biomed 2010;98:285-92.
14. Hissoiny S, Ozell B, Després P. Fast convolution-superposition dose calculation on graphics hardware. Med Phys 2009;36:1998-2005.
15. Jia X, Gu X, Sempau J, et al. Development of a GPU-based Monte Carlo dose calculation code for coupled electron-photon transport. Phys Med Biol 2010;55:3077-86.
16. Jia X, Gu X, Graves YJ, et al. GPU-based fast Monte Carlo simulation for radiotherapy dose calculation. Phys Med Biol 2011;56:7017-31.
17. Hissoiny S, Ozell B, Bouchard H, et al. GPUMCD: A new GPU-oriented Monte Carlo dose calculation platform. Med Phys 2011;38:754-64.
18. Yepes PP, Mirkovic D, Taddei PJ. A GPU implementation of a track-repeating algorithm for proton radiotherapy dose calculations. Phys Med Biol 2010;55:7107-20.
19. Kohno R, Hotta K, Nishioka S, et al. Clinical implementation of a GPU-based simplified Monte Carlo method for a treatment planning system of proton beam therapy. Phys Med Biol 2011;56:N287-94.
20. Jia X, Shuemann J, Paganetti H, et al. GPU-based fast Monte Carlo dose calculation for proton therapy. Submetted to Phys Med Biol 2012;56:577-90.
21. Badal A, Badano A. Accelerating Monte Carlo simulations of photon transport in a voxelized geometry using a massively parallel graphics processing unit. Med Phys 2009;36:4878-80.
22. Jia X, Yan H, Gu X, et al. Fast Monte Carlo simulation for patient-specific CT/CBCT imaging dose calculation. Phys Med Biol 2012;57:577-90.
23. NVIDIA. NVIDIA CUDA Compute Unified Device Architecture, Programming Guide 2011,4.0.
24. Schaffner B, Pedroni E, Lomax A. Dose calculation models for proton treatment planning using a dynamic beam delivery system: an attempt to include density heterogeneity effects in the analytical dose calculation. Phys Med Biol 1999;44:27-41.
25. Paganetti H. Range uncertainties in proton therapy and the role of Monte Carlo simulations. Phys Med Biol 2012;57:R99-117.
26. Li JS, Shahine B, Fourkal E, et al. A particle track-repeating algorithm for proton beam dose calculation. Phys Med Biol 2005;50:1001-10.
27. Kohno R, Takada Y, Sakae T, et al. Experimental evaluation of validity of simplified Monte Carlo method in proton dose calculations. Phys Med Biol 2003;48:1277-88.
28. Yepes P, Randeniya S, Taddei PJ, et al. Monte Carlo fast dose calculator for proton radiotherapy: application to a voxelized geometry representing a patient with prostate cancer. Phys Med Biol 2009;54:N21-8.
29. Fippel M, Soukup M. A Monte Carlo dose calculation algorithm for proton therapy. Med Phys 2004;31:2263-73.
30. Chen GT, Singh RP, Castro JR, et al. Treatment planning for heavy ion radiotherapy. Int J Radiat Oncol Biol Phys 1979;5:1809-19.
31. Highland V. Some practical remarks on multiple scattering. Nuclear Instruments & Methods 1975;129:497-9.
32. Agostinelli S, Allison J, Amako K, et al. GEANT4-a simulation toolkit. Nuclear Instruments & Methods 2003;506:250-303.
33. Pratx G, Xing L. GPU computing in medical physics: a review. Med Phys 2011;38:2685-97.
34. Perl J, Shin J, Schumann J, et al. TOPAS - An innovative proton Monte Carlo platform for research and clinical applications. Med Phys 2012. [Epub ahead of print].
35. Gifford KA, Horton JL, Wareing TA, et al. Comparison of a finite-element multigroup discrete-ordinates code with Monte Carlo for radiotherapy calculations. Phys Med Biol 2006;51:2253-65.
36. Lewis HW. Multiple scattering in an infinite medium. Phys Rev 1950;78:526-9.
37. Börgers C. Complexity of Monte Carlo and deterministic

dose-calculation methods. Phys Med Biol 1998;43:517-28.
38. Fogliata A, Nicolini G, Clivio A, et al. Accuracy of Acuros XB and AAA dose calculation for small fields with reference to RapidArc(®) stereotactic treatments. Med Phys 2011;38:6228-37.
39. Zourari K, Pantelis E, Moutsatsos A, et al. Dosimetric accuracy of a deterministic radiation transport based 192Ir brachytherapy treatment planning system. Part I: single sources and bounded homogeneous geometries. Med Phys 2010;37:649-61.
40. Vassiliev ON, Wareing TA, Davis IM, et al. Feasibility of a multigroup deterministic solution method for three-dimensional radiotherapy dose calculations. Int J Radiat Oncol Biol Phys 2008;72:220-7.
41. Luo Z. An overview of the bipartition model for charged particle transport. Radiation Physics and Chemistry 1998;53:305-27.
42. Luo ZM, Brahme A. An overview of the transport theroy of charged particles. Radiation Physics and Chemistry 1993;41:673-703.
43. Lewis EE, Miller WF. eds. Computational Methods of Neutron Transport. New York: Wiley, John & Sons, 1984.
44. Golub GH, van Loan CF. eds. Matrix computation. Baltimore: Johns Hopkins University Press, 1996.

Cite this article as: Jia X, Pawlicki T, Murphy KT, Mundt AJ. Proton therapy dose calculations on GPU: advances and challenges. Transl Cancer Res 2012;1(3):207-216. DOI: 10.3978/j.issn.2218-676X.2012.10.03

Review Article

Toward robust proton therapy planning and delivery

Zuofeng Li

University of Florida Proton Therapy Institute, Jacksonville, FL, USA

Correspondence to: Zuofeng Li. University of Florida Proton Therapy Institute, North Jefferson Street, Jacksonville, FL, United States. Email: zli@floridaproton.org.

DOI: 10.3978/j.issn.2218-676X.2012.10.01

Scan to your mobile device or view this article at: http://www.thetcr.org/article/view/601/html

With its significant advantages of physical dose deposition, specifically, the ability to select the energy of a proton beam such that it stops in patient at a known depth, thereby depositing no dose in tissue distal to the target, proton therapy is gaining wider acceptance as an additional modality in radiation therapy treatments. Many uncertainties, however, are associated with the clinical application of proton therapy, including calculation of beam range in patient from patient CT images; uncertainties in beam lateral scattering and penumbra values in patient; sensitivity to patient set up error and intra-fraction organ motion; and sensitivity to patient anatomical and physiological changes through the course of treatment, including tumor shrinkage and organ filling variations in stomach and bowels. Many studies have been performed to quantify and evaluate the dosimetric effects of such uncertainties. In the clinical practice of proton therapy, every effort should be made in the patient simulation, planning, and delivery process to take these uncertainties into consideration, such that proton treatments are delivered with adequate robustness and high confidence against their effects.

Uncertainty of CT number to relative stopping power ratio (RSPR) conversion

For each treatment field, the beam range required to adequately cover the target distally is calculated from the water-equivalent-path-length (WEPL) of the beam, from the location where it first enters the patient to the distal most point of the target. CT numbers of patient anatomy along the beam path is converted to tissue-to-water relative stopping power ratio (RSPR) of protons, using a pre-determined CT number conversion curve, such as the stoichiometric method of Schneider *et al.* (1). Uncertainties in the determination of such conversion curves, including accuracy of calculated RSPR of tissue-equivalent materials used to establish such curves (2); CT imaging beam hardening effect (3); and the weak dependence of CT numbers on tissue compositions; translate directly into uncertainties in beam range calculation. Clinically, proximal and distal margins of up to 3.5% have been added to the calculated beam range to accommodate for such uncertainties (4) see *Figure 1*. Schaffer and Pedroni (3) performed animal tissue stopping power measurements in comparison with the calculated values using the stoichiometric method, and found agreements to within 1.1% in soft tissues and 1.8% in bones, with CT beam hardening contributing to less than 1% of the uncertainties. Yang *et al.* (5) performed a comprehensive analysis of proton beam range uncertainties in the CT number to relative stopping power ratio conversion using the stoichiometric method. It was noted that uncertainties associated with the calculated RSPR values are highly dependent on tissue groups, ranging from 1.6% to 5.0%, with smaller values of uncertainties for soft tissues and higher values for higher-density tissue groups such as bones. The overall uncertainties of beam range determination, for most clinical disease sites, were estimated at 3.0-3.4% at 95 percentile confidence interval.

It should be noted that use of proximal and distal margins to accommodate for CT number to RSPR conversion uncertainties assumes that target coverage by the prescribed isodose distribution is prioritized at distal end of the beam: addition of a distal margin guarantees target coverage in the event that the delivered beam has a range in patient shorter than calculated from the CT number to RSPR conversion curve; while use of a proximal margin assures target coverage in the event that the delivered

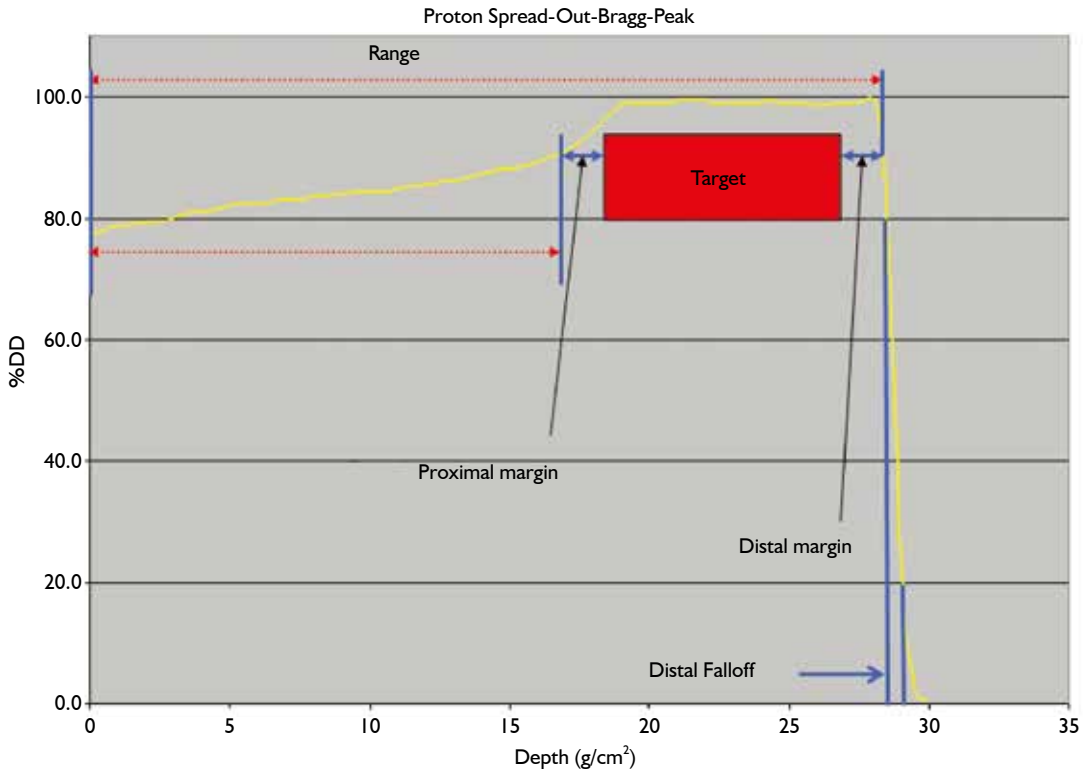

Figure 1 Use of proximal and distal margins to account for CT number to RSPR conversion uncertainties: a distal margin is included in beam range selection to assure distal CTV coverage in the event that the calculated beam range overestimates the delivered beam range; while a proximal margin is used to assure proximal CTV coverage in the event that the calculated beam range underestimates the delivered beam range

beam range is larger than calculated. In the case where delivered beam range is larger than calculated beam range, beam penetration is deeper than shown in a treatment planning system, therefore delivering a prescribed dose to an additional thickness of tissue located distal to the target than calculated by the treatment planning system. A critical organ located distal to the target may therefore receive the full prescription dose by use of a distal margin to the beam. For this reason, it is generally recommended that proton beam angles are selected to avoid having a critical organ immediately distal to the target. Proximal margins should also be adequate to assure target coverage for the case where delivered beam range is larger than calculated, especially for beams that enter target through low density tissues such as the lung (6). In addition, verification treatment plans, using the same beam range and modulation values, may be re-calculated using alternative CT number to RSPR conversion curves that are scaled up or down by the expected uncertainty limits (for example +/-3.5%), to investigate the cumulative effect of such uncertainties in terms of both target dose coverage and critical organ doses, and the original treatment plan modified if unacceptable target and critical organ doses were identified in the verification plans.

While proximal and distal margins have been the method of choice to account for CT number to RSPR conversion uncertainties for traditional, scattered broad beam proton therapy techniques, their implementation for intensity modulated proton therapy techniques using pencil or spot beam scanning techniques is not as well-established. In particular, the delivered dose distribution degradations, in terms of both dose inhomogeneities and target coverage, due to potential misplacement of individual beam spots, are not completely resolved by use of distal and proximal margins, as shown by Albertini *et al.* (7). While effect of range uncertainties may be estimated by recalculating treatment plans using CT number to RSPR conversion curves scaled up to down a given percentage (8), complete integration of such uncertainties in IMPT optimization algorithms remains unavailable in commercial treatment planning systems.

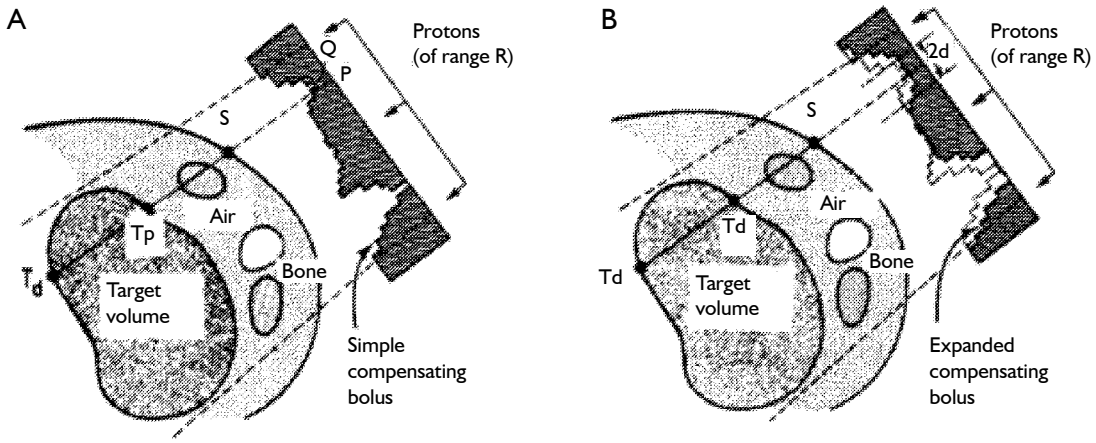

Figure 2 Modification of range compensator to account for effect of beamlet range changes due to setup errors. (A). Sample ray line along which a line integral is performed to obtain the WEPL between skin (S) and the proximal (Tp) and distal (Td) target surfaces. (B). Expansion (smearing) of range compensator to ensure target coverage in the presence of setup error and organ motion of magnitude *d*. From (15)

Inaniwa *et al.* (9) proposed an IMPT optimization algorithm that allows adequate target coverage while maintaining allowable dose distribution gradients within the target. Liu *et al.* (10) developed an IMPT optimization algorithm based on worst-case dose distributions that includes setup errors as well as range uncertainty. A total of nine different dose distributions that include the effects of these uncertainties are calculated each iteration of plan optimization, and optimization objective function evaluated based on the worst dose distribution of the 9 plans. The authors found that the proposed algorithm able to improve normal tissue sparing while maintaining plan robustness against the uncertainties considered, without using the "safety margins" of traditional PTV concept.

Dosimetric effect of setup errors and organ motion

In general, patient setup errors and organ motion tend to cause geometric misalignment of treatment field to the treatment target [clinical target volume (CTV)] in radiotherapy, resulting in part of the CTV receiving inadequate dose coverage. Traditionally, these uncertainties are compensated for in treatment planning by use of the Internal Target Volume (ITV) and Planning Target Volume (PTV) concept (11), which expand the treatment field laterally in the beam's eye view (BEV) such that the CTV or ITV is always contained within the treatment field. In proton therapy treatments, however, patient setup errors and organ motion not only affect the lateral extent of proton dose distribution, but also cause uncertainties in beam range within the treatment field. In that sense, the traditional PTV expansion, using magnitude of target motion and setup errors to calculate expansion margins, *does not* in principle apply to proton therapy. A setup error parallel to beam direction, if not associated with a corresponding WEPL change, has minimal effect on proton beam dose distribution, thus may be safely ignored in proton therapy treatment planning.

A state-of-the-art proton therapy treatment planning system for scattered and/or or uniform scanning (wobbling) proton beam dose calculations, using the pencil beam dose calculation algorithm (12,13), decomposes a broad, scattered proton beam into small pencil beamlets, and performs ray-tracing of each proton pencil beam to determine the WEPL of the pencil required for the treatment field. A range compensator (or "bolus") is used to pull back the ranges of individual pencil beams so that the board beam conforms distally to the treatment target (14,15). Patient setup errors, both translational and rotational, may change the calculated WEPL values across the treatment field, for example, increasing the WEPL of a pencil beamlet required to reach the distal side of the target if a higher density bone, absent in the path of a beamlet in the treatment planning images, moves into the path of the beamlet due to setup errors. *Figure 2* from Urie *et al.* (15) illustrates how the range compensator is "smeared" (expanded) to account for the WEPL changes of setup errors and organ motion on a given beamlet. The tissue-equivalent range compensator is calculated using ray tracing for each beamlet, and has

variable thicknesses across its profile so that all beamlets would stop at the distal surface of the target. In regions where the beam passes through high density bone segments, the range compensator has reduced thickness due to the increased WEPL through the bone (for example, line from points P through S to Td). If the bone is offset from the range compensator laterally due to patient setup errors or organ motion, then a beamlet may pass though thicker part of the compensator, as well as the bone segment, causing it to stop before reaching the distal surface of the target. The thinner part of the range compensator is therefore smeared by a given radius, called "smearing margin", the magnitude of which should be no smaller than the potential total shift of the bone relative to the compensator due to setup errors and/or organ motion (*d* in *Figure 2*).

As discussed above, range compensator design is based on geometric ray tracing of the WEPL values of beamlets within the treatment field to the distal surface of the target. This method of compensator design, however, does not adequately consider the additional scattering and range straggling of protons passing through the compensator itself. Range compensators are therefore fabricated with a tapered milling bit on a CNC milling machine, in order to introduce an tapering angle (up to 3°) that reduces the effect of protons scattering off sharp compensator edges and the resulting dose distribution inhomogeneities (hot-spots) (14). Range compensators may also be "smoothed" manually by interpolation of its thicknesses for beamlets into final grids for fabrication. This practice has been found to improve agreement of calculated *vs*. measured dose distribution, and in general improves dose distribution homogeneity (16). The effectiveness of compensator smearing is also reduced by the additional proton range straggling introduced by the compensator. To include the effect of such range straggling, Moyers *et al*. (4) included an additional term of proton lateral scattering term in their smearing margin (referred to as "bolus expansion (BE)" in the article) calculation, to arrive at an equation of

$$\mathrm{BE} = \sqrt{(IM + SM)^2 + (0.03 \times (distal\ CTV\ depth + bolus\ thickness)^2},$$

where IM is the internal organ motion radius in the direction orthogonal to beam axis, and SM is the setup error term, again in the direction orthogonal to beam axis.

The borders of the compensator which overlaps with the additional PTV and aperture margins of the treatment field will not produce intersections with the target in ray tracing. Thicknesses of the compensator in these parts are usually set to be equal to the compensator thicknesses immediately inside the target in the beam's eye view (BEV), in a practice commonly referred to as "border smoothing". The radius of border smoothing should therefore be selected to be no smaller than the margins between the field border and the target.

Adequate selection of range compensator smearing and border smoothing margin values in general assures adequate target coverage of scattered proton beam treatments. This method of increasing proton beamlet ranges to assure adequate distal target coverage, however, results in unnecessary treatment of normal tissues immediately deeper than the target for the times when the higher density tissues do not intersect the beamlets for which the smearing margin is selected. Use of smearing margins, therefore, may increase doses to critical organs located immediately distal to the target. Similar to the case of range uncertainties discussed previously, careful considerations should be given to beam angle selection to avoid such scenarios.

Calculation of proximal and distal margins, as outlined above, assumes knowledge of magnitudes of organ motion and setup errors for each patient. Magnitude of periodic organ motion, such as due to breathing, is available via use of 4-dimensional CT (4DCT) or MRI imaging techniques. Use of such data however needs to be cautioned with the understanding that their reproducibility throughout the course of a patient's radiation therapy treatment is not assured (17). Periodic repeat 4DCT scans during a patient's treatment course may be necessary to confirm the consistency of such motion data. Non-periodic organ motion, such as prostate movement due to bladder filling and rectal gases, may require separate and additional and sometimes patient-specific evaluation.

It should be further noted that the setup errors that have impact on selection of proximal and distal margins, as well as smearing margins in range compensator design, are heavily influenced by multiple factors. While in traditional photon therapy one would be concerned only with the setup error of the target itself, for proton therapy one is concerned with the setup errors of the target, as well as all tissues that lie in the path between beam entrance and the distal target, for each individual beam. Patient skin and the underlying fat/muscle tissue may not be reproducible, especially when compressed by immobilization devices. Bony structures that a beam traverses through may present different angulations between treatment fractions. Rotational setup errors, both for overall patient anatomy, as well as internal organs, such as bones and, in the thorax, the mediastinum and the heart, can cause large range errors. *Figure 3* shows the potential

Figure 3 Effect of rotation setup errors on the range of a proton beam tangential to the heart. The planned beam path, shown in red, has a WEPL value of 8.48 cm to reach the tumor. With a setup error of 2 degrees, the altered beam path, shown in yellow, has a WEPL value of 10.68 cm. This 2 degree setup error in patient roll direction therefore introduces a beam range uncertainty up to 2.2 cm

effect of rotational setup error: if an anterior-posterior (AP) beam is used for treating this lung cancer, a rotational error of 2 degrees in patient roll direction would place the beam path though a thickness of the heart (yellow line) that was not present in the planned beam path (red line). The heart tissue in the beam path causes an increase of 2.2 cm in WEPL required to reach the target. Such a sharp change in WEPL values could be compensated for by use of range compensator smearing margins, which nonetheless increases dose distribution heterogeneity. Note that this type of changes may not be due to setup errors, but can be the result of organ motion: breathing motion, as well as heart beating, can cause rotation of the heart by greater than 2 degrees. It is therefore recommended that such treatment beams be avoided in proton therapy treatment plans.

Trofimov *et al*. (18) performed detailed analysis of the effect of setup errors in the treatment of prostate cancer using proton therapy. As proton therapy fields in prostate cancer treatments typically use lateral beam entrance gantry angles, femur rotation angles, as well as thicknesses of subcutaneous tissue, in addition to prostate position and rotation, all contribute to uncertainties in the delivered proton dose distributions. The authors found substantial variations in the software tissue thicknesses in the lateral hips (up to 5 mm), and femur rotation angle deviations from initial values of greater than 10°. Selection of distal and proximal margins for beam range calculations, as well as smearing margin for the range compensator, needs to take these variations into consideration. Patient immobilization technique and daily setup tolerances, as calculated by image guidance system, should be optimized to minimize such variations. For example, the commonly used vacuum bags in lung cancer treatments can introduce over 10 mm variations in the thicknesses of soft tissue around the chest wall; and breast position in female patients can introduce additional thickness variations. It is therefore common that no such vacuum bag immobilization devices are used for treatment of tumors in the thorax region using proton therapy, and beams that enter female patient through breasts are minimally used.

While the dosimetric effect of organ motion has been traditionally accounted for by use of the ITV concept in photon-based radiation therapy, this practice is often inadequate for proton therapy, especially when the organ motion is accompanied by tissue density changes, such as in the treatment of isolated lung tumors. The solid tumor, often having near tissue RSPR value, is enclosed within low density lung tissue. The ITV volume therefore includes volumes of both low density lung tissue and higher density tumor tissue. Calculation of proton beam range that ensures adequate tumor coverage regardless where the tumor is needs to take this motion-induced RSPR change into consideration. In addition, the normal lung volume has variable RSPR values at different phases of breathing, due to the filling of lung airways and blood vessels. Several authors have described treatment planning strategies for lung cancer (4,19-21). A typical strategy would start with constructing an average CT dataset from the 10 phases of a 4DCT scan set. The ITV is then outlined on the average CT dataset, and its HU values overridden by the maximum or a representative HU value of the tumor. Beam range calculations, as well as range compensator design, is performed on this CT dataset, with appropriate proximal, distal, and compensator smearing margins applied. Note that this approach accounts for the range uncertainties caused by lung density variations in breathing, as well as ITV density variations due to tumor motion. However, the critical organ doses calculated from this CT dataset may

be underestimated. A second treatment plan is therefore calculated, using the same beam parameters (apertures, compensators, beam ranges, beam modulation widths, etc.) of the initial treatment plan, but using an average CT dataset with no override of ITV HU values. Finally, several verification plans of the initial plan may be calculated on representative phases of 4DCT images (for example maximum inhalation, mid-inhalation, and maximum exhalation phases) to confirm the adequacy of target coverage as well as critical organ protection. Treatment planning of proton lung therapy therefore calls for calculation of anywhere between 2 and 5 treatment plans, a significant increase in complexity and workload from the practice of photon-based lung radiotherapy practice.

Detailed and comprehensive consideration of the dosimetric effect of patient setup errors and organ motion is critical in the optimal design of proton therapy treatment plans. It is also a labor-intensive and time-consuming process, as state-of-the-art proton therapy treatment planning systems do not include automatic tools for this process. Much research efforts have been devoted to development of methodologies to perform this task, with greater attention paid to intensity-modulated proton therapy (IMPT) treatment planning (10,22-26). For example, Park *et al*. (27) proposed the use of beam-specific PTV (bsPTV) to account for setup errors, CT number to RSPR conversion uncertainties, as well as range uncertainties due to organ motion. In the beam axis direction, ray tracing is performed for each beamlet within a treatment field, and the WEPL values of the beamlets are expanded both proximally and distally by the effects of each of these uncertainties. Laterally the CTV is expanded in the same manner as is done traditionally to achieve PTV. Treatment planning then may proceed with range compensator design and dose calculation for each scattered or uniform scanning proton beam, or beam spot weight optimization for pencil beam scanning beam such that each beam delivers a uniform dose distribution conforming to the bsPTV.

With the increasing interests in IMPT applications, especially in treatment of tumors associated with significant organ motion such as lung tumor (28), various methods have been proposed to address the dosimetric effect of organ motion. Specifically, the interplay effect of organ motion relative to the spot-by-spot *and* layer-by-layer delivery of pencil beam proton therapy treatments has been a subject of intense research efforts (29,30). Similar to conventional photon-based radiotherapy (31), the lateral motion of treatment target in the BEV of a proton treatment field causes the delivery of a pencil beam dose to a voxel of the tumor other than the planned voxel. In addition, state-of-the-art IMPT treatments are delivered in a layer-by-layer manner, where the deepest layer is treated to the prescribed dose, followed by energy changes (range pullback) to deliver prescribed doses to shallow layers of the tumor. Tumor motion in the beam axis direction, as well as organ motion along the beam passage, may cause WEPL changes that result in doses deposited at incorrect layers of tumor or normal tissues. Simulated dose calculation studies have demonstrated dose delivery error of 34% in a single fraction (32) and 18% in 30 fractions (33) for lung treatments; and of 33% in a given fraction for liver (34). Various methods have been proposed to mitigate the dosimetric effects of organ motion in radiotherapy (29,35), including gated therapy; breath-hold; tumor-tracking; and abdominal compression. In addition, IMPT treatments may be delivered via a "repainting" technique (33,36), in which the entire volume is treated multiple times within a treatment fraction, each delivering a portion of the fractional prescribed dose. While all motion mitigation methods will potentially serve to minimize the dosimetric effect of organ motion in proton therapy treatments, they all also require additional verification of organ motion magnitudes and patterns for a given treatment fraction, so as to ensure that deviations of organ motion patterns from their assumed ones at time of patient simulation do not lead to significant dose delivery errors. Dose repainting of the target volume, at 5-10 times in a given fraction, is general considered adequate to minimize the effect of any residual motion modeling error (33,36). This strategy however also may be associated with significantly increased treatment delivery time: at a nominal average dose rate of 2 Gy/min for IMPT treatments, repainting n times would potentially increase the fractional treatment time by n times longer.

Dosimetric effect of patient anatomy variations

Tumor volume changes during course of radiotherapy treatment are common for H&N and lung cancers, and may result in increased doses to critical organs and decreased target dose coverage (37). Adaptive therapy techniques, where off-line repeat patient imaging and re-planning is performed periodically during a patient's treatment course, are used to minimize the effect of such target volume changes. For proton therapy, these volume changes may

significantly change the WEPL of treatment beams, causing even larger dosimetric deviations than would happen for photon-based radiotherapy techniques. Shi *et al*. (38,39) reported the case of a non-small-cell lung cancer patient, for whom the tumors shrank by up to 80% in volume through the course of a 75.6 Gy (RBE) proton therapy treatment, delivered in 42 daily fractions. Without adaptive re-planning, the patient would receive a lung V20 value 20% higher than originally planned; 150% higher for spinal cord; and 200% higher for esophagus. Adaptive proton therapy for treatment of cancers where the target is subject to shrinkage during the course of treatment is therefore a required component of robust proton therapy practice.

Evaluation of tumor response during radiation therapy course remains an active area of investigations. Currently there are no specific guidelines on the frequency and technique of adaptive re-planning for proton lung cancer treatments. Hui *et al*. (40) reported results of weekly repeat 4DCT imaging for 8 lung cancer patients with Stage III non-small cell lung cancer receiving IMRT treatments. Proton treatment planning studies showed a mean 4% increase of contra-lateral lung dose; and a mean 4.4 Gy (RBE) dose increase to the spinal cord. Koay *et al*. (41) reviewed the need for and results of adaptive re-planning of proton therapy for lung cancer. Of the 44 patients enrolled in their clinical trial proton therapy treatment [74 Gy (RBE) in 37 fractions] of stage III non-small cell lung cancer, 9 patients required re-planning due to tumor volume changes that were identified in repeat patient CT imaging, performed at 3-4 weeks after start of treatment. The adaptive re-planning maintained sparing of critical organs such as the esophagus and spinal cord, and prevented inadequate target coverage that would have occurred without re-planning. Beltran *et al*. (42) reported results of a study of tumor volume changes in craniopharyngioma patients. An average of 6 MRI studies was performed for these patients during their course of radiation therapy treatments. Maximum tumor volume changes ranged between –20.7% and 82%, with a mean of 28.5%. The dosimetric effects of these tumor volume changes were investigated in a subsequent study (43) of 14 similar patients. Comparisons of IMRT, scattered proton therapy, and IMPT treatment plans show higher sensitivity of IMPT than the other two techniques to tumor volume changes. The authors suggest that IMPT re-planning should be considered with a 5% change in PTV volume, while 10% and 25% changes would necessitate re-planning for IMRT and scattered proton therapy respectively.

Patient anatomy changes that impact proton therapy dose delivery accuracy may occur in all tissues along proton beam paths. Albertini *et al*. (44) reported the dosimetric effect of weight changes for two patients with para-spinal tumors. Treatments were planned and delivered using IMPT technique. Patient weight changes (gaining 1.5 kg for one patient, and losing 8 kg for another) caused WEPL changes along treatment beams, and resulted in optimized beam range changes of +8 mm and –13 mm. It was noted that maximum dose to the cauda equina, the critical organ of concern in the treatments, increased by only 2%, although as much as 80% dose differences were observed within the treated volume locally, due to the range changes. Similarly, changes of stomach and bowel contents in abdominal tumor treatments such as retroperitoneal sarcomas (45), pancreas (46), and liver tumors, may significantly alter the WEPLs of treatment beams. For beams that have to traverse through such organs with potential content changes, alternative CT image datasets are created with the CT numbers of these organs overridden by their potential values for contents that may be present alternatively. Verification plans are then calculated on the overridden image sets to estimate the extent of dosimetric uncertainties due to these organ filling changes. The initial treatment plan may be modified by increasing the proximal and distal margins of the offending treatment field. In general, multiple beams, sometimes non-coplanar, are used, with a majority of target doses delivered via beams having smaller uncertainties, if no other choices are available. Periodic repeat CT or MRI imaging sessions are also used to verify the validity of these verification plans. For prostate treatments, the rectum content may be controlled by filling the rectum with saline or saline-filled rectal balloons, to reduce the impact of daily variability of rectal filling (47).

Relative biological effectiveness (RBE)

Clinically, an RBE value of 1.10 has been assigned to protons of all beam energies, at all depths (11). The RBE of a given proton beam, however, increases significantly toward the end of its beam range (48-55). Current clinical treatment planning systems do not represent the effect of such RBE increases, and it is therefore left to the treatment planning personnel to interpret and include such effects implicitly. In particular, the increase of RBE at the distal end of a proton beam, estimated at up to an additional 25% (over the 1.10 value currently used clinically), also manifests itself in an increase of the beam range (defined to

be at the distal 90% of the depth dose) when corrected for RBE by 2 mm or greater (56). For beams that stop before a critical organ, this implies that an additional distal margin of 2 mm or above would need to be included in treatment planning for the offending beam, so that the potential effect of the increased biological dose to the critical organ is approximated in the dose distribution.

Conclusions

Accurate and safe delivery of proton therapy must take into consideration the various uncertainties associated with the calculation and delivery of proton doses. In particular, these include the uncertainties of CT number to relative stopping power ratio conversion, as well as the effect of setup error and organ motion on delivered beam ranges. For traditional scattered beam treatments, addition of distal and proximal margins, as well as use of range compensator smearing margins, has proven adequate for a large variety of tumor treatments. The specific effects of these uncertainties on intensity-modulated proton therapy, however, remain an active area of research. Delivery of IMPT treatments to targets with significant organ motion, therefore, must be done with utmost care.

Acknowledgements

Disclosure: The author declares no conflict of interest.

References

1. Schneider U, Pedroni E, Lomax A. The calibration of CT Hounsfield units for radiotherapy treatment planning. Phys Med Biol 1996;41:111-24.
2. Yohannes I, Kolditz D, Langner O, et al. A formulation of tissue- and water-equivalent materials using the stoichiometric analysis method for CT-number calibration in radiotherapy treatment planning. Phys Med Biol 2012;57:1173-90.
3. Schaffner B, Pedroni E. The precision of proton range calculations in proton radiotherapy treatment planning: experimental verification of the relation between CT-HU and proton stopping power. Phys Med Biol 1998;43:1579-92.
4. Moyers MF, Miller DW, Bush DA, et al. Methodologies and tools for proton beam design for lung tumors. Int J Radiat Oncol Biol Phys 2001;49:1429-38.
5. Yang M, Zhu XR, Park PC, et al. Comprehensive analysis of proton range uncertainties related to patient stopping-power-ratio estimation using the stoichiometric calibration. Phys Med Biol 2012;57:4095-115.
6. Chang JY, Komaki R, Wen HY, et al. Toxicity and patterns of failure of adaptive/ablative proton therapy for early-stage, medically inoperable non-small cell lung cancer. Int J Radiat Oncol Biol Phys 2011;80:1350-7.
7. Albertini F, Hug EB, Lomax AJ. Is it necessary to plan with safety margins for actively scanned proton therapy? Phys Med Biol 2011;56:4399-413.
8. Lomax AJ, Boehringer T, Coray A, et al. Intensity modulated proton therapy: a clinical example. Med Phys 2001;28:317-24.
9. Inaniwa T, Kanematsu N, Furukawa T, et al. A robust algorithm of intensity modulated proton therapy for critical tissue sparing and target coverage. Phys Med Biol 2011;56:4749-70.
10. Liu W, Zhang X, Li Y, et al. Robust optimization of intensity modulated proton therapy. Med Phys 2012;39:1079-91.
11. International Commission on Radiation Units and Measurements. ICRU Report 78: Prescribing, recording, and reporting proton-beam therapy. J ICRU 2007;7:210.
12. Hong L, Goitein M, Bucciolini M, et al. A pencil beam algorithm for proton dose calculations. Phys Med Biol 1996;41:1305-30.
13. Schaffner B, Pedroni E, Lomax A. Dose calculation models for proton treatment planning using a dynamic beam delivery system: an attempt to include density heterogeneity effects in the analytical dose calculation. Phys Med Biol 1999;44:27-41.
14. Wagner MS. Automated range compensation for proton therapy. Med Phys 1982;9:749-52.
15. Urie M, Goitein M, Wagner M. Compensating for heterogeneities in proton radiation therapy. Phys Med Biol 1984;29:553-66.
16. Li G. Experimental comparison of range compensator calculation algorithms and milling strategies. 51st Particle Therapy Collaborative Group Annual Meeting 2012.
17. Hugo G, Vargas C, Liang J, et al. Changes in the respiratory pattern during radiotherapy for cancer in the lung. Radiother Oncol 2006;78:326-31.
18. Trofimov A, Nguyen PL, Efstathiou JA, et al. Interfractional variations in the setup of pelvic bony anatomy and soft tissue, and their implications on the delivery of proton therapy for localized prostate cancer. Int J Radiat Oncol Biol Phys 2011;80:928-37.
19. Kang Y, Zhang X, Chang JY, et al. 4D Proton treatment

planning strategy for mobile lung tumors. Int J Radiat Oncol Biol Phys 2007;67:906-14.
20. Engelsman M, Rietzel E, Kooy HM. Four-dimensional proton treatment planning for lung tumors. Int J Radiat Oncol Biol Phys 2006;64:1589-95.
21. Engelsman M, Kooy HM. Target volume dose considerations in proton beam treatment planning for lung tumors. Med Phys 2005;32:3549-57.
22. Bert C, Rietzel E. 4D treatment planning for scanned ion beams. Radiat Oncol 2007;2:24.
23. Knopf A, Bert C, Heath E, et al. Special report: workshop on 4D-treatment planning in actively scanned particle therapy--recommendations, technical challenges, and future research directions. Med Phys 2010;37:4608-14.
24. Morávek Z, Rickhey M, Hartmann M, et al. Uncertainty reduction in intensity modulated proton therapy by inverse Monte Carlo treatment planning. Phys Med Biol 2009;54:4803-19.
25. Shirato H, Onimaru R, Ishikawa M, et al. Real-time 4-D radiotherapy for lung cancer. Cancer Sci 2012;103:1-6.
26. Unkelbach J, Bortfeld T, Martin BC, et al. Reducing the sensitivity of IMPT treatment plans to setup errors and range uncertainties via probabilistic treatment planning. Med Phys 2009;36:149-63.
27. Park PC, Zhu XR, Lee AK, et al. A beam-specific planning target volume (PTV) design for proton therapy to account for setup and range uncertainties. Int J Radiat Oncol Biol Phys 2012;82:e329-36.
28. Chang JY, Cox JD. Improving radiation conformality in the treatment of non-small cell lung cancer. Semin Radiat Oncol 2010;20:171-7.
29. Bert C, Durante M. Motion in radiotherapy: particle therapy. Phys Med Biol 2011;56:R113-44.
30. Lomax AJ. Intensity modulated proton therapy and its sensitivity to treatment uncertainties 2: the potential effects of inter-fraction and inter-field motions. Phys Med Biol 2008;53:1043-56.
31. Yu CX, Jaffray DA, Wong JW. The effects of intra-fraction organ motion on the delivery of dynamic intensity modulation. Phys Med Biol 1998;43:91-104.
32. Kraus KM, Heath E, Oelfke U. Dosimetric consequences of tumour motion due to respiration for a scanned proton beam. Phys Med Biol 2011;56:6563-81.
33. Seco J, Robertson D, Trofimov A, et al. Breathing interplay effects during proton beam scanning: simulation and statistical analysis. Phys Med Biol 2009;54:N283-94.
34. Zhang Y, Boye D, Tanner C, et al. Respiratory liver motion estimation and its effect on scanned proton beam therapy. Phys Med Biol 2012;57:1779-95.
35. Keall PJ, Mageras GS, Balter JM, et al. The management of respiratory motion in radiation oncology report of AAPM Task Group 76. Med Phys 2006;33:3874-900.
36. Zenklusen SM, Pedroni E, Meer D. A study on repainting strategies for treating moderately moving targets with proton pencil beam scanning at the new Gantry 2 at PSI. Phys Med Biol 2010;55:5103-21.
37. Barker JL Jr, Garden AS, Ang KK, et al. Quantification of volumetric and geometric changes occurring during fractionated radiotherapy for head-and-neck cancer using an integrated CT/linear accelerator system. Int J Radiat Oncol Biol Phys 2004;59:960-70.
38. Shi W, Nichols RC, Flampouri S, et al. Tumour shrinkage during proton-based chemoradiation for non-small-cell lung cancer may necessitate adaptive replanning during treatment. Hong Kong J Radiol 2011;14:190-4.
39. Shi W, Nichols RC, Flampouri S, et al. Proton-based chemoradiation for synchronous bilateral non-small-cell lung cancers: a case report. Thoracic Cancer 2012. [Epub ahead of print].
40. Hui Z, Zhang X, Starkschall G, et al. Effects of interfractional motion and anatomic changes on proton therapy dose distribution in lung cancer. Int J Radiat Oncol Biol Phys 2008;72:1385-95.
41. Koay EJ, Lege D, Mohan R, et al. Adaptive/Nonadaptive Proton Radiation Planning and Outcomes in a Phase II Trial for Locally Advanced Non-small Cell Lung Cancer. Int J Radiat Oncol Biol Phys 2012. [Epub ahead of print].
42. Beltran C, Naik M, Merchant TE. Dosimetric effect of target expansion and setup uncertainty during radiation therapy in pediatric craniopharyngioma. Radiother Oncol 2010;97:399-403.
43. Beltran C, Roca M, Merchant TE. On the benefits and risks of proton therapy in pediatric craniopharyngioma. Int J Radiat Oncol Biol Phys 2012;82:e281-7.
44. Albertini F, Bolsi A, Lomax AJ, et al. Sensitivity of intensity modulated proton therapy plans to changes in patient weight. Radiother Oncol 2008;86:187-94.
45. Swanson EL, Indelicato DJ, Louis D, et al. Comparison of three-dimensional (3D) conformal proton radiotherapy (RT), 3D conformal photon RT, and intensity-modulated RT for retroperitoneal and intra-abdominal sarcomas. Int J Radiat Oncol Biol Phys 2012;83:1549-57.
46. Nichols RC Jr, Huh SN, Prado KL, et al. Protons offer reduced normal-tissue exposure for patients receiving postoperative radiotherapy for resected pancreatic head cancer. Int J Radiat Oncol Biol Phys 2012;83:158-63.

47. Vargas C, Mahajan C, Fryer A, et al. Rectal dose-volume differences using proton radiotherapy and a rectal balloon or water alone for the treatment of prostate cancer. Int J Radiat Oncol Biol Phys 2007;69:1110-6.
48. Paganetti H, Niemierko A, Ancukiewicz M, et al. Relative biological effectiveness (RBE) values for proton beam therapy. Int J Radiat Oncol Biol Phys 2002;53:407-21.
49. Paganetti H. Significance and implementation of RBE variations in proton beam therapy. Technol Cancer Res Treat 2003;2:413-26.
50. Wilkens JJ, Oelfke U. Optimization of radiobiological effects in intensity modulated proton therapy. Med Phys 2005;32:455-65.
51. Tilly N, Johansson J, Isacsson U, et al. The influence of RBE variations in a clinical proton treatment plan for a hypopharynx cancer. Phys Med Biol 2005;50:2765-77.
52. Wambersie A, Hendry JH, Andreo P, et al. The RBE issues in ion-beam therapy: conclusions of a joint IAEA/ICRU working group regarding quantities and units. Radiat Prot Dosimetry 2006;122:463-70.
53. Jäkel O. The relative biological effectiveness of proton and ion beams. Z Med Phys 2008;18:276-85.
54. Frese MC, Wilkens JJ, Huber PE, et al. Application of constant vs. variable relative biological effectiveness in treatment planning of intensity-modulated proton therapy. Int J Radiat Oncol Biol Phys 2011;79:80-8.
55. Wambersie A, Menzel HG, Andreo P, et al. Isoeffective dose: a concept for biological weighting of absorbed dose in proton and heavier-ion therapies. Radiat Prot Dosimetry 2011;143:481-6.
56. Carabe A, Moteabbed M, Depauw N, et al. Range uncertainty in proton therapy due to variable biological effectiveness. Phys Med Biol 2012;57:1159-72.

Cite this article as: Li Z. Toward robust proton therapy planning and delivery. Transl Cancer Res 2012;1(3):217-226. DOI: 10.3978/j.issn.2218-676X.2012.10.01

Original Article

Comparison of tissue characterization curves for different CT scanners: implication in proton therapy treatment planning

Chee-Wai Cheng[1,2], Li Zhao[1,2], Mark Wolanski[1,2], Qingya Zhao[1,3], Josuha James[4], Kate Dikeman[4], Michael Mills[4], Mei Li[5], Shiv P. Srivastava[6], Xing Qi Lu[7], Indra J. Das[1,2]

[1]Indiana University Health Proton Therapy Center, Bloomington, IN, 47408, USA; [2]Department of Radiation Oncology, Indiana University School of Medicine, Indianapolis, IN, 46202, USA; [3]Department of Radiation Oncology, Parkview Health, Fort Wayne, IN, USA; [4]Department of Radiation Oncology, University of Louisville, Louisville, KY, 40202, USA; [5]Department of Radiation Oncology, Morristown Memorial Hospital, Morristown, NJ, 07962, USA; [6]Purdue University, West Lafayette, and Reid Hospital, Richmond, IN, 47374, USA; [7]Beth Israel Deaconess Medical Center, Harvard Medical School, Boston, MA 02215, USA

Correspondence to: Chee-Wai Cheng, Ph.D. Indiana University Health Proton Therapy Center, Bloomington, IN, 47401, USA. Email: ccheng1@iuhealth.org.

Abstract: For proton beam therapy, CT imaging is required to calculate dose based on CT pixel values of relative stopping power (RSP). The variation among CT-scanners and the phantom used to derive the relationship CT number-electron density-RSP has not been investigated. Using RMI CT phantoms, 18 CT scanners and a Tomotherapy unit, the Hounsfield unit (HU) variations and associated dosimetric uncertainty were investigated. The variation of HU was within one standard deviation (SD) of the average for 14 out of the 15 scanners tested with the same phantoms. For high density materials (>400 HU) the HU values deviated by more than 4% from the average. The HU- RSP curves of 18 scanners were fitted with a straight line in three HU intervals: –700<HU<0, 0<HU<230 and <230<HU<1,700. The dosimetric impacts of the variation of HU among scanners were <1% in DVH point dose comparisons in a prostate cancer plan. For a head and neck cancer plan the difference was up to 4% due to large inhomogeneities. Our results seem to suggest that the X-ray spectrum of a CT scanner has a smaller effect on the HU-RSP curve than the elemental compositions of the tissue substitutes used in the calibration. Furthermore, a single HU-RSP curve may suffice as a reference curve for proton treatment planning. It is found to agree with the calibration curve obtained for the specific scanner. This study does not address the issue of metallic implants included in the treatment plan.

Keywords: Proton beam; CT scanner; electron density; relative stopping power; dosimetric uncertainty

doi: 10.3978/j.issn.2218-676X.2012.11.05

Scan to your mobile device or view this article at: http://www.thetcr.org/article/view/811/html

Introduction

In modern radiation therapy, CT is used to provide the anatomical information of the targets and organs at risk (OAR) for treatment planning of a patient. To determine the dose deposited in each pixel of a CT data set, the relative electron density (RED) must be known a priori. This is enabled by a tissue characterization curve (TCC) that assigns the Hounsfield unit (HU) of each pixel to an associated RED value. Conventionally, the TCC for a given kVp of a CT scanner is generated from a calibration measurement using a tissue characterization phantom. A commonly used tissue characterization phantom is the RMI 467 (Gammex Inc., Middleton, WI) that contains a number of tissue substitutes made in the form of cylindrical rods 2.8 cm in diameter arranged in two concentric circles in a 33 cm diameter solid water phantom slab. Each tissue substitute rod has a specific elemental composition (considered as confidential information by the vendor) to reproduce the physical characteristics of the tissue it represents (for example, electron density and physical density). The HU of each tissue

substitute material averaged over a certain region-of-interest (ROI) is obtained from the CT scan. A plot of the HU of the tissue substitutes versus their corresponding RED values (supplied by the manufacturer) produces the TCC for that particular kVp for a given CT scanner.

Variations in CT numbers among different diagnostic scanners for the same materials and their locations and orientations inside the scanner were reported more than 30 years ago (1,2). With the emergence of three dimensional treatment planning in the 1990s, CT-based treatment planning became the standard of practice in radiation therapy. Subsequently, the use of TCC in treatment planning has become a norm as reported by many investigators (3-7). Thomas (7) studied TCC for a number of CT scanners and reported that using a single table for all the scanners would produce dosimetric errors of <0.8% for 6 MV X-rays. It was also reported that a 1% error in dosimetry would require errors over 8% in the bone electron density in external beam radiation therapy (7). Kilby *et al*. (6) found that a greater precision in electron density is required as the photon beam energy decreases or the tissue thickness increases. For 6 MV photons, the reported tolerance level of electron densities from Kilby *et al*. (6) are in agreement with those reported earlier by Thomas (7). However, tissue substitute materials may not accurately mimic the radiation characteristics of the real tissues due to the differences in the elemental compositions. Schneider *et al*. (8) pointed out that there is a strong dependence of the TCC on the choice of the tissue substitute materials as photon attenuation in a CT scanner depends not only on the Compton scattering, but also on the photoelectric effect and coherent scattering. A stoichiometric method to generate a more accurate TCC was proposed using both the measured HU and the chemical composition of real tissues (8). As HU is the ratio of the attenuation coefficient of a material to that of water, the value is affected by the beam hardening effect. Schneider *et al*. (8) suggested that all tissue substitute materials should be scanned at the center of the CT scanner so that each material is irradiated by the same X-ray spectrum.

For treatment planning in proton beam therapy (PBT), RED must be first converted to the corresponding relative stopping power (RSP) values. This is done using the Bethe-Bloch equation as shown by Bichsel (9):

$$RSP = \rho_e^{rel}\{\ln(2m_oc^2\beta^2/[I_t(1-\beta^2)]-\beta^2\}/\{\ln(^2m_oc^2\beta^2/[I_w(1-\beta^2)]-\beta^2\} \quad [1],$$

where ρ_e^{rel} is the RED of the material, I_t is the ionization potential of the material, m_o is the electron rest mass, c is the speed of light and β is the ratio v/c, v being the speed of proton.

The effect of the elemental composition of tissue substitutes on the TCC is more pronounced in PBT due to the energy dependence of the proton range and the stopping powers in tissue, which in turn depends on the elemental composition of the tissues. Yohannes *et al*. (10) proposed a semi-empirical model in the stoichiometric calibration based on which a new formulation of tissue substitute materials was proposed (11). These new tissue substitute materials closely resemble the radiation and physical characteristics of those of the standard real tissues in ICRU Report 44 (12) and allow the generation of an accurate TCC efficiently. The accuracy of the stoichiometric calibration has been verified in proton beam (13). On the other hand, Qi *et al*. (14) found that the CT scan technique (kilo-voltage) and the patient support table top have the most impact on the HU, whereas changing the positions of the tissue substitute rods in the RMI phantom resulted in <1% change in HU for lung and cortical bone.

With advancements in CT technology in recent years, CT scanners used in radiation oncology are mostly multi-slice high resolution scanners and some are equipped with dose and artifact reduction capabilities. A question arises: could modern technology reduce the inconsistencies in HU among the different CT scanners that have been observed earlier (1,2,7)? In other words, how different are the TCC among the different modern scanners in the radiotherapy clinics, giving the same model of the tissue characterization phantom? Alternatively, do all CT scanners produce identical TCC using the same tissue characterization phantom? Ultimately, the question we want to answer is: what is the dosimetric implication in PBT due to differences in TCC?

In this study, we have carried out a systematic study to examine the HU-RSP curves obtained from a wide array of CT scanners and to investigate the effects of the differences in HU-RSP curves on dose distributions in PBT. This study did not include CT scans containing metallic structures such as implants.

Methods

Comparison of HU variation in different RMI phantoms

Using the RMI 467 phantom, HU-RED curves were obtained from 18 different CT scanners in nine institutions for 120 kVp (mAs was not a controlled experimental variable and may have been different for different institutions). In addition, a HU-RED curve was obtained from a TomoTherapy unit operated

Table 1 List of CT scanners used in this study and the manufacturers. The numbers in parenthesis are the number of CT scanners of the same model, but from different institutions

CT scanner model	Manufacturer
Philips Brilliance 16 (2)	Philips
Philips Brilliance	
Philips PET-CT TF TOF16	
Philips iCT 256	
Philips Bigbore	
GE Hi Speed (2)	GE
GE Light Speed (2)	
GE Light Speed 16	
Siemens Biograph 16	
Siemens Cardiac 64	Siemens
Siemens Plus 4	
Siemens Sensation Open 16	
Siemens Sensation Open 48	
Toshiba	Toshiba
Picker	Picker international
Tomotherapy (MVCT)	Accuray

in a scanner mode with 1 MV x rays for imagining as advocated by Langen *et al*. (15). *Table 1* lists the CT scanners involved in this study and their respective manufacturers. A majority of the CT scanners (16/18) were from one of three vendors: Philips (Philips Healthcare, Andover, MA), GE, or Siemens (Siemens USA, Malvern, PA). The remaining two are from two separate vendors: Toshiba (Toshiba America Medical Systems, Inc., Tustin, CA) and Picker International (Picker International, Cleveland, OH).

Five RMI 467 phantoms were used to obtain the different TCC. There were two identical pairs of phantoms as they had identical RED data sheet. Thus practically, only three different RMI phantoms were used for the calibration of the CT scanners. They are labeled as RMI 1, RMI 2 and RMI 3 for identification purpose. Except for one RMI phantom (RMI 3), each of the remaining four phantoms (two under RMI 1 and two under RMI 2) were used for the calibration of more than one CT scanners. Additional inserts were used for RMI 1 to generate calibration points in the RED range between 0.936-1.137.

The RED was converted to RSP using the Bethe-Bloch formula [Eqn. 1] and ionization energies published in ICRU49 (16). The RSP values were calculated for 208 MeV proton energy, which is the maximum energy at our center. *Table 2* lists the tissue substitute materials

Table 2 A list of tissue substitute inserts in the RMI 467 tissue characterization phantom and the associated ranges of relative electron densities and relative stopping powers for the five phantoms

Tissue substitute material	Relative electron density	Relative stopping power
LN-300	0.283±0.014	0.282±0.014
LN-450	0.433±0.009	0.432±0.009
AP6	0.910±0.021	0.917±0.022
BR-12 breast	0.962±0.008	0.968±0.006
Solid water	0.990±0.002	0.991±0.001
Water	1.000	1.000
BRN-SR2 brain	1.041±0.010	1.054±0.012
LV1 liver	1.057±0.016	1.060±0.018
IB inner bone	1.087±0.014	1.074±0.016
B200 bone mineral	1.099±0.009	1.085±0.010
CB2-30%	1.276±0.003	1.260±0.005
CB2-50%	1.464±0.004	1.423±0.007
SB3-cortical bone	1.694±0.002	1.626±0.005
Polyethylene*	0.936	0.958
CB3 resin*	1.011	1.023
CB resin (CB4)*	1.106	1.109
CB2-10% $CaCO_3$*	1.132	1.132
Acrylic*	1.137	1.137

*additional inserts used by some of the CT scanners

used in the RMI phantoms, and their respective RED and RSP values averaged over the five phantoms ±1 SD. The tissue substitute materials marked with an asterisk are the additional inserts used by two institutions for their CT scanners. Since the RMI phantoms have identical RED for the tissue substitute materials, no average values and standard deviations were calculated for these additional inserts. *Table 2* shows that for the lowest density material the RED variation is about 5%. For RED between 0.4-0.99, the variation in RED values among the five phantoms is ≤2%. For RED>1, the density variation is ≤1%. For each tissue substitute material, the different HU obtained from the 18 scanners is separated into three groups based on their phantom number.

Since RSP of a material is derived from its corresponding RED value from a very complex equation [Eq. 1], it is interesting to compare the HU-RSP and its corresponding HU-RED curves. As an example, the two curves are compared for the Siemens Biograph 16 CT scanner used at the Proton Therapy Center.

Comparison of HU-RSP curves for the different CT scanners

In addition to the variation of the RED values (and hence RSP) for the tissue substitute materials among the three different RMI phantoms, the HU for a given tissue substitute material may vary from one CT scanner to another, even for the same tissue characterization phantom due mainly to the difference in the energy spectra of the X-rays. To examine the variation of the HU-RSP curves among the different CT scanners of the same vendor, the various HU-RSP curves were compared for the three vendors: Philips, GE and Siemens.

Using the same RMI phantom, the HU-RSP curves were obtained for nine CT scanners from various vendors to investigate the effect of the X-ray spectrum in the different CT scanners on the TCC.

Finally, to examine the extent of variation of the HU-RSP curves for all the scanners in the study, the 18 TCC were compared in the same graph. The portion in the TCC for some of the CT scanners which included the additional inserts was excluded from the curves so that all HU-RSP curves contained the same tissue substitute materials. The HU-RSP curve obtained from a TomoTherapy unit which is operated at 1 MV in the imaging mode is also included for comparison as well as to demonstrate the difference between tissue characterization between MVCT and kVCT. The difference is especially relevant in proton therapy for patients with metallic implants, as reported by Yang *et al*. (17).

Effect of differences in HU-RSP curves on dose distributions

In treatment planning of PBT, the RSP value associated with each pixel in a CT image is obtained from the HU-RSP curve. To study the effects of differences in the HU-RSP curves on dose distributions, instead of using all 18 HU-RSP curves in treatment planning, we elected to generate HU-RSP curves, which represent the minimum and maximum HU-RSP curves with respect to the HU axis for dose calculation. To this end, the minimum and maximum HU of each tissue substitute material and its corresponding average RSP value (RSP_{av}) are used to form two HU-RSP curves, HU_{min}-RSP_{av} and HU_{max}-RSP_{av} respectively, representing the largest change in the HU-RSP curves. In addition, a HU-RSP curve was formed by using the average HU of each material and the corresponding RSP_{av}, which is the average HU-RSP curve for the 18 scanners. For each HU-RSP curve (min, max and mean), dose distributions were calculated for a prostate and a head and neck proton treatment plan, respectively. The DVH of the GTV, PTV and a number of organs at risks were then determined and compared with those obtained from the respective 'reference plan', which was generated by using the HU-RSP curve for the IUHPTC planning system currently in use clinically.

Results

Comparison of HU variation in different RMI phantoms

Figure 1 shows the HU variation across CT scanners for three tissue substitute materials (LN-300, water and cortical bone) within each RMI phantom as examples. The HU where the X-axis intersects with the Y-axis corresponds to the mean value of the HU. The numbers on the X-axis represent the phantom number (zero is the origin on the plot). For LN-300, larger HU variations are observed for RMI-1 compared to RMI-2 as shown in *Figure 1A*. The HU for RMI-3 is unusually high compared to all other points. For water, there is an unusually low HU for one institution in RMI-1. Otherwise, most of the remaining points (14/15) are within 1SD of each other. For cortical bone, the HU shows larger variation for RMI-1 compared to those from RMI-2.

Figure 2 compares a HU-RED curve and the corresponding HU-RSP curve for the Siemens Biograph 16 CT scanner. It can be seen that the two calibration curves track each other very closely in the region from lung to an RED (RSP) value of about 200. The curves start to separate from each other with RED slightly higher than the corresponding RSP value from about 1% at HU ~450 to about 4% at HU ~1200, corresponding to the cortical bone.

Comparison HU-RSP curves for the different CT scanners

Figure 3(A-C) compares the HU-RSP curves for the Siemens, GE and Philips CT scanners involved in the study respectively. The portion of the curves circled in *Figure 3A* (magnified in the inset) contains additional calibration points in the RSP range between 0.9-1.14. These points represent phantom materials (highlighted in *Table 2*) with higher percentage of carbon but no phosphorus or calcium compared to other materials of similar RSP which have about 9% calcium and 3% phosphorus. A similar structure in the HU-RSP curve is also shown for the GE Hi Speed

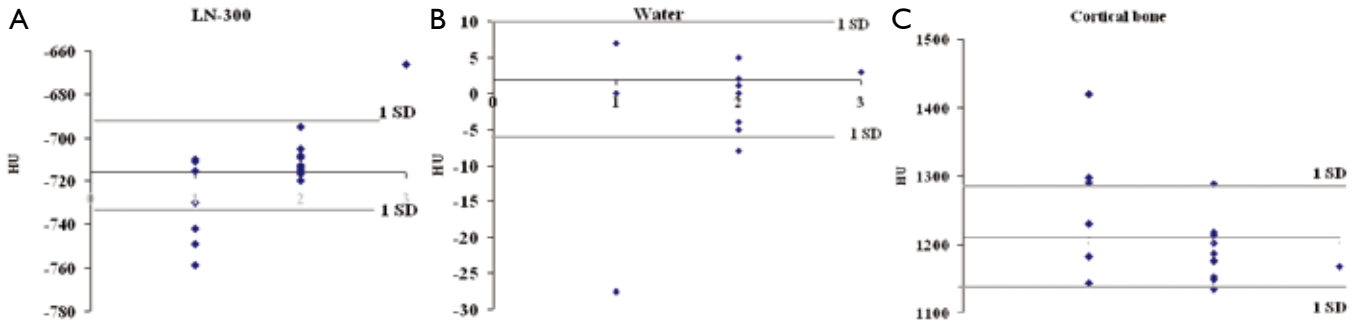

Figure 1 A. Variation of HU for the lung substitute material, LN-300, in the three RMI phantoms. The HU where the x-axis intercepts with the Y-axis is the mean HU, averaged over al l8 points. The numbers on the X-axis are the phantom numbers (the zero is the origin of the X-axis). Larger variation in HU can be observed for RMI 1, compared to those in RMI 2. HU for RMI 3 is much higher than the rest; B. Variation of HU for water in the three different RMI phantoms. The HU where the X-axis intercepts with the Y-axis is the mean HU. Note that most of the HU for water were within 1 SD of each other, except two institutions with unusually low HU; C. Variation of HU for the cortical bone in the three RMI phantoms. Again, the mean HU value is where the X-axis intersects with the Y-axis. The HU for the cortical bone show larger variation compared to those in RMI 2

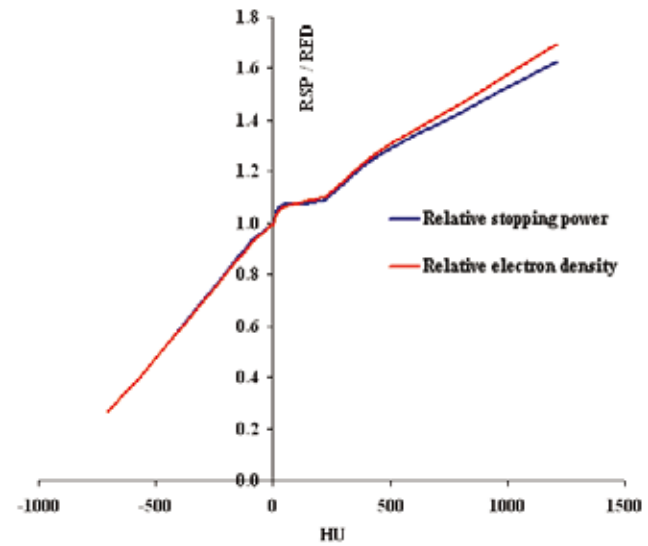

Figure 2 Comparison of HU-RED and the HU-RSP curves for the Siemens Biograph 16 CT scanner

1 in *Figure 3B* for the same reason. The presence of these points results in ambiguity in the calibration curve as a given HU in that region corresponds to more than one RSP values. The HU-RSP curves for the Philips CT scanners chosen for this study are remarkably similar as shown in *Figure 3C*.

Figure 4 compares the HU-RSP curves obtained for the same RMI phantom for nine different CT scanners. The curves look remarkably similar for all nine CT scanners in the region –700<RSP<500. Above RSP=500, the curves begin to show some separations. However, when examining closely, the largest separation occurs at RSP ~1.633 with 1 SD of the variations at about 3%. On the other hand, the SD of the HU variation is about 30% for the SR2 brain insert corresponding to RSP =1.062. The large % difference is probably due to the small HU for the brain substitute materials, in the range 8-24.

To remove the ambiguity in the HU-RSP curves as shown in the inset of *Figure 3A*, these additional points were removed from the respective calibration curves and re-plotted in *Figure 5* together with all other curves to investigate the extent of variation among the 18 HU-RSP curves. The curves generally can be represented by three straight lines in the three HU intervals: –700<HU<0, 0<HU<230 and <230<HU<1,700.

In the HU range –700 to zero, the HU-RSP curves are roughly parallel to each other. For a given RSP, the variation in HU among the 18 CT scanners is within about 10%. The region immediately above water (RSP=0) to RSP~1.1 is almost horizontal resulting in a large variation in HU for a small change in RSP. The HU changes from about 5 to 300 for RSP =1 to 1.1 (water to bone mineral region). In the RSP region corresponding to the liver substitute (RSP~ 1.05-1.07), the HU changes from a minimum of 58 to 106, depending on the model and manufacturer of the CT scanners. The mean HU value, HU_{mean} for liver was 84.3±8.30. In the bone region, corresponding to RSP>1.1, the curves start to separate from each other. For the CB2-30% substitute, the HU changes from a minimum of 407 to a maximum of 539. The HU_{mean} is 447±34.0. For the

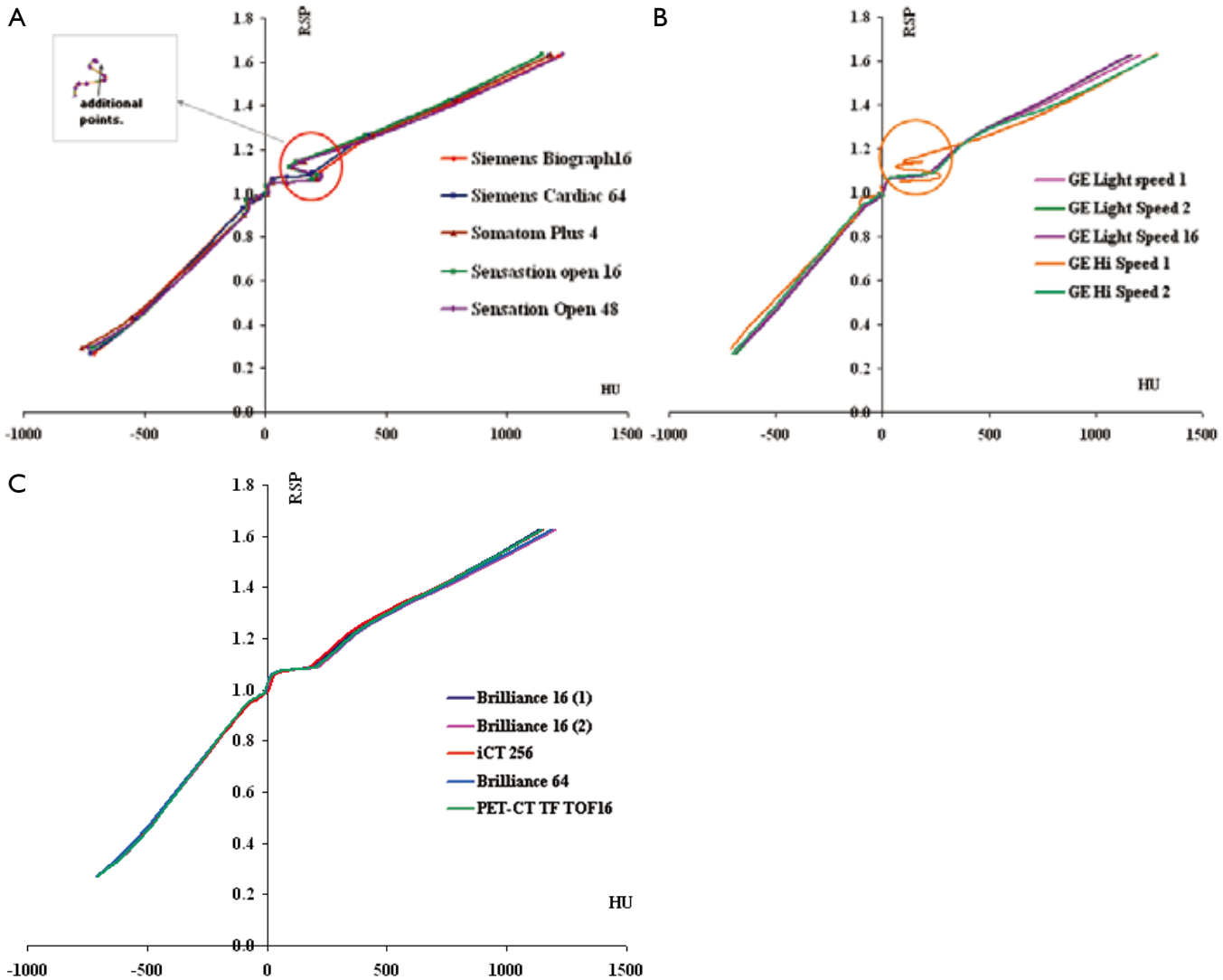

Figure 3 A. Comparison of HU-RSP curves for the different Siemens CT scanners. The region inside the circle is magnified to show the behavior of the curves due to additional inserts used to obtain the curves for some of the CT scanners; B. Comparison of HU-RSP curves for the different GE CT scanners. The strange behavior of the region inside the circle for the GE Hi Speed 1 CT scanner is due to additional inserts used to obtain the curve; C. Comparison of HU-RSP curves for the different Philips CT scanners

cortical bone which is the highest RSP point, the HU changes from 1,140 to 1,420 with a mean value of 1,210±720 (1 SD).

Two HU-RSP curves for a particular institution were distinctively different from the rest of the group (the GE Hi Speed 1 in *Figure 3B* is one of the two, the other curve is the Toshiba Aquilion scanner). If these two curves are removed, the HU-RSP curves for this group of remaining 16 CT scanners show smaller deviations from each other, especially in the RSP region >1.1 as shown in *Figure 6*. For example, for the CB2 bone, the HU_{min}=407, and the HU_{max}=490, with the HU_{mean}=438±21.1. For the cortical bone, HU_{min}=1,140, HU_{max}=1,300, with the HU_{mean}=1,190±47.3. The variations of HU with respect to RSP were then described by the two HU-RSP curves representing the minimum and maximum of the HU for a given RSP.

It is interesting to note that for the TomoTherapy unit, the HU-RSP curve is almost linear for the entire range of HU. This is due to the fact that the attenuation of MeV photons is predominantly due to Compton interaction, which has a weak dependence on Z.

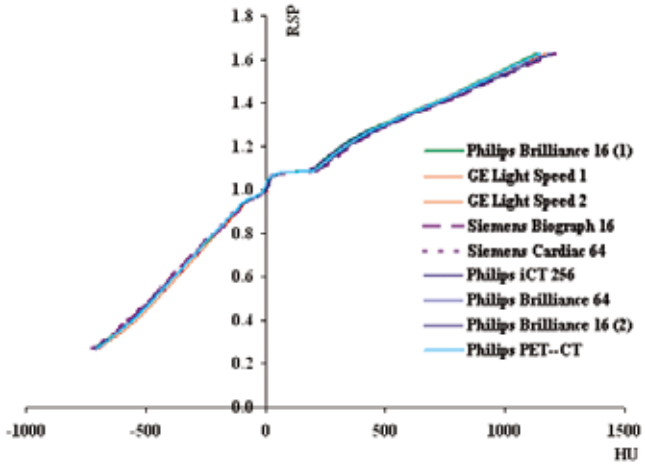

Figure 4 Comparison of HU-RSP curves for nine CT scanners obtained with the same RMI 467 phantom

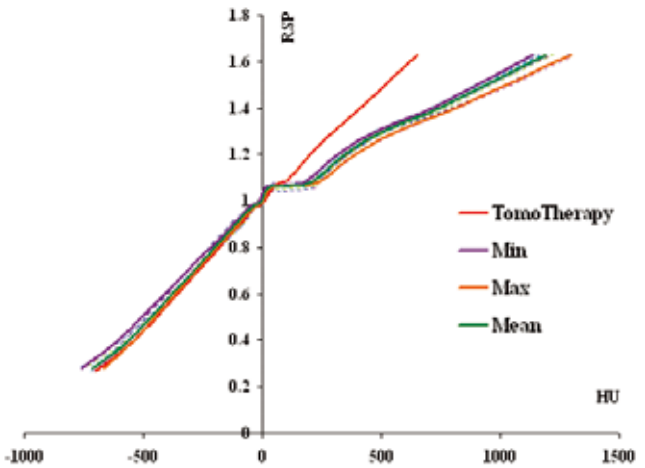

Figure 6 After removing the two HU-RSP curves from one institution which both showed distinctly different behavior from the other curves, the remaining 16 HU-RSP curves are plotted. A new set of HU_{min}-RSP_{av}, HU_{max}-RSP_{av} and HU_{mean}-RSP_{av}, curves were obtained

Effect of differences in HU-RSP curves on dose distributions

Table 3 compares the minimum, maximum and mean doses from the DVHs of the volumes of interest (GTV, PTV1, PTV2, bladder, rectum and seminal vesicle) for a prostate case. Since an opposed lateral beam configuration is used in the treatment, the major inhomogeneities involved are the femoral heads and the rectal balloon which is filled with a contrast medium of RSP=1.2. The HU-RSP curves (min, max, mean) used in the calculation were obtained without

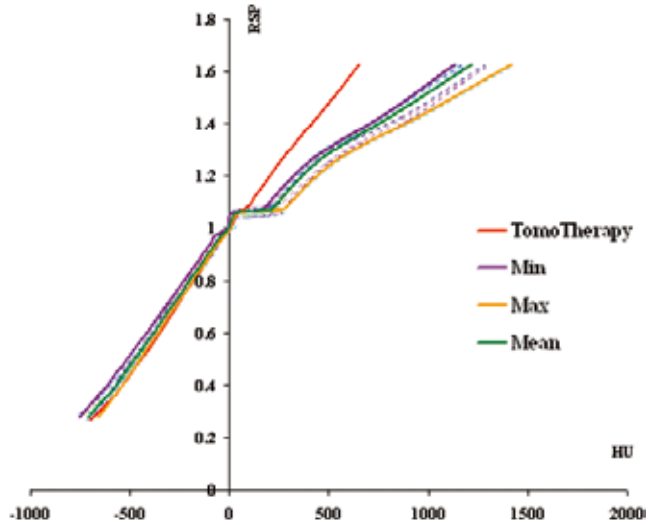

Figure 5 HU-RSP curves for all 18 CT scanners (dashed lines). The characterization curve obtained from a TomoTherapy unit is included for comparison. Also included are the three HU-RSP curves: HU_{min}-RSP_{av}, HU_{max}-RSP_{av} and HU_{mean}-RSP_{av}, labeled as min, max and mean in the graph

the two distinctly different HU-RSP curves. It can be seen that the three HU-RSP curves (min, max, mean) produce very similar DVH parameters for the volumes of interest when compared with those obtained from the clinical HU-RSP curve (labeled as IUHPTC120). Indeed, the min, max and mean doses for all the volumes of interest were within 1% for all but the minimum dose to the PTV1, which was about 4.5% smaller than that from IUHPTC120.

Table 4 compares the minimum, maximum and mean doses from the DVHs of the volumes of interest for a head and neck case. Due to the complex shape of the target volumes, complicated beam setup was used. Despite the presence of inhomogeneities such as air cavities and bone, all three HU-RSP curves (min, max, mean) yielded DVH results for the various volumes of interests to within 5% of those obtained with the clinical calibration curve for the majority of the dose parameters examined. However, deviations >10% from the IUHPTC120-based plan in the dose parameters were observed for the optic nerves and cochlea for both the HU_{minn}-RSP and HU_{max}-RSP plans. The DVHs for the HU_{mean}-RSP plan, on the other hand, agreed with the OIHPTC120 plan to within 4%.

Discussion and conclusions

We have compared the HU-RSP curves for 18 CT scanners

Table 3 Comparison of the min, max and mean doses for the different volumes of interest in a prostate plan in proton therapy

Prostate		Min dose	Max dose	Mean dose
PTV1	HU-RSP-MIN	4,627	8,168	7,333
	HU-RSP-MAX	4,839	8,132	7,348
	HU-RSP-MEAN	4,833	8,149	7,349
	IUHPRC120	4,834	8,153	7,348
PTV2	HU-RSP-MIN	5,982	8,168	7,898
	HU-RSP-MAX	5,966	8,132	7,875
	HU-RSP-MEAN	5,973	8,149	7,887
	IUHPRC120	5,970	8,153	7,888
GTV	HU-RSP-MIN	7,675	8,164	7,926
	HU-RSP-MAX	7,673	8,118	7,893
	HU-RSP-MEAN	7,679	8,137	7,908
	IUHPRC120	7,677	8,145	7,909
Bladder	HU-RSP-MIN	0	8,061	897
	HU-RSP-MAX	0	8,031	943
	HU-RSP-MEAN	0	8,045	924
	IUHPRC120	0	8,048	923
Rectum	HU-RSP-MIN	0	7,339	2,138
	HU-RSP-MAX	0	7,344	2,128
	HU-RSP-MEAN	0	7,341	2,133
	IUHPRC120	0	7,340	2,133
Seminal vesicle	HU-RSP-MIN	5,070	8,000	6,606
	HU-RSP-MAX	5,056	7,962	6,593
	HU-RSP-MEAN	5,069	7,980	6,601
	IUHPRC120	5,067	7,982	6,602

and a TomoTherapy unit operated in the imaging mode. The CT scanners were from five different manufacturers. Five RMI 467 phantoms, two of which were an identical pair, were used to generate the HU-RSP curves. Thus practically, only three different RMI phantoms were used for the 18 HU-RSP curves. Here, we assumed that the elemental compositions of the tissue substitutes were identical so long as their RED values were the same. There was a small variation (<2%) in RED (and RSP) among the three different RMI phantoms for all tissue substitute materials except for LN-300, which had about 5% variation among the three phantoms.

The variations of the HU within each RMI phantom group generally show larger variation for RMI 1 as shown by the three representative materials in *Figure 1*. If we assume that phantoms within the same group were truly identical, the variation in HU indicates the source of variation being the different x ray spectra of the different CT scanners.

Figure 3A-C shows that even for CT scanners from the same vendor, the HU-RSP curves may deviate from each other. There are two factors that may contribute to the HU variation: the difference in the x ray spectra of the CT scanners and the variation in the chemical composition of the 'same' tissue substitute materials in the different RMI phantoms. The minimum HU was in general 7-10% lower than the maximum HU, for all tissue substitute materials and for all CT scanners in the study.

On the other hand, using the same RMI phantom the HU-RSP curves for nine CT scanners from various vendors are remarkably similar as shown in *Figure 4*. For cortical bone, the minimum HU was about 5% smaller than the maximum HU. For LN-300, the minimum HU was about 2.5% smaller than the maximum HU. The results seem to indicate that the chemical compositions of the tissue substitute materials have a larger effect on the HU than the

Table 4 Comparison of the min, max and mean doses for the different volumes of interest in a head and neck plan in proton therapy

H&N		Min dose	Max dose	Mean dose	H&N	Min dose	Max dose	Mean dose
PTV	HU-RSP-MIN	4,512	6,370	5,768	R optic nerve	0	3,812	1,152
	HU-RSP-MAX	4,925	6,366	5,761		5	3,996	1,592
	HU-RSP-MEAN	4,753	6,367	5,765		2	3,890	1,391
	IUHPRC120	4,712	6,368	5,767		1	3,866	1,305
CTV	HU-RSP-MIN	5,033	6,368	5,781	Brainstem	5,264	5,950	4,622
	HU-RSP-MAX	5,039	6,366	5,771		5,250	5,960	5,612
	HU-RSP-MEAN	5,048	6,367	5,776		5,257	5,956	5,617
	IUHPRC120	5,050	6,366	5,779		5,260	5,954	5,619
GTV	HU-RSP-MIN	5,054	6,300	5,758	Cord	0	5,406	2,715
	HU-RSP-MAX	5,039	6,294	5,747		0	5,397	2,710
	HU-RSP-MEAN	5,048	6,297	5,752		0	5,402	2,713
	IUHPRC120	5,050	6,299	5,754		0	5,403	2,713
Optic chiasm	HU-RSP-MIN	3,638	5,020	4,152	L cochlea	3,559	5,969	5,229
	HU-RSP-MAX	3,667	5,370	4,506		4,904	6,045	5,736
	HU-RSP-MEAN	3,656	5,217	4,312		4,304	6,024	5,545
	IUHPRC120	3,651	5,158	4,278		3,754	5,994	5,341
L optic nerve	HU-RSP-MIN	0	3,750	1,028	R Cochlea	855	4,485	2,695
	HU-RSP-MAX	0	3,985	1,278		880	4,618	2,807
	HU-RSP-MEAN	0	3,852	1,164		862	4,553	2,747
	IUHPRC120	0	3,823	1,127		855	4,508	2,712

X-ray spectrum.

The calibration curves for all CT scanners generally exhibit similar shapes and can be described by three linear segments in three distinct HU regions: [–700, 0], [0, 1,100] and [1,100, 1,700]. The largest deviations in the HU-RSP curves among the different CT scanners occur in the bone region where RSP >1.4. The 18 HU-RSP curves showed substantial variation over the range of HU from –700 to 1,700. However, by removing the two curves from one institution, which seem to have distinctly different behavior, the variations of the HU-RSP curves for the remaining 16 scanners were substantially reduced. The HU_{min}-RSP_{av} and HU_{max}-RSP_{av} curves followed closely the envelop of the 16 curves.

Despite the relatively large variation of between the HU_{min}-RSP_{av} and HU_{max}-RSP_{av} curves, the minimum, maximum and mean doses from the DVHs of the volumes of interests for a prostate plan obtained with these two calibration curves were within 1% of those obtained with the clinical calibration curve and the HU_{mean}-RSP_{av} curve, which represent the average HU-RSP curve of all 16 CT scanners. For the head-and-neck plan, the agreement was still within 5% for most dose points for the various volumes of interests. Our results indicate that 7-10% differences between the HU-RSP curves had <5% effect even in a complex head and neck plan with the presence of several inhomogeneities.

This study did not address the issue of metallic implants as this was beyond the scope of this work. Rather it shows that while both elemental compositions of the tissue substitutes and the variation in the X-ray spectrum among the CT scanners contribute to the HU variation for a given RSP value, the effect of the X-ray spectrum, and hence the beam hardening effect is smaller than that due to difference in elemental compositions. This is in agreement with the study by Qi *et al.* (14). On the other hand, despite the large variation among the HU-RSP (min, max and mean) curves, the minimum, maximum and the mean doses for the target volume as well as for the OAR were generally in very good agreement with the reference plan. The excellent agreement between the dose calculation results using HU_{mean}-RSP_{av} and those from the clinical HU-RSP curve seems to suggest that a single HU-RSP reference curve, generated by a large number of treatment planning CT scanners, may be used for proton therapy. A similar conclusion has been reported for 6 MV

X-rays by Thomas (5).

This study does not recommend the use of a single HU-RSP curve without a CT calibration. On the contrary, a user has to do a calibration of his/her own scanner using a tissue characterization phantom and then compare the curve with the 'universal' curve to decide if the latter is suitable to be used. This is similar to the golden data offered by linac vendors. Indeed, a golden beam data has also been recently proposed for proton pencil beams used in active beam scanning (18). A clinic which purchases the golden data for a linac still has to obtain a number of beam scanning data to verify that the golden data is suitable for their clinic. Thereafter, beam data would still need to be scanned annually to confirm the suitability and stability of the beam so that the golden data could be used. A HU-RSP reference curve may be used in a similar manner.

In summary, the present work is the first study that examined a large number (18) of kVCT scanners that are newer models commonly used in the clinic. In addition, a MVCT was also studied. Further, our study is also the first to look at the differences in dose distributions in proton therapy due to variations in HU-RSP curves. Our study showed that the differences in HU-RSP curves obtained from tissue substitute materials appear to affect the minimum, maximum and mean dose parameters of a representative prostate treatment plan by less than 1% and that of a representative head and neck plan by less than 4%. This suggests the usefulness of a single 'averaged' HU-RSP reference curve.

Acknowledgements

Disclosure: This paper was partially presented as a poster in the AAPM annual meeting in 2010. None of the authors has any financial interests with any of the CT vendors.

References

1. Levi C, Gray JE, McCullough EC, et al. The unreliability of CT numbers as absolute values. AJR Am J Roentgenol 1982;139:443-7.
2. Faulkner K, Moores BM. Variations in measured computed tomography number values. Radiography 1985;51:163-7.
3. Constantinou C, Harrington JC, DeWerd LA. An electron density calibration phantom for CT-based treatment planning computers. Med Phys 1992;19:325-7.
4. Coolens C, Childs PJ. Calibration of CT Hounsfield units for radiotherapy treatment planning of patients with metallic hip prostheses: the use of the extended CT-scale. Phys Med Biol 2003;48:1591-603.
5. Cozzi L, Fogliata A, Buffa F, et al. Dosimetric impact of computed tomography calibration on a commercial treatment planning system for external radiation therapy. Radiother Oncol 1998;48:335-8.
6. Kilby W, Sage J, Rabett V. Tolerance levels for quality assurance of electron density values generated from CT in radiotherapy treatment planning. Phys Med Biol 2002;47:1485-92.
7. Thomas SJ. Relative electron density calibration of CT scanners for radiotherapy treatment planning. Br J Radiol 1999;72:781-6.
8. Schneider U, Pedroni E, Lomax A. The calibration of CT Hounsfield units for radiotherapy treatment planning. Phys Med Biol 1996;41:111-24.
9. Bichsel H. eds. Passage of charged particles through matter, In American Institute of Physics Handbook. New York: McGraw-Hill, 1972.
10. Yohannes I, Kolditz D, Kalender WA. Semiempirical analysis of materials' elemental composition to formulate tissue-equivalent materials: a preliminary study. Phys Med Biol 2011;56:2963-77.
11. Yohannes I, Kolditz D, Langner O, et al. A formulation of tissue- and water-equivalent materials using the stoichiometric analysis method for CT-number calibration in radiotherapy treatment planning. Phys Med Biol 2012;57:1173-90.
12. ICRU Report 44. Tissue substitutes in radiation dosimetry and measurement. In. Bethesda, MD: International Commission on Radiation Units and Measurements, 1989.
13. Schaffner B, Pedroni E. The precision of proton range calculations in proton radiotherapy treatment planning: experimental verification of the relation between CT-HU and proton stopping power. Phys Med Biol 1998;43:1579-92.
14. Qi ZY, Huang SM, Deng XW. Calibration of CT values used for radiation treatment planning and its impact factors. Ai Zheng 2006;25:110-4.
15. Langen KM, Meeks SL, Poole DO, et al. The use of megavoltage CT (MVCT) images for dose recomputations. Phys Med Biol 2005;50:4259-76.
16. ICRU Report 49. Stopping Powers and Ranges for Protons and Alpha Particles. In. Bethesda, MD: International Commission on Radiation Units and Measurements, 1993.
17. Yang M, Virshup G, Mohan R, et al. Improving accuracy of electron density measurement in the presence of metallic

implants using orthovoltage computed tomography. Med Phys 2008;35:1932-41.
18. Clasie B, Depauw N, Fransen M, et al. Golden beam data for proton pencil-beam scanning. Phys Med Biol 2012;57:1147-58.

Cite this article as: Cheng CW, Zhao L, Wolanski M, Zhao Q, James J, Dikeman K, Mills M, Li M, Srivastava SP, Lu XQ, Das IJ. Comparison of tissue characterization curves for different CT scanners: implication in proton therapy treatment planning. Transl Cancer Res 2012;1(4):236-246. doi: 10.3978/j.issn.2218-676X.2012.11.05

Original Article

Surgical organ displacement for proton radiotherapy

Jerry M. Jesseph[1], Markus M. Fitzek[1,2], Kambiz Shahnazi[2], Song-Chu Ko[1,2], James R. Howe[3], Allan F. Thornton[2], Andrew L. Chang[1,2]

[1]Indiana University School of Medicine, Indianapolis, IN, USA; [2]Indiana University Health Proton Therapy Center, Bloomington, IN, USA; [3]University of Iowa Carver College of Medicine, Iowa City, IA, USA

Correspondence to: Andrew L. Chang, MD. Hampton University Proton Therapy Center, 40 Enterprise Parkway, Hampton, VA 23666, USA. Email: AndrewLChangMD@gmail.com.

doi: 10.3978/j.issn.2218-676X.2012.12.05

Scan to your mobile device or view this article at: http://www.thetcr.org/article/view/855/html

Introduction

Proton radiotherapy is a method of applying high-energy particle radiation to treat cancers. Proton therapy is appealing due to its ability to deliver highly conformal dose distributions while minimizing radiation to adjacent normal tissues (1). Proton treatments first began in the 1950s using equipment added on to large nuclear physics labs. The Indiana University Health Proton Therapy Center (IUHPTC, formerly Midwest Proton Radiotherapy Institute) was built at the Indiana University Cyclotron Facility in Bloomington, Indiana, and was the third established center actively treating patients in the United States. At present, there are 10 proton centers treating patients in the US and several more around the world.

In general, the effectiveness of any form of radiation treatment is limited by the tolerances of adjacent normal tissues. The acute and chronic toxicity of radiation (especially to bowel) continues to confound our therapies (2-4). Often the morbidity and cost from the side effects of radiation treatments can become worse than the original disease (5).

While proton radiotherapy treatments can provide more precision in dose delivery, the same problem remains of damage to very closely adjacent structures; conversely, along with a greater ability to provide an intense, targeted dose of radiation to a target volume, there is also the potential to cause greater collateral damage. The authors encountered a number of patients who, despite the accuracy of proton therapy dose distributions, could not be treated adequately and safely due to closely adjacent or abutting vulnerable structures. The question became: can we change the anatomy?

The authors have collaborated in an attempt to surgically alter the patient's anatomy to make untreatable patients treatable. Here we present our initial series of surgical organ displacements performed on patients with localized cancers of the abdomen and pelvis for whom there were no other acceptable treatment options.

Methods

After obtaining IRB approval, we reviewed the charts of all patients treated at IUHPTC who had had undergone surgical organ displacement with the intention for treatment with proton radiotherapy. We reviewed the pathologic categories, diagnostic images (CT, MRI, and PET), treatment plans and available outcomes of the patients.

Planning and decisions about spacing and strategy were a combined effort of the treatment team. All patients had no evidence of metastatic disease. All patients were initially considered to be untreatable even with protons without some alteration of their anatomy due to adjacent bowel or critical structures preventing sufficient dosage to expect an adequate response. All patients were treated by laparotomy and displacement of organs using omentum and/or saline breast prostheses, anterior oophoropexy, colopexy, or diverting colostomy if required. Multiple metallic fiducial markers were placed at time of surgery to guide treatment planning and for accurate targeting during treatment.

The majority of patients had previous (often multiple) abdominal and pelvic surgical procedures and several had previous conventional radiation treatments to the area as well. There was no assurance given that the displacement procedures would accomplish what was required, and once

Table 1 Organ displacement summary

	Disease	Organs at risk	Displacement technique
1.	Recurrent bladder cancer	Urostomy, small bowel, and sigmoid colon	Breast prosthesis and diverting colostomy
2.	Recurrent bladder cancer	Small bowel and sigmoid colon	Two breast prostheses and diverting colostomy
3.	Recurrrent (3x) desmoid tumor of rectus sheath	Small bowel, ovaries, and bladder	Breast prosthesis (extraperitoneal)
4.	Recurrent rectal cancer (previously irradiated)	Small bowel	Breast prosthesis
5.	Recurrent cholaniocarcinoma of the liver	Stomach, duodenum, and colon	Omentum as spacer
6.	Hepatocellular carcinoma (unresectable)	Stomach, duodenum, and colon	Omentum as spacer
7.	Hepatocellular carcinoma (unresectable)	Stomach, duodenum, and colon	Omentum as spacer
8.	Pelvic sarcoma (unresectable)	Small bowel and colon	Breast prosthesis
9.	Recurrent sacral chordoma	Small bowel	Breast prosthesis
10.	Recurrent pancreatic cancer	Small bowel and colon	Colopexy, omentum, and breast prosthesis
11.	Recurrent pancreatic cancer	Small bowel and colon	Colopexy and omentum
12.	Cholangiocarcinoma of the liver (unresectable)	Small bowel and colon	Omentum as spacer
13.	T3 low rectal cancer	Small bowel, uterus, and ovaries	Breast prosthesis
14.	Obstructing carcinoma of the head of the pancreas	Small bowel, colon, and stomach	Colopexy, omentum, and breast prosthesis
15.	Multiply recurrent retroperitoneal desmoid tumor	Small bowel	Tissue expander and omentum

the procedures were done, the decision to treat was made independently by the radiation oncologist based on the treatment planning CT. Each patient was informed about the uncertainty of adequate displacement and the risk for complications from the displacement procedure themselves, in addition to the risks and benefits of proton radiotherapy.

Our patients ranged from 16 to 82 years of age, and are summarized on *Table 1*. They included: two recurrent bladder cancers after radical cystectomy, a thrice recurrent desmoid tumor of the rectus sheath, a multiply recurrent desmoid tumor of the retroperitoneum, a previously irradiated and locally recurrent rectal cancer after abdominoperineal resection, a cholangiocarcinoma of the liver, two unresectable hepatocellular carcinomas, an unresectable pelvic sarcoma, a recurrent sacral chordoma, two recurrent pancreatic cancers and an enlarging unresectable cholangiocarcinoma of the liver. In addition, we performed organ displacement for a 21-year-old female with a T3 low rectal cancer, who then underwent subsequent preoperative (neoadjuvant) treatment using protons, and for an 82-year-old with an obstructing carcinoma of the head of the pancreas for whom proton radiation was her only treatment. To our knowledge, the latter two patients are unique in that no such methods to treat malignancies with protons in this way had been previously attempted.

Results

No surgical complications were encountered. All patients obtained adequate displacement to allow for successful proton treatment planning. All completed their treatment course with protons except for one patient with a diagnosis of recurrent pancreatic cancer who developed a perforation of a marginal ulcer at a previous gastrojejunostomy and could not continue; the patient subsequently died of issues unrelated to his radiation or displacement procedure. Two patients had some migration of the spacers that required re-planning; one patient a primary pancreatic cancer, and another with a multiply recurrent retroperitoneal desmoids. Both were able to complete the proton radiation therapy treatment course. Data from this series of patients is shown in *Table 1*. Selected proton treatment plans are shown in *Figures 1-6*.

All patients who completed their treatment developed no radiation-related complications greater than Grade 2

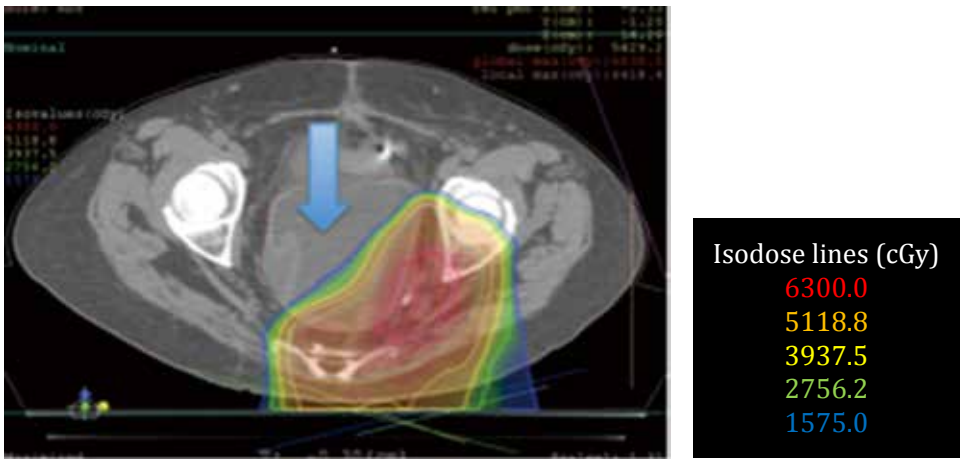

Figure 1 Recurrent rectal cancer. Arrow indicates breast prosthesis

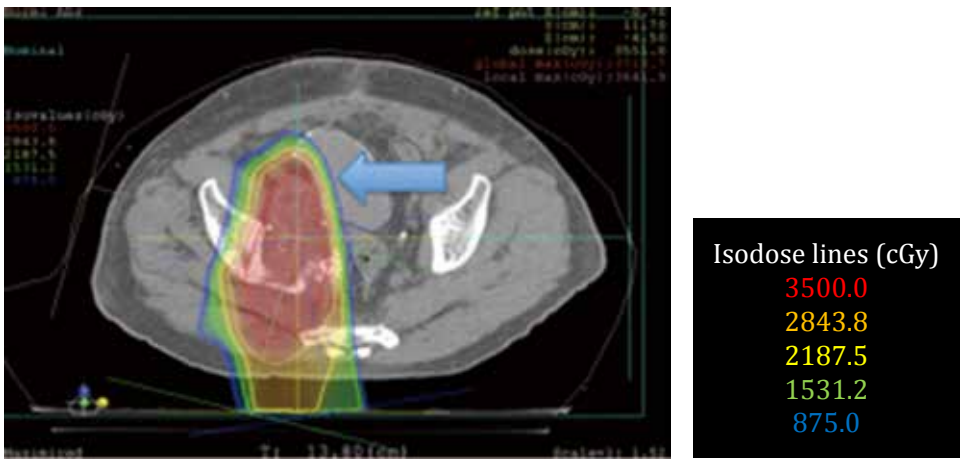

Figure 2 Recurrent bladder cancer. Arrow indicates breast prosthesis

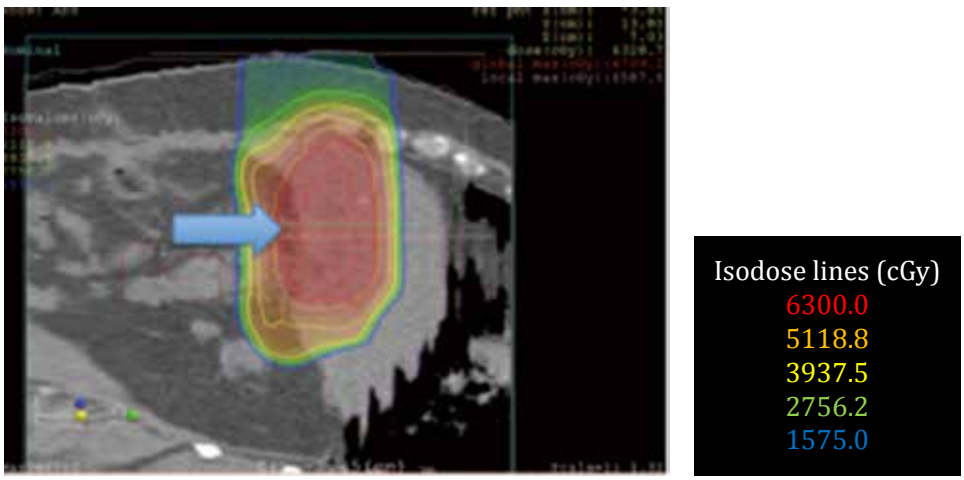

Figure 3 Unresectable cholangiocarcinoma. Arrow indicates omentum

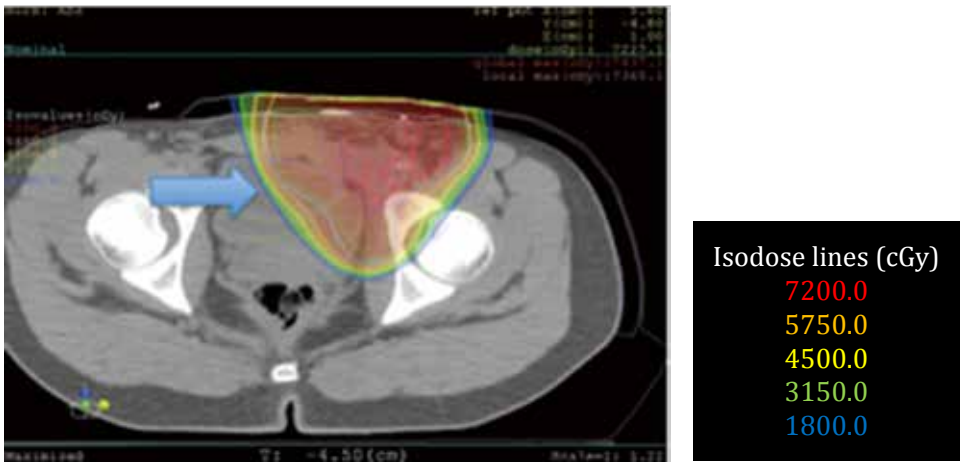

Figure 4 Recurrent desmoid tumor. Arrow indicates breast prosthesis

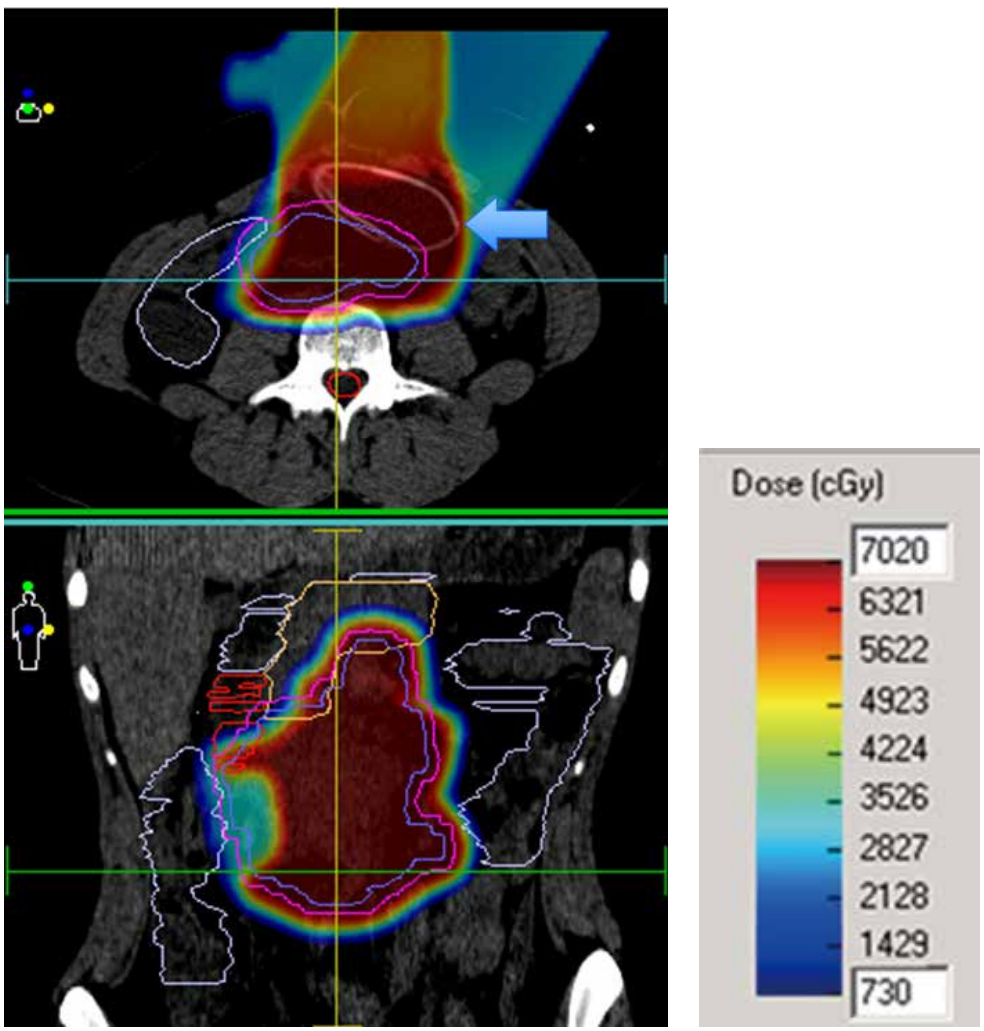

Figure 5 Multiply recurrent desmoid tumor. Arrow indicates tissue expander

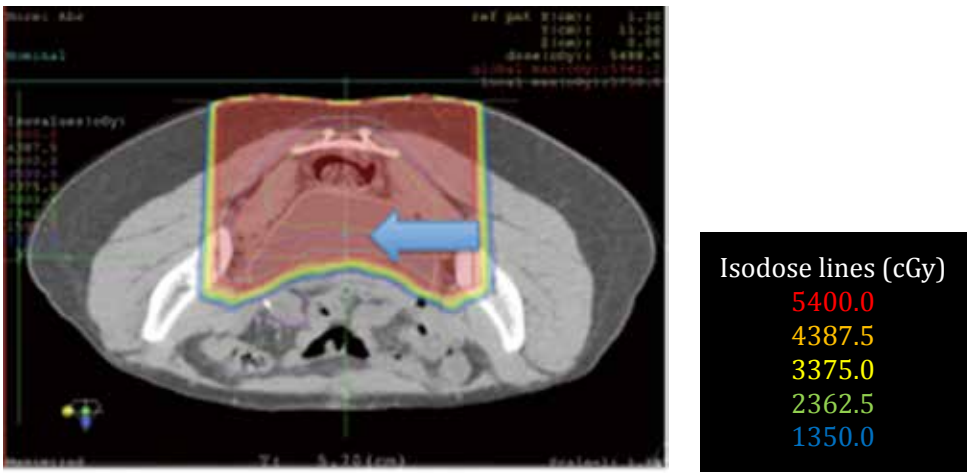

Figure 6 T3 Low rectal cancer. Arrow indicates breast prosthesis

radiation dermatitis. Mean target dose was 63 Gy(RBE) with a range of 35 to 72 Gy(RBE). The longest follow up is six years in the patient with a pelvic sarcoma. That patient is presently active and without evidence of disease.

The 19-year-old patient with the multiply recurrent retroperitoneal desmoid tumor is 2 years post-radiation and continues to have regression of her tumor. She tolerated 70.0 Gy(RBE) to the abdomen without any GI symptoms during her treatment course nor in the intervening time. She had subsequent removal of the spacer (*Figure 5*).

The 21-year-old patient who received preoperative proton treatment for a locally advanced rectal cancer after organ displacement completed her abdominoperineal resection and is doing well. She has had no gastrointestinal toxicity and continues to have regular menstrual periods (*Figure 6*).

The remaining patients are within two years of completion of proton treatment, and none has shown signs of radiation enteritis. Patients displaced for liver tumors have shown complete responses and, at present, have no evidence of disease. All patients with recurrent pelvic tumors have shown good responses to treatment thus far. The one patient who completed proton treatment for recurrent pancreatic cancer was found later to have developed evidence of metastatic disease and is awaiting decisions about further chemotherapy.

Discussion

Surgeons and radiation oncologists have collaborated quite successfully in the treatment of several malignancies. This is most apparent in our present methods of breast conserving therapy for the treatment for breast cancer. Another obvious outcome improvement from collaboration has been in the treatment of patients with locally advanced rectal cancers.

The life-long morbidity of radiation enteritis from conventional radiation treatments has motivated attempts at a variety of surgical displacement procedures in the abdomen, pelvis and retroperitoneum (6-12). Displacement of organs using omentum, tissue expanders, breast prostheses and several types of mesh has been reported, but none of these methods have gained widespread usage (13-16). In addition, techniques like oophoropexy have been employed to move radiosensitive structures out of harm's way. Despite some apparent advantages, these methods have not entered mainstream clinical practice. For conventional radiation techniques the benefit is often not worth the extra surgical morbidity. The dose to other adjacent structures usually remains high even with displacement.

However, the unique characteristics of proton therapy appeared to present an opportunity in which old ideas might prove to have new and more beneficial applications. Recently, our efforts have been supported by two published case reports demonstrating the utility of displacement methods for proton radiotherapy (17,18).

Proton radiotherapy differs in several important ways from standard external beam radiation therapy. These differences need to be well understood by surgeons and radiation oncologists alike. Conventional therapies use high-energy ionizing radiation that passes through tissues giving both an entrance dose and an exit dose. Therefore, the target volume is normally covered using multiple fields

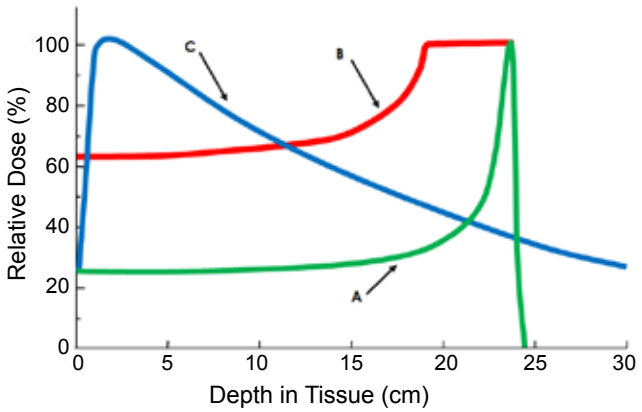

Figure 7 A. Pristine peak of a 200 MeV proton beam; B. 5 cm Spread-Out Bragg Peak (SOBP) of a 200 MeV proton beam; C. 8 MV X-ray beam (100 cm SSD)

(beam angles) to spread out the entrance and exit doses in order to lessen dosage to normal tissues and to increase the target dose where the beam paths converge.

With protons, which are positively charged particles, the entrance dose tends to be less as most of the protons pass between atomic nuclei near the speed of light. Once into the tissues, the interaction of the protons with the negatively charged electron clouds causes a slowing of the proton trajectories. As the particles slow enough, the inter-nuclear forces bring about an interaction by which the protons impart their energy to the tissues and then stop without an exit dose. This area of high dose is called the Bragg peak. By combining beam energies, this peak can be spread out in depth to cover a larger area that is referred to as the Spread-Out Bragg Peak (SOBP). As the SOBP increases in depth, the entrance dose increases as well (see *Figure* 7). As with standard radiation methods, multiple beam angles are often required to supply adequate dosage for proton treatments as well.

It is critical for surgeons to understand these differences in radiation delivery so that, with organ displacement for proton radiotherapy, one can move critical structures: (I) out of the penumbra of the beam path laterally, (II) beyond the end of the Bragg peak (out of range), and/or (III) proximal in the beam path - out of the high dose Bragg peak. In addition, knowing normal tissue tolerances, effective target dosages, range uncertainties, organ motion issues due to breathing and body motion, dose uncertainties due to air or gas within the tissues, along with constraints of beam angles and beam delivery are all necessary to engage adequately in treatment planning decisions and for proper execution of displacement procedures. This requires significant collaboration between the surgeon and treating radiation oncologist; in several cases, the radiation oncology authors were present at the time of the operation to help determine the displacement technique utilized.

Our series underscores a variety of issues of fundamental importance for treatment of recurrent and unresectable tumors of the abdomen and pelvis using protons. The biology of a specific tumor has a significant impact on our ability to improve survival and palliate symptoms. Adequate and stable displacement in the pelvis is, at present, a promising technique. The upper abdomen remains problematic due to the large number of closely associated organs as well as the motion imparted by the diaphragm. One exception is the liver, for which displacement has been clearly shown, by us and by others, to allow for adequate and safe treatment of liver lesions.

Importantly, evidence of metastatic disease makes these complex pursuits futile in most instances where there can be no significant impact on morbidity and survival. All this can make patient selection for proton radiotherapy treatment challenging.

Logistics can be challenging as well, since patients, at present, often must travel long distances from home for proton treatment at one of the few facilities offering proton radiotherapy. The addition of displacement procedures will lengthen the already lengthy process of proton treatment planning and delivery that can often span several weeks. Additionally, at first, few teams may understand or be accepting of the whole process.

The most important question to ask ourselves about organ displacement for proton radiotherapy is whether or not the risks involved (plus the time and expense) is worth the increased complexity. It is crucial for all involved to understand that the displacement procedure might not work to make proton treatment possible. Plus, the morbidity from the displacement procedure carries significant possible complications itself. We have been most fortunate in this regard thus far.

Previous reports of organ displacement for standard radiation have included complications such as, infections, movement of the spacers, spontaneous deflation or extrusion of a prosthesis, and entero-cutaneous fistulae. Although there have been no reports, concern has been raised about possible impedance of venous return.

Further work in organ displacement using minimally invasive techniques has strong theoretical appeal for use in neo-adjuvant radiation for locally advanced (T3 and greater)

rectal cancers and, possibly, for non-metastatic pancreatic cancers. The general feeling in radiation oncology is that if sufficient dosage can be applied in tumors with a high risk of local recurrence, improved outcomes can be expected. We have shown that it is feasible to apply unprecedentedly high doses while improving tissue sparing using proton radiotherapy and surgical organ displacement in both diseases.

In the case of rectal cancers, we have demonstrated that it is possible to displace small bowel and pelvic viscera to completely avoid radiation dosage. We have shown that it is possible to minimize injury to the colon and small bowel and deliver dosages to the pancreas and retroperitoneum [72 Gy(RBE)] that have never been achieved without significant morbidity.

We are presently less enthusiastic about the value of organ displacement for recurrent pancreatic cancers, largely due to our inability to accurately recognize metastatic disease early as well as the often debilitated nature of most of these patients. While there appears to be some hope to lessen local recurrence with our methods used preoperatively, recurrent pancreatic cancer remains a difficult challenge at present.

For patients with recurrent disease after prior radiation therapy, organ displacement - especially of previously irradiated healthy tissue, such as bowel, may facilitate the delivery of an additional course of radiation therapy. However, the morbidity even from an open procedure can be significant in patients that have had previous surgery and radiation; minimally invasive surgery to displace organs for recurrent disease is unlikely to be successful (and may be harmful) because of extensive adhesion formation from surgery, radiation and desmoplastic reactions. In these cases surgical experience and judgment are crucial to bring about satisfactory displacement and minimize morbidity.

The prospect of eliminating, or at least, significantly reducing radiation injury to the bowel is important considering the fact that up to sixty percent of patients receiving pelvic radiation suffer life-long consequences requiring multiple hospitalizations, diagnostic procedures (including further radiation exposure), surgical procedures, loss of work and general misery (5). The cost to the individual and to society from standard pelvic radiation is great. We see opportunity for much improvement.

Conclusions

In our small series of highly selected patients with primary or recurrent pelvic and abdominal tumors, and patients with primary liver tumors, we have convincingly shown that it is technically feasible and safe to alter the anatomical relations in these patients surgically. This can be done with minimal morbidity and convert previously untreatable patients into treatable patients who can receive relatively high doses of radiation with protons.

More significantly, we have shown that it is technically feasible to displace organs to allow neo-adjuvant treatment with particle therapy for locally advanced rectal cancer and pancreatic cancer. These combined techniques hold a double hope of more effectively treating a difficult cancer and also diminishing or eliminating the costly and disabling effects often seen with conventional radiation. We see opportunities for valuable collaboration and innovation in this area, especially in the development of minimally invasive displacement techniques.

Acknowledgements

Disclosure: The authors declare no conflict of interest.

References

1. Sui H, Urie M. Proton beams in radiation therapy. J Natl Cancer Inst 1992;83:155-64.
2. Galland RB, Spencer J. Natural history and surgical management of radiation enteritis. Br J Surg 1987;74:742-7.
3. Touboul E, Balosso J, Schlienger M, et al. Radiation injury of the small intestine. Radiobiological, radiopathological aspects; risk factors and prevention. Ann Chir 1996;50:58-71.
4. Rubio CA, Jalnas M. Dose-time-dependent histological changes following irradiation of the small intestine of rats. Dig Dis Sci 1996;41:392-401.
5. Letschert JG, Lebesque JV, Aleman BM, et al. The volume effect in radiation-related late small bowel complications: results of a clinical study of the EORTC Radiotherapy Cooperative Group in patients treated for rectal carcinoma. Radiother Oncol 1994;32:116-23.
6. Shanahan TG, Mehta MP, Bertelrud KL, et al. Minimization of small bowel volume within treatment fields utilizing customized "belly boards". Int J Radiat Oncol Biol Phys 1990;19:469-76.
7. Hindley A, Cole H. Use of peritoneal insufflation to displace the small bowel during pelvic and abdominal radiotherapy in carcinoma of the cervix. Br J Radiol 1993;66:67-73.

8. Gallagher MJ, Brereton HD, Rostock RA, et al. A prospective study of treatment techniques to minimize the volume of pelvic small bowel with reduction of acute and late effects associated with pelvic irradiation. Int J Radiat Oncol Biol Phys 1986;12:1565-73.
9. Vasilev SA, McGonigle KF, Spencer-Smith EL. Intestinal peritoneal sling as an adjunct to radical pelvic operation and pelvic irradiation. J Am Coll Surg 1995;180:568-72.
10. Rodier JF, Janser JC, Roy C, et al. Pelvic exclusion using polyglactin 910 mesh (Vicryl) for preventing radiation injuries of the small intestine Apropos of a series of 24 cases. Bull Cancer 1989;76:1121-5.
11. Evans DB, Shumate CR, Ames FC, et al. Use of Dexon Mesh for abdominal partitioning above the peritoneal reflection. Dis Colon Rectum 1991;34:833-5.
12. Chen JS, ChangChien CR, Wang JY, et al. Pelvic peritoneal reconstruction to prevent radiation enteritis in rectal carcinoma. Dis Colon Rectum 1992;35:897-901.
13. Sugarbaker PH. Intrapelvic prosthesis to prevent injury of the small intestine with high dosage pelvic irradiation. Surg Gynecol Obstet 1983;157:269-71.
14. Burnett AF, Coe FL, Klement V, et al. The use of a pelvic displacement prosthesis to exclude the small intestine from the radiation field following radical hysterectomy. Gynecol Oncol 2000;79:438-43.
15. Hong A, Stevens G, Stephen M. Protection of the small bowel during abdominal radiation therapy with a tissue expander prosthesis. Aust N Z J Surg 2000;70:690-2.
16. Hoffman JP, Lanciano R, Carp NZ, et al. Morbidity after intraperitoneal insertion of saline-filled tissue expanders for small bowel exclusion from radiotherapy treatment fields: a prospective four year experience with 34 patients. Am Surg 1994;60:473-82; discussion 482-3.
17. Fukumoto T, Komatsu S, Hori Y, et al. Particle beam radiotherapy with a surgical spacer placement for advanced abdominal leiomyosarcoma results in a significant clinical benefit. J Surg Oncol 2010;101:97-9.
18. Komatsu S, Hori Y, Fukumoto T, et al. Surgical spacer placement and proton radiotherapy for unresectable hepatocellular carcinoma. World J Gastroenterol 2010;16:1800-3.

Cite this article as: Jesseph JM, Fitzek MM, Shahnazi K, Ko SC, Howe JR, Thornton AF, Chang AL. Surgical organ displacement for proton radiotherapy. Transl Cancer Res 2012;1(4):247-254. doi: 10.3978/j.issn.2218-676X.2012.12.05

Review Article

Gold nanoparticles in radiation research: potential applications for imaging and radiosensitization

Jay F. Dorsey*, Lova Sun*, Daniel Y. Joh, Alon Witztum, Ajlan Al Zaki, Gary D. Kao, Michelle Alonso-Basanta, Stephen Avery, Andrew Tsourkas, Stephen M. Hahn

Department of Radiation Oncology, Perelman School of Medicine (JFD, LS, DYJ, AW, GDK, MAB, SA, SMH); Department of Bioengineering (AA, AT), University of Pennsylvania, Philadelphia, PA 19104, USA

*These authors contributed equally to this work.

Correspondence to: Jay F. Dorsey, M.D, Ph.D. Smilow Center for Translational Research, Perelman School of Medicine, University of Pennsylvania, Bldg. 421 Room 8-135, 3400 Civic Center Blvd, Philadelphia, PA 19104-5156, USA. Email: JayD@uphs.upenn.edu.

Abstract: The potential of gold nanoparticles (GNPs) in therapeutic and diagnostic cancer applications is becoming increasingly recognized. These biologically compatible particles can be easily synthesized, tuned to different sizes, and functionalized by conjugation to various biologically useful materials. Efficient and specific delivery to tumor tissue can then be accomplished either by passive accumulation in leaky tumor vessels and tissue, or by directly targeting tumor-specific biomarkers. Tumor-localized GNPs can serve as both adjuvants for enhancing the efficacy of radiation therapy and also as contrast agents for various imaging modalities. In this review, we will discuss recent advancements and future potential in the application of GNP as both a radiosensitizer and an imaging contrast agent. Due to their versatility and biocompatibility, gold nanoparticles may represent a novel theranostic adjuvant for radiation applications in cancer management.

Keywords: Gold Nanoparticle (GNP); theranostics; radiosensitization; nanoscale

doi: 10.3978/j.issn.2218-676X.2013.08.09

Scan to your mobile device or view this article at: http://www.thetcr.org/article/view/1547/2262

Applications of radiation in cancer imaging and treatment

Both ionizing radiation therapy and CT-based imaging modalities are mainstays of cancer treatment and diagnosis. These techniques, lifesaving as they are, have potential side effects and limitations; thus, adjuvants and complementary agents would be a welcome addition. From a therapeutic perspective, despite significant advances in technology, radiation therapy does not always achieve local control of the primary tumor, while at the same time potentially causing normal tissue toxicity. Radiosensitizing adjuvants that enhance the dose specifically absorbed by tumor tissue can result in enhanced tumor killing for any given total radiation dose compared to radiation therapy alone. From an imaging perspective, traditional iodine-based contrast agents are often limited by fast clearance, short imaging times, requirement for high doses of radiation, and insufficient contrast resolution (1). An agent with enhanced X-ray attenuation capabilities could potentially improve sensitivity and resolution of tumor imaging, while exposing patients to lower radiation doses. Gold nanoparticles (GNPs) are currently being studied in both of these therapeutic and diagnostic roles, and have thus far shown great potential clinical application.

Properties and functionalization of GNPs

Physicochemical properties of GNPs

The anti-cancer potential of GNPs stems from several advantageous physicochemical properties (*Figure 1*). First, numerous studies have established gold's safety and biocompatibility both *in vitro* and *in vivo* (2-6), suggesting

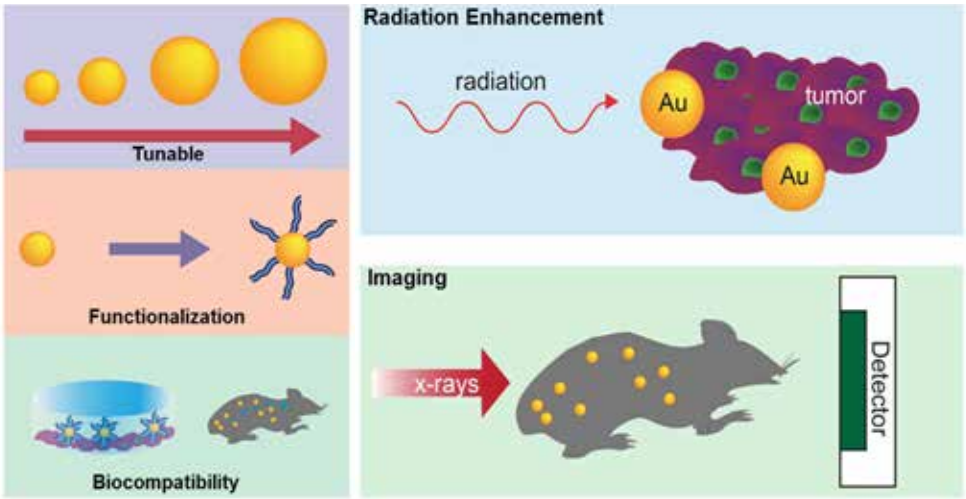

Figure 1 Versatility of Gold Nanoparticles. GNPs can be tunable to various shapes and sizes, functionalized with various biomolecules, and are generally safe and nontoxic *in vitro* and *in vivo*. They also have the ability to enhance radiation therapy of tumors, as well as serve as high-Z imaging contrast agents

that GNPs can be safely administered with minimal inflammatory activation (6) and few local or systemic side effects. Second, gold can be easily manufactured in a variety of shapes and sizes, and possesses easily controllable surface chemistry allowing functionalization with various biologically useful molecules to help evade immune detection and improve stability, tumor-targeting, and crossing of biophysical barriers such as the blood-brain barrier (7,8). Third, gold's high atomic number (Au, 79) allows high absorption and enhancement of ionizing radiation, as well as superior X-ray attenuation for imaging applications. Other physical characteristics of gold such as surface plasmon resonance and Raman scattering activity (9) have been exploited in non-radiation based cancer applications including optical imaging and photoacoustic tomography of tumors, drug delivery vehicles, tumor-specific photothermal therapy agents, antiangiogenic agents, and molecular reporters (10). In this review, we will focus on radiation-based therapeutic and diagnostic applications of GNPs.

GNP production, functionalization, and delivery to tumor tissue

Gold nanoparticles can be easily produced in uniform sizes and shapes, including nanospheres, nanorods, shells, and cages (10). Classic methods of gold nanosphere synthesis include citrate reduction of aqueous $HAuCl_4$ by the Turkevich method (11); and the Brust-Schiffrin two-phase synthesis method which uses $NaBH_4$ as a reducing agent and a mercapto-containing binding agent (12). In both methods, nanosphere size can be tuned by altering the ratio of gold to reducing substance. Other reductants have been employed to improve GNP yield and tunability; while surface ligands such as tumor-targeting antibodies, as discussed below, have been employed to modify GNP functionality and delivery.

Biological molecules such as DNA and RNA are also capable of being functionalized with GNPs. There are several ways to achieve this, including functionalization that takes advantage of the electrostatic interactions between GNPs and the target biological molecule to create GNP bioconjugates. For example, positively charged GNPs can bind through stable ionic interactions to negatively charged and nucleophilic moieties, i.e., GNPs may interact with the phosphate ester backbone of nucleic acids within DNA and RNA (13).

Targeted delivery of GNPs to tumor tissue can be accomplished in a variety of ways. Direct routes of intratumoral injection and intraperitoneal administration have been described for targeting of lung cancers (14). More clinically relevant, intravenously (IV) administered bare gold nanoparticles exhibit selective accumulation in tumor tissue due to the tumor's characteristic leaky fenestrated vasculature and impaired lymphatic clearance—the enhanced permeability and retention (EPR) effect

(15,16). For example, Hainfeld *et al*. found that a one-time injection (2.7 g Au/kg body weight) of 1.9 nm GNPs led to accumulation within tumors of up 7 mg Au/g, for a selective tumor-to-normal-tissue gold concentration ratio of 8:1 (17).

The EPR-dependent passive accumulation strategy for bare GNP delivery is limited, however, by the inherent heterogeneities of tumor vasculature, especially in necrotic poorly-vascularized areas of tumor. In addition, rapid renal clearance, opsonization, and nonspecific phagocytosis of nanoparticles by the reticuloendothelial system (RES) pose a challenge to delivery and persistence of adequate nanoparticle concentrations in the target site (7). Moreover, high interstitial pressure within tumors may also represent a barrier to the EPR effect as has been described elsewhere (18).

Various ligands and GNP surface modifications have been employed to address these limitations. Coating GNPs with polyethylene glycol (PEG), for instance, improves stability and persistence in circulation, allowing greater accumulation in tumor tissue and providing a hydrophobic barrier to RES phagocytosis and uptake (19). Work in our labs has shown that intravenously injected PEG-coated GNPs can accumulate in mouse sarcoma flank tumors to concentrations 10 times that of muscle and 50 times that of brain (data not shown).

More specific tumor-targeting can be achieved by surface conjugation of antibodies to markers overexpressed in tumors, such as EGF, HER2, and folate (20-23). Generally, functionalization of gold is accomplished either by direct thiol-modification of the targeting ligand or through the attachment of a targeting ligand to GNPs that have been modified within a coating material (e.g., polymer, lipid, etc.). Marega *et al*. used a plasma-polymerized allylamine coating to allow bioconjugation of tumor-targeting EGFR monoclonal antibodies to GNPs (20). Folic acid-conjugated GNPs have been produced by grafting on a PEG polymer chain with thioctic acid and folic acid on opposite ends (21); and Hainfeld *et al*. produced Her2-targeted GNPs by coating 15 nm GNPs with PEG and covalently coupling them to anti-Her2 antibodies (23). Other non-tumor targeting ligands have also been employed to broaden GNP functionality—for instance, Kumar *et al*. equipped ultra-small GNPs with both a therapeutic peptide (PMI/p12) and also a targeting peptide (neuropilin-1), which provided regulated membrane receptor-mediated cellular internalization (24). Furthermore, attempts have also been made to target GNPs to tumors by exploiting the unique tumor microenvironment, which may include matrix metalloprotease (MMP) expression, low pH, and elevated glucose metabolism. For example, Ayogan *et al*. have initially characterized 2-deoxy-D-glucose (2DG)-labeled GNPs for potential cancer imaging (25).

Indeed, most targeting ligands specific for overexpressed membrane receptors also have the advantage of increased receptor-mediated internalization into tumor cells (26)—an improvement upon the nonspecific cellular uptake of bare GNPs (27). The rates of internalization are also highly dependent on size and physical dimensions of nanoparticles (27). The tuning of geometry, surface modification, and tumor-targeting functionality of GNPs are under active investigation and can be accomplished in a variety of ways. Once delivered to tumor tissue, GNPs can be leveraged as multifunctional radiotherapy and imaging adjuvants, as will be discussed below.

Radiosensitization

Numerous studies have shown that gold nanoparticles delivered to tumor tissue can selectively enhance radiation therapy efficacy leading to differentially increased tumor cell killing. Though the exact mechanisms are unclear, radiosensitization is generally attributed to increased photon absorption of high-Z elements, and the resulting transfer of a larger portion of primary ionizing photon energy to tumor tissue (28). Theoretical dose enhancement achieved by gold radiosensitization as predicted by Monte Carlo studies is significant (up to 200% or more) (29,30).

The photoelectric mechanism of radiosensitization predominantly occurs at kilovoltage (kV) energies which are generally less clinically relevant (with the exception of brachytherapy); however, studies have shown dose enhancement and radiosensitization at megavoltage (MV) energies as well (5,31,32). Jain *et al*. showed cell-specific radiosensitization in breast cancer MDA-MB-231 cells, with comparable dose-enhancing ratios at kV and MV energies (32). Berbeco *et al*. suggest that GNPs can enhance the tumor-killing efficacy of 6 MV X-rays by boosting radiation dose to the tumor microvasculature and endothelial cells (31). *In vitro* work by Chitthrani showed that 50 nm GNPs radiosensitize in both lower and higher energy photon ranges, with dose modification factors (DMF) of 1.66 for 105 kVp and 1.17 for 6 MVp (33).

To test our hypothesis that GNP-induced radiosensitization is also present in the MV radiation energies, we conducted preliminary studies utilizing specialized radiochromic film to measure potential MV range energy dose enhancement in the presence of GNPs.

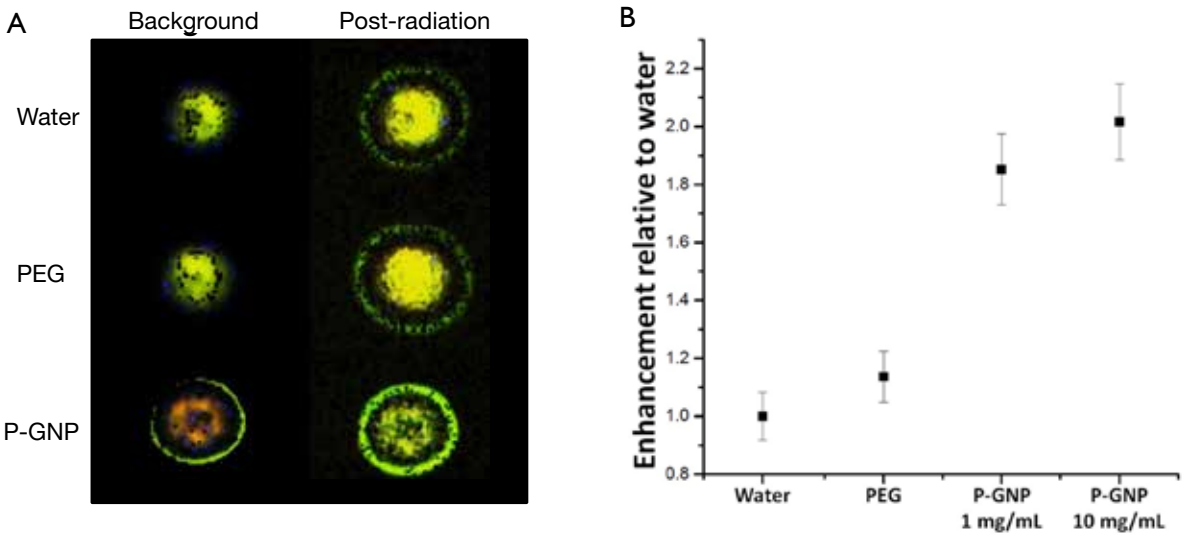

Figure 2 GNP dose enhancement in the MV range of radiation energy. A. Representative dose maps of background and post-radiation (2 Gy, 6 MV) radiochromic film in the presence of water, PEG, and 1 mg/mL PEGylated-GNP (P-GNP) as indicated. P-GNP shows an area of high density around the edge suggesting localization of GNPs. PEG alone shows an area of high density in the center which is similar to the dose map of water; B. Enhancement of PEG or P-GNPs at 2 Gy relative to water. The PEG solution alone shows no significant enhancement compared to water. The 1 and 10 mg/mL concentrations of P-GNP in contrast show significant dose enhancement (1.8-2.0 fold) compared to water alone

The dose enhancement was calculated by subtracting the background dose map before a single exposure to 2 Gy [6 MV beam energy, in the presence of water, PEG vehicle, or PEGylated-GNP (P-GNP) solution on film] from the post-radiation dose map. In a comparison of background and post-radiation dose maps of water, PEG alone, and PEG-GNPs, we preliminarily found that there is negligible enhancement due to the PEG vehicle alone compared to water as would be expected. However, as shown in a representative dose map image, P-GNPs demonstrate significant enhancement of absorbed dose in radiochromic film measurements (*Figure 2A*). We quantified these results for 2 Gy of radiation delivered by a Varian TrueBeam system in Flattening Filter Free (FFF) mode which shows significant enhancement in the presence of P-GNP compared to water or PEG alone (*Figure 2B*). Taken together, this preliminarily suggests that GNPs are capable of radiosensitization in the clinically relevant MV range of radiation energies. In terms of mechanism, short-range low-energy Auger electrons which deliver a precise lethal dose in their immediate vicinity (34,35) could help to explain higher-energy radiosensitization. Indeed, Zheng *et al*. concluded that GNP-induced radiosensitization was largely attributable to the production of low-energy secondary electrons (which are about three times more efficient than X-rays in causing DNA damage), and that this radiosensitizing mechanism operates at MV photon beam energies commonly used in radiotherapy (36).

Alternate biological mechanisms have also been proposed to account for radiosensitization seen at MV energies; beyond serving as an inert photon-absorbing element, gold may also act as a biologically active agent that enhances radiation damage by inducing cellular responses such as cell cycle acceleration (37), cytokinesis arrest, increased apoptosis (5,32), and ROS-induced DNA damage (38). Although *in vivo* studies of radiosensitization at higher energies are limited, preliminary modeling and cell line results suggest that GNPs can also be effective radiosensitizers in the MV range, with direct applicability to clinical radiation therapy.

Studies in cell line and animal models have shown various degrees of radiosensitization and tumor cell killing. Hainfeld *et al*. first showed in 2004 that intravenously injected 1.9 nm GNPs accumulated in and enhanced radiation-induced killing of mammary carcinomas in mice, leading to a 1-year survival of 86% compared to 20% with X-rays alone and 0% with gold alone (17). Chang *et al*. subsequently showed that GNPs accumulate inside melanoma cells and

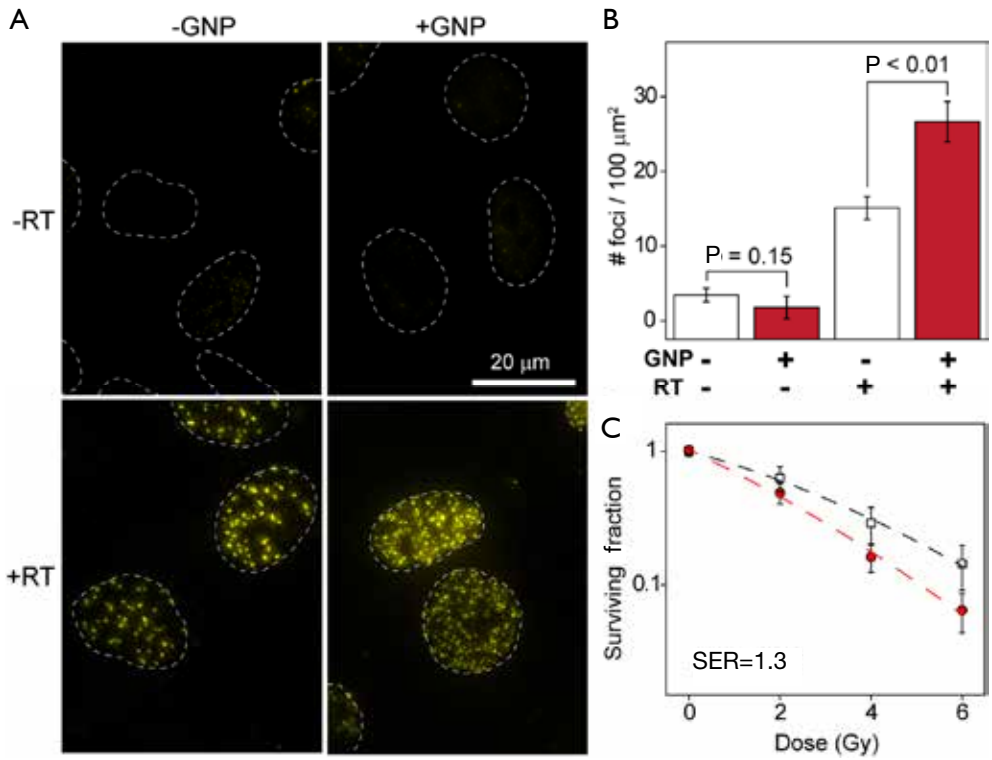

Figure 3 Assessing GNP enhancement with *in vitro* assays of radiosensitization. A. Deconvolution imaging of h2ax (marker of DNA damage) in U251 glioma cells that were mock-irradiated (upper) or irradiated with 4 Gy (lower); Cells irradiated with 1 mM GNPs display a higher density of persistent h2ax foci 24 hours after RT; B. Quantitative analysis of h2ax foci for N >100 viable nuclei. Error bars, 95% confidence interval; C. Clonogenic survival assay of U251 glioma cells treated with (red circles) and without (hollow squares) 1 mM GNPs. Error bars represent the mean survival ± s.d. of at least four replicates [adapted from Joh *et al.* PLoS One 2013;8:e62425]

enhance the efficacy of ionizing radiation, inducing tumor cell apoptosis, retarding tumor growth, and resulting in significantly increased survival in tumor-bearing mice (39). Similar GNP radioenhancement has been shown in head and neck squamous cell carcinoma (40), prostate cancer (41), and ovarian cancer (42). Work in our laboratory has shown that glioma cells and even brain tumors, despite their protection from the circulation by the blood-brain barrier, can be targeted and efficiently radiosensitized by PEGylated GNPs, leading to enhanced DNA damage, tumor cell killing (*Figure 3*), and improved survival (*Figure 4*).

Intriguingly, proton radiotherapy has also been shown to exert increased tumor-killing efficacy when directed against gold-loaded tumors. Polf *et al.* showed that prostate tumor cells with internalized gold nanoparticles exhibited increased ionization density and a lower surviving fraction when irradiated with proton beams compared with cells exposed to proton therapy alone. They approximate a clinically significant 15-20% increase in the relative biological effectiveness of proton therapy of gold-loaded tumor cells compared to proton therapy in the absence of gold, and attribute this effect to proton-Au scatter interactions and production of low energy delta-ray electrons, which result in lethal intracellular damage and lower cell survival for any given proton dose (43). More recently, Kim *et al.* used protons (10-41 Gy) to irradiate mouse tumors loaded with gold and iron nanoparticles, and found significant dose enhancement with increased intracellular ROS generation *in vitro* as well as increased tumor regression and mouse survival *in vivo*, due to release of secondary electrons and particle-induced radiation (44).

The predominant mechanisms and extent of GNP-induced radiosensitization are likely dependent on a multiple variables, including nanoparticle size and shape (33,45), surface coating (26,46), radiation dose and energy (40),

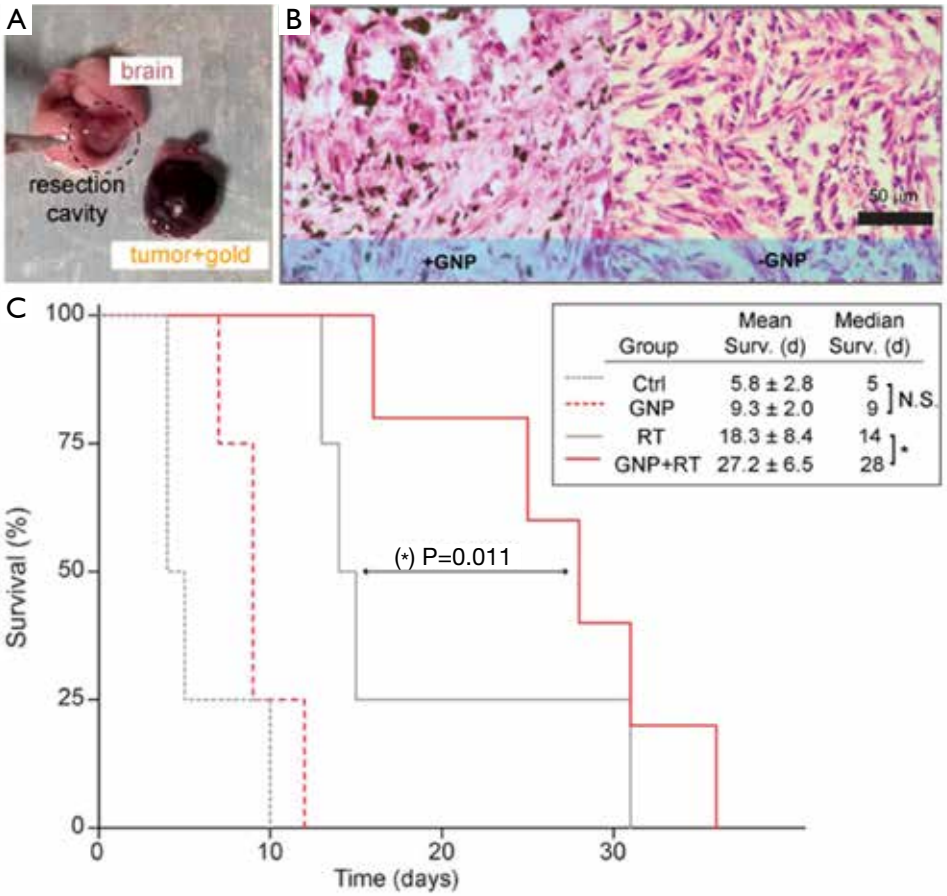

Figure 4 GNP administration in combination with RT improves survival in mice with advanced GBM tumors. A. Photograph of a brain and resected tumor 48 hours after intravenous injection of GNPs; Tumor shows darkened appearance due to extravasation due to EPR into the tumor; B. Representative H/E staining of sections from orthotopic brain tumors with (+) and without (–) GNP injection; C. Survival data in mice with advanced orthotopic GBM treated with or without GNPs, followed by no irradiation or stereotactic RT (20 Gy). Median and mean survival analysis were obtained with Kaplain-Meier analysis. Mean survival times are shown with 95% confidence intervals [adapted from Joh *et al*. PLoS One 2013;8:e62425]

and tumor type. Other GNP-assisted mechanisms, such as hyperthermia and chemosensitization, may also work in synergy with radiosensitization (40,46). Clearly, more studies are needed to optimize GNP surface architecture and elucidate mechanisms behind gold-enhanced tumor cell killing; however, the clinical applicability and therapeutic promise of GNPs as safe and effective adjuvants in radiation therapy for cancer seems increasingly clear.

Imaging

Contrast agents can improve the accuracy of tumor diagnosis, staging, and treatment planning by providing superior definition of tumor volumes and vasculature (47,48). Gold has been demonstrated as an effective experimental X-ray contrast agent that can overcome numerous obstacles of traditional iodine-based contrast agents. At energy ranges used for clinical CT imaging, gold exhibits much higher mass-energy absorption coefficient than iodine (*Figure 5*); indeed, gold's higher atomic number and X-ray absorption coefficient results in about 2.7 times greater attenuation per unit weight than iodine, which could translate to better image contrast at lower radiation doses (1). Surface modifications can enhance this effect—Kim *et al*. found the attenuation coefficient achieved by PEG-coated GNPs to be 5.7 times higher than by current iodine-based CT contrast agents (49). Gold's physical properties also allow good contrast in higher X-ray photon

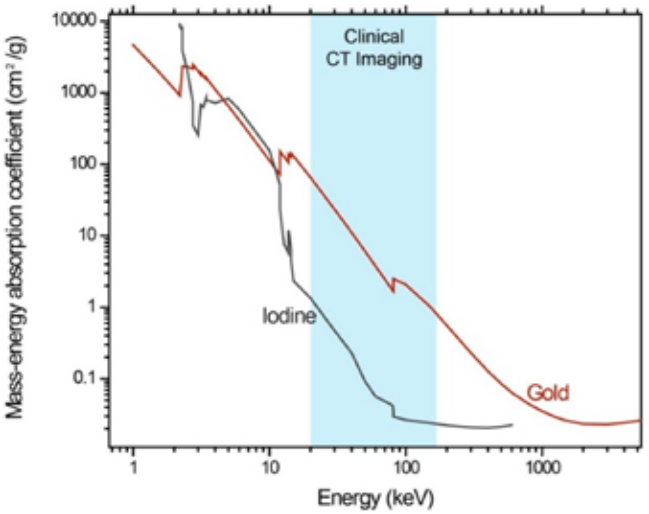

Figure 5 Mass-energy absorption coefficient of gold *vs*. iodine. At clinically relevant energies for CT imaging, gold's mass-energy absorption coefficient is superior to that of iodine (on which most traditional CT contrast agents are based); this translates into higher X-ray attenuation and contrast. (Adapted from NIST: http://physics.nist.gov/PhysRefData/XrayMassCoef/ElemTab/z79.html)

energies (80-100 keV) which exhibit lower soft tissue absorption and thus lower radiation toxicity to patients (1,50). The higher molecular weight of GNPs, along with its ability to be conjugated to various antibiofouling surface molecules such as PEG, also lends it stability and persistence in circulation, allowing longer imaging times and less renal toxicity (49).

Either by passive EPR-assisted accumulation or targeted delivery, intravenously administered GNPs can localize to tumor tissue and allow CT-assisted visualization of tumor-associated vasculature and borders. After intravenously injecting GNPs into mice implanted with breast tumors, Hainfeld *et al*. found sufficient CT contrast enhancement enabling direct imaging of GNP-loaded tumors as well as angiogenic and hypervascularized regions (23). Chien *et al*. found that bare GNPs in conjunction with heparin injection also provided sufficient contrast to allow *in vivo* detection of tumor microvessels, suggesting their application in tumor-related angiography (51). Surface modifications have also been shown to be useful—Kim *et al*. demonstrated the use of PEGylated GNPs as long-circulating contrast agents in the imaging of hepatoma (49); and Wang *et al*. showed that acetylated dendrimer-entrapped GNPs could be used for both *in vitro* and *in vivo* CT imaging of adenocarcinoma (14). Work in our laboratories have shown that PEGylated GNPs can serve as long-circulating vascular blood pool CT imaging agents as well as CT contrast agents for sarcoma tumors in mice (*Figure 6*). *Figure 6A* shows coronal CT images through a non-tumor bearing mouse before, immediately after and 20 hours post injection of PEGylated GNPs which highlight the long-circulating contrast properties of this agent. *Figure 6B* demonstrates an axial CT image of well-defined GNP-loaded, contrast-enhancing orthotopic sarcoma flank tumor. CT images can also be reconstructed in the x,y,z coordinates to create a 3-dimensional representation of GNP accumulation within tumors, as shown in *Figure 6C*, which may be useful in future studies to define the parameters and microenvironmental factors that lead to heterogenous uptake within tumors. One could also speculate that GNPs may have utility in the study of vascular renormalization that may occur with various targeted agents (52).

Gold-based contrast agents may also serve as molecular CT imaging platforms for tumors that are undetectable by structural and anatomical imaging modalities. Popovtzer *et al*. showed that immuno-targeted gold nanorods coated with tumor-selective antibodies can bind to head and neck squamous cell carcinoma cells, accumulating to concentrations sufficient to provide 5 times greater CT attenuation compared to untargeted cancer cells or normal cells (48). Additionally, this technique has the potential advantage of selectively identifying aggressive tumor cells by specifically targeting antigens overexpressed on cells with metastatic behavior (48). This molecular imaging concept has also been supported *in vivo*; Reuveni *et al*. showed that EGF-conjugated GNPs, when intravenously injected into nude mice, efficiently homed to and caused contrast enhancement of head and neck cancers too small to be detectable through conventional CT (53). Furthermore, Eck *et al*. demonstrated that anti-CD4-targeted GNPs could distinctly enhance the X-ray contrast of peripheral lymph nodes (54) which is directly relevant to the radiation treatment planning of target volumes.

In addition to their applications in CT imaging, GNPs can also be conjugated to paramagnetic elements such as iron and gadolinium to form MRI-active contrast agents. This is important for two reasons: improved sensitivity (the sensitivity of CT imaging of GNPs tends to fall off at a concentration of about 0.5 mg/mL) (23), and the potential acquisition of additional pathological or molecular information with complementary imaging techniques. A gold-iron oxide micellar formulation is

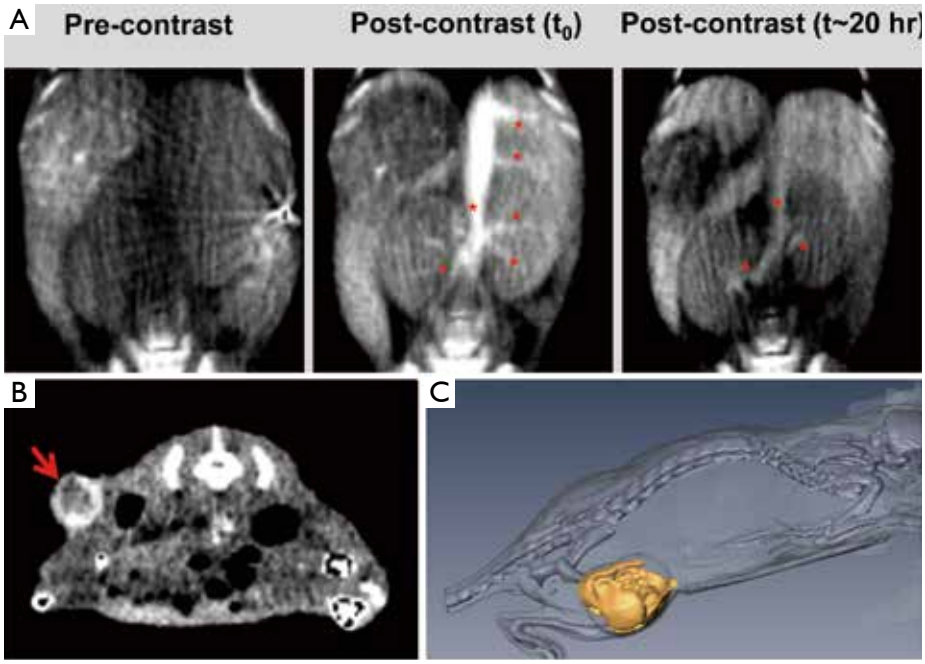

Figure 6 Pegylated GNPs as vascular blood pool and tumor-enhancing CT contrast agents. A. Immediately after GNP injection, and up to 20 hours post-injection, major vessels appear hyperintense and can be clearly visualized with CT imaging (GNP contrasted vessels indicated by red asterisks); B. Intravenously injected GNPs accumulate in flank sarcoma tumor and result in well-defined CT contrast enhancement (tumor indicated by red arrow); C. 3-Dimensional reconstruction of GNP accumulation within an orthotopic sarcoma flank tumor (tumor reconstructed in gold)

currently being investigated in our laboratories as a contrast agent for both CT and MRI imaging of tumors in mice. Choi *et al*. demonstrated the use of hybrid FePt-Au nanoparticles in molecular MR imaging and other biological detection modalities (55); and dumbbell-shaped Au-Fe_3O_4 nanoparticles have been reported as simultaneous optical and MR imaging agents (56). Similarly, Kim *et al*. showed dual-modality CT and MRI blood pool imaging using GNPs coated with Gadolinium-chelate (57). Due to its versatility and ability to be conjugated to other elements, gold may be incorporated into versatile imaging nanoplatforms capable of multimodal diagnostic applications.

Conclusions: limitations and theranostic possibilities

GNP safety

Gold has a long history of use in medical practice and continues today as treatment for conditions such as rheumatoid arthritis (58). Although bulk gold is generally accepted to be nontoxic and has been approved for clinical use in some human diseases, nanoparticle formulations of gold carry potentially more risk due to small size and ability to disseminate, penetrate, and persist in organ systems. Smaller nanoparticles have been shown to cause apoptosis, reactive oxygen species, and necrosis of various tissues due to their deeper penetration and wider systemic distribution (6,59,60).

One potential concern with the use of GNPs may be protracted elimination from the liver (61-63)—with one study reporting only 9% decrease in the content of gold in the liver from day 1 to 6 months following the intravenous injection of 40 nm GNPs (64); and another study showing inflammatory and apoptotic changes in liver tissue after injection of 13 nm PEG-GNPs (65). Nephrotoxicity is also a potential risk of GNP administration, with gold nanoparticles shown to be capable of penetrating renal cells (66) and accumulating in kidney tissue (2). Reassuringly, however, when 12.5 nm GNPs were administered to mice daily for 8 days, no evidence of toxicity was observed in terms of survival, behavior, animal

weight, organ morphology, blood biochemistry, and tissue histology over a period of two-plus months (67). In addition, the percent of GNPs uptaken by both liver and kidney decreased with increasing doses, suggesting that GNPs are in fact cleared from the body (4). *In vitro* studies have also showed that even high relatively GNP concentrations inflict little cytotoxicity on various kidney cell lines (2).

In general, nanoparticles <~6 nm are primarily renally cleared and have low circulation times. Larger particles enjoy a prolonged systemic circulation thus enhancing accumulation within tumors. These particles may remain in the reticuloendothelial system (RES) for long periods of time; however, numerous studies have suggested that larger colloidal GNPs exhibit lower cytotoxicity, possibly due to diminished binding to DNA and other key molecules (2). There is a tradeoff between the larger particle size necessary for molecular imaging (especially for targeted imaging given a limited number of surface receptors) and the effective clearance of smaller particles. This remains a hurdle for their utilization in diagnostic imaging.

Although still not fully understood, GNP persistence and toxicity is governed by factors including cell type as well as GNP functionalization and size. In any case, these concerns have not prevented the use of gold in patients with poor cancer prognoses. In fact, several GNP formulations have already entered clinical trials for cancer treatment, including CYT-6091 (www.clinicaltrials.gov: NCT00356980) and AuroShell® particles (silica core with a gold shell). More safety studies of GNPs in various formulations are needed before further clinical implementation can occur.

Theranostic possibilities

Most studies to date have investigated GNPs in either a radiosensitizing or imaging role; combined theranostic anti-cancer applications of GNPs have mainly focused on non-radiation based drug-delivery and molecular or cellular imaging modalities (68). However, studies investigating GNP-induced radiosensitization have hinted at imaging applications as well—for example, while their primary aim was to demonstrate radiosensitization of mammary carcinoma, Hainfeld *et al*. also found X-ray contrast enhancement of the gold-loaded tumor (17). Work in our laboratories has also shown that PEGylated-GNPs can function simultaneously as both a CT contrast agent and a radiosensitizer. Future studies are still needed to more fully investigate the multifunctional theranostic potential of GNPs and are currently ongoing.

Conclusions

Gold nanoparticles are novel agents with strong therapeutic and diagnostic potential in a wide variety of cancer applications. These nanoagents possess many attractive physicochemical properties including biocompatibility, easy synthesis and modification, and a high Z coefficient; however, potential safety concerns and mechanisms of radiosensitization at different energy ranges still need to be fully elucidated before clinical implementation. Although their multifunctional potential remains to be fully explored, GNPs could represent an ideal theranostic adjuvant in radiation-based diagnostic and therapeutic anti-cancer modalities. We are currently actively engaged in the studies to move these potential theranostic agents closer to clinical implementation.

Acknowledgements

This work was supported by the National Institutes of Health, National Institute of Neurological Disorders and Stroke (K08 NS076548). J.F.D. was supported on a Burroughs Wellcome Career Award for Medical Scientists (1006792).
Disclosure: The authors declare no conflict of interest.

References

1. Hainfeld JF, Slatkin DN, Focella TM, et al. Gold nanoparticles: a new X-ray contrast agent. Br J Radiol 2006;79:248-53.
2. Khlebtsov N, Dykman L. Biodistribution and toxicity of engineered gold nanoparticles: a review of in vitro and in vivo studies. Chem Soc Rev 2011;40:1647-71.
3. Connor EE, Mwamuka J, Gole A, et al. Gold nanoparticles are taken up by human cells but do not cause acute cytotoxicity. Small 2005;1:325-7.
4. Lasagna-Reeves C, Gonzalez-Romero D, Barria MA, et al. Bioaccumulation and toxicity of gold nanoparticles after repeated administration in mice. Biochem Biophys Res Commun 2010;393:649-55.
5. Coulter JA, Jain S, Butterworth KT, et al. Cell type-dependent uptake, localization, and cytotoxicity of 1.9 nm gold nanoparticles. Int J Nanomedicine 2012;7:2673-85.
6. Shukla R, Bansal V, Chaudhary M, et al. Biocompatibility

of gold nanoparticles and their endocytotic fate inside the cellular compartment: a microscopic overview. Langmuir 2005;21:10644-54.
7. Jain S, Hirst DG, O'Sullivan JM. Gold nanoparticles as novel agents for cancer therapy. Br J Radiol 2012;85:101-13.
8. Praetorius NP, Mandal TK. Engineered nanoparticles in cancer therapy. Recent Pat Drug Deliv Formul 2007;1:37-51.
9. Kah JC, Kho KW, Lee CG, et al. Early diagnosis of oral cancer based on the surface plasmon resonance of gold nanoparticles. Int J Nanomedicine 2007;2:785-98.
10. Cai W, Gao T, Hong H, et al. Applications of gold nanoparticles in cancer nanotechnology. Nanotechnol Sci Appl 2008:17-32.
11. Turkevich J, Stevenson PC, Hillier J. A study of the nucleation and growth processes in the synthesis of colloidal gold. Discuss Faraday Soc 1951;11:55-75.
12. Brust M, Walker M, Bethell D, et al. Synthesis of thiol-derivatised gold nanoparticles in a two-phase liquid-liquid system. J Chem Soc Chem Commun 1994:7;801-2.
13. De Long RK, Reynolds CM, Malcolm Y, et al. Functionalized gold nanoparticles for the binding, stabilization, and delivery of therapeutic DNA, RNA, and other biological macromolecules. Nanotechnol Sci Appl 2010;8:53-63.
14. Wang H, Zheng L, Peng C, et al. Computed tomography imaging of cancer cells using acetylated dendrimer-entrapped gold nanoparticles. Biomaterials 2011;32:2979-88.
15. Iyer AK, Khaled G, Fang J, et al. Exploiting the enhanced permeability and retention effect for tumor targeting. Drug Discov Today 2006;11:812-8.
16. Fang J, Sawa T, Maeda H. Factors and mechanism of "EPR" effect and the enhanced antitumor effects of macromolecular drugs including SMANCS. Adv Exp Med Biol 2003;519:29-49.
17. Hainfeld JF, Slatkin DN, Smilowitz HM. The use of gold nanoparticles to enhance radiotherapy in mice. Phys Med Biol 2004;49:N309-15.
18. Ruoslahti E, Bhatia SN, Sailor MJ. Targeting of drugs and nanoparticles to tumors. J Cell Biol 2010;188:759-68.
19. Cho WS, Cho M, Jeong J, et al. Size-dependent tissue kinetics of PEG-coated gold nanoparticles. Toxicol Appl Pharmacol 2010;245:116-23.
20. Marega R, Karmani L, Flamant L, et al. Antibody-functionalized polymer-coated gold nanoparticles targeting cancer cells: an in vitro and in vivo study. Journal of Materials Chemistry 2012;22:21305-12.
21. Dixit V, Van den Bossche J, Sherman DM, et al. Synthesis and grafting of thioctic acid-PEG-folate conjugates onto Au nanoparticles for selective targeting of folate receptor-positive tumor cells. Bioconjug Chem 2006;17:603-9.
22. Zhao X, Li H, Lee RJ. Targeted drug delivery via folate receptors. Expert Opin Drug Deliv 2008;5:309-19.
23. Hainfeld JF, O'Connor MJ, Dilmanian FA, et al. Micro-CT enables microlocalisation and quantification of Her2-targeted gold nanoparticles within tumour regions. Br J Radiol 2011;84:526-33.
24. Kumar A, Ma H, Zhang X, et al. Gold nanoparticles functionalized with therapeutic and targeted peptides for cancer treatment. Biomaterials 2012;33:1180-9.
25. Aydogan B, Li J, Rajh T, et al. AuNP-DG: deoxyglucose-labeled gold nanoparticles as X-ray computed tomography contrast agents for cancer imaging. Mol Imaging Biol 2010;12:463-7.
26. Kong T, Zeng J, Wang X, et al. Enhancement of radiation cytotoxicity in breast-cancer cells by localized attachment of gold nanoparticles. Small 2008;4:1537-43.
27. Chithrani BD, Ghazani AA, Chan WC. Determining the size and shape dependence of gold nanoparticle uptake into mammalian cells. Nano Lett 2006;6:662-8.
28. Hainfeld JF, Dilmanian FA, Slatkin DN, et al. Radiotherapy enhancement with gold nanoparticles. J Pharm Pharmacol 2008;60:977-85.
29. Hainfeld JF, Dilmanian FA, Slatkin DN, et al. Radiotherapy enhancement with gold nanoparticles. J Pharm Pharmacol 2008;60:977-85.
30. Cho SH. Estimation of tumour dose enhancement due to gold nanoparticles during typical radiation treatments: a preliminary Monte Carlo study. Phys Med Biol 2005;50:N163-73.
31. Berbeco RI, Ngwa W, Makrigiorgos GM. Localized dose enhancement to tumor blood vessel endothelial cells via megavoltage X-rays and targeted gold nanoparticles: new potential for external beam radiotherapy. Int J Radiat Oncol Biol Phys 2011;81:270-6.
32. Jain S, Coulter JA, Hounsell AR, et al. Cell-specific radiosensitization by gold nanoparticles at megavoltage radiation energies. Int J Radiat Oncol Biol Phys 2011;79:531-9.
33. Chithrani DB, Jelveh S, Jalali F, et al. Gold nanoparticles as radiation sensitizers in cancer therapy. Radiat Res 2010;173:719-28.
34. Butterworth KT, McMahon SJ, Currell FJ, et al. Physical basis and biological mechanisms of gold nanoparticle radiosensitization. Nanoscale 2012;4:4830-8.

35. Lechtman E, Chattopadhyay N, Cai Z, et al. Implications on clinical scenario of gold nanoparticle radiosensitization in regards to photon energy, nanoparticle size, concentration and location. Phys Med Biol 2011;56:4631-47.
36. Zheng Y, Hunting DJ, Ayotte P, et al. Radiosensitization of DNA by gold nanoparticles irradiated with high-energy electrons. Radiat Res 2008;169:19-27.
37. Roa W, Zhang X, Guo L, et al. Gold nanoparticle sensitize radiotherapy of prostate cancer cells by regulation of the cell cycle. Nanotechnology 2009;20:375101.
38. Butterworth KT, Coulter JA, Jain S, et al. Evaluation of cytotoxicity and radiation enhancement using 1.9 nm gold particles: potential application for cancer therapy. Nanotechnology 2010;21:295101.
39. Chang MY, Shiau AL, Chen YH, et al. Increased apoptotic potential and dose-enhancing effect of gold nanoparticles in combination with single-dose clinical electron beams on tumor-bearing mice. Cancer Sci 2008;99:1479-84.
40. Hainfeld JF, Dilmanian FA, Zhong Z, et al. Gold nanoparticles enhance the radiation therapy of a murine squamous cell carcinoma. Phys Med Biol 2010;55:3045-59.
41. Zhang X, Xing JZ, Chen J, et al. Enhanced radiation sensitivity in prostate cancer by gold-nanoparticles. Clin Invest Med 2008;31:E160-7.
42. Geng F, Song K, Xing JZ, et al. Thio-glucose bound gold nanoparticles enhance radio-cytotoxic targeting of ovarian cancer. Nanotechnology 2011;22:285101.
43. Polf JC, Bronk LF, Driessen WH, et al. Enhanced relative biological effectiveness of proton radiotherapy in tumor cells with internalized gold nanoparticles. Appl Phys Lett 2011;98:193702.
44. Kim JK, Seo SJ, Kim HT, et al. Enhanced proton treatment in mouse tumors through proton irradiated nanoradiator effects on metallic nanoparticles. Phys Med Biol 2012;57:8309-23.
45. Zhang XD, Wu D, Shen X, et al. Size-dependent radiosensitization of PEG-coated gold nanoparticles for cancer radiation therapy. Biomaterials 2012;33:6408-19.
46. Hébert EM, Debouttière PJ, Lepage M, et al. Preferential tumour accumulation of gold nanoparticles, visualised by Magnetic Resonance Imaging: radiosensitisation studies in vivo and in vitro. Int J Radiat Biol 2010;86:692-700.
47. Essig M, Debus J, Schlemmer HP, et al. Improved tumor contrast and delineation in the stereotactic radiotherapy planning of cerebral gliomas and metastases with contrast media-supported FLAIR imaging. Strahlenther Onkol 2000;176:84-94.
48. Popovtzer R, Agrawal A, Kotov NA, et al. Targeted gold nanoparticles enable molecular CT imaging of cancer. Nano Lett 2008;8:4593-6.
49. Kim D, Park S, Lee JH, et al. Antibiofouling polymer-coated gold nanoparticles as a contrast agent for in vivo X-ray computed tomography imaging. J Am Chem Soc 2007;129:7661-5.
50. Shilo M, Reuveni T, Motiei M, et al. Nanoparticles as computed tomography contrast agents: current status and future perspectives. Nanomedicine (Lond) 2012;7:257-69.
51. Chien CC, Chen HH, Lai SF, et al. Gold nanoparticles as high-resolution X-ray imaging contrast agents for the analysis of tumor-related micro-vasculature. J Nanobiotechnology 2012;10:10.
52. Cerniglia GJ, Pore N, Tsai JH, et al. Epidermal growth factor receptor inhibition modulates the microenvironment by vascular normalization to improve chemotherapy and radiotherapy efficacy. PLoS One 2009;4:e6539.
53. Reuveni T, Motiei M, Romman Z, et al. Targeted gold nanoparticles enable molecular CT imaging of cancer: an in vivo study. Int J Nanomedicine 2011;6:2859-64.
54. Eck W, Nicholson AI, Zentgraf H, et al. Anti-CD4-targeted gold nanoparticles induce specific contrast enhancement of peripheral lymph nodes in X-ray computed tomography of live mice. Nano Lett 2010;10:2318-22.
55. Choi JS, Jun YW, Yeon SI, et al. Biocompatible heterostructured nanoparticles for multimodal biological detection. J Am Chem Soc 2006;128:15982-3.
56. Xu C, Xie J, Ho D, et al. Au-Fe3O4 dumbbell nanoparticles as dual-functional probes. Angew Chem Int Ed Engl 2008;47:173-6.
57. Kim HK, Jung HY, Park JA, et al. Gold nanoparticles coated with gadolinium-DTPA-bisamide conjugate of penicillamine (Au@GdL) as a T1-weighted blood pool contrast agent. J Mater Chem 2010;20:5411-7.
58. Fricker S. Medical uses of gold compounds: past, present, and future. Gold Bulletin 1996;29:53-60.
59. Pan Y, Neuss S, Leifert A, et al. Size-dependent cytotoxicity of gold nanoparticles. Small 2007;3:1941-9.
60. Lim ZZ, Li JE, Ng CT, et al. Gold nanoparticles in cancer therapy. Acta Pharmacol Sin 2011;32:983-90.
61. Balasubramanian SK, Jittiwat J, Manikandan J, et al. Biodistribution of gold nanoparticles and gene expression changes in the liver and spleen after intravenous administration in rats. Biomaterials 2010;31:2034-42.
62. Goel R, Shah N, Visaria R, et al. Biodistribution of TNF-alpha-coated gold nanoparticles in an in vivo model

system. Nanomedicine (Lond) 2009;4:401-10.
63. James WD, Hirsch LR, West JL, et al. Applications of INAA to the build-up and clearance of gold nanoshells in clinical studies in mice. J Radioanal Nucl Chem 2007;271:455-9.
64. Sadauskas E, Danscher G, Stoltenberg M, et al. Protracted elimination of gold nanoparticles from mouse liver. Nanomedicine 2009;5:162-9.
65. Cho WS, Cho M, Jeong J, et al. Acute toxicity and pharmacokinetics of 13 nm-sized PEG-coated gold nanoparticles. Toxicol Appl Pharmacol 2009;236:16-24.
66. Sereemaspun A, Rojanathanes R, Wiwanitkit V. Effect of gold nanoparticle on renal cell: an implication for exposure risk. Ren Fail 2008;30:323-5.
67. Lasagna-Reeves C, Gonzalez-Romero D, Barria MA, et al. Bioaccumulation and toxicity of gold nanoparticles after repeated administration in mice. Biochem Biophys Res Commun 2010;393:649-55.
68. Heo DN, Yang DH, Moon HJ, et al. Gold nanoparticles surface-functionalized with paclitaxel drug and biotin receptor as theranostic agents for cancer therapy. Biomaterials 2012;33:856-66.

Cite this article as: Dorsey JF, Sun L, Joh DY, Witztum A, Al Zaki A, Kao GD, Alonso-Basanta M, Avery S, Tsourkas A, Hahn SM. Gold nanoparticles in radiation research: potential applications for imaging and radiosensitization. Transl Cancer Res 2013;2(4):280-291. doi: 10.3978/j.issn.2218-676X.2013.08.09

Review Article

Convergence of nanotechnology with radiation therapy—insights and implications for clinical translation

Dev Kumar Chatterjee[1]*, Tatiana Wolfe[1]*, Jihyoun Lee[1,2]*, Aaron P Brown[1]*, Pankaj Kumar Singh[1]*, Shanta Raj Bhattarai[1]*, Parmeswaran Diagaradjane[1], Sunil Krishnan[1]

[1]Department of Radiation Oncology, The University of Texas M. D. Anderson Cancer Center, Houston, Texas, USA; [2]Soon Chun Hyang University Hospital, Republic of Korea

*These authors contributed equally to this work.

Correspondence to: Sunil Krishnan. The University of Texas M. D. Anderson Cancer Center, 1515 Holcombe Boulevard, Unit-97, Houston, Texas 77030, USA. Email: skrishnan@mdanderson.org; Parmeswaran Diagaradjane. The University of Texas MD Anderson Cancer Center, 1515 Holcombe Boulevard, Unit-97, Houston, Texas 77030, USA. Email: parmesh@mdanderson.org.

Abstract: Improvements in accuracy and efficacy in treating tumors with radiation therapy (RT) over the years have been fueled by parallel technological and conceptual advances in imaging and image-guidance techniques, radiation treatment machines, computational methods, and the understanding of the biology of tumor response to RT. Recent advances in our understanding of the hallmarks of cancer and the emergence of strategies to combat these traits of cancer have resulted in an expanding repertoire of targeted therapeutics, many of which can be exploited for enhancing the efficacy of RT. Complementing this advent of new treatment options is the evolution of our knowledge of the interaction between nanoscale materials and human tissues (nanomedicine). As with the changes in RT paradigms when the field has encountered newer and maturing disciplines, the incorporation of nanotechnology innovations into radiation oncology has the potential to refine or redefine its principles and revolutionize its practice. This review provides a summary of the principles, applications, challenges and outlook for the use of metallic nanoparticles in RT.

Keywords: Cancer; nanoparticles; nanotechnology; radiation therapy (RT); review

doi: 10.3978/j.issn.2218-676X.2013.08.10

Scan to your mobile device or view this article at: http://www.thetcr.org/article/view/1546/2260

Introduction

Ionizing radiation has been used for cancer treatments since the close of the nineteenth century, fairly soon after Wilhelm Roentgen discovered X-rays [1895], Henri Becquerel discovered radioactivity [1897], and Marie and Pierre Curie discovered radium [1898]. Since these early days of radiation therapy (RT), we have witnessed incremental changes and occasional quantum leaps in treatment techniques, paradigms, and machines.

Beginning with cathode-ray tubes and advancing through gantry-mounted cobalt heads in treatment machines, megavoltage linear accelerators, and charged particle accelerators, changes in technology have occurred in close parallel with similar advances in other technical disciplines like physics and engineering. Treatment delivery has been revolutionized by the use of motorized individually controllable collimator leaves that permit modulation of the intensity of radiation in real-time during treatment. Coupling the movement of these collimators to movement of the gantry now permits faster rotational arc treatment. Other forms of RT that have evolved over these years include the use of radioactive sources placed close to or within tumors (brachytherapy), electron radiation, and heavy ion radiation (largely protons and carbon ions).

As importantly, the clinical discipline has benefited from interaction with less technological but more clinical and biological disciplines. Growing up alongside

diagnostic radiology, the field has co-opted much of the progress in imaging. Kilovoltage two-dimensional X-ray simulators have now been replaced with three- and four-dimensional computed tomographic (CT) simulators, magnetic resonance (MR) simulators, and positron emission tomographic (PET)-CT simulators to acquire images of tumors to aid the sculpting of beams aimed at them. These machines have also found their way into the treatment room and are an integral component of image-guided delivery systems. The other discipline that developed alongside RT was tumor biology (radiobiology), bringing with it the concept of optimizing the therapeutic ratio where the intent of treatment was maximal tumor control with minimal collateral damage to adjacent normal tissues. More importantly, the modern practice of RT was founded on the recognition that greater tumor control with less normal tissue toxicity can be achieved by fractionating treatments into smaller instalments rather than delivering all of it as a single large dose. In a departure from this conventional wisdom, assimilation and incorporation of sophisticated image-guided delivery techniques have resulted in increasing acceptance of short-course high-dose (stereotactic) radiation treatments. This is again a testament to the convergence of a greater understanding of radiation biology and the emergence of newer enabling technologies. These conceptual advances have benefited immensely from encounters with mathematical and statistical modelling techniques that allow prediction of the behavior of radiated tissues *a priori*. The other discipline that has grown alongside RT in the latter half of the last century is medical oncology. Increasingly, RT is interwoven with chemotherapy (concurrently and/or sequentially) to increase therapeutic efficacy without excessive toxicity. The latest entrant in this crosstalk between disciplines is the explosion in our knowledge of the biological hallmarks of cancer at the genetic and molecular level. Molecular biology continues to refine the way RT is chosen for subsets of patients with specific molecular traits, tailored to the intrinsic make-up of an individual patient's tumor, often adapting to inducible changes, or combined with molecularly targeted agents for maximum therapeutic benefit.

As illustrated above, the history of radiation oncology is replete with examples of solving research problems with multidisciplinary approaches that bridge disparate life science and physical science fields. It is within this context that we view radiation oncology's convergence with nanotechnology—the study and manipulation of matter and phenomena at a nanoscale, about 1 to 100 nm. Most applications of nanotechnology in medicine (as elsewhere) harness the unique physical and chemical properties of matter at these size regimes compared to bulk matter, and employ these particles to sense, image, measure, and manipulate biologic processes and functions. These characteristics largely arise from the large surface area to volume ratio and the tunable intense and narrow spectral absorption and scattering cross-sections when interacting with electromagnetic waves. In turn, the large surface area to volume ratio translates to greater potential for interaction with biomaterials and surfaces than single molecules, greater potential for decoration of their surface with targeting, imaging and/or therapeutic agents, and greater ability to multiplex different functionalities (an exciting new field of theranostics, i.e., the merger of therapeutics and diagnostics, borrows heavily from these properties of nanoparticles). The strong absorption and scattering properties can be clinically exploited to amplify a weaker signal from individual molecules (for instance, Raman scattering), or generate heat (for instance, plasmon resonance) that could itself be used for therapeutic purposes or could be imaged by photoacoustic imaging. From the perspective of cancer imaging and therapy, a unique feature of the tumor itself that makes it accessible to nanoparticles is the presence of leaky, immature and chaotic blood vessels with fenestrations ranging from 60-400 nm when compared to the surrounding healthy tissues. The consequent tumor-specific accumulation of intravenously administered nanoparticles is called the enhanced permeability and retention (EPR) effect, wherein nanoparticle leak out through these fenestrations and are retained within the disorganized extracellular architecture of tumors.

Nanoparticles can be fabricated with different sizes, shapes, and surface properties from numerous materials. Although organic molecules like polymers and liposomes have also found broad applicability in radiation oncology and are further along in clinical trials, this review highlights the potential for and the challenges to realizing similar clinical advances with metallic nanoparticles as conduits to improving RT.

Nanoparticle-mediated radiosensitization

Despite being an effective component of modern cancer therapy for localized disease, the ultimate utility of RT is limited by the fact that some cancer cells are resistant to ionizing radiation. Attempts to improve outcomes of RT have largely focused on (I) increasing the dose

of radiation delivered to the tumor; (II) sensitizing the radioresistant fraction of tumor cells to conventional doses of radiation; and (III) targeting cancer cells specifically while administering RT. The advent of nanotechnology in the field of biology and medicine presents versatile opportunities to overcome the limitations associated with these traditional strategies by combining multiple approaches in one unified seamless therapeutic strategy. We address some of these strategies below.

Thermoradiotherapy with metallic nanoparticles

One of the key mediators of inherent radiation resistance of tumor cells is intra-tumoral hypoxia that contributes to changes at the genetic, epigenetic and protein levels within tumor cells and tumor micro-environmental changes that eventually result in greater tumor aggressiveness. Mild temperature (<43 ℃) hyperthermia is a well-recognized therapeutic adjunct to conventional RT (thermoradiotherapy) (1-3) that exerts its radiosensitizing effects, in part, via enhanced vascular perfusion of tumors and consequent better oxygenation and reduced hypoxia (4). Despite its proven biologic and clinical efficacy, this strategy has not been widely adopted in the clinic because conventional methods of generating hyperthermia have been at least minimally invasive, lacking in means to monitor temperature non-invasively, and difficult to control and administer in a consistent and controlled manner. Current approaches to delivery of heat to tumors are based on methods which focus energy from outside the body to the tumor, like hot water bags, ultrasound, microwave, etc. (5). These approaches result in uneven temperatures within the tumor with "heat-sinks" along vasculature where cooler blood dissipates heat efficiently from the heated adjacent tumor parenchyma. Metal nanoparticles, particularly gold and iron, offer an alternative approach to tumor heating.

Gold nanoparticles (GNPs) offer a radically different approach to induce mild temperature hyperthermia in tumor tissues. GNPs have a 'cloud' of free electrons whose oscillatory motion is restricted by the shape and size of the particle, giving rise to quantized waves called polaritons. When light (electromagnetic energy) of a specific wavelength is incident on gold nanoparticles such that the incident light photons are resonant with the polaritons, the electrons absorb the incident energy to become highly energized (plasmons). This energy is then released to the immediate environment in the form of heat. This phenomenon (surface plasmon resonance) results in a net transduction of light energy to heat energy (6). Since the resonant wavelength depends on the shape and size of the nanoparticle, and since light in the near infrared (NIR) region of the electromagnetic spectrum has the greatest penetration depth in human tissues, two types of GNPs—gold nanoshells and gold nanorods with plasmon resonance tuned to peak in the NIR region have been extensively used in pre-clinical investigations, in anticipation of eventual clinical translation (7). In the case of the silica-gold core-shell nanoparticles (gold nanoshells), the ratio of the thickness of the gold shell to the diameter of the dielectric silica core can be varied to tune the plasmon resonance to the NIR region. In the case of the solid cylindrical gold nanorods, the ratio of the length to the diameter can be varied to tune the longitudinal plasmon resonance to the NIR wavelength. Seminal report on the use of gold nanoshell-mediated thermoradiotherapy demonstrated integrated antihypoxic and localized vascular disrupting effect resulting in an enhanced RT response in mouse tumor model (8). The vascular disruption effect is mediated by the sequestration of gold nanoshells (NIR activatable ones are roughly 150 nm in size, comprised of a 120 nm diameter silica core and a 15 nm thick gold shell) in the perivascular zone where temperature rise adjacent to the nanoshells is considerably more than that within tumor parenchyma which reaches mild hyperthermia range temperatures. This heterogeneity of temperature within tumors is distinctly different from that encountered when hyperthermia is generated from the "outside in" and results in "cold spots" or "heat sinks" along blood vessels. Here, the temperature increase is generated at the blood vessel-tumor interface and dissipates from the "inside out", thereby creating a "hot spot" along blood vessels. This not only results in vascular disruption but also ensures that the maximal heat is generated inside the targeted tumor with minimal heating of normal tissues and potentially accounts for the preferential sensitization of cancer stem cells residing in the perivascular niche to radiation (9). Nevertheless, the limited penetration depth of NIR light in tissues remains a great challenge reiterating the need for appropriate clinical scenarios to utilize this strategy to its maximum advantage. Superficial tumors (head and neck, skin, cavity locations reachable by endoscopes), low-attenuation tissues (e.g., breast) or post-surgical tumor beds (e.g., post-mastectomy) present ideal clinical scenarios for gold nanoparticle mediated thermoradiotherapy.

Alternatively, ferromagnetic nanoparticles that are made of various formulations of iron and/or iron oxide are ideal

candidates to induce mild-temperature hyperthermia in deep-seated tumors where an external alternative magnetic field is used to activate these particles (10,11). The alternating field heats up the ferromagnetic nanoparticles through a combination of rapid hysteresis and Neel relaxation (12,13). An additional advantage is that these particles can be imaged using magnetic resonance imaging (MRI). Although this strategy seems to be promising to heat up deep-seated tumors the major challenge associated with this method is the requirement of large amount of ferromagnetic nanoparticles to generate sufficient heat for clinical applications. Water-soluble 15 nm particles with magnetic cores and silane coats that are directly injected into tumors (and visualized by MRI for thermal dosimetry purposes) have currently obtained approval in Europe for multiple clinical trials with at least one (glioblastoma model) having completed Phase II evaluation (14-16). These approaches to thermoradiotherapy have evolved in parallel with the more widespread availability of MR thermal imaging for non-invasive monitoring of temperature and the emergence of closed-loop hyperthermia generating and thermal imaging systems (such as the MR guided focused ultrasound systems) for controlled and consistent hyperthermic treatments.

Gold nanoparticle mediated radiation dose enhancement

The biological effect of radiation interaction with tissues is generally related to the linear energy transfer (LET)—defined as the amount of energy transferred per unit distance travelled in tissues which in turn depends on the kinetic energy of electrons (17). Since the normal and tumor tissues have similar electron densities, precise treatment planning is required (as widely adopted in current RT treatment strategies), to deliver maximum dose to the tumor tissues with minimum collateral damage to normal tissues. As a corollary, enhancing the electron density in the tumor tissues could potentially have favorable benefits in improving RT treatment outcomes. Electron dense high atomic number (Z) elements offer an excellent choice to enhance the radiation interaction cross-section of the target tissues (18). Combining this characteristic of high-Z elements with the unique tumor specific accumulation of nanoparticles (in the range of 1-100 nm) opens up the prospect of delivering greater radiation dose to tumors while sparing adjacent normal tissues. Although several high-Z elements have been explored for radiosensitization, GNPs have favorable characteristics such as biocompatibility, ease of conjugation, evasion of the immune system upon PEGylation and preferential accumulation in tumors by the EPR effect (19-22). Furthermore, active targeting via decoration of these GNPs with tumor-homing moieties (peptide, antibodies, oligonucleotides, etc.) affords tumor-specificity and the potential for internalization of GNPs into tumor cell cytoplasms and possibly nuclei. In turn, the presence of GNPs in tumor cells leads to (I) physical dose enhancement induced by the interaction of secondary electrons, generated from the GNPs (often localized in the peri-nuclear region of the cell), with the nuclear DNA and (II) enhanced biological response induced by the short-lived reactive oxygen species (ROS) generated near critical organelles within the tumor cell.

Physics of gold-mediated radiation dose enhancement

When atoms are irradiated with photon energies above the ionization energy of the innermost (K) shell electrons, photoelectric absorption results in the production of photo- and Auger/Coster-Kronig electrons (23,24). Classical photoelectric interactions occur when a high-energy photon collides with an atom to eject an electron—the photoelectron—from its shell; the remaining energy (incident photon energy minus energy transferred to the photoelectron) brings the whole atom to an excited state. This excess energy is released through two mechanisms that eject photons or electrons: X-ray fluorescence and ejection of Auger electrons. In both cases, the ejected particles form tracks of ionization in the tissue. In the case of high-Z nanoparticles, these secondary particles locally enhance the physical dose delivered around the metallic nanoparticles (25). Typically, photoelectric phenomena are dominant at kilovoltage (kV) energies and directly proportional to Z^{3-4} of the material. Consequently, the photoelectric cross-sections of high-Z materials (like gold, with a Z of 79) are considerably more than that of materials such as soft tissues containing carbon (Z=6), hydrogen (Z=1), nitrogen (Z=7) and oxygen (Z=8). Computational studies have shown that the yield of electrons is increased up to 10 times when 0.1% w/w of GNPs are incorporated into biological tissue irradiated with kilovoltage radiation beams (energy <200 keV), and approximately double when the same tissue is irradiated with megavoltage clinical beams—photons with energy up to 6 MeV (26). Studies have also shown the feasibility of using Yb-169 brachytherapy sources (matching the gold K-edge energy absorption) in combination with GNPs that demonstrated a dose enhancement of 2 orders of magnitude (27). While

several macro, micro and nano-scale computations have demonstrated the radiation dose enhancement of gold using multiple photon sources (^{125}I, ^{103}Pd, ^{169}Yb, ^{192}Ir, 50 kVp, 6MV X-rays) there is no clear consensus on the optimal parameters to define the effectiveness of GNP-mediated radiosensitization (27-29). More recently, it has been demonstrated that the effectiveness of GNP-mediated radiosensitization depends on the size of GNPs, the rate of photoelectric absorption, the characteristics of the escaping Auger electrons and the location of GNPs within the cell (30,31). Despite these extensive computational investigations a complete understanding of the nanoscale effects of GNP-mediated radiosensitization remains a lingering question. Nevertheless, experimental evidence demonstrates excellent radiosensitization effects that are attributed to the biological consequences of the GNP-mediated physical radiation dose enhancement.

Biological mechanisms of gold nanoparticle radiosensitization

The interaction of ionizing radiation with tissues causes damage by depositing energy directly to biomolecules (direct effects) or by the producing ROS through radiolysis of water (indirect effect) via, superoxide ($O\cdot_2^-$), hydrogen peroxide (H_2O_2) and hydroxyl ($^{\cdot}OH$) radical. In turn, these ROS generate DNA strand breaks, the most challenging ones to repair being double strand breaks (DSBs). A fine balance between DNA damage (primarily DSBs) and DNA repair is generally considered the primary determinant of the intrinsic radiosensitivity of tissues. Consequently, the effectiveness of GNP-mediated radiosensitization is evaluated by correlating the experimental outcome with the number of unrepaired DNA DSBs. A direct correlation between the cellular damage and the number of radiation-induced γH2AX and 53BP1 foci (markers of unrepaired DSBs) was reported for 50 and 2 nm GNPs; the damage induced by 50 nm GNPs is dependent on the cellular internalization of GNPs (32,33). A more recent investigation revealed 1.7 fold enhancement in γH2AX-foci at 24 hr after irradiation of glioblastoma cells incubated with 12 nm GNPs (34). While DNA DSBs are considered as the primary markers for radiation-induced cellular damage, some studies have demonstrated the role of intracellular ROS and apoptosis in GNP-mediated radiosensitization. Elevated levels of intracellular ROS and apoptosis have been reported in ovarian cells and breast cancer cells that were treated with 14 and 1.9 nm GNPs followed by kV and MV X-ray radiation (32,35,36). Additionally, the activation of cell cycle checkpoints in G1/S and G2/M phases, which maintain genomic integrity by repairing defects or preventing cell division, is a common response to ionizing radiation. Cells incubated with 10.8 nm glucose capped GNPs and irradiated with a ^{137}Cs source demonstrated accelerated G0/G1 transition and subsequent accumulation in G2/M phase (37). Similar findings were observed in ovarian cancer cells irradiated with 6 MV X-rays following the incubation with 14 nm glucose capped GNPs (35). These experimental results suggests that factors such as modulation in cell cycle kinetics, the ability of the cells to recover from DNA/mitochondrial damage or from high levels of oxidative stresses in the cytoplasm contribute to the effectiveness of GNP-mediated radiosensitization. Even without accounting for the heterogeneity of cell populations (stem cells, endothelial cells, immune and hematopoietic cells, hypoxic cells, etc.) *in vivo* within tumors and their differing responses to radiation, these cellular effects go beyond the predictions of physical dose enhancement to modify the biological effect of a given form of radiation on tumors laden with GNPs.

Pre-clinical evidence and outlook for clinical implementation

A seminal report on GNP-mediated radiosensitization in animal tumor models demonstrated a remarkable 1-year survival rate of 86% followed by 26 Gy radiation with 250 kVp X-ray when mouse tumors were laden with 1.9 nm intravenously administered GNPs *vs*. 20% for tumors not laden with GNPs. Based on this promising result, subsequent *in vitro* and *in vivo* studies were conducted to investigate both the enhanced intracellular damage and the global tumor response to RT in the presence of GNPs. Attempts to demonstrate the feasibility of using clinically relevant radiation beams showed delayed tumor growth and increased apoptosis in mice injected intravenously with 13 nm GNPs, 24 hr prior to a radiation dose of 25 Gy from a 6 MV clinical accelerator. When combined with hyperthermia, the therapeutic outcome of GNP-mediated radiosensitization was enhanced in radiation resistant squamous cell carcinomas (38). More recent investigations on the combination of GNPs and proton radiation (40 MeV, 10 to 41 Gy) demonstrated 1-year survival of 58-100% with GNPs and 11-13% without GNPs in murine CT26 colorectal cancer models (39,40). Thus, convincing pre-clinical evidence along with *in vitro* studies suggests that radiation dose enhancement by GNPs can be accomplished using multiple types of radiation (photons,

protons, electrons) from different sources (kilovoltage and megavoltage X-rays, HDR brachytherapy, protons) with different energies (low energy kilovoltage ranging from 50-300 kVp and high energy megavoltage ranging from 6 to 160 MV) (41). Although gold nanoparticle mediated radiation therapy (GNRT) is predominantly dependent on the energy of the radiation, with clinically less significant low energy beams being more efficient in generating secondary electrons when compared to the high energy beams, the therapeutic outcome of the clinically relevant high energy megavoltage beams can be modulated by enhancing tumor-specific localization of the GNPs.

The vast majority of pre-clinical investigations accomplish tumor-specific localization of GNPs via passive targeting that is dependent on the GNP size and the EPR effect. Larger GNPs tend to extravasate and accumulate in the perivascular space without penetrating deep into tumor parenchyma or getting internalized within cells. In contrast, smaller GNPs with enhanced permeability and diffusion characteristics demonstrate enhanced accumulation within tumor tissues (1% w/w) and may be internalized by some tumor cells. These present an ideal choice to transiently increase the radiation interaction cross-section of tumors. However, very small GNPs often act as intravascular contrast agents and are rapidly extruded from vasculature into tumors and equally rapidly efflux back into circulation due to the high interstitial tumor pressure within tumors. This rapid tumor uptake and immediate wash-out necessitates delivery of radiation immediately after the intravenous infusion of GNPs for effective radiation dose enhancement. The short interval (~2 min) between GNP administration and the radiation dose delivery, and the need for such administration before each radiation fraction reduce the enthusiasm for this approach in the clinic. Therefore, for clinically meaningful radiation dose enhancement, an approach that achieves the sustained presence of GNPs at high concentrations within the tumors is desirable. This could be accomplished by the active targeting strategy where the GNPs can be conjugated to antibodies or peptides directed against tumor antigens or antigens on tumor vasculature for tumor-specific localization of these GNPs. Thereafter, receptor-mediated or other non-specific methods (caveolin-mediated, macropinocytosis, etc.) may cause internalization that could bring these GNPs within close proximity to DNA, mitochondria, and cell membranes where short-range secondary electrons emanating from irradiated GNPs could cause DNA DSBs, mitochondrial membrane depolarization or lipid peroxidation, respectively. Additionally, the intracellular localization of GNPs achieved via active targeting could potentially minimize the amount of GNPs required to induce substantial radiation dose enhancement during GNRT, with less collateral damage to surrounding normal tissues. A more recent investigation using Her2-conjugated GNPs (~54 nm) and 100 kVP X-rays demonstrated a tumor regression of breast cancer models by 46% as compared to treatment with radiation alone (42). Our unpublished data with gold nanorods conjugated with an anti-EGFR antibody or a luteinizing hormone releasing hormone (LHRH) agonist strongly support this hypothesis. Nevertheless, uncertainties related to the intratumoral biodistribution of GNPs due to the heterogeneity of EPR in tumors still persist. While attempts to delineate the parameters for an enhanced biodsitrbution within tumors have largely been confined to pre-clinical investigations using animal tumor models, understanding the EPR effect in humans remains elusive. In particular, various parameters such as the variability in tumor vascular architecture, pore dimensions within and between tumor types, the location and origin of the tumor, nature of the vascular bed and surrounding stroma, tumor size, etc. could significantly influence the heterogeneity of EPR in tumors. Hence, integration of GNP imaging with GNP treatment would not only monitor and quantify the GNP biodistribution within tumors but also permit dosimetry and prediction of effects with biophysical models that include physical dose enhancement principles and biological parameters that modify these effects.

Nanoparticle-mediated delivery of radiosensitizing drugs to tumor

Extensive studies have been devoted to address the radiation resistance of tumors using multiple potent chemical radiosensitizers (43). The well-known radiosensitizers which work through chemical or biochemical means are hydroxyurea, halopyrimidines 5-iododeoxyuridine (IUDR) (44), 5-bromo-2'-deoxyuridine (BUDR) (45), 5-fluoro-2'-deoxy-beta-uridine (FUDR), trans sodium crocetinate, hypoxic radiosensitizers (nitric oxide, tirapazamine, nitroimidazoles like nimorazole, and the anthraquinone AQ4N), topoisomerase inhibitors (camptothecin and topotecan), alkylating agents (temozolomide) and monoclonal antibodies (cetuximab). Other examples of common radiosensitizers (also used as chemotherapeutic agents) are 5-fluorouracil (5-FU), doxorubicin, taxanes, gemcitabine, and platinum-based drugs (cisplatin and carboplatin).

One major difficulty in the implementation of these agents in radiotherapy as radiosensitizers is their cytotoxic effects and off-target effects in normal tissues (46). Such limitations can potentially be overcome by designing carriers with multi-faceted characteristics that include encapsulation and controlled release, minimization of immune-clearance, penetration of biological barriers and targeting the disease site (47,48). Various micro- and nano-sized carrier systems (liposomes, nanoparticle albumin-bound (Nab), polymeric nanoparticles, dendrimers, inorganic metal nanoparticles, and molecular targeted nanoparticles) (49) have been designed to create extended release formulations of drugs at the target site, while decreasing overall systemic drug dose to levels below the toxicity threshold (50,51).

Radioimmunotherapy using nanoparticles

Radionuclides formulated as nanoparticles have the potential to accumulate preferentially within tumors through passive diffusion or active targeting and thereby irradiate from within. Liposomal formulation of radionuclides (52) contributes to passive tumor accumulation via the EPR effect. For preventing hepatic accumulation, pretreatment with non-radioactive liposomes was effective in an *in vivo* biodistribution study (53). Utilization of tumor-specific metabolic and immune processes provides an effective route to deliver radionuclides preferentially to tumor tissues. Radioactive iodine has been used in the treatment of thyroid cancer due to its characteristic of being mostly taken up by the thyroid gland after systemic administration. In radioimmunotherapy, radionuclides are attached to antibodies to target tumors. Instead of attaching one radionuclide to each antibody, producing nanoparticles containing hundreds of radioactive atoms was demonstrated to deliver up to 50 Gy to tumor cells with Y_2O_3 nanoparticles (54). Yttrium-encapsulated 8 nm apoferritin shells with biotin surface modification was shown to be an effective strategy to conjugate multiple antibodies, constructing radioactive nanoparticles for radioimmunotherapy applications (55). Selective intra-arterial instillation of radioactive microparticles (56) might be useful in treatments of hepatocellular carcinoma via hepatic artery, since the blood supply of surrounding liver parenchyma comes mainly from the portal vein. *ChemoRad* nanoparticles were also recently described in the literature as biocompatible lipid–polymer hybrid nanoparticles loaded with both the chemotherapeutic drug (doxetaxel) and radionuclides (^{111}In or ^{90}Y) for chemo- RT of prostate cancer cells (46).

Neutron capture therapy using nanoparticles

Neutron capture therapy (NCT) has been investigated in clinical trials of glioblastoma, malignant melanoma, and head and neck cancer (57-59). Essentially, this modality of RT is based on the increased nuclear interaction cross-section of thermal neutrons (epithermal neutrons slow down to this level after colliding with nitrogen and hydrogen atoms along the way) with boron atoms (isotope B_{10}). The resulting localized nuclear reaction within the tumor creates a high-energy alpha (α^{2+}) particle and a high-energy stable ^{7}Li nucleus, both of which have short path lengths shorter than the diameter of a typical cell, where they cause a dense cluster of ionizations accounting for a high LET. This localized dose delivery combined with the inability of neutron radiation by itself to damage tissue makes boron NCT a promising therapeutic modality. So it gives promising concepts for targeted radiotherapy. Among the many challenges for widespread clinical implementation of NCT, one that can potentially be solved by nanoparticulate formulation of boronated compounds is that of tumor-specific uptake of boron without significant accumulation in normal tissues. This is particularly crucial for boron NCT because the tissue damage is largely confined to the boron-containing tumor cell. Not surprisingly, nanoparticles have been shown to play a role in improving the delivery of boron atoms to cancer cells. Nanoscaled dimensions of boron-capture particles generated via ball milling techniques have been shown to facilitate cellular uptake (60). Significant tumor growth delay was observed by neutron irradiation of boron nanoparticle laden tumors in *in vivo* studies (61). Liposome formulations (smaller than 100 nm) loaded with boron atoms have demonstrated enhanced tumor uptake leading to tumor growth suppression after NCT (30). More recent research on nanoparticle based BNT includes the design of (I) multifunctional gold nanoparticles decorated with fluorescent dye, boron, and folic acid for targeted delivery to tumor tissue (31); (II) boron nitride nanotubes as theranostic probes for simultaneous MR imaging and NCT (32), similar to that of gadolinium nanoparticles (62,63). Similarly, other nanoparticle based candidates for NCT include dirhenium decacarbonyl [$Re_2(CO)_{10}$] encapsulated in poly-L-lactide

(PLLA)-based nanoparticles (64) and holmium-loaded PLLA nanoparticles (65). Lastly, NCT using holmium-containing mesoporous silica nanoparticles demonstrated enhanced survival of mice with ovarian tumors (66). It remains to be seen whether nanopar¬ticle formulations will increase accumulation of neutron-absorbing nonradioactive isotopes within tumors and thereby increase tumor dose without increasing normal tissue dose to realize the promise of enhanced therapeutic gain with NCT in a clinical setting.

Other methods of enhancing radiotherapy using nanoparticles

In addition to the methods noted above to sensitize tumors to RT using nanoparticles, there are some reports in the literature that allude to combination of photodynamic therapy with RT. Photodynamic therapy induces cytotoxicity by generating singlet oxygen species when illuminated with light in presence of a photosensitizer. Its application to cancerous or non-cancerous lesion is confined to superficial areas that light can reach, such as endobronchial, esophageal, bladder, head and neck, oropharyngeal, eye, and skin lesions. An impediment to its wide acceptance in clinic is the nonspecific distribution of photosensitizer in adjacent normal tissues. Nanotechnology has the potential to enhance photodynamic therapy by selectively delivering drug or the photosensitizer itself (67). Scintillation or persistent luminescence nanoparticles with attached photosensitizers have been synthesized such that they can be excited by RT to generate light that, in turn, stimulates the photosensitizer (68). This approach not only enables photodynamic therapy of deep-seated lesions but also enhances radiation dose effect with additional DNA damage from the photosensitizer.

Whereas the above descriptions of the use of nanotechnology have focused on sensitization of tumors to RT, improvement of the therapeutic ratio of RT can be achieved by protection of adjacent normal tissue as well. Given the EPR effect resulting in preferential accumulation of nanoparticles in tumors, it is hard to conceptualize a way to passively accumulate radioprotective nanoparticles in normal tissues. Consequently, the ideal scenario for nanoparticulate radioprotector use is when selective accumulation in normal tissues can be achieved by active targeting or when there is no tumor being radiated simultaneously (such as to mitigate radiation syndromes from accidental radiation exposure of healthy individuals). In a study of melanin-coated silica nanoparticles administered intravenously to melanoma-bearing nude mice, the radioprotective property of melanin resulted in reduction of hematological toxicity without compromising anti-tumor efficacy of subsequent radioim¬munotherapy with ^{188}Re-labeled melanin-binding antibody due to the accumulation of nanoparticles within the bone marrow (69). Amifostine, a free-radical scavenger used for prevention of xerostomia (dry mouth syndrome) from head and neck cancer RT, is effective when administered intravenously. Amifostine nanoparticles produced by polymeric encapsulation (polylactide-co-glycolide) were shown to significantly protect mice from whole body irradiation when administered orally (70). Cerium oxide (CeO_2) nanoparticles (71-73) and fullerene nanoparticles (74,75) are also being investigated as potential free radical scavengers to reduce radiation-induced pneumonitis, gut mucosal injury, xerostomia, and radiation-induced dermatitis in animal models.

Conclusions: caveats and outlook for clinical translation

Interest in using nanotechnology to treat cancer has grown explosively as a result of tremendous versatility in nanoparticle design and the potential for surface modifications to enhance their functionality. These properties can be effectively utilized for numerous applications in the diagnosis and treatment of cancer and RT is no exception. Nanoparticles can modify tumor radiation response either as radiosensitizers or radioprotectors themselves or by mediating the delivery of a payload of another radiation modifying material. In addition to these favorable characteristics, nanoparticles may also be detected using a variety of imaging modalities, potentially allowing for quantitative dosimetry and image-guided RT. Potential applications of nanoparticles in radiation oncology are illustrated in *Figure 1*. While excitement about the impact of nanotechnology on radiation oncology is growing, research in this arena is still in its infancy with most studies confined to proof-of-principle experiments and modeling.

Successful clinical translation of nanoparticles will require investigators to navigate a number of unique challenges in both preclinical evaluation and clinical trial design. The first challenge is to ensure immediate and long-term safety and tolerability in humans. Some particles, such as gold, have years of track record of safe clinical use in other diseases like arthritis. However each

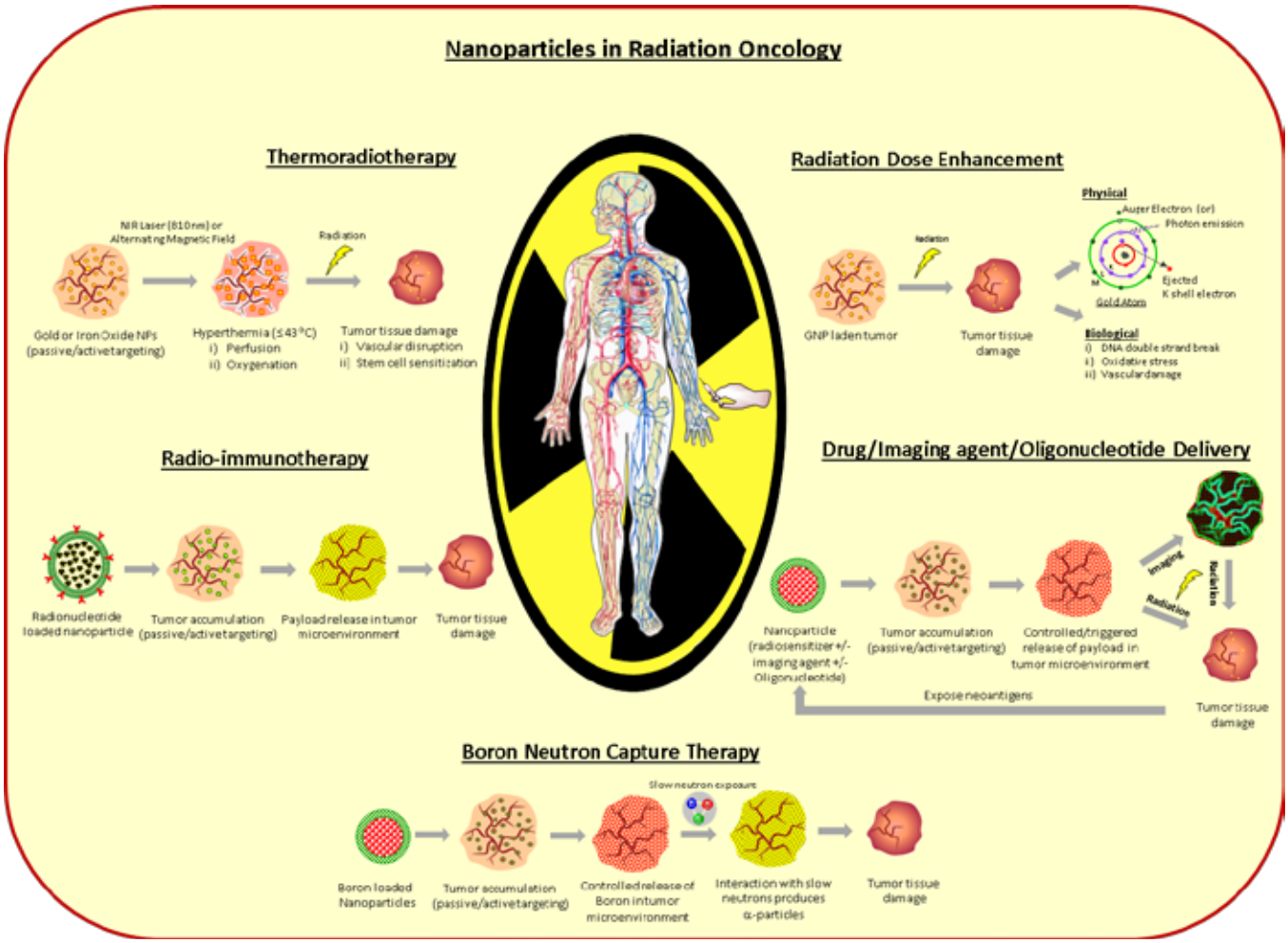

Figure 1 Potential clinical applications of nanoparticles in radiation oncology. This cartoon outlines some of the many ways in which nanoparticles can improve radiation therapy, namely thermoradiotherapy, radioimmunotherapy, radiation dose enhancement, delivery of payloads of drug/imaging agent/oligonucleotides to enhance radiotherapy efficacy or image-guidance, and boron neutron capture therapy. NIR, near infrared; DNA, deoxyribonucleic acid

new particle will require meticulous preclinical testing and documentation of safety and tolerability thresholds before advancing to early phase clinical trials. As part of this process, the pharmacokinetics, biodistribution and clearance of nanoparticles need to be thoroughly investigated. The functionality of nanoparticles might be limited by nonspecific uptake, assisted by plasma protein opsonization that clears nanoparticles via the reticulo-endothelial system (liver, spleen, lymph nodes). This nonspecific uptake could significantly minimize the circulation half-life of these particles, thus leading to less accumulation in tumors. Ways to minimize nonspecific uptake might include: (I) reducing nanoparticle size; (II) changing the shape of particles (elongated particles are more likely to extravagate from blood vessels since they travel at the periphery of a blood column, rather than spherical particles that travel at the center); (III) changing the surface charge (generally positively charged particles are cleared more rapidly by opsonization while particles with a slightly negative charge keep particles in suspension without clumping and neutral charge minimizes chemical interactions allowing particles to remain in circulation); (IV) using surface modification with a material like polyethylene glycol or dextran to evade macrophages; and (V) inhibiting Kupffer cell activation in the liver. Additionally, the unique operating constraints (type of

nanoparticle and the energy source) associated with each of the strategies sets the limitation on the use of these strategies for specific oncologic applications.

Despite the aforesaid limitations, the clinical translation of nanoparticle based strategies in radiation oncology is probably a matter of time because of the prior history of interactions between the physical and life sciences in the field of radiation oncology, the conceptual foundation of both disciplines in the quantitative sciences, and the versatile characteristics of nanoparticles that enable need-based tunability to overcome the roadblocks for specific oncologic applications. Nevertheless, a detailed understanding of the operating constraints and the nano-scale physical and biological underpinnings of nanoparticle-radiation interactions is needed to advance these strategies towards clinical translation.

Acknowledgements

This work was funded in part by grants from the National Institutes of Health (1R21CA133691-01, 1R01CA132032, 1R01CA155446, and U01CA151886), Department of Defense (PC111832), MD Anderson Institutional Research Grant to SK and NIH-Head and Neck SPORE (P50 CA097007) career development award to PD.
Disclosure: The authors declare no conflict of interest.

References

1. Roti Roti JL. Introduction: radiosensitization by hyperthermia. Int J Hyperthermia 2004;20:109-14.
2. Horsman MR, Overgaard J. Hyperthermia: a potent enhancer of radiotherapy. Clin Oncol (R Coll Radiol) 2007;19:418-26.
3. Song CW, Park HJ, Lee CK, et al. Implications of increased tumor blood flow and oxygenation caused by mild temperature hyperthermia in tumor treatment. Int J Hyperthermia 2005;21:761-7.
4. Song CW, Shakil A, Osborn JL, et al. Tumour oxygenation is increased by hyperthermia at mild temperatures. 1996. Int J Hyperthermia 2009;25:91-5.
5. Lai CY, Kruse DE, Caskey CF, et al. Noninvasive thermometry assisted by a dual-function ultrasound transducer for mild hyperthermia. IEEE Trans Ultrason Ferroelectr Freq Control 2010;57:2671-84.
6. Jain PK, Huang X, El-Sayed IH, et al. Noble metals on the nanoscale: optical and photothermal properties and some applications in imaging, sensing, biology, and medicine. Acc Chem Res 2008;41:1578-86.
7. Kennedy LC, Bickford LR, Lewinski NA, et al. A new era for cancer treatment: gold-nanoparticle-mediated thermal therapies. Small 2011;7:169-83.
8. Diagaradjane P, Shetty A, Wang JC, et al. Modulation of in vivo tumor radiation response via gold nanoshell-mediated vascular-focused hyperthermia: characterizing an integrated antihypoxic and localized vascular disrupting targeting strategy. Nano Lett 2008;8:1492-500.
9. Atkinson RL, Zhang M, Diagaradjane P, et al. Thermal enhancement with optically activated gold nanoshells sensitizes breast cancer stem cells to radiation therapy. Sci Transl Med 2010;2:55ra79.
10. Kim J, Oh J, Kang HW, et al. Photothermal response of superparamagnetic iron oxide nanoparticles. Lasers Surg Med 2008;40:415-21.
11. Kobayashi T. Cancer hyperthermia using magnetic nanoparticles. Biotechnol J 2011;6:1342-7.
12. Rosensweig RE. Heating magnetic fluid with alternating magnetic field. J Magn Magn Mater 2002;252:370-4.
13. Jordan A, Wust P, Fähling H, et al. Inductive heating of ferrimagnetic particles and magnetic fluids: physical evaluation of their potential for hyperthermia. 1993. Int J Hyperthermia 2009;25:499-511.
14. van Landeghem FK, Maier-Hauff K, Jordan A, et al. Post-mortem studies in glioblastoma patients treated with thermotherapy using magnetic nanoparticles. Biomaterials 2009;30:52-7.
15. Johannsen M, Gneveckow U, Taymoorian K, et al. Morbidity and quality of life during thermotherapy using magnetic nanoparticles in locally recurrent prostate cancer: results of a prospective phase I trial. Int J Hyperthermia 2007;23:315-23.
16. Maier-Hauff K, Rothe R, Scholz R, et al. Intracranial thermotherapy using magnetic nanoparticles combined with external beam radiotherapy: results of a feasibility study on patients with glioblastoma multiforme. J Neurooncol 2007;81:53-60.
17. Wheldon TE, O'Donoghue JA. The radiobiology of targeted radiotherapy. Int J Radiat Biol 1990;58:1-21.
18. Pignol JP, Rakovitch E, Beachey D, et al. Clinical significance of atomic inner shell ionization (ISI) and Auger cascade for radiosensitization using IUdR, BUdR, platinum salts, or gadolinium porphyrin compounds. Int J Radiat Oncol Biol Phys 2003;55:1082-91.
19. Maeda H, Nakamura H, Fang J. The EPR effect for macromolecular drug delivery to solid tumors: Improvement of tumor uptake, lowering of systemic

toxicity, and distinct tumor imaging in vivo. Adv Drug Deliv Rev 2013;65:71-9.
20. Wong C, Stylianopoulos T, Cui J, et al. Multistage nanoparticle delivery system for deep penetration into tumor tissue. Proc Natl Acad Sci U S A 2011;108:2426-31.
21. Moghimi SM, Hunter AC, Murray JC. Nanomedicine: current status and future prospects. FASEB J 2005;19:311-30.
22. Lévy R, Thanh NT, Doty RC, et al. Rational and combinatorial design of peptide capping ligands for gold nanoparticles. J Am Chem Soc 2004;126:10076-84.
23. Bernhardt P, Friedland W, Paretzke HG. The role of atomic inner shell relaxations for photon-induced DNA damage. Radiat Environ Biophys 2004;43:77-84.
24. Nikjoo H, Emfietzoglou D, Charlton DE. The Auger effect in physical and biological research. Int J Radiat Biol 2008;84:1011-26.
25. Butterworth KT, McMahon SJ, Currell FJ, et al. Physical basis and biological mechanisms of gold nanoparticle radiosensitization. Nanoscale 2012;4:4830-8.
26. Cho SH. Estimation of tumour dose enhancement due to gold nanoparticles during typical radiation treatments: a preliminary Monte Carlo study. Phys Med Biol 2005;50:N163-73.
27. Jones BL, Krishnan S, Cho SH. Estimation of microscopic dose enhancement factor around gold nanoparticles by Monte Carlo calculations. Med Phys 2010;37:3809-16.
28. Carter JD, Cheng NN, Qu Y, et al. Nanoscale energy deposition by X-ray absorbing nanostructures. J Phys Chem B 2007;111:11622-5.
29. Leung MK, Chow JC, Chithrani BD, et al. Irradiation of gold nanoparticles by x-rays: Monte Carlo simulation of dose enhancements and the spatial properties of the secondary electrons production. Med Phys 2011;38:624-31.
30. Lechtman E, Chattopadhyay N, Cai Z, et al. Implications on clinical scenario of gold nanoparticle radiosensitization in regards to photon energy, nanoparticle size, concentration and location. Phys Med Biol 2011;56:4631-47.
31. Lechtman E, Mashouf S, Chattopadhyay N, et al. A Monte Carlo-based model of gold nanoparticle radiosensitization accounting for increased radiobiological effectiveness. Phys Med Biol 2013;58:3075-87.
32. Jain S, Coulter JA, Hounsell AR, et al. Cell-specific radiosensitization by gold nanoparticles at megavoltage radiation energies. Int J Radiat Oncol Biol Phys 2011;79:531-9.
33. Chithrani DB, Jelveh S, Jalali F, et al. Gold nanoparticles as radiation sensitizers in cancer therapy. Radiat Res 2010;173:719-28.
34. Joh DY, Sun L, Stangl M, et al. Selective targeting of brain tumors with gold nanoparticle-induced radiosensitization. PLoS One 2013;8:e62425.
35. Geng F, Song K, Xing JZ, et al. Thio-glucose bound gold nanoparticles enhance radio-cytotoxic targeting of ovarian cancer. Nanotechnology 2011;22:285101.
36. Butterworth KT, Coulter JA, Jain S, et al. Evaluation of cytotoxicity and radiation enhancement using 1.9 nm gold particles: potential application for cancer therapy. Nanotechnology 2010;21:295101.
37. Roa W, Zhang X, Guo L, et al. Gold nanoparticle sensitize radiotherapy of prostate cancer cells by regulation of the cell cycle. Nanotechnology 2009;20:375101.
38. Hainfeld JF, Dilmanian FA, Zhong Z, et al. Gold nanoparticles enhance the radiation therapy of a murine squamous cell carcinoma. Phys Med Biol 2010;55:3045-59.
39. Kim JK, Seo SJ, Kim KH, et al. Therapeutic application of metallic nanoparticles combined with particle-induced x-ray emission effect. Nanotechnology 2010;21:425102.
40. Kim JK, Seo SJ, Kim HT, et al. Enhanced proton treatment in mouse tumors through proton irradiated nanoradiator effects on metallic nanoparticles. Phys Med Biol 2012;5:8309-23.
41. Polf JC, Bronk LF, Driessen WH, et al. Enhanced relative biological effectiveness of proton radiotherapy in tumor cells with internalized gold nanoparticles. Appl Phys Lett 2011;98:193702.
42. Chattopadhyay N, Cai Z, Kwon YL, et al. Molecularly targeted gold nanoparticles enhance the radiation response of breast cancer cells and tumor xenografts to X-radiation. Breast Cancer Res Treat 2013;137:81-91.
43. Brown JM. Clinical trials of radiosensitizers: what should we expect? Int J Radiat Oncol Biol Phys 1984;10:425-9.
44. Williams JA, Yuan X, Dillehay LE, et al. Synthetic, implantable polymers for local delivery of IUdR to experimental human malignant glioma. Int J Radiat Oncol Biol Phys 1998;42:631-9.
45. Doiron A, Yapp DT, Olivares M, et al. Tumor radiosensitization by sustained intratumoral release of bromodeoxyuridine. Cancer Res 1999;59:3677-81.
46. Wang AZ, Yuet K, Zhang L, et al. ChemoRad nanoparticles: a novel multifunctional nanoparticle platform for targeted delivery of concurrent chemoradiation. Nanomedicine (Lond) 2010;5:361-8.
47. Langer R. New methods of drug delivery. Science 1990;249:1527-33.

48. Wagner V, Dullaart A, Bock AK, et al. The emerging nanomedicine landscape. Nat Biotechnol 2006;24:1211-7.
49. Wang AZ, Langer R, Farokhzad OC. Nanoparticle delivery of cancer drugs. Annu Rev Med 2012;63:185-98.
50. Farokhzad OC, Langer R. Impact of nanotechnology on drug delivery. ACS Nano 2009;3:16-20.
51. Youan BB. Impact of nanoscience and nanotechnology on controlled drug delivery. Nanomedicine (Lond) 2008;3:401-6.
52. Sofou S, Thomas JL, Lin HY, et al. Engineered liposomes for potential alpha-particle therapy of metastatic cancer. J Nucl Med 2004;45:253-60.
53. Jonasdottir TJ, Fisher DR, Borrebaek J, et al. First in vivo evaluation of liposome-encapsulated 223Ra as a potential alpha-particle-emitting cancer therapeutic agent. Anticancer Res 2006;26:2841-8.
54. Bouchat V, Nuttens VE, Lucas S, et al. Radioimmunotherapy with radioactive nanoparticles: first results of dosimetry for vascularized and necrosed solid tumors. Med Phys 2007;34:4504-13.
55. Wu H, Wang J, Wang Z, et al. Apoferritin-templated yttrium phosphate nanoparticle conjugates for radioimmunotherapy of cancers. J Nanosci Nanotechnol 2008;8:2316-22.
56. Campbell AM, Bailey IH, Burton MA. Analysis of the distribution of intra-arterial microspheres in human liver following hepatic yttrium-90 microsphere therapy. Phys Med Biol 2000;45:1023-33.
57. Hiratsuka J, Fukuda H, Kobayashi T, et al. Human melanoma treated by boron neutron capture therapy: comparison of the clinical response with the predicted response. Radiat Med 1996;14:257-63.
58. Kawabata S, Miyatake S, Hiramatsu R, et al. Phase II clinical study of boron neutron capture therapy combined with X-ray radiotherapy/temozolomide in patients with newly diagnosed glioblastoma multiforme--study design and current status report. Appl Radiat Isot 2011;69:1796-9.
59. Barth RF, Vicente MG, Harling OK, et al. Current status of boron neutron capture therapy of high grade gliomas and recurrent head and neck cancer. Radiat Oncol 2012;7:146.
60. Mortensen MW, Sørensen PG, Björkdahl O, et al. Preparation and characterization of Boron carbide nanoparticles for use as a novel agent in T cell-guided boron neutron capture therapy. Appl Radiat Isot 2006;64:315-24.
61. Petersen MS, Petersen CC, Agger R, et al. Boron nanoparticles inhibit tumour growth by boron neutron capture therapy in the murine B16-OVA model. Anticancer Res 2008;28:571-6.
62. Arrais A, Botta M, Avedano S, et al. Carbon coated microshells containing nanosized Gd(III) oxidic phases for multiple bio-medical applications. Chem Commun (Camb) 2008;(45):5936-8.
63. Fujimoto T, Ichikawa H, Akisue T, et al. Accumulation of MRI contrast agents in malignant fibrous histiocytoma for gadolinium neutron capture therapy. Appl Radiat Isot 2009;67:S355-8.
64. Hamoudeh M, Fessi H, Mehier H, et al. Dirhenium decacarbonyl-loaded PLLA nanoparticles: influence of neutron irradiation and preliminary in vivo administration by the TMT technique. Int J Pharm 2008;348:125-36.
65. Hamoudeh M, Fessi H, Salim H, et al. Holmium-loaded PLLA nanoparticles for intratumoral radiotherapy via the TMT technique: preparation, characterization, and stability evaluation after neutron irradiation. Drug Dev Ind Pharm 2008;34:796-806.
66. Di Pasqua AJ, Yuan H, Chung Y, et al. Neutron-activatable holmium-containing mesoporous silica nanoparticles as a potential radionuclide therapeutic agent for ovarian cancer. J Nucl Med 2013;54:111-6.
67. Chatterjee DK, Fong LS, Zhang Y. Nanoparticles in photodynamic therapy: an emerging paradigm. Adv Drug Deliv Rev 2008;60:1627-37.
68. Chen W, Zhang J. Using nanoparticles to enable simultaneous radiation and photodynamic therapies for cancer treatment. J Nanosci Nanotechnol 2006;6:1159-66.
69. Schweitzer AD, Revskaya E, Chu P, et al. Melanin-covered nanoparticles for protection of bone marrow during radiation therapy of cancer. Int J Radiat Oncol Biol Phys 2010;78:1494-502.
70. Pamujula S, Kishore V, Rider B, et al. Radioprotection in mice following oral administration of WR-1065/PLGA nanoparticles. Int J Radiat Biol 2008;84:900-8.
71. Colon J, Herrera L, Smith J, et al. Protection from radiation-induced pneumonitis using cerium oxide nanoparticles. Nanomedicine 2009;5:225-31.
72. Colon J, Hsieh N, Ferguson A, et al. Cerium oxide nanoparticles protect gastrointestinal epithelium from radiation-induced damage by reduction of reactive oxygen species and upregulation of superoxide dismutase 2. Nanomedicine 2010;6:698-705.
73. Madero-Visbal RA, Alvarado BE, Colon JF, et al. Harnessing nanoparticles to improve toxicity after head and neck radiation. Nanomedicine 2012;8:1223-31.
74. Daroczi B, Kari G, McAleer MF, et al. In vivo

radioprotection by the fullerene nanoparticle DF-1 as assessed in a zebrafish model. Clin Cancer Res 2006;12:7086-91.
75. Brown AP, Chung EJ, Urick ME, et al. Evaluation of the fullerene compound DF-1 as a radiation protector. Radiat Oncol 2010;5:34.

Cite this article as: Chatterjee DK, Wolfe T, Lee JH, Brown AP, Singh PK, Bhattarai SR, Diagaradjane P, Krishnan S. Convergence of nanotechnology with radiation therapy—insights and implications for clinical translation. Transl Cancer Res 2013;2(4):256-268. doi: 10.3978/j.issn.2218-676X.2013.08.10

Review Article

Nanoparticles in radiation therapy: a summary of various approaches to enhance radiosensitization in cancer

Deep Kwatra[1], Anand Venugopal[1], Shrikant Anant[1,2]

[1]Department of Molecular and Integrative Physiology, [2]University of Kansas Cancer Center, University of Kansas Medical Center, Kansas City, KS 66160, USA

Correspondence to: Shrikant Anant, Ph.D. 3901 Rainbow Blvd MS 3040, Kansas City, KS 66160, USA. Email: sanant@kumc.edu.

Abstract: Acquired radiation resistance is one of the major causes of radio therapy failure and subsequent tumor relapse. Multiple approaches have been utilized to limit the radiation resistance while simultaneously enhancing the efficacy and safety of radiation therapy. The three major approaches for the improvement of radiation therapy have involved (I) ehancing radiosensitization of tumor tissue; (II) rversing of radiation resistance in tumor tissue; and (III) ehancing radioresistance of the healthy tissue. Nanoparticles have played a key role in the enhancement of the radiation therapy by acting both as a therapeutic as well as a carrier for other therapeutics. In this review we summarize the research being carried out using different species of nanoparticles for enhanced radiosensitization in cancer.

Keywords: Radiation resistance; radio protection; high-Z metal nanoparticles

doi: 10.3978/j.issn.2218-676X.2013.08.06

Scan to your mobile device or view this article at: http://www.thetcr.org/article/view/1550/2266

Introduction

A major reason for the absence of cure and subsequent tumor relapse is the development of resistance to the therapeutic modality. Radiation therapy along with surgery and chemotherapy are the major therapeutic strategies for cancer treatment. It involves the delivery of high intensity ionizing radiations with high accuracy to the tumor tissue resulting in the death of tumor cells. Radiation therapy has its disadvantages including the possibility of injury to the surrounding normal tissue. Another disadvantage is that some tumor cells are farther away from the site of radiation and hence might receive a lower intensity of the radiation beam. Moreover, the cells can develop resistance to the radiation. Usually the sensitivity of the mitotically active tumor cells is only slightly higher than that of surrounding healthy tissue. Hence the minimum dose of radiation that is sufficient to kill tumor tissue may only injure but not kill the normal tissue. However, due to development of resistance of tumor cells to the dosed radiation results in requirement of elevated doses which eventually leads to death of the healthy tissue.

High-energy ionizing radiations such as gamma rays or X-rays are mainly used to ionize cellular components and/or water. Particulate radiations such as alpha or beta particles or electron, proton or neutron beams are also used in certain specific cases to target the cancer tissue (1,2). Since water is a major component of the cells it is the major target of these ionizing radiations which result in radiation mediated lysis of the molecule. Unlike a chemical lysis, this radiolysis results in the generation of not only charged species but also free radicals such as hydrogen radical $H^{\bullet}$, hydroxyl radical $OH^{\bullet}$, Superoxides O_2^- and charged water species such as H_2O^+, and H_2O^+. DNA is the primary target of the ionizing radiations themselves along with the radicals though many other cellular components are also damaged (3). Interaction of free radicals with the membrane structures also causes structural damages resulting in induction of apoptosis. The hydroxyl ion has been reported in multiple studies to be a major source of cellular damage and it is known to induce lipid peroxidation. The interaction with lipid bilayers have also been shown make the cells highly permeable.

Though great advances have been made in the field of

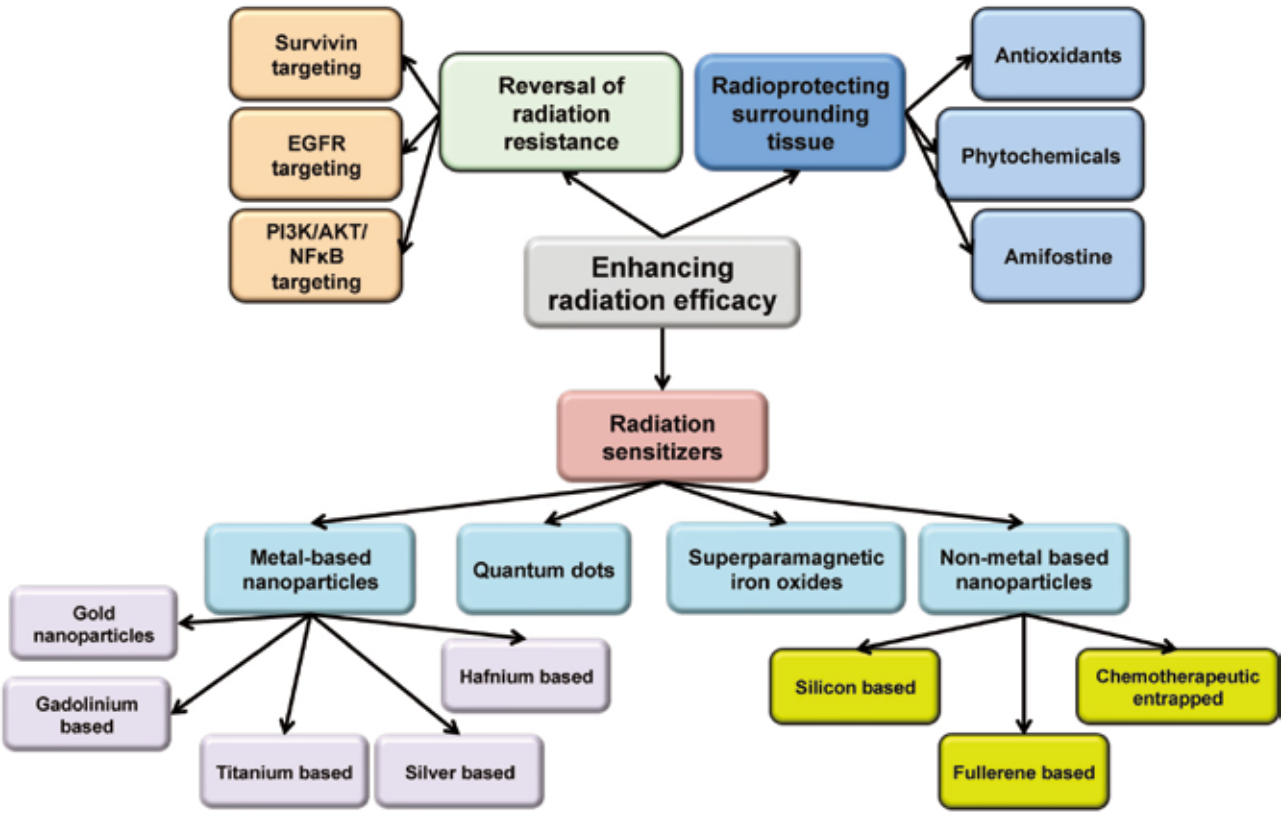

Figure 1 Summary of various approaches for enhancing the radiosensitization in cancer cells

radiation oncology resulting in better focusing and more regulated dosing of the ionizing radiation, some major issues with the therapy still remain. Radiation resistance as well as the inherent flaws of the therapeutic system still makes it a balancing act between its therapeutic advantages and physiological disadvantages. Multiple approaches have been used to enhance its efficacy while reducing the toxicity. The three major approaches that will be discussed in this mini review will be (I) ehancing radiosensitization of tumor tissue; (II) reversal of radiation resistance in tumor tissue; and (III) enhancing radioresistance of the healthy tissue. Approaches used for radiosensitization have been summarized in *Figure 1*.

Enhancing the efficacy of radiation therapy by radiosensitizers

Radiation sensitization is a process of enhancing the susceptibility of tumor tissues to injury by radiation exposure. Hence, rediosensitizers are therapeutic or otherwise inert agents that enhance the effects of radiation therapy. Over the last few years there has been a considerable increase in interest in the use of formulations to enhance radiotherapeutic effects, especially using metal (mainly gold) based nanoparticles (4). The densely packed metal particles can selectively scatter and/or absorb the high energy gamma/X-ray radiations. This allows for better targeting of cellular components within the tumor tissues allowing for more localized and consolidated damage. These also provide enriched interaction cross-section with the photons from these radiations (5,6). The photoelectron scattering upon the exposure of the surface of the metals to the gamma irradiation is also proposed to be mechanism for enhanced activity. A combination of all these phenomenon results in reduction is the therapeutic radiation dose further limiting the damage to the healthy tissue. The use of nanomaterial radiosensitizers is also called as Nanoparticle Enhanced X-ray Therapy or NEXT (7).

The earliest studies demonstrating enhanced radiation damage of the chromosomal DNA occurred in the mid-1970s when patients undergoing iodine angiography showed enhanced lymphocyte toxicity (8). *In vitro* studies

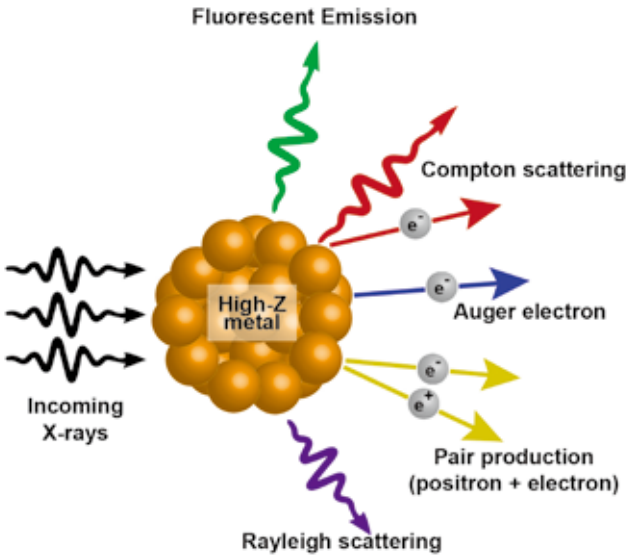

Figure 2 Interaction of X-rays with high-Z material nanoparticles

conducted during the same period also showed similar enhancements in cytotoxic effects of radiation in presence of Iodine (9). This resulted in the development of the concept in which high-Z material when incorporated into cells results in higher efficiency for radiation mediated cellular damage. In separate studies it was demonstrated that cells grown on gold film showed a multifold and significant dose enhancement effect upon irradiation. In other studies, tumor tissues injected with ≈3 μm sized gold nanoparticles showed much reduced growth post irradiation. The problem with these particles was the lack of diffusion in the cancer tissue due to their large size. Thus based on the same principles smaller sized gold nanoparticles have been extensively optimized and utilized in various cancers.

Principles of radiosensitization by metal-based formulations

When X-rays hit a metal, there are multiple possibilities of eventual outcome. Among the several emissions that occur, the most relevant to cancer radiotherapy are scattered X-rays/photons, photoelectrons, Compton electrons, Auger electrons and fluorescence photons. The incoming radiation wave imparts its energy to an electron within the atom ejecting it from its orbital with a kinetic energy equivalent of the energy of the wave minus the binding energy of the electron. This kinetic energy of the outgoing electron radiation is what decides the range of the electron within the tissue. This photoelectric effect is decided by $(Z/E)^3$ where E is the energy of the incoming photon and Z is the atomic number of the molecule being targeted. The Auger electrons or fluorescent photons are produced when the ejected electrons are replaced with electrons dropping from the higher orbits and energy is released. The fluorescent photons are low energy but have higher coverage range. The Auger electrons have much shorter range of coverage but can generate much higher ionization density at a localized area. Gold being a high-Z material (Z=79) and very inert to tissue interactions is ideal for photosensitization reactions. The interaction of X-rays with high-Z nanoparticles and the resultant outcomes have been summarized in *Figure 2*.

Properties of gold nanoparticles

The advantages of gold nanoparticles that make it an ideal material for photosensitization among high Z particles are the following (10):

- Gold being very inert, it is highly biocompatible;
- The gold nanoparticles enhance the effect of the radiation over a large area of tumor thus eliminating the need of the nanoparticles to be delivered to all the cells of the tumor tissue;
- Nanoparticles are known to have low systemic clearance as compared to low molecular contrast agents such as iodine allowing the photosensitizing material enough time to get absorbed into the tumor tissue;
- Nanoparticles are known to be well absorbed into systemic circulations, better permeation into the tumor tissue. This along with lower clearance rate results in the enhanced permeation and retention (EPR) effect;
- By attaching targeting moieties such as antibodies, large number of the gold atoms can be specifically delivered to the tumor tissue as compared to using solutions of iodine. A nanoparticle of 10-15 nm in size contains 50-75 thousand atoms within it resulting in a much higher efficiency of delivery;
- The gold nanoparticles can be varied in size or shapes (such as spheres cube, rods, cones or other 3D structures) based on the delivery requirements of the tumor tissue (such as its size and location) so as to achieve optimum delivery and effect;
- It is much easier to perform overall and tissue specific pharmacokinetic studies with the gold nanoparticles

as they are easy to image and quantify. Thus the dose levels can be optimized for best results.

Along with these advantages, there are certain disadvantages associated with the use of gold nanoparticles such as the high cost of material and formulation. Though the EPR effect has its own advantages, the long circulating half-life may not be beneficial when considered at a whole body level. Though as such gold is supposed to be inert, more detailed toxicological profile still needs to be generated. Surface coating using polymeric material has led to better regulation of the pharmacokinetic and targeting properties of the gold nanoparticles (11). The gold nanoparticle itself provides large number of ligand binding sites. The number of binding sites is directly proportional to the size of the nanoparticle. The advantage of these ligand-binding sites is that the chemistry for the attachment is relatively easy, and the surface properties allow for the binding of multiple different types of ligands to the same nanoparticle. Due to the cost associated with the therapy using gold, just modifying the size of the nanoparticles itself to adjust the pharmacokinetic properties of the formulation may not be the best approach. The use of polymeric coating may be a better approach to play around with the size of the formulation. Also the possibility of attaching multiple different ligands allows for the attachment of polymeric materials such as PEG along with other targeting moieties. PEG has been shown in multiple studies to reduce the uptake of nanoparticulate formulations by reticuloendothelial system (12). This allows for prolonged retention of the gold nanoparticles within the circulatory system. As previously mentioned, the efficacy of the metal-based formulation depends upon the energy of the radiation along with the type, amount and location of material within the tissue. Better targeting and pharmacokinetic profile of the nanoparticles will generate much more efficient therapy with reduced adverse effects to surrounding healthy tissue.

Therapeutic uses of gold nanoparticles in radiosensitization

Zheng and colleagues did a proof of principal study for the enhanced radiosensitization effects of gold nanoparticles on DNA damage induced by high energy electrons (13). They used plasmid DNA and bombarded them with 60 keV electrons either alone or in the presence of gold nanoparticles at a ratio of 1:1 or 1:2 DNA to gold nanoparticle. This increased the number of double stranded breaks by a magnitude of about 2.5 fold. The studies suggested that the enhanced effects were due to the production of low energy electrons from the gold particles and that the effects were directly proportional to the number of particles in the proximity of the DNA. Based on similar concepts, one of the first systemic optimization studies was performed by Brun and colleagues, where they further studied parameters such as size (8-92 nm) and molar ratio of the nanoparticles along with the energy of the incident X-rays (14.8-70 keV) (14). In these studies, the best results were achieved when using gold nanoparticles of large size, at high molar concentration and with 50-keV photons. This combination resulted in a 6-fold improvement relative to controls.

Additional optimization studies by Lechtman and group also had very interesting outcomes (15). Based on the results of their studies, they concluded that when using photon energies below the k-edge, auger cascade is dominant and hence small sized nanoparticles need to be located in close proximity of the eventual target sites within the cellular compartments. However, the use of photon sources above the k-edge requires a higher gold concentration in the tumor region but in these cases the size and localization of the nanoparticles is not a significant factor (15). The authors recently also generated a Monte Carlo-based model for prediction of gold nanoparticle radiosensitization, which takes into account the detailed energy deposition at the nanoscale. The claims by these authors though have been disputed by McMahon *et al*. stating there may be a potential disparity between the theoretical predictions and actual clinical outcomes (16).

The role of size in deciding the eventual sensitization outcome of nanoparticles depends of the balancing act between the effect of size on uptake as well as effect of size on photon production and range. Therefore, increasing the uptake of particles into cells, with larger diameter of the particles may have the most optimal outcome. The use of gold nanoparticles as radiosensitizing agents for low dose rate gamma radiation therapy such as with I-125 brachytherapy seeds has also been recently shown by Ngwa and colleagues (17). They found a 70-130% increase in the therapeutic efficacy in the presence of the nanoparticles. Most of the toxicological responses are due to the gold accumulation and liver toxicity. With the increased interests in the use of gold nanoparticles in cancer therapy, more sensitive detection methods have been developed allowing for more accurate dosimetry (18).

To study the effects of gold nanoparticles in combination with radiotherapy in specified cancers Joh *et al*. studied the effect of gold nanoparticles in sensitizing glioblastoma cells

and tumors to radiation therapy (19). They found that the gold nanoparticles not only enhanced the radiation effects *in vitro* but also showed significantly higher brain endothelial cell death. The treatment increased the survival rate in mice with orthotopic glioblastoma multiforme tumors. Separate studies by Bobyk and group on mice models of glioma showed a similar increase in efficacy and improved survival rate with gold nanoparticles on 1.9 nm size in combination with low energy radiation therapy (20).

To determine whether gold nanoparticles have higher activity, Xiao *et al*. coated them with thiolated undecane [S-C(11)H(23)], or with dithiolated diethylenetriaminepentaacetic (DTDTPA) or gadolinium (Gd) DTDTPA chelating agents. The studies using these coated nanoparticles showed attenuated effects as compared to the naked nanoparticles (21). These studies suggested that coatings may considerably diminish the short-range low-energy electrons emitted from gold, leading to a considerable decrease of radiosensitization. However, independent studies conducted by multiple groups using PEG coated gold nanoparticles showed increased therapeutic efficacy of the formulation for radiosensitization (22-24). Various sized nanoparticles have been studied and in each case a concentration dependent increase in efficiency of killing the cancer cells was observed. This increased efficacy was attributed to the EPR benefits of the PEG coating rather than its effects on energy redistribution. Studies in fields other than radiotherapy suggest there may be potential interference of PEG with the photon production by the gold particles. In addition, studies carried out to determine the toxicological effects of PEG coated gold nanoparticles in healthy tissue suggest that there is no enhanced toxicity associated with these coated nanoparticles (25) though these effects may be size dependent (26,27) or concentration dependent (10) or vary based on the administration route (28).

Combination of the gold nanoparticles with other radiosensitizers either by co-administration or by conjugation have also been utilized extensively so as to increase tumor cytotoxicity, while simultaneously minimizing effects on healthy surrounding tissue. Jeong and colleagues used gold nanoparticles as a carrier for delivery of ss-lapachone a novel anticancer agent displaying potent cytotoxicity against cancer cells as well excellent radiosensitizer (29). The combination was shown to have significant enhancements in activity. Further introduction of anti-EGFR antibody as a targeting moiety for cancer further enhanced the effects (29). DNA condensation by avidin has radioprotective effects in cancer (30). Moreover, the DNA:avidin interaction is reversible with biotin. Based on this theory the authors have hypothesized that by using combination of biotin and gold nanoparticles can synergistically make the target DNA more susceptible to radiation induced damage (30). Human Epidermal Growth Factor Receptor-2 (HER-2)-targeted gold nanoparticles have been synthesized by conjugating trastuzumab (Herceptin) to 30 nm gold nanoparticles. Herceptin acts as both a targeting moiety as well as a mono-therapeutic agent. These conjugated nanoparticles were able to increase the cytotoxic effects of radiation by 3.3-fold as compared to radiation alone whereas non-targeted nanoparticles showed only 1.7-fold increase in efficiency (31). Gold nanoparticles have also been studied in combination with other chemotherapeutic agents for potential synergy in activity. A multifold increase in the single and double stranded breaks was observed in DNA of the cells in presence of gold nanoparticles and radiation when they were pretreated with cisplatin (32). Cisplatin binding to guanine was shown to result in better bond dissociation by triggering the formation of transient anions. They further went on to study the various stoichiometric combinations of gold nanoparticles and cisplatin on their eventual radiosensitization (33). Binding of a single cisplatin molecule to the nanoparticle resulted in a 3-fold increase in activity whereas combination of 2 cisplatin molecules with a gold nanoparticle resulted in up to 7.5 times more double stranded breaks.

Other metal based based radiosensitizers

Gadolinium was identified as another new class of radiation sensitizers that were also very practical because they could also be easily viewed *in vivo* through the use of magnetic resonance imaging. It is known to generate long-lived pi-radical cations upon exposure to hydrated electrons. Its effectiveness was studied *in vitro* in HT-29 cells and also in a murine mammary carcinoma model and was found to be effective in both the cases (34). The effectiveness of the material as such has been subject of debate (35). Gadolinium neutron-capture therapy (NCT) is a therapeutic strategy for cancer, which utilizes the "Gadolinium neutron capture reaction" induced by thermal neutron irradiation. This reaction results in emission of long range gamma rays, internal conversion electrons, X-rays and Auger electrons with large total kinetic energy. The effectiveness of this therapy for cancer was evaluated using chitosan

nanoparticles loaded with Gadolinium-157. Mice with subcutaneous melanoma were injected with this formulation intratumorally and then thermal neutron irradiation was performed. Mice treated with the nanoparticle showed much better therapeutic response as compared to those that were dosed with just the gadolinium solution (36). Recently a detailed study was undertaken using 5 nm size gadolinium based nanoparticle on head and neck squamous cell carcinoma cells. These particles consisted of a core of gadolinium oxide, a shell of polysiloxane and were functionalized by diethylenetriaminepentaacetic acid (DTPA). These formulations were found to possess efficient in-vitro radiosensitizing properties at energy of 660 keV (37,38).

Titanium dioxide has also been shown to be useful for killing cancer cells using photocatalytic chemistry (39). Its mechanism of action involves generating reactive oxygen species upon photoexcitation by UV radiation. Again, due to limited penetration depth of UV rays, the material is less effective for deep-rooted tissues. To make them more susceptible to X-ray based stimulation titanium nanoparticles were formed containing gadolinium and further optimized with other rare earth metals. The activation of these nanoparticles by X-rays resulted in the formation of ROS, which resulted in enhanced photosensitization effects *in vivo* (40). Since elongated organic nanoparticles internalize into cells more effectively than their spherical counterparts of similar volume, titanium dioxide nanotubes were formulated and tested for their radiosensitization effects of glioblastoma (41). TiO_2 nanotubes were found to be effective radiosensitizers in SNB-19 and U87MG cells by enhancing the DNA damage and retarding the DNA repair (42). Various other techniques have also been utilized to enhance the radiosensitizing effects of TiO_2 nanoparticles such as special dye coating (43) or entrapment of other DNA intercalating chemotherapeutic agents such as doxorubicin (44). Pre-photoactivated TiO_2 nanoparticles have also been shown to possess enhance cytotoxic effects in HepG2 cells by induction of double stranded breaks (45).

Silver nanoparticles also have radiosensitizing properties, similar to that seen with gold nanoparticles (46). Silver nanoparticles utilize similar mechanisms of action for radiosensitization effects like other high Z-number atoms. They are more cost effective than gold nanoparticles but relatively less biocompatible (47). Silver nanoparticles have been utilized alone (48) or in combination of other metal oxides such as Fe_3O_4 for radiation therapy in cancer. Silver nanoparticles of nonconventional shape have also been created and studied for their effectiveness in cancer. Chitosan-coated triangular silver nanoparticles have been formulated and have been shown to possess better radiosensitizing activity when compared to conventional PEG coated gold nanoparticles on human non-small lung cancer cells (49). Silver nanoparticles with multiple different coatings have also been shown to possess additive anticancer properties when combined with IR radiations in Glioma cell lines (50).

Nanoparticles have been made using other rare earth metals and high-Z elements such as using hafnium oxide (HfO_2). HfO_2 has been shown to possess photo-luminescent properties (51,52). They cause thermal induced stress damage to cellular components. Based on these properties, HfO_2 nanoparticles have also been tried and tested for their effects on radiosensitization in HCT116 cells *in vitro* and in *in vivo* xenograft mice models. The studies showed a good biocompatibility, biodistribution as well as significant radiosensitization using these nanoparticles (53).

Quantum dots in radiosensitization

Quantum dots discovered in the early 1980s are nanocrystals made of semiconductor materials that display quantum mechanical properties due to their small size. Their semiconductor properties are less than those displayed by bulk semiconductors. Quantum dots made from CaF, LaF, ZnS or ZnO [164] have been suggested for use as radiosensitizers (54,55). Development of photosensitizing quantum dots has been a very active area of interest (56). The mechanism of action for these is based on the principle of generation of radicals upon absorption of visible light by the quantum dots. Since these light waves have much less toxicity as compared X-rays or gamma rays, the overall adverse effects of the therapy are greatly reduced. The major disadvantage of this approach is that light waves within the visible spectrum have very little penetration depth and hence the therapies designed utilizing these mechanisms will be suitable only for superficial cancers (57,58).

Superparamagnetic iron oxide nanoparticles as radiosensitizers

Superparamagnetic iron oxide nanoparticles are mainly made up of either magnetite (Fe_3O_4) or magnemite (γ Fe_2O_3). These are especially useful for their superparamagnetic properties, which allow them to be directed and localized to a particular organ by using external

magnetic force (59). These are also known to be highly biocompatible with negligible toxicity to healthy tissues allowing for usage in therapy (60). These nanoparticles can produce cytotoxic effects due to the production of ROS such as hydrogen peroxide, hydroxyl radical, hydroperoxyl radical and superoxide anion resulting in DNA and other cell organelle damage. The superparamagnetic iron oxide has been shown to enhance the radiation induced DNA damage by catalyzing the ROS production by these ionizing radiation resulting much stronger oxidative stress (61). This process was tested on MCF-7 cells by enhancing the impact of X-rays on the ROS generation for about 240% (62). Further these nanoparticles have also been used as synergistic carriers for other chemotherapeutic agents such as cisplatin (63,64) and genetic material. Superparamagnetic chitosan iron oxide nanoparticles carrying *human Adenovirus type 5 early region 1A* (E1A) gene were used to enhance the radiosensitivity of cervical cancer. The gene is known to reduce the expression of HER-2 and increase the expression in p53 both of which are known to play a role in regulating radioresistance in cancer (65). The combinations of genetic therapy with increased oxidative stress by iron oxide nanoparticles further enhance the radiosensitivity of human cervical cancer in xenograft mice (66). The iron superoxides have also been used in composition with other metal-based radiosensitizers such as silver. A multifunctional nanocomposite was generated using Fe_3O_4/Ag and conjugated with to an epidermal growth factor receptor-specific antibody (C225) (67). This composite can act as a diagnostic tool through MRI as well as a radiosensitizer. It was found to sensitize nasopharyngeal carcinoma cell lines to radiation therapy in a dose dependent manner (67).

Non-metal based radiosensitizers

Silica has been used as a carrier or coating material in nanoparticles containing heavy metals for radiosensitization such as gold (68,69), FeO_4 (70) or multicomponent cores (71-73). Moreover, nanoparticles made of silica alone have also been tested for their potential role in radiosensitization. In a recent study by Klein and colleagues, the ultrasmall uncapped and aminosilanized oxidized silicon nanoparticles were tested for their radiosensitization effects in breast cancer (MCF-7) and mouse fibroblast cells (3T3) exposed to X-rays of 3 Gy (74). Though the simple nanoparticles did not display any significant increase in ROS production upon exposure to the X-rays, the aminosilanized oxidized silicon nanoparticles exhibited significantly higher ROS production. These were shown to reach the mitochondria and cause oxidative stress damage within the organelle. Though the oxidized nanoparticles displayed increased ROS activity in both the cancer cells and the normal cells, the effects were significantly higher in the cancer cells. This indicates the relative safety of the therapeutic.

C_{60} is a fullerene, identified in the early 1990s, with unique globular structure consisting of 32 different member rings and containing a total of 60 carbon atoms. Fullerene C_{60} possesses potent anti-cancer activities and induces certain markers of autophagy in cancer cells (75). It has significant toxicity to normal tissues, which limits its use as therapeutic (76). Nanocrystals of underivatized fullerene C_{60} (Nano-C_{60}) have been used in concentrations that are non-toxic to normal cells to study their effects on radiosensitization. B16 and SMMU-7721 cell lines were tested with Nano-C_{60} and γ-radiation and were found to show enhanced membrane damage and induced apoptotic cell death (77). Nano-C_{60} has also been shown to possess chemosensitizing activity and hence can serve as a potential adjuvant therapeutic in cancer (75).

Polymeric nanoparticles have also been formulated using various chemotherapeutic agents either alone or in combination to serve as radiosensitizers. Paclitaxel is a potent chemotherapeutic agent that is also known to be a cell cycle specific radiosensitizer (78). This is because it arrests cell cycle progression at G2/M, a stage in which the cells are most susceptible to radiation induced damage. Similarly Etanidazole is a nitroimidazole hypoxic radiosensitizer. The studies were performed with PLGA nanoparticles of the drugs either alone or both together to test for their potential radiosensitizing effects (79). Both the individual drugs and their combination enhanced the susceptibility of the cells to the radiation. The prolonged release of the drug from the formulation allowed radiosensitization of hypoxic cells, which are generally more resistant to radiation induced injury. The combination was found to be more effective than the individual drugs. Genexol-PM, a clinically approved formulation of paclitaxel, was studied as a radiosensitizer using non-small cell lung cancer mouse xenograft models. Again, this formulation was found to be both a better radiosensitizer than the normal drug (with effective concentration half of that of the free drug) as well as a safer therapeutic with much reduced exposure of the drug to the health lung tissue (80).

Other chemotherapeutic agents such as doxorubicin have also been used as radiosensitizers. A nanomiceller composite formulation of doxorubicin displayed significantly enhanced

radiation sensitivity in multicellular spheroid of A549 lung cancer cell line (81). The formulation cells treated showed significantly higher radio toxicity as compared to cells treated with drug alone. Biodegradable lipid polymer nanoparticles have also been made using docetaxel as the entrapped drug and targeted to cancer tissue using folate. The studies showed that the targeted nanoparticles showed better radiosensitizing properties as compared to drug alone or unmodified nanoparticles. The studies also showed that the radiosensitizing effects using nanoparticulate formulations depend significantly on the time gap between the dosing of the formulation and the radiation (82).

Enhanced efficacy of radiation therapy by radioprotection of surrounding healthy tissue

Since the major targets of radiation therapy are water and DNA, and these are also present in healthy tissue making them susceptible to injury and significant damage if the energy waves are not properly directed to the targeted tissue. The efficacy of the radiation therapy can be increased and its adverse effects decreased if somehow the surrounding healthy tissue can either be protected from this damage or made less radiation sensitive. Molecules with potential radioprotective effects have been an area of interest for scientists since the World War II. Molecules such as amino acid cysteine have also been known to have radiation protective effects. Studies performed in rats showed that the animals dosed with cysteine were able to withstand normally lethal doses of X-rays (83) and showed much less damage to essential organs (84). Certain natural compounds such as curcumin have been shown to exert a dual mode of action after irradiation depending on its dose (85). It protects the cells against the damaging effects of radiation by reducing oxidative stress and inhibiting transcription of genes related to oxidative stress and inflammatory responses at lower doses in healthy cells. Its radiosensitizing effects in cancer cells maybe due to the upregulation of genes responsible for cell death. Antioxidants have also been shown extensively to be radioprotective especially from the reactive oxygen species induced damage (86).

Amifostine is an adjuvant used in cancer chemotherapy to reduce the incidence of neutropenia-related fever and infection induced by DNA-binding chemotherapeutic agents. It has been studied since late 80s for its potential use as a protectant against radiation induced DNA damage (87,88). Orally administered Amifostine did not show any significant radioprotective activity (89). To remedy this, polymeric nanoparticles of Amifostine were prepared that have revealed to have significant radiation desensitizing effects when administered orally (89). Nanostructural combination of Amifostine and fullerenol C_{60} has also been shown to possess radioprotective effects in both mammalian cells as well as rats undergoing radiation exposure (90,91). Fullerenol C_{60} alone also has been shown to diminish the radiosensitivity in single cellular eukaryotes as well as in zebra fish models (92). Amifostine has also been found to restore transcriptional activity of p53 enhancing the apoptotic responses to radiation (93).

Neuroprotective agent citicoline when delivered in the form of transferrin coupled liposomes has been shown to possess protective effects in human ovarian adenocarcinoma cells exposed to radiation but not as much in endothelial cells. Thus though the drug formulation has radiprotective effects, its usefulness in increasing the efficacy of radiation therapy is questionable (94). Cerium oxide nanoparticles act as free radical scavengers by changing the charge state on their surface. Thus they help in protecting the cells from free radical damage caused by radiation. They have been shown to increase the longevity of cells by reducing hydrogen peroxide and ultraviolet radiation induced injury (95). Nitroxide Tempol has also been shown to impart radioprotection of the salivary glands in C3H mice (96).

Enhanced efficacy of radiation therapy by reversal of radiation resistance

There are multiple biological pathways that get activated in cancer that make them either inherently resistant to radiation therapy or acquire resistance upon exposure to radiation. These pathways are especially active in cancer stem cells which are normally quiescent cells within the tumor responsible for maintaining and regenerating of a tumor after therapeutic intervention (97,98). Various drugs and treatment strategies are being designed so as to target these specific pathways making the cancer cells more susceptible to radiation therapy. Survivin is one such target protein which is overexpressed in most human tumors, but its levels are barely detectable in normal tissues (99). It is a regulator of cell division, apoptosis, cellular stress response, and also in the regulation of cell migration and metastasis. Increased survivin expression has been directly linked to acquired resistance to chemotherapeutic agents as well as radiation therapy (100). Though novel small molecular therapies are being worked upon (101,102), most of the therapies currently designed for attacking surviving involve

macromolecular approaches such as the use of siRNA or peptides which suffer from multiple drug delivery issues (103,104). To overcome these delivery issues human serum albumin-based nanoparticulate carrier system for plasmid-mediated RNA interference (RNAi) have been designed and tested for their efficacy in reversing surviving mediated radioresistance. Gaca and colleagues tested 220 nm sized nanoformulations for their effects of inhibition of surviving expression and its overall effects on radiosensitization. The results were found to be promising with up to 50% decrease in surviving expression as well as a significant increase in radiation susceptibility of SW480 colorectal cancer cells (105). Survivin siRNA cross-linked iron oxide nanoparticles (CLIO)-Cy5.5 have also been designed which can be better targeted using magnetic fields, but their efficacy in reversing radiation resistance has not yet been tested. Dual targeting of survivin and X-linked IAP (XIAP) by using siRNA was found to be even more effective in reversing the radiation resistance of the colorectal cancer cells. Hence the use of nanotechnology and siRNA in targeting surviving can be a productive approach in the future.

Another major target for reversal of radiation resistance is the epidermal growth factor receptor (EGFR). It is known to be a protooncogene that regulates multiple cellular processes, such as proliferation, differentiation, survival, blood vessel formation, and DNA repair (106,107). EGFR has been shown to be over expressed in multiple cancer types such as squamous cell carcinoma of the head and neck (108). Anti EGFR treatments have been shown to increase therapeutic activity of radiation therapy. Along with the antitumor activity of anti EGFR treatment the combination of radiation further results in strong synergy (109). To test this synergy PLGA nanoparticle encapsulated antisense EGFR oligonucleotides were combined with radiotherapy and the relative radiosensitivity of the SCCVII squamous cells was tested. The results showed that antisense EGFR nanoparticles enhanced radiosensitivity by inhibition of EGFR-mediated mechanisms of radioresistance (110). This is very useful as both the therapies complement each other and cell death can be achieved in cells that are resistant to either EGFR therapy or to radiation.

As mentioned earlier, curcumin has been shown to possess both radiosensitizing as well as radioprotective effects based on the cell types and concentrations. Curcumin is also known to act on multiple essential pathways in cancer responsible for radiation resistance. Inhibition of PI3K/AKT-NF-κB pathway with curcumin has been shown to enhance the radiation-induced apoptosis in human Burkitt's lymphoma (111). It has also been known to interact with Sonic Hedgehog signaling pathway to elicit its radiosensitizing effects (112). Hence a targeted PLGA nanoparticle formulation of curcumin was developed and tested for its effects on chemotherapeutic and radioresistant effects on cisplatin resistant ovarian cancer cell lines. Other extracts such as raspberry extract and neem leaf extract have also been shown to have increased radiosensitization effects (77). Hence, there is a lot of scope in developing formulations with ingredients from natural products for potential radiosensitization activity.

Acknowledgements

Disclosure: The authors declare no conflict of interest.

References

1. Hogle WP. The state of the art in radiation therapy. Semin Oncol Nurs 2006;22:212-20.
2. Mallick I, Waldron JN. Radiation therapy for head and neck cancers. Semin Oncol Nurs 2009;25:193-202.
3. Halliwell B, Aruoma OI. DNA damage by oxygen-derived species. Its mechanism and measurement in mammalian systems. FEBS Lett 1991;281:9-19.
4. Herold DM, Das IJ, Stobbe CC, et al. Gold microspheres: a selective technique for producing biologically effective dose enhancement. Int J Radiat Biol 2000;76:1357-64.
5. Park YS, Liz-Marzán LM, Kasuya A, et al. X-ray absorption of gold nanoparticles with thin silica shell. J Nanosci Nanotechnol 2006;6:3503-6.
6. Carter JD, Cheng NN, Qu Y, et al. Nanoscale energy deposition by X-ray absorbing nanostructures. J Phys Chem B 2007;111:11622-5.
7. Praetorius NP, Mandal TK. Engineered nanoparticles in cancer therapy. Recent Pat Drug Deliv Formul 2007;1:37-51.
8. Adams FH, Norman A, Mello RS, et al. Effect of radiation and contrast media on chromosomes. Preliminary report. Radiology 1977;124:823-6.
9. Matsudaira H, Ueno AM, Furuno I. Iodine contrast medium sensitizes cultured mammalian cells to X rays but not to gamma rays. Radiat Res 1980;84:144-8.
10. Jeremic B, Aguerri AR, Filipovic N. Radiosensitization by gold nanoparticles. Clin Transl Oncol 2013;15:593-601.
11. Larson TA, Joshi PP, Sokolov K. Preventing protein adsorption and macrophage uptake of gold nanoparticles via a hydrophobic shield. ACS Nano 2012;6:9182-90.

12. Wang M, Thanou M. Targeting nanoparticles to cancer. Pharmacol Res 2010;62:90-9.
13. Zheng Y, Hunting DJ, Ayotte P, et al. Radiosensitization of DNA by gold nanoparticles irradiated with high-energy electrons. Radiat Res 2008;169:19-27.
14. Brun E, Sanche L, Sicard-Roselli C. Parameters governing gold nanoparticle X-ray radiosensitization of DNA in solution. Colloids Surf B Biointerfaces 2009;72:128-34.
15. Lechtman E, Chattopadhyay N, Cai Z, et al. Implications on clinical scenario of gold nanoparticle radiosensitization in regards to photon energy, nanoparticle size, concentration and location. Phys Med Biol 2011;56:4631-47.
16. McMahon SJ, Prise KM, Currell FJ. Comment on 'implications on clinical scenario of gold nanoparticle radiosensitization in regard to photon energy, nanoparticle size, concentration and location'. Phys Med Biol 2012;57:287-90; discussion 291-5.
17. Ngwa W, Korideck H, Kassis AI, et al. In vitro radiosensitization by gold nanoparticles during continuous low-dose-rate gamma irradiation with I-125 brachytherapy seeds. Nanomedicine 2013;9:25-7.
18. Alqathami M, Blencowe A, Yeo UJ, et al. Novel multicompartment 3-dimensional radiochromic radiation dosimeters for nanoparticle-enhanced radiation therapy dosimetry. Int J Radiat Oncol Biol Phys 2012;84:e549-55.
19. Joh DY, Sun L, Stangl M, et al. Selective targeting of brain tumors with gold nanoparticle-induced radiosensitization. PLoS One 2013;8:e62425.
20. Bobyk L, Edouard M, Deman P, et al. Photoactivation of gold nanoparticles for glioma treatment. Nanomedicine 2013. [Epub ahead of print].
21. Xiao F, Zheng Y, Cloutier P, et al. On the role of low-energy electrons in the radiosensitization of DNA by gold nanoparticles. Nanotechnology 2011;22:465101.
22. Liu CJ, Wang CH, Chien CC, et al. Enhanced x-ray irradiation-induced cancer cell damage by gold nanoparticles treated by a new synthesis method of polyethylene glycol modification. Nanotechnology 2008 Jul;19:295104.
23. Liu CJ, Wang CH, Chen ST, et al. Enhancement of cell radiation sensitivity by pegylated gold nanoparticles. Phys Med Biol 2010;55:931-45.
24. Zhang XD, Wu D, Shen X, et al. Size-dependent radiosensitization of PEG-coated gold nanoparticles for cancer radiation therapy. Biomaterials 2012;33:6408-19.
25. Cho WS, Kim S, Han BS, et al. Comparison of gene expression profiles in mice liver following intravenous injection of 4 and 100 nm-sized PEG-coated gold nanoparticles. Toxicol Lett 2009;191:96-102.
26. Zhang XD, Wu D, Shen X, et al. Size-dependent in vivo toxicity of PEG-coated gold nanoparticles. Int J Nanomedicine 2011;6:2071-81.
27. Coulter JA, Jain S, Butterworth KT, et al. Cell type-dependent uptake, localization, and cytotoxicity of 1.9 nm gold nanoparticles. Int J Nanomedicine 2012;7:2673-85.
28. Zhang XD, Wu HY, Wu D, et al. Toxicologic effects of gold nanoparticles in vivo by different administration routes. Int J Nanomedicine 2010;5:771-81.
29. Jeong SY, Park SJ, Yoon SM, et al. Systemic delivery and preclinical evaluation of Au nanoparticle containing beta-lapachone for radiosensitization. J Control Release 2009;139:239-45.
30. Riva P, Franceschi G, Riva N, et al. Role of nuclear medicine in the treatment of malignant gliomas: the locoregional radioimmunotherapy approach. Eur J Nucl Med 2000;27:601-9.
31. Chattopadhyay N, Cai Z, Kwon YL, et al. Molecularly targeted gold nanoparticles enhance the radiation response of breast cancer cells and tumor xenografts to X-radiation. Breast Cancer Res Treat 2013;137:81-91.
32. Zheng Y, Hunting DJ, Ayotte P, et al. Role of secondary low-energy electrons in the concomitant chemoradiation therapy of cancer. Phys Rev Lett 2008;100:198101.
33. Zheng Y, Sanche L. Gold nanoparticles enhance DNA damage induced by anti-cancer drugs and radiation. Radiat Res 2009;172:114-9.
34. Young SW, Qing F, Harriman A, et al. Gadolinium(III) texaphyrin: a tumor selective radiation sensitizer that is detectable by MRI. Proc Natl Acad Sci U S A 1996;93:6610-5.
35. Bernhard EJ, Mitchell JB, Deen D, et al. Re-evaluating gadolinium(III) texaphyrin as a radiosensitizing agent. Cancer Res 2000;60:86-91.
36. Tokumitsu H, Hiratsuka J, Sakurai Y, et al. Gadolinium neutron-capture therapy using novel gadopentetic acid-chitosan complex nanoparticles: in vivo growth suppression of experimental melanoma solid tumor. Cancer Lett 2000;150:177-82.
37. Mowat P, Mignot A, Rima W, et al. In vitro radiosensitizing effects of ultrasmall gadolinium based particles on tumour cells. J Nanosci Nanotechnol 2011;11:7833-9.
38. Rima W, Sancey L, Aloy MT, et al. Internalization pathways into cancer cells of gadolinium-based radiosensitizing nanoparticles. Biomaterials 2013;34:181-95.
39. Sotter E, Vilanova X, Llobet E, et al. Niobium-doped titania nanopowders for gas sensor applications. J

Optoelectron Adv Mater 2005;7:1395-8.
40. Townley HE, Kim J, Dobson PJ. In vivo demonstration of enhanced radiotherapy using rare earth doped titania nanoparticles. Nanoscale 2012;4:5043-50.
41. Gratton SE, Ropp PA, Pohlhaus PD, et al. The effect of particle design on cellular internalization pathways. Proc Natl Acad Sci U S A 2008;105:11613-8.
42. Mirjolet C, Papa AL, Créhange G, et al. The radiosensitization effect of titanate nanotubes as a new tool in radiation therapy for glioblastoma: A proof-of-concept. Radiother Oncol 2013;108:136-42.
43. Blatnik J, Luebke L, Simonet S, et al. Dye surface coating enables visible light activation of TiO2 nanoparticles leading to degradation of neighboring biological structures. Microsc Microanal 2012;18:134-42.
44. Hong C, An S, Son M, et al. In-vitro cell tests using doxorubicin-loaded polymeric TiO2 nanotubes used for cancer photothermotherapy. Anticancer Drugs 2012;23:553-60.
45. Petković J, Küzma T, Rade K, et al. Pre-irradiation of anatase TiO2 particles with UV enhances their cytotoxic and genotoxic potential in human hepatoma HepG2 cells. J Hazard Mater 2011;196:145-52.
46. Ma J, Xu R, Sun J, et al. Nanoparticle surface and nanocore properties determine the effect on radiosensitivity of cancer cells upon ionizing radiation treatment. J Nanosci Nanotechnol 2013;13:1472-5.
47. Coulter JA, Hyland WB, Nicol J, et al. Radiosensitising nanoparticles as novel cancer therapeutics - pipe dream or realistic prospect? Clin Oncol (R Coll Radiol) 2013;25:593-603.
48. Zheng Q, Yang H, Wei J, et al. The role and mechanisms of nanoparticles to enhance radiosensitivity in hepatocellular cell. Biomed Pharmacother 2013. [Epub ahead of print].
49. Boca SC, Potara M, Gabudean AM, et al. Chitosan-coated triangular silver nanoparticles as a novel class of biocompatible, highly effective photothermal transducers for in vitro cancer cell therapy. Cancer Lett 2011;311:131-40.
50. Xu R, Ma J, Sun X, et al. Ag nanoparticles sensitize IR-induced killing of cancer cells. Cell Res 2009;19:1031-4.
51. Brezesinski T, Smarsly B, Iimura K, et al. Self-assembly and crystallization behavior of mesoporous, crystalline HfO2 thin films: a model system for the generation of mesostructured transition-metal oxides. Small 2005;1:889-98.
52. Mendoza JG, Frutis MA, Flores GA, et al. Synthesis and characterization of hafnium oxide films for thermo and photoluminescence applications. Appl Radiat Isot 2010;68:696-9.
53. Maggiorella L, Barouch G, Devaux C, et al. Nanoscale radiotherapy with hafnium oxide nanoparticles. Future Oncol 2012;8:1167-81.
54. Juzenas P, Chen W, Sun YP, et al. Quantum dots and nanoparticles for photodynamic and radiation therapies of cancer. Adv Drug Deliv Rev 2008;60:1600-14.
55. Wang YH, Chen Z, Zhou XQ. Synthesis and photoluminescence of ZnS quantum dots. J Nanosci Nanotechnol 2008;8:1312-5.
56. Bakalova R, Ohba H, Zhelev Z, et al. Quantum dots as photosensitizers? Nat Biotechnol 2004;22:1360-1.
57. Shao L, Gao Y, Yan F. Semiconductor quantum dots for biomedicial applications. Sensors (Basel) 2011;11:11736-51.
58. Chatterjee DK, Fong LS, Zhang Y. Nanoparticles in photodynamic therapy: an emerging paradigm. Adv Drug Deliv Rev 2008;60:1627-37.
59. Wadajkar AS, Menon JU, Kadapure T, et al. Design and Application of Magnetic-based Theranostic Nanoparticle Systems. Recent Pat Biomed Eng 2013;6:47-57.
60. Mikhaylov G, Vasiljeva O. Promising approaches in using magnetic nanoparticles in oncology. Biol Chem 2011;392:955-60.
61. Huang G, Chen H, Dong Y, et al. Superparamagnetic iron oxide nanoparticles: amplifying ROS stress to improve anticancer drug efficacy. Theranostics 2013;3:116-26.
62. Klein S, Sommer A, Distel LV, et al. Superparamagnetic iron oxide nanoparticles as radiosensitizer via enhanced reactive oxygen species formation. Biochem Biophys Res Commun 2012;425:393-7.
63. Huang C, Neoh KG, Xu L, et al. Polymeric nanoparticles with encapsulated superparamagnetic iron oxide and conjugated cisplatin for potential bladder cancer therapy. Biomacromolecules 2012;13:2513-20.
64. Kettering M, Zorn H, Bremer-Streck S, et al. Characterization of iron oxide nanoparticles adsorbed with cisplatin for biomedical applications. Phys Med Biol 2009;54:5109-21.
65. Raybaud-Diogène H, Fortin A, Morency R, et al. Markers of radioresistance in squamous cell carcinomas of the head and neck: a clinicopathologic and immunohistochemical study. J Clin Oncol 1997;15:1030-8.
66. Shen LF, Chen J, Zeng S, et al. The superparamagnetic nanoparticles carrying the E1A gene enhance the radiosensitivity of human cervical carcinoma in nude mice. Mol Cancer Ther 2010;9:2123-30.

67. Zhao D, Sun X, Tong J, et al. A novel multifunctional nanocomposite C225-conjugated Fe3O4/Ag enhances the sensitivity of nasopharyngeal carcinoma cells to radiotherapy. Acta Biochim Biophys Sin (Shanghai) 2012;44:678-84.
68. Mallick S, Sun IC, Kim K, et al. Silica coated gold nanorods for imaging and photo-thermal therapy of cancer cells. J Nanosci Nanotechnol 2013;13:3223-9.
69. Elbialy N, Mohamed N, Monem AS. Preparation and characterization of SiO2-Au nanoshells: in vivo study of its photo-heat conversion. J Biomed Nanotechnol 2013;9:158-66.
70. Li J, Jiang H, Yu Z, et al. Multifunctional uniform core-shell Fe3O4@mSiO2 mesoporous nanoparticles for bimodal imaging and photothermal therapy. Chem Asian J 2013;8:385-91.
71. Wang Y, Chen L, Liu P. Biocompatible triplex Ag@SiO2@mTiO2 core-shell nanoparticles for simultaneous fluorescence-SERS bimodal imaging and drug delivery. Chemistry 2012;18:5935-43.
72. Zhao Z, Han Y, Lin C, et al. Multifunctional core-shell upconverting nanoparticles for imaging and photodynamic therapy of liver cancer cells. Chem Asian J 2012;7:830-7.
73. Zhang Z, Wang L, Wang J, et al. Mesoporous silica-coated gold nanorods as a light-mediated multifunctional theranostic platform for cancer treatment. Adv Mater 2012;24:1418-23.
74. Klein S, Dell'Arciprete ML, Wegmann M, et al. Oxidized silicon nanoparticles for radiosensitization of cancer and tissue cells. Biochem Biophys Res Commun 2013;434:217-22.
75. Zhang Q, Yang W, Man N, et al. Autophagy-mediated chemosensitization in cancer cells by fullerene C60 nanocrystal. Autophagy 2009;5:1107-17.
76. Sayes CM, Gobin AM, Ausman KD, et al. Nano-C60 cytotoxicity is due to lipid peroxidation. Biomaterials 2005;26:7587-95.
77. Veeraraghavan J, Natarajan M, Lagisetty P, et al. Impact of curcumin, raspberry extract, and neem leaf extract on rel protein-regulated cell death/radiosensitization in pancreatic cancer cells. Pancreas 2011;40:1107-19.
78. Tishler RB, Geard CR, Hall EJ, et al. Taxol sensitizes human astrocytoma cells to radiation. Cancer Res 1992;52:3495-7.
79. Jin C, Bai L, Wu H, et al. Radiosensitization of paclitaxel, etanidazole and paclitaxel+etanidazole nanoparticles on hypoxic human tumor cells in vitro. Biomaterials 2007;28:3724-30.
80. Werner ME, Cummings ND, Sethi M, et al. Preclinical evaluation of Genexol-PM, a nanoparticle formulation of paclitaxel, as a novel radiosensitizer for the treatment of non-small cell lung cancer. Int J Radiat Oncol Biol Phys 2013;86:463-8.
81. Xu WH, Han M, Dong Q, et al. Doxorubicin-mediated radiosensitivity in multicellular spheroids from a lung cancer cell line is enhanced by composite micelle encapsulation. Int J Nanomedicine 2012;7:2661-71.
82. Werner ME, Copp JA, Karve S, et al. Folate-targeted polymeric nanoparticle formulation of docetaxel is an effective molecularly targeted radiosensitizer with efficacy dependent on the timing of radiotherapy. ACS Nano 2011;5:8990-8.
83. Patt HM, Tyree EB, Straube RL, et al. Cysteine Protection against X Irradiation. Science 1949;110:213-4.
84. Bari WA. Cysteine protection against the morphologic effects of x-irradiation on mouse spleen. Pathol Microbiol (Basel) 1968;32:205-18.
85. Jagetia GC. Radioprotection and radiosensitization by curcumin. Adv Exp Med Biol 2007;595:301-20.
86. Kumar KS, Srinivasan V, Toles R, et al. Nutritional approaches to radioprotection: vitamin E. Mil Med 2002;167:57-9.
87. Murray D, Altschuler EM, Hunter N, et al. Protection by WR-3689 against gamma-ray-induced intestinal damage: comparative effect on clonogenic cell survival, mouse survival, and DNA damage. Radiat Res 1989;120:339-51.
88. Capizzi RL, Oster W. Chemoprotective and radioprotective effects of amifostine: an update of clinical trials. Int J Hematol 2000;72:425-35.
89. Pamujula S, Kishore V, Rider B, et al. Radioprotection in mice following oral delivery of amifostine nanoparticles. Int J Radiat Biol 2005;81:251-7.
90. Theriot CA, Casey RC, Moore VC, et al. Dendro[C(60)] fullerene DF-1 provides radioprotection to radiosensitive mammalian cells. Radiat Environ Biophys 2010;49:437-45.
91. Trajković S, Dobrić S, Jaćević V, et al. Tissue-protective effects of fullerenol C60(OH)24 and amifostine in irradiated rats. Colloids Surf B Biointerfaces 2007;58:39-43.
92. Hwang M, Yong C, Moretti L, et al. Zebrafish as a model system to screen radiation modifiers. Curr Genomics 2007;8:360-9.
93. Maurici D, Monti P, Campomenosi P, et al. Amifostine (WR2721) restores transcriptional activity of specific p53 mutant proteins in a yeast functional assay. Oncogene 2001;20:3533-40.
94. Suresh Reddy J, Venkateswarlu V, et al. Radioprotective

effect of transferrin targeted citicoline liposomes. J Drug Target 2006;14:13-9.
95. Tarnuzzer RW, Colon J, Patil S, et al. Vacancy engineered ceria nanostructures for protection from radiation-induced cellular damage. Nano Lett 2005;5:2573-7.
96. Vitolo JM, Cotrim AP, Sowers AL, et al. The stable nitroxide tempol facilitates salivary gland protection during head and neck irradiation in a mouse model. Clin Cancer Res 2004;10:1807-12.
97. Bütof R, Dubrovska A, Baumann M. Clinical perspectives of cancer stem cell research in radiation oncology. Radiother Oncol 2013. [Epub ahead of print].
98. Peitzsch C, Kurth I, Kunz-Schughart L, et al. Discovery of the cancer stem cell related determinants of radioresistance. Radiother Oncol 2013. [Epub ahead of print].
99. Zaffaroni N, Pennati M, Daidone MG. Survivin as a target for new anticancer interventions. J Cell Mol Med 2005;9:360-72.
100. Grdina DJ, Murley JS, Miller RC, et al. A survivin-associated adaptive response in radiation therapy. Cancer Res 2013;73:4418-28.
101. Yamada T, Horinaka M, Shinnoh M, et al. A novel HDAC inhibitor OBP-801 and a PI3K inhibitor LY294002 synergistically induce apoptosis via the suppression of survivin and XIAP in renal cell carcinoma. Int J Oncol 2013;43:1080-6.
102. Ling X, Cao S, Cheng Q, et al. A novel small molecule FL118 that selectively inhibits survivin, Mcl-1, XIAP and cIAP2 in a p53-independent manner, shows superior antitumor activity. PLoS One 2012;7:e45571.
103. Pennati M, Millo E, Gandellini P, et al. RNA interference-mediated validation of survivin and Apollon/BRUCE as new therapeutic targets for cancer therapy. Curr Top Med Chem 2012;12:69-78.
104. Zhang M, Mukherjee N, Bermudez RS, et al. Adenovirus-mediated inhibition of survivin expression sensitizes human prostate cancer cells to paclitaxel in vitro and in vivo. Prostate 2005;64:293-302.
105. Gaca S, Reichert S, Rödel C, et al. Survivin-miRNA-loaded nanoparticles as auxiliary tools for radiation therapy: preparation, characterisation, drug release, cytotoxicity and therapeutic effect on colorectal cancer cells. J Microencapsul 2012;29:685-94.
106. Jakus J, Yeudall WA. Growth inhibitory concentrations of EGF induce p21 (WAF1/Cip1) and alter cell cycle control in squamous carcinoma cells. Oncogene 1996;12:2369-76.
107. Schmidt-Ullrich RK, Contessa JN, Lammering G, et al. ERBB receptor tyrosine kinases and cellular radiation responses. Oncogene 2003;22:5855-65.
108. Rubin Grandis J, Melhem MF, Gooding WE, et al. Levels of TGF-alpha and EGFR protein in head and neck squamous cell carcinoma and patient survival. J Natl Cancer Inst 1998;90:824-32.
109. Patel JD. Epidermal growth factor receptor pathway targeted therapy in patients with aerodigestive malignancies. Curr Opin Oncol 2006;18:609-14.
110. Ping Y, Jian Z, Yi Z, et al. Inhibition of the EGFR with nanoparticles encapsulating antisense oligonucleotides of the EGFR enhances radiosensitivity in SCCVII cells. Med Oncol 2010;27:715-21.
111. Qiao Q, Jiang Y, Li G. Inhibition of the PI3K/AKT-NF-κB pathway with curcumin enhanced radiation-induced apoptosis in human Burkitt's lymphoma. J Pharmacol Sci 2013;121:247-56.
112. Elamin MH, Shinwari Z, Hendrayani SF, et al. Curcumin inhibits the Sonic Hedgehog signaling pathway and triggers apoptosis in medulloblastoma cells. Mol Carcinog 2010;49:302-14.

Cite this article as: Kwatra D, Venugopal A, Anant S. Nanoparticles in radiation therapy: a summary of various approaches to enhance radiosensitization in cancer. Transl Cancer Res 2013;2(4):330-342. doi: 10.3978/j.issn.2218-676X.2013.08.06

Review Article

Role of p53 in regulating tissue response to radiation by mechanisms independent of apoptosis

Chang-Lung Lee[1], Jordan M. Blum[2], David G. Kirsch[1,2]

[1]Department of Radiation Oncology, [2]Pharmacology & Cancer Biology, Duke University Medical Center, Durham, North Carolina 27710, USA
Correspondence to: David G. Kirsch. Duke University Medical Center, Box 91006, Durham, NC 27708, USA. Email: david.kirsch@duke.edu.

Abstract: Radiation exposure leads to diverse outcomes in vivo across different tissues and even within the same cell lineage. The diversity of radiation response in vivo is at least partially attributable to the status of the tumor suppressor p53, a master regulator of cellular response to stress, and activation of its transcriptional targets. In certain cells, such as hematopoietic progenitors and transit amplifying cells in the gastrointestinal (GI) epithelium, activation of p53 by radiation triggers the intrinsic pathway of apoptosis. However, in many other cells, activation of p53 by radiation does not result in apoptosis, which underscores the importance of understanding the role of p53 in regulating radiation response through alternative mechanisms. In this review, we summarize recent studies using genetically engineered mice to dissect the role of p53 in (I) cells where its activation is dissociated from the intrinsic pathway of apoptosis, such as hematopoietic stem cells (HSCs) and vascular endothelial cells and (II) tissues where activation of the intrinsic pathway of apoptosis does not promote the acute radiation syndrome, such as the GI epithelium. We highlight findings showing that the apoptosis-independent response of p53 to radiation in vivo can contribute to death or survival in a cell-type dependent manner, which underscores the complexity by which p53 regulates the cellular and tissue response to radiation.

Keywords: Apoptosis; cell cycle arrest; normal tissue injury; p53, radiation

doi: 10.3978/j.issn.2218-676X.2013.09.01
Scan to your mobile device or view this article at: http://www.thetcr.org/article/view/1638/html

Introduction

The tumor suppressor p53 is a master regulator of cellular response to radiation (1-3). p53 is a multifunctional transcription factor containing two transcriptional activation domains that can independently enhance transcription of downstream target genes, and a DNA binding domain responsible for sequence-specific binding of p53 to its response elements (4). Upon radiation exposure, activation of the DNA damage response increases the level of p53 protein in cells primarily by promoting protein translation (5) and inhibiting protein degradation (6). Accumulation of p53 protein in the nucleus induces a variety of downstream signaling pathways that mediate cellular response to stress (7,8). Activation of p53-mediated signaling can cause cell cycle arrest and facilitate DNA repair, which promote cell survival, or induce the intrinsic pathway of apoptosis and cell senescence, which augment cell death. Therefore, p53 plays a crucial role in controlling cellular fate after irradiation.

Several factors influence the p53 response following irradiation, including the intensity of stress, the presence of co-factors that interact with p53, and DNA binding cooperativity of p53 (7,9). Additionally, it has been shown in mice that total-body irradiation induces p53 and its downstream signaling *in vivo* in a tissue-dependent manner (8,10,11). For example, activation of p53 results in dramatically increased pre-mitotic apoptosis in tissues that have a rapid turnover rate such as the hematopoietic system and the gastrointestinal (GI) epithelium. To the contrary, in tissues with a slower turnover rate, such as the myocardium, accumulation of p53 following radiation does not cause a

significant increase in pre-mitotic apoptosis, but instead induces genes that control cell-cycle checkpoints such as the cyclin-dependent kinase inhibitor p21. Moreover, recent studies in the hematopoietic system suggest that p53 activation results in a distinct response in stem cells versus progenitors (12,13). Thus, these findings reveal the diversity of p53 response following radiation *in vivo* and underscore the significance of dissecting the mechanisms by which p53 controls radiation response in a cell-type specific manner.

To dissect the role of p53 in response to radiation *in vivo*, several groups have performed mechanistic studies using mice that either lack p53 or its transcriptional targets, or using the Cre-loxP system (14) to spatially and/or temporally disrupt p53 in mice. In this review, we summarize recent advances in understanding the role of p53-mediated signaling in regulating radiation response through mechanisms that are independent of apoptosis in the hematopoietic system, the GI epithelium and vascular endothelial cells.

Role of p53 in controlling radiation response in hematopoietic stem and progenitor cells

Radiation causes acute and long-term toxicity in the hematopoietic compartment

The hematopoietic system is very sensitive to radiation. After irradiation, a rapid increase in pre-mitotic apoptosis ablates hematopoietic progenitor cells and more differentiated hematopoietic cells (15), leading to acute hematological radiation toxicity due to the short-term loss of functioning blood cells (16,17). The overall response of the hematopoietic compartment is mediated by apoptosis in the acute phase following radiation exposure, coupled with long-term defects in hematopoietic stem cells (HSCs) after the recovery phase (18). The reduction in fitness of irradiated HSCs, which is associated with cell senescence (18-20), has been demonstrated using competitive repopulation assays. HSCs from mice that are exposed to lethal or sub-lethal doses of total-body irradiation have a dramatic decrease in long-term engraftment in the bone marrow compared to unirradiated HSCs (19,21,22). Collectively, these results demonstrate that radiation exposure causes short-term and long-term damage to the hematopoietic compartment. While acute hematological radiation toxicity is primarily attributed to apoptosis, chronic hematological toxicity is at least partially caused by apoptosis-independent mechanisms.

Loss of p53 ameliorates acute hematological radiation toxicity by blocking apoptosis

Radiation induces the DNA damage response to active p53 in hematopoietic stem cells and progenitors (HSPCs) (12,13,23). However, the response of p53 to radiation varies between stem and progenitor cells. While p53 activation engages radiation-induced apoptosis in hematopoietic progenitors, activation of p53 in short-term HSCs does not induce the intrinsic pathway of apoptosis. Moreover, radiation does not induce detectable levels of phosphorylated p53 in long-term HSCs (13). It has been shown that p53 is necessary to promote radiation-induced apoptosis in hematopoietic cells because deletion of p53 in mice ($p53^{-/-}$ mice) dramatically abrogates radiation-induced apoptosis and ameliorates acute hematological radiation toxicity (24-26). The essential role of p53-mediated apoptosis in acute hematopoietic toxicity is further demonstrated using mice that lack PUMA (p53 upregulated modulator of apoptosis), a transcriptional target of p53 that activates the intrinsic pathway of apoptosis (27,28). Compared to $PUMA^{+/+}$ mice, both $PUMA^{+/-}$ and $PUMA^{-/-}$ mice are resistant to acute hematological radiation toxicity due to a dramatic decrease in apoptosis in hematopoietic progenitor cells (29,30).

Loss of p53 improves long-term engraftment potential of irradiated HSCs

It has been challenging to study long-term effects of radiation on the hematopoietic system in $p53^{-/-}$ mice due to the extremely high penetrance of spontaneous lymphomas (31,32). Recent studies investigated how p53 controls long-term fitness of HSPCs after total-body irradiation using bone marrow chimeric mice that harbor only a small portion of p53-deficient cells. Marusyk *et al*. generated bone marrow chimera containing approximately 15% GFP-tagged $p53^{-/-}$ cells. After 2.5 Gy total-body irradiation, the percentage of $p53^{-/-}$ peripheral blood cells in chimeric mice increased significantly compared to unirradiated controls, indicating that p53 disruption confers radioresistance and facilitates clonal expansion of HSPCs (33). These results indicate that deletion of p53 in HSPCs improves their clonogenic capacity after irradiation over HSPCs with wild-type p53 because radiation-induced apoptosis is blocked in progenitors and because stem/progenitor cells are protected from radiation-induced loss of fitness.

To address a similar question, Bondar *et al*. generated a

novel conditional allele in which a GFP-tagged oncogenic p53 mutant R172H (mp53) can be temporally induced in the whole animal by tamoxifen. Injection with a single dose of tamoxifen created bone marrow chimeric mice that contain a small portion (<5%) of mp53 cells in peripheral blood. After exposure to 2.5 Gy total-body irradiation, the percentage of mp53 blood cells increased dramatically and even persisted 200 days after irradiation, demonstrating the expansion of mp53 cells in the long-term HSC pool (34). Interestingly, induction of mp53 either two days before or seven days after irradiation, when the DNA damage response is diminished, significantly increased the percentage of mp53 cells in hematopoietic cells. These results indicate that in addition to the DNA damage response, stress stimuli that are secondary to radiation, such as increased reactive oxygen species (22,35,36), impair the fitness of HSPCs that have functional p53. In addition, deletion of cyclin-dependent kinase inhibitor 2A gene, which transcribes both $p16^{INK4a}$ and $p19^{ARF}$ in mice (37), partially improves the clonogenic capacity of p53-wild type HSPCs after irradiation, suggesting that senescence contributes to radiation-induced defects in HSPCs. Together, these findings indicate that a permanent change in p53 activity improves the fitness of HSPCs by blocking acute apoptosis, which is induced by the DNA damage response and by suppressing delayed senescence, which may be induced by an altered microenvironment after irradiation.

Deletion of p21 allows human fibroblasts to bypass senescence in response to DNA damage (38), suggesting that p21 may also play a role in regulating radiation-induced senescence *in vivo*. However, different groups have shown that loss of p21 exacerbates defects in long-term engraftment potential of irradiated HSCs (13,39). These data indicate that p21 is necessary to protect HSCs against radiation. Interestingly, Insinga and colleagues found that radiation upregulated p21 in short-term HSCs and long-term HSCs via p53-dependent and p53-independent mechanisms, respectively (13). In addition, p21 protein actually suppressed radiation-induced p53 activation in long-term HSCs because deletion of p21 in long-term HSCs increased phosphorylated of p53 protein and apoptosis after irradiation. These results indicate that p21 regulates the response to radiation in HSCs through mechanisms that either dependent or independent of p53. Further studies are warranted to understand the mechanisms by which radiation induces p21 in a p53-independent manner and how p21 suppresses p53 activation in long-term HSCs after irradiation.

Summary

A reduced level of p53 in the hematopoietic compartment promotes radiation resistance, making p53 a promising target for preventing the acute hematopoietic syndrome and/or residual bone marrow toxicity. However, the manner in which p21 cooperates with p53 to regulate radiation response in short-term and long-term HSCs remains to be better understood (*Figure 1A*). In addition, there is a concern about the long-term consequences of reducing p53 (such as thymic lymphoma) during radiation because of its function as a tumor suppressor (46). Therefore, further studies are warranted to evaluate the effect of temporarily blocking p53 during irradiation on radiation toxicity of the hematopoietic system and radiation-induced cancer.

Role of p53-mediated signaling in the radiation-induced GI syndrome

Loss of p53 sensitizes mice to the radiation-induced GI syndrome

Exposure of the GI tract to radiation causes acute GI toxicity or the GI syndrome (47). The GI syndrome is caused by destruction of the GI epithelium, which leads to infection and loss of fluid and electrolytes (48,49). The integrity of the small intestine is dependent on a constant state of renewal driven by the stem cells residing in the crypts. Radiation impairs the regeneration of intestinal epithelium predominantly by inducing cell death in crypt epithelial cells (50,51). Crypt epithelial cells are highly sensitive to radiation-induced pre-mitotic apoptosis, which occurs within a few hours after irradiation (50). It has been shown that p53-mediated signaling plays a pivotal role in promoting pre-mitotic apoptosis of crypt epithelial cells because crypt epithelial cells in $p53^{-/-}$ mice are dramatically resistant to radiation-induced apoptosis that occurs 4 to 6 hours after irradiation (41,42).

While crypt epithelial cells in $p53^{-/-}$ mice are resistant to radiation-induced apoptosis, $p53^{-/-}$ mice are surprisingly more sensitive to the radiation-induced GI syndrome (26). Detailed time course studies after radiation exposure show that $p53^{-/-}$ mice have a delayed onset of cell death in crypt epithelial cells that occurs approximately 24 hours after irradiation (52). Thus, it is possible that loss of p53 sensitizes crypt epithelial cells to mitotic death, which results from aberrant segregation of the genomic DNA during mitosis (53,54). Mitotic catastrophe is frequently observed in cells that have a defect in cell

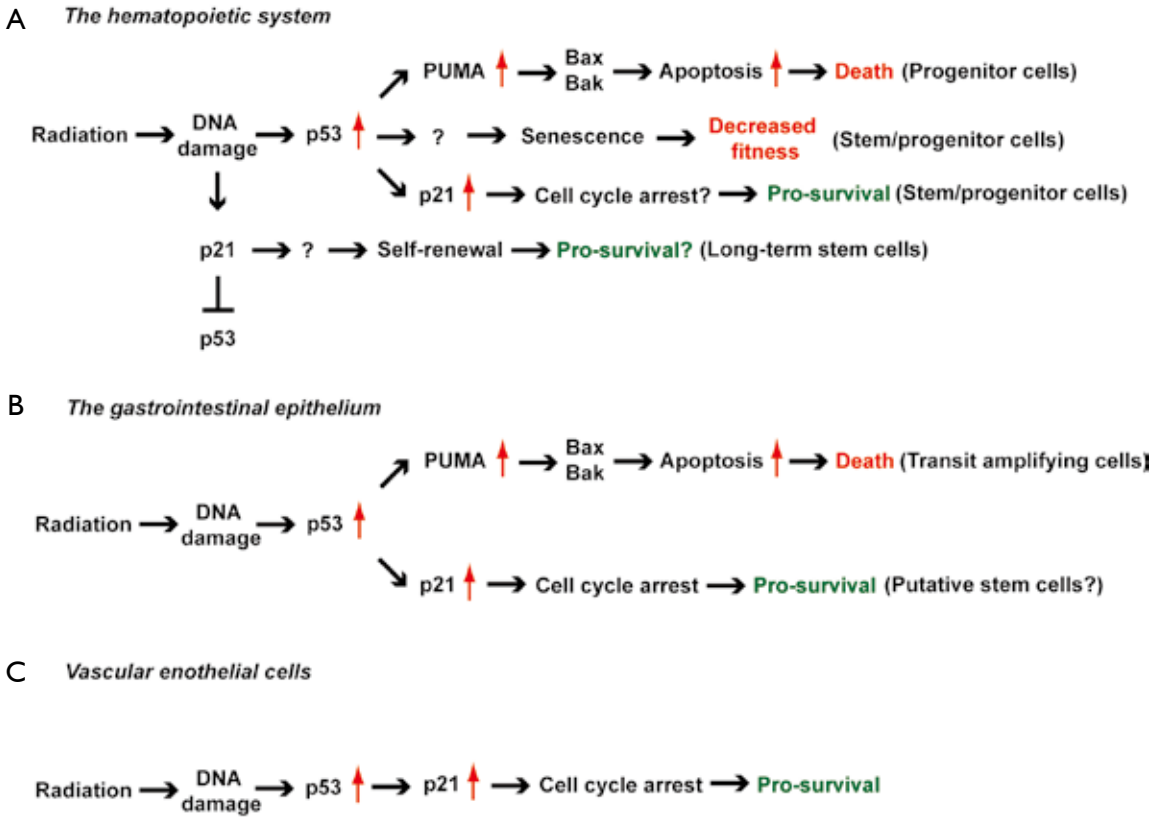

Figure 1 The diverse role of p53 in regulating cellular response to radiation *in vivo*. Schematic diagram summarizing the results of studies investigating the role of genes in the p53 pathway in the cellular response to radiation. A. Mice that lack p53 (26) or PUMA (29,30) are resistant to hematopoietic radiation toxicity because of decreased radiation-induced apoptosis in hematopoietic progenitor cells. In addition, mice with hematopoietic cell-specific deletion of Bax and Bak are also resistant to radiation-induced acute hematopoietic toxicity (40), which recapitulates the phenotype observed in $p53^{-/-}$ and $PUMA^{-/-}$ mice. In addition to suppressing apoptosis, deletion of p53 increases the fitness of hematopoietic stem/progenitor cells after irradiation (33,34) through mechanisms that are partially dependent on blocking radiation-induced senescence. Conversely, deletion of the cyclin-dependent kinase inhibitor p21 decreases the fitness of hematopoietic stem/progenitor cells after irradiation (13,39), which is likely due to defects in cell cycle arrest. In long-term HSCs (LT-HSCs), radiation induces p21 in a p53-independent manner, which improves self-renewal of stem cells. Moreover, deletion of p21 increases p53 levels in LT-HSCs after irradiation, suggesting that p21 negatively regulates p53 in LT-HSCs (13). B. Deletion of p53 in the whole animal (41,42) or in the GI epithelium (40) suppresses radiation-induced apoptosis, which is mediated by PUMA (43) and Bax/Bak (40), in transit amplifying cells in the GI epithelium. However, loss of p53 in the GI epithelium exacerbates the radiation-induced GI syndrome (26,40) because of defects in p21-mediated cell cycle arrest, which leads to mitotic catastrophe in putative intestinal stem cells that are responsible for tissue regeneration after radiation. C. Deletion of p53 sensitizes endothelial cells to radiation (44,45) due to defects in p21-mediated cell cycle arrest. Damage of cardiac endothelial cells by radiation leads to myocardial hypoxia and cardiac ischemia, which cause radiation-induced cardiac injury (45).

cycle checkpoints (54). Indeed, in the first 24 hours after irradiation, crypt epithelial cells of $p53^{+/+}$ mice show a decrease in cell proliferation; however, crypt epithelial cells of $p53^{-/-}$ mice have a defect in cell cycle arrest and continue to proliferate (26,52). Collectively, these results indicate a diverse role of p53 in regulating the survival of crypt epithelial cells.

The intrinsic pathway of apoptosis in GI epithelial cells does not contribute to the radiation-induced GI syndrome

To specifically investigate the role of the intrinsic pathway

of apoptosis in the radiation-induced GI syndrome, we utilized the Cre-loxP system to generate mice with GI epithelium-specific deletion of Bak (Bcl-2 homologous antagonist killer) and Bax (Bcl-2 associated X protein) (VillinCre; $Bax^{FL/-}$; $Bak^{-/-}$) (40). Bak and Bax are key pro-apoptotic proteins that govern mitochondrial outer membrane permeabilization to irreversibly initiate the intrinsic pathway of apoptosis (55,56). Remarkably, deletion of both Bak and Bax in the GI epithelium decreased radiation-induced apoptosis in crypt epithelial cells, but it did not protect mice from the radiation-induced GI syndrome (40). In contrast, specific deletion of p53 in the GI epithelium significantly exacerbated the GI syndrome, which recapitulates the phenotype that was observed in $p53^{-/-}$ mice (40). Moreover, deletion of Bak and Bax did not rescue the radiation sensitivity of the GI tract resulting from loss of p53. Together, these results demonstrate that (I) survival from the GI syndrome is not increased by blocking the intrinsic pathway of apoptosis in GI epithelial cells and (II) loss of p53 sensitizes GI epithelial cells to radiation through mechanisms that are independent of pre-mitotic apoptosis.

Loss of PUMA protects mice from the GI syndrome via the cyclin-dependent kinase inhibitor p21

Other groups also investigated the role of p53-mediated apoptosis in controlling the radiation-induced GI syndrome using mice with whole animal knockout of PUMA (43). Remarkably, $PUMA^{-/-}$ mice not only showed a defect in radiation-induced apoptosis in the crypts, but also had improved survival from the GI syndrome (43). These results suggest that blocking PUMA-mediated apoptosis may protect mice from the GI syndrome, which appears to contradict the results using mice with GI epithelium-specific deletion of Bak and Bax. However, because PUMA functions upstream of Bak and Bax to initiate pre-mitotic apoptosis (10), it is possible that deletion of PUMA protects mice from the GI syndrome through mechanisms that are independent of its role in regulating apoptosis (57). Indeed, through mechanisms that are not well understood, the GI epithelium of $PUMA^{-/-}$ mice has elevated levels of the cyclin-dependent kinase inhibitor p21 (43,58). Thus, up-regulation of p21 may function in the resistance to the radiation-induced GI syndrome resulting from deletion of PUMA.

The role of p21 in the radiation-induced GI syndrome has been examined in several studies using $p21^{-/-}$ mice. The results from these studies demonstrate that $p21^{-/-}$ mice are more sensitive to the radiation-induced GI syndrome than mice retaining functional p21 (26,40,58), indicating that p21-mediates signaling is necessary to prevent mice from developing the GI syndrome. To elucidate whether p21 is necessary for the resistance of $PUMA^{-/-}$ mice to the GI syndrome, Leibowitz *et al.* investigated the radiation-induced GI syndrome in $p53^{-/-}$, $PUMA^{-/-}$, $p21^{-/-}$ and $PUMA^{-/-}$; $p21^{-/-}$ (double knockout) mice (58). Their results showed that $PUMA^{-/-}$; $p21^{-/-}$ mice developed the radiation-induced GI syndrome significantly faster than $PUMA^{-/-}$ mice, indicating that p21 is also necessary to confer resistance to the GI syndrome in $PUMA^{-/-}$ mice. Remarkably, although $p53^{-/-}$, $p21^{-/-}$ and $PUMA^{-/-}$; $p21^{-/-}$ mice were more sensitive to the GI syndrome compared to wild-type mice; these mice all had a significantly higher number of regenerated crypts in the small intestine 72 hours after irradiation, which is likely due to compromised cell cycle arrest (59,60). Defects in cell cycle arrest in these mice elicit a higher percentage of crypt cells that undergo aberrant mitosis or mitotic catastrophe, which results in delayed cell death after irradiation (58). Consistent with this model, we found that "super p53 mice", which harbor an extra copy of p53 (61), are more resistant to the radiation-induced GI syndrome via a mechanism that is also dependent on p21 (14,62). Taken together, these results demonstrate a pivotal role of the p53/p21 axis in protecting mice against the radiation-induced GI radiation syndrome by preventing crypt cells from premature mitotic entry after irradiation.

Mitotic catastrophe contributes to cell death in intestinal stem cells after irradiation

The increased sensitivity of $p53^{-/-}$ and $p21^{-/-}$ mice to GI syndrome reveals that certain types of intestinal stem cells (ISCs) (63) essential to regenerate the GI epithelium after radiation injury may be killed through mitotic catastrophe. Indeed, in the small intestine of wild-type mice, radiation not only induces pre-mitotic apoptosis, but also causes aberrant mitosis and mitotic death in crypt epithelial cells (40,64). To elucidate the mechanisms by which ISCs die from radiation, a recent study (65) investigated the radiosensitivity of $Lgr5^{+}$ crypt base columnar cells (CBCs), a group of ISCs that can reconstitute at least part of the GI tract (66). Hua and colleagues found that radiation exposure caused a dose-dependent decrease in CBCs in the small intestine. In addition, an irreversible loss of CBCs in the small intestine was observed at a radiation dose that caused the GI syndrome (15 Gy). Remarkably, the majority of CBCs

Table 1 Summary of studies that use knockout mice to study the role of p53-mediated signaling in regulating the radiation-induced GI syndrome

Deletion of genes	Radiation-induced pre-mitotic apoptosis	Radiation-induced GI syndrome	References
p53 (whole animal)	Decreased	Sensitive	(26,41,42,58)
p53 (GI epithelium)	Decreased	Sensitive	(40)
Bax and Bak (GI epithelium)	Decreased	No change	(40)
PUMA (whole animal)	Decreased	Resistant	(43,58)
p21 (whole animal)	No change	Sensitive	(26,40,58)
PUMA and p21 (whole animal)	Decreased	Sensitive	(58)

were depleted around 1 to 3.5 days, rather than a few hours, after 15 Gy, suggesting that the majority of CBCs died from mitotic death after irradiation. Together, these results reveal a strong association between mitotic catastrophe of CBCs and the onset of the radiation-induced GI syndrome.

Summary

The diverse effect of p53-mediated signaling on radiosensitivity of the GI epithelium reveals the complex biology of the radiation-induced GI syndrome (*Table 1*). While some crypt epithelial cells are highly sensitive to radiation-induced apoptosis, which is largely dependent on p53 activation, blocking the intrinsic pathway of apoptosis in the GI epithelium does not significantly influence the GI syndrome. In contrast, studies with $p53^{-/-}$ and $p21^{-/-}$ mice demonstrate the significance of the p53/p21-mediated cell cycle arrest pathway in preventing mitotic catastrophe in crypt epithelial cells after irradiation (*Figure 1B*). Given that multiple types of ISCs may contribute to regeneration of the small intestine after radiation injury (67), future studies using mouse genetics to manipulate p53 expression in specific types of ISCs would provide insight into how p53-mediated apoptosis and cell cycle arrest cooperate to regulate the radiation-induced GI syndrome.

Role of p53-mediated signaling in response of endothelial cells to radiation

The vascular endothelium is critical to maintain the architecture and function of blood vessels. Damage to endothelial cells significantly contributes to the pathogenesis of acute and late effects of radiation (68,69). For example, animal models show that radiation causes ultrastructural endothelial degeneration and a substantial decrease in microvessel density in the myocardium, which occurs prior to the onset of radiation-induced myocardial injury (70-74). Radiation causes endothelial cell death or dysfunction through a variety of mechanisms including apoptosis (75), senescence (76,77) and mitotic death (77). *In vitro* studies using endothelial cells from different sources indicate that radiation induces expression of p53 protein and its transcriptional targets, such as the cyclin-dependent kinase inhibitor p21. However, the mechanism through which p53 influences radiation response in endothelial cells is controversial. Some studies indicate that blocking p53-mediated signaling improves survival of endothelial cells *in vitro* by suppressing apoptosis or senescence (76,78), while others using endothelial cells isolated from $p53^{-/-}$ mice to show that deletion of p53 sensitizes endothelial cells to radiation *in vitro* (44).

Burdelya *et al*. evaluated the effect of blocking p53 in tumor stroma, which contains endothelial cells, on tumor response to radiation *in vivo*. They used mouse tumorigenic packaging cells that produce a retrovirus encoding a dominant-negative mutant p53 to generate xenograft tumors with p53-deficient stroma (44). Tumors with p53-deficient stroma showed markedly prolonged growth delay compared to tumors with p53-wild type stroma. A similar level of growth delay was also observed in tumors that were treated with a p53 inhibitor, PFTα, in combination with radiation. In addition, blocking p53 in tumor stroma resulted in a significant decrease in vessel density in tumors, suggesting that inhibition of p53 sensitizes tumor-associated endothelial cells to radiation *in vivo*.

To specifically investigate the effect of blocking p53 in endothelial cells on radiation-induced heart disease, we used the Cre-loxP system to delete p53 in endothelial cells using Tie2Cre and VE-Cadherin-Cre mice (45). We observed that after whole-heart irradiation, mice in which both alleles of p53 are deleted in endothelial cells (i.e., Tie2Cre; $p53^{FL/-}$ or VECre; $p53^{FL/-}$ mice) were sensitized to radiation-induced

myocardial injury compared to mice that retained one allele of p53 in endothelial cells (i.e., Tie2Cre; $p53^{FL/+}$ or VECre; $p53^{FL/+}$ mice). After whole-heart irradiation, both Tie2Cre; $p53^{FL/-}$ and VECre; $p53^{FL/-}$ mice showed a focal decrease in microvessel density in the myocardium, which leads to cardiac ischemia and myocardial necrosis. The progression of myocardial necrosis resulted in systolic dysfunction and heart failure. In addition, *in vitro* studies using primary endothelial cells showed that after irradiation a higher percentage of p53-deficient endothelial cells displayed early entry into mitosis and contained micronuclei with positive γ-H2AX foci, which result from improper segregation of genomic DNA after radiation. Together, these results demonstrate that p53 protects cardiac endothelial cells from radiation *in vivo* by preventing the formation of aberrant mitosis or mitotic catastrophe.

Because radiation induces p21 expression in cardiac endothelial cells in a p53-depedent manner, we also studied radiation-induced heart disease in $p21^{-/-}$ mice. Remarkably, after whole heart irradiation $p21^{-/-}$ mice phenocopy the sensitivity of Tie2Cre; $p53^{FL/-}$ and VECre; $p53^{FL/-}$ mice to radiation-induced myocardial injury. Similar to Tie2Cre; $p53^{FL/-}$ and VECre; $p53^{FL/-}$ mice, $p21^{-/-}$ mice developed a reduction in microvessel density, increased vascular permeability and myocardial hypoxia prior to the onset of cardiac dysfunction. These data demonstrate a crucial role of the p53/p21 axis in protecting cardiac endothelial cells from radiation (*Figure 1C*).

Summary

Results from studies in mice indicate that blocking p53 *in vivo* through either pharmacological inhibition or genetic deletion dramatically increases radiosensitivity of endothelial cells in tumors and in the heart. These findings suggest that p53 may generally play a pro-survival role in endothelial cell *in vivo*. Thus, genetically engineered mice with endothelial cell-specific deletion of p53 may be useful tools to mechanistically study the impact of vascular injury on acute and late effects of radiation. Given the diversity of gene expression profiles in human endothelial cells isolated from different tissues (79), further studies are warranted to dissect how p53 functions in endothelial cells to regulate the radiation response of different organs.

Conclusions and perspectives

Radiation activates p53-mediated signaling in a variety of cells; however, the consequence of p53 activation is cell-type dependent. Using genetically engineered mouse models to manipulate the expression of p53 in specific cell types *in vivo*, several groups have begun to mechanistically dissect the role of p53 in regulating radiation response of different organs in a cell-type specific manner. The findings summarized in this review demonstrate how response of p53 to radiation can vary across different organs or even within the same cell lineage (*Figure 1*). The complexity by which p53 regulates cellular and tissue response to radiation underscores the importance of understanding mechanisms through which individual cell types respond to radiation. These findings may be critical for developing better strategies to ameliorate normal tissue injury from radiation therapy or radiation disasters.

Acknowledgements

We thank David Van Mater and Katherine Castle for critically reviewing the manuscript. This work was supported by NIAID grant R01 AI080488 (D.G.K).
Disclosure: The authors declare no conflict of interest.

References

1. Gudkov AV, Komarova EA. The role of p53 in determining sensitivity to radiotherapy. Nat Rev Cancer 2003;3:117-29.
2. Gudkov AV, Komarova EA. Pathologies associated with the p53 response. Cold Spring Harb Perspect Biol 2010;2:a001180.
3. Lindsay KJ, Coates PJ, Lorimore SA, et al. The genetic basis of tissue responses to ionizing radiation. Br J Radiol 2007;80 Spec No 1:S2-6.
4. Brady CA, Attardi LD. p53 at a glance. J Cell Sci 2010;123:2527-32.
5. Takagi M, Absalon MJ, McLure KG, et al. Regulation of p53 translation and induction after DNA damage by ribosomal protein L26 and nucleolin. Cell 2005;123:49-63.
6. Brooks CL, Gu W. p53 ubiquitination: Mdm2 and beyond. Mol Cell 2006;21:307-15.
7. Schlereth K, Charles JP, Bretz AC, et al. Life or death: p53-induced apoptosis requires DNA binding cooperativity. Cell Cycle 2010;9:4068-76.
8. Murray-Zmijewski F, Slee EA, Lu X. A complex barcode underlies the heterogeneous response of p53 to stress. Nat Rev Mol Cell Biol 2008;9:702-12.
9. Purvis JE, Karhohs KW, Mock C, et al. p53 dynamics control cell fate. Science 2012;336:1440-4.

10. Fei P, Bernhard EJ, El-Deiry WS. Tissue-specific induction of p53 targets in vivo. Cancer Res 2002;62:7316-27.
11. MacCallum DE, Hupp TR, Midgley CA, et al. The p53 response to ionising radiation in adult and developing murine tissues. Oncogene 1996;13:2575-87.
12. Mohrin M, Bourke E, Alexander D, et al. Hematopoietic stem cell quiescence promotes error-prone DNA repair and mutagenesis. Cell Stem Cell 2010;7:174-85.
13. Insinga A, Cicalese A, Faretta M, et al. DNA damage in stem cells activates p21, inhibits p53, and induces symmetric self-renewing divisions. Proc Natl Acad Sci U S A 2013;110:3931-6.
14. Kirsch DG. Using genetically engineered mice for radiation research. Radiat Res 2011;176:275-9.
15. Dainiak N. Hematologic consequences of exposure to ionizing radiation. Exp Hematol 2002;30:513-28.
16. Mauch P, Constine L, Greenberger J, et al. Hematopoietic stem cell compartment: acute and late effects of radiation therapy and chemotherapy. Int J Radiat Oncol Biol Phys 1995;31:1319-39.
17. Williams JP, Brown SL, Georges GE, et al. Animal models for medical countermeasures to radiation exposure. Radiat Res 2010;173:557-78.
18. Wang Y, Schulte BA, Zhou D. Hematopoietic stem cell senescence and long-term bone marrow injury. Cell Cycle 2006;5:35-8.
19. Wang Y, Schulte BA, LaRue AC, et al. Total body irradiation selectively induces murine hematopoietic stem cell senescence. Blood 2006;107:358-66.
20. Meng A, Wang Y, Van Zant G, et al. Ionizing radiation and busulfan induce premature senescence in murine bone marrow hematopoietic cells. Cancer Res 2003;63:5414-9.
21. Chua HL, Plett PA, Sampson CH, et al. Long-term hematopoietic stem cell damage in a murine model of the hematopoietic syndrome of the acute radiation syndrome. Health Phys 2012;103:356-66.
22. Marusyk A, Casas-Selves M, Henry CJ, et al. Irradiation alters selection for oncogenic mutations in hematopoietic progenitors. Cancer Res 2009;69:7262-9.
23. Pant V, Quintas-Cardama A, Lozano G. The p53 pathway in hematopoiesis: lessons from mouse models, implications for humans. Blood 2012;120:5118-27.
24. Lotem J, Sachs L. Hematopoietic cells from mice deficient in wild-type p53 are more resistant to induction of apoptosis by some agents. Blood 1993;82:1092-6.
25. Oren M. Relationship of p53 to the control of apoptotic cell death. Semin Cancer Biol 1994;5:221-7.
26. Komarova EA, Kondratov RV, Wang K, et al. Dual effect of p53 on radiation sensitivity in vivo: p53 promotes hematopoietic injury, but protects from gastro-intestinal syndrome in mice. Oncogene 2004;23:3265-71.
27. Villunger A, Michalak EM, Coultas L, et al. p53- and drug-induced apoptotic responses mediated by BH3-only proteins puma and noxa. Science 2003;302:1036-8.
28. Nakano K, Vousden KH. PUMA, a novel proapoptotic gene, is induced by p53. Mol Cell 2001;7:683-94.
29. Yu H, Shen H, Yuan Y, et al. Deletion of Puma protects hematopoietic stem cells and confers long-term survival in response to high-dose gamma-irradiation. Blood 2010;115:3472-80.
30. Shao L, Sun Y, Zhang Z, et al. Deletion of proapoptotic Puma selectively protects hematopoietic stem and progenitor cells against high-dose radiation. Blood 2010;115:4707-14.
31. Harvey M, McArthur MJ, Montgomery CA Jr, et al. Spontaneous and carcinogen-induced tumorigenesis in p53-deficient mice. Nat Genet 1993;5:225-9.
32. Jacks T, Remington L, Williams BO, et al. Tumor spectrum analysis in p53-mutant mice. Curr Biol 1994;4:1-7.
33. Marusyk A, Porter CC, Zaberezhnyy V, et al. Irradiation selects for p53-deficient hematopoietic progenitors. PLoS Biol 2010;8:e1000324.
34. Bondar T, Medzhitov R. p53-mediated hematopoietic stem and progenitor cell competition. Cell Stem Cell 2010;6:309-22.
35. Shao L, Li H, Pazhanisamy SK, et al. Reactive oxygen species and hematopoietic stem cell senescence. Int J Hematol 2011;94:24-32.
36. Wang Y, Liu L, Pazhanisamy SK, et al. Total body irradiation causes residual bone marrow injury by induction of persistent oxidative stress in murine hematopoietic stem cells. Free Radic Biol Med 2010;48:348-56.
37. Serrano M, Lee H, Chin L, et al. Role of the INK4a locus in tumor suppression and cell mortality. Cell 1996;85:27-37.
38. Brown JP, Wei W, Sedivy JM. Bypass of senescence after disruption of p21CIP1/WAF1 gene in normal diploid human fibroblasts. Science 1997;277:831-4.
39. van Os R, Kamminga LM, Ausema A, et al. A Limited role for p21Cip1/Waf1 in maintaining normal hematopoietic stem cell functioning. Stem Cells 2007;25:836-43.
40. Kirsch DG, Santiago PM, di Tomaso E, et al. p53 controls radiation-induced gastrointestinal syndrome in mice independent of apoptosis. Science 2010;327:593-6.

41. Merritt AJ, Potten CS, Kemp CJ, et al. The role of p53 in spontaneous and radiation-induced apoptosis in the gastrointestinal tract of normal and p53-deficient mice. Cancer Res 1994;54:614-7.
42. Clarke AR, Gledhill S, Hooper ML, et al. p53 dependence of early apoptotic and proliferative responses within the mouse intestinal epithelium following gamma-irradiation. Oncogene 1994;9:1767-73.
43. Qiu W, Carson-Walter EB, Liu H, et al. PUMA regulates intestinal progenitor cell radiosensitivity and gastrointestinal syndrome. Cell Stem Cell 2008;2:576-83.
44. Burdelya LG, Komarova EA, Hill JE, et al. Inhibition of p53 response in tumor stroma improves efficacy of anticancer treatment by increasing antiangiogenic effects of chemotherapy and radiotherapy in mice. Cancer Res 2006;66:9356-61.
45. Lee CL, Moding EJ, Cuneo KC, et al. p53 functions in endothelial cells to prevent radiation-induced myocardial injury in mice. Sci Signal 2012;5:ra52.
46. Kemp CJ, Wheldon T, Balmain A. p53-deficient mice are extremely susceptible to radiation-induced tumorigenesis. Nat Genet 1994;8:66-9.
47. Shadad AK, Sullivan FJ, Martin JD, et al. Gastrointestinal radiation injury: symptoms, risk factors and mechanisms. World J Gastroenterol 2013;19:185-98.
48. Moore JV. The 'gastrointestinal syndrome' after chemotherapy: inferences from mouse survival time, and from histologically- and clonogenically-defined cell death in intestinal crypts. Br J Cancer Suppl 1986;7:16-9.
49. Somosy Z, Horvath G, Telbisz A, et al. Morphological aspects of ionizing radiation response of small intestine. Micron 2002;33:167-78.
50. Potten CS. Extreme sensitivity of some intestinal crypt cells to X and gamma irradiation. Nature 1977;269:518-21.
51. Booth C, Potten CS. Gut instincts: thoughts on intestinal epithelial stem cells. J Clin Invest 2000;105:1493-9.
52. Merritt AJ, Allen TD, Potten CS, et al. Apoptosis in small intestinal epithelial from p53-null mice: evidence for a delayed, p53-independent G2/M-associated cell death after gamma-irradiation. Oncogene 1997;14:2759-66.
53. Vakifahmetoglu H, Olsson M, Zhivotovsky B. Death through a tragedy: mitotic catastrophe. Cell Death Differ 2008;15:1153-62.
54. Vitale I, Galluzzi L, Castedo M, et al. Mitotic catastrophe: a mechanism for avoiding genomic instability. Nat Rev Mol Cell Biol 2011;12:385-92.
55. Antignani A, Youle RJ. How do Bax and Bak lead to permeabilization of the outer mitochondrial membrane? Curr Opin Cell Biol 2006;18:685-9.
56. Dewson G, Kluck RM. Mechanisms by which Bak and Bax permeabilise mitochondria during apoptosis. J Cell Sci 2009;122:2801-8.
57. Clarke AR. Puma: mauling the intestinal crypt. Cell Stem Cell 2008;2:517-8.
58. Leibowitz BJ, Qiu W, Liu H, et al. Uncoupling p53 functions in radiation-induced intestinal damage via PUMA and p21. Mol Cancer Res 2011;9:616-25.
59. Bunz F, Dutriaux A, Lengauer C, et al. Requirement for p53 and p21 to sustain G2 arrest after DNA damage. Science 1998;282:1497-501.
60. Brugarolas J, Chandrasekaran C, Gordon JI, et al. Radiation-induced cell cycle arrest compromised by p21 deficiency. Nature 1995;377:552-7.
61. García-Cao I, García-Cao M, Martín-Caballero J, et al. "Super p53" mice exhibit enhanced DNA damage response, are tumor resistant and age normally. EMBO J 2002;21:6225-35.
62. Sullivan JM, Jeffords LB, Lee CL, et al. p21 protects "Super p53" mice from the radiation-induced gastrointestinal syndrome. Radiat Res 2012;177:307-10.
63. Barker N, van Oudenaarden A, Clevers H. Identifying the stem cell of the intestinal crypt: strategies and pitfalls. Cell Stem Cell 2012;11:452-60.
64. Hendry JH, Potten CS. Intestinal cell radiosensitivity: a comparison for cell death assayed by apoptosis or by a loss of clonogenicity. Int J Radiat Biol Relat Stud Phys Chem Med 1982;42:621-8.
65. Hua G, Thin TH, Feldman R, et al. Crypt base columnar stem cells in small intestines of mice are radioresistant. Gastroenterology 2012;143:1266-76.
66. Barker N, van Es JH, Kuipers J, et al. Identification of stem cells in small intestine and colon by marker gene Lgr5. Nature 2007;449:1003-7.
67. Yan KS, Chia LA, Li X, et al. The intestinal stem cell markers Bmi1 and Lgr5 identify two functionally distinct populations. Proc Natl Acad Sci U S A 2012;109:466-71.
68. Wang J, Boerma M, Fu Q, et al. Significance of endothelial dysfunction in the pathogenesis of early and delayed radiation enteropathy. World J Gastroenterol 2007;13:3047-55.
69. Stewart FA, Hoving S, Russell NS. Vascular damage as an underlying mechanism of cardiac and cerebral toxicity in irradiated cancer patients. Radiat Res 2010;174:865-9.
70. Fajardo LF, Stewart JR. Pathogenesis of radiation-induced myocardial fibrosis. Lab Invest 1973;29:244-57.
71. Fajardo LF, Stewart JR. Experimental radiation-induced

heart disease. I. Light microscopic studies. Am J Pathol 1970;59:299-316.
72. Lauk S, Kiszel Z, Buschmann J, et al. Radiation-induced heart disease in rats. Int J Radiat Oncol Biol Phys 1985;11:801-8.
73. Yeung TK, Lauk S, Simmonds RH, et al. Morphological and functional changes in the rat heart after X irradiation: strain differences. Radiat Res 1989;119:489-99.
74. Seemann I, Gabriels K, Visser NL, et al. Irradiation induced modest changes in murine cardiac function despite progressive structural damage to the myocardium and microvasculature. Radiother Oncol 2012;103:143-50.
75. Paris F, Fuks Z, Kang A, et al. Endothelial apoptosis as the primary lesion initiating intestinal radiation damage in mice. Science 2001;293:293-7.
76. Lee MO, Song SH, Jung S, et al. Effect of ionizing radiation induced damage of endothelial progenitor cells in vascular regeneration. Arterioscler Thromb Vasc Biol 2012;32:343-52.
77. Mendonca MS, Chin-Sinex H, Dhaemers R, et al. Differential mechanisms of x-ray-induced cell death in human endothelial progenitor cells isolated from cord blood and adults. Radiat Res 2011;176:208-16.
78. Nübel T, Damrot J, Roos WP, et al. Lovastatin protects human endothelial cells from killing by ionizing radiation without impairing induction and repair of DNA double-strand breaks. Clin Cancer Res 2006;12:933-9.
79. Chi JT, Chang HY, Haraldsen G, et al. Endothelial cell diversity revealed by global expression profiling. Proc Natl Acad Sci U S A 2003;100:10623-8.

Cite this article as: Lee CL, Blum JM, Kirsch DG. Role of p53 in regulating tissue response to radiation by mechanisms independent of apoptosis. Transl Cancer Res 2013;2(5):412-421. doi: 10.3978/j.issn.2218-676X.2013.09.01

Review Article

Molecular mechanisms involved in tumor repopulation after radiotherapy

Wooi-Loon Ng, Qian Huang, Xinjian Liu, Mary Zimmerman, Fang Li, Chuan-Yuan Li

Department of Dermatology, Duke University Medical Center, Durham, NC 27710, USA

Correspondence to: Chuan-Yuan Li, Ph.D. Duke University Medical Center, Box 3155, Durham, NC 27710, USA. Email: Chuan.Li@duke.edu.

Abstract: Radiotherapy remains one of most important treatment modalities for solid tumors. Current radiotherapy is mostly based on a set of concepts called the 4"R"s, which were established when there was lack of understanding of the underlying molecular mechanisms. However, progress made in the past two decades are beginning to allow us to see some of the molecular details involved in tumor response to radiation therapy. In this review, we will attempt to summarize some of the key discoveries in molecular radiation biology that have direct relevance to radiotherapy. We will focus our discussion on areas such as radiation induced tumor vasculogenesis, stem cell mobilization, and cellular repopulation. We hope our discussion will stimulate further studies in this important area of cancer research.

Keywords: Radiation therapy; 4"R"s; tumor repopulation; vasculogenesis; phoenix rising pathway

doi: 10.3978/j.issn.2218-676X.2013.10.03

Scan to your mobile device or view this article at: http://www.thetcr.org/article/view/1676/html

Introduction

Ionizing radiation was used as a means to treat cancer soon after Wilhelm Roentgen discovered X-rays. Modern radiation therapy was based on a fractionated scheme instead of a single high dose of radiation. The fractionated dose scheme was based on the well known ram's testes experiments in 1927 by Regaud and Ferroux done in France (1). In their experiments, when a ram's testes were irradiated for sterilization, a single dose exposure failed to sterilize the ram despite severe scrotum skin injury. On the other hand, a fractionated dose scheme was successful in sterilizing the ram. This fundamental discovery were gradually adopted in the filed of radiation oncology worldwide in the form of fractionated radiotherapy which is still the norm in radiation oncology. At the theoretical level, fractionated radiotherapy was based on the theory of the 4"R"s (2) (repair, redistribution, reoxygenation and repopulation) which are described briefly here.

Repair is correlated with the cell's ability to form DNA strand breaks. Treatment to use fractionated doses (usually 1.8-2.0 Gy/day) with a time interval (0.5-24 hrs depending on cell types) will allow cells to recover from most of the sublethal damage after the irradiation. It has been assumed that normal healthy cells will be able to activate their checkpoint mechanisms and repair the "sublethal" damage. On the other hand, most types of cancer cells have deficiencies in their checkpoint mechanisms and thus less able to repair DNA damage. Therefore multiple fractions of radiation allow normal cells to carry out repair while allowing tumor cells to be exposed to higher level of radiation. Redistribution refers to radiation-induced cell cycle effects. Because cancer cells are more sensitive in G2/M phases of the cell cycle than G1/S and they tend to pile up in G2/M due to a functional G2 checkpoint after being exposed to radiation, they are more likely to be killed during subsequent irradiation. In comparison, normal cells are mostly in G0/G1 due to a G1 checkpoint and are thus less susceptible to this type of sensitization (3). Re-oxygenation refers to the changes in oxygen tension within the irradiated tumor mass. In low LET photon radiotherapy, oxygen molecule is key for radiation induced cell killing because it facilitates the formation of free radical species that are responsible for most of radiation induced DNA damage (4). Hypoxic tumor cells are thus

much more difficult to kill than well oxygenated ones. If radiation treatment is fractionated, the hypoxic cells will be allowed to reoxygenate due to reduced demand from dying tumor cells and the subsequent fractions will be much more efficient to eliminate the reoxygenated tumor cells. Repopulation is the rapid proliferation of surviving tumor cells after radiation induced cell killing (5). The influence of repopulation on the outcome of radiotherapy is self-evident. Effective suppression of tumor cell repopulation is therefore key for the success of radiotherapy.

In this review, we summarize some of the key recent discoveries that have added significantly to our knowledge base of tumor response to radiotherapy. We hope the discussion can stimulate fresh new endeavors into this important area of cancer research.

The importance of tumor vasculature *vs.* tumor cells in radiotherapy

One notable recent controversy in molecular radiation biology is the relative importance of tumor cells *vs.* tumor vasculature. Most of 4"R"s are mainly centered on how to sensitize tumor cells to radiation. In a study published in 2003 (6), Kolesnick and colleagues demonstrated that tumor vasculature could play a key role. Using a transgenic mouse model that was rendered resistant to apoptosis induction in the endothelial cell compartment due to knockout (KO) of the asmase or Bax genes, the authors demonstrated that tumors were significantly more resistant to radiation when their vasculature was rendered more resistant to apoptosis. In addition, they showed that when a higher dose of radiation was used to kill the endothelial cells in the KO mice, tumors would be effectively controlled. This study caused controversy because it challenged established, tumor cell-centric concepts in radiobiology. The data were also quite different from an earlier study (7) that showed the tumor control dose (TCD_{50}) in a radiation sensitive mouse (SCID) background was not significantly different from that in a non-sensitive (nude) background. In that same study, however, it was shown that stroma sensitivity to radiation did cause significant tumor growth delay. In a more recent study, Gerweck *et al.* (8) showed that tumor cells that were deficient in the DNA-PKcs gene and thus very sensitive to radiation, showed significantly less growth delay after irradiation when compared with its genetically identical counterpart with the DNA-PKcs gene. The results were interpreted as indicating that tumor cell sensitivity did matter for overall tumor response to radiotherapy. In a further paper combining genetically identical tumor cells lines with or without DNA-PKcs and host mice with or without DNA-PKcs deficiency (9), it was shown that radiation sensitivities of both tumor cells and stromal tissues play important roles in determining the outcome of radiotherapy.

Importance of bone marrow derived cells in tumor response to radiotherapy

Since Garcia-Barros *et al.* (6) demonstrated the importance of tumor endothelial cells in determining the outcome of radiotherapy, other studies have shown that additional non-tumor cells also play significant roles. For example, Ahn and colleagues have shown that vasculogenesis, the *de novo* formation of blood vessels, to be important in tumor recovery. They showed a crucial role for matrix metalloproteinase-9 (MMP-9) in mediating tumor vasculogenesis (10). MMP-9 is a protein involved in extracellular matrix degradation and a member of zinc-containing endopeptidases (11). In a MMP-9 KO mouse model, tumor growth were completely inhibited in pre-irradiated hosts but restored after wild-type bone marrow cells were transplanted into the MMP-9 KO mice (10). Surprisingly, they found that BM-derived $CD11b^+$ myelomonocytic cells were the most recruited to X-irradiated tumor for vasculogenesis rather than epithelial progenitor cells, which had previously been shown to be important for tumor blood vessel development (12). Other studies have shown that tumors recruited myeloid cells via secretion of VEGF (13) and M-CSF (14) through VEGF receptor-1 (15) and M-CSF receptor (16) respectively to activate their migration to the tumor. Subsequently, myeloid cells might produce proangiogenic cytokine, including stromal derived factor-1 (SDF-1), VEGF, TGF-β. Of note is an additional study by Kioi *et al.* (17) which demonstrated in a mouse glioma model that radiation activated HIF-1 which stimulated the transcription of SDF-1 that caused the homing in of bone marrow derived CD11b+ myelomonocytes to induce vasculogenesis. A small molecule drug AMD3100 appears to be effective in suppressing tumor growth when used in combination with radiotherapy.

HIF-1 as a major regulator of tumor response to hypoxia and radiotherapy

Hypoxia, a condition of oxygen tension below the physiological norm, has long been recognized as a common

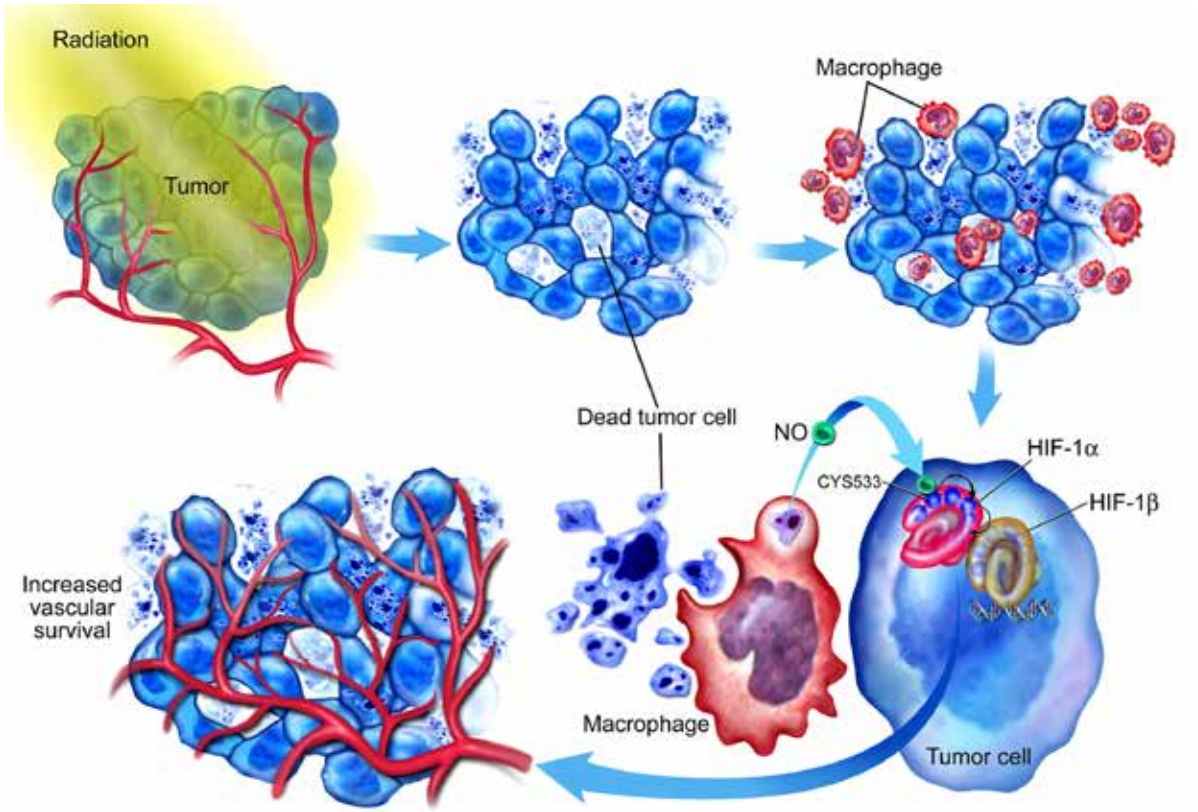

Figure 1 Radiation induced HIF-1α stabilization through nitrosylation of C533 by macrophage derived nitric oxide (adapted from reference 25).

feature of the tumor microenvironment. Hypoxia in itself can significantly increase radiation resistance of tumor cells due to its ability to reduce radiation induced free radicals, which are the main effectors in radiation induced cell killing. In addition, at the biological level, hypoxia induces profound changes in tumor cells that allow it to be more angiogenic and metastatic (18-20). Previously, it has been identified that HIF-1 transcription factor is the master regulator that coordinate cellular response to hypoxia (21,22). A rich body of literature has established HIF-1α as the key factor that plays a central role in tumor angiogenesis and tumor proliferation under hypoxic conditions. Under normoxic conditions, HIF-1α is hydroxylated by proline hydroxylases (PhDs) in an oxygen-dependent manner. The hydroxylation key proline residues in HIF1α leads to rapid recognition by VHL and subsequent ubiquitylation of HIF-1α, which leads to proteasome-mediated degradation (23). Under hypoxic conductions, HIF-1α is not hydroxylated and the protein remains stabilized and able to activate downstream genes. In addition to the oxygen-dependent activation, studies have shown that HIF-α could be activated in a hypoxia-independent manner by radiotherapy (24). It was shown that irradiation of tumor cells could result in increased nuclear accumuation and enhanced translation of HIF-1α after radiation induced depolymerizaton of "stress granules" (24). In another study, Li *et al*. showed that after radiotherapy, tumor associated macropahges mediate hypoxia independent activation of HIF-1α through a nitric oxide mediated mechanism (25). They showed that L-NAME, a potent inhibitor of NO synthases (NOS), can attenuate HIF-1α activity in 4T1 murine breast tumors, which suggested that, NOS was likely to be the source of NO in enabling radiation induced HIF-1α stabilization. They further identified that iNOS (inducible NOS) in the tumor-associated macrophages (TAMs) was the source of NO production after radiotherapy (*Figure 1*). NO was shown to nitrosylate the Cys533 residue in the HIF-α oxygen-dependent domain in mouse cells (correspond to Cys520 in human HIF-1α). Nitrosylation of HIF-1α at Cys533 protected HIF-1α from degradation by preventing its binding to von Hippel-Lindau (vHL). The discovery of an NO-based HIF-1α activation mechanism in response

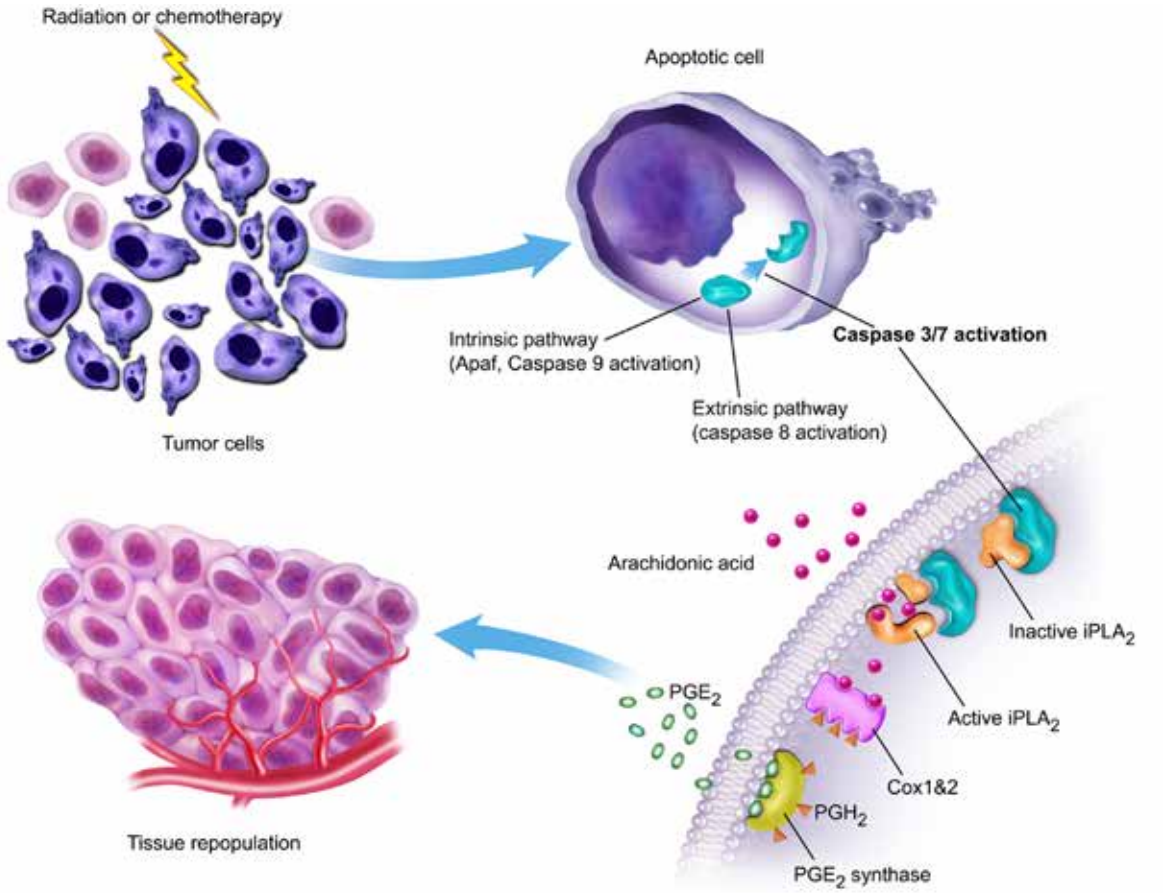

Figure 2 The "phoenix rising" pathway of cell death-mediated stimulation of tumor repopulation during cancer radiotherapy (adapted from reference 26).

to radiation has opened up an option to use NOS inhibitor to attenuate tumor HIF-1α activation and suppress tumor growth (25).

The unexpected roles of caspase 3 in tumor cell repopulation after radiotherapy

Tumor repopulation is an important mechanism through which tumors growth back after radiotherapy (2). Despite the recognition of its importance for decades, the mechanism for repopulation, especially accelerated tumor repopulation (5) in some cancer patients undergoing radiotherapy, is not clear. A recent study from our group shows that one of the key signals for tumor repopulation after radiotherapy is actually cell death induced by radiation (26). We show that lethally irradiated tumor or fibroblast cells can stimulate the rapid proliferation of non-irradited tumor cells in tissue culture or in mice. In addition, we show that caspase 3 activation in the dying cells is key for the growth-stimulating signals. In casp3-/- MEF cells, the growth-stimulation effect is significantly attenuated. Given that caspase 3 itself is considered a cellular "excutioner" whose normal function is to get rid of damaged or unwanted cells, its positive regulation of a signal that stimuates tumor cell repopulation is especially surprising. Further experiments show that one of the major downstream factors that regulate cell growth is calcium-independent phospholipase A_2 ($iPLA_2$), which is cleaved and activated by caspase 3. Caspase 3-mediated activataion of $iPLA_2$ leads to increased production of arachidonic acid, which in turn boosts the production of PGE_2 that stimulates tumor growth (*Figure 2*). We named this newly discovered tumor cell repopulation mechanism the "phoenix rising" pathway. In a separate study, we show that the "phoenix rising" pathway is a fundamental mechanism for wound healing and tissue regeneration (27). Our discovery in the normal tissue is consistent with earlier

discoveries in lower organisms that were characterized as "compensatory proliferation" (28,29).

Involvement of cancer stem cells in tumor response to radiation therapy

One of the major new concepts emerging in the past decade is cancer stem cells. Cancer stem cells were initially described by John Dick and colleagues in human acute myeloid leukemia (30). At earlier times cancer cells in a tumor mass were largely treated as clonal and mostly identical, except for rare mutants. The discovery of cancer stem cells completely changed this viewpoint. Cancer stem cells rapidly become a focal point of attention because they are the putative cells responsible for tumor cell self-renewal. Targeting cancer cells would be akin to eradicating the roots of the tree. Eliminating of cancer stem cells alone may be sufficient to suppress the growth of the whole tumor. Earlier studies do show that human cancer stem cells possess remarkable ability to form tumors in nude mice. For example, it was shown that as few as 100 CD44+CD24- breast cancer stem cells could form tumors in a nude mouse (31). In contrast 10^5 non-stem cells could not form tumors in the same mice. Another important characteristic of cancer stem cells appears to be their resistance to chemotherapy and radiation therapy. It was shown in animal models that cytoxic treatment of cancers increased the percentage of cancer stem cells, indicating their relative resistance to these agents. At the mechanistic level, it was shown that glioma stem cells had the ability to upregulate their DNA repair capacity to deal with DNA damage inflicted on them by exposure to radiation (32). Similer radiation-resistant properties of cancer stem cells were reported in breast cancer cells. By use of colony forming assay, it was shown that cancer cells bearing stem cell markers were significantly more radio-resistant than those cells without the markers (33). These appeared to provide strong rationale for developing strategies to target cancer stem cells during conventional chemotherapy or radiation therapy.

Counter-arguments against sole targeting of cancer stem cells during cancer therapy

Despite signicant enthusiasms among the cancer research community towards cancer stem cells as key targets in cancer therapy, there are also increasing evidence that there are complicated biology and confusion that need to be sorted out. One area that has generated a lot of controveries is the assay system for the "stemness" of cancer stem cells. Currently the "gold standard" is the ability to form tumors in immunodeficient mice. However, Quintana *et al*. show that the use of different mouse strains may lead to drastically different estimation of the frequencies of cancer stem cell in patient-derived melanoma samples. For example the use of NOD/SCID mice, which of the host of choice for estimating the frequencies of cancer stem cells in patient tumor samples, often leads to an estimate of 1 in a million (0.00001%) human melanoma cells as tumorigenic. However, if the same samples were itradiated in NSD (NOD/SCID interleukin 2-receptor gamma chain null) mice, the frequency of stem cells can be as high as one in three (34). These data strongly suggest that previous estimates of cancer stem cell frequencies are very much subjected to the assay system. The other area of confusion is the markers used to define stem cells. Different groups have used different markers for the same type of tumor, most of them on cellular surface (e.g., ABCB5, CD166, CD271 for melanoma), a few based on intracellular enzyme staining (ALDH1, or side population). Therefore, there is no consensus on a set of markers that can be universally applied to isolate cancer stem cells from tumor samples. This led to many problems that include wildly different estimates of the frequency of cancer stem cells. It could also lead to problems in efforts to target cancer stem cells because of the lack of consensus cancer stem cell markers and mechanisms.

Epigenetic reprogramming, a further issue that complicates the cancer stem cell field

Much of the intial enthusiasm on cancer stem cells is based on the initial assumption of a strict hierarchical structure in cancer cells in a tumor mass, similar to those found in normal tissues such as the hematopoietic system. However, there are several studies now indicating that the percieved hierarchy structure may not exist in cancer cells. For example, it was found that in melanoma tissues, the putative non-stem cell faction could form tumors equally as well as the stem cell faction. In addition, the newly formed tumors contain cancer cells that now possess the stem cell markers, indicating the plasticity of the cancer stem cell marker expression (35). Consistently, in another study it was found that ionzing radiation could induce the expression of stem cell genes such as *Oct4*, *Sox2*, *Nanog*, or *Klf4* in breast cancer cells (36). This finding, in

particular, calls for the re-examination of previous studies that reported the enrichment of cancer stem cells after treatment with conventional chemotherapeutic agents. It is possible that the observed increase in stem cells fraction may come from reprogramming of relatively differentiated cancer cells instead of expansion of pre-existing cancer stem cells. Indeed, other several other stimuli such as hypoxia condition (37) and nitric oxide-induced notch signaling (38) have been shown to induce epigenetic reprogramming in gliomablastoma cells. Interestingly, in a published study from our own laboratory, we observed that caspases 3&8 are activated by the transduction of the so-called Yamanada factors. Furthermore, we show that activation of the caspases facilitated the reprogramming of human fibroblasts into induced pluripotent stem cells instead of killing the cells (39). Therefore, it is conceivable that during cancer therapy induced caspase activation could faciliate cellular reprogramming if the cells somehow survive the caspase activation.

Conclusions

The classical 4"R"s have served the field of radiation cancer therapy very well. In the past two decades, we are beginning to understand the genetic, epigentic, and microenvironmental mechanisms underpining the 4"R"s. We hope the new insights gained will provide the basis for the development novel therapeutic agents and approaches that can significantly enhance current radiotherapy.

Acknowledgements

This work is supported by grants CA131408, CA136748, and CA155270 from the US National Institutes of Health (C-Y L).
Disclosure: The authors declare no conflict of interest.

References

1. Regaud C, Ferroux R. Disordance des effets de rayons X, d'une part dans le testicule, par le fractionnenment de la dose. Comptes Rendus Societe Biologique, 1927;97:431.
2. Withers HR. The 4 R's of radiotherapy, in Advances in radiation biology. Lett JT, Alder H. eds. Vol 5. New York: Academic Press, 1975;5:241-71.
3. Sinclair WK. Cyclic x-ray responses in mammalian cells in vitro. Radiat Res 1968;33:620-43.
4. Hall EJ. Radiobiology for the radiologist. 4 ed. Philadelphia: Lippincott, 1994.
5. Withers RH. Treatment-induced accelerated human tumor growth. Semin Radiat Oncol 1993;3:135-43.
6. Garcia-Barros M, Paris F, Cordon-Cardo C, et al. Tumor response to radiotherapy regulated by endothelial cell apoptosis. Science 2003;300:1155-9.
7. Budach W, Taghian A, Freeman J, et al. Impact of stromal sensitivity on radiation response of tumors. J Natl Cancer Inst 1993;85:988-93.
8. Gerweck LE, Vijayappa S, Kurimasa A, et al. Tumor cell radiosensitivity is a major determinant of tumor response to radiation. Cancer Res 2006;66:8352-5.
9. Ogawa K, Boucher Y, Kashiwagi S, et al. Influence of tumor cell and stroma sensitivity on tumor response to radiation. Cancer Res 2007;67:4016-21.
10. Ahn GO, Brown JM. Matrix metalloproteinase-9 is required for tumor vasculogenesis but not for angiogenesis: role of bone marrow-derived myelomonocytic cells. Cancer Cell 2008;13:193-205.
11. Heissig B, Hattori K, Friedrich M, et al. Angiogenesis: vascular remodeling of the extracellular matrix involves metalloproteinases. Curr Opin Hematol 2003;10:136-41.
12. Lyden D, Hattori K, Dias S, et al. Impaired recruitment of bone-marrow-derived endothelial and hematopoietic precursor cells blocks tumor angiogenesis and growth. Nat Med 2001;7:1194-201.
13. Du R, Lu KV, Petritsch C, et al. HIF1alpha induces the recruitment of bone marrow-derived vascular modulatory cells to regulate tumor angiogenesis and invasion. Cancer Cell 2008;13:206-20.
14. Kubota Y, Takubo K, Shimizu T, et al. M-CSF inhibition selectively targets pathological angiogenesis and lymphangiogenesis. J Exp Med 2009;206:1089-102.
15. Beck H, Raab S, Copanaki E, et al. VEGFR-1 signaling regulates the homing of bone marrow-derived cells in a mouse stroke model. J Neuropathol Exp Neurol 2010;69:168-75.
16. Ikeda O, Sekine Y, Muromoto R, et al. Enhanced c-Fms/M-CSF receptor signaling and wound-healing process in bone marrow-derived macrophages of signal-transducing adaptor protein-2 (STAP-2) deficient mice. Biol Pharm Bull 2008;31:1790-3.
17. Kioi M, Vogel H, Schultz G, et al. Inhibition of vasculogenesis, but not angiogenesis, prevents the recurrence of glioblastoma after irradiation in mice. J Clin Invest 2010;120:694-705.
18. Rofstad EK, Danielsen T. Hypoxia-induced metastasis of human melanoma cells: involvement of vascular

endothelial growth factor-mediated angiogenesis. Br J Cancer 1999;80:1697-707.
19. Rofstad EK, Halsør EF. Hypoxia-associated spontaneous pulmonary metastasis in human melanoma xenografts: involvement of microvascular hot spots induced in hypoxic foci by interleukin 8. Br J Cancer 2002;86:301-8.
20. Harris AL. Hypoxia--a key regulatory factor in tumour growth. Nat Rev Cancer 2002;2:38-47.
21. Wang GL, Jiang BH, Rue EA, et al. Hypoxia-inducible factor 1 is a basic-helix-loop-helix-PAS heterodimer regulated by cellular O2 tension. Proc Natl Acad Sci U S A 1995;92:5510-4.
22. Wang GL, Semenza GL. General involvement of hypoxia-inducible factor 1 in transcriptional response to hypoxia. Proc Natl Acad Sci U S A 1993;90:4304-8.
23. Jaakkola P, Mole DR, Tian YM, et al. Targeting of HIF-alpha to the von Hippel-Lindau ubiquitylation complex by O2-regulated prolyl hydroxylation. Science 2001;292:468-72.
24. Moeller BJ, Cao Y, Li CY, et al. Radiation activates HIF-1 to regulate vascular radiosensitivity in tumors: role of reoxygenation, free radicals, and stress granules. Cancer Cell 2004;5:429-41.
25. Li F, Sonveaux P, Rabbani ZN, et al. Regulation of HIF-1alpha stability through S-nitrosylation. Mol Cell 2007;26:63-74.
26. Huang Q, Li F, Liu X, et al. Caspase 3-mediated stimulation of tumor cell repopulation during Cancer radiotherapy. Nat Med 2011;17:860-6.
27. Li F, Huang Q, Chen J, et al. Apoptotic cells activate the "phoenix rising" pathway to promote wound healing and tissue regeneration. Sci Signal 2010;3:ra13.
28. Ryoo HD, Gorenc T, Steller H. Apoptotic cells can induce compensatory cell proliferation through the JNK and the Wingless signaling pathways. Dev Cell 2004;7:491-501.
29. Chera S, Ghila L, Dobretz K, et al. Apoptotic cells provide an unexpected source of Wnt3 signaling to drive hydra head regeneration. Dev Cell 2009;17:279-89.
30. Bonnet D, Dick JE. Human acute myeloid leukemia is organized as a hierarchy that originates from a primitive hematopoietic cell. Nat Med 1997;3:730-7.
31. Al-Hajj M, Wicha MS, Benito-Hernandez A, et al. Prospective identification of tumorigenic breast Cancer cells. Proc Natl Acad Sci U S A 2003;100:3983-8.
32. Bao S, Wu Q, Mclendon RE, et al. Glioma stem cells promote radioresistance by preferential activation of the DNA damage response. Nature 2006;444:756-60.
33. Phillips TM, Mcbride WH, Pajonk F. The response of CD24(-/low)/CD44+ breast cancer-initiating cells to radiation. J Natl Cancer Inst 2006;98:1777-85.
34. Quintana E, Shackleton M, Sabel MS, et al. Efficient tumour formation by single human melanoma cells. Nature 2008;456:593-8.
35. Quintana E, Shackleton M, Foster HR, et al. Phenotypic heterogeneity among tumorigenic melanoma cells from patients that is reversible and not hierarchically organized. Cancer Cell 2010;18:510-23.
36. Lagadec C, Vlashi E, Della Donna L, et al. Radiation-induced reprogramming of breast Cancer cells. Stem Cells 2012;30:833-44.
37. Heddleston JM, Li Z, Mclendon RE, et al. The hypoxic microenvironment maintains glioblastoma stem cells and promotes reprogramming towards a Cancer stem cell phenotype. Cell Cycle 2009;8:3274-84.
38. Charles N, Ozawa T, Squatrito M, et al. Perivascular nitric oxide activates notch signaling and promotes stem-like character in PDGF-induced glioma cells. Cell Stem Cell 2010;6:141-52.
39. Li F, He Z, Shen J, et al. Apoptotic caspases regulate induction of iPSCs from human fibroblasts. Cell Stem Cell 2010;7:508-20.

Cite this article as: Ng WL, Huang Q, Liu X, Zimmerman M, Li F, Li CY. Molecular mechanisms involved in tumor repopulation after radiotherapy. Transl Cancer Res 2013;2(5):442-448. doi: 10.3978/j.issn.2218-676X.2013.10.03

Review Article

Cancer stem cells in glioma: challenges and opportunities

Jialiang Wang[1,2], Yufang Ma[1], Michael K. Cooper[3,4]

[1]Department of Neurological Surgery, [2]Department of Cancer Biology, and [3]Department of Neurology, Vanderbilt University Medical Center, Nashville, TN, USA; [4]Neurology Service, Veterans Affairs TVHS, Nashville, TN 37212, USA

Correspondence to: Jialiang Wang. Vanderbilt University, USA. Email: jialiang.wang@vanderbilt.edu; Michael K. Cooper. Vanderbilt University, USA. Email: michael.cooper@vanderbilt.edu.

Abstract: The discovery of cancer stem cells in glioma has created a paradigm shift in our understanding of this deadly disease. Glioma stem cells exhibit sustained self-renewal and potent tumorigenic potential and differ from their more differentiated progeny in response to current therapies. Recurrent disease is likely derived from glioma stem cells or progeny reprogrammed to gain stem cell-like phenotypes, indicating that the stem cell phenotype is a crucial therapeutic target. While debate over cancer stem cell and clonal evolution models persists, important knowledge has been gained over the past decade from glioma stem cells investigation and clinical impact is expected.

Keywords: Glioma; cancer stem cells

doi: 10.3978/j.issn.2218-676X.2013.08.01

Scan to your mobile device or view this article at: http://www.thetcr.org/article/view/1415/html

Introduction

Malignant gliomas constitute a heterogeneous group of highly infiltrative primary brain tumors with distinct histopathological and molecular features. Each year in the United States, approximately 15,750 individuals are diagnosed with a malignant glioma and an estimated 12,740 patients succumb to this disease (1). These statistics highlight the particularly lethal nature of malignant gliomas and important need for enhanced therapeutic efficacy. Current classifications of glioma are based upon the seminal work of Bailey and Cushing, who in the 1920s named and divided glial tumors according to a putative cell type of origin and stage of cellular development (2). Likewise, efforts to provide more effective therapies continue to be driven by the studies of glioma cells of origin and underlying mechanisms of cellular development and growth. Paramount to these efforts is an evolving understanding of the cellular heterogeneity within gliomas. Thus, while the predominant cell type within an astrocytoma or oligodendroglioma may resemble an astrocyte or oligodendrocyte, respectively, each type of glioma is composed of morphologically, phenotypically and genetically heterogeneous cells.

In this review, two seemingly though not necessarily competing views of glioma heterogeneity are discussed, the stochastic and cancer stem cell models. How recent studies of microenvironmental cues, developmental signaling pathways, and treatment resistance inform our views of glioma heterogeneity, growth and therapy will also be reviewed.

Hierarchical organization *vs.* clonal evolution

Although most cancers, including glioma, appear to be of monoclonal origin, at the time of diagnosis, tumors are composed of genetically and phenotypically heterogeneous clones (3-7). Intratumoral heterogeneity has traditionally been viewed according to a stochastic model outlined by Peter Nowell in 1976 (8). By this perspective, cancer heterogeneity and growth is an evolutionary process whereby neoplasms arise from a single cell of origin and tumor progression results from random accumulation of somatic mutations in genetically unstable cell populations with sequential selection of malignant subclones by environmental constraints (*Figure 1A*). In accordance with this model, it was proposed that each cancer may

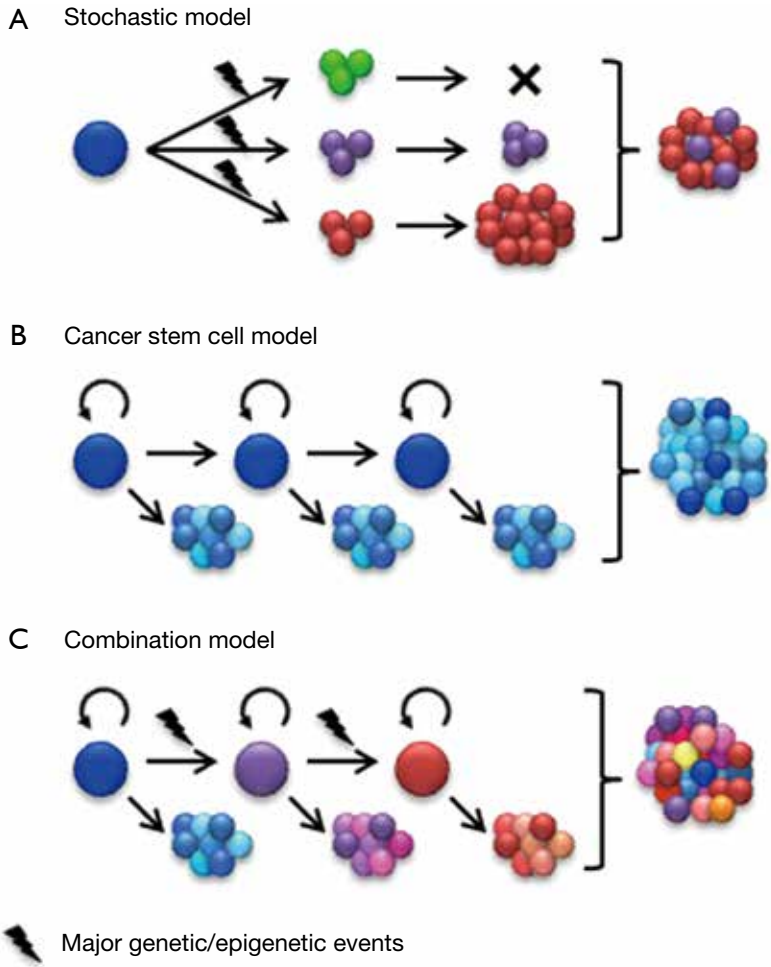

Figure 1 Modeling cellular heterogeneity of cancer. (A) The stochastic model assumes that cancer cell phenotypes are primarily defined by intrinsic factors, in particular driver mutations. It indicates a clonal evolution of cancer. However, this model may not adequately address phenotypic variations within individual clones; (B) The cancer stem cell model assumes that cancer is organized in a hierarchical structure that, at least in part, resembles that of the tissue of origin. Tumorigenic potential is limited to the cancer stem cell subpopulation. In addition, cellular heterogeneity of the cancer is a product of multipotent cancer stem cells. However, the maintenance of coexisting genetically distinct clones in most late-stage cancers has not been adequately addressed by this model; (C) Emerging evidence suggests a combination of these two models in which cancers are driven by one or multiple dominating clones, some of which may be organized in a hierarchical manner. However, at the time of diagnosis, the original hierarchy may be altered due to acquisition of genetic or epigenetic events that promote tumorigenic capacity and impair differentiation.

require individual-specific therapy due to the multitude of potentially random mutations that might drive tumor growth and emergence of treatment resistant subclones from neoplastic cells with roughly equal tumorigenic potential (8).

Recent advances in genomic mapping have unambiguously demonstrated the complex genetic landscape in a wide variety of human tumors (9). Genetic heterogeneity in glioma was initially demonstrated by the presence of subclones with differing karyotype (10). More recent studies show that some glioblastoma tumors comprise subclones carrying amplifications of different receptor tyrosine kinases (RTKs, e.g., *EGFR*, *MET*, *PDGRFA*) in a mutually exclusive manner (11,12). The clonal heterogeneity RTK gene amplification in glioma suggests a mechanism for inherent resistance to agents that target only a single RTK. While clonal heterogeneity has been extensively documented in glioma and many other cancers, accumulating evidence suggests an additional level of

functional heterogeneity based upon cellular differentiation.

Functional heterogeneity among cancer cells was documented decades ago by the demonstration that only a small subset of the cells within a tumor are capable of clonogenic growth in mice or soft agar (13,14). The cancer stem cell (CSC) model suggests a hierarchical organization of functional heterogeneity, with self-sustaining CSCs at the apex giving rise to heterogeneous transit-amplifying and differentiated cancer cell types (*Figure 1B*) (15). Two key outcomes of CSC divisions are differentiation into heterogeneous cancer cell types or self-renewal to sustain a cancer stem cell pool. Compelling evidence that the tumorigenic capacity may be restricted to cancer cells with stem cell phenotype was demonstrated by John Dick and colleagues in their seminal studies of human acute myelogenous leukemia (AML) (16). These landmark studies are supported in other tumor types by xenotransplantation assays showing that tumorigenic cells can be prospectively identified by selection for stem cell markers, whereas the remaining tumor cells are depleted of tumorigenic potential (15).

A fundamental implication of the hierarchical model is that CSCs sustain and fuel tumor growth and that their eradication is crucial to effective therapy. Many aspects of the CSC model remain intensely debated, such as the cell of origin, cell surface markers, and the relative frequencies of CSCs. Nevertheless, several recent lineage-tracing studies provide crucial support of a hierarchical structure in some human cancers, including malignant glioma. These studies demonstrate that the majority of tumor cells have limited proliferative potential and are derived from a subpopulation of cancer cells that exhibit stem cell-like features (17-20). Luis Parada and colleagues crossed one strain of mice genetically engineered to develop gliomas with another strain expressing green fluorescent protein (GFP) under the control of the neural stem cell marker Nestin. In the resulting gliomas, the fraction of tumor cells expressing GFP were relatively quiescent and fulfilled key stem cell features. More importantly, following treatment with temozolomide, the recurrent tumors were derived from GFP-positive cells. Selective depletion of the GFP-positive subpopulation extended survival of experimental animals and improved tumor response to temozolomide (20). Hans Clevers and coworkers identified a minor population of cells expressing the intestinal stem cell marker Lgr5 as the stem cell fraction of intestinal adenoma (18). A cellular hierarchy resembling the organization of normal epidermis has also been revealed by lineage tracing studies in skin papilloma and squamous cell carcinoma (19). Interestingly, the genetically marked CSC pool expanded in malignant squamous cell carcinoma in comparison to benign papilloma (19), suggesting that hierarchical architecture may not be fixed during tumor progression. These results may explain some of the controversy regarding differences in CSC frequencies measured for the same tumor types by different investigators.

While the clonal evolution model and the CSC model interpret intratumoral heterogeneity in different ways, it is important to note that they are not mutually exclusive. Major genetic events continuously accumulate in CSCs and their progenies, which progressively gives rise to genetically distinguished new clones. These new clones may or may not be organized in a hierarchical structure. Therefore, the diversity in reported phenotypes of CSCs may in part reflect complexities of cancer genomes. Two recent studies analyzed the genetic diversity of CSCs in acute lymphoblastic leukemia driven by either BCR-ABL (breakpoint cluster region protein-Abelson murine leukemia viral oncogene homolog 1) or ETV6-RUNX1 (Ets Variant 6-Runt-related transcription factor 1) fusion genes (21,22). In these relatively less complex blood cancers, CSCs exhibited significant genetic diversity that reflects a branching clonal evolution. Importantly, xenografts and recurrent tumors were not always derived from the dominant clones, suggesting that CSCs of minor subclones may also be of clinical significance (21,22). On the other hand, CSCs isolated from different tumor types may share common phenotypes irrespective of their tissue background. For example CD133 expression is associated with CSCs from brain tumors and a wide range of other malignancies (23). Although direct experimental evidence is still emerging, the cellular complexity of many human cancers is likely the result of a combination of clonal genetic events and hierarchical differentiation (*Figure 1C*). The existence of genetically and phenotypically distinct cell populations within an individual's tumor represents significant challenges to develop effective targeted therapies. Genetic diversity needs to be taken into account as we gain a better understanding of mechanisms commonly implicated in tumorigenic potential, therapeutic resistance, and other crucial phenotypes of CSCs.

Identity of glioma stem cells

A major advance in study of CSC is the ability to identify them among the rest of the tumor cells by phenotypic

markers. Glioma stem cells (GSCs) were first identified by selection for the neural and hematopoietic stem cell marker, CD133 (prominin) (24,25). In these seminal studies, 100 CD133+ glioma cells were sufficient to develop xenografted tumors that recapitulated the heterogeneity of the original tumor, while CD133- tumor cells were effectively depleted for tumorigenic potential. Subsequent studies have either substantiated or challenged the specificity of CD133 as the GSC marker. Tumorigenic CD133- cells have been identified in different samples or even within the same tumors that contain CD133+ GSCs (26-29). These controversial observations can only be partially explained by a lack of technical consensus. Alternatively, the role of CD133 as the stem cell marker may vary in different molecular subtypes of glioma. Multiple groups have shown that gliomas driven by CD133+ cells exhibit transcription profiles resembling the proneural subtype, whereas CD133- GSCs may be associated with gliomas of the mesenchymal subtype (30-32). Further, Heidi Philips and colleagues have provided evidence for a more complex hierarchy driven by CD133- GSCs, which give rise to CD133+ intermediate progenitors and then CD133- differentiated progenies (33). In addition to CD133, a variety of other markers have been described, such as CD15, L1CAM, integrin α6, and A2B5 (28,34-36). Robust methods that can reproducibly identify and enrich for GSCs are of paramount importance to the field. However, it is conceivable that genetically and phenotypically diverse GSCs cannot be encompassed by a universal marker. With advances in high-throughput technologies for genomics and epigenomics, markers selective for subtypes of GSCs may be anticipated.

The crosstalk between glioma stem cells and their niche

Stem cell number and growth rate are tightly regulated by microenvironmental cues (a.k.a. niche). Like their normal counterparts, CSCs are affected by microenvironment factors. Therefore, disrupting the crosstalk between CSCs and their niches appear to be attractive therapeutic strategies. At least two types of niches have been identified for GSCs. Each is associated with a pathological hallmark of this disease, namely aberrant vascular proliferation and hypoxia-associated necrosis (37). Glioma is a highly angiogenic tumor, and GSCs are enriched in perivascular regions (38), where a variety of regional signals have been found to promote CSC phenotypes. Endothelial cells express Notch ligands, such as jagged1 (JAG1) and delta-like ligand 4 (DLL4) that activate Notch signaling in GSCs residing in perivascular region (39). The perivascular region is also enriched for extracellular matrix proteins that are capable of promoting proliferation, survival and migration of GSCs. For example, integrin α6 is highly expressed in perivascular GSCs and possibly functions as the receptor of laminin in the perivascular niche (35,40). GSCs are not passive residents of their niche, rather these cells play active roles in shaping tumor vasculature. GSCs produce high levels of pro-angiogenic factors, such as vascular endothelia growth factor (VEGF) (41). GSCs also produce differentiated progenies that exhibit features of endothelial cells and contribute to formation of cancer-specific vasculature (42-44). Similar observations have been made in other cancers, such as melanoma (45). More recently, Bao and colleagues demonstrate that GSCs are also a source of vascular pericytes (46). While it has been well documented that malignant cells are actively involved in cancer vasculature (a.k.a. vasculogenic mimicry) (47), these emerging results suggest that CSCs are key regulators of this process. Blood vessels formed by cancer cells may be pathologically important when proliferation of normal endothelial cells is not sufficient to sustain tumor growth or suppressed by factors such as anti-angiogenic therapy. The VEGF neutralizing antibody, bevacizumab, mitigates many symptoms in patients with recurrent glioblastoma (48). However, treatment with bevacizumab fails to improve patient survival. The ability of GSCs to generate functional blood vessels is one potential hurdle to anti-angiogenic therapy and suggests that it may need to be combined with other treatments that block the transdifferentiation of GSCs.

Malignant glioma, and in particular glioblastoma, is associated with widespread hypoxia (49). Necrosis is a histologic hallmark of glioblastoma and predictor of poor prognosis (50), suggesting that necrosis may promote tumor progression and therapeutic resistance. The necrotic regions of glioblastoma are characterized by severe hypoxia. Low oxygen tension has been shown to promote self-renewal for various types of normal stem cells (51). Emerging evidence further suggests that hypoxia promotes stem cell-like phenotypes in glioma, thus hypoxic regions function as an important niche factor for GSCs (52). The hypoxia inducible factors (HIF) family of transcription factors is a central regulator of tumor response to hypoxia. In particular, HIF2α appears to be a key player in maintenance of stem cells in glioma (53,54). GSCs express higher levels of HIF2α in comparison to non-stem glioma cells and normal neural progenitors (54). Knockdown of HIF2α

specifically compromise proliferation and survival of GSCs, while HIF1α may have important functions in non-stem glioma cells as well (54). Prolonged hypoxic stresses not only stimulate expansion of CD133+ GSCs but also exhibit the potential to reprogram non-stem glioma cells to a CSC-like phenotype (55,56). However, these results should not be over-interpreted, as HIF may directly activate expression of CD133 (57,58). The ability of GSCs to expand under hypoxic condition imposes additional challenges to anti-angiogenic therapy, as reduction in vascular supply may have limited impact on these cells. In fact, compromised tumor vasculature may mobilize GSCs, as a number of anti-angiogenic therapies have been found to stimulate cancer invasion and metastasis (59,60). The plasticity of GSCs to co-opt drastically different tumor microenvironments, again, suggests that combinatorial approaches will be required to effectively disrupt their putative niches.

GSCs and pathways that direct cell fate determination

Vogelstein and colleagues analyzed the seemingly innumerable genetic alterations identified by comprehensive genomic studies in human cancer to identify those that significantly promote or "drive" tumorigenesis. Through this effort, they distilled driver genes into 12 signaling pathways that regulate core cellular processes of cell fate determination, proliferation, survival, and genome maintenance. Key among the signaling pathways regulating cell fate are Notch, Hedgehog, and Wnt (61). These three pathways are instrumental in embryonic development and adult tissue homeostasis. Aberrant activation of these pathways promotes stem cell-like phenotypes in cancer and dampens CSC differentiation (62). Although components of these three pathways are not frequently mutated in glioma, they appear to be crucial GSCs niche factors and thus attractive therapeutic targets.

Notch signaling pathway

The Notch signaling pathway is an evolutionarily conserved mechanism that regulates cell fate determination across many tissue types (63). Notch receptors are activated by ligands expressed on the surface of neighboring cells. The intracellular domains of activated Notch receptors are proteolytically released by the γ-secretase complex, translocate into nucleus, and subsequently activate transcription of Notch-responsive target genes. During embryonic development, Notch signaling plays critical roles to maintain neural stem cell proliferation, survival and self-renewal (64). In contrast, EGFR activation leads to expansion of progenitor cells (65). Crosstalk between the Notch and EGFR pathways regulates a crucial balance between neural stem and progenitor cells. Disruption of Notch signaling in the embryonic mouse brain by knockout of the DNA binding subunit RBPJ/CBF1 (recombining binding protein suppressor of hairless) or the catalytic subunit of γ-secretase (presenilin-1) promotes premature neuronal differentiation with profound consequences on neural development (66,67). Notch signaling also regulates stem cells in adult tissue homeostasis, including the brain (68), and aberrant Notch signaling has been widely implicated in cancer.

The oncogenic function of Notch pathway activation is best exemplified by the presence of activating mutations in Notch1 in more than half of human T-cell acute lymphoblastic leukemias (69). While genetic alterations of the Notch pathway are rare in glioma, Notch signaling can be activated by a variety of microenvironmental cues. In xenotransplantation assays, the addition of human brain microvascular endothelial cells improves the tumorigenic potential of glioblastoma sphere cells, and the effect is abolished upon knockdown of Notch ligands, JAG1 or DLL4, in endothelial cells (39). In colorectal cancer, endothelial cells produce a soluble form of JAG1 that promotes CSC phenotypes (70). In addition to the expression of Notch ligands, endothelial cells also produce nitric oxide that induces Notch activation in perivascular glioma cells (71). Blockade of Notch signaling by γ-secretase inhibitors (GSIs) reduces proliferation, neurosphere formation, and tumorigenic potential of GSCs (72). In addition to these effects on GSC proliferation, it is worth noting that Notch inhibition compromises the ability of GSCs to resist radiation as well as temozolomide (73,74).

Multiple GSIs have entered clinical trials. The first clinical evidence for potential efficacy came from a recent phase I clinical trial of a Merck GSI, MK-0752, in patients with advanced solid tumors that included glioma. Stable disease was reported in about 24% of patients with advanced glioma in addition to a complete response in one patient with a grade III glioma (75). Of particular interest in this trial, clinical response of MK-0752 was predominantly found in adult patients with glioma. However, the efficacy of MK-0752 in refractory pediatric brain cancers was not significant (76). Another GSI, RO4929097 (Roche), also exhibited moderate clinical efficacy in a phase I trial, though

the trial was not focused on glioma (77). Trials combining GSIs with other therapeutic modality are currently ongoing in glioblastoma and other cancers (e.g., clinicaltrials.gov identifier-NCT01119599 and NCT01098344).

Wnt signaling pathway

The Wnt family of secreted signaling proteins and their receptors have important functions in embryonic development, particularly in tissue patterning (78). The central player of the canonical Wnt signaling is the cytoplasmic protein β-catenin. In the absence of Wnt pathway stimulation, β-catenin is constitutively degraded by a destruction complex and Wnt target gene expression is repressed by DNA-bound TCF/LEF (T-cell factor and lymphoid enhancing factor) transcription factors. Binding of Wnt ligands to the Frizzled family of receptors inhibits kinase activity of the destruction complex, leading to stabilization and nuclear translocation of β-catenin. Nuclear β-catenin converts TCF/LEF into a transcription activator of Wnt target genes that induce downstream signaling (79). The function of the Wnt pathway in tumorigenesis is best documented in colorectal cancer. Mutational inactivation of Adenomatous polyposis coli (APC), a scaffolding protein of the destruction complex, plays a key role in development of hereditary and sporadic colorectal cancer (80,81). Lgr5, a Wnt receptor, is preferentially expressed in both normal and malignant stem cells of colon and intestine (18,82). Though the roles of Wnt signaling in glioma are less understood, β-catenin is essential for neuronal progenitor cell proliferation (83) and the expression of Wnt1, β-catenin, and the downstream target cyclin D1 has been demonstrated in a considerable percentage of gliomas and correlate with increasing World Health Organization tumor grade (84). PLAGL*2* (pleomorphic adenoma gene-like 2) is a recently identified proto-oncogene that is amplified in glioma and promotes proliferation and self-renewal of GSCs (85). The ability of PLAGL2 to regulate "stemness" in glioma and normal neural tissues is attributable in part to activation of the Wnt pathway (85). Like PLAGL2, additional transcription factors overexpressed in glioblastoma, such as Forkhead box protein M1 (FOXM1) and Achaete-scute homolog 1 (ASCL1), also cooperate with the Wnt/β-catenin pathway to regulate stemness of GSCs (86,87). However, controversial results have been reported. In primary glioblastoma cells, activation of Wnt signaling promotes neuronal differentiation and compromises malignant phenotypes of CD133+ glioblastoma cells, particularly in a hypoxic microenvironment (88). These effects appear to be mediated, at least in part, via antagonism of Notch signaling (88). The different roles of Wnt signaling in glioma may reflect the genetic heterogeneity of this disease. A recent study showed that the Wnt pathway is a downstream target of MET in glioblastoma stem cells (89). MET is a tyrosine receptor kinase frequently amplified in glioblastoma and associated with the mesenchymal subtype (90,91). Therefore, the functions of Wnt signaling may vary in different molecular subtype of glioma, which demands further investigation.

Hedgehog signaling pathway

Hedgehog secreted signaling proteins are critical for embryonic tissue development (patterning) and postnatal tissue homeostasis (92,93). Aberrant activation of the Hedgehog pathway has been implicated in the growth of many malignancies in a role that is largely attributed to action of the pathway on stem or progenitor cells (94). Cellular responses to Hedgehog signaling are regulated through the primary cilium by the transmembrane proteins Patched-1 (PTCH1) and Smoothened (SMOH) (95). PTCH1 functions to suppress the activity of Smoothened. Hedgehog ligand binding to PTCH1 inhibits this function to activate the GLI family of transcription factors. *PTCH1* and *GLI1* are transcriptional gene targets of Hedgehog signaling, and in the proper context their expression levels can be used to monitor Hedgehog pathway activity in malignancies.

A role for aberrant Hedgehog signaling in tumorigenesis was first appreciated by the series of discoveries that mutations in the Hedgehog signal transduction components PTCH1 and SMOH may confer ligand-independent pathway activation in heritable (Gorlin or basal cell nevus syndrome) and sporadic forms of medulloblastoma and basal cell carcinoma (BCC) (96-99). Shortly afterwards, studies of an acquired form of cyclopia (100,101) identified the teratogen cyclopamine as a potent inhibitor of Hedgehog signal reception through direct binding and antagonism of SMOH (102-104). Cyclopamine is a plant-derived alkaloid and several synthetic SMOH antagonists have since been identified that appear to bind the same sight as cyclopamine but with enhanced efficacy for inhibiting SMOH bearing oncogenic mutations (105). Some of the SMOH antagonists have progressed into clinical trial and one, vismodegib (GDC-0449; Genentech), has received approval by the FDA for treatment of adults with metastatic BCC or locally

advanced disease who are not candidates for surgery or radiation (106). Enthusiasm for dramatic initial response to GDC-0449 in a patient with metastatic medulloblastoma was dampened by the emergence of treatment resistance with disease relapse (107). Gene sequencing of the recurrent disease, however, identified acquisition of a SMOH missense mutation that decreased GDC-0449 binding affinity (108), demonstrating the critical importance of Hedgehog pathway activation for tumor growth and offering hope for the efficacy of other mechanistically diverse Hedgehog inhibitors.

In contrast to medulloblastoma and BCC in which the Hedgehog pathway is constitutively activated by pathway component mutation, ligand-dependent activation of the Hedgehog pathway in the absence of mutation has been identified in a broader array of malignancies (109). In these tumors, the Hedgehog pathway appears to be activated in a small population of cells that have been proposed to have stem or progenitor-like features (92). Although the Hedgehog transcription factor GLI1 was first discovered (and named) as a gene that was amplified in a glioblastoma cell line (110), *GLI1* gene amplification or other genomic alterations in Hedgehog pathway components are generally absent in gliomas (91,111). Instead, the Hedgehog pathway is activated by a ligand-dependent mechanism in gliomas (112-114). Activation of the pathway in GSCs regulates tumor growth and inhibition of the pathway in preclinical animal models confers a significant survival advantage (112,113,115).

In contrast to Wnt signaling, where pathway component expression levels correlate with tumor grade, Hedgehog component and gene target expression is higher among grades II and III gliomas than in grade IV gliomas (113,114). Further, the Hedgehog pathway is not operant in all malignant gliomas (114,115) and thus the clinical utility of targeting this pathway could be enhanced by clear identification of Hedgehog-responsive glioma subtypes. Somatic mutations in the isocitrate dehydrogenase (IDH) gene have recently emerged as a surrogate marker for identifying gliomas with an operant Hedgehog pathway (116). In adult gliomas, *IDH* mutations occur in more than 70% of diffuse astrocytomas, oligodendrogliomas, oligoastrocytomas and secondary glioblastomas that evolve from lower grade astrocytomas (117,118). Conversely, *IDH* mutation occurs in less than 7% of primary glioblastomas, which occur without evidence or antecedent disease and represent greater than 95% of glioblastomas. Increasing evidence suggests that *IDH* mutation is an early genetic alteration in a common cell of origin for astrocytic or oligodendroglial tumors that is distinct from the cellular origin for primary glioblastoma (119,120). The Hedgehog pathway is frequently activated in secondary glioblastoma and lower-grade gliomas carrying *IDH* mutations. Taken together, these observations suggest an interesting model whereby lower grade infiltrating gliomas and secondary glioblastoma arise from Hedgehog-dependent cell types and primary glioblastoma from cell types that are not Hedgehog responsive (116).

Glioma stem cells and resistance to radiation

Adult gliomas are highly infiltrative and cannot be completely removed by surgery. Radiation and temozolomide are the primary adjuvant therapies for malignant gliomas. Response to chemoradiotherapy in malignant glioma is generally short-lived, and the almost universal recurrence suggests inadequate eradication of tumorigenic cells (121). Identification of CSCs in glioma provides fresh mechanistic insights into intrinsic resistance to radiation and chemotherapy. GSCs appear to substantially differ in response to radiation in comparison to differentiated cancer cells, although some controversy persists (122). The percentage of CD133+ cells within malignant gliomas markedly increases following radiotherapy (123). CD133+ cells are also enriched in glioma tumorsphere cultures and orthotopic tumors following radiation, potentially due an inherent capacity of GSCs to more effectively repair radiation-induced DNA damage (122). In addition, the CD133+ subpopulation is preferentially protected in a physiologically relevant microenvironment, associated with fewer phosphorylated histone H2AX (γH2AX) and TP53 binding protein 1 (53BP1) loci than CD133- cells within the same tumor (124). Ropolo and colleagues found no difference in DNA base excision, single-strand break repair, or γH2AX foci resolution between patient-derived glioblastoma spheroid cultures and differentiated cells or established cell lines grown in serum-containing medium (125). However, enhanced basal activation of DNA damage checkpoint kinases Chk1 and Chk2 in CD133+ cells may protect these cells against radiation (125). In addition to DNA damage repair mechanisms, a variety of signaling pathways that are preferentially activated in GSCs may protect these cells from radiation-induced toxicity. Ionizing radiation activates Notch in GSCs, and Notch signaling confers protection from radiation via an Akt-mediated mechanism (73). Wnt and MET also exhibits radioprotective functions in GSCs

(126,127) as well as breast CSCs (128). Conflicting results have been reported comparing the radiation response between GSCs and non-stem glioma cells. For example, McCord and colleagues observed that CD133+ GSCs derived from surgical specimens were more radiosensitive than established glioma cell lines based on clonogenic assays (129). The CD133+ primary cultures actually exhibited a defective DNA damage checkpoint (129). Pallini and colleagues found significantly higher percentage of CD133+ cells in recurrent specimens based on examination of 37 paired glioblastoma samples (130). Interestingly, the percentage of CD133+ cells correlated with longer survival after tumor recurrence. Further studies suggested that a significant portion of the CD133+ cells in recurrent glioblastoma specimens were normal neural stem cells with potential antineoplastic activity (130). Discrepancies with regard to the radiation responses of GSCs may reflect technical difficulties of identifying GSCs, thus highlighting significant challenges in this field of study. Genetic heterogeneity in samples generates additional difficulties in interpreting these results. Lineage tracing assays provide an alternative strategy to interrogate therapeutic response of specific cellular subpopulations.

Conclusions and outlooks

While not all cancers may contain hierarchical organization, the existence of CSCs in glioma has been extensively documented and validated by rigorous measures including serial transplantation and *in vivo* lineage tracing assays (20,25). Introduction of the CSC concept into brain cancer research has led to a paradigm shift and significant advances in the field. For example, it has been convincingly demonstrated that the genomic integrity and cellular heterogeneity of patient tumors cannot be maintained in widely used established glioma cell lines (131). In contrast, culture conditions designed for normal neural progenitors and GSCs preserve the phenotypes and genotypes of patient tumors and thus represent a more physiologically relevant *in vitro* model (132). The ability of GSCs to repopulate the original tumor following treatment and their inherent potentials for conferring treatment resistance indicate that GSCs are crucial targets for novel therapeutics. Over the past decade, a rapidly growing list of novel targets has been identified by interrogating the biology of GSCs, including the developmental signaling pathways, Notch, Wnt and Hedgehog. Other targets in GSCs have emerged, such as the epigenetic regulators-EZH2 (133,134), kinases-bone marrow X-linked (BMX) and maternal embryonic leucine-zipper kinase (MELK) (135,136), and transcription factors like STAT3, REST, and MYC (137-139). Notably, and potentially introducing another layer of complexity, in the majority of these studies, the glioma molecular subtypes are not determined, and thus the roles of these novel targets among gliomas of different molecular subtypes remain unclear. Future studies of GSC-targeted therapy will need to establish links with glioma molecular subtypes in order to design more selective and effective clinical trials.

Lastly, it is important to note that while GSCs represent crucial therapeutic targets, differentiated glioma cells are not merely bystanders. Although there is still a lack of direct experimental evidence, the hierarchical structure of glioma may not be as strict as that of normal tissues. Both mature astrocytes and neurons can be genetically reprogramed to confer stem and glioma-initiating properties (140-142). Reprogramming might also be induced by environmental factors, such as low pH, hypoxia and even stem cell culture condition (56,143,144). Dedifferentiation may even be accelerated by treatments that change the microenvironment and increase mutations rates.

Recent advances in the study of the cancer genome and epigenome are rapidly transforming research in the field of neuro-oncology. Studies of GSCs in malignant gliomas with defined genetic backgrounds will likely offer greater success in identifying important drug targets that are tailored for individual glioma subtypes. In addition, targeting the microenvironment may more broadly impact GSCs irrespectively of genetic background and possibly reduce the rate of dedifferentiation. To considerably improve outcomes of clinical trials, combinations of multiple therapeutic modalities that target GSCs as well as their microenvironment appear to be essential.

Acknowledgements

Disclosure: This work is supported in part by the National Institutes of Health grant 1R01CA166492 (to J.W.) and the Department of Veterans Affairs grant 1I01BX000744-01 (to M. K. C.). The contents do not represent the views of the Department of Veterans Affairs or the United States Government.

References

1. Dolecek TA, Propp JM, Stroup NE, et al. CBTRUS statistical report: primary brain and central nervous system

tumors diagnosed in the United States in 2005-2009. Neuro Oncol 2012;14:v1-49.
2. Bailey P, Cushing H. A classification of the tumors of the glioma group on a histogenetic basis with a correlated study of prognosis. Philadelphia:Lippincott.1926.
3. Greaves M, Maley CC. Clonal evolution in cancer. Nature 2012;481:306-13.
4. Campbell PJ, Pleasance ED, Stephens PJ, et al. Subclonal phylogenetic structures in cancer revealed by ultra-deep sequencing. Proc Natl Acad Sci U S A 2008;105:13081-6.
5. Ding L, Ellis MJ, Li S, et al. Genome remodelling in a basal-like breast cancer metastasis and xenograft. Nature 2010;464:999-1005.
6. Navin N, Kendall J, Troge J, et al. Tumour evolution inferred by single-cell sequencing. Nature 2011;472:90-4.
7. Marusyk A, Polyak K. Tumor heterogeneity: causes and consequences. Biochim Biophys Acta 2010;1805:105-17.
8. Nowell PC. The clonal evolution of tumor cell populations. Science 1976;194:23-8.
9. Aparicio S, Caldas C. The implications of clonal genome evolution for cancer medicine. N Engl J Med 2013;368:842-51.
10. Shapiro JR, Yung WK, Shapiro WR. Isolation, karyotype, and clonal growth of heterogeneous subpopulations of human malignant gliomas. Cancer Res 1981;41:2349-59.
11. Little SE, Popov S, Jury A, et al. Receptor tyrosine kinase genes amplified in glioblastoma exhibit a mutual exclusivity in variable proportions reflective of individual tumor heterogeneity. Cancer Res 2012;72:1614-20.
12. Snuderl M, Fazlollahi L, Le LP, et al. Mosaic amplification of multiple receptor tyrosine kinase genes in glioblastoma. Cancer Cell 2011;20:810-7.
13. Bruce WR, Van Der Gaag H. A quantitative assay for the number of murine lymphoma cells capable of proliferation in vivo. Nature 1963;199:79-80.
14. Hamburger AW, Salmon SE. Primary bioassay of human tumor stem cells. Science 1977;197:461-3.
15. Clarke MF, Dick JE, Dirks PB, et al. Cancer stem cells--perspectives on current status and future directions: AACR Workshop on cancer stem cells. Cancer Res 2006;66:9339-44.
16. Lapidot T, Sirard C, Vormoor J, et al. A cell initiating human acute myeloid leukaemia after transplantation into SCID mice. Nature 1994;367:645-8.
17. Humphries A, Cereser B, Gay LJ, et al. Lineage tracing reveals multipotent stem cells maintain human adenomas and the pattern of clonal expansion in tumor evolution. Proc Natl Acad Sci U S A 2013;110:E2490-9.
18. Schepers AG, Snippert HJ, Stange DE, et al. Lineage tracing reveals Lgr5+ stem cell activity in mouse intestinal adenomas. Science 2012;337:730-5.
19. Driessens G, Beck B, Caauwe A, et al. Defining the mode of tumour growth by clonal analysis. Nature 2012;488:527-30.
20. Chen J, Li Y, Yu TS, et al. A restricted cell population propagates glioblastoma growth after chemotherapy. Nature 2012;488:522-6.
21. Anderson K, Lutz C, van Delft FW, et al. Genetic variegation of clonal architecture and propagating cells in leukaemia. Nature 2011;469:356-61.
22. Notta F, Mullighan CG, Wang JC, et al. Evolution of human BCR-ABL1 lymphoblastic leukaemia-initiating cells. Nature 2011;469:362-7.
23. Mizrak D, Brittan M, Alison M. CD133: molecule of the moment. J Pathol 2008;214:3-9.
24. Singh SK, Clarke ID, Terasaki M, et al. Identification of a cancer stem cell in human brain tumors. Cancer Res 2003;63:5821-8.
25. Singh SK, Hawkins C, Clarke ID, et al. Identification of human brain tumour initiating cells. Nature 2004;432:396-401.
26. Beier D, Hau P, Proescholdt M, et al. CD133(+) and CD133(-) glioblastoma-derived cancer stem cells show differential growth characteristics and molecular profiles. Cancer Res 2007;67:4010-5.
27. Nishide K, Nakatani Y, Kiyonari H, et al. Glioblastoma formation from cell population depleted of Prominin1-expressing cells. PLoS One 2009;4:e6869.
28. Ogden AT, Waziri AE, Lochhead RA, et al. Identification of A2B5+CD133- tumor-initiating cells in adult human gliomas. Neurosurgery 2008;62:505-14; discussion 514-5.
29. Wang J, Sakariassen PØ, Tsinkalovsky O, et al. CD133 negative glioma cells form tumors in nude rats and give rise to CD133 positive cells. Int J Cancer 2008;122:761-8.
30. Lottaz C, Beier D, Meyer K, et al. Transcriptional profiles of CD133+ and CD133- glioblastoma-derived cancer stem cell lines suggest different cells of origin. Cancer Res 2010;70:2030-40.
31. Joo KM, Kim SY, Jin X, et al. Clinical and biological implications of CD133-positive and CD133-negative cells in glioblastomas. Lab Invest 2008;88:808-15.
32. Mao P, Joshi K, Li J, et al. Mesenchymal glioma stem cells are maintained by activated glycolytic metabolism involving aldehyde dehydrogenase 1A3. Proc Natl Acad Sci U S A 2013;110:8644-9.
33. Chen R, Nishimura MC, Bumbaca SM, et al. A hierarchy

of self-renewing tumor-initiating cell types in glioblastoma. Cancer Cell 2010;17:362-75.
34. Son MJ, Woolard K, Nam DH, et al. SSEA-1 is an enrichment marker for tumor-initiating cells in human glioblastoma. Cell Stem Cell 2009;4:440-52.
35. Lathia JD, Gallagher J, Heddleston JM, et al. Integrin alpha 6 regulates glioblastoma stem cells. Cell Stem Cell 2010;6:421-32.
36. Bao S, Wu Q, Li Z, et al. Targeting cancer stem cells through L1CAM suppresses glioma growth. Cancer Res 2008;68:6043-8.
37. Filatova A, Acker T, Garvalov BK. The cancer stem cell niche(s): the crosstalk between glioma stem cells and their microenvironment. Biochim Biophys Acta 2013;1830:2496-508.
38. Calabrese C, Poppleton H, Kocak M, et al. A perivascular niche for brain tumor stem cells. Cancer Cell 2007;11:69-82.
39. Zhu TS, Costello MA, Talsma CE, et al. Endothelial cells create a stem cell niche in glioblastoma by providing NOTCH ligands that nurture self-renewal of cancer stem-like cells. Cancer Res 2011;71:6061-72.
40. Lathia JD, Li M, Hall PE, et al. Laminin alpha 2 enables glioblastoma stem cell growth. Ann Neurol 2012;72:766-78.
41. Bao S, Wu Q, Sathornsumetee S, et al. Stem cell-like glioma cells promote tumor angiogenesis through vascular endothelial growth factor. Cancer Res 2006;66:7843-8.
42. Ricci-Vitiani L, Pallini R, Biffoni M, et al. Tumour vascularization via endothelial differentiation of glioblastoma stem-like cells. Nature 2010;468:824-8.
43. Soda Y, Marumoto T, Friedmann-Morvinski D, et al. Transdifferentiation of glioblastoma cells into vascular endothelial cells. Proc Natl Acad Sci U S A 2011;108:4274-80.
44. Wang R, Chadalavada K, Wilshire J, et al. Glioblastoma stem-like cells give rise to tumour endothelium. Nature 2010;468:829-33.
45. Lai CY, Schwartz BE, Hsu MY. CD133+ melanoma subpopulations contribute to perivascular niche morphogenesis and tumorigenicity through vasculogenic mimicry. Cancer Res 2012;72:5111-8.
46. Cheng L, Huang Z, Zhou W, et al. Glioblastoma stem cells generate vascular pericytes to support vessel function and tumor growth. Cell 2013;153:139-52.
47. Folberg R, Hendrix MJ, Maniotis AJ. Vasculogenic mimicry and tumor angiogenesis. Am J Pathol 2000;156:361-81.
48. Kunnakkat S, Narayana A. Bevacizumab in the treatment of high-grade gliomas: an overview. Angiogenesis 2011;14:423-30.
49. Evans SM, Judy KD, Dunphy I, et al. Hypoxia is important in the biology and aggression of human glial brain tumors. Clin Cancer Res 2004;10:8177-84.
50. Barker FG 2nd, Davis RL, Chang SM, et al. Necrosis as a prognostic factor in glioblastoma multiforme. Cancer 1996;77:1161-6.
51. Davy P, Allsopp R. Hypoxia: are stem cells in it for the long run? Cell Cycle 2011;10:206-11.
52. Li Z, Rich JN. Hypoxia and hypoxia inducible factors in cancer stem cell maintenance. Curr Top Microbiol Immunol 2010;345:21-30.
53. Seidel S, Garvalov BK, Wirta V, et al. A hypoxic niche regulates glioblastoma stem cells through hypoxia inducible factor 2 alpha. Brain 2010;133:983-95.
54. Li Z, Bao S, Wu Q, et al. Hypoxia-inducible factors regulate tumorigenic capacity of glioma stem cells. Cancer Cell 2009;15:501-13.
55. Soeda A, Park M, Lee D, et al. Hypoxia promotes expansion of the CD133-positive glioma stem cells through activation of HIF-1alpha. Oncogene 2009;28:3949-59.
56. Heddleston JM, Li Z, McLendon RE, et al. The hypoxic microenvironment maintains glioblastoma stem cells and promotes reprogramming towards a cancer stem cell phenotype. Cell Cycle 2009;8:3274-84.
57. Ohnishi S, Maehara O, Nakagawa K, et al. Hypoxia-Inducible Factors Activate CD133 Promoter through ETS Family Transcription Factors. PLoS One 2013;8:e66255.
58. Griguer CE, Oliva CR, Gobin E, et al. CD133 is a marker of bioenergetic stress in human glioma. PLoS One 2008;3:e3655.
59. Pàez-Ribes M, Allen E, Hudock J, et al. Antiangiogenic therapy elicits malignant progression of tumors to increased local invasion and distant metastasis. Cancer Cell 2009;15:220-31.
60. Ebos JM, Lee CR, Cruz-Munoz W, et al. Accelerated metastasis after short-term treatment with a potent inhibitor of tumor angiogenesis. Cancer Cell 2009;15:232-9.
61. Vogelstein B, Papadopoulos N, Velculescu VE, et al. Cancer genome landscapes. Science 2013;339:1546-58.
62. Takebe N, Ivy SP. Controversies in cancer stem cells: targeting embryonic signaling pathways. Clin Cancer Res 2010;16:3106-12.
63. Bolós V, Grego-Bessa J, de la Pompa JL. Notch signaling in development and cancer. Endocr Rev 2007;28:339-63.
64. Lathia JD, Mattson MP, Cheng A. Notch: from neural

development to neurological disorders. J Neurochem 2008;107:1471-81.
65. Aguirre A, Rubio ME, Gallo V. Notch and EGFR pathway interaction regulates neural stem cell number and self-renewal. Nature 2010;467:323-7.
66. Handler M, Yang X, Shen J. Presenilin-1 regulates neuronal differentiation during neurogenesis. Development 2000;127:2593-606.
67. Imayoshi I, Sakamoto M, Yamaguchi M, et al. Essential roles of Notch signaling in maintenance of neural stem cells in developing and adult brains. J Neurosci 2010;30:3489-98.
68. Ables JL, Breunig JJ, Eisch AJ, et al. Not(ch) just development: Notch signalling in the adult brain. Nat Rev Neurosci 2011;12:269-83.
69. Weng AP, Ferrando AA, Lee W, et al. Activating mutations of NOTCH1 in human T cell acute lymphoblastic leukemia. Science 2004;306:269-71.
70. Lu J, Ye X, Fan F, et al. Endothelial cells promote the colorectal cancer stem cell phenotype through a soluble form of Jagged-1. Cancer Cell 2013;23:171-85.
71. Charles N, Ozawa T, Squatrito M, et al. Perivascular nitric oxide activates notch signaling and promotes stem-like character in PDGF-induced glioma cells. Cell Stem Cell 2010;6:141-52.
72. Fan X, Khaki L, Zhu TS, et al. NOTCH pathway blockade depletes CD133-positive glioblastoma cells and inhibits growth of tumor neurospheres and xenografts. Stem Cells 2010;28:5-16.
73. Wang J, Wakeman TP, Lathia JD, et al. Notch promotes radioresistance of glioma stem cells. Stem Cells 2010;28:17-28.
74. Gilbert CA, Daou MC, Moser RP, et al. Gamma-secretase inhibitors enhance temozolomide treatment of human gliomas by inhibiting neurosphere repopulation and xenograft recurrence. Cancer Res 2010;70:6870-9.
75. Krop I, Demuth T, Guthrie T, et al. Phase I pharmacologic and pharmacodynamic study of the gamma secretase (Notch) inhibitor MK-0752 in adult patients with advanced solid tumors. J Clin Oncol 2012;30:2307-13.
76. Fouladi M, Stewart CF, Olson J, et al. Phase I trial of MK-0752 in children with refractory CNS malignancies: a pediatric brain tumor consortium study. J Clin Oncol 2011;29:3529-34.
77. Tolcher AW, Messersmith WA, Mikulski SM, et al. Phase I study of RO4929097, a gamma secretase inhibitor of Notch signaling, in patients with refractory metastatic or locally advanced solid tumors. J Clin Oncol 2012;30:2348-53.
78. Clevers H, Nusse R. Wnt/β-catenin signaling and disease. Cell 2012;149:1192-205.
79. Reya T, Clevers H. Wnt signalling in stem cells and cancer. Nature 2005;434:843-50.
80. Fodde R. The APC gene in colorectal cancer. Eur J Cancer 2002;38:867-71.
81. Kinzler KW, Vogelstein B. Lessons from hereditary colorectal cancer. Cell 1996;87:159-70.
82. Barker N, van Es JH, Kuipers J, et al. Identification of stem cells in small intestine and colon by marker gene Lgr5. Nature 2007;449:1003-7.
83. Zechner D, Fujita Y, Hülsken J, et al. beta-Catenin signals regulate cell growth and the balance between progenitor cell expansion and differentiation in the nervous system. Dev Biol 2003;258:406-18.
84. Liu C, Tu Y, Sun X, et al. Wnt/beta-Catenin pathway in human glioma: expression pattern and clinical/prognostic correlations. Clin Exp Med 2011;11:105-12.
85. Zheng H, Ying H, Wiedemeyer R, et al. PLAGL2 regulates Wnt signaling to impede differentiation in neural stem cells and gliomas. Cancer Cell 2010;17:497-509.
86. Rheinbay E, Suvà ML, Gillespie SM, et al. An aberrant transcription factor network essential for Wnt signaling and stem cell maintenance in glioblastoma. Cell Rep 2013;3:1567-79.
87. Zhang N, Wei P, Gong A, et al. FoxM1 promotes β-catenin nuclear localization and controls Wnt target-gene expression and glioma tumorigenesis. Cancer Cell 2011;20:427-42.
88. Rampazzo E, Persano L, Pistollato F, et al. Wnt activation promotes neuronal differentiation of glioblastoma. Cell Death Dis 2013;4:e500.
89. Kim KH, Seol HJ, Kim EH, et al. Wnt/ -catenin signaling is a key downstream mediator of MET signaling in glioblastoma stem cells. Neuro Oncol 2013;15:161-71.
90. Phillips HS, Kharbanda S, Chen R, et al. Molecular subclasses of high-grade glioma predict prognosis, delineate a pattern of disease progression, and resemble stages in neurogenesis. Cancer Cell 2006;9:157-73.
91. Verhaak RG, Hoadley KA, Purdom E, et al. Integrated genomic analysis identifies clinically relevant subtypes of glioblastoma characterized by abnormalities in PDGFRA, IDH1, EGFR, and NF1. Cancer Cell 2010;17:98-110.
92. Beachy PA, Karhadkar SS, Berman DM. Tissue repair and stem cell renewal in carcinogenesis. Nature 2004;432:324-31.
93. Varjosalo M, Taipale J. Hedgehog: functions and

mechanisms. Genes Dev 2008;22:2454-72.
94. Barakat MT, Humke EW, Scott MP. Learning from Jekyll to control Hyde: Hedgehog signaling in development and cancer. Trends Mol Med 2010;16:337-48.
95. Rohatgi R, Scott MP. Patching the gaps in Hedgehog signalling. Nat Cell Biol 2007;9:1005-9.
96. Aszterbaum M, Rothman A, Johnson RL, et al. Identification of mutations in the human PATCHED gene in sporadic basal cell carcinomas and in patients with the basal cell nevus syndrome. J Invest Dermatol 1998;110:885-8.
97. Hahn H, Wicking C, Zaphiropoulous PG, et al. Mutations of the human homolog of Drosophila patched in the nevoid basal cell carcinoma syndrome. Cell 1996;85:841-51.
98. Johnson RL, Rothman AL, Xie J, et al. Human homolog of patched, a candidate gene for the basal cell nevus syndrome. Science 1996;272:1668-71.
99. Reifenberger J, Wolter M, Weber RG, et al. Missense mutations in SMOH in sporadic basal cell carcinomas of the skin and primitive neuroectodermal tumors of the central nervous system. Cancer Res 1998;58:1798-803.
100. Keeler RF, Binns W. Teratogenic compounds of Veratrum californicum (Durand). I. Preparation and characterization of fractions and alkaloids for biologic testing. Can J Biochem 1966;44:819-28.
101. Keeler RF, Binns W. Teratogenic compounds of Veratrum californicum (Durand). V. Comparison of cyclopian effects of steroidal alkaloids from the plant and structurally related compounds from other sources. Teratology 1968;1:5-10.
102. Chen JK, Taipale J, Cooper MK, et al. Inhibition of Hedgehog signaling by direct binding of cyclopamine to Smoothened. Genes Dev 2002;16:2743-8.
103. Cooper MK, Porter JA, Young KE, et al. Teratogen-mediated inhibition of target tissue response to Shh signaling. Science 1998;280:1603-7.
104. Taipale J, Chen JK, Cooper MK, et al. Effects of oncogenic mutations in Smoothened and Patched can be reversed by cyclopamine. Nature 2000;406:1005-9.
105. Lin TL, Matsui W. Hedgehog pathway as a drug target: Smoothened inhibitors in development. Onco Targets Ther 2012;5:47-58.
106. Axelson M, Liu K, Jiang X, et al. U.S. Food and Drug Administration approval: vismodegib for recurrent, locally advanced, or metastatic basal cell carcinoma. Clin Cancer Res 2013;19:2289-93.
107. Rudin CM, Hann CL, Laterra J, et al. Treatment of medulloblastoma with hedgehog pathway inhibitor GDC-0449. N Engl J Med 2009;361:1173-8.
108. Yauch RL, Dijkgraaf GJ, Alicke B, et al. Smoothened mutation confers resistance to a Hedgehog pathway inhibitor in medulloblastoma. Science 2009;326:572-4.
109. Rubin LL, de Sauvage FJ. Targeting the Hedgehog pathway in cancer. Nat Rev Drug Discov 2006;5:1026-33.
110. Kinzler KW, Bigner SH, Bigner DD, et al. Identification of an amplified, highly expressed gene in a human glioma. Science 1987;236:70-3.
111. Bigner SH, Wong AJ, Mark J, et al. Relationship between gene amplification and chromosomal deviations in malignant human gliomas. Cancer Genet Cytogenet 1987;29:165-70.
112. Bar EE, Chaudhry A, Lin A, et al. Cyclopamine-mediated hedgehog pathway inhibition depletes stem-like cancer cells in glioblastoma. Stem Cells 2007;25:2524-33.
113. Clement V, Sanchez P, de Tribolet N, et al. HEDGEHOG-GLI1 signaling regulates human glioma growth, cancer stem cell self-renewal, and tumorigenicity. Curr Biol 2007;17:165-72.
114. Ehtesham M, Sarangi A, Valadez JG, et al. Ligand-dependent activation of the hedgehog pathway in glioma progenitor cells. Oncogene 2007;26:5752-61.
115. Sarangi A, Valadez JG, Rush S, et al. Targeted inhibition of the Hedgehog pathway in established malignant glioma xenografts enhances survival. Oncogene 2009;28:3468-76.
116. Gerardo Valadez J, Grover VK, Carter MD, et al. Identification of Hedgehog pathway responsive glioblastomas by isocitrate dehydrogenase mutation. Cancer Lett 2013;328:297-306.
117. Hartmann C, Meyer J, Balss J, et al. Type and frequency of IDH1 and IDH2 mutations are related to astrocytic and oligodendroglial differentiation and age: a study of 1,010 diffuse gliomas. Acta Neuropathol 2009;118:469-74.
118. Yan H, Parsons DW, Jin G, et al. IDH1 and IDH2 mutations in gliomas. N Engl J Med 2009;360:765-73.
119. Watanabe T, Nobusawa S, Kleihues P, et al. IDH1 mutations are early events in the development of astrocytomas and oligodendrogliomas. Am J Pathol 2009;174:1149-53.
120. Lai A, Kharbanda S, Pope WB, et al. Evidence for sequenced molecular evolution of IDH1 mutant glioblastoma from a distinct cell of origin. J Clin Oncol 2011;29:4482-90.
121. Wen PY, Kesari S. Malignant gliomas in adults. N Engl J Med 2008;359:492-507.
122. Bao S, Wu Q, McLendon RE, et al. Glioma stem cells promote radioresistance by preferential activation of the

DNA damage response. Nature 2006;444:756-60.
123. Tamura K, Aoyagi M, Wakimoto H, et al. Accumulation of CD133-positive glioma cells after high-dose irradiation by Gamma Knife surgery plus external beam radiation. J Neurosurg 2010;113:310-8.
124. Jamal M, Rath BH, Tsang PS, et al. The brain microenvironment preferentially enhances the radioresistance of CD133(+) glioblastoma stem-like cells. Neoplasia 2012;14:150-8.
125. Ropolo M, Daga A, Griffero F, et al. Comparative analysis of DNA repair in stem and nonstem glioma cell cultures. Mol Cancer Res 2009;7:383-92.
126. Joo KM, Jin J, Kim E, et al. MET signaling regulates glioblastoma stem cells. Cancer Res 2012;72:3828-38.
127. Kim Y, Kim KH, Lee J, et al. Wnt activation is implicated in glioblastoma radioresistance. Lab Invest 2012;92:466-73.
128. Woodward WA, Chen MS, Behbod F, et al. WNT/beta-catenin mediates radiation resistance of mouse mammary progenitor cells. Proc Natl Acad Sci U S A 2007;104:618-23.
129. McCord AM, Jamal M, Williams ES, et al. CD133+ glioblastoma stem-like cells are radiosensitive with a defective DNA damage response compared with established cell lines. Clin Cancer Res 2009;15:5145-53.
130. Pallini R, Ricci-Vitiani L, Montano N, et al. Expression of the stem cell marker CD133 in recurrent glioblastoma and its value for prognosis. Cancer 2011;117:162-74.
131. Li A, Walling J, Kotliarov Y, et al. Genomic changes and gene expression profiles reveal that established glioma cell lines are poorly representative of primary human gliomas. Mol Cancer Res 2008;6:21-30.
132. Lee J, Kotliarova S, Kotliarov Y, et al. Tumor stem cells derived from glioblastomas cultured in bFGF and EGF more closely mirror the phenotype and genotype of primary tumors than do serum-cultured cell lines. Cancer Cell 2006;9:391-403.
133. Kim E, Kim M, Woo DH, et al. Phosphorylation of EZH2 Activates STAT3 Signaling via STAT3 Methylation and Promotes Tumorigenicity of Glioblastoma Stem-like Cells. Cancer Cell 2013;23:839-52.
134. Suvà ML, Riggi N, Janiszewska M, et al. EZH2 is essential for glioblastoma cancer stem cell maintenance. Cancer Res 2009;69:9211-8.
135. Gu C, Banasavadi-Siddegowda YK, Joshi K, et al. Tumor-specific activation of the C-JUN/MELK pathway regulates glioma stem cell growth in a p53-dependent manner. Stem Cells 2013;31:870-81.
136. Guryanova OA, Wu Q, Cheng L, et al. Nonreceptor tyrosine kinase BMX maintains self-renewal and tumorigenic potential of glioblastoma stem cells by activating STAT3. Cancer Cell 2011;19:498-511.
137. Kamal MM, Sathyan P, Singh SK, et al. REST regulates oncogenic properties of glioblastoma stem cells. Stem Cells 2012;30:405-14.
138. Sherry MM, Reeves A, Wu JK, et al. STAT3 is required for proliferation and maintenance of multipotency in glioblastoma stem cells. Stem Cells 2009;27:2383-92.
139. Wang J, Wang H, Li Z, et al. c-Myc is required for maintenance of glioma cancer stem cells. PLoS One 2008;3:e3769.
140. Friedmann-Morvinski D, Bushong EA, Ke E, et al. Dedifferentiation of neurons and astrocytes by oncogenes can induce gliomas in mice. Science 2012;338:1080-4.
141. Bachoo RM, Maher EA, Ligon KL, et al. Epidermal growth factor receptor and Ink4a/Arf: convergent mechanisms governing terminal differentiation and transformation along the neural stem cell to astrocyte axis. Cancer Cell 2002;1:269-77.
142. Dai C, Celestino JC, Okada Y, et al. PDGF autocrine stimulation dedifferentiates cultured astrocytes and induces oligodendrogliomas and oligoastrocytomas from neural progenitors and astrocytes in vivo. Genes Dev 2001;15:1913-25.
143. Kang SK, Park JB, Cha SH. Multipotent, dedifferentiated cancer stem-like cells from brain gliomas. Stem Cells Dev 2006;15:423-35.
144. Hjelmeland AB, Wu Q, Heddleston JM, et al. Acidic stress promotes a glioma stem cell phenotype. Cell Death Differ 2011;18:829-40.

Cite this article as: Wang J, Ma Y, Cooper MK. Cancer stem cells in glioma: challenges and opportunities. Transl Cancer Res 2013;2(5):429-441. doi: 10.3978/j.issn.2218-676X.2013.08.01

Review Article

Normal tissue protection for improving radiotherapy: Where are the Gaps?

Pataje G.S. Prasanna, Helen B. Stone, Rosemary S. Wong, Jacek Capala, Eric J. Bernhard, Bhadrasain Vikram, C. N. Coleman

Radiation Research Program, Division of Cancer Treatment and Diagnosis, National Cancer Institute, Bethesda, MD 20892, USA

Correspondence to: Pataje G.S. Prasanna. National Cancer Institute, Division of Cancer Treatment and Diagnosis, Radiation Research Program, Executive Plaza North (EPN)/6015A, 6130 Executive Blvd., MSC 7440, Bethesda, MD 20892-7440, USA. Tel: ++1(301) 496-9360; Fax: ++1(301) 480-5785. Email: Pat.Prasanna@nih.gov.

Abstract: Any tumor could be controlled by radiation therapy if sufficient dose were delivered to all tumor cells. Although technological advances in physical treatment delivery have been developed to allow more radiation dose conformity, normal tissues are invariably included in any radiation field within the tumor volume and also as part of the exit and entrance doses relevant for particle therapy. Mechanisms of normal tissue injury and related biomarkers are now being investigated, facilitating the discovery and development of a next generation of radiation protectors and mitigators. Bringing recent research advances stimulated by development of radiation countermeasures for mass casualties, to clinical cancer care requires understanding the impact of protectors and mitigators on tumor response. These may include treatments that modify cellular damage and death processes, inflammation, alteration of normal flora, wound healing, tissue regeneration and others, specifically to counter cancer site-specific adverse effects to improve outcome of radiation therapy. Such advances in knowledge of tissue and organ biology, mechanisms of injury, development of predictive biomarkers and mechanisms of radioprotection have re-energized the field of normal tissue protection and mitigation. Since various factors, including organ sensitivity to radiation, cellular turnover rate, and differences in mechanisms of injury manifestation and damage response vary among tissues, successful development of radioprotectors/mitigators/treatments may require multiple approaches to address cancer site specific needs. In this review, we discuss examples of important adverse effects of radiotherapy (acute and intermediate to late occurring, when it is delivered either alone or in conjunction with chemotherapy, and important limitations in the current approaches of using radioprotectors and/or mitigators for improving radiation therapy. Also, we are providing general concepts for drug development for improving radiation therapy.

Keywords: Acute radiation effects; radiotherapy; radiation mitigator; radioprotector; oral mucositis; lung fibrosis; radiation-induced brain damage

DOI: 10.3978/j.issn.2218-676X.2012.05.05

Scan to your mobile device or view this article at: http://tcr.thepbpc.org/article/view/372/725

Introduction

Radiotherapy is an important treatment modality for many malignancies and is also used as a part of combined modality therapy with (I) conventional chemotherapeutic agents often used in modified schedules accommodating radiation, (II) molecular targeted therapy, (III) immunotherapy, and (IV) as a part of immune suppression for stem cell and organ transplantation. New technologies in radiation therapy in the past decade have led to significant improvements in tailoring the radiation dose distribution more precisely to the shape of the tumor and minimizing the dose to sensitive normal tissues. These advances also allow higher

dose delivery to a defined tumor sub-volume called "dose-painting" to areas deemed having greater tumor burden and/or increased radio-resistance due to hypoxia. Molecular and functional imaging linked to physical CT scanned images are used to guide radiation targeting and adapt treatment to tumor and normal tissue changes during a course of therapy. These novel approaches reduce collateral normal tissue damage and improve the therapeutic ratio. However, the location of the tumor within the organ, errors in treatment delivery such as incorrect patient positioning, and patient movement during treatment can result in excessive doses to normal tissues. Changes in treatment plans may be required during the course of treatment to accommodate changes in location, size and shape of the tumor and the organs at risk. A key factor to the risk of radiation injury is the relationship between dose and volume treated.

Many patients suffer adverse effects from radiation therapy. These side effects may be acute, occurring during or within a few weeks after therapy, or intermediate to late, occurring months to years after therapy. Acute radiation toxicity is primarily due to cell killing, but inflammation or infection may also be contributing factors. Intermediate and late effects result from complex responses as tissues attempt to heal or fail to heal, and may be exacerbated by trauma or infection. There is a need to reduce radiation toxicity and thus provide a therapeutic benefit and improve overall quality of life. Understanding the mechanisms through which radiation toxicity develops would provide clues for developing effective radioprotectors, mitigators or treatments (1). In this review, we discuss examples of important adverse effects of radiotherapy (acute and intermediate to late-occurring, including consequential effects (2), delivered either alone or in conjunction with chemotherapy, and important limitations in the current approaches of using radioprotectors and/or mitigators for improving radiation therapy. *Table 1*, modified from Vikram *et al*. (1) illustrates important cancer types, current treatment approaches, mortality, median survival, and important adverse effects of radiation therapy either alone or as an adjuvant to chemotherapy to emphasize how development of radioprotectors can help improve radiation therapy.

There are three categories of intervention for radiation damage: Protectors are agents given before radiation to prevent damage; mitigators are given during or shortly after a course of radiation therapy, before symptoms of toxicity appear; and treatments are given after symptoms of toxicity appear (4). Since various factors, including organ sensitivity to radiation, cellular turnover rate, and differences in mechanisms of injury manifestation and damage response vary among tissues successful development of radioprotectors/mitigators/treatments may require multiple approaches. In addition, patients cured of their primary malignancies may be susceptible to the development of secondary malignancies several years to decades after treatment. This risk is higher in younger patients in part because they have longer life expectancy for developing late effects. This review, however, will exclude carcinogenesis, and instead focus on the acute and intermediate to long-term toxicities from radiotherapy and potential strategies for protection, mitigation and treatment. Proposed general drug development process for radioprotectors to improve radiation therapy is illustrated in *Figure 1* taking into consideration important adverse effects in current treatment approaches for major cancer types.

Skin and mucosal damage

Damage to skin and mucosa represents one of the most common acute adverse effects of radiotherapy and/or chemotherapy. Mucosal damage may occur in the mouth, pharynx, esophagus, and bowel. It is a particular problem in head and neck cancer, where a significant number of patients report oral mucositis as the most debilitating adverse effect of radiotherapy (5,6). Oral mucositis often results in poor treatment outcome, reduced quality of life, and increased medical costs (7). Treatment regimens involving altered fractionation, such as hyperfractionation, accelerated radiotherapy, and concomitant boost accelerated radiation, improve therapy outcome, but invariably produce severe mucositis. Prevalence, patient-associated variables, pathobiology, risk factors, impact and current management approaches of oral mucositis have been reviewed (8). The World Health Organization (WHO) distinguishes four grades of oral mucositis, Grade 0 to 4 (9). The risk factors for developing severe mucosal injury include patients' age, sex, ethnicity, body mass index, individual radiation sensitivity, etc.

Extent of radiation-induced damage and recovery in the cell renewal systems of skin and mucosa is determined by radiation sensitivity and the cellular turnover rate. A biological model for treatment induced oral mucositis has been proposed by Sonis (10). Accordingly, the onset,

Table 1 Important adverse effects after conventional radiotherapy (1) (modified to emphasize development of radioprotectors to improve radiation therapy)

Cancer Type	Treatment	Mortality	Median Survival (mo)	Adverse Effects	
				Acute Effects	Likely intermediate to late effects
Glioblastoma	Temozolomide	73.5% by 2 yr	14.6	Gr. 3-4 non hematologic, Fatigue, rashes and vision, nausea, vomiting	Cognitive defects (3)
Head and Neck (locally advanced, unresectable)	Cetuximab	45% by 3 yr	49	Gr 3-5 mucosal toxicity (56%), Gr 3-5 dyspahgia (26%), Gr 3-5 dermatitis (23%)	Cognitive defects (3)
Head and Neck (locally advanced, resected)	Cisplatin	Not available	48	Gr. 4-5 non hematologic in 27% including mucositis, pharyngitis, nausea, vomiting, skin toxicity	Cognitive defects (3)
Larynx (locally advanced)	Cisplatin	24% by 2 yr	Not available	Gr 3/4 non hematologic toxicity in 77% including mucositis, pharyngitis, esophagitis, laryngitis	Persistant dysphagia in 15% at 2 years
Lung, non small-cell locally advanced	Continuous hyperfractionated accelerated radiation therapy	71% by 2 yr	16.5	Symptomatic acute pneumonitis (10%)	Persistent severe dysphagia in 7% at 2 years
Lung, non small-cell locally advanced	Chemotherapy before irradiation	68% by 2 yr	13.2	Acute 3-5 toxicity (52%)	Late Gr 3-5 toxicity (3%)
Lung small-cell limited disease	Chemotherapy	74% by 5 yr	23	Acute Gr 3-5 esophagitis (32%), Infection, fever, vomiting, pulmonary effects	Fibrosis

development, and healing of oral mucositis occurs in five sequential and overlapping steps: initiation, upregulation, message generation, ulceration, and healing. Initiation is via generation of reactive oxygen species (ROS) and direct damage to cells, tissues and blood vessels, and a cascade of reactions contributing to tissue damage (11). Up-regulation involves activation of transcription factors (e.g., nuclear factor-κβ), leading to a local increase in pro-inflammatory cytokines (IL-6) and tumor necrosis factor (TNF). A positive feedback mechanism results in an amplification and acceleration of the process leading to ulceration, allowing oral bacteria to colonize denuded connective tissue. It is now believed that treatment-induced mucositis is not restricted to direct epithelial damage in regions surrounding the treatment area, but affects the entire alimentary tract and involves the connective tissue (12). Compared to chemotherapy, radiotherapy-induced mucositis follows a relatively more gradual clinical course, as the latter is administered in fractions over weeks (8). Not surprisingly, given this overlap in toxicity, chemoradiotherapy-induced mucositis can be quite severe.

The incidence, duration and severity of radiation-induced oral mucositis increases with dose (13). In general, radiation-induced oral mucositis begins at an accumulated

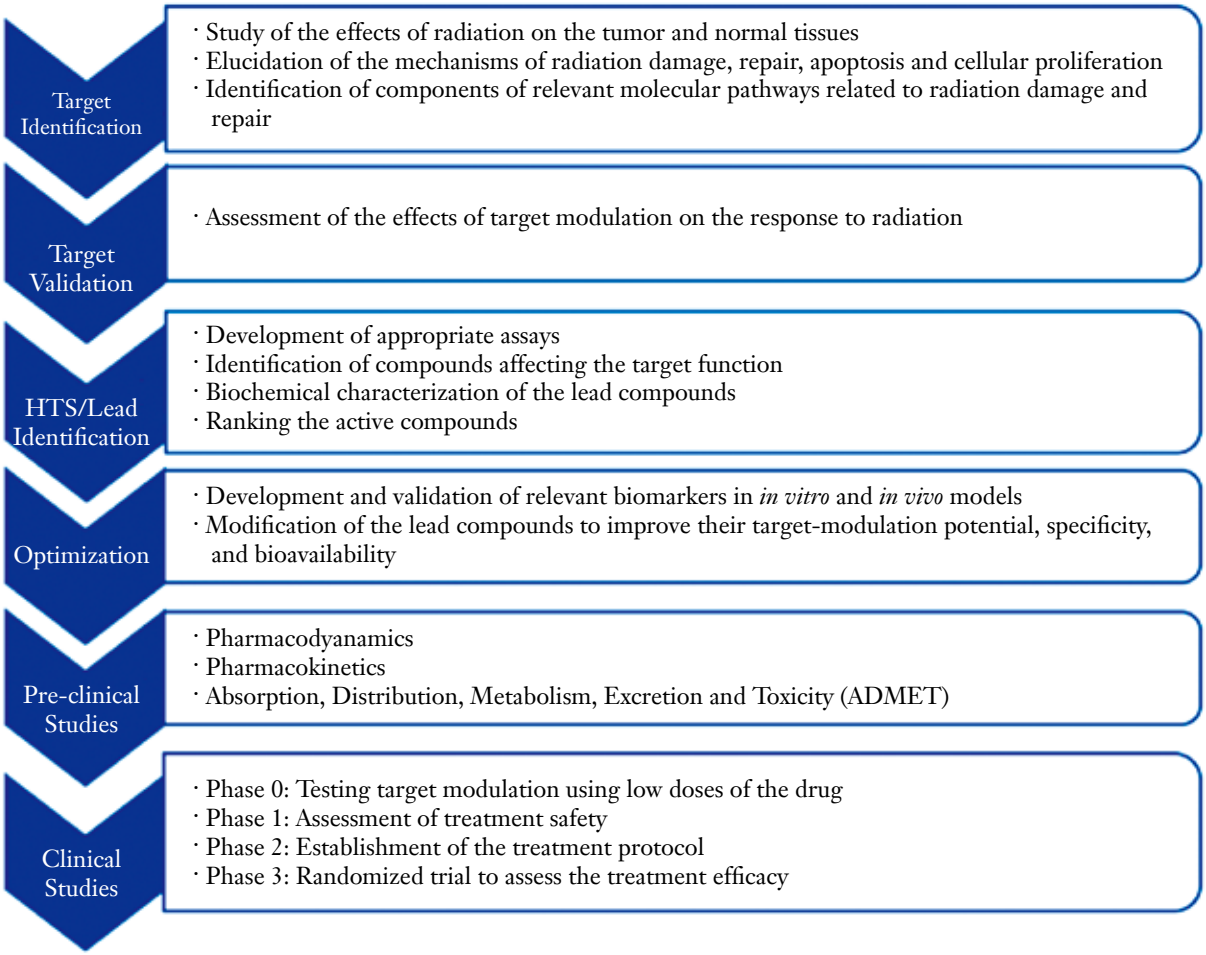

Figure 1 Proposed general drug development process for radioprotectors to improve radiation therapy

dose of 10 Gy during treatment, and intensifies in severity around 30 Gy, lasting for weeks to months. The highest rates of severe mucositis are seen among patients who receive a total body irradiation of 12 Gy as a preparative regimen in combination with high dose chemotherapy before blood stem cell transplantation (14).

Current approaches in the treatment of oral mucositis

Microbial colonization exacerbates oral mucositis. Current therapies for oral mucositis therefore include non-pharmacological approaches such as maintenance of oral health and hygiene in addition to oral cryotherapy as well as pharmacological treatment regimens. Benzydamine, a non-steroidal, anti-inflammatory analgesic and antimicrobial compound, is used for palliation and to reduce microbial colonization (15,16).

Management of radiation-induced oral mucositis with drugs such as the radioprotector amifostine, KGF (keratinocyte growth factor, palifermin), benzydamine treatment, and other investigational therapies does not provide consistent results, as described below.

Amifostine, given 15-30 min before each fraction of radiation, was not effective in preventing oral mucositis in a randomized large clinical trial involving over 300 patients undergoing treatment for squamous head and neck cancer, but both acute and delayed xerostomia were reduced (17).

KGF acts specifically on epithelial cells, promoting proliferation and decreasing apoptosis. It also causes thickening of the mucosa. It was effective in reducing chemotherapy-induced oral mucositis (14,18). Based on this effect, it was FDA-approved for prophylaxis of mucositis in patients receiving etoposide,

cyclophosphamide and total body irradiation of 12 Gy prior to hematopoietic stem cell transplantation for hematological malignancies (14). However, in a clinical study assessing the efficacy and safety of prophylactic KGF given to patients for three days before receiving concurrent chemoradiotherapy (CRT) for advanced head and neck squamous cell carcinoma and weekly treatment after completion of CRT, it appeared to reduce mucositis, dysphagia, and xerostomia during hyperfractionated radiotherapy, but not during standard radiation therapy (19). In a subsequent multinational, randomized, placebo controlled, double-blinded trial with (n=188) patients with locally advanced head and neck cancers, a higher dose of KGF (180 μg/kg), when administered in weekly doses throughout the treatment with conventional chemoradiation, reduced the incidence of severe oral mucositis from 69% to 54%. The median duration of mucositis was reduced from 26 to 5 days and time to onset delayed from 35 to 47 days. The side effects were tolerable (20).

Thus, the majority of current treatment approaches for oral mucositis involve palliation or treatment after manifestation of symptoms, inducing proliferative activity of the mucosal layer to enhance repair of damage. Few attempts to prevent damage to the normal mucosa during radiation treatment have been made, largely because of the possibility of tumor protection, enhanced tumor proliferation, development of tumor resistance to other cytotoxic therapies, or inter-individual variability in response to radiation.

Standardization of dose, route, and time of administration is also essential to development and application of agents to reduce the incidence and severity of oral mucositis. These are constrained by side effects of the agents themselves, as was the case with amifostine (17). Common adverse events related to the administration of this drug included nausea/vomiting, hypotension, facial flushing and phlebitis.

Prevention of mucosal damage is preferable to mitigation, which is preferable to treatment after symptoms develop, to allow either the uninterrupted delivery of the prescribed radiation dose or dose escalation to the tumor. Phenylbutyrate, an antitumor histone deacetylase inhibitor, was recently shown in a pilot study to mitigate oral mucositis, during radiotherapy or chemoradiotherapy (21). Further development of normal-tissue-specific radioprotectors is needed. It is also important to develop and validate predictive markers useful for determining radiation sensitivity of the mucosa in individual patients in order to optimize the balance between tumor control and normal tissue toxicity.

Radiotherapy-induced lung damage

More than 60% of patients with Non-Small Cell Lung Cancer (NSCLC) are treated with radiation therapy (22). Radiation-induced lung damage is an intermediate to late-occurring side effect of radiation therapy. This damage appears as pneumonitis at the earlier times, with fibrosis occurring as a late effect.

Pneumonitis

Pneumonitis occurs at about 1-3 months after radiotherapy in some patients undergoing thoracic irradiation for cancers of lung, esophagus, breast, and lymphatic systems. The symptoms are congestion, cough, dyspnea, fever, and chest pain. Pneumonitis generally subsides after several weeks and can be treated with steroids.

Pneumonitis involves interstitial pulmonary inflammation, although the molecular mechanisms are not yet fully understood. Stone *et al.* (23) reviewed radiation-induced damage to lung and described the mechanisms of its onset, development, and contributing factors. At the molecular level, several cytokines such as TGF-β1 (24,25), IL-1 and IL-6 (26) seem to play important roles. Kong *et al.* (27) proposed a mechanism of regulation of pneumonitis and fibrosis. Accordingly, repetitive stimuli from fractionated irradiation and chemotherapy induce local damage to lung cells causing release of regulatory molecules such as cytokines that attract fibroblasts, circulating fibrocytes, and bone marrow stem cells that contribute to tissue healing and functional recovery (28). It is likely that interactions among multiple cell systems within a network of cellular and supra-cellular signaling pathways drive the processes leading to radiation-induced lung damage. Serial plasma specimens analyzed for changes in circulating cytokines before, during, and up to 12 weeks after irradiation indicated that both IL-1α and IL-6 levels were significantly higher before, during, and after radiotherapy in patients who developed pneumonitis (26).

While new conformal techniques are helpful in limiting normal tissue radiation doses, increasing lung doses will also increase the risk of developing radiation pneumonitis. This relationship is linear-quadratic from 5 to 30 Gy (27).

New information on dose-volume relationships indicates that doses of radiation higher than those traditionally administered can be delivered to a majority of patients with non-small cell lung cancer (NSCLC) (29). This could allow dose escalation based on risk of toxicity in individual patients, combined with information on the lung volumes to be irradiated (29,30). Radiation toxicity to the lung can be markedly exacerbated by concurrent use of chemotherapy. For example, when gemcitabine and docetaxel were combined with radiation therapy, the combination regimen was extremely toxic with 8% deaths and 23% grade-3 lung toxicity compared to 1.6-2.1% deaths from radiotherapy alone (31). Combined modality toxicity is an ongoing concern with the advent of particle therapies, as proton therapy trials are being considered for treatment of lung and esophageal cancers using combined modality therapy. Whether the toxicities will be equivalent to standard therapies is not yet known.

Fibrosis

Recently, Hill *et al.* (32) concluded that radiation-induced inflammation in lung cells occurs through production of ROS contributing to DNA damage over prolonged periods. Individual patient factors including genetic predisposition, autoimmune conditions, or comorbidities can lead to aberrant wound healing, resulting in pulmonary fibrosis. Fibrosis often follows pneumonitis months to years after irradiation. It is diagnosed radiographically and in many patients does not cause clinical symptoms. It occurs after doses above about 30-40 Gy, depending on the fractionation scheme of radiation therapy and the use of chemotherapy. Fibrosis is characterized by vascular damage and collagen deposition (27).

Current approaches of treatment or mitigation of radiation pneumonitis and fibrosis

Although pneumonitis and pulmonary fibrosis are associated, the existence of pneumonitis-prone and fibrosis-prone strains of mice suggests that different mechanisms are involved in their development (33), and therefore, different approaches may be required. Since the lung is the most sensitive tissue for the delayed effects of acute radiation exposure (DEARE) following whole body exposure in terrorism and also bone-marrow transplantation, radioprotective and/or mitigation strategies could benefit all these patients. Several drugs have been evaluated, including amifostine, agents that target the renin-angiotensin system (RAS); angiotensin converting enzyme inhibitors (ACEI) and angiotensin II receptor agonists (AT_2RA), genistein, pentoxyfiline, and manganese superoxide dismutase/plasmid liposomes. Some examples are reviewed below.

A Phase III randomized study by the Radiation Therapy Oncology Group (RTOG) evaluated the benefits of amifostine administration in 180 patients with stages II-III non-small-cell lung cancer receiving induction paclitaxel and carboplatin, and then concurrently with hyperfractionated radiation therapy from pretreatment to 6 weeks post-treatment. Results indicated that the use of amifostine significantly reduced pain after chemoradiation (34% *vs.* 21%), less difficulty in swallowing during chemoradiation, and less weight loss compared to patients not receiving amifostine. However, physician-rated assessments of dysphagia were not significantly different between the treatment arms. No other quality of life or symptom changes were found with respect to treatment arm, smoking status, alcohol use, or gender (34).

Robbins and Diz (35) reviewed the role of the RAS as a target for the modulation of radiation-induced late effects. RAS is a complex blood-borne hormonal system in which the substrate (angiotensinogen) and enzyme (renin) are released into the circulation from the liver and kidneys, respectively (35,36). Angiotensin-converting enzyme (ACE) converts angiotensin I to the active form, angiotensin II (ANG II), by binding to G protein-coupled receptors, AT_1R and AT_2R (37), that are widely distributed in various tissues. ACE inhibitors (ACEI) and angiotensin II receptor antagonists (AT_2RA), routinely used to manage hypertension, mitigated radiation-induced lung injury in preclinical models. In irradiated Sprague Dawley rats, administration of ACEIs captopril, CL 24817, enalapril, and CGS 13945, prevented expression of markers of endothelial dysfunction. Angiotensin II appears to play an important role in the regulation of TGF-β and α-smooth muscle actin (SMA), two proteins involved in the pathogenesis of pulmonary fibrosis (38). The AT_2RA 158,809 and the ACEIs, captopril and enalapril, significantly ameliorated the effects of radiation and cytoxan treatment-induced lung injury. Thus, ACEI and an AT_2RA were effective in protecting lungs from radiation-induced pneumonitis and the development of lung fibrosis (39).

However, administration of ACEI during radiotherapy did not reduce the risk of radiation-induced pneumonitis in a retrospective analysis of 213 eligible patients receiving 3D-CRT for lung cancer with curative intent (40). Because

a relatively small fraction of patients develop pneumonitis following thoracic radiation therapy it is important to develop predictive biomarkers that will help to identify those at risk prior to initiating trials evaluating treatments with ACEIs. On the positive side, the incidence of Grade 2 or higher pneumonitis was significantly lower in 62 patients with stage I through III who were taking ACEIs during thoracic irradiation treatment compared to 100 non-users (2% *vs.* 11%) (39). This is consistent with preclinical evidence, but warrants further investigation in a prospective study.

Hill *et al.* (32) demonstrated that post-irradiation administration of EUK-207, a SOD catalase mimetic and genistein, an isoflavone with anti-inflammatory properties, decreased the frequency of radiation-induced micronuclei, a marker of radiation damage, in lung cells in mice. Similarly, genistein reduced the incidence of micronuclei in primary fibroblast cultures from female mice, indicating protection against radiation-induced genotoxicity (41). It also prevented radiation-induced reduction of COX-2 expression, TGF-β receptor (TGF-βR) I and II, and other potential biomarkers of pulmonary injury at 90 days after irradiation (41). It is hypothesized that genistein would reduce the levels of inflammatory cytokines and ROS after irradiation, resulting in reduced DNA damage and functional deficits (42).

TNF-α knockout mice had a smaller radiation-induced increase in breathing rate than wild-type mice and less severe radiation pneumonitis, indicating that TNF-α plays an important role in the development of inflammation in lung following irradiation.

Manganese superoxide dismutase-plasmid liposomes (MnSOD-PL) also protects lung from local radiation injury (43,44). It appears to stabilize antioxidant pools, including glutathione and total thiols, within cells and in normal tissues (43). Tumor radiosensitization, not protection, was observed in mice with orthotopic Lewis lung carcinomas following intratracheal administration of MnSOD-PL (45). The onset of alveolitis/pulmonary fibrosis was delayed and its extent was reduced (43). Mice treated with inhalation delivery of MnSOD-PL showed a plasmid dose-dependent increase in expression of MnSOD transgene product over the range of 250 μg to 2.5 mg. Treatment with MnSOD-PL 24 hr before 20 Gy to the lungs had slightly longer survival than irradiated controls (44).

The initial interim analysis of RTOG 0617 comparing standard 60 Gy plus chemotherapy to the higher 74 Gy plus chemotherapy + cetuximab for treatment of inoperable Stage III NSCLC, was reported at the 2011 ASTRO meeting showing no overall survival advantage with dose escalation to 74 Gy. It was also reported that there was no significant difference in treatment-related toxicities between the two radiation treatment arms after a median follow-up time of only 11 months (unpublished at the time this paper was written: http://journals.lww.com/oncology-times/blog/onlinefirst/pages/post.aspx?PostID=316). Any benefits from further dose escalation beyond 74 Gy remain to be determined, but tumor motion, location and normal tissue effects must also be considered. Normal tissue protection will be useful for improving cure rates and decreasing patient morbidity if dose escalation is to be pursued. Physical dose-volume relationships that are required for effective treatment but increase the likelihood of lung injury will need to be defined. Since the cohort that develops radiation pneumonitis is relatively small, the development of early predictive biomarkers of pneumonitis would aid in identifying the patient population that could benefit from the administration of radioprotectors or mitigators. Therefore, clinical trials are necessary to determine whether normal tissue protectors and mitigators will permit use of higher radiation doses and whether these can lead to a survival advantage in patients with non-small cell lung cancer (46).

Radiation-induced brain damage

The American Cancer Society predicts that there will be 22,910 new brain cancer cases and 13,700 deaths in 2012. Additionally, about 30% of cancer survivors will develop brain metastases. In fact over 200,000 patients/year in the US with malignant brain tumors, including primary and metastatic tumors, are treated with radiation therapy for cure and palliation. Over 100,000 of these long-term survivors (>6 months) will develop brain injury that affects their quality of life (47). In the brain, as in other tumor sites, radiation dose prescriptions and probability of tumor control are constrained by normal tissue tolerance, despite the use of state-of-the-art radiation delivery techniques and improved modeling of dose distributions. New stereotactic radiotherapy techniques that use high doses per fraction may provide benefit in the treatment of metastases, but their impact on treatment of glioblastoma may be mitigated by tumor extension beyond what is detectable in imaging.

Radiation injury to brain develops months to years after therapy, and is severe and irreversible. In the past, delayed radiation injury was thought to be solely due to a

reduction in surviving clonogens of parenchymal or vascular target cell populations; this hypothesis now appears to be simplistic. Radiation injury is dynamic and involves not only loss of parenchymal and stromal cells, including vascular cells, but also impaired proliferation of precursor cells, reactive oxygen species (ROS) and waves of pro-inflammatory cytokines and leads to tissue damage and functional deficits (11,48). Research into the mechanisms of cognitive impairment presents opportunities for development of novel therapeutic intervention strategies (35). Studies in rodent models indicate that irradiation of the brain leads to a significant reduction in neurogenesis (49), inflammation of the neurons (50,51), and progressive cognitive impairment (52). Neural progenitors within the subgranular zone of the dentate gyrus are among the most radiosensitive cell types in the adult brain. Damage to these cells reduces neurogenesis and correlates with cognition deficits (50). Neural precursor cells in culture exhibit an acute dose-dependent apoptosis accompanied by an increase in ROS persisting over a 3-4-week period. Radiation also activates cell cycle checkpoints that delay or prevent cell division (42). Proliferating precursor cells and their progeny (i.e. immature neurons) exhibit a dose-dependent reduction in cell number, which is less severe in Trp53-null mice, suggesting that the apoptotic and ROS responses may be tied to Trp53-dependent regulation of cell cycle control and stress-activated pathways (51).

Histological characteristics of brain injury appear to be non-specific to radiation, but after high doses, white matter necrosis with demyelination is a prominent histopathological feature. Endothelial cell loss appears to contribute to the demyelination, because significant demyelination was observed and neural precursor cell populations were reduced when endothelial cells were selectively irradiated using boron neutron capture therapy employing a boron compound that remained within the vasculature (53,54). Also, excessive generation of ROS, including oxygen radicals, free radicals, and inorganic and organic peroxides, causes an "oxidative stress" and overwhelms the "antioxidant defense system", resulting in the development of delayed effects in the brain (55). Gradual upregulation of vascular endothelial growth factor (VEGF) occurs several weeks prior to manifestation of tissue pathology (56), which seems to gradually diminish the integrity of blood brain barrier (BBB) (57). This leads to a vicious cycle of reduction in endothelial cell density and disruption of BBB, ultimately causing functional deficits.

The RAS described previously is also found in the brain (35), where it is involved in brain-specific functions, including modulation of the BBB, pain perception, stress, memory, and cognition (58,59).

Therapeutic strategies for radiation-induced brain damage

Drugs currently used in animal models to counter radiation-induced brain damage block pro-inflammatory cytokines and prevent formation of ROS. These include ACEIs, statins, superoxide mimetics, and VEGF inhibitors.

An ACEI, ramipril, ameliorated demyelination of optic nerves in a rat model of optic neuropathy after a single stereotactic dose of 30 Gy (60) and preserved the functional integrity of the nerve (61). Putative mechanisms of amelioration of radiation-induced brain injury, including cognitive impairment, by RAS inhibitors include a blockade of Ang II/NADPH oxidase-mediated oxidative stress and neuro-inflammation and a change in the balance of angiotensin (Ang) peptides from the pro-inflammatory and pro-oxidative Ang II to the anti-inflammatory and anti-oxidative Ang-1-7 (62). Treatment with the AT_1RA L-158,809 before, during, and after, fractionated whole-brain irradiation prevents or ameliorates radiation-induced cognitive deficits in adult rats, although it does not appear to modulate chronic inflammatory mechanisms (63,64). Both ACEIs and AT_1RAs are routinely prescribed for hypertension and are well-tolerated drugs that also exhibit some antitumor properties and can prevent/ameliorate radiation-induced brain injury (62).

Statins, a class of drugs routinely used to treat hypercholesterolemia and atherosclerosis, have pleiotropic effects, which may include neuroprotection and promotion of tissue repair via modulation of endothelial nitric oxide synthetase (eNOS) antioxidant and anti-inflammatory pathways (65-68). Jenrow *et al.* (69) investigated whether atorvastatin, administered alone or in combination with the ACEI, ramipril, following radiation injury, protects progenitors and/or preserves neurogenic potential within the subgranular zone of the dentate gyrus. Although chronic administration of atorvastatin alone was relatively ineffective as a mitigator, its combination with ramipril appeared to interact synergistically to mitigate radiation-induced disruption of neurogenic signaling. Cognitive functions were not evaluated in this study in adult male rats.

Since oxidative stress via excessive generation of ROS appears to play a role in the development of delayed effects

in brain (55), it was speculated that superoxide dismutase (SOD), may help mitigate late effects of irradiation on brain. VEGF family of signal proteins stimulates vasculogenesis and angiogenesis, which promote tumor growth. Anti-VEGF therapies have been found useful in the treatment of certain cancer types, but their benefit in protecting against radiation-induced normal tissue damage and/or mitigation is not clear. Winkler *et al*. (70) showed that VEGF receptor 2 (VEGFR2) blockade creates a "normalization window", because of a transient stabilization of blood vessels and improved oxygen delivery to hypoxic regions within a rat orthotopic glioma tumor in which radiation therapy may be more effective. The benefit to counter radiation-induced normal tissue damage in brain is not clear. Bevacizumab, alone and in combination with other agents, was found to reduce radiation necrosis by decreasing capillary leakage and the associated brain edema in a clinical trial involving a very small number of patients (n=15) with malignant brain tumors, but these findings need to be confirmed in a randomized trial (71).

Development of radioprotectors/mitigators - translational path to clinic

Decades of preclinical and clinical research efforts have been spent with the aim of protecting normal tissue from acute radiation-induced damage and mitigating intermediate to late effects with some limited success such as with amifostine. The importance of developing agents that protect or mitigate radiation-induced damage in normal tissue, improve survival and quality of life, as well as improve palliative care in cancer patients was emphasized in an NCI workshop, "Advanced Radiation Therapeutics - Radiation Injury Mitigation". The proceedings of this workshop include guidelines for preclinical (72) and clinical development (73) of promising agents for reducing the adverse effects of radiation therapy.

A three-stage approach is recommended for preclinical radioprotector/mitigator development (74). In Stage I, maximum tolerated dose (MTD) and toxicity of the agent is determined using Good Laboratory Practices (GLP). In stage II, protective/mitigative effects are determined using both *in vitro* and *in vivo* testing in both normal tissues and tumors. If both absence of tumor protection and sufficient normal tissue protection/mitigation is found, then the mechanism of action should be identified, if not already available. In Stage III, comprehensive toxicological and pharmacological testing is performed to address the regulatory requirement for data on Absorption, Distribution, Metabolism, Excretion and Toxicity profiles (ADMET) before proceeding to the clinical investigation (73). A consensus was reached among the workshop participants on (I) best practices for agent evaluation for normal tissue protection and radiation injury mitigation in cancer patients, (II) clinical trial designs that could efficiently and empirically move the most promising agents into appropriate clinical trials, and (III) scientific rationale that might be applied by regulatory agencies to evaluate agents for investigational new drug (IND) applications and approval. An algorithm to guide clinical trials for such agents in patients receiving radiotherapy or chemotherapy has already been published (73).

The search for a universal radioprotector that works across all tissue types and anatomical sites is likely to yield limited success, because various organs and tissues differ in such factors as radiation sensitivity, DNA damage response, proliferative and oxygenation status of tissue, vasculature, drug uptake, and activation, release, and response to inflammatory cytokines. For example, the radioprotection afforded to normal tissues by amifostine varies widely, with some of the most responsive tissues showing low levels of absorbed drug and vice versa, possibly due to differences in oxygen tension (74). In addition, tumors can also affect the biology and radiation response of normal tissues, before, during, and after irradiation. Therefore, although there may be some commonality among tissues, efforts must be focused on discovering and developing radioprotectors/mitigators that are specific to each anatomical site.

The extent of initial DNA damage induced by a given radiation dose to different tissues will be similar in the absence of differences in tissue oxygenation, although differences in DNA conformation resulting from cell cycle differences might occur. The outcome of this damage will largely be determined by DNA damage responses in the different tissues. There is significant inter-individual variation in responses and susceptibility to radiation effects on normal tissues, doubtless influenced by genetic factors. These are at present not well defined, but are the subject of active investigation. In the absence of mutation in DNA damage response genes, the response to DNA damage will be influenced by the proliferative status, cell cycle distribution and propensity for apoptosis of the cells in the irradiated tissue. More rapidly dividing tissues with a higher rate of cell turnover, such as those of the oral mucosa and lung epithelial lining will demonstrate greater

acute reactions and consequential late effects, while the more slowly dividing CNS tissues (brain and spinal cord) are susceptible to late effects including leukoencephalopathies and radiation necrosis (75). The protection and mitigation strategies for these two types of responses could, in the future, differ as a result. For example, while anti-apoptotic approaches might be applied to epithelium, they could be of limited benefit in neural injury.

The principal factors currently determining therapeutic approach are the location and accessibility of these tissues. While both pneumonitis and CNS inflammation can be treated with steroids, epithelial surfaces in the lung, oral and upper aerodigestive mucosa are candidates for topical approaches including the application of radical scavengers. This could not be used in the CNS. Soy isoflavones and SOD mimetics have been proposed for prevention of pneumonitis (76). Bevacizumab has recently been proposed as a treatment to prevent the vascular endothelial dysfunction that contributes to radiation necrosis in the CNS (77).

It is well known that hypoxic cells, which are present in many tumors, are radioresistant. Because these may give the tumor a survival advantage, any additional potential for protection of tumors in relation to normal tissue, whose oxygen levels also vary, is a concern in the radioprotector field. Assays for tumor protection using cultured cell lines do not translate well into *in vivo* studies and hence to the clinic, because they do not mimic oxygen levels and other microenvironmental factors that affect the responses of tumors and normal tissues *in situ*. Functional radiobiological endpoints for cell killing such as the clonogenic assay are necessary to fully assess the impact of any protector/mitigator for normal and cancer cell lines. Since irradiated cells may remain metabolically viable and undergo several cell divisions before they die (78), assays based on uptake or exclusion of dyes are inappropriate (79).

Differential radioprotection may be achieved if the normal tissue selectively takes up the radioprotector or if it has mechanisms of tissue protection not utilized by the tumor. Therefore, data demonstrating a higher concentration of the drug in the target normal tissue than the tumor in *in vivo* models are essential. Studies of structure-activity relationships using analogs of lead compounds can aid in understanding mechanisms of action and finding the most effective radioprotectors. Preclinical and/or early phase clinical studies demonstrating safety, efficacy, dose, schedule, pharmacokinetics (PK), pharmacodynamics (PD), and metabolism is necessary. It is important to demonstrate that an effective concentration of an agent in the target tissue can be achieved. This may differ among various organs. For example, the normal tissues in which the highest concentrations of amifostine are achieved include kidney, salivary gland, bone marrow, liver, heart, lung and small intestine (80). Not surprisingly, the most impressive clinical benefits were reported for amifostine for protecting kidneys and preventing xerostomia (81). Exploitable differences between tumors and normal tissues may include differences in vasculature and membrane properties related to drug or prodrug uptake and conversion to an active metabolite.

Protectors and mitigators, especially those intended for use in patients treated with radiotherapy, must be evaluated in relevant *in vitro* and *in vivo* systems to determine whether they also protect tumors or increase metastasis while protecting normal tissue or aiding normal tissue recovery. In addition, they should have limited normal tissue toxicity. The protective/mitigative effect of the candidate agents ideally should be determined using *in vivo* human orthotopic xenograft mouse models (82), where possible to demonstrate protection/mitigation in the target tissue, but not the tumor.

Finally, a clear understanding of regulatory requirements including a regulatory plan with key steps such as a pre-IND meeting with FDA, submitting an investigational new drug (IND) application, approval of clinical trial design, and ultimately drug registration also are critical.

Phase zero trials

Traditionally new drugs in oncology undergo Phase I trials for evaluating their toxicity profile, then Phase II trials for demonstrating efficacy proof-of-principle, followed by Phase III trials for the evaluation of efficacy. The most common reason that drugs fail is lack of efficacy in Phase II or III trials. That may be due to inadequate biological understanding of the underlying mechanisms, inadequate animal models, inadequate understanding of the optimal scheduling of the drug and/or suboptimal design of the clinical trial itself.

Toxicity is a major concern for many cancer drugs. The Phase 0 trial is a new approach for evaluating the PK and PD properties of a new investigational agent in a small number of patients before initiating larger, traditional Phase I trials (83). It involves administration of very low doses of the new drug over a short time period and measuring the effect of the drug on its molecular target and/or pathways in humans employing procedures validated in preclinical models.

FDA Exploratory IND Guidance may be found at:

(http://www.fda.gov/downloads/Drugs/Guidance.%20Compliance%20Regulatory%20Information/Guidances/ucm078933.pdf). Because of the low doses involved, Phase 0 trials require less preclinical toxicity data than for traditional first-in-human phase I studies. Issues to be addressed in the design of such trials for radioprotectors and mitigators will include obtaining relative distribution of candidate drugs in tumor *vs*. normal tissue and the identification of appropriate biomarkers.

Acknowledgements

National Cancer Institute's Radiation Research Program supported the manuscript preparation.
Disclosure: This manuscript is not being submitted for consideration of publication elsewhere. All authors do not have any financial interests in any or all of the companies that are mentioned in this manuscript.

References

1. Vikram B, Coleman CN, Deye JA. Current status and future potential of advanced technologies in radiation oncology. Part 1. Challenges and resources. Oncology 2009;23:279-83. Williston Park.
2. Dörr W, Hendry JH. Consequential late effects in normal tissues. Radiother Oncol 2001;61:223-31.
3. Johannesen TB, Lien HH, Hole KH, et al. Radiological and clinical assessment of long-term brain tumour survivors after radiotherapy. Radiother Oncol 2003;69:169-76.
4. Coleman CN, Blakely WF, Fike JR, et al. Molecular and cellular biology of moderate-dose (1-10 Gy) radiation and potential mechanisms of radiation protection: report of a workshop at Bethesda, Maryland, December 17-18, 2001. Radiat Res 2003;159:812-34.
5. Rose-Ped AM, Bellm LA, Epstein JB, et al. Complications of radiation therapy for head and neck cancers. The patient's perspective. Cancer Nurs 2002;25:461-7.
6. Bellm LA, Epstein JB, Rose-Ped A, et al. Patient reports of complications of bone marrow transplantation. Support Care Cancer 2000;8:33-9.
7. Nonzee NJ, Dandade NA, Patel U, et al. Evaluating the supportive care costs of severe radiochemotherapy-induced mucositis and pharyngitis: results from a Northwestern University Costs of Cancer Program pilot study with head and neck and nonsmall cell lung cancer patients who received care at a county hospital, a Veterans Administration hospital, or a comprehensive cancer care center. Cancer 2008;113:1446-52.
8. Raber-Durlacher JE, Elad S, Barasch A. Oral mucositis. Oral Oncol 2010;46:452-6.
9. World Health Organization. WHO handbook for reporting results of cancer treatment. Geneva, [Albany, N.Y.: World Health Organization; sold by WHO Publications Centre USA]; 1979.
10. Sonis ST. Mucositis as a biological process: a new hypothesis for the development of chemotherapy-induced stomatotoxicity. Oral Oncol 1998;34:39-43.
11. Rubin P, Johnston CJ, Williams JP, et al. A perpetual cascade of cytokines postirradiation leads to pulmonary fibrosis. Int J Radiat Oncol Biol Phys 1995;33:99-109.
12. Sonis ST. A biological approach to mucositis. J Support Oncol 2004;2:21-32.
13. Russo G, Haddad R, Posner M, et al. Radiation treatment breaks and ulcerative mucositis in head and neck cancer. Oncologist 2008;13:886-98.
14. Spielberger R, Stiff P, Bensinger W, et al. Palifermin for oral mucositis after intensive therapy for hematologic cancers. N Engl J Med 2004;351:2590-8.
15. Kim JH, Chu FC, Lakshmi V, et al. Benzydamine HCl, a new agent for the treatment of radiation mucositis of the oropharynx. Am J Clin Oncol 1986;9:132-4.
16. Sonis ST, Clairmont F, Lockhart PB, et al. Benzydamine HCL in the management of chemotherapy-induced mucositis. I. Pilot study. J Oral Med 1985;40:67-71.
17. Brizel DM, Wasserman TH, Henke M, et al. Phase III randomized trial of amifostine as a radioprotector in head and neck cancer. J Clin Oncol 2000;18:3339-45.
18. Rosen LS, Abdi E, Davis ID, et al. Palifermin reduces the incidence of oral mucositis in patients with metastatic colorectal cancer treated with fluorouracil-based chemotherapy. J Clin Oncol 2006;24:5194-200.
19. Brizel DM, Murphy BA, Rosenthal DI, et al. Phase II study of palifermin and concurrent chemoradiation in head and neck squamous cell carcinoma. J Clin Oncol 2008;26:2489-96.
20. Le QT, Kim HE, Schneider CJ, et al. Palifermin reduces severe mucositis in definitive chemoradiotherapy of locally advanced head and neck cancer: a randomized, placebo-controlled study. J Clin Oncol 2011;29:2808-14.
21. Yen SH, Wang LW, Lin YH, et al. Phenylbutyrate mouthwash mitigates oral mucositis during radiotherapy or chemoradiotherapy in patients with head-and-neck cancer. Int J Radiat Oncol Biol 2012;82:463-70.
22. Tyldesley S, Boyd C, Schulze K, et al. Estimating the need for radiotherapy for lung cancer: an evidence-based,

epidemiologic approach. Int J Radiat Oncol Biol Phys 2001;49:973-85.
23. Stone HB, Coleman CN, Anscher MS, et al. Effects of radiation on normal tissue: consequences and mechanisms. Lancet Oncol 2003;4:529-36.
24. Anscher MS, Kong FM, Marks LB, et al. Changes in plasma transforming growth factor beta during radiotherapy and the risk of symptomatic radiation-induced pneumonitis. Int J Radiat Oncol Biol Phys 1997;37:253-8.
25. Yuan X, Liao Z, Liu Z, et al. Single nucleotide polymorphism at rs1982073:T869C of the TGFbeta 1 gene is associated with the risk of radiation pneumonitis in patients with non-small-cell lung cancer treated with definitive radiotherapy. J Clin Oncol 2009;27:3370-8.
26. Chen Y, Williams J, Ding I, et al. Radiation pneumonitis and early circulatory cytokine markers. Semin Radiat Oncol 2002;12:26-33.
27. Kong FM, Ten Haken R, Eisbruch A, et al. Non-small cell lung cancer therapy-related pulmonary toxicity: an update on radiation pneumonitis and fibrosis. Semin Oncol 2005;32:S42-S54.
28. Greenberger JS. Gene therapy approaches for stem cell protection. Gene Ther 2008;15:100-8.
29. Marks LB, Bentzen SM, Deasy JO, et al. Radiation dose-volume effects in the lung. Int J Radiat Oncol Biol Phys 2010;76(Suppl):S70-6.
30. Kong FM, Ten Haken RK, Schipper MJ, et al. High-dose radiation improved local tumor control and overall survival in patients with inoperable/unresectable non-small-cell lung cancer: long-term results of a radiation dose escalation study. Int J Radiat Oncol Biol Phys 2005;63:324-33.
31. Kouroussis C, Mavroudis D, Kakolyris S, et al. High incidence of pulmonary toxicity of weekly docetaxel and gemcitabine in patients with non-small cell lung cancer: results of a dose-finding study. Lung Cancer 2004;44:363-8.
32. Hill RP, Zaidi A, Mahmood J, Jelveh S. Investigations into the role of inflammation in normal tissue response to irradiation. Radiother Oncol 2011;101:73-9.
33. Skwarchuk MW, Travis EL. Murine strain differences in the volume effect and incidence of radiation-induced colorectal obstruction. Int J Radiat Oncol Biol Phys 1998;41:889-95.
34. Sarna L, Swann S, Langer C, et al. Clinically meaningful differences in patient-reported outcomes with amifostine in combination with chemoradiation for locally advanced non-small-cell lung cancer: an analysis of RTOG 9801. Int J Radiat Oncol Biol Phys 2008;72:1378-84.
35. Robbins ME, Diz DI. Pathogenic role of the renin-angiotensin system in modulating radiation-induced late effects. Int J Radiat Oncol Biol Phys 2006;64:6-12.
36. Lavoie JL, Sigmund CD. Minireview: overview of the renin-angiotensin system--an endocrine and paracrine system. Endocrinology 2003;144:2179-83.
37. Nakajima M, Hutchinson HG, Fujinaga M, et al. The angiotensin II type 2 (AT2) receptor antagonizes the growth effects of the AT1 receptor: gain-of-function study using gene transfer. Proc Natl Acad Sci USA 1995;92:10663-7.
38. Molteni A, Wolfe LF, Ward WF, et al. Effect of an angiotensin II receptor blocker and two angiotensin converting enzyme inhibitors on transforming growth factor-beta (TGF-beta) and alpha-actomyosin (alpha SMA), important mediators of radiation-induced pneumopathy and lung fibrosis. Curr Pharm Des 2007;13:1307-16.
39. Kharofa J, Cohen EP, Tomic R, et al. Decreased Risk of Radiation Pneumonitis with Incidental Concurrent Use of Angiotensin-Converting Enzyme Inhibitors and Thoracic Radiation Therapy. Int J Radiat Oncol Biol Phys. DOI: S0360-3016(11)03501-2 [pii] 10.1016/j.ijrobp.2011.11.013.
40. Wang LW, Fu XL, Clough R, et al. Can angiotensin-converting enzyme inhibitors protect against symptomatic radiation pneumonitis? Radiat Res 2000;153:405-10.
41. Day RM, Barshishat-Kupper M, Mog SR, et al. Genistein protects against biomarkers of delayed lung sequelae in mice surviving high-dose total body irradiation. J Radiat Res (Tokyo) 2008;49:361-72.
42. Calveley VL, Jelveh S, Langan A, et al. Genistein can mitigate the effect of radiation on rat lung tissue. Radiat Res 2010;173:602-11.
43. Greenberger JS, Epperly MW. Review. Antioxidant gene therapeutic approaches to normal tissue radioprotection and tumor radiosensitization. In Vivo 2007;21:141-6.
44. Carpenter M, Epperly MW, Agarwal A, et al. Inhalation delivery of manganese superoxide dismutase-plasmid/liposomes protects the murine lung from irradiation damage. Gene Ther 2005;12:685-93.
45. Guo H, Epperly MW, Bernarding M, et al. Manganese superoxide dismutase-plasmid/liposome (MnSOD-PL) intratracheal gene therapy reduction of irradiation-induced inflammatory cytokines does not protect orthotopic Lewis lung carcinomas. In Vivo 2003;17:13-21.
46. Rosenman J. Can the use of amifostine improve cure rates for patients with advanced non-small cell lung cancer? Semin Oncol 2004;31:52-8.

47. American Cancer Society I. Learn about cancer. American Cancer Society; 2012 [updated 01/05/2012; cited 2012 05/05/2012]; Available from: http://www.cancer.org/Cancer/BrainCNSTumorsinAdults/DetailedGuide/brain-and-spinal-cord-tumors-in-adults-key-statistics.
48. Kim JH, Brown SL, Jenrow KA, et al. Mechanisms of radiation-induced brain toxicity and implications for future clinical trials. J Neurooncol 2008;87:279-86.
49. Ramanan S, Kooshki M, Zhao W, et al. The PPARalpha agonist fenofibrate preserves hippocampal neurogenesis and inhibits microglial activation after whole-brain irradiation. Int J Radiat Oncol Biol Phys 2009;75:870-7.
50. Limoli CL, Rola R, Giedzinski E, et al. Cell-density-dependent regulation of neural precursor cell function. Proc Natl Acad Sci USA 2004;101:16052-7.
51. Limoli CL, Giedzinski E, Rola R, et al. Radiation response of neural precursor cells: linking cellular sensitivity to cell cycle checkpoints, apoptosis and oxidative stress. Radiat Res 2004;161:17-27.
52. Raber J, Rola R, LeFevour A, et al. Radiation-induced cognitive impairments are associated with changes in indicators of hippocampal neurogenesis. Radiat Res 2004;162:39-47.
53. Coderre JA, Morris GM, Micca PL, et al. Late effects of radiation on the central nervous system: role of vascular endothelial damage and glial stem cell survival. Radiat Res 2006;166:495-503.
54. Otsuka S, Coderre JA, Micca PL, et al. Depletion of neural precursor cells after local brain irradiation is due to radiation dose to the parenchyma, not the vasculature. Radiat Res 2006;165:582-91.
55. Robbins ME, Zhao W. Chronic oxidative stress and radiation-induced late normal tissue injury: a review. Int J Radiat Biol 2004;80:251-9.
56. Schuller BW, Binns PJ, Riley KJ, et al. Selective irradiation of the vascular endothelium has no effect on the survival of murine intestinal crypt stem cells. Proc Natl Acad Sci USA 2006;103:3787-92.
57. Li YQ, Ballinger JR, Nordal RA, et al. Hypoxia in radiation-induced blood-spinal cord barrier breakdown. Cancer Res 2001;61:3348-54.
58. McKinley MJ, Albiston AL, Allen AM, et al. The brain renin-angiotensin system: location and physiological roles. Int J Biochem Cell Biol 2003;35:901-18.
59. Gard PR. The role of angiotensin II in cognition and behaviour. Eur J Pharmacol 2002;438:1-14.
60. Kim JH, Brown SL, Kolozsvary A, et al. Modification of radiation injury by ramipril, inhibitor of angiotensin-converting enzyme, on optic neuropathy in the rat. Radiat Res 2004;161:137-42.
61. Ryu S, Kolozsvary A, Jenrow KA, et al. Mitigation of radiation-induced optic neuropathy in rats by ACE inhibitor ramipril: importance of ramipril dose and treatment time. J Neurooncol 2007;82:119-24.
62. Robbins ME, Zhao W, Garcia-Espinosa MA, et al. Renin-angiotensin system blockers and modulation of radiation-induced brain injury. Curr Drug Targets 2010;11:1413-22.
63. Conner KR, Payne VS, Forbes ME, et al. Effects of the AT1 receptor antagonist L-158,809 on microglia and neurogenesis after fractionated whole-brain irradiation. Radiat Res 2010;173:49-61.
64. Robbins ME, Payne V, Tommasi E, et al. The AT1 receptor antagonist, L-158,809, prevents or ameliorates fractionated whole-brain irradiation-induced cognitive impairment. Int J Radiat Oncol Biol Phys 2009;73:499-505.
65. Lu D, Goussev A, Chen J, et al. Atorvastatin reduces neurological deficit and increases synaptogenesis, angiogenesis, and neuronal survival in rats subjected to traumatic brain injury. J Neurotrauma 2004;21:21-32.
66. Shishehbor MH, Brennan ML, Aviles RJ, et al. Statins promote potent systemic antioxidant effects through specific inflammatory pathways. Circulation 2003;108:426-31.
67. Shishehbor MH, Patel T, Bhatt DL. Using statins to treat inflammation in acute coronary syndromes: Are we there yet? Cleve Clin J Med 2006;73:760-6.
68. Chen J, Zhang ZG, Li Y, et al. Statins induce angiogenesis, neurogenesis, and synaptogenesis after stroke. Ann Neurol 2003;53:743-51.
69. Jenrow KA, Liu J, Brown SL, et al. Combined atorvastatin and ramipril mitigate radiation-induced impairment of dentate gyrus neurogenesis. J Neurooncol 2011;101:449-56.
70. Winkler F, Kozin SV, Tong RT, et al. Kinetics of vascular normalization by VEGFR2 blockade governs brain tumor response to radiation: role of oxygenation, angiopoietin-1, and matrix metalloproteinases. Cancer Cell 2004;6:553-63.
71. Gonzalez J, Kumar AJ, Conrad CA, et al. Effect of bevacizumab on radiation necrosis of the brain. Int J Radiat Oncol Biol Phys 2007;67:323-6.
72. Movsas B, Vikram B, Hauer-Jensen M, et al. Decreasing the adverse effects of cancer therapy: National Cancer Institute guidance for the clinical development of radiation injury mitigators. Clin Cancer Res 2011;17:222-8.
73. Ryan JL, Krishnan S, Movsas B, et al. Decreasing the adverse effects of cancer therapy: an NCI Workshop on the preclinical development of radiation injury mitigators/protectors. Radiat Res 2011;176;688-91.

74. Yuhas JM, Afzal SM, Afzal V. Variation in normal tissue responsiveness to WR-2721. Int J Radiat Oncol Biol Phys 1984;10:1537-9.
75. Rane N, Quaghebeur G. CNS effects following the treatment of malignancy. Clin Radiol 2012;67:61-8.
76. Sonis ST. Mucositis: The impact, biology and therapeutic opportunities of oral mucositis. Oral Oncol 2009;45:1015-20.
77. Matuschek C, Bolke E, Nawatny J, et al. Bevacizumab as a treatment option for radiation-induced cerebral necrosis. Strahlenther Onkol 2011;187:135-9.
78. Thompson LH, Suit HD. Proliferation kinetics of x-irradiated mouse L cells studied with time-lapse photography. Int J Radiat Biol Relat Stud Phys Chem Med 1969;15:347-62.
79. Brown JM, Wouters BG. Apoptosis, p53, and tumor cell sensitivity to anticancer agents. Cancer Res 1999;59:1391-9.
80. Rasey JS, Nelson NJ, Mahler P, et al. Radioprotection of normal tissues against gamma rays and cyclotron neutrons with WR-2721: LD50 studies and 35S-WR-2721 biodistribution. Radiat Res 1984;97:598-607.
81. Cassatt DR, Fazenbaker CA, Bachy CM, et al. Preclinical modeling of improved amifostine (Ethyol) use in radiation therapy. Semin Radiat Oncol 2002;12:97-102.
82. Rubio-Viqueira B, Hidalgo M. Direct in vivo xenograft tumor model for predicting chemotherapeutic drug response in cancer patients. Clin Pharmacol Ther 2009;85:217-21.
83. Murgo AJ, Kummar S, Rubinstein L, et al. Designing phase 0 cancer clinical trials. Clin Cancer Res 2008;14:3675-82.

Cite this article as: Prasanna PGS, Stone HB, Wong RS, Capala J, Bernhard EJ, VikramB, Coleman CN. Normal tissue protection for improving radiotherapy: Where are the Gaps? Transl Cancer Res 2012;1(1):35-48. DOI: 10.3978/j.issn.2218-676X.2012.05.05

Meet the Professor

Featured interviews with the global key opinion leaders in medical fields

AME Publishing Company

ASVIDE AME Surgical Video Database

PBPC

ISBN: 978-988-12997-2-7 (hardback)
ISBN: 978-988-12997-3-4 (eBook)

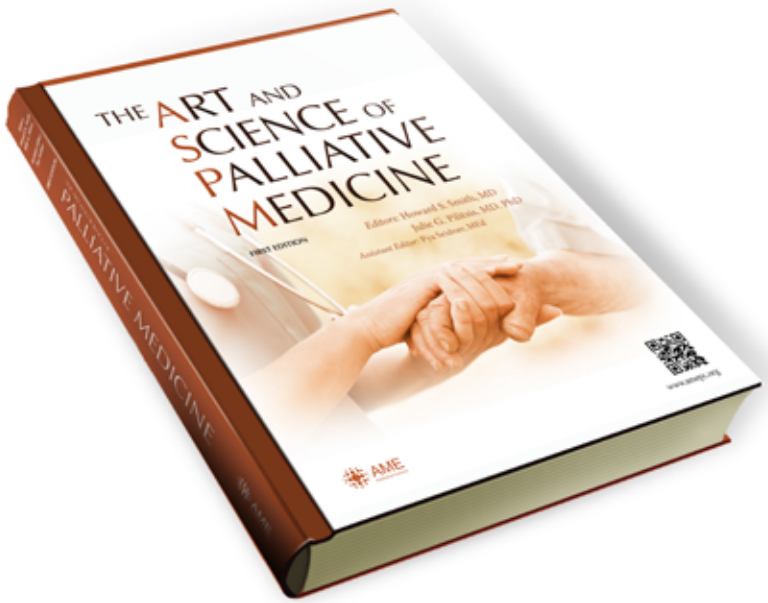

Editors:
Howard S. Smith, MD
Julie G. Pilitsis, MD, PhD

Assistant Editor:
Pya Seidner, MEd

Page count: 598

The goal of the book was to provide a resource that is usable in all countries, providing straightforward data as well as food for thought for providers worldwide. Its design by Howard Smith, MD, was brilliant in its simplicity as well as its breadth of coverage. It is useful both for the student and resident physician being first exposed to death and ding as well as the palliative care specialist that may be an expert in one facet of the patient's disease, but not in others. After reading this book, it was Dr. Smith's goal to arm the reader with a new set of tools in their daily responsibility and to be the best provider possible for their patients. It is meant to spawn interest in further reading on topics of interest and to promote future directions of study.

Julie G. Pilitsis, MD, PhD
Albany, NY, USA

"... to cure sometimes, to relieve often, to comfort always."
Attributed to Dr. Edward Livingston Trudeau, founder of a 19th century tuberculosis sanatorium, this could easily be a defining slogan for palliative care because nearly all care models highlight the reigning importance of the individual as the central point of care.

Amy P. Abernethy, M.D., Ph.D.
Current President, American Academy of Hospice & Palliative Medicine;
Duke University School of Medicine, Durham, USA

Please scan the above code for purchase information, or contact apm@amepc.org.

OPEN ACCESS

PEER-REVIEWED ACADEMIC JOURNALS

FOR THE PRACTICING CLINICIAN & RESEARCHERS

AME Publishing Company | PBPC

More online at www.thepbpc.org and www.amepc.org

Gold Anchor™

small size **big impact**

Unique marker design
Superior tissue attachment
Less artifacts
Enhanced MRI visibility

Super fine needle
Significantly improved safety with 25G and 22G needles

Improve positioning
Use markers safely in any inner organ, not only in prostate.

Shorten lead times
Obtain CT or MR for treatment plan on same day as marker implantation.

Reduce cost
Position patients faster with orthogonal kV-images.
Reduce complication rates from marker implantation.
Use standard MR sequences to fuse MR and CT images.

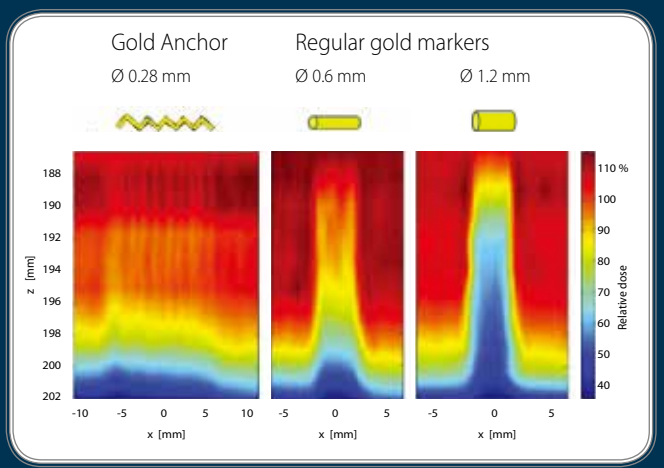

Great for proton therapy

The thinner (0.28 mm diameter) Gold Anchor markers cause very little dose perturbation when they are implanted with a line shape.

The high density material - gold - provides good visibility with kV imaging

These film measurements show dose perturbation for a Gold Anchor implanted with a line-shape (assumed to form more of a zigzag shape) vs. regular gold markers.

For more information, see
FineNeedleMarker.com/proton-treatments.html

CE marked and FDA cleared. Available from Naslund Medical AB (Sweden), Naslund Medical Inc. (USA), or one of our distributors.

Gold Anchor™
The fine needle marker - By Naslund Medical

Contact us for more information at info@FineNeedleMarker.com